UNIVERSITAT POLITÈCNICA DE VALÈNCIA

Contribution to the study of thermal, biological and photo degradation of polylactide

Doctoral Thesis

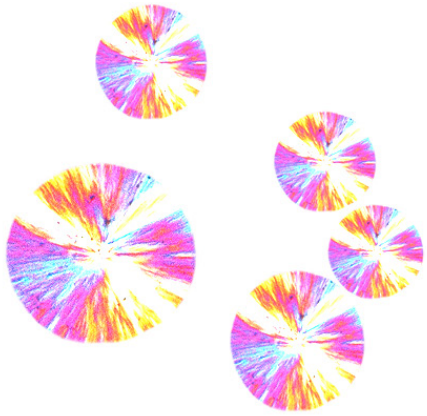

Presented by:
Laura Santonja Blasco

Directed by:
Dr. Amparo Ribes Greus

Valencia, June 2012

UNIVERSITAT POLITÈCNICA DE VALÈNCIA

Contribution to the study of thermal, biological and photo degradation of polylactide

Institut Tecnològic de Materials

Universitat Politècnica de València

Tesi Doctoral

Presentada per:
Laura Santonja Blasco

Dirigida per:
Dra.Amparo Ribes Greus

València 2012

Als meus pares

Declaration

This is a doctoral thesis submitted to the Univesitat Politècnica de València for the requeriments for the degree of Doctor in Engineering and Industrial Production with International mention.

This work has not been previously submitted for any degree and is believed to be wholly original. The research has been carried out by me in the Univesitat Politècnica de València (Spain), Florida State University (USA) and University of Bologna (Italy)

Acknowledgments

Quan una etapa tant intensa i important acaba u recorda amb emoció tota la gent que ha format part d'eixe recorregut.

En primer lloc agrair la labor de la meua guia professional la Dra. Amparo Ribes Greus, pel seu constant estímul, per transmitir-me la seua passió per l'aprenentatge continu en la investigació i docència, per confiar amb mi i incitar-me cada dia a nous reptes. T'agreix l'orientació i dedicació rebuda al llarg d'estos anys de doctorat i convivència.

El meu agraïment a la Dra. Rufina Alamo per la seua acollida durant les meues estades breus en la Florida State University desde 2009 a 2012. Gràcies per la seua implicació en el meu treball i en la meua formació, per submergir-me al món de la cristal·lització de polímers i motivar-me a créixer com a investigadora.

També agrair la direcció rebuda pel Dr. Andrea Saccani durant la direcció de la meua Master Thesis en la Università di Bologna.

Ha sigut un gran privilegi compartir estos anys amb Amparo i amb els companys en la UPV, eixa gran família "india" que sempre m'acompanya, de la que he aprés valors que m'han fet millor treballadora i persona.

Gràcies Fran per la teua energia i bons consells, recorde amb gust les teues vingudes a València i la teua implicació en el treball. Gràcies Rosana per tantes vivències que hem compartit a nivell personal i professional, per contagiar-me la teua motivació i optimisme.

Alf t'agraeix els teus consells, l'entusiasme que em transmiteixes, la teua professionalitat i la teua capacitat de fer-nos mirar sempre endavant amb il·lusió. Gràcies Jose per compartir PLA-talks, per l'alegria i positivisme que m'aportes, pel teu compromís i saber fer dins del nostre equip. Als dos especialment vos agreix la vostra ajuda en estos últims anys. T'agraix Roberto que sempre tingues una solució "informàtica-electrònica" increïble a qualsevol problema, per la teua implicació en el grup i per "traure'ns" als japos. Gràcies Cristina per la teua dedicació, pel teu afany en els nous projectes i per la teua vitalitat. Volia agrair-te Marta la entrega i cura amb la portes endavant nous desafiaments que fan que el lab estiga tan actiu. Soraia t'agraeix que ens hajes portat tanta "química" al laboratori, per la teua disposició i implicació...Vamos equipo...estem ahí!.

També vull agrair als estudiants amb els que he treballat i que m'han ajudat a créixer a nivell professional, especialment a Cristina. Amb ells he anat aprenent el que significa el compromís i l'alegria dels resultats finals.

Als meus companys en FSU, Asif, Linda, Diamond, Madhavi, Eduardo, Juan Mari gràcies per la vostra amabilitat i companyerisme. Especialment el meu agraïment a Carolina i Papatya per tota la ajuda proporcionada a nivell personal i científic. A Zeena Mae, Carolina, Jesús, Patty i Mark, gràcies a tots per aconseguir que les estades doctorals a USA hagen sigut una forma de vida inoblidable. A Mariado, des del dia que ens pujarem l'avió gràcies per els bons moments compartits.

Als amics i amigues repartits per diferents ciutats, especialment en Bocairent i “contornà”, gràcies per les estones compartides durant estos anys, per carregar-me les piles quan més ho necessite, per sempre estar apunt per fer una sopaeta i per mantindre el contacte actiu després de tants “no puc quedar” per la meua part. El meu agraïment a Sara i Mónica, els anys de Zariñena quan començava la tesi, van ser increïbles haver compartit eixos anys convivència amb vosaltres.

Estos anys han sigut complets gràcies a la presència i recolzament de la meua família, als meus sogres, tios/as, cunyats/des, cosins/es, nebots/es, heu jugat un paper fonamental estos anys ja que amb una paella, un sopar, les vostres aportacions a la nostra despensa i amb el somriure dels nebodets es supera tot l’estrés. Gràcies per estar ahí i animar-me sempre. Un agraïment a mon tio Ximo el primer politècnic de la família que em va aconsellar sobre els obstacles i gratituds d’esta carrera. I com no a les meues iaies, Araceli i Maria, per els divendres a casa, els berenars quan torne de València, per la energia que em transmitiu i pel gran exemple que sou en la meua vida.

Gràcies infinites a ma mare, mon pare i la meua germana, sempre hem fet una pinya per superar els moments més durs i per gaudir al màxim els bons. Paqui i Juan sou els meus pilars i ho sereu sempre, sou exemple d’il·lusió, sacrifici i superació, heu peleat dur en la vostra vida perquè no ens falte de res i ho heu aconseguit, el que ens heu brindat no té preu. Silvia, com agrair-te els consells, la teua estima i la teua incondicionalitat, quatre rialles i alguna cançó distorsionada canvien un moment dur, gràcies per estar ahí sempre i per dissenyar-me la portada de la tesi.

I com no gràcies Isidro, per brindar-me el teu recolzament, entusiasme i fer-me gaudir de la vida. En estos anys hem emprés projectes i construït llars en diferents barris, ciutats i països i sempre amb la força que et caracteritza i que fa que xicotets gests es converteixen en un motor de vida.

Summary

The purpose of this PhD thesis is to study the effect of thermal, biological and photo degradation on polylactide (PLA) to characterize the changes occurring under different conditions during its life cycle. This biodegradable polymer is obtained from renewable resources and is considered an excellent candidate to substitute other polymeric materials with scarce degradability. The decrease on the polylactide molar mass was monitored by Gel Permeation Chromatography (GPC) and Viscometry. Additionally, Fourier Transform Infrared Spectroscopy (FTIR) was used to determine the degradation mechanisms and their effect on the chemical structure of PLA. Moreover, the impact of each type of degradation on the morphology and the thermal and viscoelastic properties of PLA was also determined. Thermogravimetric Analysis (TGA) was applied to monitor changes in the thermal stability of the materials caused by the different degradation types, by using several parameters such as the maximum thermal degradation rate or the activation energy. The effect of bio and photo degradation on the material surface was evaluated by Scanning Electron Microscopy (SEM), revealing variations exclusively caused by biological degradation. The thermal and viscoelastic properties were measured by Dynamic Mechanical Thermal Analysis (DMTA), Differential Scanning Calorimetry (DSC) and Optical Microscopy (OM). The decrease of molar mass with biodegradation time follows a first order process ($M_n = M_{no}\, e^{-kt}$) while the molar mass of specimens tested during thermal and photo degradation follows a second order law ($1/M_n = (1/M_{no})+k \cdot t$). Several characteristic parameters were obtained to determine their variation with degradation and molar mass and the effect of each type of degradation. The dependence of the molar mass with the spherulites growth rate is especially acute in bio and photo degraded samples, following an exponential law typical of semicrystalline polymers. The results have shown that each degradation is controlled by several factor that affect differently the morphological, thermal and mechanical properties of PLA, highlighting that degradation cannot be explained by a solely effect of chains breakage and molar mass reduction. The appearance of new functional groups is fundamental to control the crystallization of the material. Furthermore the formation and size of crystals are the most significant parameters to describe the macroscopic properties, and therefore establish the PLA degradation. In particular, the results obtained are of great interest to design a controlled management of PLA disposal and to estimate the time to reach considerable reduced molar masses. This study offers a complete characterisation of each degradation type, through the combination of all the techniques under use, by creating a methodology capable to predict the behaviour of polymers potentially degradable at long exposure times.

Resum

L'objectiu de la present tesi doctoral és l'estudi de l'efecte de la degradació tèrmica, biològica i fotolítica a la polilactida (PLA) per caracterització dels canvis que ocorren sota diferents condicions durant la seua vida útil. Aquest polímer biodegradable procedeix de fonts renovables i està considerat un excel·lent candidat per substituir altres materials polimèrics amb escassa degradabilitat. La monitorització del descens de massa molar de polilactida es realitzà mitjançant Cromatografia de Permeació en Gel (GPC) i Viscosimetria. Addicionalment, es va emprar l'Espectroscòpia Infraroja amb Transformada de Fourier (FTIR) per establir els mecanismes que controlen la degradació i llur efecte a la estructura química de la polilactida. Tanmateix s'ha determinat l'impacte dels tipus de degradació a la morfologia i a les propietats tèrmiques i mecàniques del PLA. La Termogravimetria (TGA) va permetre monitoritzar canvis a la estabilitat tèrmica del material deguts als diferents tipus de degradació, emprant paràmetres com la temperatura de màxima velocitat de degradació tèrmica o l'energia d'activació. El resultat de la degradació biològica i fotolítica a la superfície del material va ser avaluat mitjançant Microscòpia Electrònica de Rastreig (SEM), observant-se únicament canvis atribuïbles a la degradació biològica. Les propietats viscoelàstiques i tèrmiques es van analitzar per Anàlisi Dinàmic-Mecànic-Tèrmic (DMTA), Calorimetria Diferencial de Rastreig (DSC) i Microscòpia Òptica (OM). El descens de la massa molar de les mostres biodegradades amb el temps segueix un procés de primer ordre ($M_n = M_{no}\, e^{-kt}$) mentre que en el cas de la degradació tèrmica i fotolítica aquest segueix un procés de segon ordre ($1/M_n = (1/M_{no}) + k \cdot t$). De cada tècnica d'estudi s'han obtingut els paràmetres més rellevants per discernir les diferències entre els tres processos de degradació. La dependència de la massa molar amb la velocitat de creixement lineal de les esferulites és especialment notable en les mostres degradades biològica i fotolíticament, seguint una relació exponencial característica dels polímers semi-cristal·lins. Els resultats han mostrat que cada degradació està controlada per diversos factors que afecten de diferent forma les propietats morfològiques, tèrmiques i mecàniques del PLA, remarcant d'aquesta forma que no és únicament la ruptura de cadenes i la reducció de la massa molar el fenomen que regula les degradacions. L'aparició de nous grups funcionals resulta fonamental per a controlar el procés de cristal·lització del material. Tanmateix s'ha comprovat que la aparició i grandària dels cristalls és el paràmetre més significatiu per descriure les propietats macroscòpiques i per tant per establir la degradació del PLA. Particularment, els resultats obtinguts són de utilitat per dissenyar una gestió controlada de deposició del PLA i per estimar el temps al que el material abasta masses molars molt reduïdes. Aquest estudi ofereix una caracterització de cada tipus de degradació mitjançant la combinació de totes les tècniques utilitzades, creant una metodologia capaç de predir el comportament de polímers potencialment degradables a tems llargs d'exposició.

Resumen

El propósito de la presente tesis doctoral es el estudio del efecto de la degradación térmica, biológica y fotolítica en la polilactida (PLA) para caracterizar los cambios que tienen lugar bajo diferentes condiciones durante su vida útil. Este polímero biodegradable procede de fuentes renovables y está considerado un excelente candidato para sustituir a otros materiales poliméricos con escasa degradabilidad. La monitorización del descenso de masa molar de polilactida se realizó tanto mediante Cromatografía de Permeación en Gel (GPC) como por Viscosimetría. Adicionalmente se utilizó la Espectroscopía Infrarroja con Transformada de Fourier (FTIR) para establecer los mecanismos que controlan la degradación y su efecto en la estructura química de la polilactida. Asimismo, se ha determinado el impacto de cada tipo de degradación en la morfología y en las propiedades térmicas y mecánicas del PLA. La Termogravimetría (TGA) permitió monitorizar los cambios en la estabilidad térmica del material debidos a los diferentes tipos de degradación, utilizando parámetros como la temperatura de máxima velocidad de degradación térmica o la energía de activación. El resultado de la degradación biológica y fotolítica en la superficie del material fue evaluado mediante Microscopía Electrónica de Barrido (SEM), observándose únicamente cambios debidos a la degradación biológica. Las propiedades viscoelásticas y térmicas se analizaron mediante Análisis Dinámico-Mecánico-Térmico (DMTA), Calorimetría Diferencial de Barrido (DSC) y Microscopía Óptica (OM). El descenso de la masa molar de las muestras biodegradadas con el tiempo sigue un proceso de primer orden ($M_n = M_{no}\, e^{-kt}$) mientras que en el caso de la degradación térmica y fotolítica éste sigue un proceso de segundo orden ($1/M_n = (1/M_{no}) + k \cdot t$). De cada una de las técnicas se ha obtenido los parámetros más relevantes para discernir las diferencias entre los tres procesos de degradación. La dependencia de la masa molar con la velocidad de crecimiento linear de las esferulitas, es especialmente notable en las muestras degradadas biológicas y fotolíticamente, siguiendo una relación exponencial característica de polímeros semicristalinos. Los resultados muestran que cada degradación está controlada por diversos factores que afectan de diferente forma a las propiedades morfológicas, térmicas y mecánicas del PLA, enfatizando así que no es únicamente la ruptura de cadenas y la reducción de la masa molar el fenómeno que regula dichas degradaciones. La aparición de nuevos grupos funcionales resulta fundamental para controlar el proceso de cristalización del material. Asimismo se ha comprobado que la formación y tamaño de los cristales es el parámetro más significativo para describir las propiedades macroscópicas y por tanto establecer la degradación del PLA. En particular, los resultados obtenidos son de utilidad para diseñar una gestión controlada de deposición del PLA y para estimar el tiempo en que el material alcanza masas molares muy reducidas. Este estudio ofrece una caracterización de cada tipo de degradación mediante la combinación de todas las técnicas utilizadas, creando una metodología capaz de predecir el comportamiento de polímeros potencialmente degradables a tiempos largos de exposición.

Glossary

A	Pre-exponential factor
α_f	Thermal expansion coefficient
ΔHc	Crystallization enthalpy
ΔH_m	Melting enthalpy
ATR	Attenuated total reflectance
β	Heating rate
DMTA	Dynamic Mechanical Thermal Analysis
DSC	Differential Scanning Calorimetry
E'	Storage modulus
E''	Loss modulus
Ea	Activation energy
$f(\alpha)$	Differential function of the kinetic model
ϕ	Relative free volume
FTIR	Fourier Transform Infrared Spectroscopy
$g(\alpha)$	Integral function of the kinetic model
G	Growth rate
GPC	Gel Permeation Chromatography
η	Intrinsic viscosity
I	Intensity
MMD	Molar Mass Distribution
M_n	Number-average molar mass
M_w	Weight-average molar mass
M_v	Viscosity molar mass
PLA	Polylactide
OM	Optical microscopy
ROP	Ring Opening Polymerization
SEM	Scanning Electron Microscopy
$Tan\ \delta$	Loss tangent
T_c	Crystallization temperature
T_m	Melting temperature
T_g	Glass transition temperature
TGA	Thermogravimetric Analysis
T_{max}	Temperature of the maximum loss modulus
T_{peak}	Maximum temperature of thermal decomposition

Contents

Chapter 3: Experimental Part

Chapter 4: Results and discussion

Chapter 5: Conclusions

Annex: Publications during the research period **289**

Chapter 1

State of the Art Motivation and Aim

1.1 Polymer production and waste management in packaging

During the last decades the overall society has increased the consumption of polymers to satisfy the requirements of the different economic sectors. Among the different existing polymers, thermoplastics and thermosetting plastics are especially relevant because of their huge production volumes. Figure 1-1 summarizes the most recent data regarding worldwide plastic production [1].

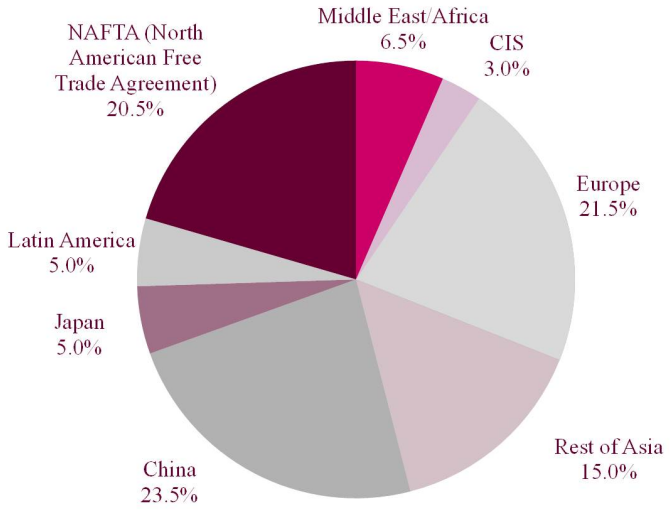

Figure 1-1 World plastic production during 2010; the values are given in percentage of the 265 million of tons (Mt) annual.

Annual plastics production reached approximately 57 Mt in 2010, only in Europe, whereas worldwide production leapt to 265 Mt in the same year. China is the principal producer (23.5% world production) closely followed by Europe (21.5% world production) and North American Free Trade Agreement (20.5% world production). Germany is the major European producer, accounting for 7.0% of global production followed by Benelux (3.5%), France (3.0%), Italy (2.0%), the UK and Spain (1.5%) and others (3%). The "Compelling Facts About Plastics 2011" report, by the Plastics Europe organization, predicted to exceed 300 Mt of world consumption in 2011 [1].

Plastics demand by converters in Europe was 46.4 Mt in 2010, being polyethylene (PE's), polypropylene (PP), polyvinylchloride (PVC) and polystyrene (PS) the most required (see Figure 1-2) In general, all of them are designed and manufactured to resist environmental degradation.

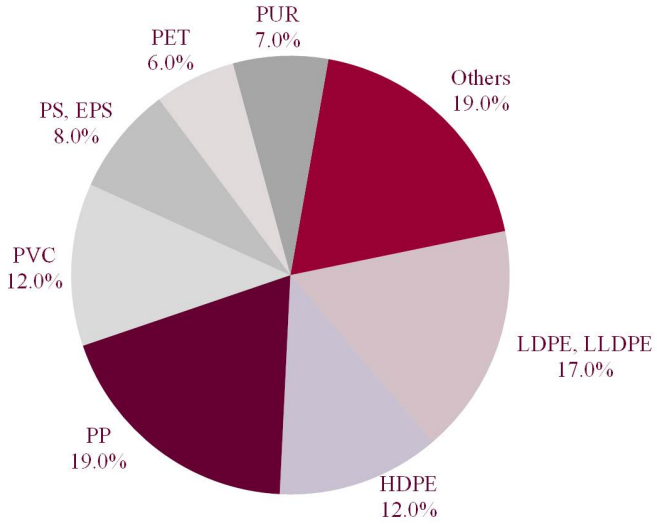

Figure 1-2 Plastics demand in Europe 2010 by types. Source: Plastics Europe Market Research Group (PEMRG) [1].

Plastics are applied in different industrial sectors, as Figure 1-3 shows. Packaging is the principal industrial sector, followed by building and construction.

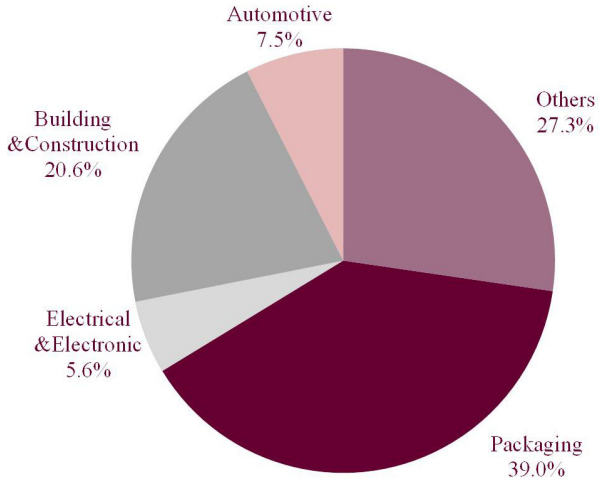

Figure 1-3 Plastics demand in Europe 2010 by economic sectors. Source: Plastics Europe Market Research Group (PEMRG) [1].

Materials used for packaging present fast disposal, due to their short service life. Furthermore, they are designed to be resistant to environmental degradation. Both characteristics result in a significant increase of packaging plastic waste. This problem concerns, not only the richest countries, but also less technologically developed regions due to the impact of tourism, exportation and the increase of resources demand. Thus, the increase in plastic production and demand consequently implies that society has to face two main problems: the increase of plastic waste accumulation and a faster decrease of the traditional resources [2,3].

A number of strategies may be used to respond to uncontrolled plastic waste accumulation. The options traditionally used for plastic waste management, but less recommended are:

- Landfill disposal is still the main destination for plastic waste, representing 42% of the post-consumer plastic waste in Europe [1]. However, it does not ensure protection of the environment, especially of soil and water, since the materials take hundreds of years to completely degrade, without any energy recovery.

- Incineration is also used, representing 34% of the plastic waste [1]. Despite the benefits of energy recovery and the possibility to generate electricity from combustion, this option is not recommended due to strong air pollution.

More recently, several efforts have been made to guarantee suitable waste management thereby reinforcing environmental protection:

- Recycling is the most suitable option within the different widespread techniques. Mechanical recycling entails re-melting of classified plastic wastes into new plastic options, allowing for energy recovery during the process. New valuable materials are obtained, usually with modified mechanical properties, but still suitable for other purposes. The total material recycling rate of post-consumer plastics in Europe was 24% during 2010 [1].

The application of these strategies for plastic waste management is always difficult, especially in countries with less investment. Cities in Africa, South America and Asia only collect between the 50% and 80% of waste generated. Open dumping is then the only disposal method available, with the consequent environment (soil, water, air...) and health (citizens) impact [4,5,6].

Recently, the use of polymers designed to be degraded by the environment with harmless sub-products has been developed as an interesting alternative for waste managing. The production of biodegradable polymers is an emerging sector of industrial biotechnology, especially for product niche markets such as packaging or car-interior fittings.

Biodegradable polymers from renewable resources (such as wheat, potatoes, corn, sugar cane, etc.) stand out as a reliable alternative to commodities in packaging applications, as most of them are hydrolytically degradable polymers [7]. Some of these new polymers are currently used as components of drug delivery systems, degradable sutures and orthopedic supports [8]. The use of biodegradable polymers from renewable sources can reduce the dependence from fossil sources and open new fields of research, and may also contribute to mitigate uncontrolled disposal of plastics worldwide.

Nowadays, bioplastics (including biodegradable and non-biodegradable polymers from renewable resources) represent around 0.30 % of the World Plastics Production (724000 tonnes, 2010) [9]. Figure 1-4 shows the distribution of Bioplastics World production [10]. Within the overall bioplastics production, the biodegradable polymers represented the 59% in 2011 [10].The largest production of biodegradable polymers is occupied by starch based thermoplastic (SBT), polylactide (PLA) and polyhydroxyalcanoate (PHA). Figure 1-5 schematically summarizes the interrelations between the different raw plastic sources, the polymer transformation and the disposal options when plastic is used for packaging.

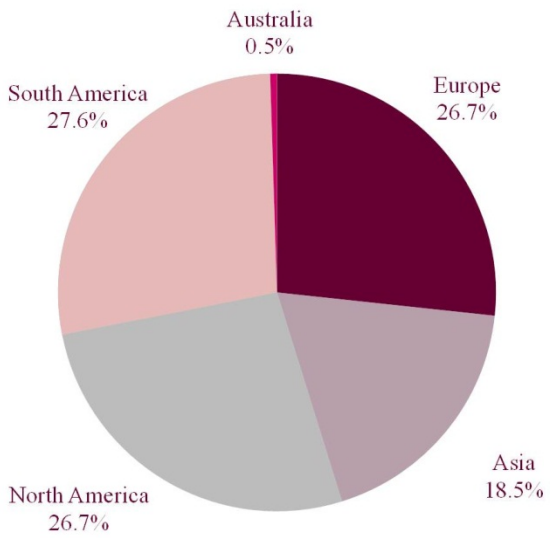

Figure 1-4 Bioplastic production in the world in 2011 [9].

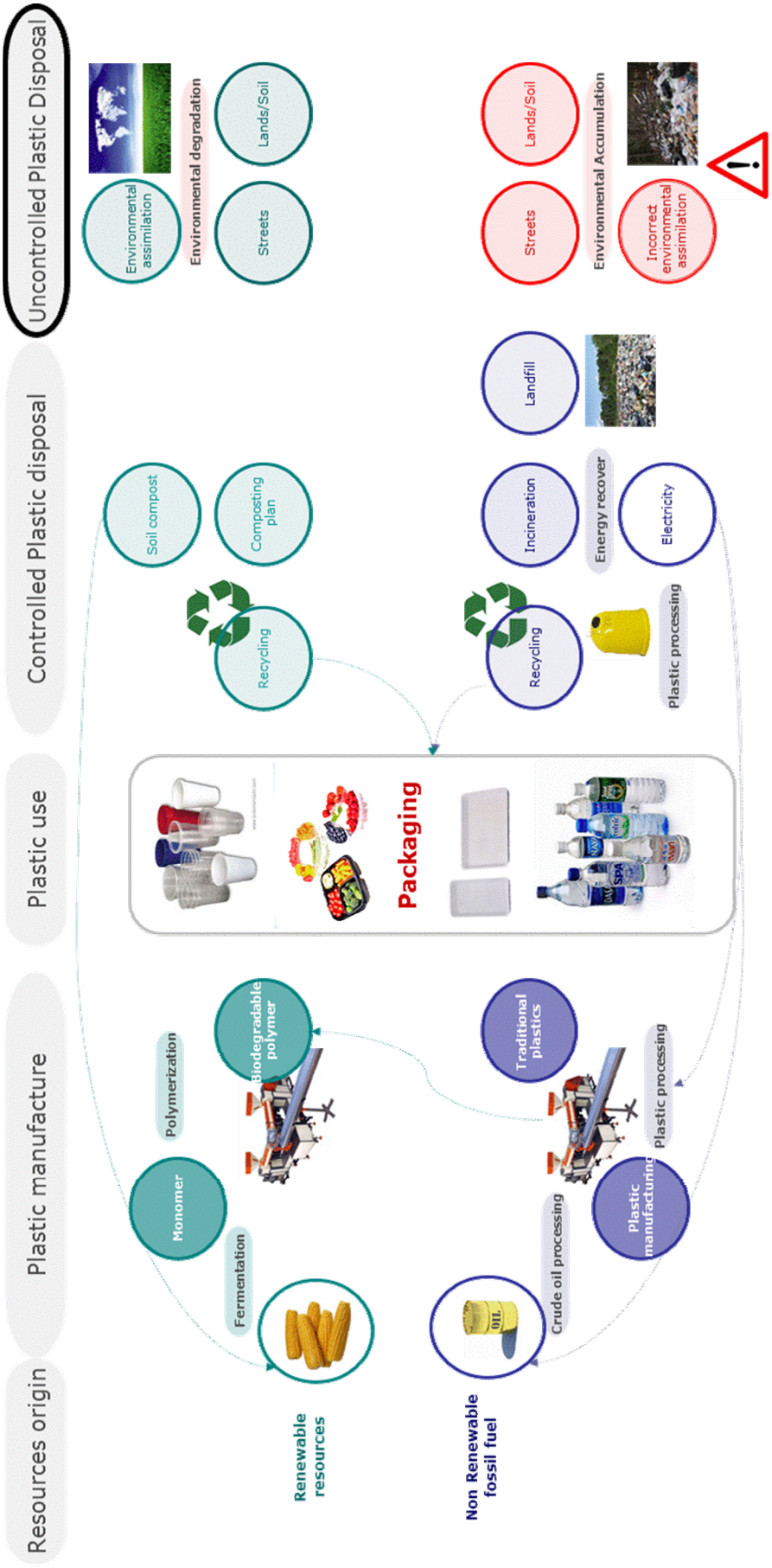

Figure 1-5 Life cycle of plastics from different resources used for packaging.

1.2 Biodegradable polymers. Polylactide

1.2.1 Definitions

Efforts to reduce environment impact of plastic waste have been translated into research in new material sources and production of eco-friendly products made from renewable raw materials. Even though terms as *biopolymers*, *biodegradable polymer*s and *bioplastics* are indistinctly used for designing polymers obtained from non-fossil sources, each of them have different meanings.

A *biopolymer* is defined as a polymer involving living organisms in its synthesis process, according to ASTM D6866-06 [11]. It therefore has a partial or total biochemical origin whereby it can be partially or totally produced from natural, renewable materials (biomasses) and can be potentially biodegradable (ASTM D6400-04) [12]. *Biopolymers (*or biobased polymers*)* can be grouped into the three following categories:

a) Polymers extracted directly from biomass and further processed. Examples of this category are starch modified polymers and polymers derived from cellulose.

b) Polymers produced directly by microorganisms in their natural or genetically modified state, such as polyhydroxyalcanoates (PHAs).

c) Polymers obtained with the participation of bio-intermediaries, produced with renewable raw materials. Some examples are polylactide (PLA) from the polymerization of lactic acid obtained from natural products as starch; bio-polyethylene (BPE), from the polymerization of ethylene produced from bio-ethanol; bio-nylons via diacids from biomass; and bio-polyurethanes, incorporating polyols of vegetal origin.

Biodegradable polymers are defined as those that undergo microbial induced chain excision leading to their mineralization. Specific conditions in terms of pH, humidity, oxygen content and the presence of some metals are usually required to ensure biodegradation of such polymers [13]. Biodegradable polymers can be produced from biosources as corn, wood cellulose, etc., or can be synthesized by bacteria from small molecules [14].

Alternatively, some biodegradable polymers can be derived from petroleum sources or also be obtained from mixed sources of biomass and petroleum [15]. The best known petroleum source-derived biodegradable polymers are aliphatic polyesters or aliphatic-aromatic copolyesters. However biodegradable polymers made from renewable resources are attracting much more interest since they are environmental friendly, in contrast to the fully petroleum based.

The American Society for Testing and Materials (ASTM, D6400 standard) alternatively defines a *biodegradable polymer* as a degradable material where the degradation results from the action of microorganisms such as bacteria, fungi, and algae. Biodegradable polymers can degrade in composting facilities and break down into water, methane, carbon dioxide and biomass [16]. The degradation process of the polymers by microorganisms in soil or compost can be then measured by standard tests over specified time-frames.

Finally, *Bioplastics* can be defined based in two criteria [10]

1. The first criterion **is the raw materials basis**. *Bioplastics* are materials that contain biopolymers in various percentages, although there is no consensus regarding the specific minimum bio-derivative content. These materials can be molded by heat and pressure, and some of them can persist to microbial degradation, such as polythioesters [17].

2. The second criterion is focused on **their functionality, "compostability"**. It is accepted that all biodegradable plastics are considered bioplastics, even if they are totally composed of petrochemical polymers. This means that polymers from fossil sources, such as polycaprolactone (PCL), polybutyleneadipate/ terephthalate (PBAT), are considered bioplastics but not biopolymers [18].

Thus, *Bioplastic* is a general term used in industry because concerns non-biodegradable biopolymers, polymers with different concentration of biopolymers and biodegradable polymers from non-renewable sources.

1.2.2 Classification of biodegradable polymers

Biodegradable polymers can be classified according to different features: the synthesis and processing methods, chemical composition, economic importance, applications, etc. Each of these classifications provides different and useful information. Figure 1-6 shows a classification of biodegradable polymers according to their origin: polymers coming from renewable resources obtained totally or partially by living microorganisms and petroleum based polymers obtained by chemical synthesis.

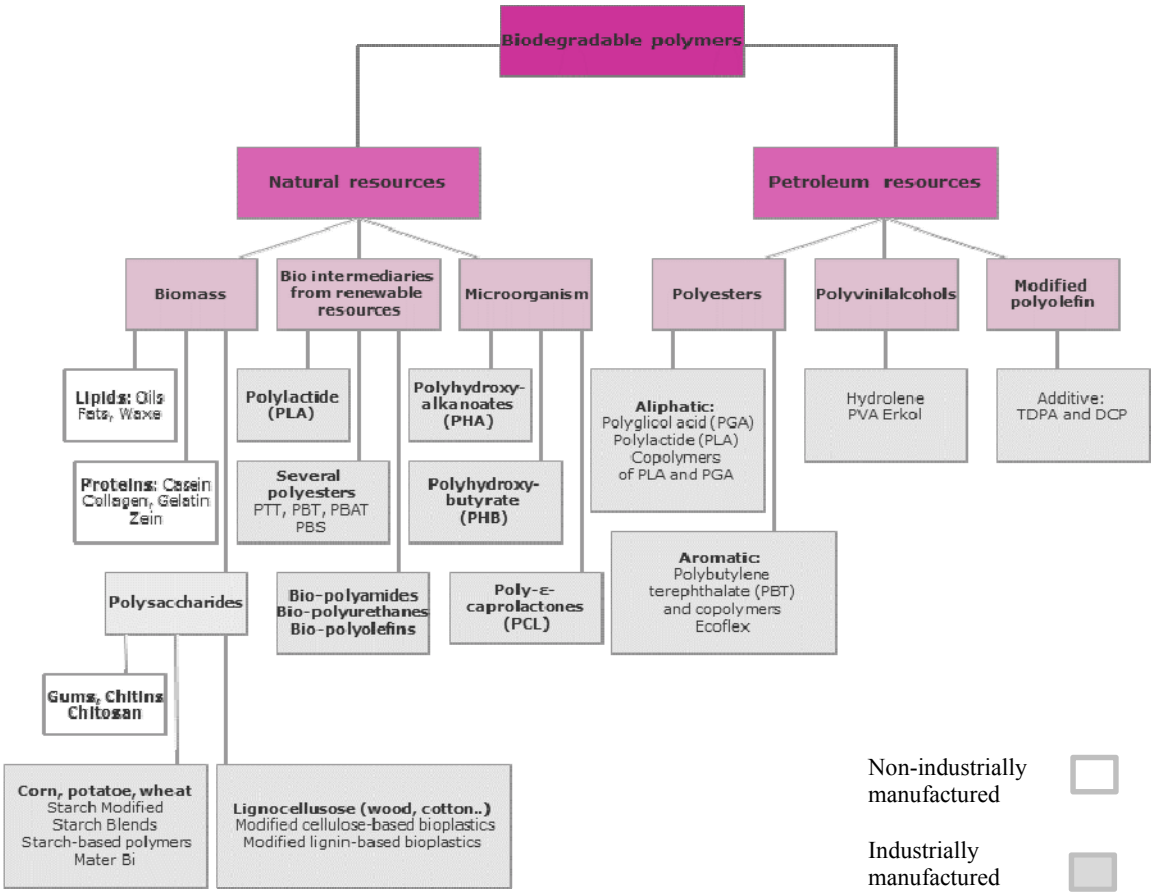

Figure 1-6 Classification of biodegradable polymers.

The penetration of bioplastic industry into the market relies on offering products favorable to the environment. The added value of these products is based on several features: a lower energy demand in processing than ordinary plastics, the release of CO_2 and water only after degradation, potential use as compost and the possibility to incorporate exclusively renewable raw materials in the production processes. The most commercialized biodegradable polymers, such as starch-based thermoplastics or polylactide, possess the

previous features. Considering their good thermal and mechanical properties, these polymers are potential alternatives to conventional thermoplastic polymers of petrochemical origin, such as polyolefins, despite the scale world production is still very low.

1.2.3 Structure and main features of polylactide

Polylactide (PLA) is a versatile compostable and bio-assimilable polymer that is made from 100% renewable resources, such as corn, sugar beets or rice. It is considered a major alternative to petroleum-based products for disposable uses, as there is a huge variety of PLA commercial products [19].

Polylactide is an aliphatic polyester with lactic acid as the fundamental constitutional unit (Figure 1-7). The majority of lactic acid is made by bacterial fermentation of carbohydrates or chemical synthesis. Lactic acid (2-hydroxy propionic acid) is the simplest hydroxyl acid with an asymmetric carbon atom and it exists in two optically active configurations, the L(+) and D(-) isomers (see Figure 1-8).

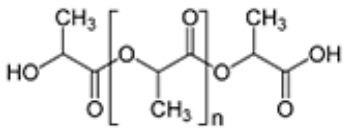

Figure 1-7 PLA structure.

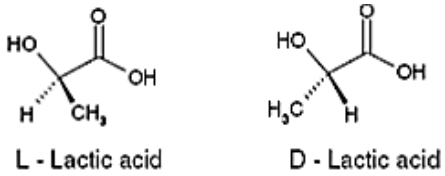

Figure 1-8 Different isomeric forms of lactic acid.

There are three main processing methods of PLA, which will finally determine its molar mass [20], they are summarized in Figure 1-9.

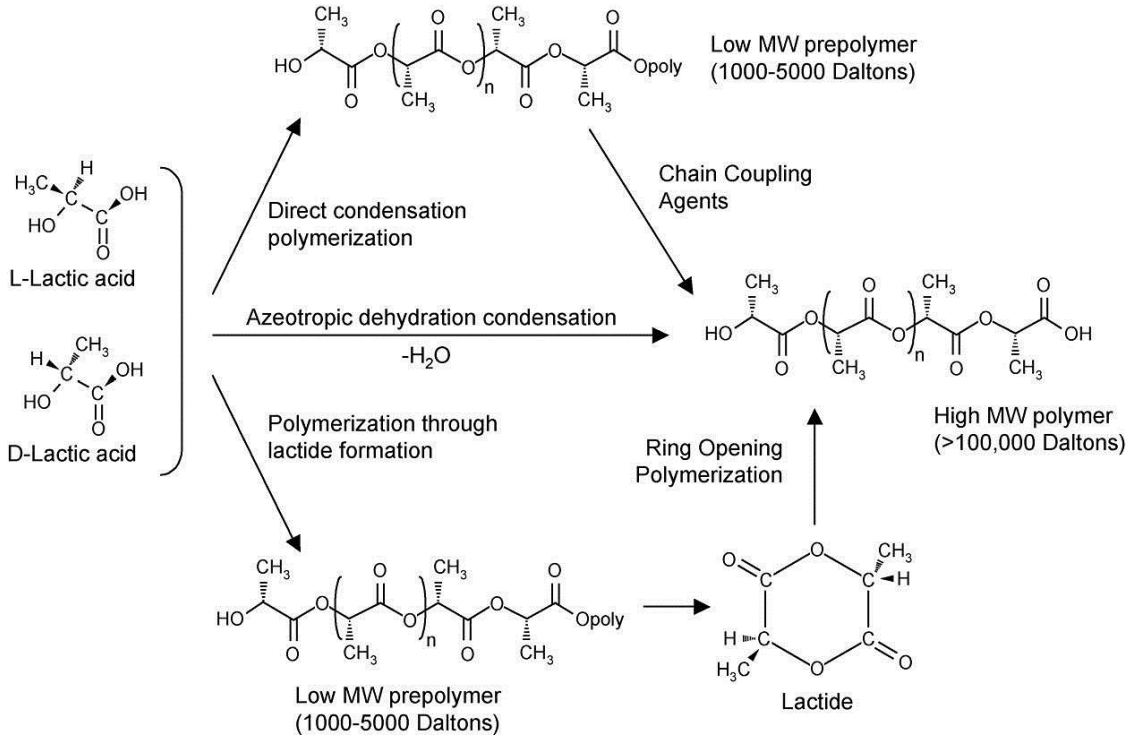

Figure 1-9 Synthesis methods for obtaining PLA (Figure from *ref. 21* adapted from *ref.26*).

1. *Direct condensation polymerization*. Polycondensation is well-established due to its simplicity, since the main reaction simply involves loss of water. This process leads to low molar mass PLAs, and thus low reaction yields, but results effective when the main objective is to have large amounts of the material with no stereospecificity [22,23].

2. *Azeotropic dehydrative condensation*. Azeotropic dehydrative condensation of lactic acid can yield high molar mass PLAs without the use of chain extenders or adjuvants [24,25].

3. *Ring Opening Polymerization (ROP)* of lactide. Lactide is the cyclic dimer of lactic acid, and is formed by condensation of two lactic acid molecules, catalytically converted to three different stereoisomers [26,27] (Figure 1-11): L-lactide (two L-lactic acid molecules), D-lactide (two D-lactic acid molecules) and meso-lactide (one L-lactic acid and one D-lactic acid molecule). Polymerization through lactide was first demonstrated by Carothers in 1932 [28], was patented by Cargill Inc. in 1992 and is the benchmark method used for PLA production [29]. This method, which is

schematically shown in Figure 1-10, leads to polymers of high molar mass with a high degree of stereo-regulation.

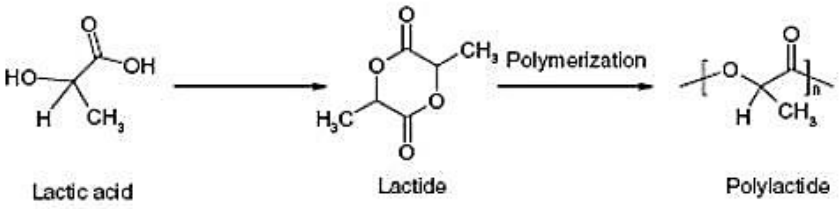

Figure 1-10 Polylactide formation by Ring Opening Polymerization (ROP) (Reproduced from *ref.* 30).

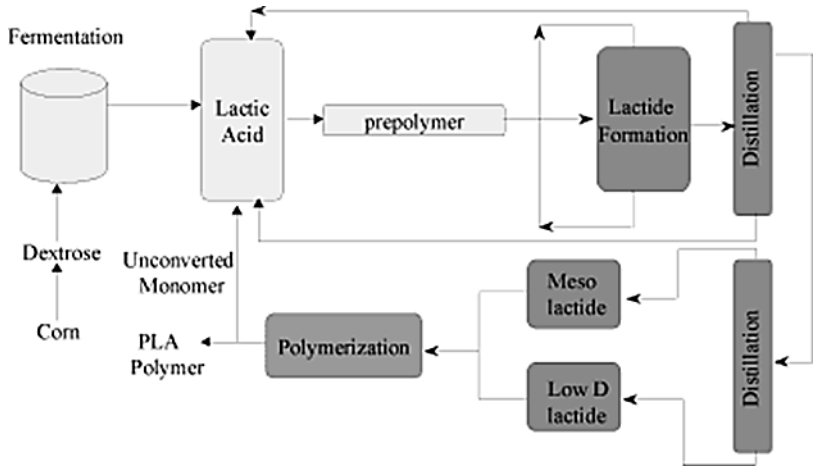

Figure 1-11 Lactide formation (Reproduced from *ref.* 31).

While the product of the first two methods is referred as poly(lactic acid), the product resulting from *Ring Opening Polymerization (ROP)* of lactide is called polylactide. Both products are generally referred to as PLA.

Polylactide has demonstrated to be competitive in industrial, agricultural or medical applications, because it is easily processed on standard equipment, representing 43% of the bio-based polymers market [32]. As an example, NatureWorks LLC has a manufacturing plant with capacity to produce 140000 metric tons of polylactide polymers per year, under the trademarks NatureWorks® PLA and Ingeo® fibers. Market advance has allowed a decrease in the price of polylactide from 2.20 - 3.40 € in 2003 to nearly 1.6 € per kg, currently [33]. It is also worth remarking that the carbon dioxide emission is 1.8 kg CO_2, / kg PLA, nearly half of the emissions generated in LDPE production [34,35]. The company has forecast to

commercialize PLA in several sectors, including fibers and fabrics, packaging, transportation market and electric and electronics.

1.2.4 Barrier properties of polylactide

Packaging is an important application sector of PLA, due to its combination of service life properties and biodegradable character. In general, packaging products are designed to yield efficient processing, to achieve competitive markets, and fulfill healthy requirements and environmental guidelines. Packaging materials must possess appropriate barrier properties respect to moisture and oxygen in order to preserve the package contents.

PLA has high odor and flavor barrier properties. It also has high resistance to grease and oil, thus finding application in the packaging of viscous oily liquids. It is also suitable for packaging of dry and short shelf-life products, although not for carbonated beverages (poor CO_2 barrier). Despite PLA pellets are hygroscopic [36], PLA foils present good moisture barrier properties, even better than starch-based polymers, which highlights the importance of processing on the final PLA properties. The medium water barrier can be of interest for some applications; *i.e*. in clothing where high water transmission for fabrics is a desirable property [29]. Also, some additives can be incorporated to PLA in order to improve its barrier properties respect to, for example, gas transport [37].

1.2.5 Thermal properties of polylactide

Selection of different processing conditions yields to PLAs with a wide range of physical and chemical properties [38,39]. In particular, the thermal behavior of polylactide is very dependent on the molar mass and the stereochemical constitution of the backbone. This stereochemical makeup can be controlled by the polymerization (and copolymerization) of D-lactide, L-lactide and *meso*-lactide, leading to different polymer forms of PLA (PLLA, PDLA, PDLLA). On the other hand, the molar mass is directly controlled by the addition of hydroxylic compounds (*i.e.* lactic acid, water, alcohols) [26]. More generally, the properties of the resulting polymer also depend on the reaction time and temperature [8].

Due to the semi-crystalline nature of polylactide, temperature has important effects on their amorphous or crystalline structures [40]. The control on the processing temperature will have severe effects on crystallization and will consequently affect important features of PLA, since crystallinity has a remarkable effect in the physical and mechanical properties.

The crystallization behavior induced by thermal treatment of polylactides depends on the following factors:

- The *molar mass* has strong influence on the molecular mobility [41,42]. Crystallization from the melt is then easily induced in PLAs with low molar masses.

- The *thermal history* induces changes in both the crystalline/amorphous ratio and the structural relaxation effects on the glassy amorphous phase [[43,44]. Controlling the thermal program (annealing, quenching, cooling/heating rates) is crucial to define the resulting properties of PLA and its ultimate applications.

- *Stereosequence distribution of the molecules* [45]. The stereo-composition of the PLAs has strong effects on the crystallinity. A 72% purity threshold is required to obtain crystalline polylactides [45], and pure homopolymers (PLLA and PDLA) have approximately the same melting point, around 207ºC [46]. On the other hand, copolymers undergo substantially lower degrees of crystallinity, melting temperatures and spherulite growth rates when increasing D-lactide and meso-lactide contents [46]. In the case of a PLLA and PDLA blend (1:1 proportion), the resulting material is amorphous, but yields an insoluble gel formed by stereocomplexation of two polymers during the crystallization process. This stereocomplex melts at 230ºC [47], solely when the molar masses of PLLA and PDLA are both in the order of 10^3-10^4 [48].

- *Amount and type of additives*, acting as nucleating agents [49].

In addition, excessive temperatures can also promote degradation of PLA upon melt processing, as 40% losses of the initial M_w have been recently reported in polylactides

processed at 200ºC during 30 minutes [50]. Such thermal degradation can be mitigated by drying the samples prior to processing or by mixing under inert nitrogen atmosphere [51].

1.2.6 Mechanical properties of polylactide

Mechanical stability and durability of polylactide may be required during its service life, and thus several parameters such as high impact strength, good processing performance and stiffness must be assessed, for example, in packaging applications. PLA microstructure and morphology, including its crystallinity [52], will have strong effects on its mechanical performance, and this will be observed in changes in many physical properties, such as tensile strength, yield strength, elastic modulus or heat stability [53]. In general, an increase on crystallinity results in stiffness and heat resistance improvements, and this can be yielded by nucleation, annealing or stretching in an orientation process.

Due to their viscoelastic nature, polymers present strong sensitivity to time and temperature during stress/strain solicitations, and therefore temperature will have a strong impact on the linear elastic behavior and plastic deformation. Polylactide behaves like a hard, brittle, elastic solid below T_g with a high modulus, and there is essentially no yield point. In this glassy region, the motion of polymer chains is frozen and strain occurs by the stretching of bonds. While structural applications clearly require a polymer T_g above room temperature, the opposite occurs for applications where material flexibility is important. Modification of the T_g of PLA is then prompted by addition of plasticizers or by blending with other biodegradable polymers, depending on the final use. Since packaging is the most current application of polylactide, PLA films require T_g values to be below room temperature. On the other hand, high hardness, stiffness, impact strength and elasticity are required for applications such as beverage flasks, showing PLA similar to values as PET.

Higher molar masses broaden the rubbery temperature range of PLA, retarding viscous flow, by the presence of a major number of entanglements. Therefore, for high molar mass polylactides, the melting temperature is high and the rubbery plateau broad, whereas for low molar mass polymers the rubbery plateau is very short or even absent.

Finally, stereochemistry also affects the mechanical properties of PLA, and stereoregularity usually promotes improvements on the mechanical parameters [26].

1.3 Motivation and Aim of the PhD Thesis

The most common polymers used in packaging, agriculture, furniture, etc., are polyolefins, also known as commodities. Due to the vast production volume involved in these and other industrial sectors, disposal of synthetic polymeric materials has become a very important environmental problem caused by their resistance to degradation by different agents: weathering, compost, temperature, etc.

Nowadays, much interest is focused on the replacement of conventional synthetic polymeric materials by biodegradable materials capable to be competitive both in terms of production cost and performance [54]. The development of biodegradable polymers offers an effective approach for reducing polymer waste [55,56]. Biodegradable polymers from natural resources address a wide range of environmental concerns associated with conventional polymers such as greenhouse gas emissions, sustainability, etc.

However, the incorporation of biodegradable polymers will result in an increase of a new source of polymer waste that is designed to easily degrade in environmental conditions [57,58,59]. Therefore, the correct management of biodegradable polymer disposal must involve the determination of their degradability performance in several degradation conditions.

Aliphatic polyesters produced from renewable resources such as sugar cane, wheat, rice, corn, etc., have promising applications in packaging, consumer goods and fibers based on their good mechanical properties, transparency and compostability [60,61]. One of these polyesters which first attracted the attention was Polylactide, PLA, for biomedical applications. More recently, biodegradable polylactide and its random copolymers and blends have been raised as potential substitutes of polypropylene and other polyolefins in packaging and agricultural uses, among others [58,60,61].

As part of an integrated plan for waste managing of biodegradable polymers, implementing PLA in such new applications requires understanding the structural changes caused by different degradation processes during its life-cycle [62,63,64,65]. The existing

studies associate the thermal, hydrolytic, biological or photo degradation of PLA with chain scission, and hence, with a significant change of the molar mass [66,67,68,69,70,71].

Thermal degradation studies are applied to analyze all stages of processing and for modeling service life. PLA may degrade during a first extrusion or compression molding process leading to a rapid reduction of molar mass and mechanical strength. Such degradation will depend on several factors, such as the operation temperature, residence time, among others [50,52,72,73],. On the other hand, the service life of the material can be modeled by submitting the polymer to controlled temperature cycles [62,74].

The *biodegradation* mechanisms of PLA and its copolymers have been studied under controlled conditions, such as *in vitro* degradation with selected cultures, soil or composting [75,76,77,78]. PLA biodegradation is regulated by a first stage of hydrolysis, either acid or basic [66,79], thus water diffusion plays a central role [80,81,82,83,84]. Studies of degradation in soil of the polylactides are more limited and usually based on simple monitoring of the weight loss up to relatively low times [83,85,86]. Biodegradation under composting conditions takes place more rapidly than degradation in soil, and such difference is attributed to the higher temperatures and water content which enhance hydrolysis and assimilation processes [83,86,85].

Photodegradation is another source of PLA degradation when exposed to outdoor conditions. Most of the existing studies concern the effect of ultraviolet (UV) radiation, while the effect of sunlight radiation on PLA has been less studied, possibly because of the generally lower sensitivity that polymers have to this radiation [87,88,89].

All these degradation processes result in chain excision and temporal decrease of molar mass [71,90], which has an important effect on the crystallization rate, morphology and final performance of PLA. The aim of this PhD thesis is to assess the degradation of polylactide under different environmental conditions, namely thermal, bio and photo degradation, in order to understand their individual degradation mechanisms and their effect on the molar mass, thermal and viscoelastic properties.

The contributions of this PhD thesis are exposed in several chapters. First, the most relevant aspects related to the different degradation processes applied to PLA are presented in **Chapter 2**.

The experimental methodology involves a combination of several spectroscopic, microscopic and thermal techniques and is exposed with detail in **Chapter 3.** The experimental strategy is summarized in Figure 1-12.

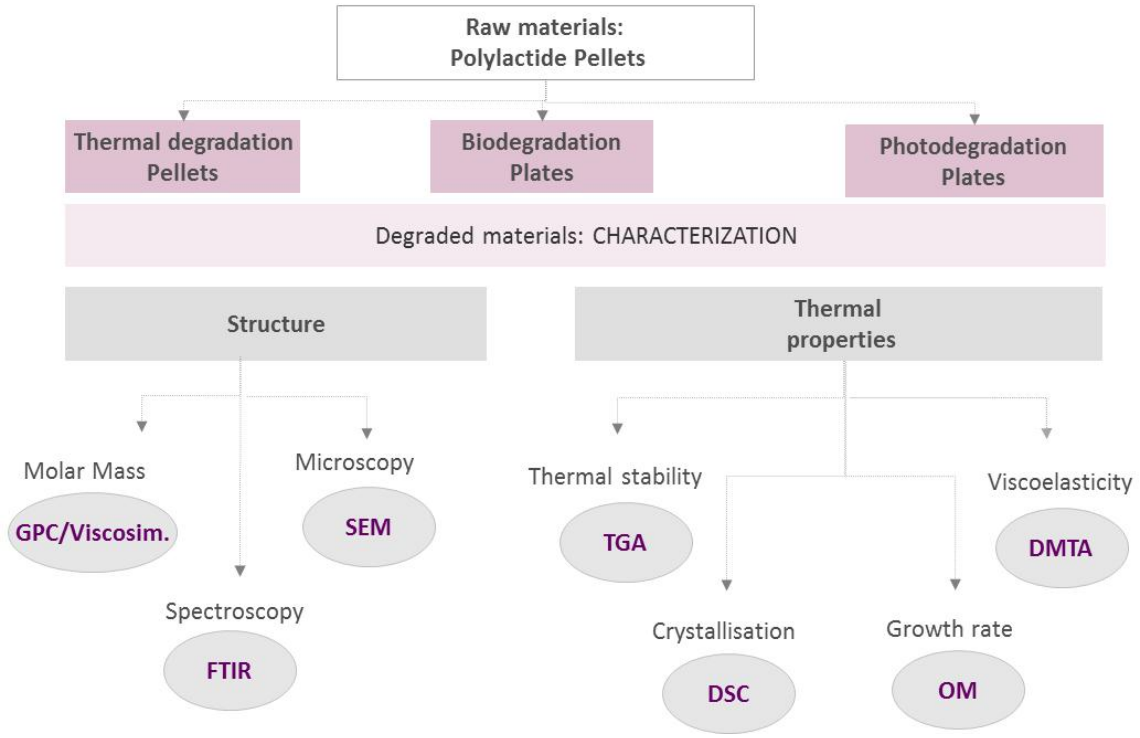

Figure 1-12 Summary of the methodology applied for the material characterization.

The reduction on molar mass promoted by degradation was determined by Gel Permeation Chromatography (GPC) and Viscometry. Thus, the effect of molar mass on several properties of polylactide was studied by a combination of analytical techniques. This includes variations on the chemical structure by Fourier Transformed Infrared Spectroscopy (FTIR), on the thermal stability by Thermogravimetric Analysis (TGA), modification on the surface of the samples by Scanning Electron Microscopy (SEM) and variation in the viscoelastic behavior by Dynamic Mechanical Thermal Analysis (DMTA). Finally the crystallization of PLA from the glass and from the melt was examined by Differential Scanning Calorimetry (DSC) and Optical Microscopy (OM), respectively.

The analysis of the effect of each type of degradation on the polylactide structure is described and discussed in detail in **Chapter 4.** With that purpose, several characteristic parameters were obtained from different experimental techniques. The molar mass decay has been modeled for each degradation type, following either first or second order functions. The experimental parameters were monitored as a function of the degradation time and the molar mass. The variation in molar mass is the greatest effect in the degradation process, regardless of the agent; therefore it was expected to find analogous crystallization rates for PLAs of equivalent molar masses. Comparative crystallization studies of specimens subject to the three degradation types evidence differences in the crystallization rates. Such effect is especially prominent when the linear growth rates of specimens subjected to bio or photo degradation are compared. The analysis of the crystallization kinetics provides further information of the type of crystallites formed upon solidification of PLA of different molar mass [42], and serves as reference to extract relevant processing parameters. The discussion is then focused on the different effects of the thermal, biological and photodegradation on the properties of PLA, and the potential existence of synergies.

The final remarks of this PhD thesis are summarized in **Chapter 5**, underlying new understanding on the effect of degradation in the properties of the polylactide developed in this thesis. The differences between random chain excisions promoted by the three types of degradation are highlighted, leading to some differences in the algebraic functionality, and this was applicable for the literature data. Such differences, within the degradation types, in the parameters studied reinforces the idea that degradation of PLA cannot be explained by a solely outcome of chains breakage and molar mass reduction. These results may be considered when designing new strategies to understand the structure/properties relations of new bio-degradable polymers, and more particularly PLA-based materials.

1.4 Bibliographical references

[1] The Compelling Facts About Plastics 2011 An analysis of European plastics production, demand and recovery for 2010

[2] Huang SJ. Polymer waste management-biodegradation, incineration and recycling. Polym Mater Sci Eng 1990;63:633–636.

[3] Tallman JW. More plastic use means more waste, which means?. Waste Age, 1987:8;141.

[4] WELL Fact Sheet-Nov 2005: Solid Waste Disposal in Ghana.

[5] UNIDO 2002; Municipal Solid Waste Management in Asia and Africa; A Comparative Analysis.

[6] Wilson DC, Velis C, Cheeseman C, Role of informal sector recycling in waste management in developing. Habitat Int 2006;30,4:797–808.

[7] Tsuji H, Ikada Y. Physical propertied of polylactides. In:DeVries KL et al., editors. Editorial advisory board. Current trends in polymer science, vol. 4. Trivandrum, India:Research Trends, 1999 p. 27–46.

[8] Migliaresi C, Cohn D, De Lollis A, Fambri L. Dynamic mechanical and calorimetric analysis of compression-molded PLLA of different molecular weights: effect of thermal treatments. J Appl Polym Sci 1991;43:83–95.

[9] European Bioplastics. Driving the evolution of plastics 2010.

[10] European Bioplastics. Bioplastics Frequently Asked Questions (FAQs). June 2008 www.european-bioplastics.org

[11] ASTM Standard D6866-06, "Standard Test Methods for Determining the Biobased Content of Natural Range Materials Using Radiocarbon and Isotope Ratio Mass Spectrometry Analysis" ASTM International, West Conshohocken, PA, www.astm.org (last accessed October 2008).

[12] ASTM Standard D6400-04, "Standard Specification for Compostable Plastics," ASTM International, West Conshohocken, PA, www.astm.org (last accessed October 2008).

[13] Sinha Ray S, Bousmina M, Biodegradable polymers and their layered silicate nanocomposites: In greening the 21st century materials world. Progr Mater Sci 2005;50,8:962–1079.

[14] Bastioli C; Handbook of Biodegradable Polymers. Shrewsbury: Rapra Technology, 2005.

[15] Vikman M; Itavaara M, Poutanen K, Biodegradation of starch-based materials. J Macromol Sci Pure Appl Chem 1995;A32:863–866.

[16] Narayan R, Mojo S, Summary of ASTM D6400-99 Test Methods and Correlation to Composting Trials.

[17] Steinbüchel A. Non-biodegradable biopolymers from renewable resources: perspectives and impacts, Curr Opin Biotech 2005;16:607–613.

[18] Lunt J. Progress in Standards for Biobased and Biodegradable Polymers in China, In The 2nd European Bioplastic Conference, Paris, November 2007 pp 21–22.

[19] Vert M, Schwarch G, Coudane J, Present and future of PLA polymers. J Macromol Sci Pure Appl Chem 1995;A32:787–796.

[20] Södergård A, Stolt M. Properties of lactic acid based polymers and their correlation with composition. Prog Polym Sci 2003;27:1123–1163.

[21] Auras R, Harte B, Selke S. An overview of polylactides as packaging materials. Macromol Biosci 2004;4:835–64.

[22] Bonsignore PV. Production of high molecular weight poly(lactic acid). US Patent No. 5470944; 1995.

[23] Spinu M. L-D Polylactide copolymers with controlled morphology. US Patent No.5270400; 1993.

[24] Ajioka M, Enomoto K, Suzuki K, Yamaguchi A. Basic properties of polylactic acid produced by the direct condensation polymerization of lactic acid. Bull Chem Soc Jpn 1995;68:2125–2131.

[25] Enomoto K, Ajioka M, Yamaguchi A. US Patent No. 310865; 1994.

[26] Hartmann MH, in Kaplan DL (Ed.), Biopolymers from Renewable Resources, Springer-Verlag, Berlin, 1998 pp. 367–411.

[27] Lowe CE. U.S. Patent No. 2668162; 1954.

[28] Carothers WH, Dorough GL, Van Natta FJ. Studies of polymerization and ring formation. X. The reversible polymerization of six-membered cyclic esters. J Amer Chem Soc 1932;54:761–772.

[29] Gruber P, O'Brien M. Polylactides NatureWorks™ PLA. In: Doi Y, Steinbüchel A, editors. Biopolymers in 10 volumes, volume 4, polyesters III applications and commercial products. Weinheim: Wiley-VCH; 2002 pp 235–49.

[30] Gupta AP, Kumar V. New emerging trends in synthetic biodegradable polymers – Polylactide: A critique. Eur Polym J 2007,43: 4053–4074.

[31] Drumright RE, Gruber PR, Henton DE. Polylactic Acid Technology. Adv Mater 2000;12,23:1841–1846.

[32] The future global markets for biodegradable packaging-report, source: www.PRW.com.

[33] Technical Report December 2005. EUR 22103 EN Catalogue number: LF-NA-22103-EN-C. ISBN: 92-79-01230-4.

[34] Vink ETH, Rabago KR, Glassner DA, Gruber PR. Applications of life cycle assessment to NatureWorks polylactide (PLA) production. Polym Degrad Stab 2003;80:403–419.

[35] Narayan R, Patel M. Review and Analysis of Bio-based Product LCA's. Internet resources 2004.

[36] Personal Communication with Dieter Scheidecker of Treofan Group, Trespaphan GmbH & Co. KG. on 18 Nov, 2003. Raunheim, Germany.

[37] Petersen K. Nielsen PV, Bertelsen G, Lawther M, Olsen MB, Nilsson NH, Mortensen G. Potential of bio-based materials for food packaging. Trends Food Sci Tech 1999;10:52–68.

[38] Garlotta D. A Literature Review of Poly(Lactic Acid). J Polym Environ 2002;9,2:63–84.

[39] Mayer J.M, Kaplan D. L, Materials: Balancing degradability and performance, Trends Pol Sci 1994;2,7:227–235.

[40] Kalb B, Pennings AJ, General crystallization behaviour of poly (L-lactic acid). Polymer 1980;21:607–612.

[41] Abe H, Kikkawa Y, Inoue Y, Doi Y. Morphological and kinetic analyses of regime transition for poly[(S)-lactide] crystal growth. Biomacromolecules 2001;2:1007–1014.

[42] Vasanthakumari R, Pennings AJ. Crystallization kinetics of poly(L-lactic acid). Polymer 1983;24:175–178.

[43] Tsuji H, Ikada Y. Properties and morphologies of poly(L-lactide): 1. Annealing condition effects on properties and morphologies of poly(L-lactide). Polymer 1995;36:2709–2716.

[44] Celli A, Scandola M. Thermal properties and physical ageing of poly(L- lactic acid). Polymer 1992;33:2699–2703.

[45] Thakur KAM, Kean RT, Hall E.S, Kolstad JJ, Lindgren TA, Doscotch MA, Siepmann JI, Munson EJ. Solid-State 13C CP-MAS NMR Studies of the Crystallinity and Morphology of Poly(L-lactide). Macromol 1996;29:8844–8851.

[46] Bouapao L, Tsuji H, Tashiro K, Zhang JM, Hanesak M. Crystallization, spherulite growth, and structure of blends of crystalline and amorphous poly(lactide)s. Polymer 2009; 50:4007–4017.

[47] Tsuji H, Ikada Y. Crystallization from the melt of poly(1actide)s with different optical purities and their blends. Macromol Chem Physic 1996;197,10:3483–3499.

[48] Tsuji H, Ikada Y. Stereocomplex formation between enantiomeric poly(lactic acids). 9. Stereocomplexation from the melt. Macromolecules 1993;26,25:6918–6926.

[49] Brochu S, Prud'homme RE, Barakat I, Jérôme R. Stereocomplexation and morphology of polylactides. Macromolecules 1995;28:5230–5239.

[50] Signori F, Coltelli MB, Bronco S. Thermal degradation of poly(lactic acid) (PLA) and poly(butylene adipate-co-terephthalate) (PBAT) and their blends upon melt processing. Polym Degrad Stab 2009;94:74–82.

[51] Wang YM, Steinhoff B, Brinkmann C, Alig I. In-line monitoring of the thermal degradation of poly(L-lactic acid) during melt extrusion by UV–vis spectroscopy. Polymer 2008;49,5:1257–65.

[52] Lim L-T, Auras R, Rubino M. Processing technologies for poly(lactic acid). Prog Polym Sci 2008;33,8:820–852.

[53] Qin D, Kean RT. Crystallinity Determination of Polylactide by FT-Raman Spectrometry. Appl Spectrosc 1998;52,4:488–495.

[54] Scott G editor, Biodegradable Polymers. Principles and applications, 2nd ed. Dordrecht, The Netherlands: Kluwer Academic Publishers, 2002.

[55] Albertsson AC; Huang SJ, Eds. Degradable Polymers, Recycling and Plastics Waste Management; Marcel Dekker: New York, 1995.

[56] Smits M. Polymer products and Waste Management. New York: Marcel Dekker, 1995.

[57] Kim DY,·Rhee YH. Biodegradation of microbial and synthetic polyesters by fungi. Appl Microbiol Biotechnol 2003;61:300–308.

[58] Hakkarainen M. Aliphatic polyesters: abiotic and biotic degradation and degradation products. Adv Polym Sci 2002;157:113–38.

[59] Shogren RL, Doane WM, Garlotta D, Lawton JW, Willett JL. Mechanical and thermal properties of starch-filled poly(D,L -lactic acid)/poly(hydroxy ester ether) biodegradable blends. Polym Degrad Stab 2003;79:405–11.

[60] Osawa S, Tsukegi T, Ogawa T, Urai T. Biodegradation behavior of molded poly(l-lactic acid)/starch blend in a land-fill test. Materials Life 2000;12:199–205.

[61] Calmon A, Guillaume S, Bellon-Maurel V, Feuilloley P, Silvestre F. Evaluation of material biodegradability in real conditions—development of a burial test and an analysis methodology based on numerical vision. J Environ Polym Degrad 1999;7:157–166.

[62] Badia JD, Vilaplana F, Karlsson S, Ribes-Greus A. Thermal analysis as a quality tool for assessing the influence of thermo-mechanical degradation on recycled poly(ethylene terephthalate). Polym Test 2009;28,2:169–175.

[63] Santonja-Blasco L, Moriana R, Badía JD, Ribes-Greus A. Thermal analysis applied to the characterization of degradation in soil of polylactide: I. Calorimetric and viscoelastic analyses. Polym Degrad Stab 2010;95:2185–2191.

[64] Badia JD, Santonja-Blasco L, Moriana R, Ribes-Greus A. Thermal analysis applied to the characterization of degradation in soil of polylactide: II. On the thermal stability and thermal decomposition kinetics. Polym Degrad Stab 2010;95:2192–2199.

[65] Badia JD, Strömberg E, Ribes-Greus A, Karlsson S. Assessing the MALDI-TOF MS sample preparation procedure to analyze the influence of thermo-oxidative ageing and thermo-mechanical degradation on poly (lactide). Eur Polym J 2011;47:1416–1428

[66] De Jong SJ, Arias ER, Rijkers DTS, van Nostrum CF, Kettenes-van den Bosch JJ, Hennink WE. New insights into the hydrolytic degradation of poly(lactic acid): Participation of the alcohol terminus. Polymer 2001;42:2795–2802.

[67] Proikakis C.S, Mamouzelos N.J, Tarantili P.A, Andreopoulos A.G. Swelling and hydrolytic degradation of poly(D,L-lactic acid) in aqueous solutions. Polym Degrad Stab 2006;91,3:614-619.

[68] Migliaresi C, Fambri L, Cohn D. A study on the in vitro degradation of poly (lactic acid). J Biomater Sci Polym 1994;4:591–606.

[69] Tsuji H, Mizuno A, Ikada Y. Properties and morphology of poly(L-lactide). III. Effects of initial crystallinity on long-term in vitro hydrolysis of high molecular weight poly(L-lactide) film in phosphate-buffered solution. J Appl Polym Sci 2000;77:1452–64.

[70] Ikada E. Photo descomposition of aliphatic polyesters. V. J Photopolym Sci Technol 1998;2,1:23–28.

[71] Ikada E. Photo-and bio-degradable polyesters. Photodegradation behaviours of aliphatic polyesters. J Photopolym Sci Technol 1997;10,2:265–270.

[72] Wachsen O, Platkowski K, Reichert K-H. Thermal degradation of poly-L-lactide-studies on kinetics, modelling and melt stabilization. Polym Degrad Stab 1997;57:87–94.

[73] Taubner V, Shishoo R. Influence of processing parameters on the degradation of poly(L-lactide) during extrusion. J Appl Polym Sci 200179;12:2128–2135.

[74] Vilaplana F, Ribes-Greus A, Karlsson S. Analytical strategies for the quality assessment of recycled high-impact polystyrene: a combination of thermal analysis, vibrational spectroscopy, and chromatography. Anal. Chim. Acta 2007; 604,18–28.

[75] Pranamuda H, Tokiwa Y, Tanaka H. Polylactide degradation by an Amycolatopsis sp. Appl Environ Microbiol 1997;63:1637–1640.

[76] Goheen RP, Wool RP. Degradation of polyethylene-starch blends in soil. J Appl Polym Sci. 1991;42:2691–2701.

[77] Pitt CG, Gratzel MM, Kimmel GL, Surles J, Schindler A. Aliphatic polyesters II. The degradation of poly (DL-lactide), poly (ε-caprolactone), and their copolymers in vivo. Biomaterials 1981;2:215–220.

[78] Lofgren A, Albertsson AC. Copolymers of 1,5-dioxepan-2-one and L- or D,L-dilactide: Hydrolytic degradation behavior. J Appl Polym Sci 1994;52:1327–38.

[79] Lucas N, Bienaime C, Belloy C, Queneudec M, Silvestre F, Nava-Saucedo J-E. Polymer biodegradation: Mechanisms and estimation techniques. Chemosphere 2008;73,4:429–442.

[80] Badia JD, Santonja-Blasco L, Martínez-Felipe A, Ribes-Greus A. Hygrothermal ageing of reprocessed polylactide**.** Polym Degrad Stab . *Doi* 10.1016/j.polymdegradstab.2012.06.001

[81] Li S. Hydrolytic degradation characteristics of aliphatic polyesters derived from lactic and glycolic acids. J. Biomed Mater Res 1999;48:342–353.

[82] Vert M, Mauduit J, Li S. Biodegradation of PLA/GA polymers: increasing complexity. Biomaterials 1994;15:1209–1213.

[83] Torres A, Li SM, Roussos S, Vert M. Microbial degradation of a poly (lactic acid) as a model of synthetic polymer degradation mechanisms in outdoor conditions. Biopolymers. Chapter 14 Utilizing nature's advanced materials, ACS Symp Ser 1999 Vol. 723 pp 218–226.

[84] Siparsky GL, Voorhees KJ, Dorgan J.R, Schilling K. Water transport in polylactic acid (PLA), PLA/polycaprolactone copolymers, and PLA/polyethylene glycol blends. J Environ Polym Degrad 1997;5:125–136.

[85] Ho KLG, Pometto III AL, Hinz PN. Effects of temperature and relative humidity on polylactic acid plastic degradation. J. Environ Polym Degrad 1999;7:83–92.

[86] Urayama H, Kanamori T, Kimura Y. Properties and biodegradability of polymer blends of poly(l-lactide)s with different optical purity of the lactate units. Macromol Mater Eng 2002;287:116–121.

[87] Feldman D. Polymer Weathering: Photo-Oxidation. J Polym Environ 2002;10,4:163–173.

[88] Janorkar AV, Metters AT, Hirt DE. Degradation of poly(L-lactide) films under ultraviolet-induced photografting and sterilization conditions. J Appl Polym Sci 2007;106:1042–1047.

[89] Bocchini S, Fukushima K, Di Blasio A, Fina A, Frache, Geobaldo F. Polylactic acid and polylactic acid-based nanocomposite photooxidation. Biomacromolecules, 2010;11,11:2919–26.

[90] Saha SK, Tsuji H. Effects of molecular weight and small amounts of D-lactide units on hydrolytic degradation of poly(L-lactic acid)s. Polym Degrad Stab 2006;91,8:1665–1673.

Chapter 2 Introduction

2.1 Background in polymer degradation

Degradation is a general term used to describe changes on the chemical and physical properties of materials promoted by different agents during a period of time. More precisely, *Schnabel* [1] relates degradation to chemical reactions which cause variations in physical properties of polymers. These reactions involve the cleavage of bonds in the main chain or in side groups of the macromolecules. Bonds excision is considered the main process in polymer degradation and can be caused by different forms of energy. More concretely, the American Society for Testing and Materials (ASTM) standard defines a degradable plastic as a plastic designed to undergo a significant change in its chemical structure, resulting in a loss or change of some properties as measured by standard test methods appropriate to the material and the application in service life [2].

Degradation is included in the general term "Environmental disintegration", which considers all the changes occurring in the properties of polymers due to environmental exposure. A distinction is made between physical changes (leading to deterioration) and chemical modifications (leading to degradation) [3]. Depending on the predominant factor, the degradation can be then classified into various subcategories, as shown in Figure 2-1. Polymeric materials exposed to outdoor conditions (*i.e.* weather, ageing or burying) can undergo transformations (mechanical, light, thermal, and chemical) which can ultimately modify their potential to be degraded.

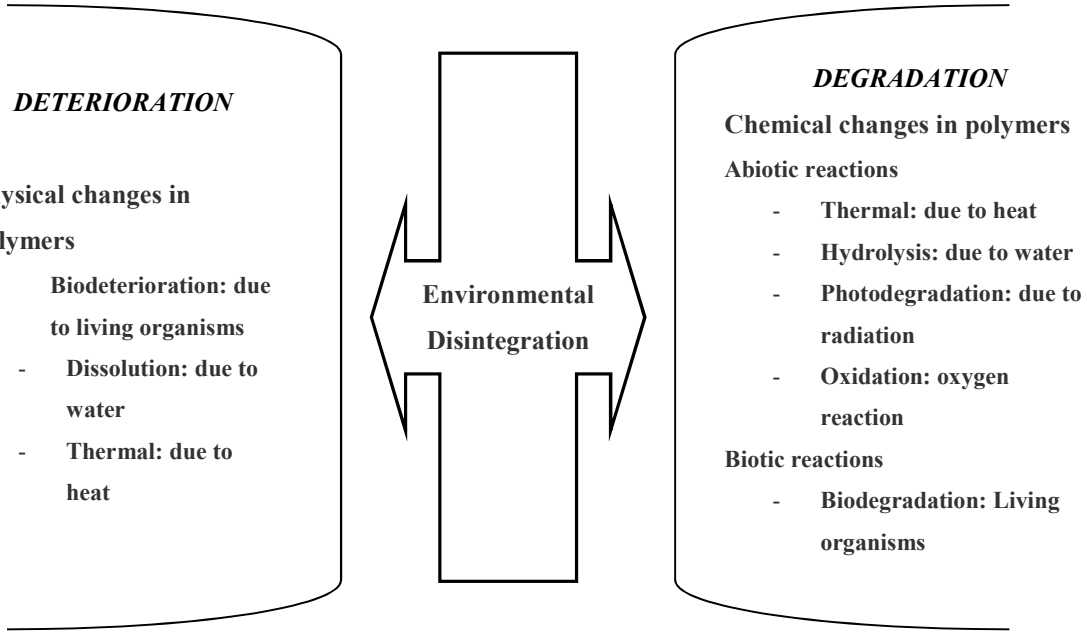

Figure 2-1 Definitions of Environmental Disintegration, Deterioration and Degradation.

2.1.1 Classification of polymer degradation

The degradation processes can be classified according to the agents activating them, which can act either individually or synergistically. The most common mechanisms of polymer degradation are now explained.

a) Thermal degradation

When a polymer is submitted to high temperatures undergoes several chemical changes. At low temperatures, volatile products are initially released. At higher temperatures, heat treatment promotes the thermal degradation of the polymer essentially following two patterns involving cleavage of the main chain (first pattern) or the substituent side chains (second pattern). In general, the excision of the polymer structure often generates free radicals, smaller fractions that undergo cyclisation, substituent reactions and several side-chain breakages. All these reactions usually end up with a decrease of the molar mass.

The first pattern of thermal degradation involves depolymerization, and this process can be more or less complex depending on the polymer structure [4], see Scheme 2-1. The breakage is initiated with homolysis of the polymer chain and the extent of the process depends on a combination of two factors: the reactivity of the macroradicals formed and the occurrence of transfer reactions. The products of decomposition essentially consist of monomers, oligomers, or a mixture of both.

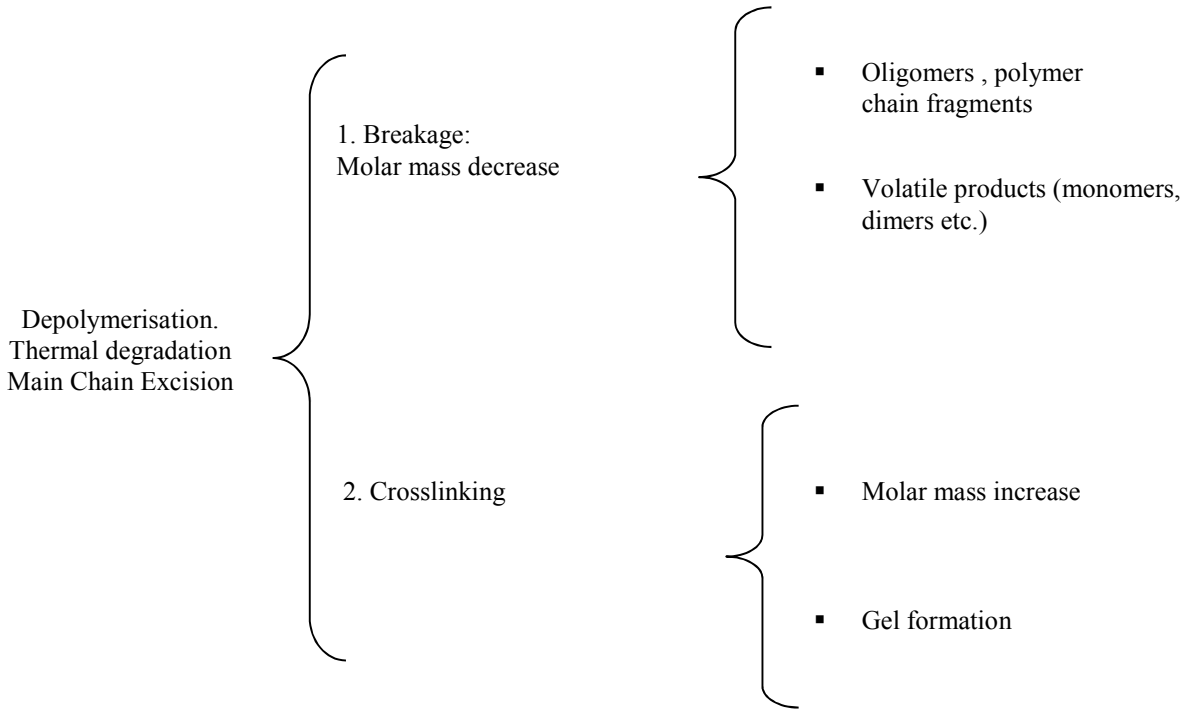

Scheme 2-1 Products of depolymerisation of homopolymers.

The second thermal degradation pattern is more complex and involves modification in the initial polymer structure through elimination and cyclisation reactions of the functional side groups (Scheme 2-2).

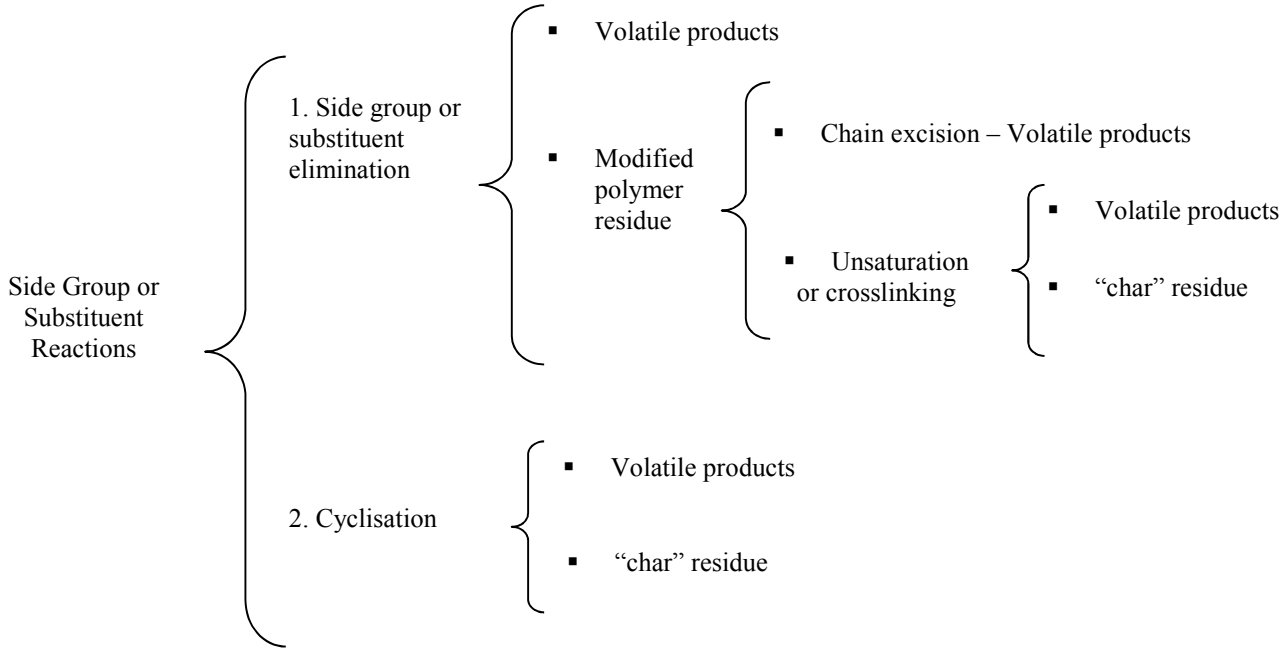

Scheme 2-2 Products of side group or substituent reaction.

b) Hydrolysis

Hydrolysis is another type of abiotic chemical degradation [5,6]. Polymers susceptible to hydrolysis must contain hydrolysable covalent bonds, such as ester, ether, anhydride, amide, carbamide, ester amide groups and so forth. Hydrolysis depends on several parameters such as water activity, temperature, pH and time. The design of polymers with controlled life span requires the selection of monomeric compositions providing with appropriate hydrophilic characteristics [7,8]. A rational design of organized molecular structures (crystalline domains) can prevent from the diffusion of O_2 and H_2O, as a strategy to avoid hydrolysis and further chemical degradation. In general, hydrolytic degradation on a given material takes place preferentially within disorganized molecular regions (amorphous domains).

c) Biodegradation

Biodegradation is defined by *Albertsson and Karlsson* [9] as a chemical decomposition process promoted through the action of living organisms (bacteria, fungi, etc.) and their enzymes. Abiotic processes such as hydrolysis, photodegradation or oxidation, can contribute to initiate biodegradation by weakening the polymeric structure [10,11,12]. It is then necessary to take into account such abiotic conditions for a reliable estimation of the polymer durability.

There are four main strategies to tailor the properties of polymers to a wide range of uses and predetermined service life [9]:

1. The ***addition of biodegradable or photooxidizable components to*** economic, synthetic, bulk polymers (*commodities*).
2. ***Chemical modification*** of the backbone of synthetic polymers by the introduction of hydrolysable or oxidizable groups.
3. The use of ***biodegradable polymers*** and their derivatives.
4. Preparation of tailor-made ***new hydrolysable structures***, *i.e*. polyesters or polycarbonates

Other essential term in polymer biodegradation is compostability. The ASTM D6400 standard defines compostable plastics as materials capable to undergo degradation by biological processes to yield carbon dioxide, water, inorganic compounds and biomass and producing no toxic residue. A plastic is considered compostable if over 30 percent of the sample is converted to carbon dioxide after 180 days in a proper compost environment [13].

Alternatively, biodegradability can be studied by submitting the polymers to a degradation in soil procedure under the international normative ISO 846 1997 [14]. In this case, the action of the microorganisms is slower than in compost or in controlled biodegradation cultures. Much effort has been made recently in monitoring the degradation in soil of different polymers by means of a combination of thermal analyses techniques [15,16,17,18,19,20].

d) Weathering

Weathering is a wide concept applied to describe the changes occurring when a material is submitted to outdoor environmental conditions. Some of the main ambient factors producing degradation are sunlight radiation, temperature, humidity (especially rain), wind, oxygen, among others. Weathering is particularly severe for organic materials since it combines the photo-physical and photo-chemical effects of ultraviolet (UV) radiation with the oxidative effects of atmospheric oxygen and the hydrolytic effects of water.

The critical factors affecting weathering are:

- *Sunlight radiation* from >250 nm wavelength. Especially, UV wavelength in the 250 - 400 nm range affects the chemical structure of polymers and consequently their properties.

- *Oxygen* is the principal degradation agent of polymers through the generation of free radicals together with other sub-products that easily absorb UV radiation.

- *Temperature.* The drastic variations between night and day temperatures enhance degradation, being especially acute when photooxidation occurs.

- *Relative humidity and water condensation.* Humidity can easily penetrate the amorphous phases of a polymer triggering hydrolysis. In addition, water condensation can drag other particles affecting the properties of the polymer.

- *Pesticides and air pollutants* may react with the polymer and generate chromophore groups capable to absorb the UV radiation and ultimately affect its service life.

e) Photodegradation

Photodegradation is produced by the controlled exposure of a polymer to either ultraviolet or sunlight radiation. Photodegradation is considered the most efficient abiotic degradation process occurring by environment exposure and contributes considerably to weathering. Several polymeric materials are photosensitive as the energy carried by photons can create unstable states in various functional groups. Energy transfer can be then accomplished by photo-ionization, luminescence, fluorescence or thermal radiation. From the degradability standpoint, photosensitive molecular structures can be added into the polymer with the aim to induce macromolecular degradation by light (*i.e.* pro-oxidants agents that can be activated depending on the light intensity and time exposure) [21,22]. Several experimental tests are used to simulate the effects of the polymer exposure to sunlight by controlling parameters such as irradiation, temperature and humidity [23,24].

f) Oxidative reactions

Oxidation is yet another important agent in abiotic degradation, since atmospheric pollutants and agrochemicals may interact with polymers in the presence of oxygen [24]. The atmospheric forms of oxygen (*i.e.* O_2 or O_3) attack covalent bonds thus producing free radicals, usually in synergy with light radiation exposure. The oxidative degradation depends on the polymer structure and is facilitated by the presence of unsaturated links and branched chains [25]. Peroxyl radicals resulting of the oxidative degradation can lead to crosslinking reactions and/or chain excisions, following Norrish mechanisms.

2.1.2 Polymer characteristics affecting the degradation processes

Degradation is a rather complex process that is influenced by several external parameters (as those explained in the previous section) and also the intrinsic characteristics of the polymers.

More precisely, the main polymer characteristics affecting degradation are:

- ***The chemical structure***. The reactivity between the external agents and the functional groups chains is the ultimate cause of the different categories of polymer degradation. As an example, the in-chain ketone groups can act as sensitizers by UV light absorption and they are used to activate oxidative and photodegradation**.** Another relevant example is the presence of RCOOH groups that accelerate hydrolysis by autocatalysis [26,27].

- ***Polymer morphology*** is one of the most important factors influencing degradation, due to the relevance of several phenomena which depend on the polymer supramolecular structure and free volume [28]. In semicrystalline materials the amorphous phase is first degraded, in part due to a more favorable solvent transport, and the degradation velocity depends on the number, size and shape of the crystals.

- ***Molar mass and molecular size.*** The molar mass distribution (represented by the weigh average molar mass, M_w, or the number average molar mass, M_n) of a polymer has strong influence on its degradation. Solubility, crystallinity and other physical parameters that influence the degradation are directly dependent on the molar mass. In general, shorter polymer chains will facilitate microorganism assimilation. In the case of polyesters, lower molecular sizes may increase the concentration of carboxylic acids at the chain ends, which will result in enhancement of hydrolysis [29].

- Polymers with ***small repetition units*** and regular microstructures present compact morphologies less accessible to the enzymes.

In the particular case of **biodegradation**, the main characteristics are:

- ***The hydrophilic–hydrophobic balance*** influences biodegradation as most of the reactions involved are catalyzed by enzymes in aqueous medium. The microorganism assimilation can be enhanced by a proper combination of hydrophilic and hydrophobic regions, which can be achieved by the introduction of hydrolysable groups in the polymer backbone, such as amides or esters.

- ***The flexibility of the polymer chain*** is required to facilitate the enzymes attack to the degradation sites.

- ***High exposure areas*** to microorganism media will increase biodegradation susceptibility.

- ***The complex biological environment***. Many different classes of bacteria, algae, fungi, protozoa etc. are collectively responsible for the biodegradation of polymers. The microbial population and activity of each microorganism will depend on particular conditions regarding several environment factors, such as pH, light, humidity, oxygen, or the presence of salt and metals.

2.2 Degradation mechanisms of polylactide

This section describes the potential of polylactide to be degraded following some of the previous processes. More concretely, this work has focused on the study of thermal, bio and photo degradation of PLA.

2.2.1 Thermal degradation of polylactide

Degradation of PLA due to thermal effects has been studied by several authors. *McNeill and Leiper* [30,31] reported thermal degradation of polylactide in the 230 to 440ºC range, while mass losses were detected by *Jamshidi et al* [32] at lower temperatures (T ≈ 190ºC).

The PLA thermal degradation at low temperatures is mainly occurring by non-radical intramolecular transesterifications, resulting in cyclic oligomers of lactic acid, lactide, acetaldehyde and carbon monoxide, as Figure 2-2 shows [33,34]. Ester interchange can occur through reactions R1, R2 and R3, specified in Figure 2-2. The size of the cycles determines the generation of oligomers (if n≥1) or lactide (if n=0) together with other sub-products, such as acetaldehyde and carbon monoxide, through reaction R3. Further studies also proposed the occurrence of cis-elimination (R4) leading to acrylic acid [35]. Cis-elimination and transesterification are then the main pyrolysis mechanisms for polyesters below 230 ºC, which results in polylactide cyclic chains with lower molar mass.

At higher temperatures, radical reactions are activated (T > 270ºC) [32], together with some non-radical intermolecular transesterifications (see Figure 2-3). The radical reactions are assumed to start with either an alkyl-oxygen (*O=CH*), see Figure 2-4 or an acyl-oxygen (*O=C-O*), see Figure 2-5.

Recently, the thermal oxidation of polylactide has been also reported for samples reprocessed by injection until five times at 190ºC. The authors detected by MALDI-TOF [36] the presence of predominant cyclic and linear oligomers of lactide as products of intra and intermolecular transesterifications, as it happened in PLA pyrolysis. However further reprocessing promotes the appearance of new linear oligomers with methoxy ends, probably

induced by intermolecular transesterification. The results confirm the combination of inter and intramolecular mechanisms in the thermal degradation of polylactide.

a. Non Radical reactions

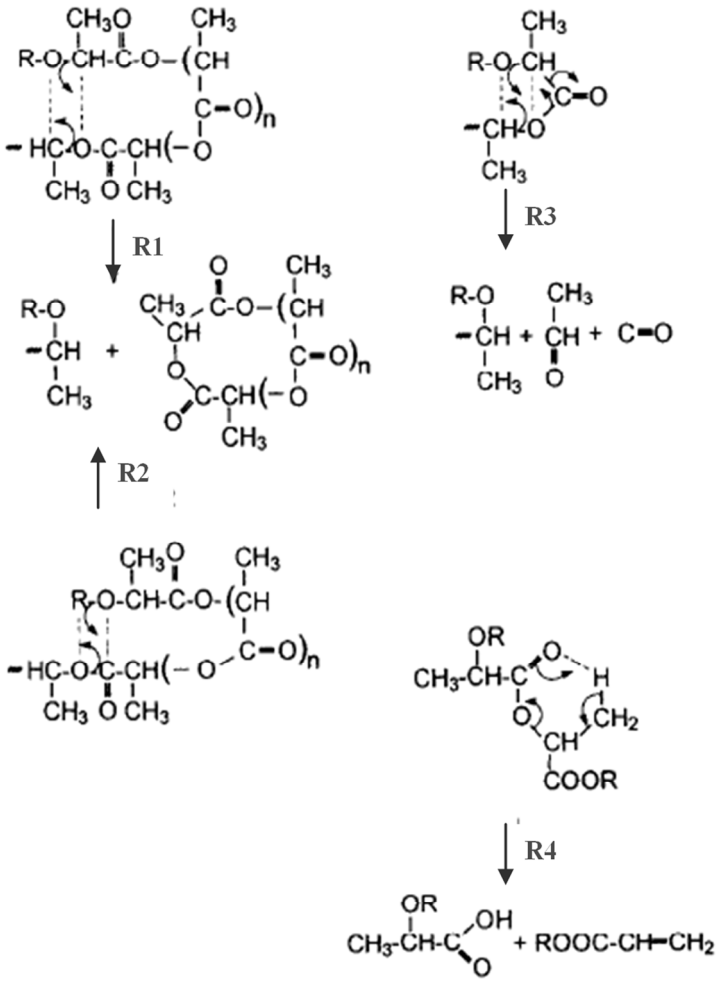

Figure 2-2 Postulated reaction of polylactide degradation. Intramolecular transesterification (back-biting) R1, R2 and R3 and cis-elimination R4 where R is H (Reproduced from *ref.* 32).

Figure 2-3 Intermolecular thermal decomposition of polylactide (Reproduced from *ref.* 34).

b. Radical reactions or the homolysis

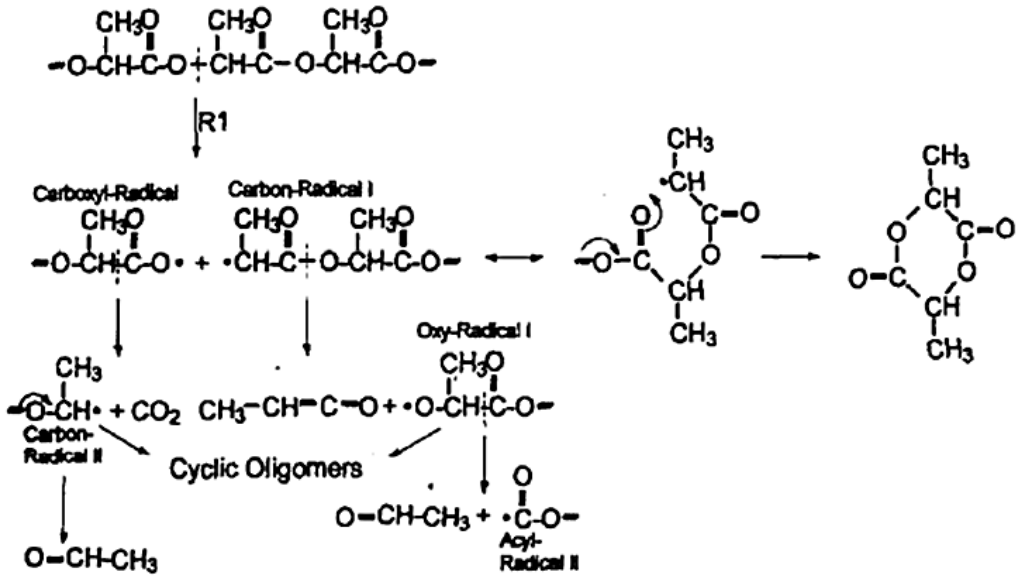

Figure 2-4 Possible radical reactions of the PLA decomposition, starting with alkyl-oxygen homolysis (Reproduced from 33 based on *ref.* 30).

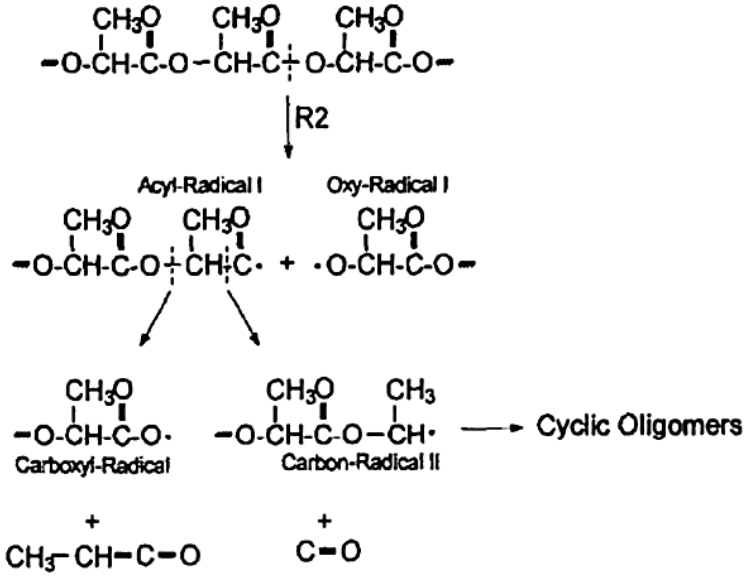

Figure 2-5 Possible radical reactions of the PLA decomposition, starting with acyl-oxygen homolysis (Reproduced from 33 based on *ref.* 30).

2.2.2 Biodegradation of polylactide

As a potential degradable commodity, PLA must be stable during service life but quickly degrade after disposal. Biodegradation process of polylactide is considered a combination of two mechanisms: abiotic hydrolysis and the action of enzymes and/or live microorganisms [37]. The velocity of the biodegradation process depends on a variety of factors, such as the purity of the sample, temperature, humidity, the amount of oxygen and nutrients, the crystalline structure, the lamellar thickness and the morphology.

Due to its importance on biodegradation, understanding the hydrolysis process is paramount to design PLA materials with controllable degradation properties. Initial abiotic degradation shortens the polymer chain lengths enhancing ulterior biotic degradation.

De Jong et al. studied the hydrolytic degradation of monodisperse lactic acid oligomers [38]. They concluded that pH influences the hydrolysis significantly. Two mechanisms have been proposed for hydrolysis depending on the pH.

Figure 2-6, mainly occurring randomly or *via* end chains. Electrophilic attack to a hydroxyl end-group (second carbonyl group) leads to ring formation. A secondary reaction can then occur when the lactide molecule produced is further hydrolyzed into two molecules of lactic acid. On the other hand, random alkaline attack on ester groups produces new molecules with low molar mass.

Figure 2-7 shows the acid hydrolysis of PLA, which can also occur randomly or at the chain-ends. Protonation of the hydroxyl end-group forms intramolecular hydrogen bonds, which permits the hydrolysis of the ester group and the release of a lactic acid molecule. An intramolecular random protonation of the ester group conduces also to the hydrolysis of ester linkages and the formation of oligomers or PLA with reduced degrees of polymerization [39].

In both cases, degradation causes an increase in the number of carboxylic acid chain ends which autocatalyze ester hydrolysis.

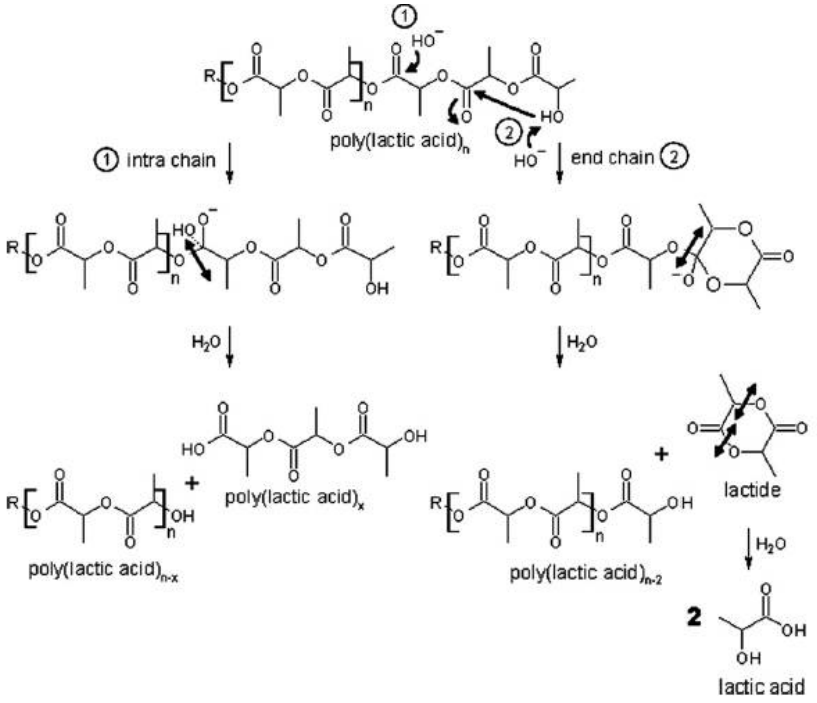

Figure 2-6 Hydrolysis of the PLA in alkaline conditions (Reproduced from *ref.* 39).

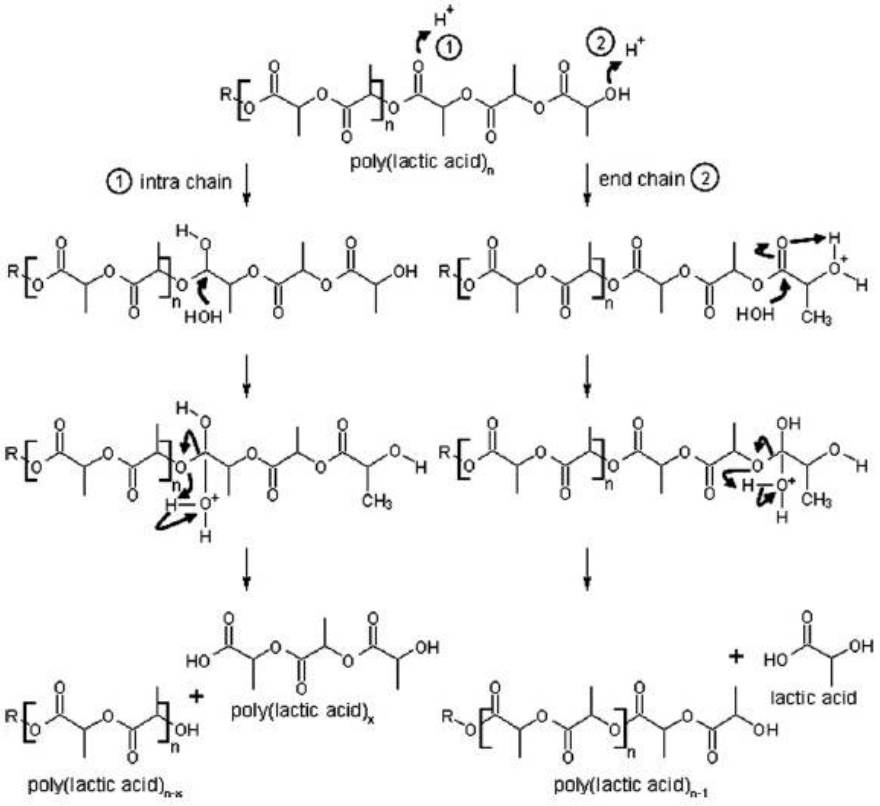

Figure 2-7 Hydrolysis of the PLA in acidic conditions (Reproduced from *ref.* 39).

Physical conditions may also influence the hydrolytic degradation of solid polymers. The initial polymer morphology will affect water uptake and ultimately determine the degradation rate. In the case of surface eroded matrices, the polymer degradation is much faster than water intrusion into the polymer bulk and degradation occurs mainly in the outermost polymer layers [40].

Initially, only the molecules at the surface, and in contact with the aqueous medium, can be hydrolyzed, and the resulting oligomers transferred into the surrounding, see Figure 2-8 [41]. As degradation proceeds, water penetrates into the bulk polymer, and hydrolysis occurs at the inner parts of the material. Some oligomers located in the core of the matrix remain entrapped and this produces an increase on the carboxylic groups and a consequent autocatalytic effect, especially acute far from the material surface. At more advanced degradation stages, the size of the oligomers is small enough to be either be assimilated by the microorganisms or transported to the surroundings.

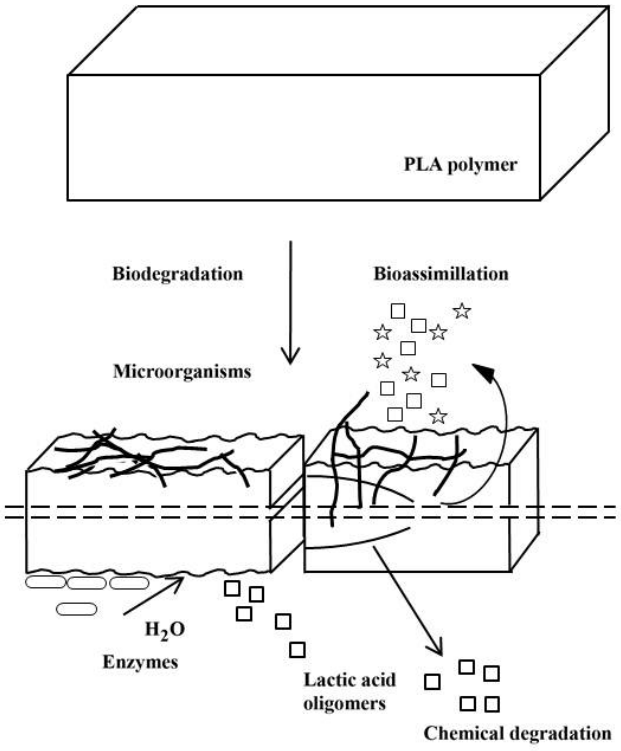

Figure 2-8 Degradation mechanism proposed for polylactide in solid state (Adapted from *ref.*41).

The relative rates of hydrolysis, bio-assimilation, transport of water or oligomers, etc., are fundamental to determine biodegradation, since these factors will promote changes in the PLA morphology. In particular, changes in the crystallinity of PLA are especially relevant due to variation on the existing amorphous regions more labile for degradation.

Biodegradation of PLA bio-packages has been reported and correlated to visual changes and variation in physical properties of the materials [42,43].Composting is one of the most commonly used methods to describe the biodegradability of polymers. The composting conditions are governed by several factors, such as temperature, pH, and relative humidity of the compost pile, which promote marked molar mass decrease. The effect of hydrolysis and bio-assimilation is very fast in compost conditions, leading to totally disintegration of the polymer in few weeks. The compostability of several commercial polylactides has been certified by the Biodegradable Products Institute (BPI), assessing complete degradation in a maximum of six months in compost, in accordance with ASTM D6400 compostability standards [44].

Alternatively, PLA degrades slower in tests performed in soil at room temperature, most likely due to the conditions of low temperature and humidity. Characterization of the degradation is commonly carried out by measuring the molar mass or the mass loss changes with degradation time. For selected examples, *Ho et al*. [45] found that about 20% of a PLA film was mineralized to CO_2 after 182 days in a laboratory respirometer charged with soil at 28ºC. *Calmon et al.* [46] reported weight losses varying from 0 to 100% of PLA films after burial in soil for 24 months, depending on PLA type and location. In contrast *Urayama et al*. [47] only observed a 20% molar mass decrease of PLA (100% L-content) plates after 20 months in soil. In addition, it has been argued that traditional techniques for studying polymer biodegradation, mostly based on the measurement of the mass loss changes, have some limitations. The adhesion of soil and fungi to the polymer, especially acute after 3 months, can mask real results and thus induce misleading information [48,49].

A complete sustainable design of PLA materials must comprise stability during storage and service life, biodegradability after disposal, and more generally, a proper balance of the resources (energy, materials) involved in the production/disposal cycle [50, 51].

The functionality of the new PLA products must accomplish resistance to exposure to environmental factors such as solar radiation, temperature variations, water, as well as to microbial colonization. On the other hand, environmental sustainability is usually assessed by the Life Cycle Assessment (LCA) [52]. In short, efficient new sustainable products must: (i) have similar functionalities as the original products with competitive costs, without degradation in quality or performance; (ii) be made from renewable resources; (iii) have minimum environmental and health impact; (iv) achieve a proper balance with all the resources involved in their life-cycle.

LCA demonstrates that, in the long-term, PLA production can promote the use of alternative and renewable energy sources. The processes involved will become competitive only with significant investment in more research, effort and capital. In order to obtain a global view of all the impacts of PLA production, LCA can serve as a tool for monitoring return on these investments over time.

2.2.3 Photodegradation of polylactide

As it was mentioned above, initial abiotic degradation can be used to accelerate posterior biodegradation. This happens when the material is exposed to sunlight in non-controlled disposal. There are not many studies related to the effect of sunlight radiation on polylactide, due to the low radiation absorbance of polymers in the visible wavelength range [53]. Instead, bonds of many polymers are more sensitive to UV radiation and most of the photodegradation studies are focused on this range. Typical bonds of saturated compounds, such as C-C, C-H, O-H and C-Cl, absorb light at wavelengths below 200 nm. On the other hand, the maxima absorption of C=O and C=C bonds are in the 200 to 300 nm range [54].

Photodegradation of polylactide due to UV radiation is explained by *Ikada* by a Norrish II mechanism located at the carbonyl groups, Figure 2-9. The mechanism involves the formation of C=C bonds that can be easily detected by infrared spectroscopy at 990 cm^{-1} [55]. The same author also studied the effect of sunlight exposure on some polyesters, and suggested different mechanisms for photodegradation of polylactide by UV and sunlight radiation, in part due to the absence of C= C bands in the sub-products of the later [56].

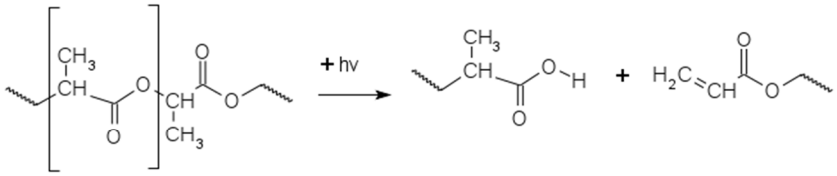

Figure 2-9 Photodegradation mechanism of polylactide (Adapted from 55).

Other authors [55,57] proposed alternative mechanisms for the UV degradation of PLA (Figure 2-10). Mechanism (A) involves a photolysis reaction leading to cleavage of the C-O bond from the backbone with the formation of methyl chain ends by hydrogen transfer, following a Norrish type II mechanism and in concordance with *Copinet et al* at 315 nm [58]. On the other hand, mechanism (B) involves the formation of a hydroperoxide derivative and its subsequent degradation to compounds containing a carboxylic acid and diketone end groups [57]. In addition, some authors have studied the influence of photosensitizers on the UV degradation of PLA films, observing considerable molar masses reductions and increase in brittleness after short exposure times (12 h) [59,60].

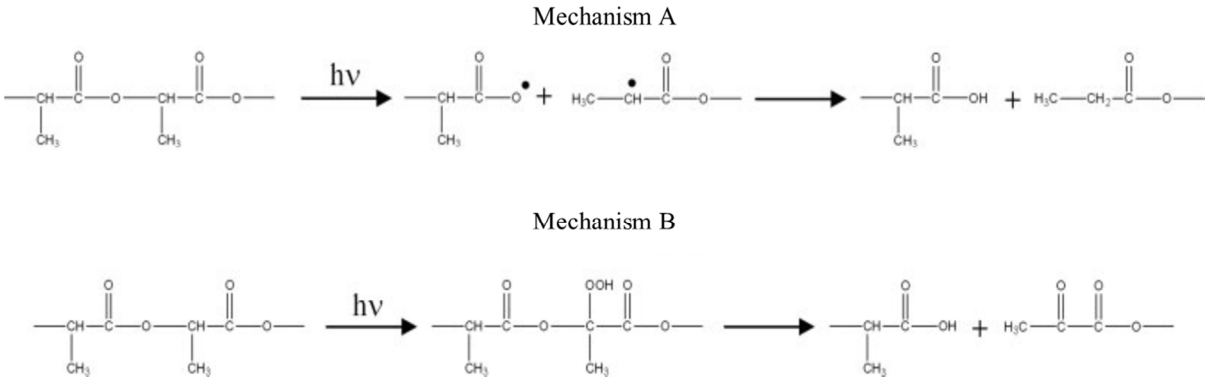

Figure 2-10 Photodegradation mechanisms of polylactide (Reproduced from *ref.* 57).

More recently *Bocchini et al.* proposed a new mechanism for PLA photodegradation under outdoor conditions (sunlight exposure) [61]. According to these authors, polymer degradation occurred through the random formation of anhydride groups in four steps, shown in Figure 2-11. Step 1) involves the formation of a tertiary radical (P•) in the polymer chain (PH) (1), which reacts with oxygen to give a peroxide radical 2). This later reacts with a new PLA molecule to form a hydroperoxide and a new radical P• 3). The hydroperoxide can then undergo photolysis 4) with the formation of HO• and PO• radicals. The PO• radical can then give 3 radical species after β-excision, containing several anhydride groups (5a-b-c). The most probable reaction, considering the stability of the subproducts, is the formation of molecules containing anhydrides following the path 5b).

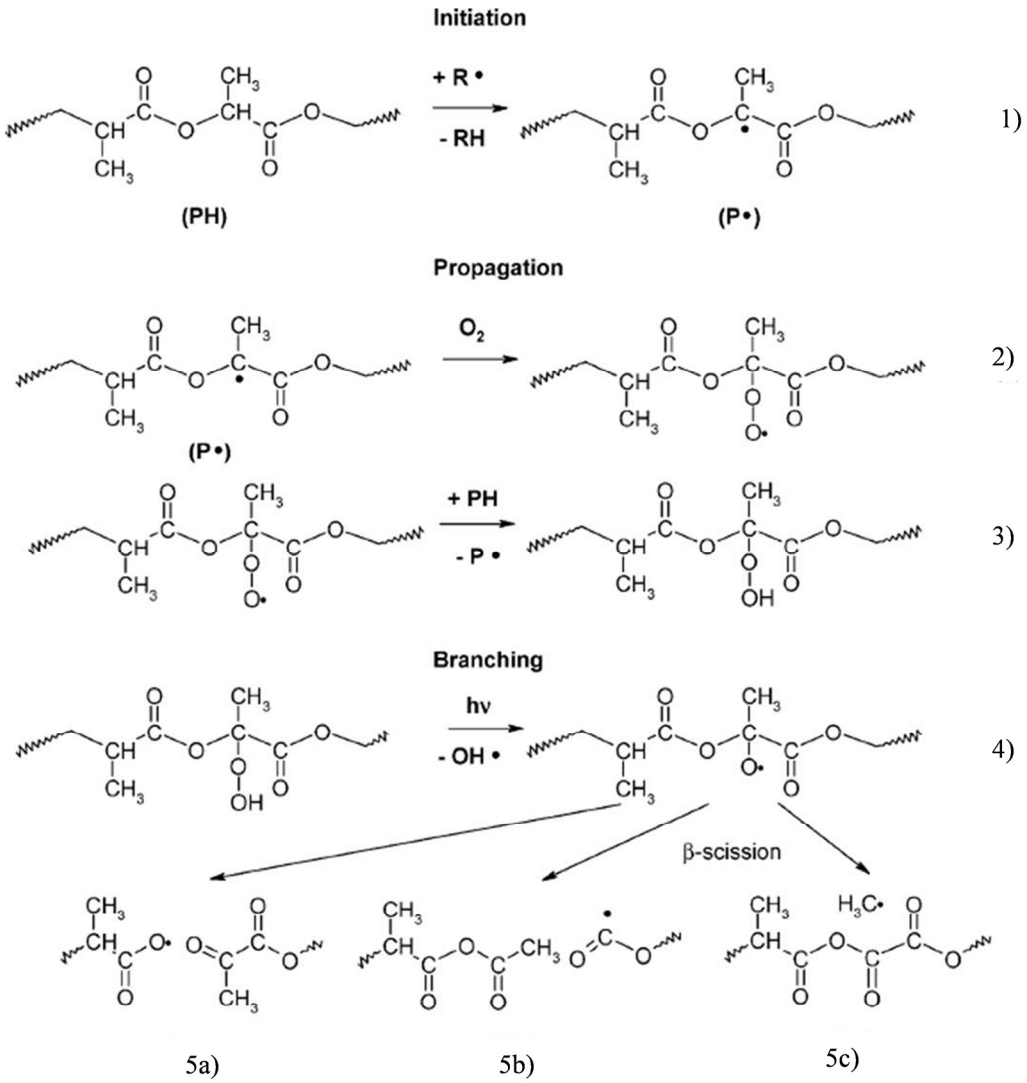

Figure 2-11 Photodegradation mechanism of polylactide (Reproduced from *ref.61*).

2.3 Importance of crystallization in the degradation processes

Molar mass decrease is the most relevant effect caused by the degradation processes. Variations in molar mass induce changes in crystallization, which affects the thermal and mechanical properties, and ultimately the degradability of the material. Thus, it is important to understand the nature of the crystalline regions and the crystallization process as a way to rationalize the degradation of PLA.

2.3.1 Crystallinity in polymers

Polymers can exhibit ordered (crystalline, liquid crystalline) or amorphous (liquid) states, depending on the capability of the macromolecules to arrange or not into regular structures. In some conditions of temperature, pressure, stress or solvent presence a spontaneous ordering of some of the chains can take place assuming favored specific orientation or rotation states. In this case, the chain molecules of the polymer can crystallize and display a three dimensional order similar to low molar mass materials. At sufficiently high temperatures, the intermolecular forces can be destroyed and an isotropic (amorphous) melt is formed. On the other hand, in amorphous polymers, the time required for the configuration changes involved to order the molecules is too high to compensate for the intermolecular interactions, and the polymer remains disordered. Many polymers can exhibit coexisting crystalline and amorphous regions, and are designated as semicrystalline.

The crystalline state is characterized by a three-dimensional order over a sufficient length range involving a least a portion of the chains. By comparing the crystalline and the liquid (amorphous) states, the former is relatively inelastic and rigid. The molecules are organized into a regular three-dimensional array irrespective of the unit cell and ordered chain dimensions. The morphology of this ordered structure can vary substantially, as can range from fully extended structure to well-known helical structures. A general prerequisite is aligning of long chains parallel to each other in order to achieve a regular arrangement.

This semicrystalline nature of the polymers, such as PLA, relies on the difficulty of long polymeric molecules to disentangle from each other from the disordered and entangled state (amorphous). The crystalline phase contains therefore only the fraction of the molecules capable to disentangle and form the ordered state. There is an interface connecting the

crystalline and amorphous regions, characterized by different chain conformations, as represented in Figure 2-12.

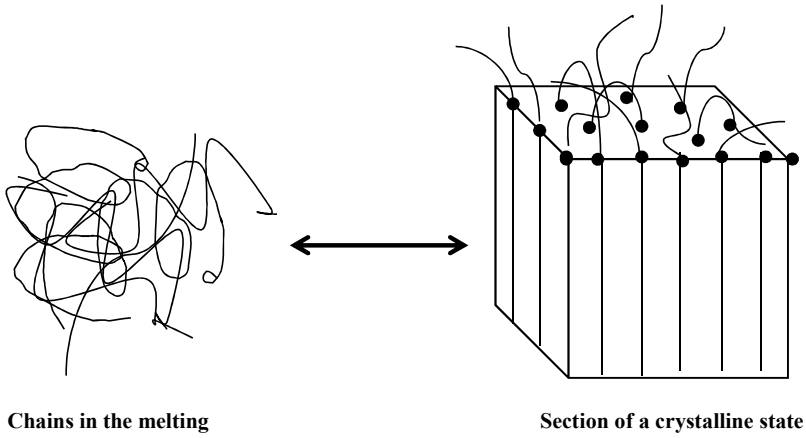

Figure 2-12 Representation of the semi-crystalline lamellae (Adapted from *ref.* 62).

The highly crystallizable and flexible linear polymers in bulk commonly crystallize in the form of spherulites, which are aggregates of molecules composed principally of chain-folded lamellae radiating from a central point, see Figure 2-13. *Fisher* was the first to show the extent of lamellar structures in melt crystalized polymers [63] and the work was followed by several authors [64,65,66,67]. The spherulite is composed of different lamellae branches forming the three dimensional spherical shape, as shown in Figure 2-13 [68]. Under polarized optical microscope, spherulites are observed as particular maltese crosses. The spherulites are formed by initial nucleation at different points of the sample, followed by growth and final impingement with the adjacent ones. Further introduction of chain irregularities in the backbone, such as branches, reduces the ability of chains to achieve the order required for the formation of stable crystals, and inhibits crystallization.

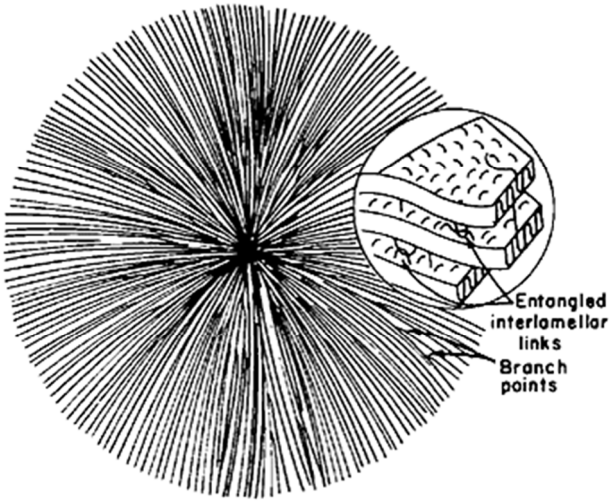

Figure 2-13 Polymer spherulite with inset of interlamellar regions (Reproduced from *ref.* 68).

Crystallization of a polymer depends on the temperature (thermodynamics) and time (kinetics). For macromolecules, the conditions of polymer mobility and thermal energy required to achieve crystallization are found only above the glass transition temperature and below the melting temperature [69]. Moreover, kinetically favorable crystallization requires appropriate selection of the crystallization time. An overview of the phenomena and the interrelation between its different aspects is shown in Scheme 2-3.

The thermal and mechanical properties of a polymer depend on the molecular morphology, which in turn is determined by the crystallization mechanism. Therefore the information about crystallization kinetics is relevant to determine the final functionalities of the materials.

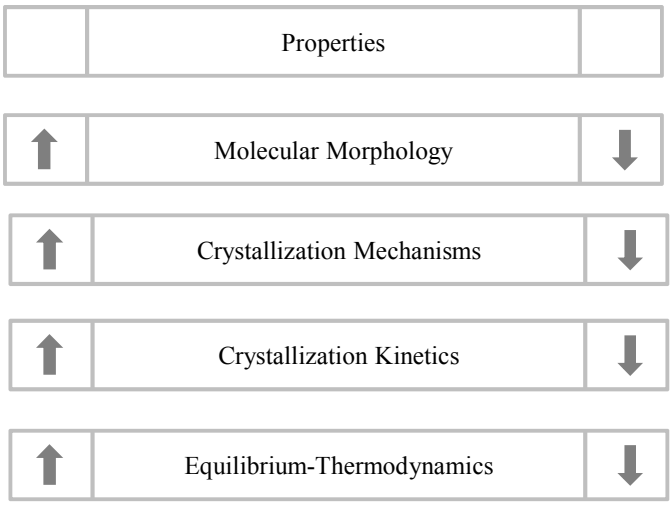

Scheme 2-3 Interrelation of problematic areas in the study of crystalline polymers (Adapted from*ref.* 70).

2.3.2 The thermodynamics of the crystallization

The crystallization phenomenon is explained by different thermodynamic theories. The classical theories of lateral and normal crystal growth modes, typically used to explain crystallization in small molecules, can be also applied in polymer crystallization [71].

The most common model for crystallization is presented in two steps, nucleation and growth. The parameter used to assess the process is the Gibbs free energy (G), which also defines the equilibrium conditions. The free energy of any system is related to the enthalpy and entropy at a given temperature T. So, the variation in free energy, ΔG, of the crystallization process at constant temperature T, is given by the following equation

$$\Delta G = \Delta H - T \cdot \Delta S \qquad (2\text{-}1)$$

where ΔH is the enthalpy change and ΔS is the change in the entropy during the phase change from liquid to solid.

A polymer melt consists of randomly coiled and entangled chains, and this corresponds to higher entropy than in a state where the molecules chains are extended, since more conformations are possible. When samples are crystallized from the melt, the order is stabilized, leading to a reduction in the entropy (less configurations available). The crystallization will be thermodynamically favored at a temperature lower than the melting temperature, only when the enthalpy reduction (ΔH_m) is higher than the product of the melting temperature and the entropy change ($T_m \cdot \Delta S_m$). When samples are quickly cooled from the melt, crystallization is largely controlled by kinetics, because the thermodynamics process is very slow (quasi-statics) and crystals nucleation and growth rates become essential.

The primary nucleation (first step) involves packing side-by-side of a few molecules to form a small cylindrical crystalline embryo. The formation of new crystal surface promotes an increase in the free energy (ΔG), since the surface-to volume ratio is high causing high surface energies. As more molecules are integrated in the crystal, *i.e.* crystal growth (second step), the embryo becomes larger the surface to volume ratio decreases. A critical size is achieved above which ΔG starts to decrease and eventually the free energy will be less than that of the original melt. Once the nucleus is greater than the critical size it will grow

spontaneously as this will cause ΔG to decrease. The result of these two competing factors is illustrated in Figure 2-14 as a function of crystal size.

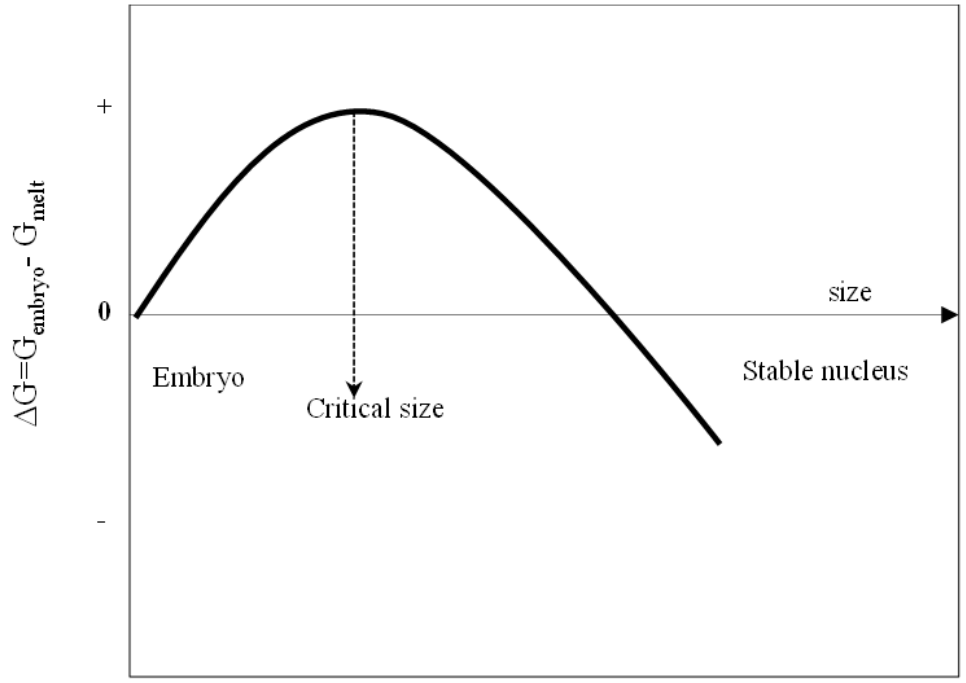

Figure 2-14 Schematic representation of change in free energy for the nucleation process during polymer crystallization. (Adapted from *ref.* 72).

The secondary nucleation was proposed by *Lauritzen* and *Hoffmann* [73] and envisages the polymer crystals growth as a process starting from a pre-existing crystal surface from the primary nucleation. This model assumes that the chains inside the nucleus are regularly folded. The secondary nucleation is similar to the primary but less primary surfaces per unit are created, resulting in lower activation energy barrier. The first step in the secondary nucleation process is laying down of a molecular strand on the crystal surface. This is followed by the subsequent addition of further segments through a chain-folding process, and extended-chain crystals are obtained from more rigid molecules. The secondary nucleation is schematically represented in Figure 2-15.

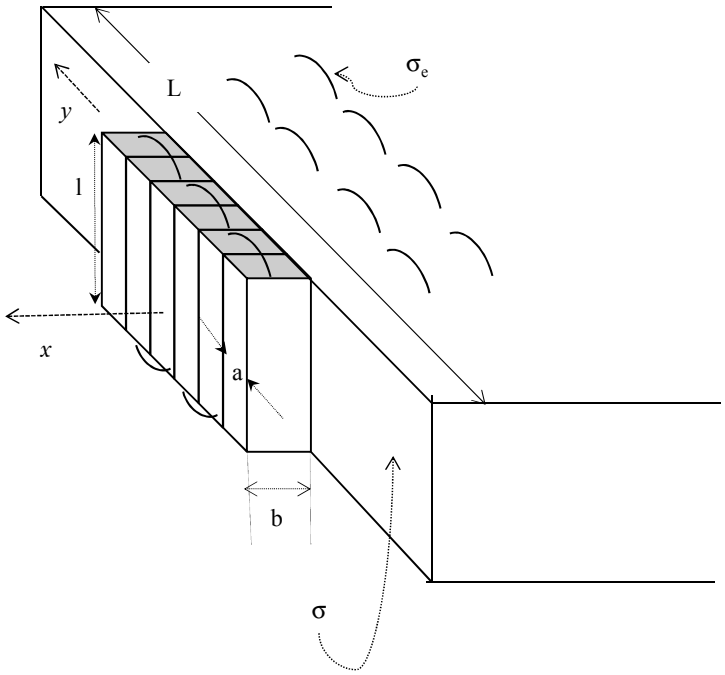

Figure 2-15 Model of the growth of a lamellar polymer crystal through the successive surface nucleation of adjacent strands. (Adapted from *ref.* 74).

The basic energetics of the crystallization process can be developed if it is assumed that the polymer lamellae has a fold surface energy σ_e, a lateral surface energy of σ and the free-energy change on crystallization is ΔG_v per unit volume. A prismatic strand geometry of a x b x l dimensions is considered, according to Figure 2-15.

Surface nucleus formation starts with a first stem formed by polymer segments from the undercooled melt, involving energy of $4bl\sigma$, The molecule then folds back and start to crystallize in an adjacent position, as this is the most probable site for reentry after folding. This new step requires an additional energy term from the basal surface free energy, $2ba\sigma_e$. By repeating this step, the nucleus spreads in the y direction. The energy involved also considers the reduction in free energy because of the formation of the first molecular strand:

$$\Delta G(1st nucleus) = 4bl\sigma + 2ba\sigma_e - abl\cdot\Delta G_v \qquad (2\text{-}2)$$

The increase in the free energy involved in laying down n adjacent molecular strands of length l is given by:

$$\Delta G(surface) = 2bl\sigma + 2nba\cdot\sigma_e \qquad (2\text{-}3)$$

There will be a reduction in free energy because of the incorporation of the molecular strands in the crystal given by

$$\Delta G(crystal) = -nabl \cdot \Delta G_v \tag{2-4}$$

Therefore, the total free energy change that is incurred in forming a regularly folded chain nucleus from the melt is given by

$$\Delta G = 2bl \cdot \sigma + 2nba\sigma_e - nabl\Delta G_v \tag{2-5}$$

The value of ΔG_v can be easily calculated at the equilibrium melting temperature T_m^0, which is the temperature at which a crystal without any surface would melt. At this temperature the change in free energy of crystallization can be calculated as:

$$\Delta G_v = \Delta H_v - T_m^0 \cdot \Delta S_v \tag{2-6}$$

where ΔH_v and ΔS_v are the melting enthalpy and entropy per unit volume respectively. At T_m^0 there is no change in free energy for the idealized boundary crystal thus, $\Delta G_v = 0$ $\Delta S_v = \Delta H_v / T_m^0$ can be incorporated to the general formula Equation (2-1) obtained per unit volume given Equation (2-7):

$$\Delta G_v = \Delta H_v - T(\Delta H_v / T_m^0) \tag{2-7}$$

Since the undercooling is given by $\Delta T = (T_m^0 - T_c)$, the Equation (2-7) can be organized as

$$\Delta G_v = \Delta H_v \cdot \Delta T / T_m^0 \tag{2-8}$$

For a given value of *n*, ΔG has a maximum value when *l* is small. By setting $\left(\frac{\partial \Delta G}{\partial l}\right)_n$ and $\left(\frac{\partial \Delta G}{\partial n}\right)_l$ equal to zero, the values of the critical size to form a stable nucleus are obtained:

$$n^* = \frac{2 \cdot \sigma}{a \cdot \Delta G_v} \tag{2-9}$$

$$l^* = \frac{2 \cdot \sigma_e}{\Delta G_v} \tag{2-10}$$

Thus ΔG^* is the change in free energy required to form a nucleus of critical size with n^* strands and length l^*:

$$\Delta G^* = \frac{4 \cdot \sigma_e \cdot \sigma}{\Delta G_v} \tag{2-11}$$

The previous analysis is important to understand the main aspects of the kinetic approach of polymer crystallization.

2.3.3 Crystallization kinetics

The formation of crystals is determined by the combination between kinetic factors involved in the transformation and thermodynamic requirements for equilibrium. Therefore, crystallization occurs in a metastable state, since the equilibrium conditions are difficult to achieve. Isothermal crystallization depends on the selection of the crystallization temperature (T_c). The crystallization rate is very slow when T_c is close to the equilibrium melting temperature T_m^0 and passes through a maximum at lower T_c values, before decreasing again when approaching the glass transition, T_g. The lateral crystal growth model involves a nucleation controlled process, on an atomically flat surface, with exponentially increasing rates with undercooling. Oppositely, in the normal crystal growth model, the molecule adds onto an atomically rough surface resulting in a linear change of crystal growth rate at low undercooling and an exponential growth rate at high undercooling.

The crystallization kinetics has been modeled by several authors. The most elementary expression of the liquid to crystalline phase transition was developed by *Von Goler* and *Sachs* [75] assuming a free growth approximation in which a mechanism of termination was not included. *Avrami* modified the expression taking into account that the growing nuclei decrease when increasing the impingement of the mass transformed [76,77,78]. The classical *Avrami* analysis is typically applied to explain the phenomenology of crystallization, but does not give comprehension into the processes involved in nucleation

and growth of the polymer crystals at a molecular level. The fraction of mass transformed 1-$\lambda(t)$, at time t, can be written as:

$$1 - \lambda(t) = \left[1 - \exp\left(-\frac{\rho_c}{\rho_l} \int_0^t V(t,\tau) \cdot N(\tau)\, d\tau \right) \right] \qquad (2\text{-}12)$$

where τ is the time in which a given nucleus center is initiated ($\tau<t$), $V(t,\tau)$ is the volume growth rate, $N(\tau)$ is the nucleation rate per unit of untransformed volume and ρ_c and ρ_l are the densities of the crystalline and liquid phase, respectively.

The integral can be evaluated by specifying the laws of nucleation and growth, providing many possible solutions since the solution is dependent on the expressions used for $V(\tau)$ and $N(\tau)$ as a function of τ. Different analytical expressions are obtained for the nucleation and volume growth rates, which will also depend on several factors such as geometry, time and dimensionality.

By considering that the steady-state nucleation rate is achieved at t=0 and remains constant with the fraction of material transformed, $N(\tau)$ is constant and other conditions that growth rate are linear and constant, the *Avrami* expression is obtained from (2-12):

$$1 - \lambda(t) = 1 - \exp\left(-kt^n\right) \qquad (2\text{-}13)$$

where k and n are the *Avrami* rate constant and exponent, respectively. k is proportional to the nucleation rate, $N(\tau)$, and the three dimensional growth rate, $V(\tau)$. n describes the types of nucleation and growth, specifically the geometry of the growth; for example theoretically n=2 represents homogenous nucleation with one dimensional growth and with diffusion controlled growth. This expression is theoretically developed for crystallization of a monomeric system (homopolymer) with complete transformation, but can be used with some modifications for polymers with incomplete transformation.

One of the limitations of the *Avrami* expression for polymers is that the k value is not an integer number and follows Arrhenius-type expressions. The temperature coefficient of the

crystallization rate can be analyzed according to the most general aspects of nucleation theory, without specific information of the nucleus structure or the crystallization process.

The T*urnbull and Fischer* equation [79] describes the steady-state rate for the formation of nuclei of critical size, which includes the temperature dependence explicitly. The model is irrespective of the type of nucleation, the shape of the nucleus or disposition of the chains within the nucleus:

$$N = No \cdot \exp\left(\frac{-E_D(T)}{RT_c} - \frac{\Delta G_n^*}{RT_c}\right) \tag{2-14}$$

where N is the constant nucleation rate, T_c is the crystallization temperature, E_D represents the activation energy for transport across the liquid-crystal interface and ΔG_n^* represents the barrier of free energy that must be overcome in order to form stable nuclei that allow crystallization to proceed.

Following similar basis, the growth rate (G) for secondary nucleation and lamellar growth via molecular deposition on a surface (see Section 4.2) was proposed by *Lauritzen* and *Hoffman* [68]:

$$G = Go \cdot \exp\left(\frac{-E_D(T)}{RT_c} - \frac{\Delta G^*}{RT_c}\right) \tag{2-15}$$

Transport term **Nucleation term**

where G_0 is the front constant and ΔG^* is associated with the free energy term for the formation of a nucleus on a pre-existing surface.

In Equation (2-15), transport is described by Arrhenius-activation term, but fails at temperatures 50-80ºC above the glass transition [80]. E_D can be also formulated using a Vogel type expression typically applied for viscous flow of amorphous polymers, leading to:

$$G = Go\exp\left(\frac{-U^*}{R(T_c - T_\infty)} - \frac{\Delta G^*}{RT}\right) \tag{2-16}$$

with $E_D = U^* \cdot T_c/(T_c - T_\infty)$, where $T_\infty = T_g - C_2$, represents the temperature below which the required segmental motion becomes infinitely slow, C_2 is a constant and U^* is the activation energy for transportation of segments to the crystallization site [81,82]. Equation (2-16) represents the growth rate using the Vogel form equation for the transport term [83].

Introducing $\Delta G_v = \Delta H_v \Delta T / T_m^0$ and $\Delta G^* = \frac{4\sigma_e \sigma}{\Delta G_v}$ in Equations (2-15) and (2-16) the expression of G can be written as:

$$G = Go\cdot\exp\left(\frac{-E_D}{RT_c} - \frac{4\cdot\sigma_e\cdot\sigma\cdot T_m^0\cdot b_0}{\Delta H_m\cdot R\cdot\Delta T\cdot T_c}\right) = Go\cdot\exp\left(\frac{-E_D}{R(T_c - T_\infty)} - \frac{Kg}{\Delta T\cdot T_c}\right) \tag{2-17}$$

$$G = Go\cdot\exp\left(\frac{-U^*}{R(T_c - T_\infty)} - \frac{4\cdot\sigma_e\cdot\sigma\cdot T_m^0\cdot b_0}{\Delta H_m\cdot R\cdot\Delta T\cdot T_c}\right) = Go\cdot\exp\left(\frac{-U^*}{R(T_c - T_\infty)} - \frac{Kg}{\Delta T\cdot T_c}\right) \tag{2-18}$$

where b_0 is the layer thickness and k the *Boltzmann* constant (R/N_A where N_A is the Avogrado's number). These parameters have been included in order to get Kg in appropriate units. Values of 30 K and 51.6 K have been used for C_2 from the Vogel equation in in order fit the data using the previous expressions.

2.4 Bibliographical references

[1] Schnabel W. Polymer Degradation Principles and Practical Applications. Hanser Publishers Munich 1992.

[2] Narayan R, Pettigrew CA. ASTM Impact of Standards Paper Contest, 1998.

[3] Dekker M. Handbook of polymer degradation, 2nd edition edited by S. Halim Hadim 2000.

[4] McNeill IC, in Eastmond G, Ledwith A, Russo S and Sigwalt P (Eds). Comprehensive Polymer Science Vol. 6. Fergamon. London, 1989 pp. 451–500.

[5] Muller RJ, Witt U, Rantze E, Deckwer WD. Architecture of biodegradable copolyesters containing aromatic constituents. Polym Degrad Stab.1998;59:203–208.

[6] Tsuji H, Ikada Y. Properties and morphology of poly(L-lactide) 4. Effects of structural parameters on long-term hydrolysis of poly(L-lactide) in phosphate buffered solution. Polym Degrad Stab 2000;67,1:179–189.

[7] Le Digabel F, Averous L. Effects of lignin content on the properties of lignocellulose-based biocomposites. Carbohydr Polym 2006;66:537–545.

[8] Yew GH, Mohd Yusof AM, Mohd Ishak ZA, Ishiaku US. Water absorption and enzymatic degradation of poly(lactic acid)/rice starch composites. Polym Degrad Stab 2006;90,3:488–500.

[9] Albertsson A-C, Karlsson S, in Chemistry and Technology of Biodegradable Polymers, Blackie, Glasgow, 1994 Chap. 2, pp. 48.

[10] Helbling C, Abanilla M, Lee L, Karbhari VM. Issues of variability and durability under synergistic exposure conditions related to advanced polymer composites in civil infrastructure. Compos Part A-Appl Sci 2006;37,8:1102–1110.

[11] Ipekoglu B, Böke H. Cizer O. Assessment of material use in relation to climate in historical buildings. Build Environ 2007;42:970–978.

[12] Jakubowicz I, Yarahmadi N, Petersen H, Evaluation of the rate of abiotic degradation of biodegradable polyethylene in various environments. Polym Degrad Stab 2006;91,6:1556–1562.

[13] ASTM D6400-04 Standard Specification for Compostable Plastics.

[14] ISO 846, 1997. Plastics–determination of behaviour under the action of microoganisms. Evaluation by visual examination or measurement of changes in mass or physical properties.

[15] Santonja-Blasco L, Contat-Rodrigo L, Moriana-Torró R, Ribes-Greus A. Thermal characterization of polyethylene blends with a biodegradable masterbatch subjected to thermo-oxidative treatment and subsequent soil burial test. J Appl Polym Sci 2007;106:2218–2230.

[16] Moriana-Torró R, Contat-Rodrigo L, Santonja-Blasco L, Ribes-Greus A. Thermal characterisation of photo-oxidized HDPE / Mater-Bi and LDPE / Mater-Bi blends buried in soil. J Appl Polym Sci 2008;109:1177–1188.

[17] Santonja-Blasco L, Moriana R, Badía JD, Ribes-Greus A. Thermal analysis applied to the characterization of degradation in soil of polylactide: I. Calorimetric and viscoelastic analyses. Polym Degrad Stab 2010;95:2185–2191.

[18] Badia JD, Santonja-Blasco L, Moriana R, Ribes-Greus A. Thermal analysis applied to the characterization of degradation in soil of polylactide: II. On the thermal stability and thermal decomposition kinetics. Polym Degrad Stab 2010;95:2192–2199.

[19] Badia JD, Vilaplana F, Karlsson S, Ribes-Greus A. Thermal analysis as a quality tool for assessing the influence of thermo-mechanical degradation on recycled poly(ethylene terephthalate). Polym Test 2009;28,2:169–175.

[20] Moriana R, Vilaplana F, Karlsson S, Ribes-Greus A. improved thermo-mechanical properties by the addition of different natural fibres in starch-based sustainable biocomposites. Composites Part A 2011;42:30-40.

[21] Kounty M, Lemaire J, Delort AM. Biodegradation of polyethylene films with prooxidant additives. Chemosphere 2006;64:1243–1252.

[22] Wiles DM, Scott G. Polyolefins with controlled environmental degradability. Polym Degrad Stab 2006;91:1581–1592.

[23] Morancho JM, Ramis X, Fernandez X, Cadenato A, Salla JM, Vallès A, Contat L, Ribes A. Calorimetric and thermogravimetric studies of UV-irradiated polypropylene/ starch-based materials aged in soil. Polym Degrad Stab 2006;91,1:44–51.

[24] Briassoulis D. The effects of tensile stress and the agrochemicals Vapam on the ageing of low density polyethylene (LDPE) agricultural films. Part I. Mechanical behaviour. Polym Degrad Stab 2005;86:489–503.

[25] Duval C. Matériaux dégradables in matières plastiques et environnement recyclage, valorisation, biodégradabilité, écoconception. 2004 DUNOD, Paris.

[26] Pitt CG, Gratzel MM, Kimmel GL, Surles J, Schindler A. Aliphatic polyesters II. The degradation of poly (DL-lactide), poly (ε-caprolactone), and their copolymers in vivo. Biomaterials 1981;2:215–220.

[27] Pitt CG. Non microbial degradation of polyesters: mechanisms and modifications. Vert M, Feijen J, Albertsson AC, Scott G, Chiellini E. (Eds) Biodegradable polymers and plastics. Royal Society of Chemistry, Cambridge, 1992 pp.7-19.

[28] Carter BK and Wilkes GL in Shalaby SW, Hoffman AS, Ratner BD and Horbert TA eds. Polymers as Biomaterials, Plenum Press, New York, 1984 pp. 67–92.

[29] Mauduit J, Bukh N, Vert M. Gentamycin/poly (lactic acid) blends aimed at sustained release local antibiotic therapy administered per-operatively. III. The case of gentamycin sulfate in films prepared from high and low molecular weight poly (DL-lactic acids). J Control Rel 1993;25:43–49.

[30] McNeill IC and Leiper HA. Degradation studies of some polyesters and polycarbonates 1. Polylactide: general features of the degradation under programmed heating conditions. Polym Degrad Stab 1985;11:267–285.

[31] McNeill IC and Leiper HA. Degradation studies of some polyesters and polycarbonates 2. Polylactide: degradation under isothermal conditions, thermal degradation mechanism and photolysis of the polymer. Polym Degrad Stab 1985;11:309-326.

[32] Jamshidi K, Hyon SH, Ikada Y, Thermal characterization of polylactides. Polymer 1988;29:2229–2234.

[33] Kopinke FD, Remmler M, Mackenzie K, Moder M, Wachsen O. Thermal decomposition of biodegradable polyesters. 2. Poly(lactic acid). Polym Degrad Stab 1996;53,3:329–342.

[34] Wachsen O, Reichert K.H, Kruger R.P, Much H. and Schulz G, Thermal decomposition of biodegradable polyesters- III. Studies on the mechanisms of thermal degradation of oligo-L-lactide using SEC, LACCC and MALDI-TOF-MS. Polym Degrad Stab 1997;55:225–231.

[35] Kopinke FD, Mackenzie K. Mechanistic aspects of the thermal degradation of poly(lactic acid) and poly(beta-hydroxybutyric acid). J Anal Appl Pyrolysis 1997;41:43–53.

[36] Badia JD, Strömberg E, Ribes-Greus A, Karlsson S. Assessing the MALDI-TOF MS sample preparation procedure to analyze the influence of thermo-oxidative ageing and thermo-mechanical degradation on poly (lactide). Eur Polym J 2011;47:1416–1428.

[37] Merkli A, Tabatabay C, Gurny R, Heller J. Biodegradable polymers for the controlled release of ocular drugs. Prog Polym Sci 1998;23,3:563–80.

[38] De Jong SJ, Arias ER, Rijkers DTS, van Nostrum CF, Kettenes-van den Bosch JJ, Hennink WE. New insights into the hydrolytic degradation of poly(lactic acid): Participation of the alcohol terminus. Polymer 2001;42:2795–2802.

[39] Lucas N, Bienaime C, Belloy C, Queneudec M, Silvestre F, Nava-Saucedo J-E. Polymer biodegradation: Mechanisms and estimation techniques. Chemosphere 2008;73,4:429–442.

[40] Siepmann J, Göpferich A. A. Mathematical modeling of bioerodible, polymeric drug delivery systems. Adv Drug Delivery Rev 2001;4,2-3:229–47.

[41] Torres A, Li S M, Roussos S, Vert M. Poly (lactic acid) degradation in soil or under controlled conditions. J Appl Polym Sci 1996;62,13:2295–2302.

[42] Kale G, Auras R, Singh SP. Comparison of the degradability of Poly(lactide) packages in composting and ambient exposure conditions. Packag Technol Sci 2007;19:49–70.

[43] Kale G, Auras R, Singh SP, Narayan R. Biodegradability of polylactide bottles in real and simulated conditions. Polym Test 2007:26:1049–1061.

[44] BPI Logo Program, http://www.bpiworld.org/ October 2005.

[45] Ho KLG, Pometto III AL, Hinz PN. Effects of temperature and relative humidity on polylactic acid plastic degradation. J. Environ Polym Degrad 1999;7:83–92.

[46] Calmon A, Guillaume S, Bellon-Maurel V, Feuilloley P, Silvestre F. Evaluation of material biodegradability in real conditions-development of a burial test and an analysis methodology based on numerical vision. J Environ Polym Degrad 1999;7:157–166.

[47] Urayama H, Kanamori T, Kimura Y. Properties and biodegradability of polymer blends of poly(l-lactide)s with different optical purity of the lactate units. Macromol Mater Eng 2002;287:116–121.

[48] Iman HS. Adhesive properties of a symbiotic bacterium from a wood-boring shipworm. Appl Environ Microbiol 1990;56:1317–1322.

[49] Goheen RP, Wool RP. Degradation of polyethylene-starch blends in soil. J Appl Polym Sci. 1991;42:2691–2701.

[50] Albertsson AC, Karlsson S. Macromolecular architecture-nature as a model for degradable polymers. J Macromol Sci Pure Appl Chem 1996; 33,10:1565–1570.

[51] Mohanty AK, Misra M, Drzal LT. Natural fibers, biopolymers and biocomposites. 2005 CRC Press by Taylor & Francis Groups, Boca Raton FL.

[52] Vink ETH, Rábago KR, Glassner DA, Gruber PR, Applications of life cycle assessment to NatureWorks™ polylactide (PLA) production. Polym Degrad Stab 2003:80;403–419.

[53] Feldman D. Polymer degradation: thermo-oxidation. J Polym Environ, 2002; 10,4:163-173.

[54] Kelen T. Polymer Degradation, Van Nostrand Reinhold Co, 1983, New York.

[55] Ikada E. Photo- and bio- degradable polyesters. Photodegradation behaviours of aliphatic polyesters. J Photopolym Sci Technol 1997;10,2:265–270.

[56] Ikada E. Relationship between photodegradability and biodegradability of some aliphatic polyesters. J Photopolym Sci Technol 1999;12,2:251–256.

[57] Janorkar AV, Metters AT, Hirt DE. Degradation of poly(L-lactide) films under ultraviolet-induced photografting and sterilization conditions. J Appl Polym Sci 2007;106:1042–1047.

[58] Copinet A, Bertrand C, Govindin S, Coma V, Couturier Y. Effects of ultraviolet light (315 nm), temperature and relative humidity on the degradation of polylactic acid plastic films. Chemosphere 2004:55;763–773.

[59] Sakai W, Sadakane T, Nishimoto W, Nagata M, Tsutsumi N. Photosensitized degradation and crosslinking of linear aliphatic polyesters studied by GPC and ESR. Polymer 2002;43:6231–6238.

[60] Tsuji H, Echizen Y, Saha SK, Nishimura Y. Photodegradation of poly (L-lactic acid):effects of photosensitizer. Macromol Mater Eng 2005;290:1192–1203.

[61] Bocchini S, Fukushima K, Di Blasio A, Fina A, Frache, Geobaldo F. Polylactic acid and polylactic acid-based nanocomposite photooxidation. Biomacromolecules, 2010;11,11:2919–2926.

[62] Flory PJ. On the morphology of the crystalline state in polymers. J Am Chem Soc 1962;84:2857–2867.

[63] Fisher EW. Stufen- und spiralförmiges Kristallwachstum bei. Hochpolymeren Z.Naturforsch. 1957;12a:753–754.

[64] Keith HD, Padden FJ. The optical behavior of spherulites in crystalline polymers. Part I: Calculation of theoretical extinction patterns in spherulites with twisting crystalline orientation. J Polym Sci 1959;39,135:101–103.

[65] Keith HD, Padden FJ. The optical behavior of spherulites in crystalline polymers. Part II. The growth and structure of the spherulites. J Polym Sci 1959;39,135:123–138.

[66] Keith HD, Padden FJ. A phenomenological theory of spherulitic crystallization. J.App. Phys. 1963;34:2409-2421.

[67] Keith HD, Padden FJ. Banding in polyethylene and other spherulites, Macromolecules 1996,;29:7776–7786.

[68] Hoffman JD, Davis GT, Lauritzen, JL. Jr. The rate of crystallization of linear polymers with chain folding. In Treatise on Solid State Chemistry Hannay, N. B., Ed.; Plenum Press: New York, 1976; Vol. 3; Chapter 7, pp 566.

[69] Gupta RK. Fundamentals of Polymer Engineering, Revised and Expanded (Plastics Engineering). 2nd edition 2003, ISBN-10: 0824708679.

[70] Mandelkern L. Relation between properties and molecular morphology of semicrystalline polymers. Faraday Discuss. Chem. Soc. 1979;68:310–319.

[71] Rosenberger F. Proceedings of the NATO Advanced Study Institute (ed. B. Mutaftschiev), 1982, pp. 315-363. Dordrecht: Reidel.

[72] Young RJ, Lovell PA, Introduction to Polymers, Second edition, 1991, Chapan and Hall

[73] Lauritzen JI Jr, Hoffman JD. Theory of formation of polymer crystals with folded chains in dilute solution. J Res Nat Bur Stand 1960:64A;73–102.

[74] Hoffman JD, Davis GT, Lauritzen JI Jr. In treatise on solid state chemistry. Hannay NB,Ed. Plenum Press New York, 1976.

[75] Von Goler F, Sachs G, Zur Kinetick von kristallisations- vorgangen. Pysik, Z 1932;77: 281.

[76] Avrami M. Kinetics of phase change. I: general theory. J Chem Phy. 1939;7:1103–1112.

[77] Avrami M. Kinetics of phase change. II: transformation-time relations for random distribution of nuclei. J Chem Phys 1940;8:212–224.

[78] Avrami M. Kinetics of phase change. III: granulation, phase change an microstructure. J. Chem. Phys. 1941;9:177–184.

[79] Turnbull D, Fischer J. Rate of nucleation in condensed systems. J Chem Phys 1949;17:71–73.

[80] Suzuki T, Kovacs A. Temperature dependence of spherulitic growth rate of isotactic polystyrene. Polymer J 1970;1,1:82–100.

[81] Vogel H. The temperature dependence law of the viscosity of fluids. Phys Z 1921;22:645.

[82] Fulcher GS. Analysis of recent measurements of the viscosity of glasses. J Am Ceram Soc 1925;8:339–355.

[83] Williams ML, Landel RF, Ferry JD. The temperature dependence of relaxation mechanism in amorphous polymers and other glass-forming liquids. J Am Ceram Soc 1955;77:3701–3707.

Chapter 3 Experimental Part

3.1 Material

The material used was a commercial Polylactide (PLA), NatureWorks® PLA 2002D supplied by NatureWorks (Blair, NE, USA), and prepared by ring opening polymerization (ROP) of lactic acid previously obtained from renewable resources. The D-content of the PLA of study is reported around 4% [1,2]. The majority of NatureWorks® PLA grades, including 2002D, are semi-crystalline polymers with relatively slow nucleation and crystallization rates. As a result, most extruded objects from these grades such as sheet and pellets are 100% amorphous after normal quenching operations.

Five different types of samples were analyzed in this thesis: the original 2002D pellets, melt pressed plates (so-called "plates"), thermally degraded pellets, melt pressed plates degraded in soil and photodegraded melt pressed plates. Figure 3-1 shows the scheme of the samples studied.

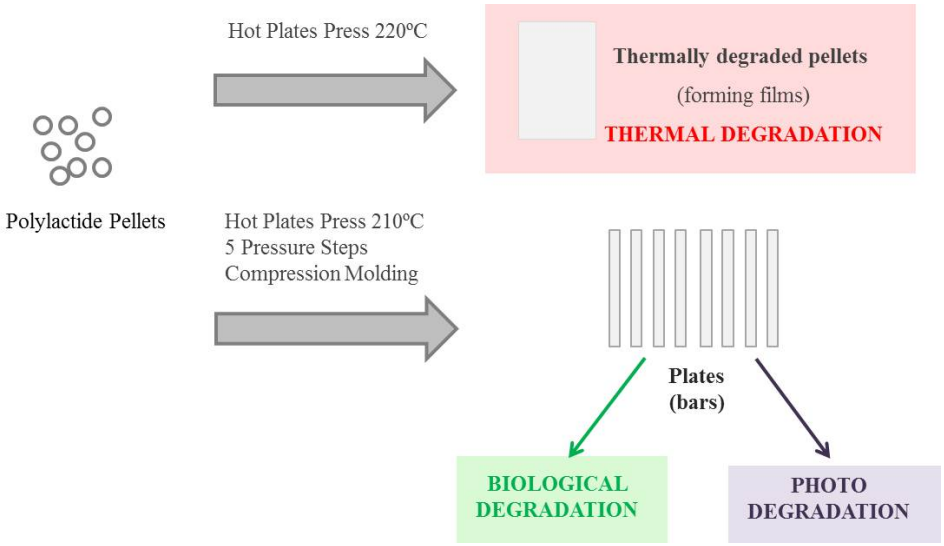

Figure 3-1 Scheme of the samples studied for each degradation process.

The thermal degraded samples were obtained by melting the pellets. The PLA plates for bio and photo degradation were obtained from the PLA pellets by compression molding. The pellets were previously dried with demoisturized air at 80ºC during 4 hours. Rectangular plates of 10x4x0.1 cm were prepared by melt compression in a Collin PCS-GA Type Press 800 (GA, USA) at 210ºC in five pressure steps as follows: 4 minutes at 2 bar, 2 minutes at 30 bar, 3 minutes at 50 bar, 5 minutes at 180 bar, and 12 minutes at 40 bar and tap water

cooling. Specimens of 6x1x0.1 cm for photo and bio degradation tests were cut from the melt-pressed plates. Additionally, several PLA plates (non-degraded) were taken as the reference during all the present study, since this work pertains to the degradation of consumer goods in landfill soil which are obtained by means of, at least, one processing step.

3.2 Degradation tests

3.2.1 Thermal degradation test

Thermal degradation was studied by heating the PLA pellets at 220ºC ± 10ºC during 3, 30, 62, 120 and 330 minutes (at atmospheric pressure) in a Carver Press and further quenching to room temperature. Two 5x5 cm Teflon sheets of 10 μm thickness were used to avoid sticking of material to the press plates. A set of thermally degraded PLA plates of around 225 μm thickness was obtained.

3.2.2 Biodegradation test

Several PLA plates were subjected to degradation in soil test under controlled conditions (temperature, water content and pH), following the ISO 846-1997 International Norm, method D [3]. Samples were buried in biologically active soil and kept in a Heraeus B12 (Hanau, Germany) culture oven at 28 ºC, Figure 3-2. The soil used in the tests was a commercial culture soil and its microbial activity was checked with cotton along the duration of the experiment. The soil was maintained at approximately pH 5. The relative humidity was kept between the 60-80% of the maximum of water retained by the soil which value was 0.87 g water/g wet soil. To ensure oxygenation of the soil, a protocol of periodical aeration was followed.

Figure 3-2 Soil burial test in a culture oven at 28 ºC.

The burial in soil test was extended to 60 months. Test specimens were extracted at 1, 5, 10, 15, 20, 24, 30, 35, 40 and 60 months, cleaned with water and soap and kept in a desiccator during 4 days in order to ensure water desorption prior to their characterization. The PLA samples underwent a progressive visual change, clearly distinguished after 60 months in soil, evidencing an extremely high fragility (see Figure 3-3).

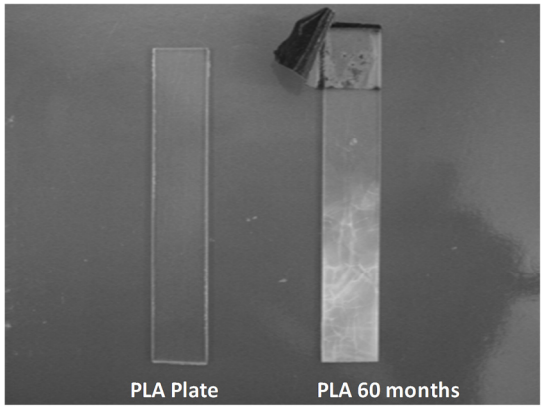

Figure 3-3 Plate and sample most degraded at 60 month in soil.

3.2.3 Photodegradation test

Photodegradation tests were carried out by an accelerated exposure test, using a Suntest XLS+ (Atlas) radiation-accelerated equipment (Figure 3-4). During all the experiments the temperature of the black panel was kept at T=50ºC, applying an irradiance of 478 W/m^2. The filter used simulates sunlight radiation higher than 290 nm (high UV-sunlight-low infrared). Samples (PLA plates) were exposed during different radiation times simulating real exposure by considering the minimum annual sun radiation in Spain, 5000 MJ/m^2 [4]. The total radiant exposure in J/m^2 was calculated by multiplying the experimental exposure time in the

accelerated test (in seconds, s) by the irradiance 478 J/(s·m^2). Division of such value by 5000 MJ/m^2·year allows obtaining the period of outdoor exposure in 12 months. Thus the different stages of photodegradation studied in this thesis are: 400 hours (1.7 months), 800 hours, (3.3 months), 1850 hours (7.7 months), 2250 hours (9.4 months), 3000 hours (12.6 months), 4100 hours (17.2 months) and 5100 hours (21.4 months). During photodegradation slight visual changes were observed, accompanied with greater brittleness of the materials at increasing times of exposure.

Figure 3-4 Suntest XLS+ Xenon Exposure System.

3.3 Characterization techniques

3.3.1 Viscometry

The molar mass of the PLA specimens was obtained by using viscometry and gel permeation chromatography. The viscosity average molar mass of different thermally and photo degraded PLA samples (M_v) was estimated from the intrinsic viscosity values (η). Measurements were carried out by solving the samples in tetrahydrofuran (THF) at 30°C, using a Cannon Freske viscometer Serie 25 from Schott Gerate Type 513 00 App.Nr. 1026 753, shown in Figure 3-5. The concentrations ranged between 0.25 to 2 g/dl. This viscometer consists of two branches connected by a capillary. The first branch is a reservoir where the polymer solution is initially introduced. The second branch includes the measuring bulb and a second bulb on top used as reservoir for the solution before the measurement starts. The pressure driving the liquid through the capillary is determined by the difference in height between the liquid in the reservoir and the measuring bulb, and therefore is essential to use the same volume of liquid for each measurement in order to compare them. The viscosity value is provided by measuring the time of flow of the solution through the two reference points in the measuring bulb.

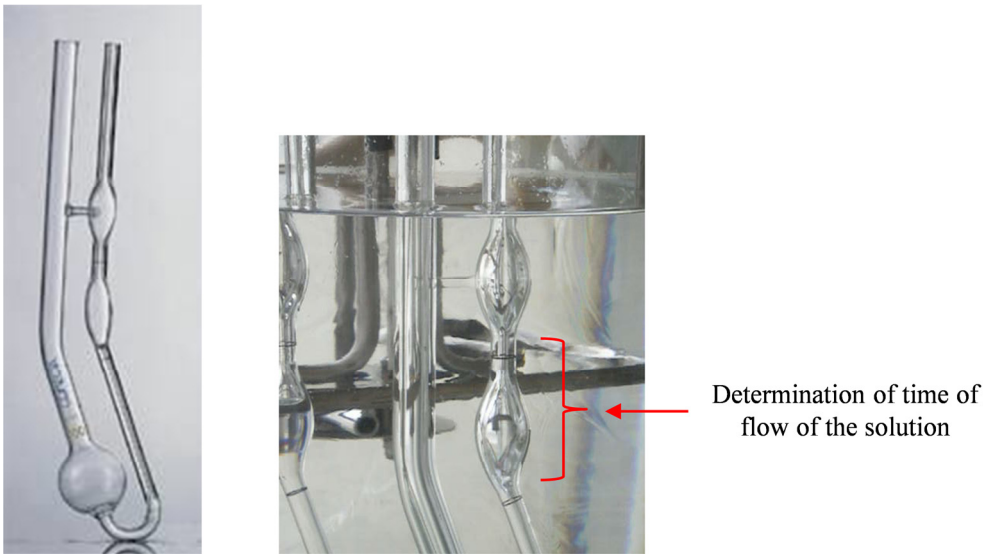

Figure 3-5 Viscometer Cannon-Freske

The viscosity of the polymers solutions can vary dramatically depending of the type of solvent, the polymer concentration, molar mass and temperature. Although to date there is not a complete theory explaining such dependences, there are several empirical relations to determine the molar mass of a polymer sample from measuring the viscosity of the solution. The Mark-Houwink-Sakurada equation was applied for the calculation of the intrinsic viscosity, $[\eta] = KM_v^{\alpha}$ [5], considering the specific parameters K and α of amorphous Poly (L-Lactide) PLLA[6]:

$$[\eta] = 1.74 \cdot 10^{-4} \times M_v^{0.736} \tag{3-1}$$

The flow rate of liquid through a capillary of radius r and length l is given by *Poiseuille's* equation:

$$\frac{dV}{dt} = \frac{\pi \cdot p \cdot r^4}{8 \cdot \eta \cdot l} \tag{3-2}$$

where η is the viscosity of the liquid, p is the pressure causing the flow and dV/dt is the volume of liquid flowing through the capillary in unit time. Since the pressure continually decreases during an experiment, it is convenient to define an average pressure . A constant volume of liquid V is normally used and Equation (3-2) is expressed as

$$\frac{V}{t} = \frac{\pi \cdot \dot{p} \cdot r^4}{8 \cdot \eta \cdot l} \tag{3-3}$$

where t is the time of flow of the solution through the capillary. The subscript ($_0$) is used when referred to the values of the solvent, and Equation (3-3) is rewritten as $\frac{V}{t_0} = \frac{\pi \cdot \dot{p}_0 \cdot r^4}{8 \cdot \eta_0 \cdot l}$ where η_0 *is* the viscosity of the solvent.

The average pressure is given by the standard relation:

$$\dot{p} \cdot = \rho \cdot g \cdot \hbar \qquad (3\text{-}4)$$

where ρ is the density of the liquid, $\hbar$ is the flow rate of the liquid and g is the acceleration due to gravity. Equation (3-4) can be used to determine the viscosity of a polymer solution if the viscometer is calibrated with solvents of known viscosity. However, normally the key parameter is the increase in viscosity of the solvent caused by the presence of the polymer molecules, instead of the absolute viscosity of the solution. A parameter of considerable importance is then the viscosity ratio or relative viscosity, η_r *,* which is defined as (η/η_0) and can be related to the times of flow t and t_0 through Equations (3-3) and (3-4):

$$\eta_r = \eta/\eta_0 = t\rho/t_0 \cdot \rho_0 \qquad (3\text{-}5)$$

This later equation can be further simplified since for a dilute solution $\rho \approx \rho_0$ and so η_r is normally taken as t/t_0. Since η_r becomes unity for an infinitely dilute solution, it is more useful to define the specific viscosity, η_{sp} which is given by:

$$\eta_{sp} = (\eta_r - 1) = (t - t_0)/t_0 \qquad (3\text{-}6)$$

The specific viscosity corresponds to the fractional increase in viscosity of the solvent due to the presence of the polymer molecules. It is obvious that the increase in viscosity will depend upon the concentration of polymer molecules in the solution (*c)*, and such dependence can be expressed as a power series in concentration:

$$\eta_{sp} = [\eta] \cdot c + \cdot k' \cdot [\eta]^2 c^2 + \ldots \qquad (3\text{-}7)$$

where *k'* is a constant. The division of the previous equation (3-7) by the polymer concentration gives the viscosity number or reduced viscosity, η_{red}*:*

$$\eta_{red} = \eta_{sp}/c = [\eta] + k'' \cdot [\eta]^2 \, c + \ldots \qquad (3\text{-}8)$$

In the previous equation, the intrinsic viscosity, $[\eta]$ (also termed limiting viscosity number), represents the capability of the polymer molecules to increase the viscosity of the solvent in the absence of any intermolecular interactions. The second term of the sum represents the interaction between the different molecules in the solution. The calculation of $[\eta]$ is made by measuring series of solutions at different polymer concentrations. The inherent viscosity, η_{inh}, is also defined as the ratio of the natural logarithm of the relative viscosity and the concentration.

$$\eta_{inh} = \ln(\eta_r)/c = = [\eta] + k_K \cdot [\eta]^2 \, c + \ldots \quad (3\text{-}9)$$

When the concentration tends to zero $\eta_{red} = [\eta] = \eta_{inh}$, the intrinsic viscosity can be estimated using the Huggins (η_{red} vs. c) and the Kraemer (η_{inh} vs. c) plots, as has been exemplified in Figure 3-6 for the 120 min thermally degraded sample.

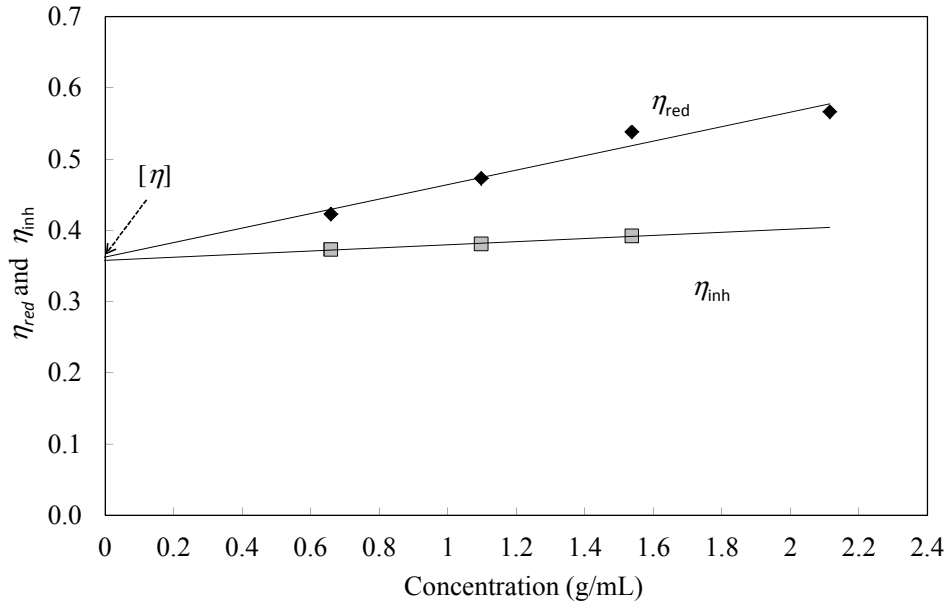

Figure 3-6 Calculation of $[\eta]$ by using the Huggins (η_{red} vs. c) and the Kraemer (η_{inh} vs. c) plots of the thermally degraded sample at 120 minutes.

3.3.2 Gel Permeation Chromatography (GPC)

Gel Permeation Chromatography (GPC) is applied to calculate the weight-average molar mass (M_w) and the number-average molar mass (M_n), as well as the molar mass distribution (*MMD*) of the samples. The following assumptions are applied to correlate the viscosity molar mass with the number and weight average molar masses for polydisperse polymers, such as the case of PLA:

1. $\eta_{sp} = \sum_i \eta_{sp}$
2. $(\eta_{sp})_i = [\eta]_i \cdot c_i$
3. $[\eta]_i = K \cdot M_i^{\alpha}$

The first assumption is that the total specific viscosity is the sum of the specific viscosities for each component, *i*, (*i.e.*, each molar mass of the polymer). The second assumption states that the specific viscosity of each component can be calculated from the intrinsic viscosity due to that component. The third assumption was that intrinsic viscosity and molar mass are correlated.

From these assumptions it is possible to write:

$$\frac{\eta_{sp}}{c} = \frac{\sum_i K \cdot c_i \cdot M_i^{\alpha}}{c} = \frac{\sum_i K \frac{N_i \cdot M_i}{V} M_i^{\alpha}}{\sum_i \frac{N_i \cdot M_i}{V}} = \frac{\sum_i K \cdot N_i \cdot M_i^{1+\alpha}}{\sum_i N_i \cdot M_i} \tag{3-10}$$

By extracting *K* from the summation term, and considering the limit of zero concentration:

$$\lim_{c \to 0} \frac{\eta_{sp}}{c} = K \cdot M_v^{\alpha} \tag{3-11}$$

where M_v is the viscosity average molar mass, defined as:

$$M_v = \left(\frac{\sum_i N_i M_i^{1+\alpha}}{\sum_i N_i \cdot M_i} \right)^{\frac{1}{\alpha}} \tag{3-12}$$

When $\alpha = 1$, M_v corresponds to the weight average molar mass, M_w; otherwise, M_v lies between the weight and number average, $M_n \leq M_v \leq M_w$. For typical α values ranging from 0.5 to 0.8, M_v is closer to M_w than to M_n. This result is expected since viscosity properties are likely to be a function of size and not only of the number of polymers.

GPC measurements were carried out in tetrahydrofuran (THF) at room temperature using:

1. A Waters Alliance 2690 GPC (Milford, MA, USA)connected to Viscotek software program along with UV absorbance and differential refractive index detector.
2. A Column Set (Polymer Laboratories): Three Polymer Labs PLgel Mixed-B with a series of well-characterized, narrow-fraction molar mass standards of known peak molecular weight (M_p).

The experimental conditions were:

- GPC Solvent: (THF) containing 50ppm of butylated hydroxy toluene fiugh a 0.45 mm Teflon filter.
- GPC oven temperature: 35ºC
- Auto sampler temperature: room temperature
- Flow rate: 1.00 ml/min.
- Dissolution solvent: THF
- Sample concentration: 2.0 mg/ml
- Sample dissolution temperature: room temperature
- Sample dissolution time: 35 minutes
- Sample injection size: 150 μL

GPC calibration

The separation efficiency of the column set was calibrated using a series of narrow *MMD* polystyrene standards, which defines the expected molar mass range for samples and the exclusion limits of the column set. More precisely, twenty five individual polystyrene standards, ranging from M_p ~580 to 7300000, were used to generate the calibration curve.

The polystyrene standards were obtained from Polymer Laboratories (Amherst, MA, USA). To assure internal consistency, the flow rate was corrected for each calibrant run. A common peak position was obtained for the flow rate marker before determining the retention volume for each polystyrene standard. The flow marker peak position was thus assigned and was further applied to correct the flow rate when analyzing the samples. A calibration curve ($\log(M_p)$ vs. retention volume) was generated by recording the retention volume at the peak in the differential refractometer (DRI) signal for each PS standard.

The molar masses of the PLA samples were referred to Polystyrene (PS) as standard using the following Mark-Houwink coefficients ($\log K$=-3.903, α=0.715).

3.3.3 Fourier Transform Infrared Spectroscopy (FTIR)

Fourier Transform Infrared Spectroscopy was applied to study the chemical functional groups of PLA and their changes throughout the degradation process. Analysis of the infrared (IR) spectra enables the identification of functional groups through the vibrations generated within bonds in the sample. The different peaks in a spectrum represent absorptions corresponding to vibrational transitions with different energy. In particular, FTIR spectrometers use the Fourier transform to process the information mathematically.

Some examples of molecular vibrations are:

In plane stretching:

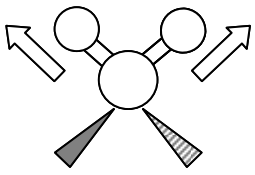

Symmetric

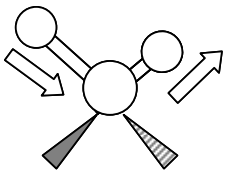

Antisymmetric

In plane bending:

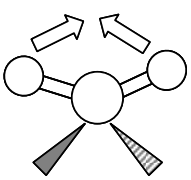

Scissoring

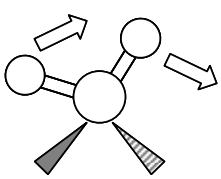

Rocking

Out of plane bending:

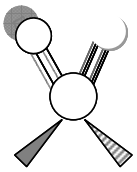

Twisting

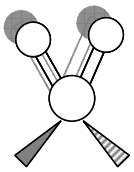

Wagging

The infrared spectrum of a sample is collected by passing a beam in the infrared frequency range through the sample. Examination of the transmitted light reveals the fraction of energy that the sample absorbed at each wavelength. By using a Fourier Transform instrument, a measurement of all wavelengths is taken at once. FTIR spectra typically show the absorption capacity of infrared radiation of the sample on the *y*-axis with respect to the wavenumber (frequency, cm^{-1}). The absorption capacity of the sample is defined as a function of absorbance (A) or transmittance (T), being these parameters defined as follows:

$$A = \log \frac{T_0}{T}$$

The FTIR spectra were obtained using a Thermo Nicolet 5700 spectrometer (Thermo Fisher Corporation, MA, USA), in the 400 to 4000 cm^{-1} region, with a 4 cm^{-1} resolution, and using an Attenuated Total Reflectance (ATR**)** modulus. The use of ATR was necessary to mitigate the excessive absorbance (and signal saturation) obtained in direct transmission experiments caused by the great thickness of the polylactide samples (Figure 3-7). Specimens were placed between a crystal (with a high refractive index) and a clamp. The IR beam is transmitted through the crystal and partially absorbed by the sample, generating the so-called evanescent wave. In order to obtain accurate results, 64 scans were performed to complete each spectrum at 7 locations on the sample, and the average was obtained. Furthermore a baseline correction and ATR correction (considering the refractive index) were applied to the spectra. Any interference with the environment surrounding the ATR spectrometer (dirt, dust, etc.) was eliminated by collecting background spectra before testing each sample.

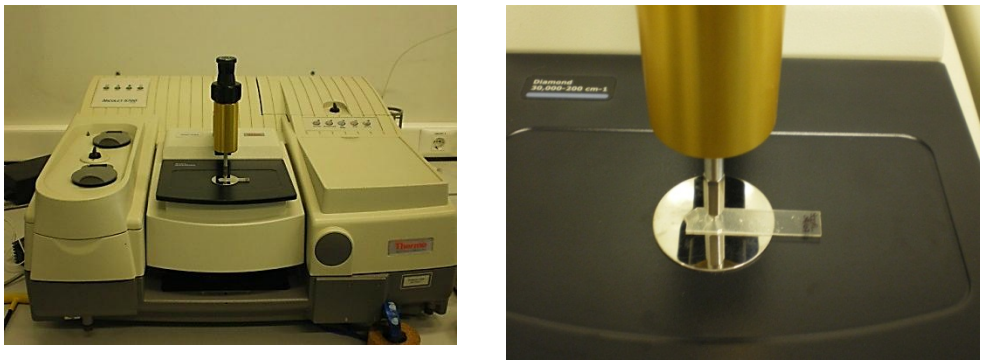

Figure 3-7: IR Spectrometer with ATR incorporated.

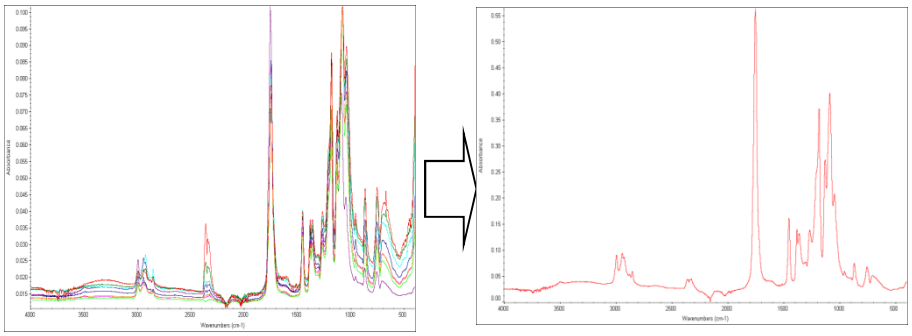

Figure 3-8 Average of the 7 spectrum collected of each sample.

3.3.4 Thermogravimetric Analysis/Thermogravimetry (TGA)

Thermogravimetric experiments were carried out using a Mettler-Toledo TGA/SDTA 851^e modulus (Columbus, OH, USA). The tests consisted in heating ramps from 25 to 750ºC at different heating rates β = 5, 7, 10, 12, 15, 20, 25, 30 ºC/min. The experiments were conducted under constant flow of 50 mL/min of argon atmosphere and nitrogen purge in the equipment of 200 mL/min, using Al_2O_3 crucibles containing 3.5 to 5 mg of sample.

Thermogravimetric analysis (TGA) is a technique used to study the thermal stability and the fraction of volatile components in a sample by monitoring the change in mass as it is heated. TGA measurements can be performed in either inert (argon or nitrogen) or oxidant atmosphere (air or oxygen). Output data are collected as changes in mass as a function of increasing temperature (dynamic experiments) or time (isothermal experiments). It is also very common to calculate the derivative thermogravimetric curve (DTG), corresponding to the derivative of the actual mass (or mass percentage) respect to time or temperature. Typical TG thermograms and DTG curves are shown in Figure 3-9. Individual processes of mass loss (solvent desorption, thermal degradation…) correspond to sigmoidal steps in the TG curves and peaks in the DTG curves. The amount of mass remaining at the end of the experiment is assigned to the residue or undegraded sample.

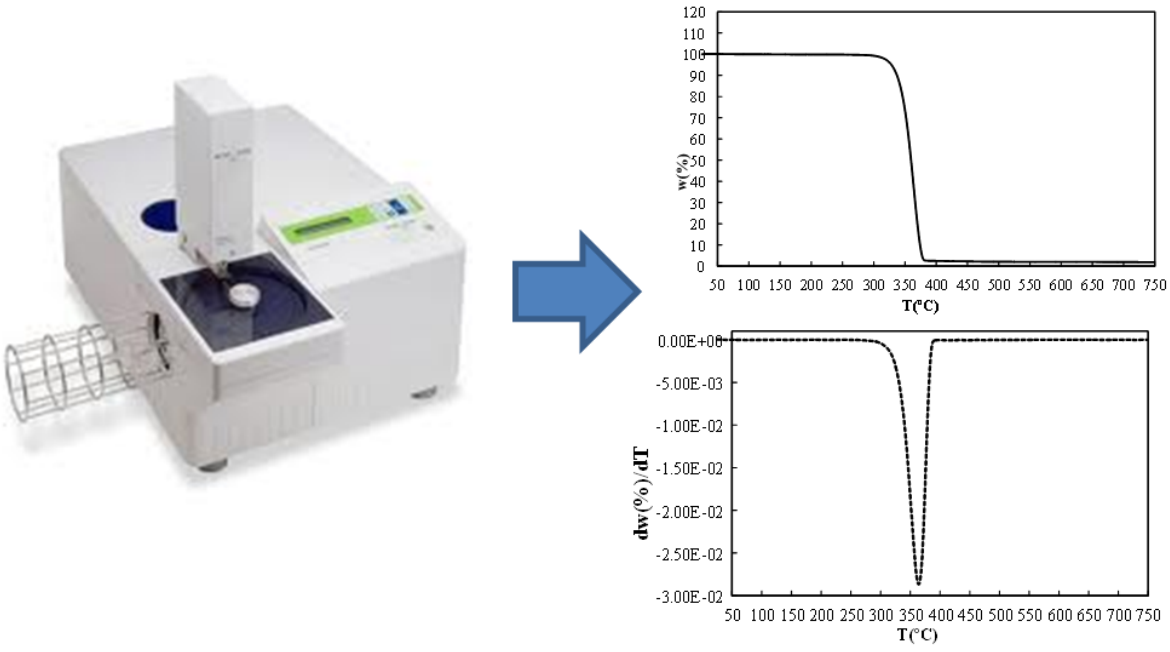

Figure 3-9 TGA Equipment (left) and TG and DTG curves of PLA (right)

Theoretical background of the kinetic analysis

The thermal stability of the samples is described by the different decomposition processes, mass loss associated, their temperature ranges, residual values, etc. In addition, it is common to apply kinetic analyses to obtain further information on the thermal degradation of polymers, by using isoconversional and non-isoconversional methods [7,8]. The completion of the kinetic triplet (the kinetic model function *f (α),* apparent activation energy (*Ea*), and pre-exponential factor (*A*)) provides with further understanding of the thermal decomposition behavior of polylactides and the effect of each degradation process on its structure [9].

In the thermal degradation study it is assumed that the decomposition rate is proportional to the sample mass measured during the experiment (ω). For the calculation of the kinetic parameters the conversion degree α is defined as:

$$\alpha = \frac{\omega_i - \omega}{\omega_i - \omega_f} \tag{3-13}$$

being: ω_i and ω_f the initial and final experimental mass, respectively.

As conversion is a function of the mass loss, it can be related to the temperature and time, and a kinetic model can be used to study the thermal degradation of the system. The basic kinetic equation separates the contribution of temperature and conversion degree as:

$$\frac{d\alpha}{dt} = k(T) \cdot f(\alpha) \tag{3-14}$$

where *k(T)* is the temperature-dependent rate constant, and *f(α)* depends on the particular decomposition mechanism.

Considering an Arrhenius model for the temperature activation of the reaction rate:

$$k(T) = A \cdot e^{\frac{-Ea}{R \cdot T}} \tag{3-15}$$

where A is the pre-exponential factor, Ea is the apparent decomposition activation energy and R is the constant of gases.

Combining equations (3-14) and (3-15), the reaction rate can be expressed as:

$$\frac{d\alpha}{dt} = A \cdot e^{\frac{-Ea}{R \cdot T}} \cdot f(\alpha) \tag{3-16}$$

In a dynamic regime experiment, temperature varies through a constant and controlled heating rate ($\beta = dT/dt$), and thus:

$$\frac{d\alpha}{dt} = \frac{d\alpha}{dT} \cdot \frac{dT}{dt} = \beta \cdot \frac{d\alpha}{dT} \tag{3-17}$$

Leading to:

$$\frac{d\alpha}{dT} = \frac{1}{\beta} \cdot A \cdot e^{\frac{-Ea}{R \cdot T}} \cdot f(\alpha) \tag{3-18}$$

Separating the terms and integrating the previous equation from the initial temperature T_0 (corresponding to the initial conversion α_0) to the peak temperature T_p (with a conversion degree α_p):

$$\int_{\alpha_0}^{\alpha_p} \frac{d\alpha}{f(\alpha)} = \frac{A}{\beta} \cdot \int_{T_0}^{T_p} e^{\frac{-Ea}{R \cdot T}} \, dT \tag{3-19}$$

The previous equation (3-16) describes the conversion function $f(\alpha)$ for a solid-state reaction, which depends on the reaction mechanism. A typical expression for $f(\alpha)$ is the so-called *Sesták-Berggren* equation:

$$f(\alpha) = \alpha^m \cdot (1 - \alpha)^n \cdot [-\ln (1 - \alpha)]^p \tag{3-20}$$

where m, n and p are empirically obtained exponent factors, one of them always being zero [10,11]. *Sesták* suggested the notation of the additional term $[-\ln (1 - \alpha)]^p$ as "accommodation coefficient", necessary to modify the reaction for heterogeneous systems. When $p = 0$, a simpler expression is obtained [11]:

$$\frac{d\alpha}{dt} = k(T) \cdot \alpha^m \cdot (1-\alpha)^n \quad (3\text{-}21)$$

The values of *m* and *n* determine the relative contributions from the acceleratory and decay regions. The sigmoid form of the $\boldsymbol{\alpha}$ -time curve expressed by Equation (3-21) is similar in shape to those derived from the *Avrami-Erofeev equation*, and is usually cataloged as one of them [12].

If T_0 is very small, it is possible to assume $\alpha_0 = 0$ and the integral function of the degree of conversion $g(\alpha)$ can be defined as follows [13]:

$$\boldsymbol{g(\alpha) = \int_0^{\alpha_p} \frac{d\alpha}{f(\alpha)} = \frac{A}{\beta} \cdot \int_0^T e^{\frac{-Ea}{R \cdot T}} \, dT} \quad (3\text{-}22)$$

The kinetic triplet *A*, *Ea* and $f(\alpha)$ can be experimentally determined, being $g(\alpha)$ the integral of $f(\alpha)$.

Different expressions of $f(\alpha)$ and $g(\alpha)$ are valuable to estimate the reaction mechanisms from the dynamic curves [14] and are grouped according of the α-time curves as acceleratory, sigmoid or decelerator. Among the different rate equations, the *Prout-Tompkins* equation produces sigmoid α-time dependences, upon the suggestion that $m=n=1$ and $p=0$:

$$\frac{d\alpha}{dt} = k(T) \cdot \alpha \cdot (1-\alpha) \quad (3\text{-}23)$$

This equation (3-23) clearly shows the dependence of the rate on both the amount of remaining reactant (α) and product formed $(1-\alpha)$, which is assigned to autocatalytic processes. In most polymers the thermal degradation follows a sigmoid function.

Table 3-1 lists different degradation mechanisms of bulk polymers [15,16,17]. The study of the macroscopic kinetics has controversy due to the complexity of the reactions involving simultaneous multiple steps [18]. Some abbreviated methods consider that the degradation of the samples can be described by a single mechanism that permits the calculation of *Ea* of the process. However it should be taken into account that the activation energy can vary with the conversion degree.

Recently many authors have established isoconversional methods to evaluate *Ea* by integration or differentiation of the general Equation (3-18) [18,19]. Isoconversional methods require measurements at different heating rates, and are based on the hypothesis that at a constant extent of conversion α, the decomposition rate $d\alpha/dt$ is a function only of temperature. Therefore it is not necessary to assume any conversion model at the initial stages of the analysis. The most powerful differential methods for the determination of kinetic parameters obtained from equation (3-16) are the *Kissinger* [20] and *Friedman* [21] methods, which are independent of the degradation mechanism. It is worth noting that in such methods the equations are obtained by considering $f(\alpha) = (1-\alpha)^n$.

Table 3-1 List of common kinetic functions to explain the thermal decomposition mechanisms in bulk polymers.

Symbol	*f(α)*	*g(α)*	Model	Rate-determining mechanism
Sigmoid rate equation or random nucleation and subsequent growths				
A_2	$2\,(1-\alpha)(-\ln(1-\alpha))^{\frac{1}{2}}$	$[-\ln(1-\alpha)]^{\frac{1}{2}}$	Avrami-Erofeyev	Assumed random nucleation and its subsequent growth n=2
A_3	$3\,(1-\alpha)(-\ln(1-\alpha))^{\frac{2}{3}}$	$[-\ln(1-\alpha)]^{\frac{1}{3}}$	Avrami-Erofeyev	Assumed random nucleation and its subsequent growth n=3
A_4	$4\,(1-\alpha)(-\ln(1-\alpha))^{\frac{3}{4}}$	$[-\ln(1-\alpha)]^{\frac{1}{4}}$	Avrami-Erofeyev	Assumed random nucleation and its subsequent growth n=4
An	$\propto(1-\alpha)$	$\ln(\propto/(1-\alpha))$	Prout-Tompkins	Branching nuclei (Autocatalysis)
Deceleratory rate equations. Phase boundary reaction				
R_1, F_0	1	α	Power law ($F_0/R_1/n = 0$)	Contracting disk
R_2	$2\,(1-\alpha)^{\frac{1}{2}}$	$\left[1-(1-\alpha)^{\frac{1}{2}}\right]$	Power law (R_2, $F_{1/2}$)	Contracting cylinder (cylindrical symmetry
R_3	$3\,(1-\alpha)^{\frac{2}{3}}$	$\left[1-(1-\alpha)^{\frac{1}{3}}\right]$	Power law (R_3, $F_{2/3}$)	Contracting sphere (spherical symmetry
Deceleratory rate equations. Diffusion models				
D_1	$\frac{1}{2\,\alpha}$	α^2	Parabola low	Unidimensional Diffusion
D_2	$\frac{-1}{\ln(1-\alpha)}$	$(1-\alpha)\ln(1-\alpha) + \alpha$	Valensi equation	Bidimensional Diffusion
D_3	$\frac{3\,(1-\alpha)^{\frac{2}{3}}}{2\left(1-(1-\alpha)^{\frac{1}{3}}\right)}$	$\left[1-(1-\alpha)^{\frac{1}{3}}\right]^2$	Jander Equation	Three-dimensional diffusion,spherical symmetry
D_4	$\frac{3}{2\left((1-\alpha)^{-\frac{1}{3}}-1\right)}$	$\left(1-\frac{2}{3}\alpha\right) - (1-\alpha)^{\frac{2}{3}}$	Ginstling-Brounshtein Equation	Three-dimensional diffusion,cylindrical symmetry
Chemical process or mechanism non-invoking equations				
F_1,A_1	$(1-\alpha)$	$-\ln(1-\alpha)$	First-order (n=1)	Chemical reaction
F_2	$(1-\alpha)^2$	$\frac{1}{1-\alpha}$	Second-order (n = 2)	Chemical reaction
F_3	$\frac{1}{2\,(1-\alpha)^3}$	$\frac{1}{(1-\alpha)^2}$	Third-order (n = 3)	Chemical reaction

- ***Kissinger method***

This method is based on the differentiation of the general reaction rate equation (3-16):

$$\frac{d^2\alpha}{dt^2} = \frac{Ea \cdot \beta}{R \cdot T^2} \cdot \frac{d\alpha}{dt} + A \cdot e^{-\frac{R}{R \cdot T}} \cdot f'(\alpha)\frac{d\alpha}{dt} = \left[\frac{Ea \cdot \beta}{R \cdot T^2} + A \cdot e^{-\frac{Ea}{R \cdot T}} \cdot f'(\alpha)\right]\frac{d\alpha}{dt} \qquad (3\text{-}24)$$

If this equation is particularized to the inflection point temperature or peak temperature, T_p, at which the degradation rate is maximum, $\frac{d^2\alpha}{dt^2} = 0$:

$$0 = \frac{Ea \cdot \beta}{R \cdot T_m^2} + \ln\left[f'(\alpha_m) \cdot \frac{A \cdot R}{Ea}\right] \qquad (3\text{-}25)$$

by rearranging and taking logarithms, the equation takes the following form:

$$\ln\left(\frac{\beta}{T_m^2}\right) = -\frac{Ea}{R \cdot T_m} + \ln[f'(\alpha_m) \cdot \frac{A \cdot R}{Ea}] \qquad (3\text{-}26)$$

The Kissinger method provides global activation energy and does not require previous determination of the reaction order (n).

By considering a function, $f(\alpha) = (1 - \alpha)^n$, typical of polymers, and repeating the above mathematical process:

$$\frac{d\alpha}{dT} = \frac{A}{\beta} \cdot e^{\frac{-Ea}{R \cdot T}} \cdot f(\alpha) = \frac{A}{\beta} \cdot e^{\frac{-Ea}{R \cdot T}} \cdot (1 - \alpha)^n \qquad (3\text{-}27)$$

Deriving the previous equation:

$$\begin{aligned}\frac{d^2\alpha}{dT^2} &= \frac{A}{\beta} \cdot e^{\frac{-Ea}{R \cdot T}} \cdot \frac{Ea}{R \cdot T^2} \cdot (1 - \alpha)^n - \frac{A}{\beta} \cdot e^{\frac{-Ea}{R \cdot T}} \cdot (1-\alpha)^{n-1}\, n \frac{d\alpha}{dT} \\ &= \frac{A}{\beta} \cdot e^{\frac{-Ea}{R \cdot T}} \frac{Ea}{R \cdot T^2} \cdot (1 - \alpha) - \frac{A}{\beta} \cdot e^{\frac{-Ea}{R \cdot T}} \cdot \frac{(1-\alpha)^n}{(1-\alpha)} \cdot n \cdot \frac{d\alpha}{dT} \\ &= \frac{A}{\beta} \cdot e^{\frac{-Ea}{R \cdot T}} \cdot (1-\alpha)^n \left[\frac{Ea}{R \cdot T^2} - \frac{n}{(1-\alpha)} \frac{d\alpha}{dT}\right]\end{aligned} \qquad (3\text{-}28)$$

Obtaining:

$$\frac{d\alpha^2}{dT^2} = \frac{d\alpha}{dT}\left[\frac{Ea}{R \cdot T^2} - \frac{n}{(1-\alpha)}\frac{d\alpha}{dT}\right] \quad (3\text{-}29)$$

which has the following expression at T_p

$$\frac{Ea}{R \cdot T_p^2} = \frac{n}{1-\alpha_p}\frac{d\alpha}{dT_p} \quad (3\text{-}30)$$

The terms $d\alpha/T_p$, $\alpha_p$and T_p are experimental data from the DTG curves. Combining equations (3-27) and (3-30):

$$\frac{Ea}{R \cdot T_p^2} = \frac{A}{\beta} \cdot e^{\frac{-Ea}{R \cdot T_p}} \cdot (1-\alpha_p)^n \cdot \frac{n}{1-\alpha_p} = \frac{A}{\beta} \cdot e^{\frac{-Ea}{R \cdot T_p}} \cdot n \cdot (1-\alpha_p)^{n-1} \quad (3\text{-}31)$$

Kissinger assumes that the product $n\cdot(1\text{-}\alpha_p)^{n\text{-}1}$ is independent of β and the previous expression can be derived :

$$\ln\left(\frac{\beta}{T_p^2}\right) = \ln\left[\frac{A \cdot R}{Ea}\, n \cdot (1-\alpha)^{n-1}\right] - \frac{Ea}{R \cdot T_p} \quad (3\text{-}32)$$

Thus, plots of $\ln(\beta/T^2_p)$ versus $1/T_p$ allows the determination of the *Ea* values from the slopes. The *Ea* obtained from the Kissinger method was referred as $\boldsymbol{Ea_K}$.

Although in this thesis the order of reaction *n* and the particular kinetic function was calculated following other consideration it should be remarked that Kissinger [20] developed a procedure to calculate the reaction order, based on the measurement of peak asymmetry (from the 1st derivative curve). It was proposed that the increase in the asymmetry was correlated to a reaction order decrease. According to this fact, the dominant factor controlling the shape and position of the 1st derivative peak is the nature of the reaction itself. To quantitatively describe the peak shape, a shape factor (S) was defined as the absolute value of the ratio of the slopes of the tangents to the DTG curve at the inflexion points. This supposition is inconsistent when the height of the first peak is very small. Some other authors proposed an alternative novel procedure calculating the peak area instead of the peak height, method is very useful because it takes into consideration both peak shape and width and it does not need corrector coefficient for calculating the reaction order [22].

- ***Friedman method***

This method is directly based on the natural logarithm of equation (3-16):

$$\ln\left(\frac{d\alpha}{dt}\right) = \ln\left(\beta \cdot \frac{d\alpha}{dT}\right) = \ln A + n \cdot \ln(1-\alpha) - \frac{Ea}{R \cdot T} \tag{3-33}$$

From this equation, one individual Ea value is obtained for each conversion, α, from the representations of $\ln[\beta \cdot d\alpha/dT]$ versus $1/T$. The global activation energy, called $\boldsymbol{Ea_F}$ for the Friedman method, is obtained after averaging Ea at the different α values.

Alternatively, integral methods involve an approximate integration of equation (3-21). The Flynn–*Wall–Ozawa* method [23,24] (also independent from the degradation mechanism) and the *Coats–Redfern* method are used in this thesis [25,26].

- ***Flynn–Wall–Ozawa method***

Considering the previous expression (3-22) and integrating with initial conditions α=0 in T=T_0:

$$g(\alpha) = \int_0^{\alpha} \frac{d\alpha}{(1-\alpha)^n} = \frac{A}{\beta}\int_{T_0}^{T} e^{\frac{Ea}{R \cdot T}}\, dT \tag{3-34}$$

This method introduces a new variable $x = \frac{Ea}{R \cdot T}$, therefore $T = \frac{Ea}{R \cdot x}$ and $dT = -\frac{Ea}{R\,x^2}\, dx$. In this case the integration limits are:

$$\begin{cases} T \to 0 & \Longrightarrow \quad x \to \infty \\ T \to T & \Longrightarrow \quad x \to \frac{Ea}{R \cdot T} \end{cases}$$

After substituting the previous variables in equation (3-34), the resulting integral is:

$$g(\alpha) = \int_{\infty}^{x} \frac{A}{\beta} \cdot \left(-\frac{Ea}{R}\right) \cdot \frac{e^{-x}}{x^2}\, dx = \frac{A \cdot Ea}{\beta \cdot R} \cdot p\,(x) \tag{3-35}$$

where $p(x) = \int_{\infty}^{0} \frac{e^{-x}}{x^2}$

In the literature there are several approaches to solve this integral [27,28]. One of the most common series used to estimate the polynomial is the *Schlömilch* approximation,

$$p(x) = \frac{e^{-x}}{(1+x)\cdot x}\cdot\left(1 - \frac{1}{x+2} + \frac{2}{(x+2)\cdot(x+3)} - \frac{3}{(x+2)\cdot(x+3)\cdot(x+4)} + \ldots\right)$$

Doyle approached the polynomial by only using the first term of each series, and the approximation was written as $p(x) = \frac{e^{-x}}{x\cdot(x+2)}$ [25]. The approximation also considers that for $x > 20$, taking logarithms, $\log p(x) \approx -2.315 - 0.457 \cdot x$.

Flynn –Wall and *Ozawa* used the previous considerations to determine *Ea*, being *n* unknown:

$$g(\alpha) = \frac{A \cdot Ea}{\beta \cdot R}\frac{e^{-x}}{x\cdot(x+2)} \tag{3-36}$$

Taking logarithms and rearranging:

$$\log g(\alpha) = \log\left(\frac{A\cdot Ea}{R}\right) - \log\beta + \log p\left(\frac{Ea}{R\cdot T}\right) \tag{3-37}$$

Using the Doyle approximation, the previous equation can be simplified as:

$$\log g(\alpha) = \log\left(\frac{A\cdot Ea}{R}\right) - \log\beta + 2.315\left(\frac{0.457\cdot Ea}{R\cdot T}\right) \tag{3-38}$$

Ea can be calculated from the plot of $\log(\beta)$ versus $(1/T)$ for each conversion. The global $\boldsymbol{Ea_{FWO}}$ is obtained after doing the average of *Ea* at the different *α*.

- ***Coats–Redfern method***

This method utilizes the asymptotic series expansion for approximating the exponential integral in Equation (3-35), giving:

$$\ln\left(\frac{\beta}{T_p^2}\right) = \ln\left[\frac{A\cdot R}{Ea}\cdot n\cdot(1-\alpha)^{n-1}\right] - \frac{Ea}{R\cdot T_p} \tag{3-39}$$

This expression can be transformed into:

$$\ln g(\alpha) = \frac{A \cdot R \cdot T^2}{\beta \cdot Ea}\left(1 - \frac{2 \cdot R \cdot T}{Ea}\right) e^{\frac{-Ea}{R \cdot T}} \quad (3\text{-}40)$$

Taking natural logarithms:

$$\ln g(\alpha) = \ln\frac{A \cdot R}{\beta \cdot Ea} + 2 \cdot \ln T + \ln\left(1 - \frac{2 \cdot R \cdot T}{Ea}\right) - \frac{Ea}{R \cdot T} \quad (3\text{-}41)$$

When $x = \frac{Ea}{R\,T} > 20$, $\ln\left(1 - \frac{2\,R\,T}{E}\right)$ can be approximated to zero, resulting in:

$$\ln \frac{g(\alpha)}{T^2} = \ln\frac{A \cdot R}{\beta \cdot Ea} - \frac{Ea}{R \cdot T} \quad (3\text{-}42)$$

The *g(α)* function can be calculated for the different conversion, α, degrees at a constant heating rate (β), considering the models in Table 3-1. The activation energy for each heating rate can be calculated from the linear fit of $\ln\frac{g(\alpha)}{T^2}$ versus ($1/T$) as is named $\boldsymbol{Ea_C}$.

In the *Friedman* and *Flynn-Wall-Ozawa* methods, the *Ea* at constant *α* can be obtained from the slopes of the linear regions. Likewise, the "model free kinetic" method established by *Kissinger* is widely employed by many authors in order to assess their results. Instead, the *Coats-Redfern* method offers a more complete calculation of the apparent activation energy *Ea*, in which *f(α)* should be known in advance.

With that aim, *Criado et al*. proposed a method to calculate *f(α)*, based on the comparison of experimental data and theoretical reduced master-curves [29,17].

A new function was proposed for to represent the conversion degree, *z(α)*.

$$z(\alpha) = \frac{d\alpha/dt}{\beta}\, p(x)\, T \quad (3\text{-}43)$$

where $x = Ea/R \cdot T$ and $p(x)$ is an approximation of the temperature integral which cannot be solved by analytical methods. In this case, using the fourth rational expression of *Senum and Yang* [30], with an η lower than 10^{-5} % for $x > 20$:

$$p(x) = \frac{x^3+18x^2+88x+96}{x^4+20x^3+120x^2+240x+120} \quad (3\text{-}44)$$

If the value of the apparent activation energy is known, the kinetic model of the process can be determined by this method.

Combining equations (3-14) and (3-22):

$$z(\alpha) = f(\alpha)\cdot g(\alpha) \quad (3\text{-}45)$$

The reduced curve at $\alpha = 0.5$ can be expressed as :

$$\frac{z(\alpha)}{z(0.5)} = \frac{f(\alpha)\cdot g(\alpha)}{f(0.5)\cdot g(0.5)} = \left(\frac{T_\alpha}{T_{0.5}}\right)^2 \cdot \frac{(\frac{d\alpha}{dt})_\alpha}{(\frac{d\alpha}{dt})_{0.5}} \quad (3\text{-}46)$$

The $(f(\alpha)g(\alpha))/(f(0.5)g(0.5))$ term in the previous expression is a reduced theoretical curve, which is characteristic of each reaction mechanism, while the right side term of the equation is related to the reduced rate from experimental data. A comparison of both sides of Equation (3-46) indicates which kinetic model describes one experimental reactive process. As an example, Figure 3-10 shows the plot of $\frac{z(\alpha)}{z(0.5)}$ versus α for some selected functions at 10ºC/min corresponding to a polylactide sample.

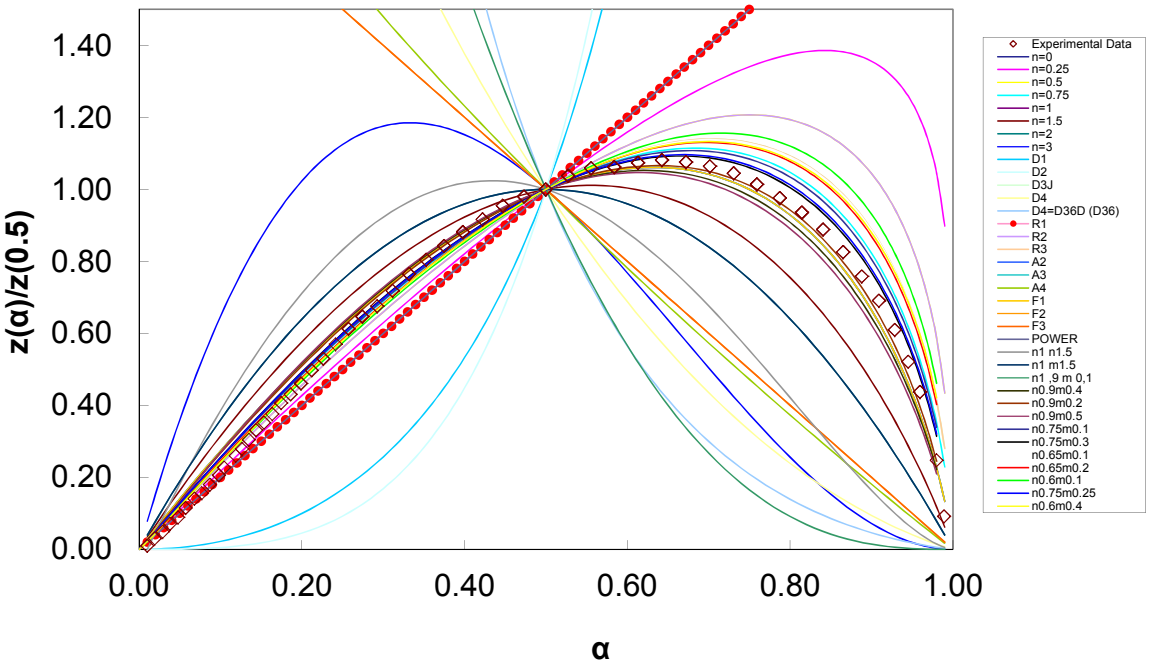

Figure 3-10 Plot of $\frac{z(\alpha)}{z(0.5)}$ versus α for some functions for a polylactide sample at 10ºC/min based in Criado model.

If the values of apparent activation energy *Ea* obtained by the *Friedman* (Ea_F), *Flynn-Wall-Ozawa* (Ea_{FWO}) and *Kissinger* (Ea_K) methods show similar results, then the average activation energy, Ea_{iso}, can be calculated. This value will be decisive in the selection of the *f(α)* function predicted by *Criado*, as Ea_{iso} must be in coherence with the corresponding *Ea* values calculated by *Coats-Redfern*. This methodology has been previously applied to other biodegradable materialsincluding PLA, offering consistency within different methods [31,32,33,34].

To summarize, Figure 3-11 schematically represents the theoretical description of these methods and the kinetic strategy followed.

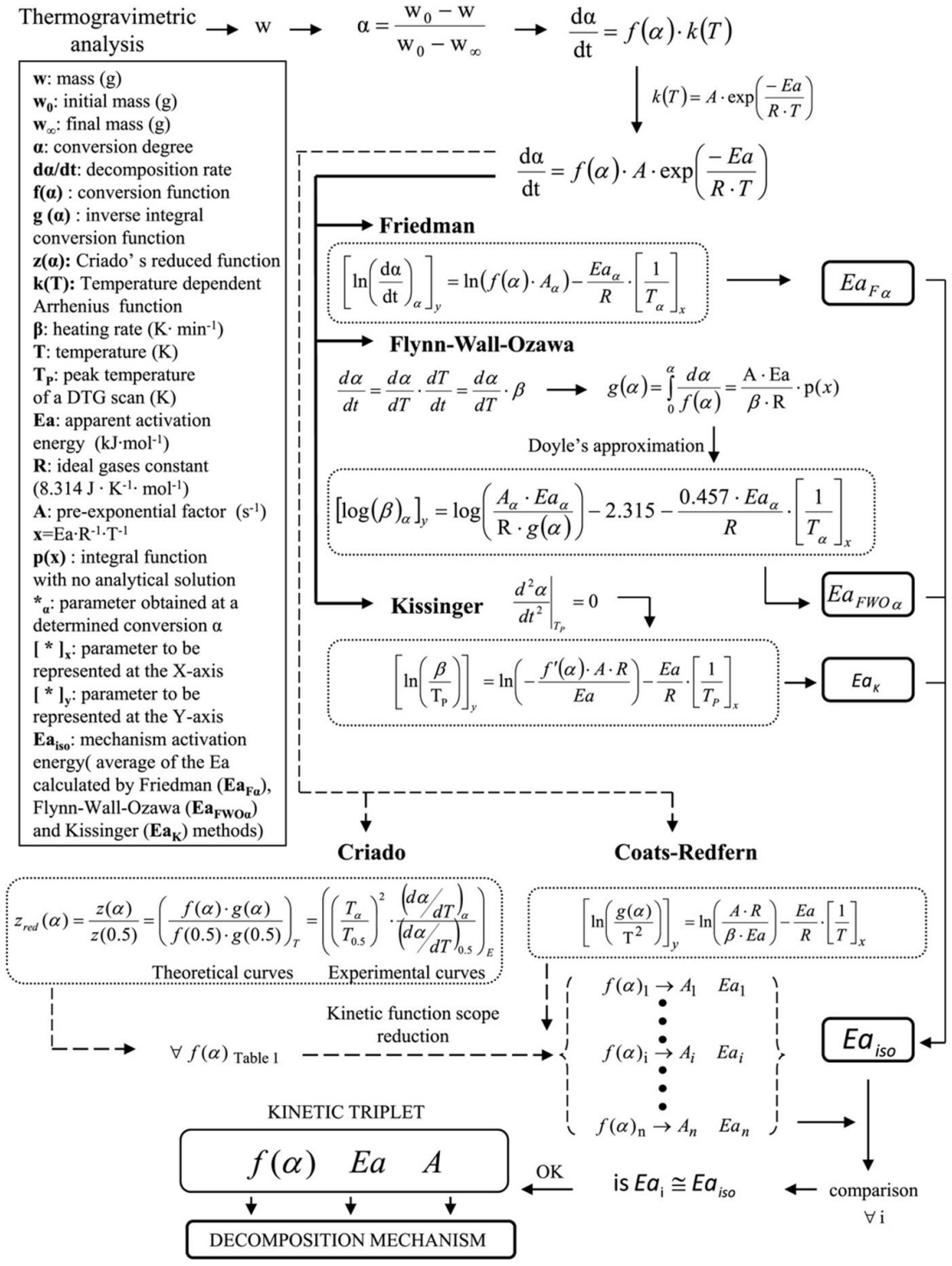

Figure 3-11 Methodology applied for the characterisation of the thermal decomposition kinetics of PLA reproduced from ref 33.

3.3.5 Scanning Electron Microscopy (SEM)

Morphological investigations of bio and photo degraded PLA samples were carried out on the surface of PLA specimens coated with aluminum by using a Philips XL 20 Scanning Electron Microscopy (SEM) (Eindhoven, The Netherlands) equipped by secondary electrons detector. Examination was carried out on the surfaces exposed directly to the contact with soil and to sunlight radiation. Small particles on the samples surfaces were removed by air-blowing. Operating conditions were set at 10 kV with a probe current of 9 ± 2 nA; and vacuum conditions (pressure below 10^{-4} Torr.).

SEM is a technique that displays the surface of a sample in three-dimensions by scanning a beam of electrons. Electrons are very small and easily deflected by gas molecules in the air. Therefore, it is necessary to work under vacuum conditions. When the electron beam hits the sample, the interaction of the beam electrons from the filament and the sample atoms generates a variety of signals. Depending on the sample the signal generated is transmitted to create a profile of the image.

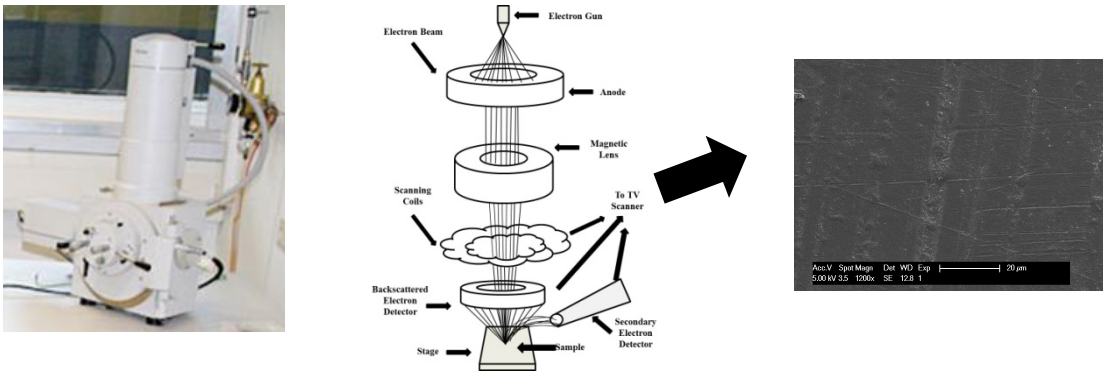

Figure 3-12 SEM equipment (left), SEM principles (central) and micrograph (right).

3.3.6 Dynamic Mechanical Thermal Analysis (DMTA)

The viscoelastic properties of the PLA materials under study were studied by Dynamic Mechanical Thermal Analysis (DMTA), using a Rheometric Scientifics Dynamic-Mechanical-Thermal Analyzer Mark IV (Piscataway, USA) (Figure 3-13). The deformation force was set at 0.01 N and the displacement was checked before each measurement. Experiments were performed by using dual cantilever clamping in bending mode. Specimens of 4 x 1 x 0.2 cm were heated from 35 to 150ºC in iso-step mode every 2ºC in the frequency (*f*) range from 0.1 to 39 Hz, measuring 5 points per decade. The storage modulus, *E'*, and delta tangent, *tan(δ)*, were measured.

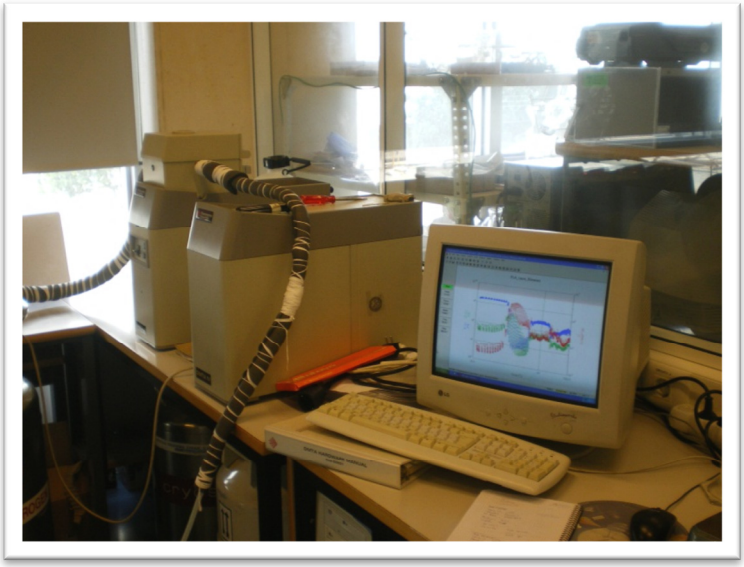

Figure 3-13 DMTA Mark IV.

This technique is based on the application of a precisely measured strain to deform a sample and subsequent evaluation of the stress developed. The stress can be then related to the material properties through the Hooke's and Newton's laws, in terms of elastic and viscous response, respectively.

The elastic component is referred to the capability of the material to store deformational energy and to recover its original shape after being deformed. Hooke's law describes the mechanical behavior of an ideal elastic solid: a proportional stress, σ, is obtained when a strain, ε, is applied to the material:

$$\sigma = E \cdot \varepsilon \tag{3-47}$$

E is the proportionality constant, known as stress or Young modulus, and is a measure of the rigidity or resistant to deformation of the materials.

On the other hand, the viscosity is a measure of the ability of the material to flow and deform. Newton's law describes the mechanical behavior of an ideal viscous fluid. The stress, σ, in this case, is proportional to the strain rate, $d\varepsilon/dt$, through the viscosity, η:

$$\sigma = \eta \cdot \frac{d\varepsilon}{dt} \tag{3-48}$$

For the polymers, the relation between stress and strain is intermediate between these two limiting cases, and the response to an applied force exhibits commonly a combination of both elastic and viscous mechanisms.This viscoelastic behavior of a material is characterized by the fact that adaptation to the stress-strain is not instantaneous and is time-dependent, and is characterized by the relaxation time parameter.

The long term performance of a polymeric material can be predicted by using the time-temperature superposition. Since materials are exposed to variable loading at different frequencies, it is appropriate to consider their behavior during this deformation process. This phenomenon is most easily analyzed when an oscillating sinusoidal load is applied to a sample at a selected frequency. The stress (σ) varies as a function of time according to the Newton's law:

$$\sigma = \sigma_0 \sin(\omega t) \tag{3-49}$$

where ω is the angular frequency (2π times the frequency in Hz, *f*). The corresponding strain for an elastic material obeying Hooke's law is:

$$\varepsilon = \varepsilon_0 \sin(\omega t) \tag{3-50}$$

Nevertheless, for viscoelastic materials like polymers, the strain lags slightly behind the stress (*e.g.* during creep). This can be considered as a damping process and the result is a

strain signal out of phase with the applied stress. This definition provides that the variation of stress and strain with time has the following expressions:

$$\varepsilon = \varepsilon_0 \sin \omega t\text{-} \tag{3-50}$$

$$\sigma = \sigma_0 \sin(\omega t + \delta) \tag{3-51}$$

where δ is the "phase angle" or "lag angle" *i.e.* the relative angular displacement of the stress and strain. The stress can be then expressed as a sum of two contributions or components:

$$\sigma = \sigma_0 \ \sin(\omega t) \cos\delta + \sigma_0 \ \cos(\omega t) \sin\delta \tag{3-52}$$

The first component, $\sigma_0 \cos(\delta)$, is in phase with the strain while the second one, $\sigma_0 \sin(\delta)$, is $^{\pi}/_{2}$ out of phase. It is then possible to define two dynamic moduli: E', in phase with the strain, and E'', $^{\pi}/_{2}$ out of phase. Since $E' = (\sigma_0 / \varepsilon_0 \cos(\delta)$ and $E'' = (\sigma_0 / \varepsilon_0 \sin(\delta)$ the previous equation becomes:

$$\sigma = \varepsilon_0 \, E' \sin(\omega t) + \varepsilon_0 \, E'' \cos(\omega t) \tag{3-53}$$

The phase angle is then given by:

$$\tan\delta = {}^{E''}/_{E'} \tag{3-54}$$

Since these are orthogonal contributions, in most of the cases the complex notation is used for the representation of the dynamic mechanical properties of viscoelastic materials. The stress and strain are then given by:

$$\varepsilon = \varepsilon_0 \exp(i \, \omega t) \tag{3-55}$$

$$\sigma = \sigma_0 \ \exp(\ i \, (\omega t + \delta)) \tag{3-56}$$

where $i = (-1)^{1/2}$. The overall complex modulus $E^* = {}^{\sigma}/_{e}$ is given by:

$$E^* = \frac{\sigma_0}{\varepsilon_0} \exp \ i\delta = \frac{\sigma_0}{\varepsilon_0} (\cos\delta \ + i \sin\delta) = E' + iE'' \tag{3-57}$$

The real part of the complex modulus is known as the storage modulus, E', can be identified with the in-phase elastic component of deformation. Elastic materials can "store" energy during deformation and release it on unloading, it represents the elastic portion. The imaginary part E'' is then called "loss modulus" since it gives a measure of the energy dissipated during each cycle, represents the viscous portion. Normally, isothermal experiments provide values of the two moduli as a function of the testing frequency

Time-temperature superposition

The principle of time-temperature superposition establishes equivalence between time and temperature in the viscoelastic properties of polymers. Representations of the modulus of a rubbery polymer as a function of the frequency evidence that the material behaves as a glass when the temperature is reduced or the frequency (ω) is increased. The opposite effect is observed when the material is glass-like, and the temperature is increased or the frequency decreased. It is found empirically that the frequency/temperature curves could be superposed by shifting them by different amount parallel to de logarithmic frequency axis.

Considering an arbitrary reference temperature T_s , ω_s is the frequency of a different curve with the same compliance, the shift required to superpose the two curves is a displacement of (log ω_s -log ω) along the frequency axis:

$$\log a_T = \log \omega_s - \log \omega = \log (\omega_s / \omega) \tag{3-58}$$

It is worth highlighting that, for viscoelastic relaxations occurring at temperatures below the glass transition, the dependence of a_T with the temperature follows typical Arrhenius behavior:

$$\log a_T = \frac{Ea_D}{2.303 \cdot R} \cdot \left(\frac{1}{T_1} - \frac{1}{T_2} \right) \tag{3-59}$$

being T_1 and T_2 the temperatures at which the relaxation occurs and Ea_D the activation energy for the motions of the molecules Taking into account that the definition of a_T is deduced from the dependence of the relaxation time with temperature:

$$\tau = \tau_0 \cdot \exp \frac{Ea_D}{R \cdot T} \tag{3-60}$$

Taking logarithms and considering $\tau = 1 / \omega$

$$\ln \omega = \ln \omega_0 - \frac{Ea_D}{R \cdot T} \tag{3-61}$$

At temperatures close to the glass transition, much of the work upon time-temperature superposition for the viscous flow [35], viscoelastic response [36], dielectric dispersion [37], nuclear magnetic response [38] and dynamic light scattering [39] was done by Williams, Lander and Ferry (WLF) and they proposed the following equation for a_T,

$$\log a_T = \frac{-C'_1 \cdot (T - Ts)}{-C'_2 + (T - Ts)} \tag{3-62}$$

C_1' and C_2' are constants and T is the temperature. Initially those values were thought to be universal constants, but they could not be applied to several distinct polymers. The previous equation is known as the WLF equation and was developed empirically. It holds well for a wide range of polymers in the vicinity of the glass transition and considering $Ts = T_g$:

$$\log a_T = \frac{-C_1 \cdot (T - T_g)}{-C_2 + (T - T_g)} \tag{3-63}$$

Resulting in new constants, C_1 and C_2, which are considered as "universal" with values of 17.4 and 51.6 K regardless of some changes depending of the polymer.

The WLF can be rationalized theoretically from considerations of free volume, V_f, which is the space in solid or liquid samples which is not occupied by molecules. Free volume is very sensitive to changes in temperature. Thus most of the thermal expansion of polymer rubbers or melts can be accounted by a change in V_f. As the temperature is lowered from the melt, free volume decreases until reaching a threshold at the glass transition temperature, when the values remains constant due to hindering of molecular motions (see Figure 3-14).

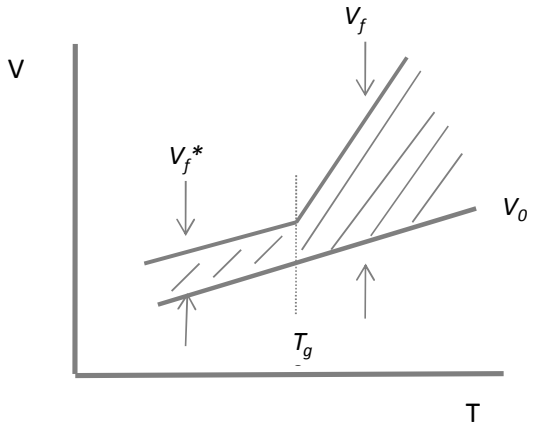

Figure 3-14 Specific volume variation with temperature of polymers. The free volume is represented by the hatched area.

Considering the total Volume, V, as the addition of the volume occupied by molecules V_0 and the free volume V_f, physical processes are expressed more conveniently in terms of fractional free volume, ϕ, which is defined as $\phi = V_f / V_0$ when temperature is below T_g, ϕ is given as $\phi_f = V_f^* / V_0$, and can be considered as being effectively constant. Above T_g there will be an important contribution to V_f due to the expansion of the melt:

$$V_f = V_f^* + (T - \mathrm{T_g}) \cdot \left(\frac{\partial V}{\partial T} \right) \tag{3-64}$$

Dividing by V:

$$\phi = \phi_g + (T - T_g) \cdot \alpha_f \tag{3-65}$$

where α_f is the thermal expansion coefficient given by the difference between the thermal expansion coefficients of the rubbery and glassy states in the vicinity of T_g. The equation for the fractional free volume will only be strictly valid over small increments of temperature above T_g.

There are several possible derivations of the WLF equation. The simplest is assuming that the polymer follows a viscoelastic behavior with a relaxation time τ_0 . From the Maxwell model $\tau_0 = \eta / E$ where η is the viscosity of the dashpot and E is modulus of the

spring. It can be assumed that only η varies with temperature, being E temperature independent. Considering the shift factor of the time-temperature superposition:

$$a_T = \frac{\tau_0(T)}{\tau_0(T_g)} = \frac{\eta(T)}{\eta(T_g)} \tag{3-66}$$

if T_g is used as the reference temperature. It is possible to relate the viscosity to the free volume through a semi-empirical equation developed by Doolittle from the study of the viscosities of liquids. Thus for a liquid, η is related to the free volume, V_f, through an equation with the form:

$$\ln\eta = \ln A + B\cdot(V - V_f)/V_f \tag{3-67}$$

where V is the total volume and A and B are constants. This equation (3-56) can be rearranged to give:

$$\ln\eta(T) = \ln A + B\cdot(1/\phi - 1) \tag{3-68}$$

and at T_g:

$$\ln\eta(T_g) = \ln A + B\cdot(1/\phi_g - 1) \tag{3-69}$$

Substituting ϕ in equation (3-68) and subtracting equation (3-69) from (3-68):

$$\log\frac{\eta(T)}{\eta(T_g)} = B\left(\frac{1}{\phi_g + \alpha_f\cdot(T - T_g)} - \frac{1}{\phi_g}\right) \tag{3-70}$$

which can be rearranged to give an identical form as the WLF equation:

$$\log\frac{\eta(T)}{\eta(T_g)} = \log a_T = \frac{-(B/2.303\cdot\phi_g)\cdot(T - T_g)}{\phi_g/\alpha_f + (T - T_g)} = -C_1\left(\frac{T - T_g}{C_2 + (T - T_g)}\right) \tag{3-71}$$

where $C_1 = B/2.303 f_g$ y $C_2 = \phi_g/\alpha_f$. This means that ϕ_g and α_f should be similar for different polymers. It has been found that ϕ_g is of the order of 0.025 and $\alpha_f \approx 4.8 \cdot 10^{-4}$ K^{-1} for most of the amorphous polymers, and this implies that $C_2 \approx 52$ K. This is only an approximate value in which molecular motions are supposed to be completely constricted; the most common values used for C_2 are 51.6 K and 30 K, obtained for poly(hexane-1) [40] and PP(atactic) [41], respectively. These values are taken as universal.

By adding and subtracting C_2 in equation (3-71):

$$\log a_T = -C_1 + \left(\frac{C_1 C_2}{C_2 + (T - T_g)} \right) \tag{3-72}$$

Changing to natural logarithm:

$$\ln a_T = A' + \frac{m_v}{T - T_\infty} \tag{3-73}$$

where $T_\infty = T_g - C_2$, $A' = -2.303 \quad C_1 = -B/\phi_g$ and $m_v = 2.303 C_1 C_2$.

This expression of the WLF equation is known as the empirical *Vogel-Fulcher-Tammann-Hesse* (*VFTH*) equation [42,43,44], where $\tau = 1/\omega$:

$$\ln \omega = A - \frac{m_v}{T - T_\infty} \tag{3-74}$$

and:

$$m_v = 2.3 \cdot C_1 \cdot C_2 = \frac{B}{\phi_g}(T_g - T_\infty) = \frac{B}{\alpha_f} \tag{3-75}$$

Since $A = -A'$, and making $\phi_\infty = 0 = \phi_g + (T_\infty - T_g) \cdot \alpha_f$, then:

$$\alpha_f = \frac{B}{m_v} \tag{3-76}$$

3.3.7 Differential Scanning Calorimetry (DSC)

The thermal transitions of polylactide were analyzed by Differential Scanning Calorimetry (DSC). The DSC experiments were performed using a Mettler Toledo DSC 822 Differential Scanning Calorimeter (Columbus, OH, USA). Samples of about 4 mg were placed in aluminum pans with pierced tops to facilitate evacuation of volatiles. The DSC thermograms were obtained from 3 temperature scans (preheating, cooling and subsequent reheating) at heating/cooling rates of ±10ºC/min, in the temperature range of 0 to 200ºC, and under N_2 atmosphere. Temperature and heat flow calibrations were carried out with indium and zinc as standards. Measurements were performed by triplicate for assessing reproducible results.

DSC is a thermo analytical technique based on the different amounts of heat required to equalize the temperature of a sample and a reference, within a temperature profile. This is usually conducted by placing the sample under study in one pan and leaving a second pan empty as the reference. A computer regulates heat flow of both pans and monitors temperature with high precision. DSC experiments are based on applying different temperature programs and calculating the heat necessary to maintain the temperatures of sample and reference equal (null balance).

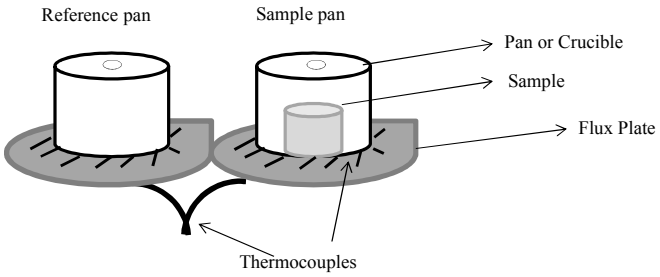

Figure 3-15 DSC scheme.

Typical results from DSC experiments display heat flow as a function of the temperature or time, which are denoting different thermal transitions of the sample under study. More particularly, the use of this technique allows for the observation of the melting, crystallization and glass transition transitions and the corresponding temperatures. Figure 3-16 shows a DSC trace extracted from PLA.

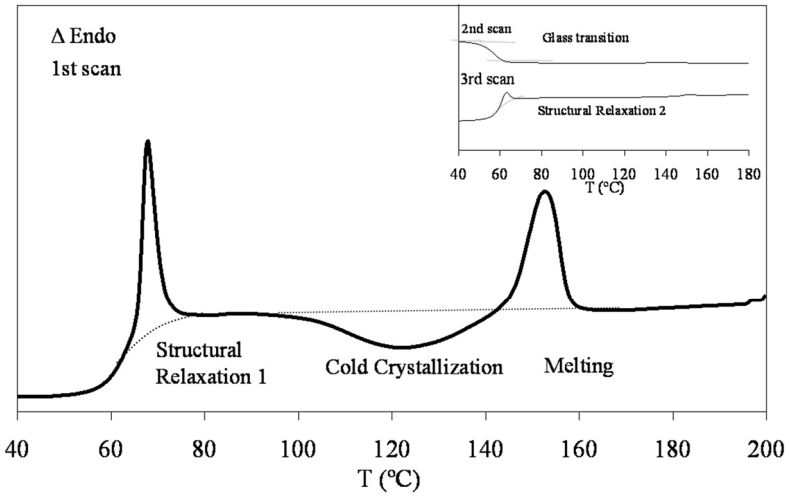

Figure 3-16 DSC trace for PLA.

When the polymers crystallize when heating from the glass, the phenomenon is known as cold crystallization. This phenomenon can be distinguished for the polylactide. There are many factors that affect the rate and extent of crystallization, the rate of cooling(heating), the presence of orientation in the melt, the melting temperatures, the tacticity, the molar mass, the amount of chain branching and the presence of additives[45,46].

3.3.8 Optical Microscopy (OM)

The spherulite radius of the PLA samples versus time was measured by Optical Microscopy, OM, in isothermal crystallization conditions, and the linear growth rates (G) were obtained from the corresponding slopes. Radius were measured in 50 μm thick films (melt-pressed from each specimen using a Carver Press at 180 ºC, 2 min) using an Olympus BH-2 microscope fitted with an Olympus DP/2 digital camera and a Linkam hot stage TP-93 with cryogenic cooling. The temperature was controlled with a precision of ±0.1ºC. The films were prepared using three aluminum foils of controlled thickness; a circle was cut in the central foil to serve as thickness control after melt pressing. A piece of film was placed between two microscope cover slips and heated from room temperature to 180 ºC (β = 40ºC/min) for 2 min to eliminate any crystalline history

The temperature was then lowered at a rate of 40 ºC/min to the different isothermal crystallization temperatures, which were in a range from 100ºC to 140 ºC. Figure 3-17 shows the diameter of the spherulites measured as a function of crystallization time, after consecutive measurements in the same specimen. Some thermal degradation was observed in subsequent measurements, which can be associated with the occurrence of chain excision of PLA. Therefore, to ensure reproducibility, measurements were carried out in a fresh piece of film at each temperature.

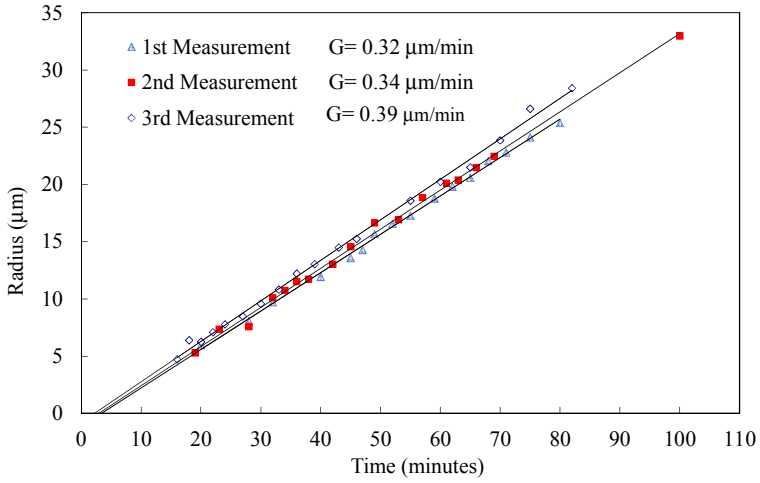

Figure 3-17 Measurement reproducibility of the same sample piece for pellets evaluated at 113.5ºC.

The principle of polarized Optical Microscopy (OM) is based on the isotropic character of light and the changes alignment occurring when passing through an anisotropic crystalline material. A polarized light microscope has two disc accessories made up of polarizing plastic that permits light vibrating in one plane to pass (Figure 3-18).

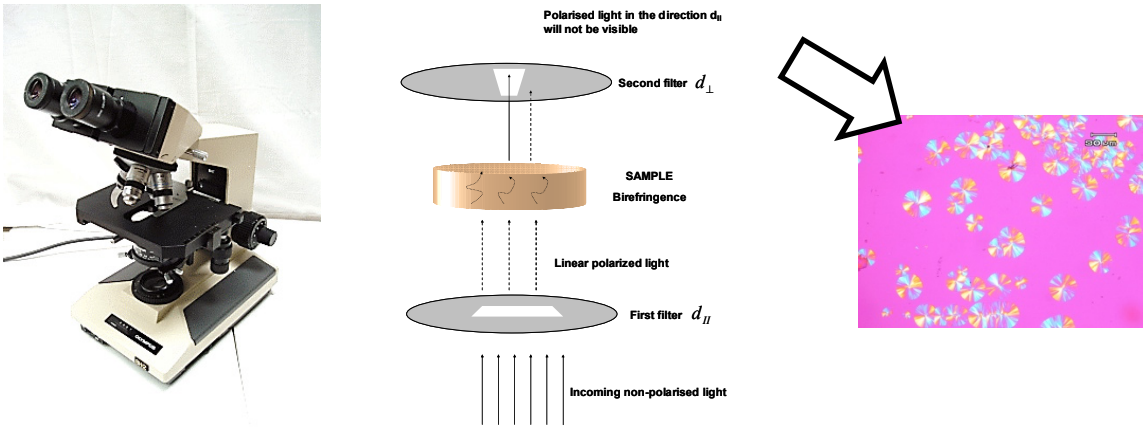

Figure 3-18 Optical microscope equipment (left), basis (central) and micrograph (right).

The first disc polarizes the light in one fixed direction (polarizer) before passing through the sample, and the second disc, placed in the top part of the microscope (analyzer), cuts off all the light vibrating in a perpendicular plane to the polarizer. Hence, when both discs are in place, no light can pass thought the eyepieces, giving a dark background. If an isotropic material is placed between the two discs, the polarization of the light according to the polarizer will not be changed (preferential contributions will be cancelled) and then no light will pass through the analyzer. If an anisotropic material is under study, then the polarized light will be re-polarized according to the material birefringence, and some light may pass through the analyzer, providing optical signal. Such is the case of crystalline polymers or liquid crystals

3.4 Bibliographical references

[1] Pantani R, De Santis F, Sorrentino A, De Maio F, Titomanlio G. Crystallization kinetics of virgin and processed poly lactic acid. Polym Degrad Stab 2010;95:1148-59.

[2] Carrasco F; Pages P; Gámez-Pérez J; Santana O.O; Maspoch, M.L**.** Processing of poly(lactic acid): Characterization of chemical structure, thermal stability and mechanical properties Polym Degrad Stab 2010;95:116-25.

[3] ISO 846, 1997. Plastics–determination of behaviour under the action of microoganisms. Evaluation by visual examination or measurement of changes in mass or physical properties.

[4] Normativa Española Edificación: Documento básico HE de Ahorro de Energía del Código Técnico de la Edificación (CTE) 2006.

[5] Stevens, M. P. Polymer Chemistry: An Introduction, 3rd ed.; Oxford University Press: New York, 1999.

[6] Dorgan J, "Rheology of poly(lactic acid)," in poly(lactic acid): Synthesis, structures, properties, processing and applications, edited by Auras R, Lim LT, Selke SEM and Tsuji H. John Wiley & Sons, Inc, 2010 pp. 125-139.

[7] Álvarez VA, Vázquez A. Thermal degradation of cellulose derivatives/starch blends and sisal fibre biocomposites. Polym Degrad Stab 2004;84:13-21.

[8] Ramis X C, Salla J M, Morancho J M, Vallés A, Contat L, Ribes A. Thermal degradation of polypropylene/starch-based materials with enhanced biodegradability. Polym Degrad Stab 2004;86:483–491.

[9] Sánchez-Jimenez PE, Pérez-Maqueda LA, Perejon A, Criado JM. Constant rate analysis for thermal stability studies of polymer. Polym Degrad Stabil 2011;96:974–981.

[10] Vlaev L, Georgieva V, Genieva S. Products and kinetics of non-isothermal decomposition of vanadium (IV) oxide compounds. J Therm Anal Calorim, 2007;88: 805–812.

[11] Šestak J, Berggren G: Study of the kinetics of the mechanism of solid-state reactions at increasing temperatures. Thermochim Acta, 1971;3:1–12.

[12] Erofeev BV. Reactivity of Solids, Proc. 4th Int. Symp. Elsevier, Amsterdam, 1961 pp. 273–282.

[13] Núñez L, Fraga F, Fraga L, Rodríguez JA. Activation energies and rate constants for an epoxy/cure agent reaction. Variation in peak exotherm temperature. J Therm Anal 1996;47,3:743.

[14] Šestak J, Berggren G. Study of the kinetics of the mechanism of solid-state reactions at increasing temperatures. Thermochim Acta, 1971;3,1:1–12.

[15] Ma S, Hill JO, Heng S. A kinetic analysis of the pyrolysis of some Australian coals by non-isothermal thermogravimetry. J Therm Anal 1991;37:1161–1177.

[16] Brown ME. Introduction to thermal analysis. Technique and applications, 1st Ed., Ed Chapman and Hall, Great Britain 1998.

[17] Criado J, Maikel J, Ortega A. Applicability of the master plots in kinetic analysis of non-isothermal data. Thermochim Acta 1989;147:377–385.

[18] Techniques and Applications. In: Brown M, editor. Introduction to thermal analysis. 2nd ed. Secaucus, NJ, USA: Kluwer Academic Publishers 2001.

[19] Brown ME, Vyazovkin S, Nomen R, Sempere J, Burnham A, Opfermann J. Computational aspects of kinetic analysis. Part A: the ICTAC kinetics project data, methods and results. Thermochim Acta 2000;355:125–143.

[20] Kissinger HE. Reaction kinetics in differential thermal analysis. Anal Chem 1957;29(11):1702–1706.

[21] Friedman HL. Kinetics and gaseous products of thermal decomposition of polymers. J Macromol Sci (Chem) 1967;1(1):57–79.

[22] Carrasco F, Pagès P, Gámez-Pérez J, Santana OO, Maspoch ML. Kinetics of the thermal decomposition of processed poly(lactic acid). Polym Degrad Stabil 2010;10:2508-2514.

[23] Ozawa T. Kinetic analysis of derivative curves in thermal analysis. J Therm Anal 1970;2:301.

[24] Flynn JH, Wall LA. A quick, direct method for the determination of activation energy from thermogravimetric data. J Polym Sci. Part C 1966; 4:323–342.

[25] Doyle CD. Series approximations to the equation of thermogravimetric data. Nature 1965;207:290–291.

[26] Coats AW, Redfern JP. Kinetic parameters from thermogravimetric data. Nature 1964; 201, 4914:68–69.

[27] Brown ME, Dollimore D, Galwey AK. Reactions in the solid state comprehensive chemical kinetic, Elsevier, Amsterdam 1980, vol. 22.

[28] Kassman AJ. Evaluation and optimization of integral methods for the analysis of thermogravimetric data. Thermochim Acta 1985;84:89–99.

[29] Criado JM. Kinetic analysis of DTG data from master curves. Thermochim Acta 1978;24:186–189.

[30] Senum G.I**,** Yang**,** RT. Rational approximations of the integral of the Arrhenius function J**.** Therm**.** Anal**.** Calorim**.** 1977;11**:**445–447.

[31] Badia JD, Santonja-Blasco L, Martínez-Felipe A, Ribes-Greus A. A methodology to assess the energetic valorization of bio-based polymers from the packaging industry: Pyrolysis of reprocessed polylactide. Bioresource Technol 2012:111: 468–475.

[32] Badia JD, Vilaplana F, Karlsson S, Ribes-Greus A. Thermal analysis as a quality tool for assessing the influence of thermo-mechanical degradation on recycled poly(ethylene terephthalate). Polym Test 2009;28:169–175.

[33] Badia JD, Santonja-Blasco L, Moriana R. Ribes-Greus A. Thermal analysis applied to the characterization of degradation in soil of polylactide: II. On the thermal stability and thermal decomposition kinetics Polymer Degradation and Stability 2010; 95:2192–2199.

[34] Moriana R, Vilaplana F, Karlsson S, Ribes-Greus A. Improved thermo-mechanical properties by the addition of natural fibres in starch-based sustainable biocomposites. Composites: Part A 2011;42 :30–40.

[35] Berry GC, Fox TG. The viscosity of polymers and their concentrated solutions. Adv Polymer Sci 1968;5:261–357.

[36] Ferry DJ. Viscoelastic Properties of Polymers, 3rd ed. (John Wiley & Sons, New York). 1980, pp. 277–279.

[37] Hofmann A, Kremer K, Fischer EW, Schönhals, The scaling of the α- and β-relaxation in low molecular weight and polymeric glassforming systems. A disorder effects on relaxational processes, edited by Richert R and Blumen A. Springer-Verlag, Berlin and Heidelberg. 1994, pp. 309–331.

[38] Spiess HW. 2D NMR: elucidation of molecular dynamics in complex systems. J Non-Cryst Solids 1991;766:131–133.

[39] Fytas G and Meier G. in Dynamic Light Scattering, the Method and Some Applications, edited by W. Brown (Clarendon Press, Oxford). 1993, pp. 427.

[40] Kurath SF, Passaglia E, Pariser R. The Dynamic Mechanical Properties of Polyhexene-1. J Appl Phys 1957;28:499.

[41] Zemke K, Schmidt-Rohr K, Speiss HW. Polymer conformational structure and dynamics at the glass transition studied by multidimensional ^{13}C NMR. Acta Polymer 1994;45:148-159.

[42] Vogel H. The temperature dependence law of the viscosity of fluids, Phys Z 1921;22:645-646.

[43] Fulcher GS. Analysis of recent measuremnts of viscosity of glasses. J Am Ceram Soc. 1925:8;339-355.

[44] Tammann G and Hesse G. The dependence of viscosity upon temperature of supercooled liquids. Z Anorg Allg Chem 1926;156:245-257.

[45] Mandelkern L. Crystallization of Polymers, vol. 1, 2nd ed Cambridge University Press, Cambridge, 2002.

[46] Mandelkern L. Crystallization of Polymers, vol. 2, 2nd ed Cambridge University Press, Cambridge, UK, 2004.

Chapter 4 Results and discussion

4.1 Molar mass assessment

4.1.1 Molar mass results

Figure 4-1 shows the molar mass (M) distributions of the PLA pellets, plates, bio and photo degraded samples obtained by Gel Permeation Chromatography (GPC) where Wf is the cumulative weight fraction. From these distributions several parameters were calculated, such as the Full Width at Half Height ($FWHH$) of the curves, the values of weight-average molar mass (M_w), the number-average molar mass (M_n) and the polydispersity (M_w/M_n). The results are gathered in Table 4-1.

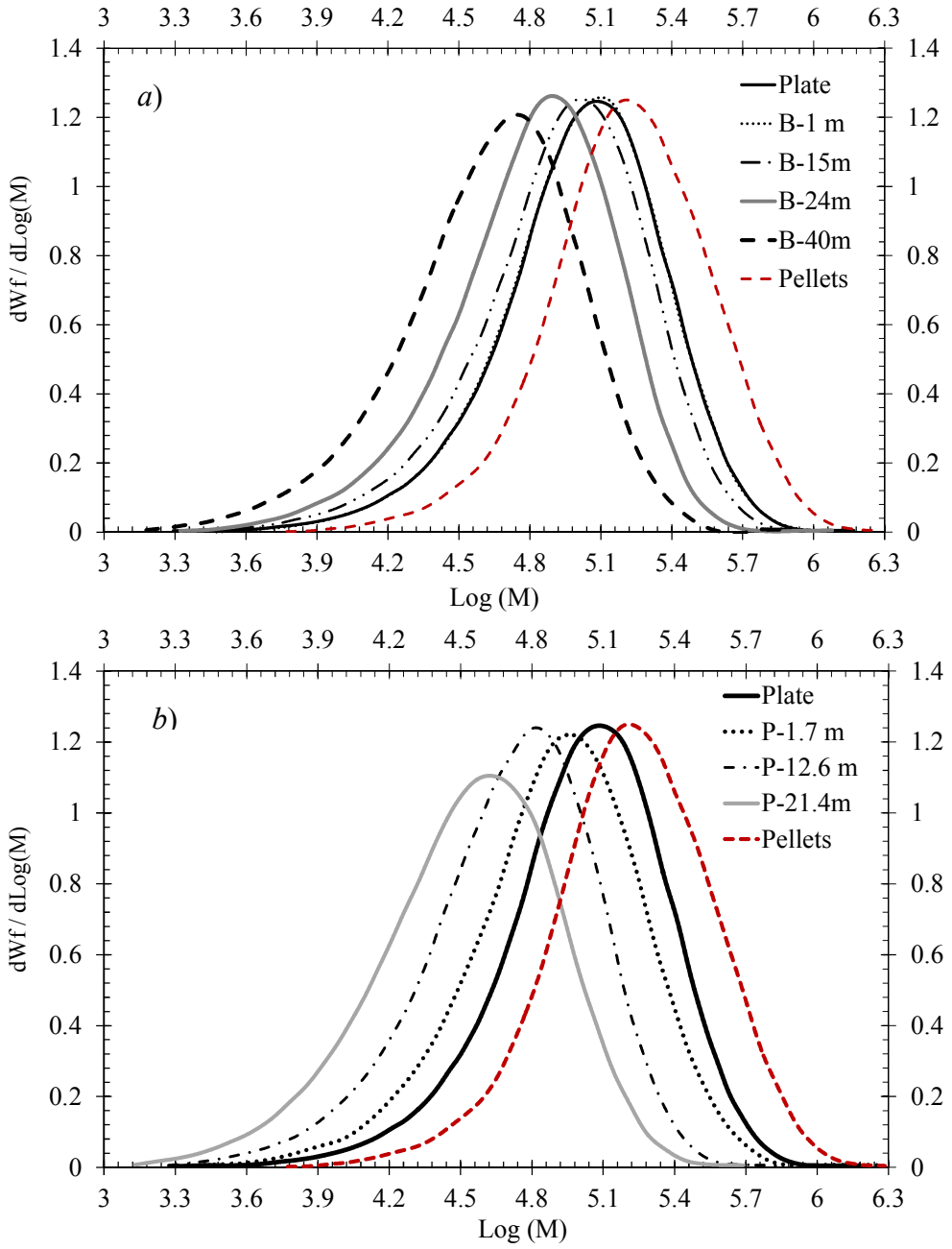

Figure 4-1 Molar mass distributions for *a*) biodegraded samples and *b*) photodegraded samples.

Table 4-1 Molar mass results obtained by GPC.

Sample Name	M_w (Da)	M_n (Da)	M_w/M_n
Pellets	221900	126800	1.75
Plates	134700	73200	1.84
Biodegraded-B (m-months)			
1 m	136300	74600	1.83
15 m	113600	60200	1.89
24 m	84100	45600	1.84
40 m	55600	29100	1.91
60 m	39700	20300	2.01
Photodegraded-P (h-hours- m-months)			
400h-1.7m	104100	56300	1.85
2250h-9.4m	80700	42600	1.89
3000h-12.6m	66200	35100	1.89
5100h-21.4m	45400	22200	2.05

Table 4-1 highlights the decrease in the M_w and M_n values after processing from pellets to plates; the initial melt compression reduced M_w from 221900 to 134700. It is also worth mentioning that a slight increment on the polydispersity was observed only for those samples highly degraded. The molar mass distributions of the plates and degraded samples were shifted to lower values, and also some changes were visible in the shapes of the curves, respect to the pellets. In Figure 4-2 the evolution of Full Width at Half Height (FWHH) of the distributions versus the degradation time for the bio and photo degraded samples was plotted. The FWHH values for photodegradation were higher than for biodegradation indicating more heterogeneous distributions at similar degradation times. Such differences can be attributed to a possible crosslinking process occurring by the radiation exposure, according to other authors who reported such effect when a photosensitizer was present [1,2]. As an attempt to check this phenomenon, the photodegraded samples were dissolved in chloroform (99.8% ACS reagent), at room temperature during two hours. Since these samples were completely dissolved, the evidence of crosslinking could not be confirmed.

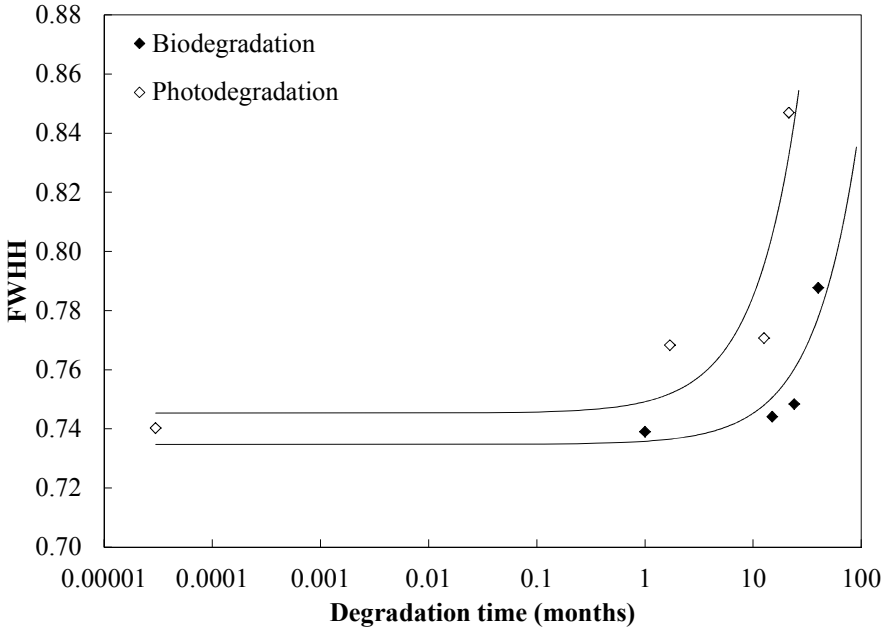

Figure 4-2 Full Width at Half Height for samples submitted to bio and photodegradation.

In Figure 4-3, M_w *was* plotted versus M_n for the plates, bio and photo degraded samples; providing a linear relation with a slope of 1.82, representing the average polydispersity of all the degraded samples.

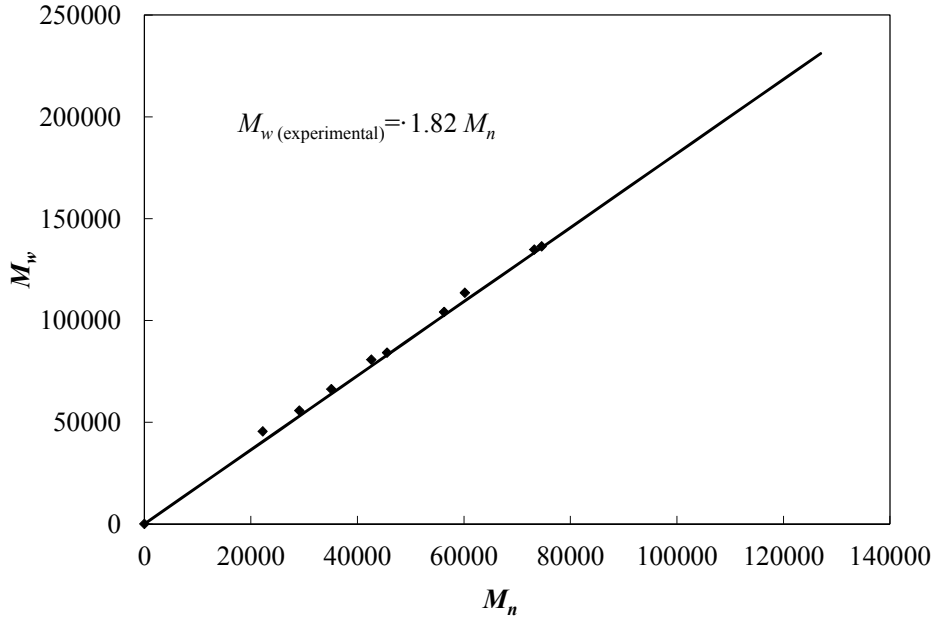

Figure 4-3 Plot of the M_w vs M_n obtained by GPC for the bio and photodegraded samples.

The molar mass changes in the thermally degraded samples could not be evaluated by means of GPC. Alternatively, M_v was calculated by measuring the intrinsic viscosity, η, and applying the Mark-Houwink-Sakurada equation $[\eta] = K \cdot M_v^{\alpha}$ [3]. Many values for the constants K and α are proposed in the literature, as reviewed by *Garlotta*, and are summarized for different temperatures and solvents [4,5]. However, these values were recently discussed and a new pair more consistent was proposed by *Dorgan* [6]:

$$[\eta] = 6.40 \text{ x } 10^{-4} \times M_v^{0.68} \text{ (}ref.\text{ 5)} \quad (4\text{-}1)$$

$$[\eta] = 1.74 \text{ x } 10^{-4} \times M_v^{0.736} \text{ (}ref.\text{ 6)} \quad (4\text{-}2)$$

Table 4-2 shows the experimental values of η and the values of M_v calculated using the specific parameter K (in *dl/g*) and α for amorphous Poly (L-Lactide) from both references, corresponding to the thermally degraded samples.

Table 4-2 Molar mass results obtained by viscometry for the thermally degraded samples.

Sample Name	***η (dl/g/)***	***M_v ref.* 5**	***M_v ref.* 6**
Pellets	1.347	77100	192190
Thermally degraded-T (time in min)			
3 min	1.260	69800	175500
30 min	0.740	31900	85170
62 min	0.560	21400	58400
120 min	0.360	11100	32000
330 min	0.230	5700	17400

The values of M_v (obtained by viscometry) and M_n (obtained by GPC) were correlated for those samples where the two molar masses were evaluated. The values of η and M_v and M_n obtained for the PLA pellets, plates and three photo degraded samples are shown in Table 4-3.

Table 4-3 Molar mass results obtained by viscometry.

Sample Name	η (dl/g)	M_v ref. 6	M_v ref. 5	M_n from GPC
Pellets	1.347	192190	77100	126800
Plates	1.148	154670	60880	73200
Photodegraded samples				
400h-1.7m	0.805	95490	36100	56300
2250h-9.4 m	0.800	94690	36500	42600
3000h-12.6 m	0.580	61170	22330	35100

Figure 4-4 shows a plot of M_v from ref 5 versus M_n for the samples from Table 4-3; the results were fitted to a linear trend, as the Flory's relation predicts. For a polydispersity (M_w/M_n) of 2, Flory envisaged a linear relation between M_v, M_n and M_w, according to the following Equation (4-3) [7]:

$$M_n/M_v/M_w = 1: [(1 + \alpha)\Gamma(1 + \alpha)]^{1/\alpha} :2 \quad (4\text{-}3)$$

Where $\Gamma(\alpha)$ is the gamma function [8] and α is the Mark Houwink parameter.

Table 4-4. Gamma function, $\Gamma(\alpha)$ corresponding to each α

α	$\Gamma(\alpha)$	α	$\Gamma(\alpha)$
1.00	1.00000000	1.52	0.88703878
1.04	0.97843820	1.56	0.88963920
1.08	0.95972531	1.60	0.89351535
1.12	0.94359019	1.64	0.89864203
1.16	0.92980307	1.68	0.90500103
1.20	0.91816874	1.72	0.91258058
1.24	0.90852106	1.76	0.92137488
1.28	0.90071848	1.80	0.93137488
1.32	0.89464046	1.84	0.94261236
1.36	0.89018453	1.88	0.95507085
1.40	0.88726382	1.92	0.96877431
1.44	0.88580506	1.96	0.98374254
1.48	0.88574696	2.00	1.00000000

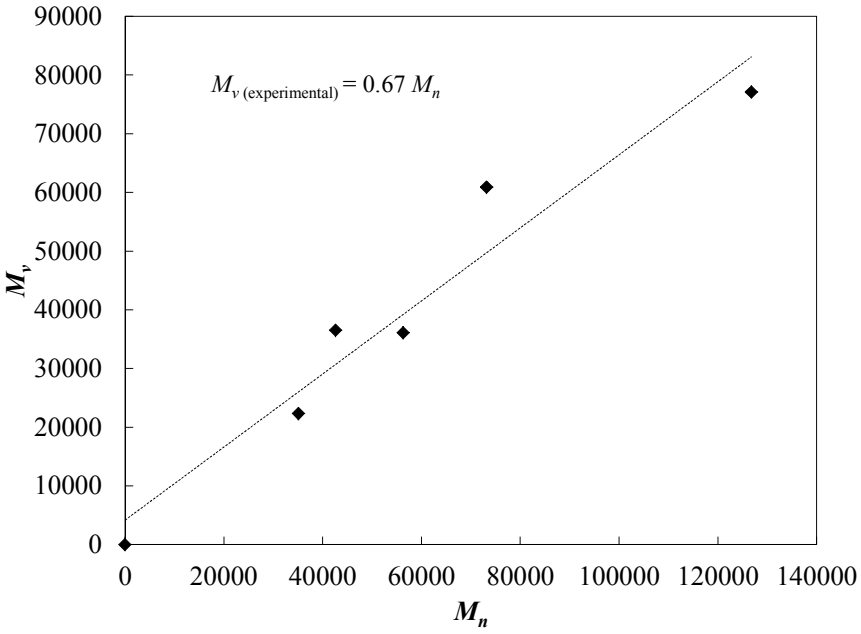

Figure 4-4 Plot of M_v versus M_n of the pellets, plates, photo 400 h, photo 2250 hours and photo 3000 hours using M_v from *ref.* 5.

The experimental value $\frac{Mv}{Mn} = 0.67$, obtained, did not accomplish the trend $M_w > M_v > M_n$. Figure 4-5 shows the same plot for data from *ref.* 6.

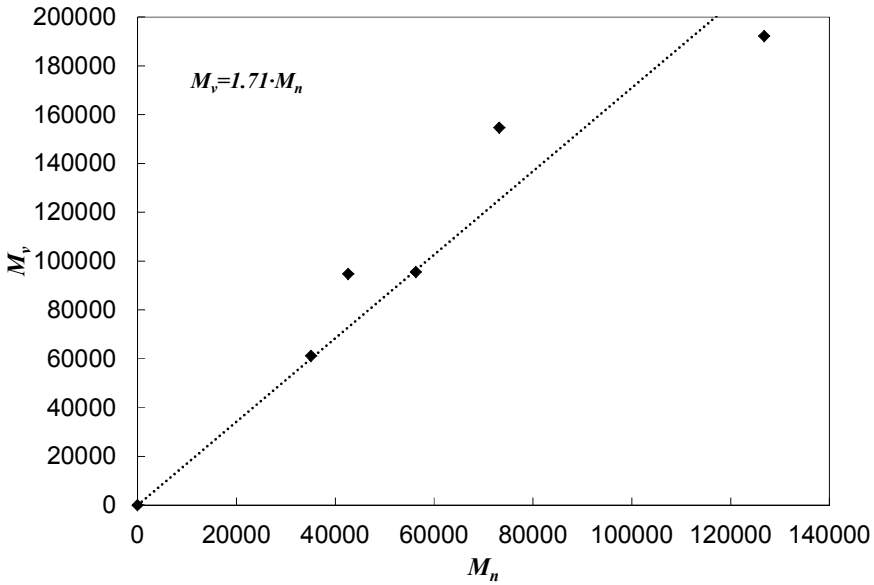

Figure 4-5 Plot of M_v versus M_n of the pellets, plates, photo 400 h, photo 2250 hours and photo 3000 hours using M_v from *ref.* 6.

The results of M_v/M_n=1.71 obtained by *ref.* 6 follows the trend $M_w > M_v > M_n$.. The slope 1.71, obtained from the data in Figure 4-5 is very close to the theoretical value M_v/M_n = 1: $[(1 + \alpha)\Gamma(1 + \alpha)]^{1/\alpha}$ =1.88 , obtained from the Flory's equation. The explanation of

such deviation may be due to the differences between the polydispersity calculated for the samples (M_w/M_n=1.82) and the Flory's conditions (M_w/M_n=2).

Equation (4-4) was chosen for the estimation of M_n from M_v in the thermally degraded samples, and the results are shown in Table 4-5.

$$M_v = 1.71 \cdot M_n \quad (4\text{-}4)$$

Table 4-5 M_n of the thermally degraded samples calculated (M_{n_calc}) from the experimental relation of M_v versus M_n

Sample Name	M_{n_calc}	M_n from GPC	$\lvert M_{n\_calc} - M_n$ GPC $\rvert$
Pellets	112590	126800	14210
Plates	90500	73200	17300
Thermally degraded			
3 min	102600		
30 min	49800		
62 min	34200		
120 min	18700		
330 min	10200		
Photo degraded			
400h-1.7m	55900	56300	400
2250h-9.4m	55400	42600	12800
3000h-12.6m	35800	35100	700

It is noticeable how processing from pellets to plates caused a decrease on molar mass and also how thermal and photodegradation could promote equivalent reductions on the molar mass of PLA, under different conditions.

4.1.2 Functionalizing the molar mass with time

The values of M_v (and consequently M_n) of the thermally degraded samples decrease with degradation time. Assuming that thermal degradation of polylactide follows a random chain scission mechanism of the ester group, *Liu et al.* [9] described the decrease of the molar mass as a 2nd order equation taking several considerations. If *s* are the bones broken in a single chain of *X* repeat units, then degree of splitting α can be defined by:

$$\alpha = \frac{s}{X_0 - 1} \tag{4-5}$$

where X_0 is the number-average degree of polymerization of polymer at the initial time.

Considering the degradation as a single molecular process the degradation rate ds/dt is proportional to the concentration of ester bonds, where the thermal degradation starts.

$$\frac{ds}{dt} = k_x \cdot (X_0 - 1 - s) \tag{4-6}$$

where *k* is the reaction rate constant. The integration of Equation (4-6) provides the following equation:

$$s = (X_0 - 1)(1 - \exp(-k_x \cdot t)) \tag{4-7}$$

Combining Equations (4-7) and (4-5):

$$\alpha = 1 - \exp(-k_x \cdot t) \tag{4-8}$$

According to the definition of the number-average degree of polymerization:

$$X_t = X_0/(s + 1) \tag{4-9}$$

where X_t is the number-average degree of polymerization at time *t*. Combining Equations (4-7) and (4-9), and eliminating *s*, one arrives to:

$$\frac{X_t - 1}{X_t} = \frac{X_0 - 1}{X_o} \exp(-k_x \cdot t) \tag{4-10}$$

The logarithmic form of Equation (4-10) is given by:

$$\ln\left[\frac{X_t - 1}{X_t}\right] = \ln\left[\frac{X_0 - 1}{X_o}\right] - k_x \cdot t \tag{4-11}$$

According to the property of logarithmic function

$$\ln\left[\frac{\mathrm{X}_t - 1}{\mathrm{X}_t}\right] = \frac{-1}{\mathrm{X}_t} - \frac{\left(\frac{1}{\mathrm{X}_t}\right)^{\frac{1}{2}}}{2} - \cdots - \frac{\left(\frac{1}{\mathrm{X}_t}\right)^{\frac{1}{n}}}{n} - \cdots \approx \frac{-1}{\mathrm{X}_t} \tag{4-12}$$

if $1/\mathrm{X}_t \ll 1$, the previous equation can be simplified and the expression has the form of Equation (4-13):

$$\frac{-1}{\mathrm{X}_t} + \frac{1}{\mathrm{X}_o} = -k_x \cdot t \tag{4-13}$$

This expression represents a linear relation between $1/X_t$ and t. If both sides of the Equation (4-13) are multiplied by 1/W, where W is the molar mass of the repeating unit:

$$-\frac{1}{\mathrm{W} \cdot \mathrm{X}_t} + \frac{1}{\mathrm{W} \cdot \mathrm{X}_o} = -(k_x \cdot \mathrm{W})t \tag{4-14}$$

$$\frac{1}{M_0} - \frac{1}{M_t} = -k \cdot \mathrm{t} \tag{4-15}$$

where M_0 and M_t are the molar mass of the polymer at time equal to 0 and at t, respectively, and k is the apparent rate constant.

The application of the previous equations to the viscous molar mass of the thermal degraded samples, $1/M_v$ versus time, is displayed in Figure 4-6 where M_{v0} is the initial molar mass of pellets.

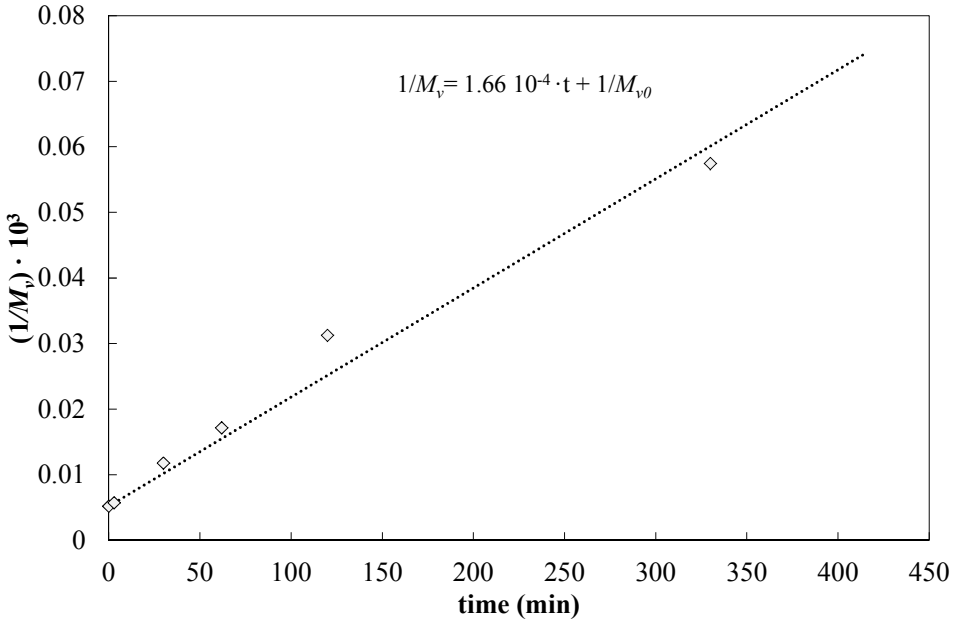

Figure 4-6 $1/M_v$ variation with degradation time (in minutes) for thermal degradation.

The data properly fit to the 2nd order equation and the values obtained are displayed in Equation (4-16), with $k_{Tv,}$ in mol/kg·min , ($k_{Tv,}$ is the apparent rate constant for the thermally degraded samples calculated from the M_v). This trend is in agreement with that proposed by other authors [10].

$$\frac{1}{M_v} = 1.66 \cdot 10^{-4} t + \frac{1}{192.2} \qquad (4\text{-}16)$$

The same experimental data can be fitted too using the M_n values (calculated from M_v =1.71M_n), were the units of k_{Tn}=2.82·10^{-4} are mol/kg·min ($k_{Tn,}$ is the apparent rate constant for the thermally degraded samples calculated from the M_n):

$$\frac{1}{M_n} = 2.82 \cdot 10^{-4} t + \frac{1}{112.6} \qquad (4\text{-}17)$$

The previous results indicate that thermal degradation can be described by a single molecular process based on the ester bond breakage.

In order to study the evolution of the molar mass for the bio and photodegradation, the values of M_n were plotted as a function of the degradation time in Figure 4-7**.**

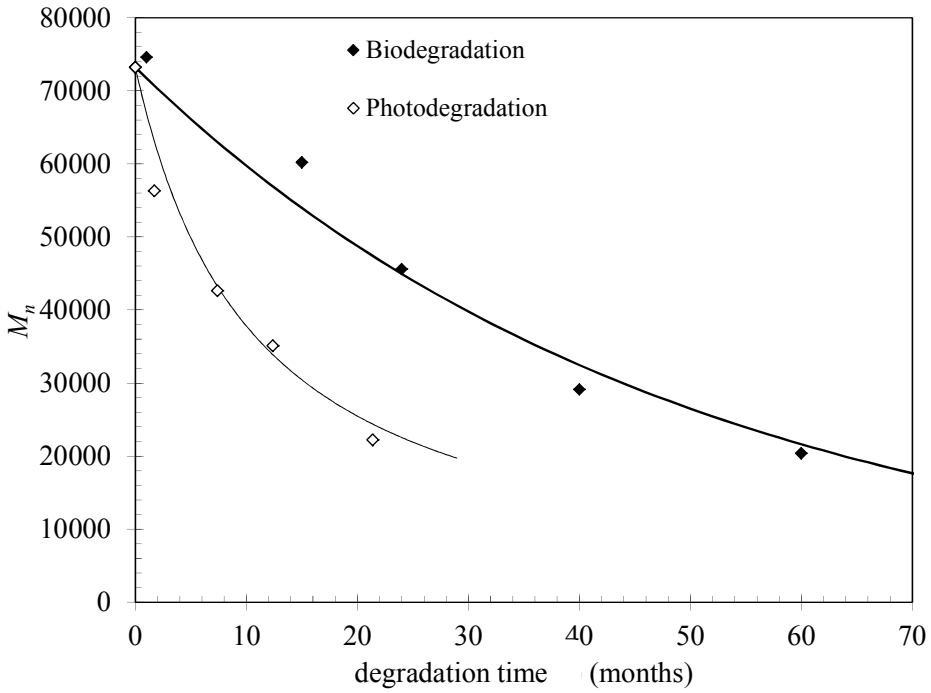

Figure 4-7 M_n variation with degradation time for bio and photo degradation.

The comparison between the curves indicates that photodegradation is faster than biodegradation, since provides lower values of M_n at a given time. Even though the non-linear molar mass decay was apparently similar in the three degradation processes, the profiles shown during biodegradation were rather different than those given by thermal and photo degradation.

The temporal variation of the molar mass of biodegraded specimens (up to 60 months) followed an exponential model ($\boldsymbol{M_n = M_{n0} \cdot e^{-k_B t}}$), typical of a 1st order degradation process, as can be seen in Figure 4-8, where $\boldsymbol{M_{n0}}$ is the initial molar mass of the plates, t the degradation time in months and k_B the biodegradation rate constant in months^{-1}. The same exponential temporal functionality was reported in hydrolysis and composting biodegradation studies, regardless of the different degradation conditions [11 ,12]. The calculated parameters, after fitting to the logarithm form, are shown in Equation (4-18):

$$\ln M_n = \ln(73.2) - 0.021 \cdot t \qquad (4\text{-}18)$$

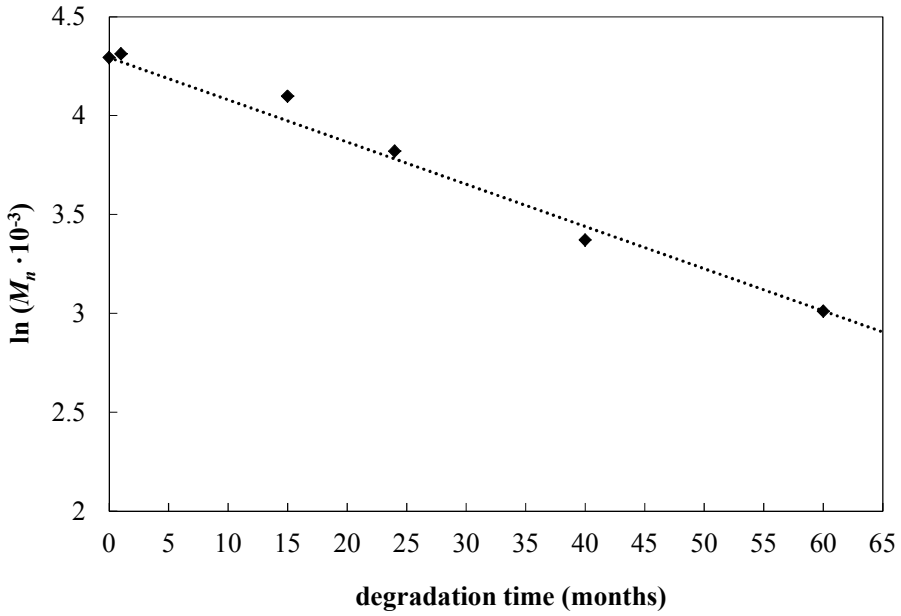

Figure 4-8 ln (M_n) variation with degradation time for biodegradation.

Like for the thermally degraded samples, the photodegradation of polylactide follows a 2nd order equation, $\frac{1}{M_{n0}} - \frac{1}{M_n} = -k_P \cdot t$, for the decrease of molar mass, as given in Figure 4-9, where M_{n0} is initial molar mass of plates, k_P is the rate constant for photodegradation in mol/kg·month and t is the time in months of outdoor sunlight exposure. The fitting parameters are displayed in Equation (4-19):

$$\frac{1}{M_n} = 1.37 \cdot 10^{-3} \cdot \mathrm{t} + \frac{1}{73.2} \tag{4-19}$$

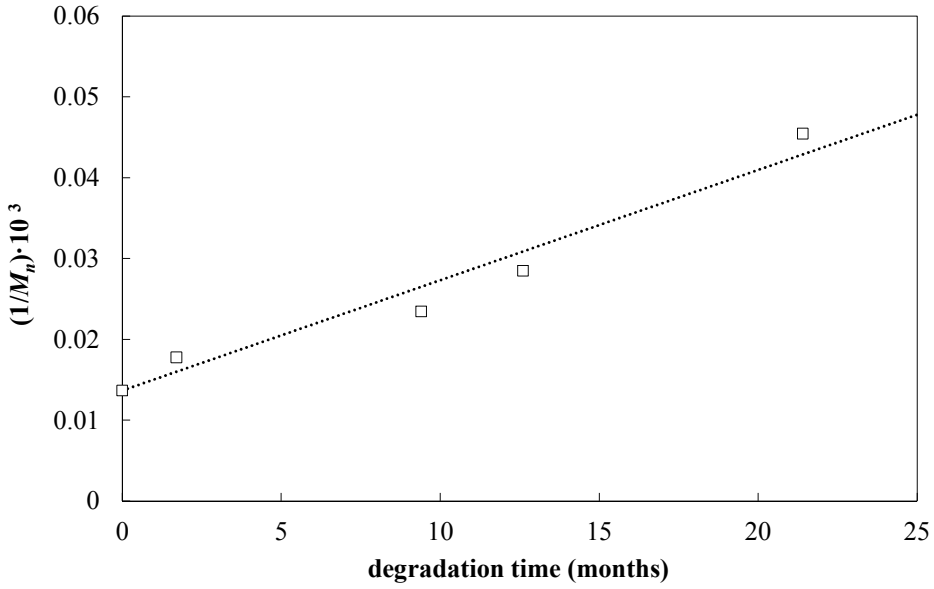

Figure 4-9 1/M_n variation with degradation time for photodegradation.

Equations (4-18) and (4-19) allow for the calculation of the molar masses of the rest of degraded samples at different times, which are shown in Table 4-5.

Table 4-6 M_n of the rest of bio and photo degraded samples calculated by Equation (4-18) and Equation (4-19) respectively.

Biodegraded samples	M_n
5 m	65900
10 m	59300
20 m	48100
30 m	39000
35 m	35100
Photodegraded samples	
800h -3.3m	55000
1850h-7.7m	41300
4100h-17.2m	26700

The differences between the degradation mechanisms could be indicative of a change on the kinetic reaction order:

- The mechanism of thermal degradation at 230 ° C is considered to occur mainly through a non-radical reaction mainly caused by intramolecular transesterification leading to cyclic oligomers, lactide, acetaldehyde and carbon monoxide [32,33] (see Figure 2-2 in Chapter 2)

- Two different mechanisms were proposed for PLA hydrolysis: random intra-chain and one chain end reaction (see Figure 2-7 of Chapter 2). Some authors reported the chain-end cleavage as the predominant in acid medium [13,14]. Considering that this is the predominant mechanism, the majority random (intra-chain) ester groups would not be susceptible to rupture.

- The photodegradation mechanism considers all the ester groups as labile to suffer cleavage, as shown in Figure 2-11 of Chapter 2.

In thermal and photo degradation, all the ester groups of the polymer chain are randomly labile to undergo degradation, which could explain why these processes follow 2nd order, in opposition to the 1st order observed for hydrolysis, which can involve selective breakage of ester groups, probably from the chain-ends as some authors reported as the predominant in the acidic media [13,14].

Figure 4-10 collects the temporal evolution of molar mass (M_n) of the PLA samples submitted to thermal, bio and photo degradation. The different time-scales permit comparing the degradation time required to achieve a certain molar mass, by the three different degradation types. According to this plot, the thermal degradation at 220ºC (slightly higher than the processing temperatures) took place much faster than bio and photodegradation. For instance, exposing the PLA pellets to thermal degradation during ~50 min would provide the same molar mass reduction as biodegradation after ~38 months or photodegradation after ~12 months of real exposure (3000 hours in sunlight radiation chamber).

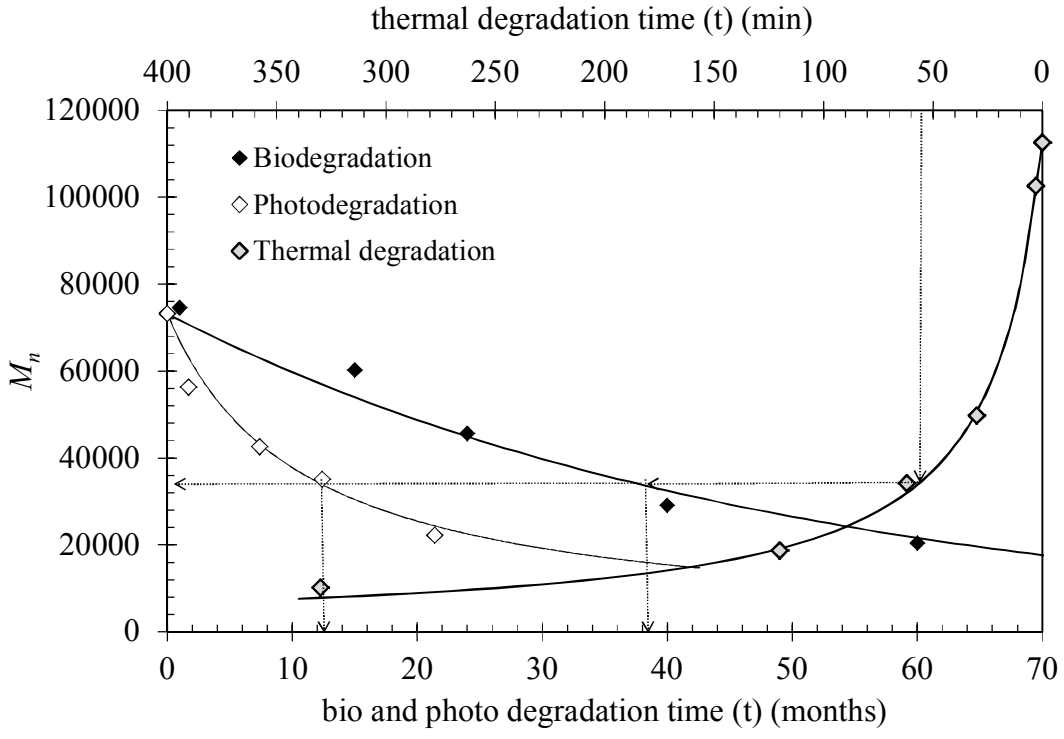

Figure 4-10 M_n versus time in the different scales studied, for thermal, bio and photo degradation.

As a summary, the equations with the evolution of the molar mass with time for all the degradation processes are now listed:

- Thermal degradation 2nd order
  - $\frac{1}{M_v} = 1.66 \cdot 10^{-4} \cdot \mathrm{t} + \frac{1}{192.2}$
  - $\frac{1}{M_n} = 2.82 \cdot 10^{-4} \cdot \mathrm{t} + \frac{1}{112.6}$
- Biodegradation 1st order: $\ln M_n = \ln(73.2) - 0.021 \cdot t$
- Photodegradation 2nd order $\frac{1}{M_n} = 1.37 \cdot 10^{-3} \cdot \mathrm{t} + \frac{1}{73.2}$

4.1.3 Literature data of molar mass decay due to degradation

It is of interest to test if the functionality of the decay of M_v and M_n, which was modeled by the previous equations, represents a universal behavior. In other words, does literature data agree this functionality for similar or longer times? In order to assess its validity, several published experimental data regarding different degradation of PLA were fitted to the previous functions.

a) Thermal degradation

Figure 4-11 shows the molar mass decay profiles obtained during the thermal degradation, in comparison with those of obtained by *Liu et al*. [10] at different temperatures. The temporal units were given in *hours* due to the longer extend of the experimental conditions used in that work The data was successfully fitted to the 2nd order equation as Figure 4-11 shows. The values of the parameter k_{Tv} (in different units) obtained from Liu's work are summarized in Table 4-7, together with those obtained from the experimental data of this current work.

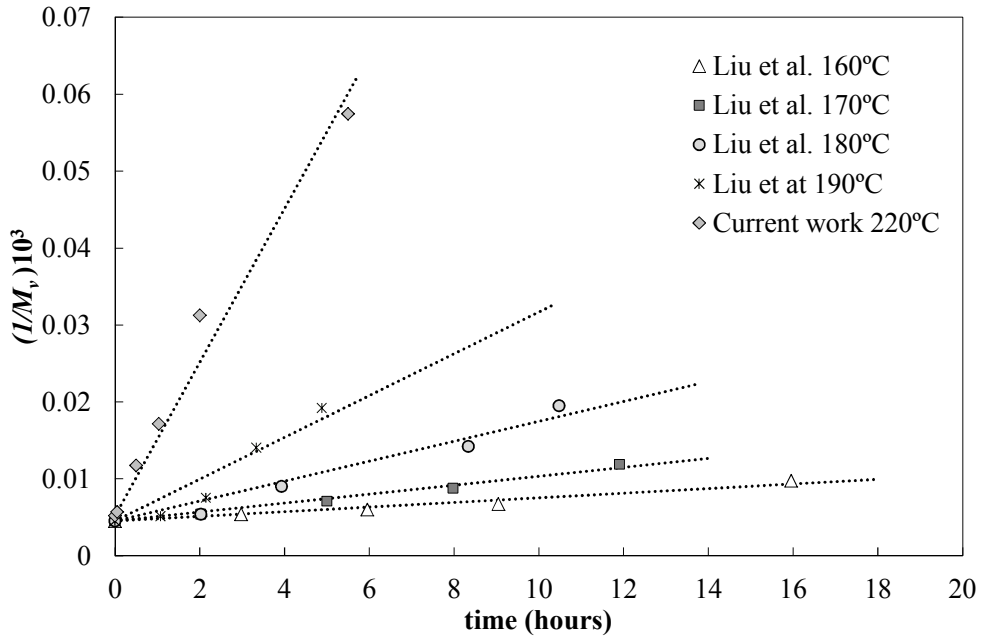

Figure 4-11 $1/M_n$ versus thermal degradation time in hours for the experimental data and the data obtained in *ref* 10 the dotted lines are the fitted tendency with the 2nd order equation.

Table 4-7 Fitting parameters from the 2nd order equation.

Reference	Temperature (ºC)	M_{v0}·10^{-3}	$k_{Tv,}$ (mol/kg·hour)	$k_{Tv,}$ (mol/kg·min)
Liu et al. [10]	160	220.6	3.01·10^{-4}	5.01·10^{-6}
	170		5.81·10^{-4}	9.68·10^{-6}
	180		1.29·10^{-3}	2.16·10^{-5}
	190		2.72 10^{-3}	4.53 10^{-5}
Current work	220	192.2	9.99 10^{-3}	1.66 10^{-4}

Once the values of k_{Tv} were obtained, their dependence with the temperature was evaluated by means of Arrhenius plots and thus the experimental ln(k_{Tv}) values were plotted versus $1/T$ (K^{-1}). Figure 4-12 evidences that the experimental points follow a linear trend, typical of Arrhenius behavior, $k_{Tv} = k_{Tvo} \cdot \exp^{(-Ea_A / RT)}$, with k_{Tvo} is a pre-exponential factor and Ea_A the activation energy obtained from the Arrhenius plot.

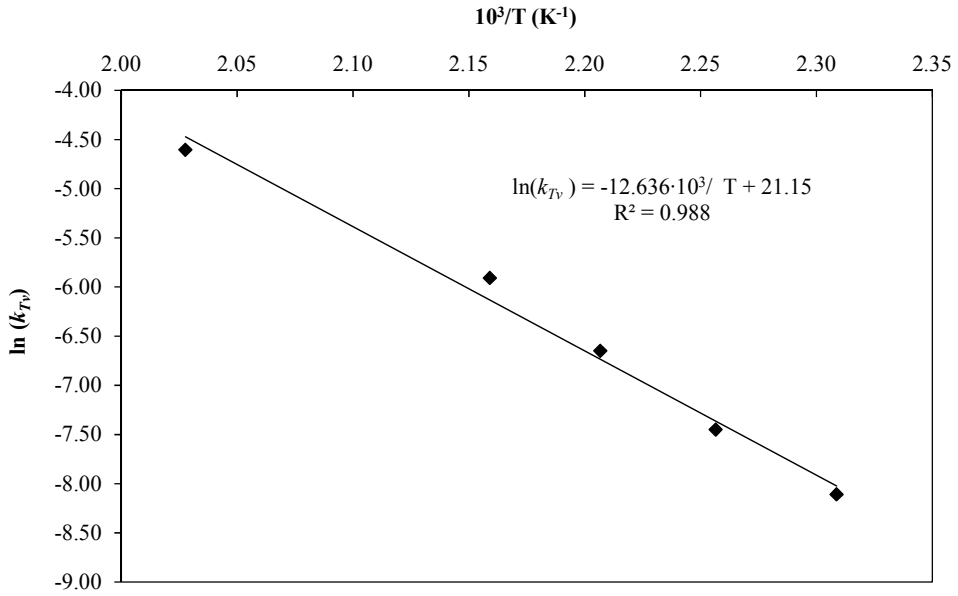

Figure 4-12 Plot of ln(k_{Tv}) versus $1/T$ (K^{-1}) for the current data (220ºC) and data of ref. 10 (at 160, 170, 180 and 190ºC).

The parameters of the Arrhenius equation were calculated and incorporated into the Mass decay second-order equation (4-16), giving the following expression Equation (4-20), that relates the molar mass with degradation and temperature.

$$\frac{1}{M_v} = e^{\left(\frac{-12.64}{T}+21.15\right)} \cdot \mathrm{t} + \frac{1}{192.2} \qquad (4\text{-}20)$$

The activation energy for the thermal degradation process, obtained in isothemal conditions in the 190 to 220ºC range, was calculated from the slope of the Arrhenius plot, providing a value of $E_{a,A}$= 105 kJ/mol. This value was in good agreement with the values of PLLA given for isothermal degradation in similar temperature conditions by *Sodergard et al* (~119 kJ/mol) and by *Wachsen et al*. for the decomposition step (~120 kJ/mol) [15,33]. A slightly higher value was also referred for PDLLA (~131 kJ/mol), obtained in similar conditions in the 160 to 190ºC range [10].

b) Biodegradation

The application of the model for molar mass decay to data obtained in biodegradation studies in the literature requires considering the different experimental conditions. In general, hydrolysis of amorphous PLA homopolymers, copolymers and blends follows an exponential behavior, while a linear trend is observed in the case of crystalline PLA without catalytic agents [16,17,18]. The hydrolysis of polylactide amorphous was faster than that of the crystalline polylactide [17,19,20,21]. In conditions of composting, an exponential behavior is been reported for amorphous PLA (4% D-lactide) [12].

The functionality of the molar mass decrease of PLA was applied to the results reported in three different studies in the literature: one involving hydrolysis [11], considered the first step in biodegradation, another reporting degradation in soil up to 15 months [22] and finally a composting study [12], which is considered the fastest biodegradation process. The characteristics of the materials used in such studies are summarized in Table 4-8.

Figure 4-13 shows the molar mass decay profiles of the data in the cited studies, together with experimental results obtained in the current work. All data fit well to the exponential decay function ln (M_n)=ln (M_{n0})-k·t and the parameters calculated are

summarized in Table 4-8. The values of rate constant *k* confirm that composting is the fastest process, followed by pure hydrolysis and by degradation in soil. The resulting rate of biodegradation may then be a combination of several synergetic effects, including water content, the initial molar mass [23], thickness [24] and the microbiological activity and conditions of the soil [25,26] or the D- content [11].

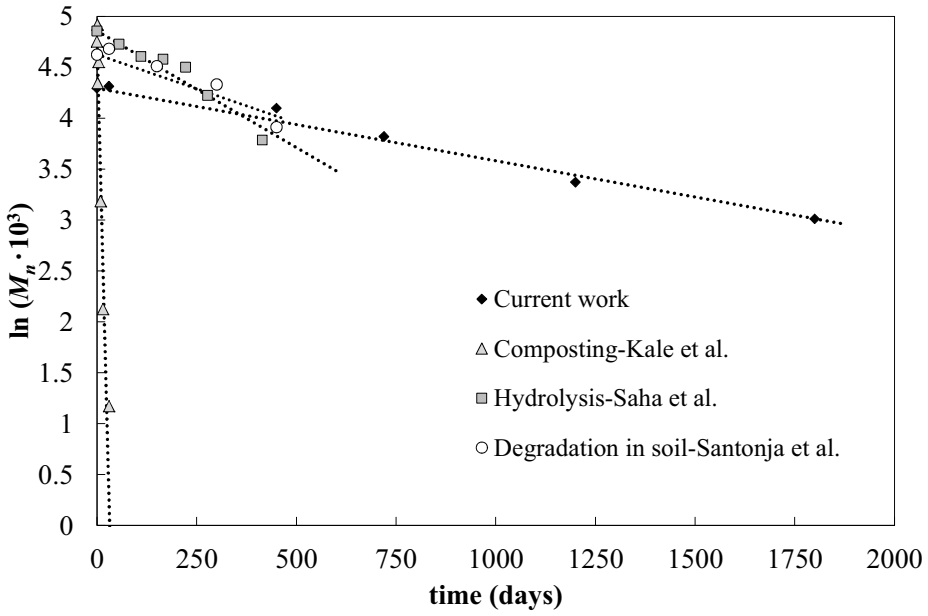

Figure 4-13 Plot of ln (M_n) versus time (in days) for the current work and the literature references for biodegradation.

Table 4-8 Data summary from the literature of biodegradation of polylactide.

Reference	Amorphous PLA	Thickness (mm)	M_{n0} 10^{-3}	Days of study	k_B (days^{-1})	k_B (months^{-1})
Current work 60m-soil T=28ºC & pH 4-5	4%D	1	102.0	1800	$7.12\ 10^{-4}$	$2.10\ 10^{-3}$
15m-Soil T=28ºC & pH 7 [*ref.* 22]	4%D	2	198.0	450	$1.34\ 10^{-3}$	$4.02 \cdot 10^{-2}$
Hydrolysis T=37ºC & pH 7.4 [*ref.* 11]	1.2% D	0.25-0.1	122.6	415	$2.29\ 10^{-3}$	$6.87\ 10^{-2}$
Compost T=65.±5ºC & pH 8.5 ± 0.5 [*ref.* 12]	4% D	Around 1	115.9	31	$1.50\ 10^{-1}$	4.50

c) Photodegradation

The great variety of experimental conditions must be also taken into account when applying the model of molar mass decay for photodegradation. *Tsuji et al* observed an exponential tendency for the M_n decrease of polylactide submitted to UV radiation [27]. On the other hand, most of the studies performed in experimental conditions of high UV wavelengths similar to the present work, report data without any fitting. *Janorkar et al* found a 40% decrease in molar mass of a PLA sample with thickness of 0.125 mm after 12 hours of UV exposition from 250 to 450 nm at 255 W/m^2 [28]. *Ikada* reported a 97% decrease of the molar mass after 12 hours in a range of UV exposure from 200 to 600 nm in samples obtained by casting [29]. Other work performed by *Zaidi et al* in real outdoor exposure reported a molar mass decrease of about 40% after 130 days [30].

The work of *Zaidi et al*. [30] was the only one not performed in accelerate chamber, and to properly compare with the rest of the results, some suppositions were assumed:

- Similar total minimum radiation per year for Algeria (location of the outdoor exposure) and Spain: 5000 MJ/m$^{2.}$
- The samples were exposed in the same chamber and submitted to the same radiation, 478 W/m^2, as the present work

Taking into account the previous considerations, the data adaptation for that particular reference can be seen in Table 4-9.

Table 4-9 Adapted photodegradation data from *ref. 30*.

Real days of outdoor exposure (from *ref 30*)	**years=** days/365	**Outdoor MJ/m^2=** (5000 MJ/m^2 *per year)* · (years)	**Outdoor J/m^2 =** Outdoor MJ/m^2) ·(1000000)	**Time in chamber (s):(**Outdoor J/m^2)/ (478 J/s·m^2)	**Hours in the chamber** *: s·3600 s/h
0	$2.74 \cdot 10^{-8}$	$1.37 \cdot 10^{-4}$	$1.37 \cdot 10^{2}$	0	**0**
30	$8.22 \cdot 10^{-2}$	$4.11 \cdot 10^{2}$	$4.11 \cdot 10^{8}$	859747	**239**
60	$1.64 \cdot 10^{-1}$	$8.22 \cdot 10^{2}$	$8.22 \cdot 10^{8}$	1719493	**478**
130	$3.56 \cdot 10^{-1}$	$1.78 \cdot 10^{3}$	$1.78 \cdot 10^{9}$	3725569	**1035**

*Theoretical time in the accelerated chamber correlated with the real days of exposure.

The experimental conditions of the photodegradation tests from the literature are summarized in Table 4-10.Several remarks should be made regarding the different experimental conditions:

- The data from *ref. 29* were obtained in wavelengths between 200 and 600 nm, but the maximum energy of the lamp corresponds to 300 nm, the same radiation was considered for all the lamps.
- In the same *ref. 29* the initial molar mass was higher than in the other studies.

Figure 4-14 shows the mass decay of the photodegradation tests from the literature data together with the results obtained in the current work, with the exposure time expressed in hours. All the data were fitted successfully to the 2nd order law, according to Equation (4-15). The corresponding rate constants (k_P) were calculated, and the results are shown in Table 4-10.

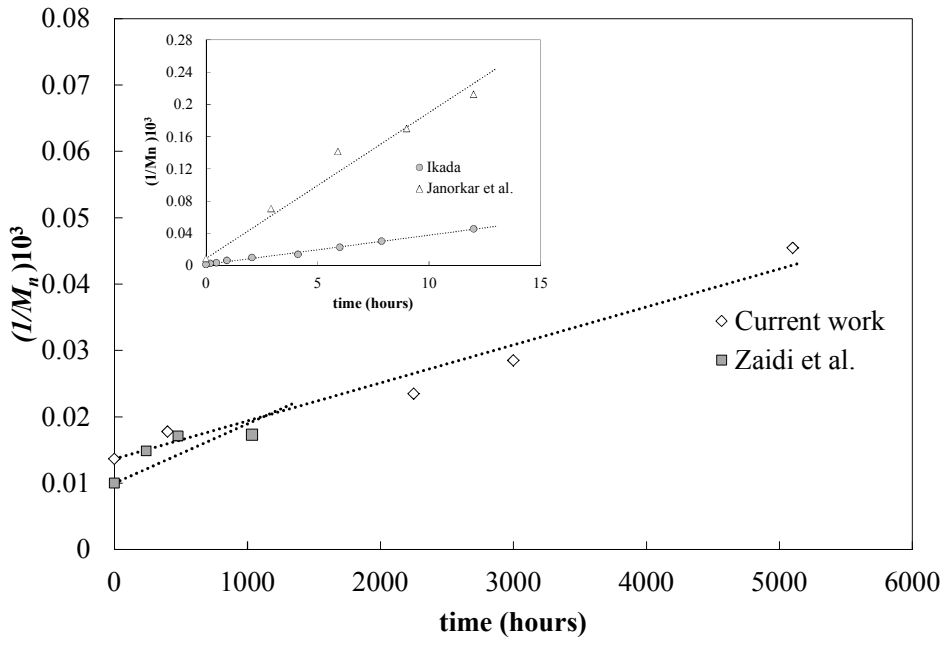

Figure 4-14 Plot of $1/M_n$ versus time (in hours of chamber exposure) for the current work and the literature references for photodegradation.

The results indicate considerable differences in the molar mass decay for the different systems, remarking the importance of the tests parameters on the photodegradability of PLA. In order to investigate such parameters, the values of rate constant, k_P, were plotted

as a function of the sample thickness and initial molar mass in Figure 4-15 *a* and *b*, respectively.

Table 4-10 Data summary from the literature data of photodegradation of polylactide.

Reference	$M_{n0} \cdot 10^{-3}$	Wavelengths (nm)	thickness (mm)	k_P (mol/kg·h)
29	645.3	>200	≈0.05-0.15	$3.63 \cdot 10^{-3}$
28	111.8	>254	0.125	$1.81 \cdot 10^{-2}$
30	100.0	>295	0.05	$8.94 \cdot 10^{-6}$
Current work	73.2	>290	1	$5.73\ 10^{-6}$

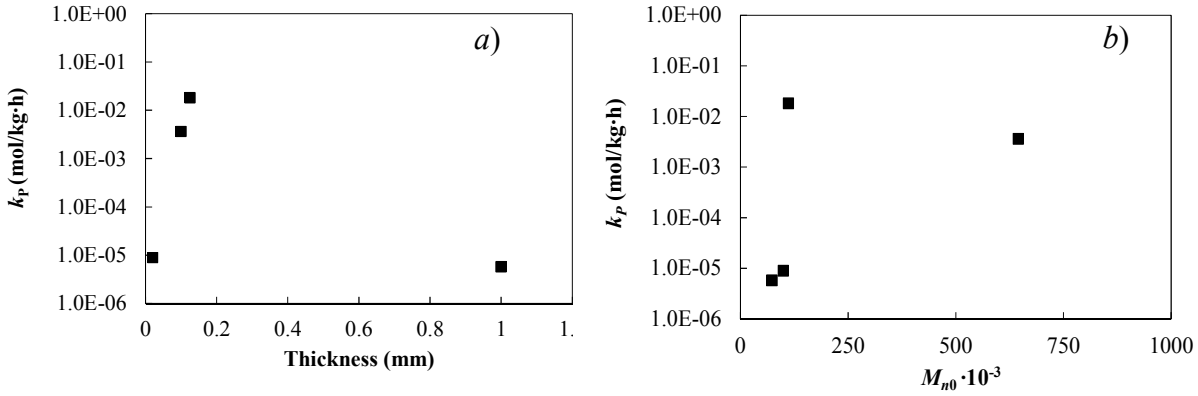

Figure 4-15 k_P versus the thickness *a*) and the M_{n0} *b*) for the current work and the literature data.

There is no apparent correlation between k_P and neither the initial molar masses nor the thicknesses. Considering the results in Table 4-10, the differences in k_P may be then attributed to the effect of radiation wavelength (200 – 400 nm). For samples submitted to wavelengths lower than 295 nm the order of magnitude of k_P is three times lower than for samples exposed at 295 nm. This means that the effect of radiation is at least three times higher at low UV wavelengths.

4.2 Analysis of the chemical structure

The study of the molar mass decay of PLA, by GPC and viscometry, suggested different functionalities depending on each degradation process. However, it is necessary to assess the changes in the PLA structure to determine the mechanism of each degradation type.

The possible modifications on the PLA structure by the different types of degradation are explained in Chapter 2. The thermal degradation of polylactide below 270ºC is a non-radical process mainly attributed to intramolecular transesterification and also to cis-eliminations. The products are cyclic oligomers, lactide, acetaldehyde and carbon monoxide [31,32,33] and olefinic double bond plus a carboxyl group with acrylic acid [34]. The mechanism essentially leads to cyclic polylactide chains with lower molar mass.

On the other hand, biodegradation of polylactide is a combination of two processes: abiotic hydrolysis followed by the action of enzymes and/or microorganisms (bacteria, fungi, etc.) or its secretion products [35,36]. After initial hydrolysis, the molar mass decreases and the material becomes bio-assimilable (<10000)[12]. Since PLA is hydrolyzed in acidic conditions, see Figure 4-16, the chain end reaction starts with the protonation of the hydroxyl end-group and the formation of an intramolecular hydrogen bond. The hydrolysis of the ester group releases a lactic acid molecule with a consequent decrease on the degree of polymerization. The mechanism can also proceed via intra-chain protonation of the carbon of one random ester group. In both cases, hydrolysis produces different fragments of lower molar mass [37]. Moreover, bulk hydrolysis of polylactide is considered heterogeneous, due to the autocatalytic character of the chain end groups and water transport effects [38,39]. The effect of hydrolysis during degradation in soil is expected to be less acute respect to pure hydrolysis or composting, mostly by lower water concentration.

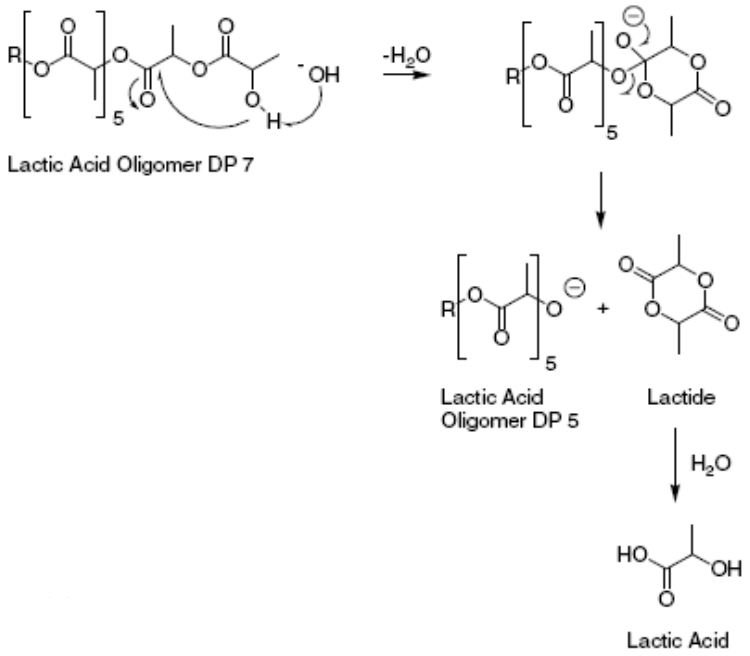

Figure 4-16 Summarized mechanism of the acidic hydrolysis of PLA oligomers.

Finally, UV photodegradation of pure poly (L-lactide) (PLLA) proceeds *via* the Norrish II mechanism and provokes chain cleavage with formation of C=C double bonds and carboxyl end groups [29], as seen in Figure 4-17. Other mechanisms propose the formation of diketone groups, which promote homolytic cleavage of the C-C bonds and ultimately activate new radical reactions [28]. Alternatively, a new mechanism applicable for outdoor conditions (sunlight) involves the formation anhydride groups, as described by *Bocchini et al.* [40] and represented in Figure 4-18.

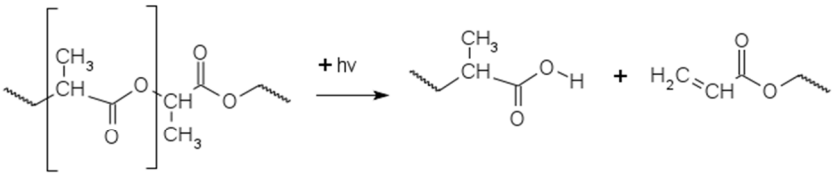

Figure 4-17 Photodegradation Norrish II mechanism of polylactide proposed in *ref.* 29.

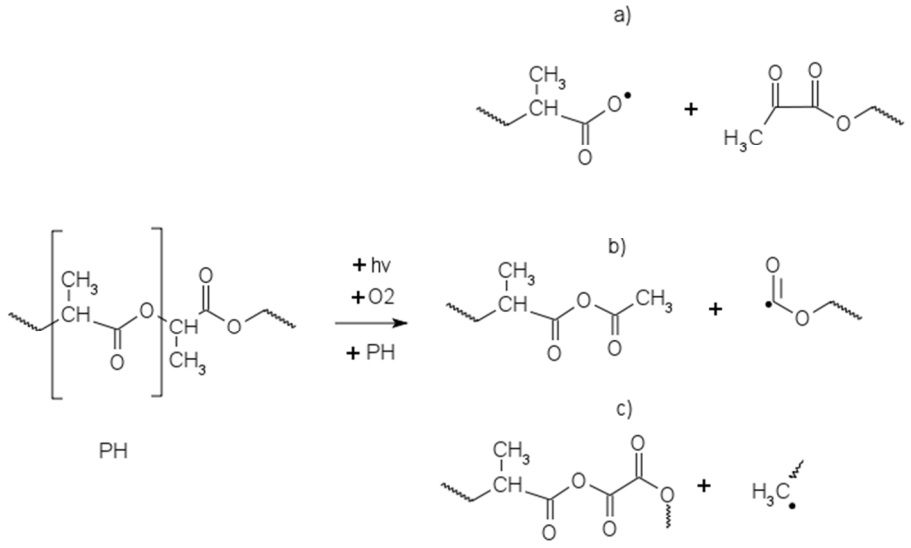

Figure 4-18 Photodegradation mechanism of polylactide proposed in *ref.* 40.

Fourier Transform Infrared Spectroscopy (FTIR) was used to study the changes on the PLA chemical structure due to the thermal, bio and photo degradation. Figure 4-19 shows the PLA characteristic IR bands associated to its most representative groups [41]. This band assignation is also valid for the thermally, bio and photo degraded samples. Only in the case of pellets, an additional weak band is visible at 921 cm^{-1} representative of the PLA crystalline structure (Figure 4-20) [42] .

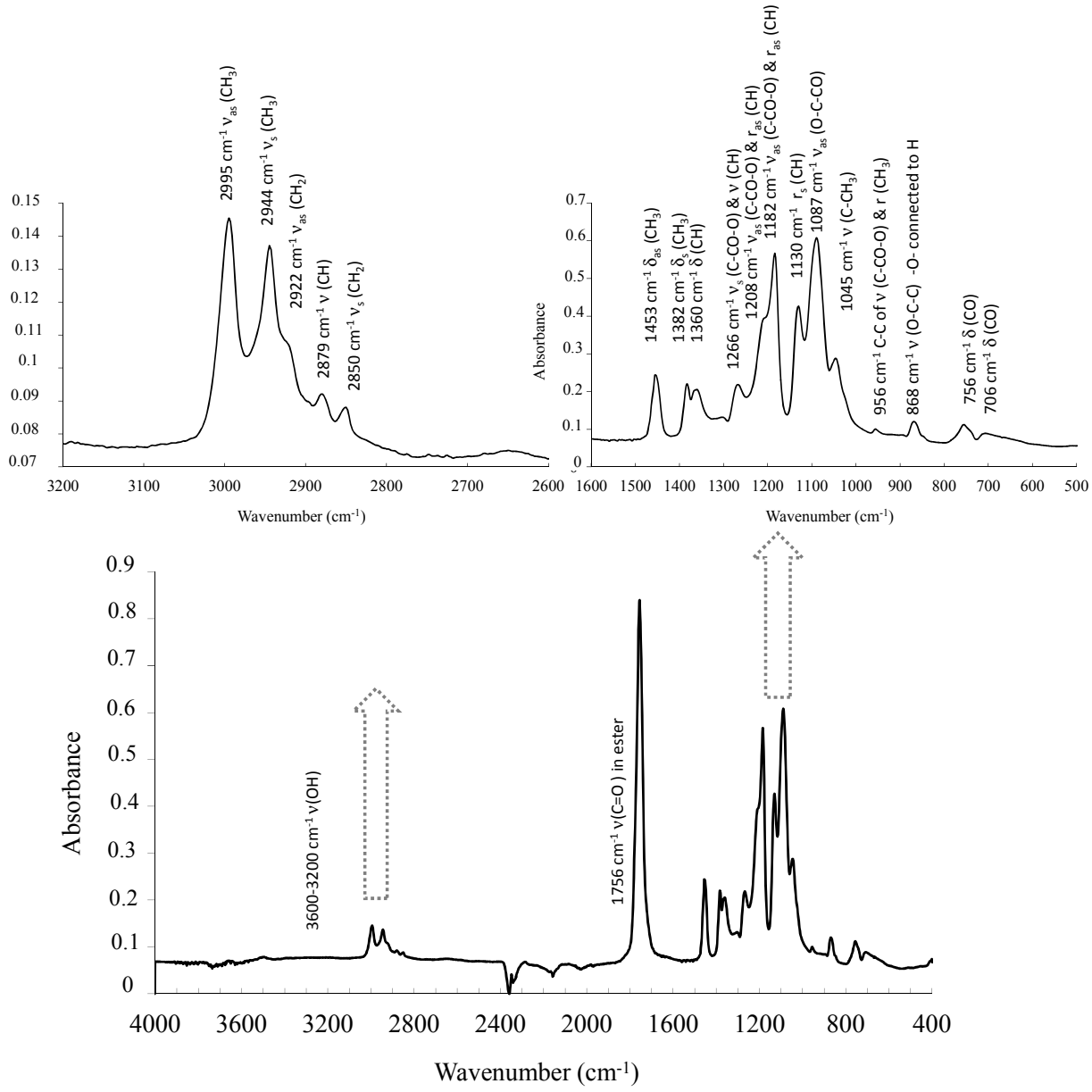

Figure 4-19 Characteristic IR bands of the polylactide plates.

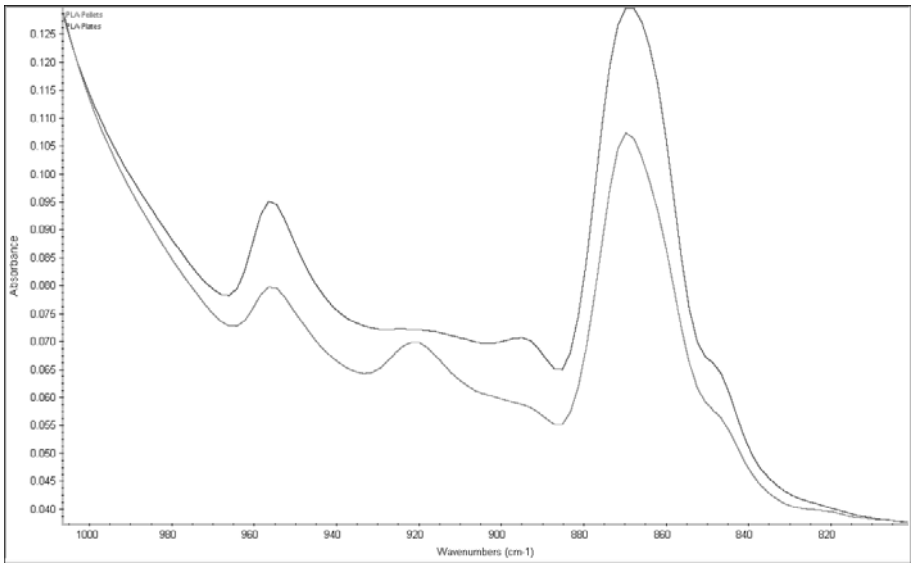

Figure 4-20 1000-800 cm^{-1} region corresponding to PLA pellets (lower line) and plates (upper line).

The most representative bands are found in several IR regions:

- *3600-3200 cm^{-1} region.*

In this region a broad band related to the OH stretching vibration is usually expected (carboxyl acids and alcohols), although this band is not well-defined in the polylactide.

- *3100-2800 cm^{-1} region.*

Several overlapping bands are visible related to the stretching vibrations of the C-H bonds of the polymeric chain:

ν = 2995 cm^{-1} stretching asymmetric vibration of CH from CH_3.

ν = 2944 cm^{-1} stretching symmetric vibration of CH from CH_3.

ν = 2922 cm^{-1} stretching asymmetric vibration of CH_2.

ν = 2879 cm^{-1} weak CH stretching vibration.

ν = 2850 cm^{-1} stretching symmetric vibration of CH_2.

The bands at 2995, 2944 and 2980 cm^{-1} are attributed to the vibration of the CH and CH_3 groups of PLA [31,40,43], while additional bands are also visible at 2922 cm^{-1}and 2850 cm^{-1}. Although the origin of these bands is yet unclear, other authors assigned them to CH_2 groups from either impurities or sub-products of degradation, already existing in the raw materials. Due to the non-reproducibility of the bands in the samples, they were not studied in any of the degradation processes.

- *1600-1800 cm^{-1} region*

A prominent band appears centered at ν=1754 cm^{-1} associated to the stretching vibration of the carbonyl group C=O in the ester linkage.

- *1460-1300 cm^{-1}*

Several bands can be observed in this IR region which can be attributed to the vibration of the C-C bonds of the polymeric chain.

ν= 1453 cm^{-1} asymmetric bending of the CH_3.

ν= 1382 cm^{-1} symmetric bending of the CH_3

ν= 1360 cm^{-1} related to the CH bending (wagging)

- *1300-800 cm^{-1}*

In this region several bands related to st. C-O vibrations appear overlapped with contributions from the C-H bonds (rocking). In the case of PLA, the ester CO-O bond can be in resonance with the carbonyl group of the same ester (C-O_{ester})or with a neighboring ester group (C-$O_{C\alpha-O}$) (Figure 4-21), leading to different IR signals [44]:

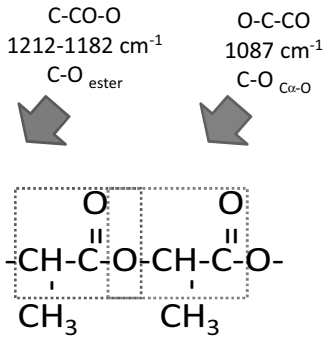

Figure 4-21 C-O vibration modes in PLA

ν= 1266 cm^{-1} symmetric stretching vibration of the C-CO-O and stretching of CH.

ν= 1208 cm^{-} and ν= 1182 cm^{-1} asymmetric stretching vibration of the C-CO-O and asymmetric rocking of CH_3.

ν= 1130 cm^{-1} symmetric rocking of CH_3.

ν= 1087 cm^{-1} related to the asymmetric stretching vibration of O-C-CO.

ν=1045 cm^{-1} related to the stretching of C-CH_3.

ν=956 cm^{-1} C-C backbone stretching of C-CO-O and the CH_3 rocking, (this band is in 921 cm^{-1} when sample has crystalline α(or α') form with a 10_3 helix conformation).

ν= 868 cm^{-1}, assigned to O–C–C in phase stretch which the –O– connected to H.

ν= 756 and 706 cm^{-1} bending of CO.

In all the degraded samples, the study has been focused on the evolution of selected IR bands related to some representative groups to monitor the changes than undergo during degradation.

4.2.1 Thermal degradation

Figure 4-22 displays the IR spectra of PLA samples thermally degraded at different times. Thermal degradation promotes the cyclation of the PLA molecules, and thus a decrease on the OH groups is expected. However, no significant changes were observed in the area or intensity of the corresponding OH st. band (>3000 cm^{-1}). This fact can be explained by the high concentration of backbone groups of the samples compared to the chain end (-OH). For PLA degraded in similar circumstances, *McNeill and Leiper* detected the products of degradation by thermal volatilization analysis (TVA), but showed no evidence of the variation of -OH, -COOH or formation of new end structures by neither NMR nor FTIR[31]. Furthermore in a recent study by *Carrasco et al.* processed polylactide at 210ºC does not present modifications on the chemical composition studied by ^{1}NMR and ^{13} C NMR [43].

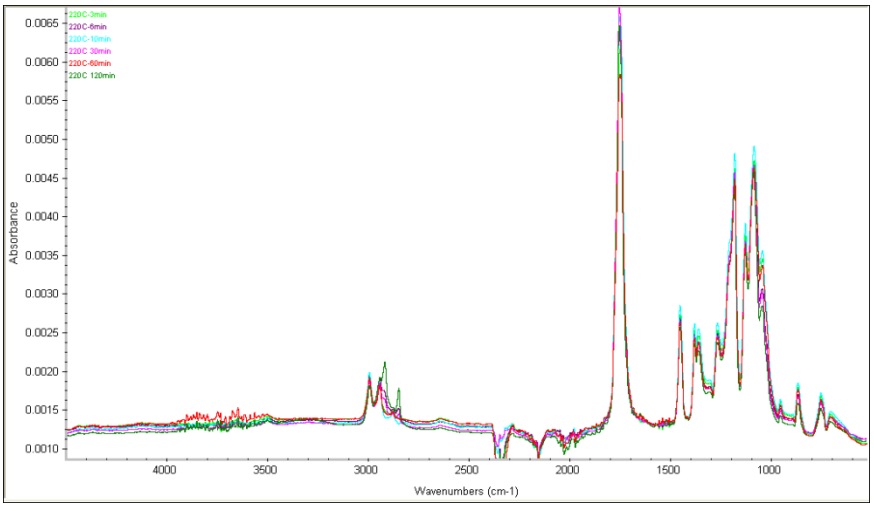

Figure 4-22 FTIR overlapped spectra of the thermally degraded samples.

On the other hand, there was no variation in the IR C=C stretching region (1620-1680 cm^{-1}), which indicates that the products of the cis-elimination ($CH=CH_2$, acrylic end group at the end of the molecule) could not be detected. This result can be attributed to the absence of such mechanism in the thermal degradation of the current samples or to the low concentration of acrylic oligomers expected at such low temperatures (less than 5% of the total sub-product) [32]

Figure 4-23 shows the 2000 – 600 cm^{-1} IR region with more detail. A deconvolution of the region was performed with the aim to follow the changes in the areas of C=O and C-CO-O with degradation time (Figure 4-24).

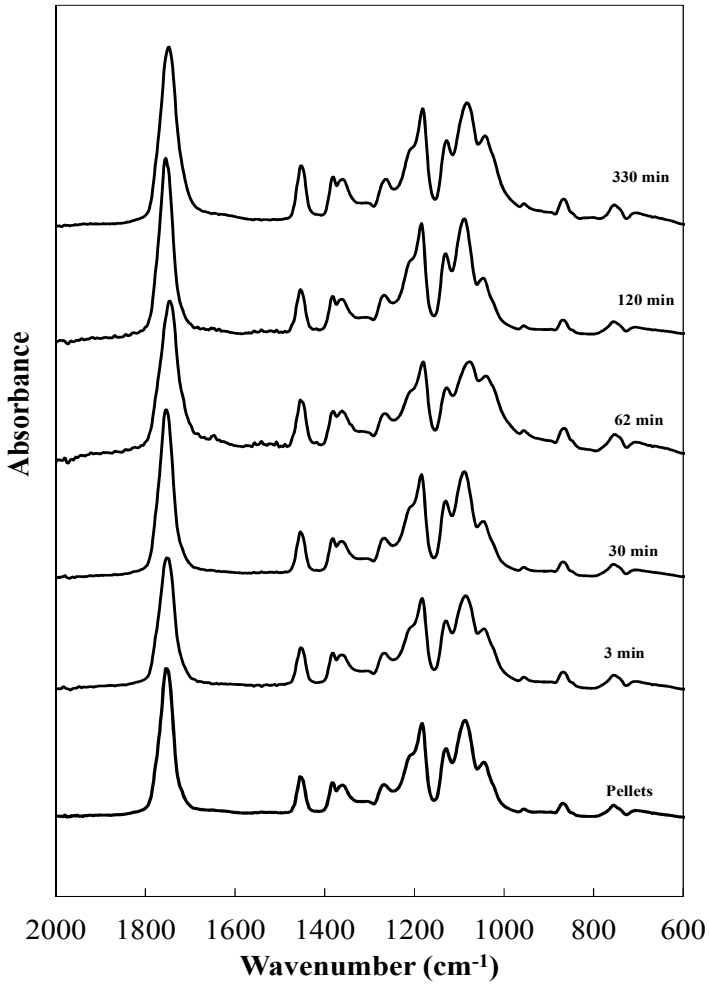

Figure 4-23 FTIR of the thermally degraded samples.

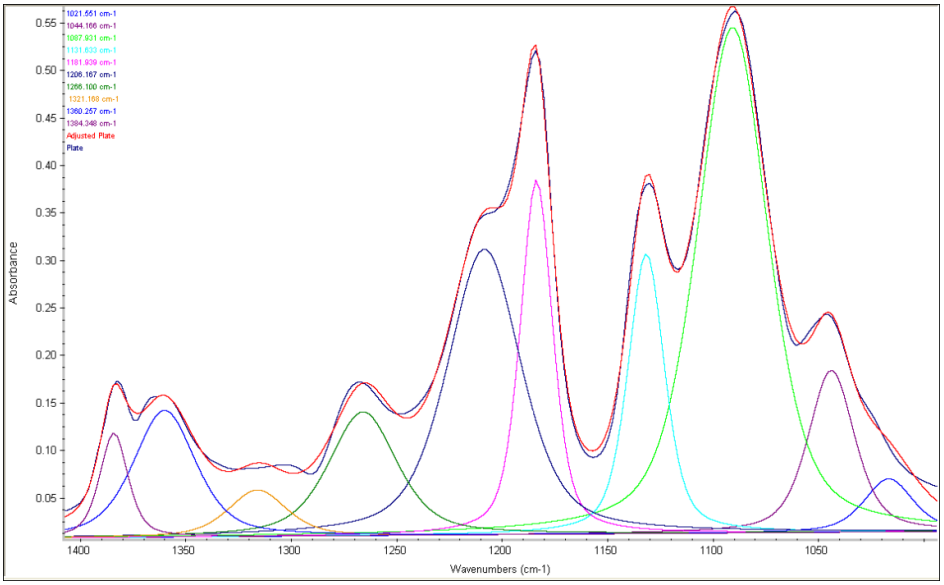

Figure 4-24 Deconvolution bands of the region 1400 to 900 cm^{-1} .

No considerable variations were detected within this area after thermal degradation, and this was confirmed by the quantitative analyses of the relative intensities of the different individual bands. Cyclation of the PLA chains is expected to modify the relative contribution of ester groups in the samples. However, only the cyclation of short chains may produce enough new ester groups to be detected by IR, and this view is in coherence with the invariability of the IR OH band.

4.2.2 Biodegradation

The products expected by acidic hydrolysis (ester removal) are mainly shorter molecules of polylactide with the formation of new carboxylic acid groups. Thus the principally groups affected by hydrolysis are O-H (3600-3200 cm^{-1}), C=O (1756 cm^{-1}) and C-CO-O (1212-1182 cm^{-1}). However, non-significant variations were observed in the OH bands of the biodegraded samples, maybe due to the high concentration of ester groups in the native molecules.

The relative contribution of the OH groups to the PLA chains is important to determine the significance of the IR band in the spectra. It was considered that groups representing less than 1% of the mass of the polymer molecule will not be detected by FTIR. Considering that the molar mass of a polylactide repeating unit -O–CH-(-CH_3)-CO- is 72, a polymer with 1 % of OH (wt.) in the chain should contain 200 repeating units and M_n = 14400. For instance, in the case of PLA plates, M_n = 73200 and thus there are two –

OH ends in 1016 repeating units, representing around the 0.20% (mass) of the polymer chain.

The percentage of molecules with lower sizes that M_n =14400 in the samples is defined by the integration of the molar mass distribution curve. Such percentages were 0.2% for pellets, 0.8% for plates, 1.0% for 1 month sample, 1.6% for 15 months sample, 3.3% for 24 months sample and 7.8% for 40 months sample. These low values explain the absence of changes in the OH bands.

On the other hand, the C=O and CO stretching regions were studied in Figure 4-25 with more detail.

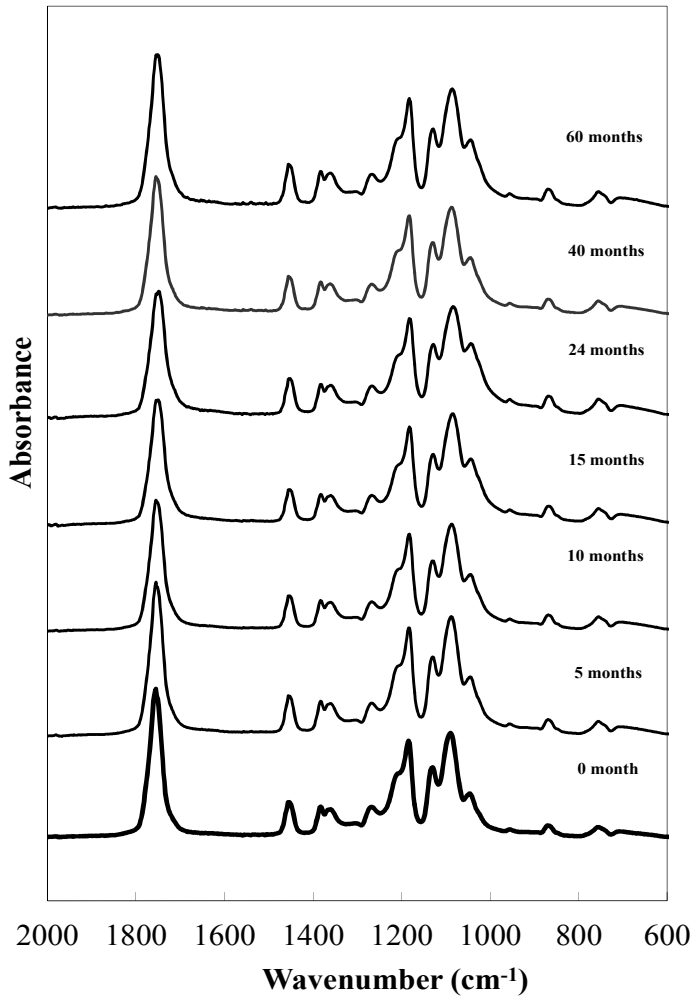

Figure 4-25 FTIR of the biodegraded samples.

Although no apparent changes are observed in the spectra at different biodegradation times, the relative absorbance (A) of the 1182 cm^{-1} (O-C-CO) and 1756 cm^{-1} (C=O) bands were further studied. The absorbance at 1360 cm^{-1} related to the CH bending was taken as a reference, due to its invariance with time:

$$A_{\frac{1182\,cm^{-1}}{1360\,cm^{-1}}} = \left(\frac{A_{\nu = 1182 cm^{-1}}}{A_{\nu = 1360 cm^{-1}}} \right) \qquad A_{\frac{1756\,cm^{-1}}{1360\,cm^{-1}}} = \left(\frac{A_{\nu = 1756 cm^{-1}}}{A_{\nu = 1360 cm^{-1}}} \right)$$

The evolution of these ratios versus biodegradation time is shown in Figure 4-26 and Figure 4-27, without evidencing significant changes or tendencies. These results are in agreement with the previous calculations of the OH relative weight in the polymer chains, as the decreases in C-O and C=O concentrations may only be detected at very small molar masses.

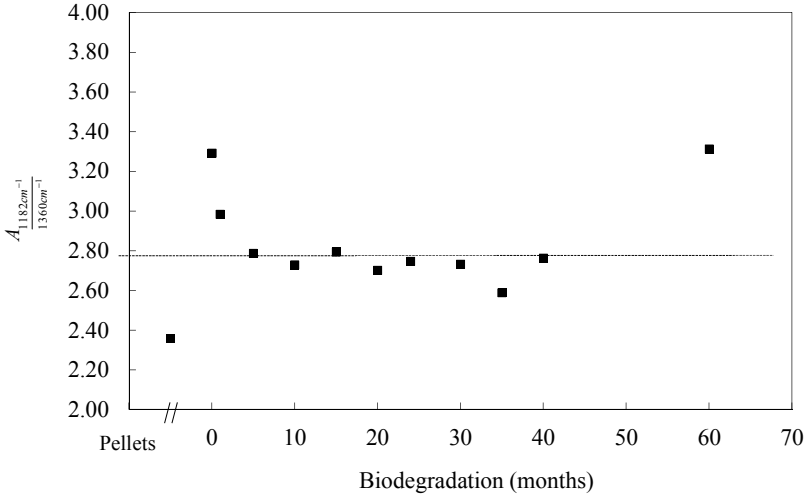

Figure 4-26 Plot of $A_{\frac{1182cm^{-1}}{1360cm^{-1}}}$ versus the biodegradation time.

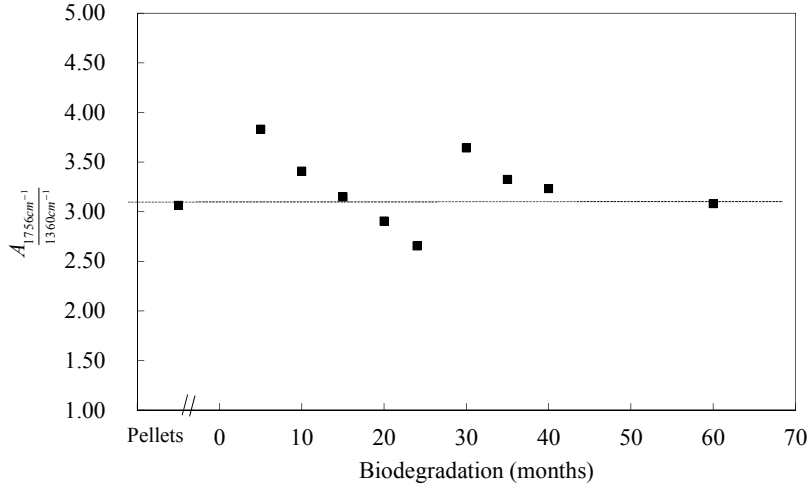

Figure 4-27 Plot of $A_{\frac{1756cm^{-1}}{1360cm^{-1}}}$ versus the biodegradation time.

4.2.3 Photodegradation

The study of the possible mechanism of photodegradation of polylactide due to sunlight exposure was also followed by FTIR. The groups involved in the proposed mechanisms are OH (3600-3200 cm^{-1}), C=C (1620-1680 cm^{-1}), CH_2 (2922-2850 cm^{-1}) and anhydride (1845 cm^{-1}) [28,40]. Figure 4-28 shows the spectra of all the photodegraded samples at the different photodegradation times. Only the bands in the 2000 to 400 cm^{-1} region has been considered for study, since no significant changes were detected at higher wavenumbers (2800-3500 cm^{-1}).

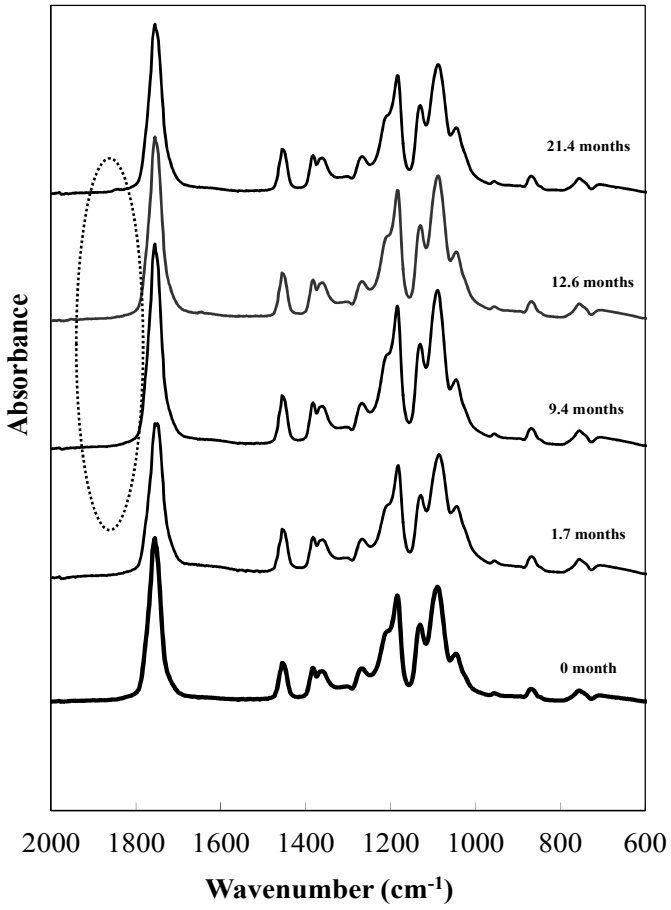

Figure 4-28 FTIR of the photodegraded samples.

No changes are observed in the OH or C=C groups after photodegradation, as it happened to the biodegraded samples. Following a similar discussion as for the OH groups in the case of biodegradation, the M_n threshold for IR determination of the C=C groups is 7200 (only present in one end-chain). Taking into account the molar mass distributions, the

percentages of chains with M_n < 7200 are 0.1% for pellets, 0.5% for plates, 1.3% for 1.7 months sample, 2.3% for 12.6 months sample and 5.3% for 21.4 months sample. These results indicate that the presence of C=C formed by photodegradation of PLA will be hardly detected by FTIR.

The results also indicate the formation of new anhydride groups during photodegradation, by the appearance (Figure 4-29) and growth (Figure 4-30) of a new band with low intensity at 1845 cm^{-1} [40]. Other IR contributions of this group (1756 cm^{-1}) may be obscured by the prominent carbonyl band.

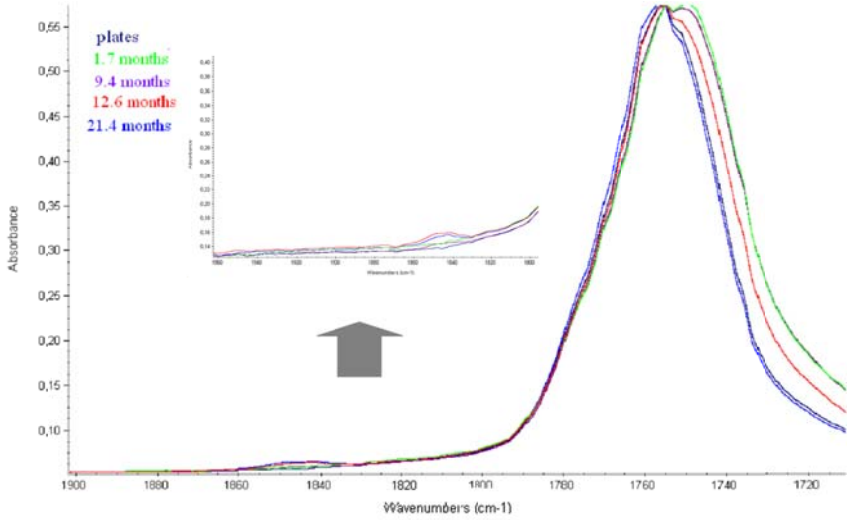

Figure 4-29 Plot of the 1845 cm^{-1} band corresponding to the anhydride group formed by photodegradation.

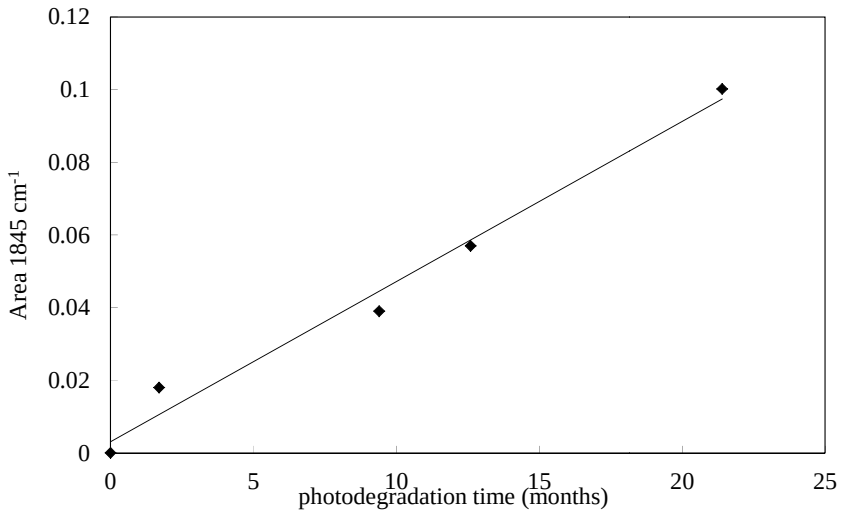

Figure 4-30 Evolution of the area corresponding to the anhydride group versus de photodegradation time in months shows the areas of the 1845 cm^{-1} band, after subtracting the area corresponding to the plates.

There was no evidence by FTIR of the formation of new groups in the case of thermal and biodegradation mechanisms, while anhydride groups were detected in photodegraded samples. This can be due to the random mechanism proposed by *Bocchini et at*., in opposition to the mechanisms involving end-chain cleavage. A more sensitive analysis requires the use of alternative techniques [40].

4.3 Thermal stability study

4.3.1 Study of the temperature variation

Thermogravimetry was applied to study how the structural changes promoted by degradation affect the thermal decomposition of polylactide.

The thermograms (TG) and their first-order derivative curves (DTG) of the pellets and plates are shown in Figure 4-31 *a* and *b*, respectively, evidencing one solely decomposition process.

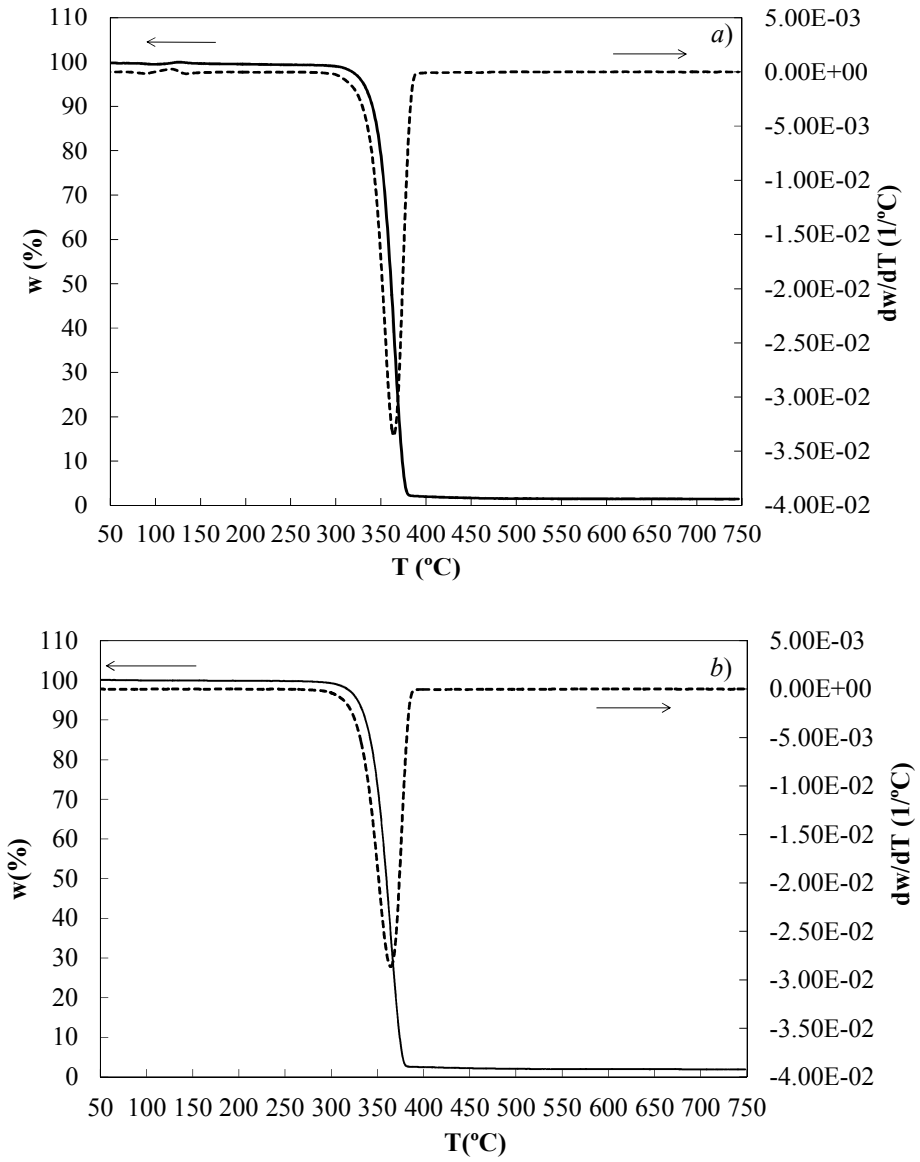

Figure 4-31 TG and DTG curves at 10ºC/min for *a*) pellets and *b*) plates.

The thermograms corresponding to plates, obtained at different heating rates (β) are shown in Figure 4-32. As expected, the thermograms and DTG curves are shifted to higher temperatures at increasing β.

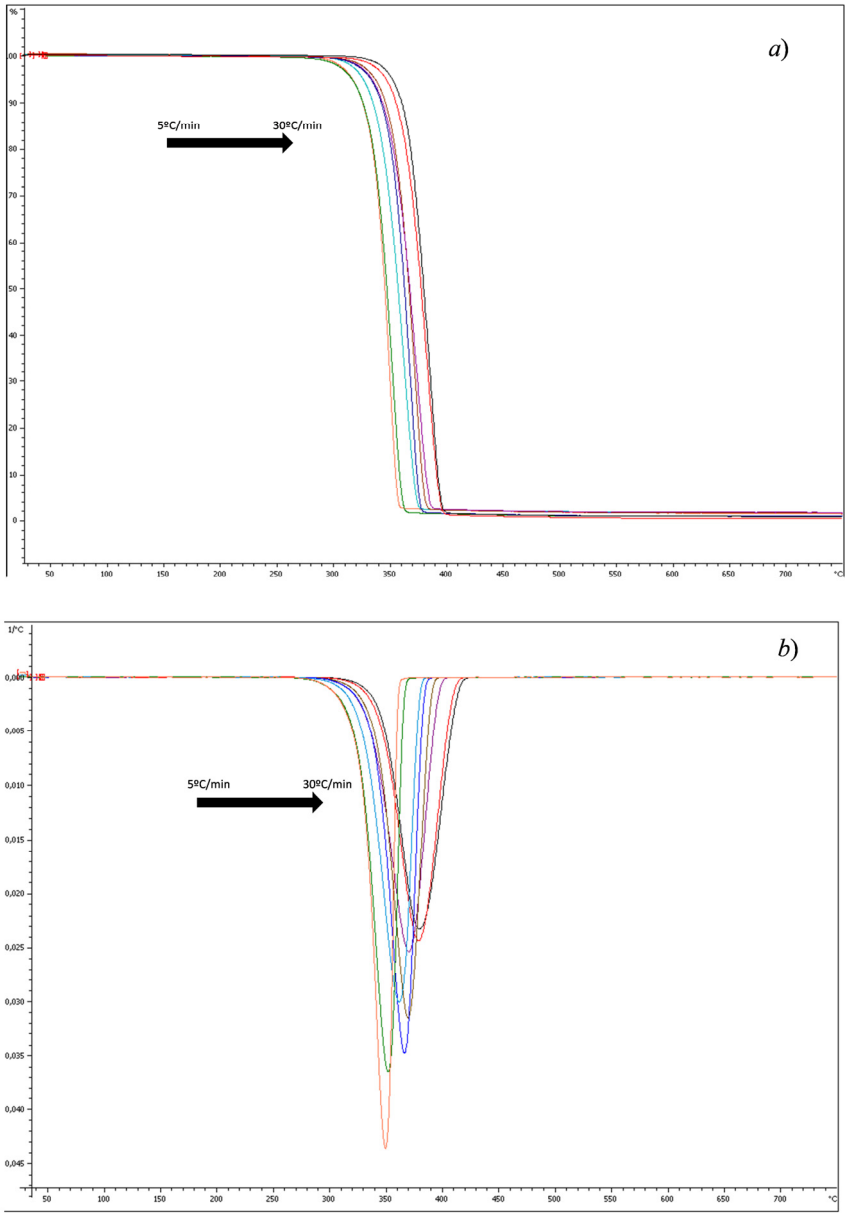

Figure 4-32 *a*) TG in *w(%)* vs *T(ºC)* and *b*) DTG *dw(%)/dT(ºC)* vs. *T(ºC)* of the plates at different heating rates.

The corresponding decomposition onset and endset temperatures of the degradation step (T_o and T_e, respectively) can be obtained by a tangential intercept method onto the TG curve, as indicated in Figure 4-33. The onset temperature ($T_o \approx$ 340-346ºC, at 10ºC/min) corresponds to a mass loss of 2-2.5%. Likewise, the minimum peak temperature of the DTG curve, which is related to the inflection temperature of the TG curve ($T_p \approx$ 365-371ºC, at 10ºC/min) was also evaluated. The mass loss was around 98-99% in all the studied samples.

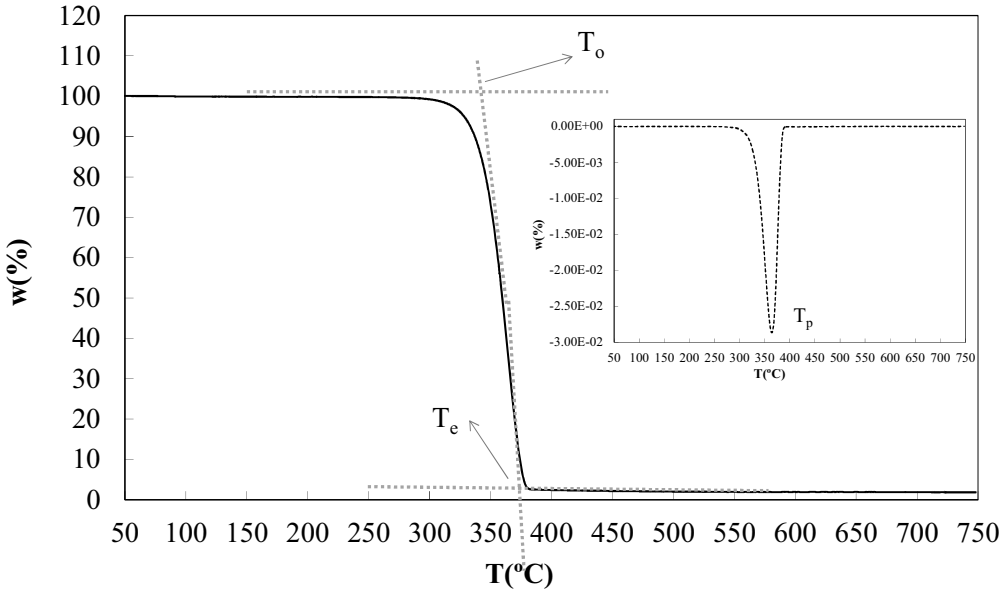

Figure 4-33 Characteristic temperatures calculated form TG and DTG curves.

Figure 4-34 *a* and *b* displays the TG and DTG curves, respectively, corresponding to the PLA samples submitted to the different degradation types during the maximum times. For the sake of comparison, the curves of the pellet and plates are also included.

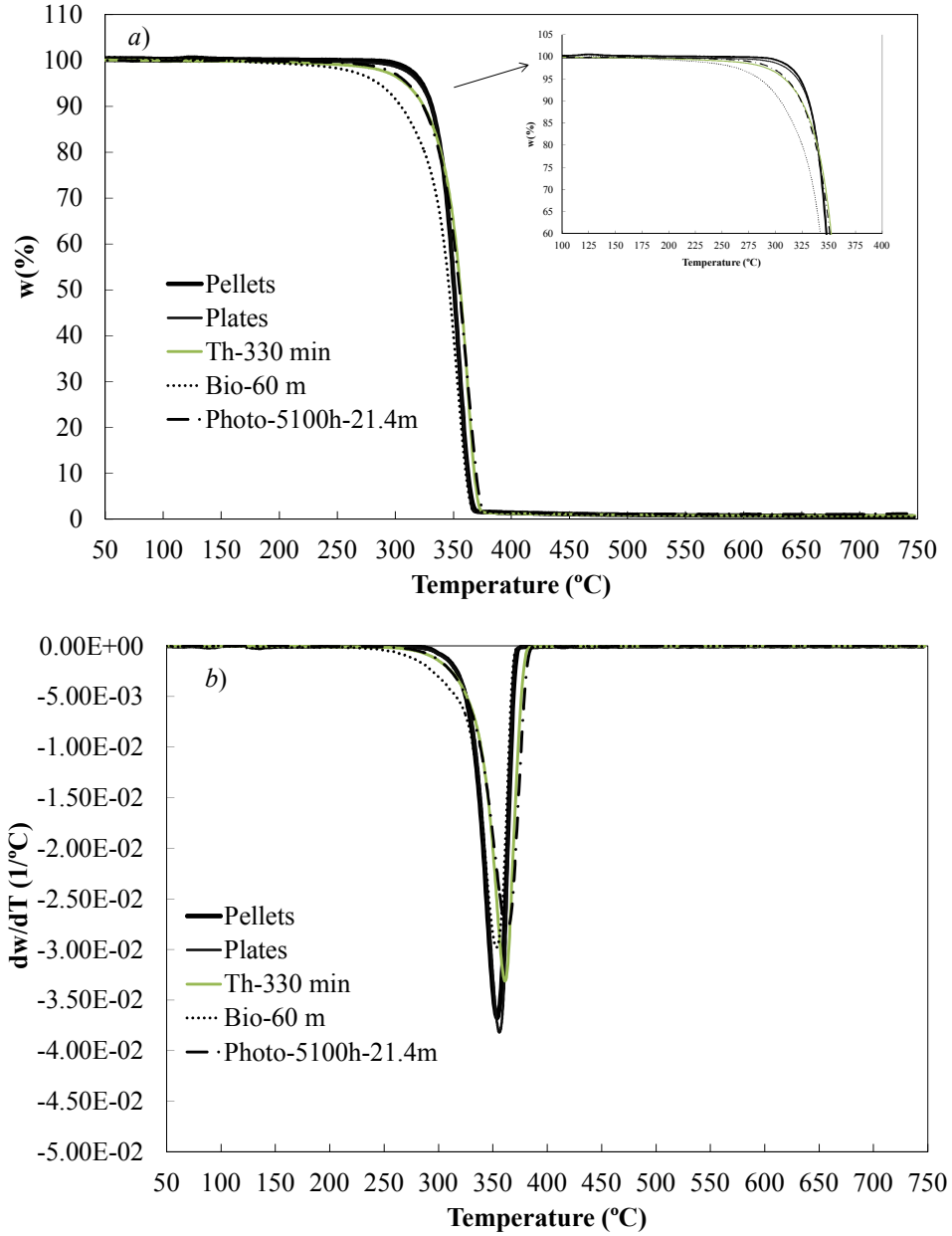

Figure 4-34 *a*)TG and *b*) DTG curves at 10ºC/min for pellets, plates, thermal 330min, bio-60m and photo-5100h-21.4m.

All the PLA samples undergo one simple thermal decomposition step, with slight shifts in the position of the maximum. In order to perform a quantitative analysis, the representative parameters of the TG and DTG curves were obtained. In the case of plates, Table 4-11 summarizes the values obtained at different heating rates, while for the biodegraded samples the results are plotted as a function of the degradation time in Figure 4-35. The parameters (T_p, T_o, T_e) presented the same tendency regardless of the heating rate, and this applies for all the samples and all degradation types. Thus, the curves

obtained at β=10ºC/min were selected for comparing the results of the degraded samples, as this is commonly used in standard thermal analysis measurements.

Table 4-11 Parameters from the TG and DTG curves for the plates at the different heating rates (β).

β (ºC/min)	T_p (ºC)	T_o (ºC)	T_e (ºC)	Mass loss (%)	Residue (%)
5	355	339	362	99.4	0.6
7	357	338	365	99.0	1.0
10	371	347	377	98.0	2.0
12	366	348	378	99.1	0.9
15	374	358	386	98.4	1.6
20	381	365	393	98.7	1.3
25	375	360	389	99.1	0.9
30	382	368	398	98.9	1.1

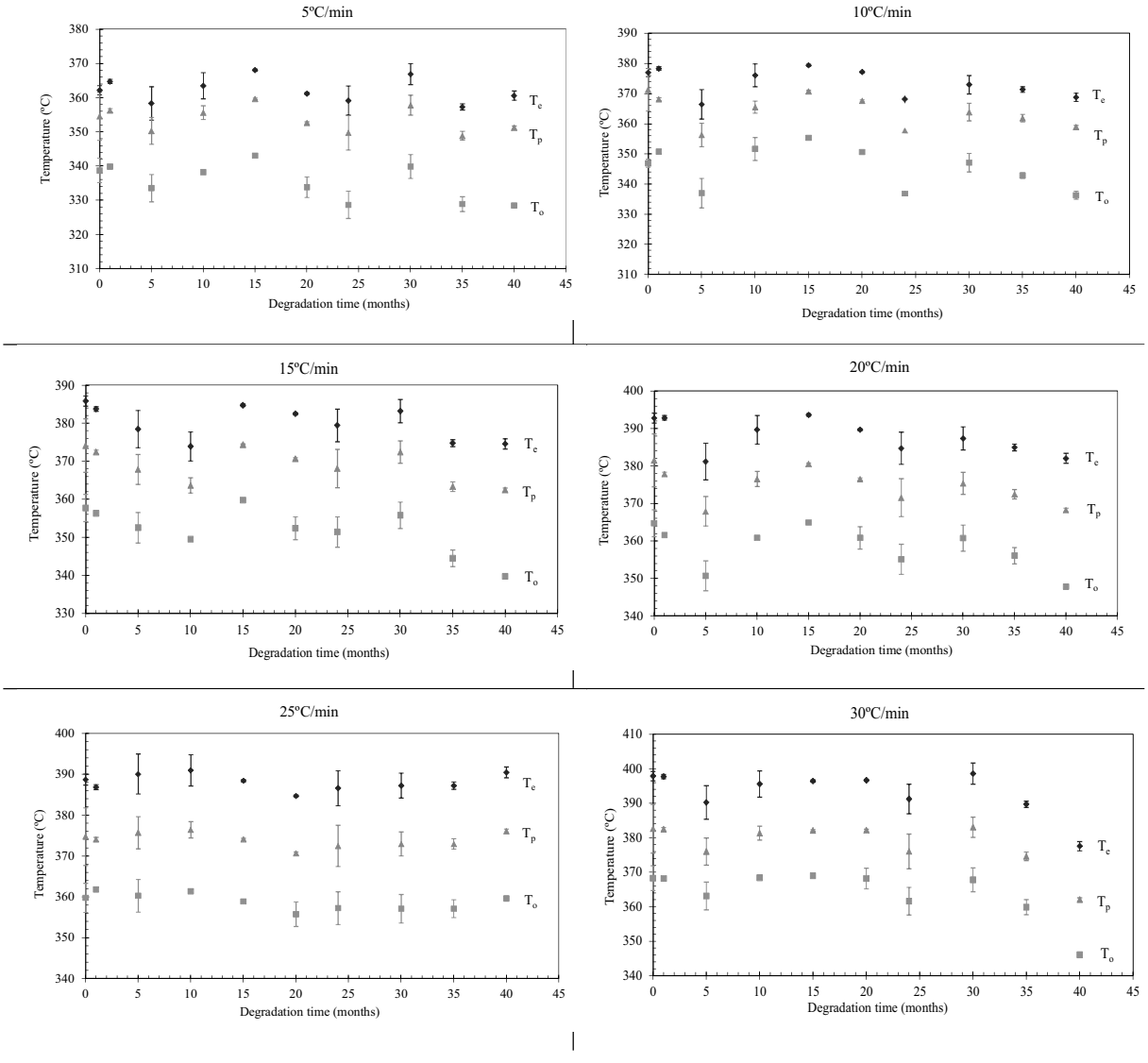

Figure 4-35 Variation of temperatures for the biodegraded samples at different heating rates.

The characteristic temperatures, obtained at β=10ºC/min, were plotted versus time and versus molar mass to study their influence of each degradation process.

The temperature results corresponding to the thermally degraded samples at 220ºC are plotted in Figure 4-36. All temperatures calculated from the TG and DTG curves undergo an increase after 30 minutes of thermal degradation at 220ºC, followed by a decrease (t = 62 min), reaching similar values as pellets at 330 min.

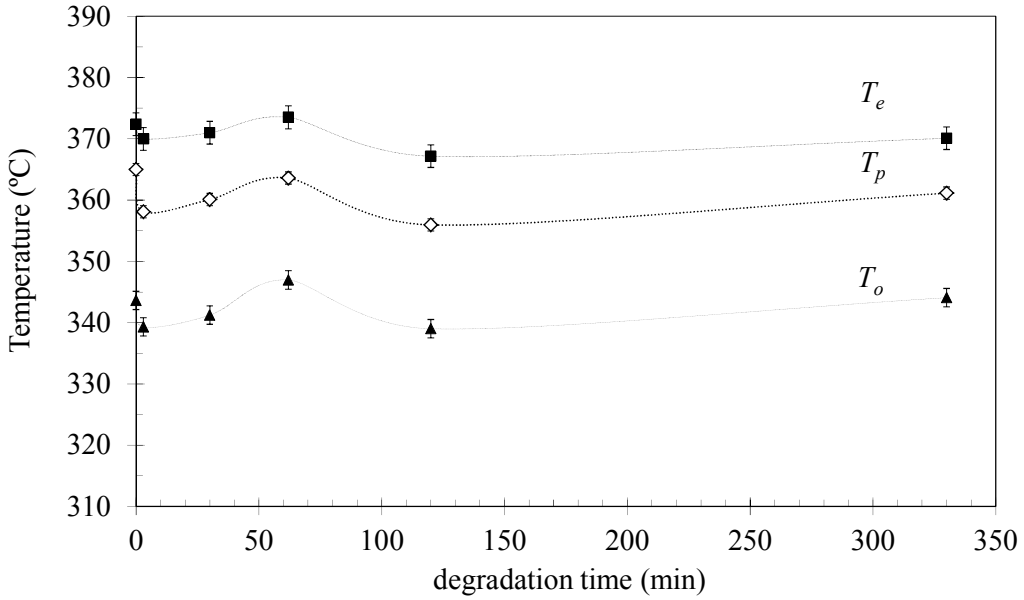

Figure 4-36 Thermal stability versus time at 10ºC/min for the thermally degraded samples at 220ºC.

The thermal parameters corresponding to the thermal decomposition of the biodegraded samples (including the plates and pellets) at 10ºC/min are plotted as a function of time in Figure 4-37. The degradation in soil did not provoke significant changes in the representative temperatures ($\Delta T \leq 8$ºC), although a sinusoidal tendency is observed, reaching a maximum at 15 months. It is worth noting that all these parameters show not very different values after 60 months of degradation, compared to the initial values (plates).

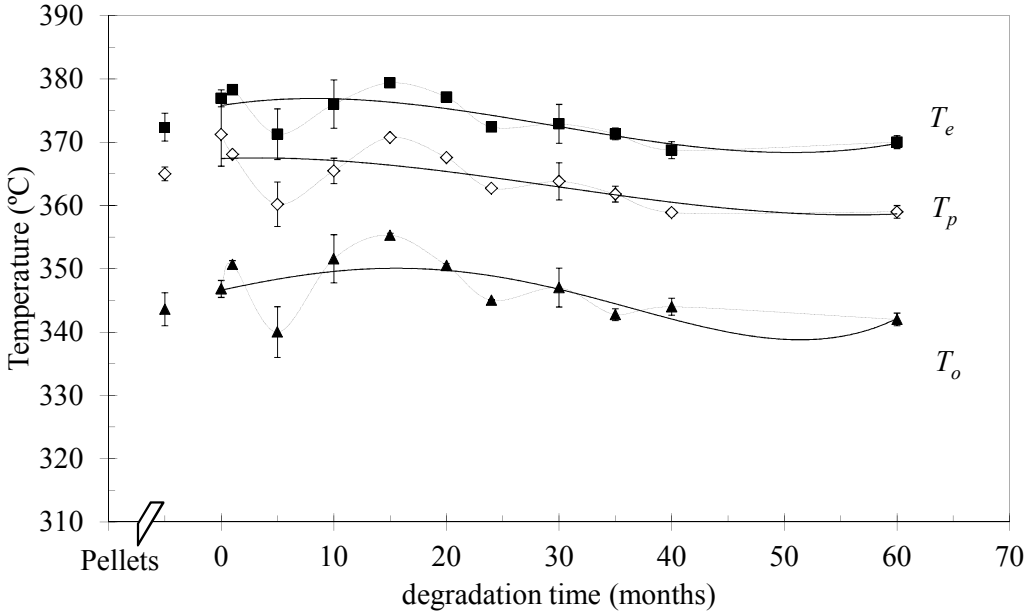

Figure 4-37 Thermal stability versus time for the biodegraded samples, pellets, and plates.

Figure 4-38 shows the evolution of T_o, T_p and T_e with the photodegradation time (at β=10ºC/min). The temperatures exhibit a sinusoidal trend with time and after 5 months of exposure a decrease in all the temperatures was observed. This fact was especially visible for T_o and T_p, which undergo decreases of 15ºC and 10ºC respect to the plates respectively.

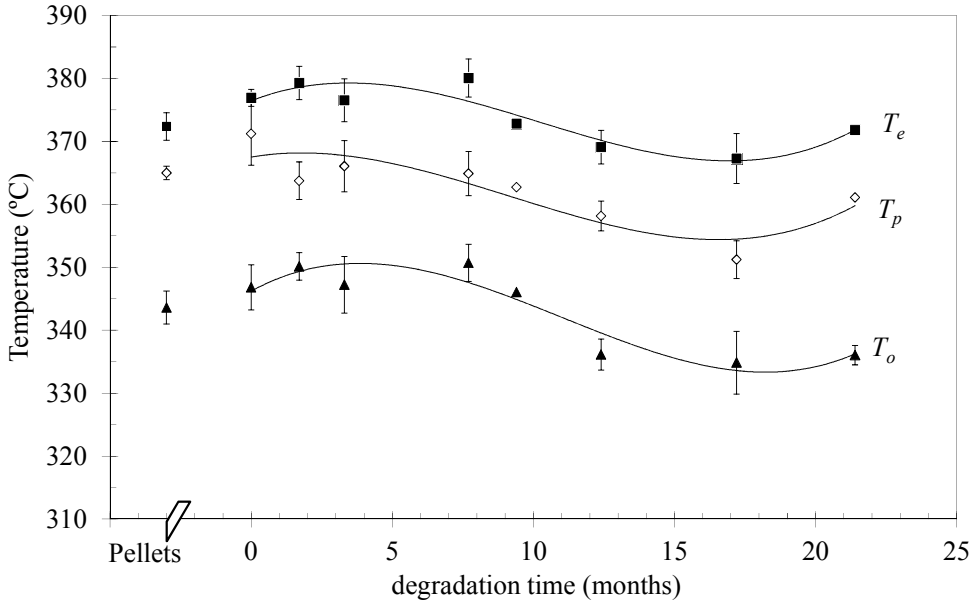

Figure 4-38 Thermal parameters versus time (β=10ºC/min) for the photodegraded samples, plates and pellets.

The temperatures related to the thermal decomposition of the degraded PLA samples showed sinusoidal behavior, and this was observed for all the types of degradation. This fact, which was especially visible in the T_o values of the photodegraded samples, was reported by other authors in the degradation studies of several polymers [45,46]. The results also suggest that photodegradation seems to cause the most marked effects on the thermal stability of PLA.

The variation on the thermal decomposition parameters with the molar mass is now studied. The parameter T_o, T_p and T_e (as obtained at β = 10ºC/min) are plotted as a function of the molar mass from Figure 4-38 to Figure 4-41.

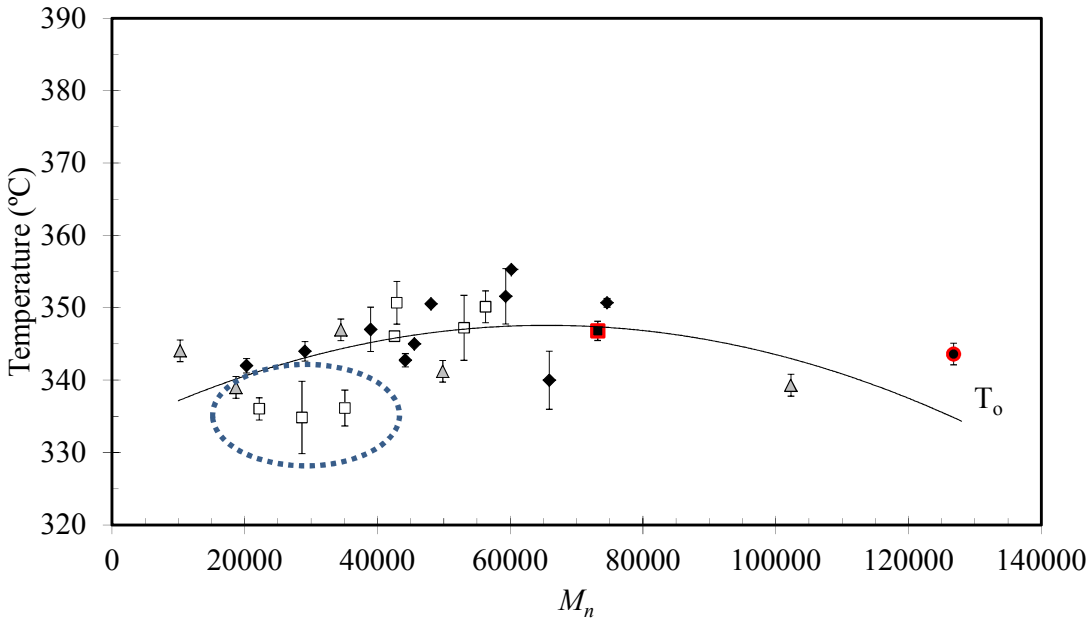

Figure 4-39 T_o vs. M_n at 10ºC/min for (●) Pellets, (■) Plates, (△) Thermal degradation (◆) Biodegradation and (□) Photodegradation.

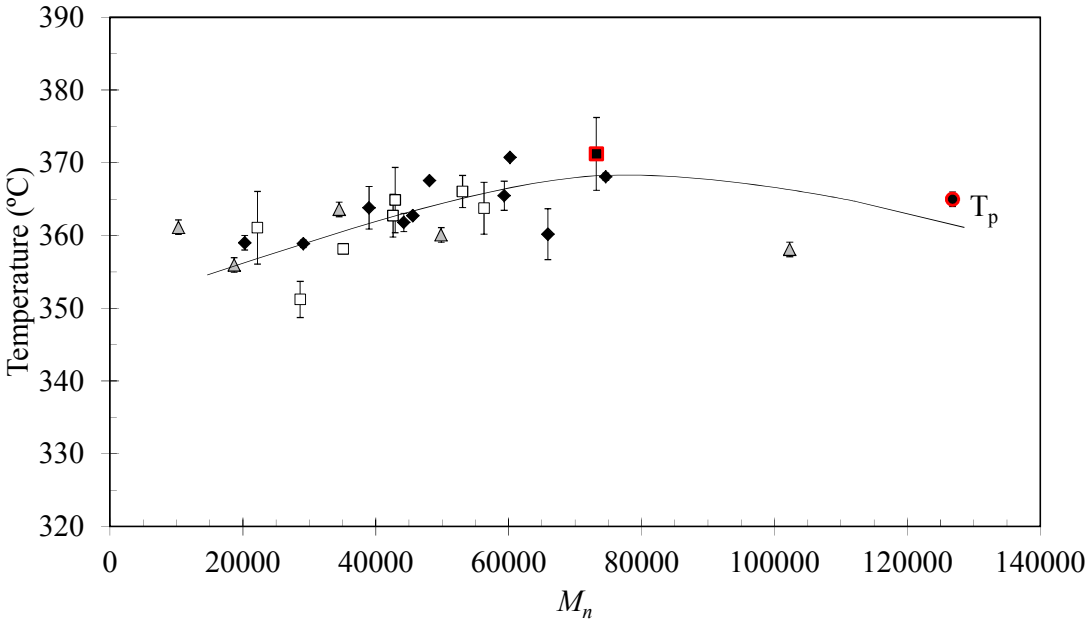

Figure 4-40 T_p vs. M_n at 10ºC/min for (●) Pellets, (■) Plates, (△) Thermal degradation (◆) Biodegradation and (□) Photodegradation.

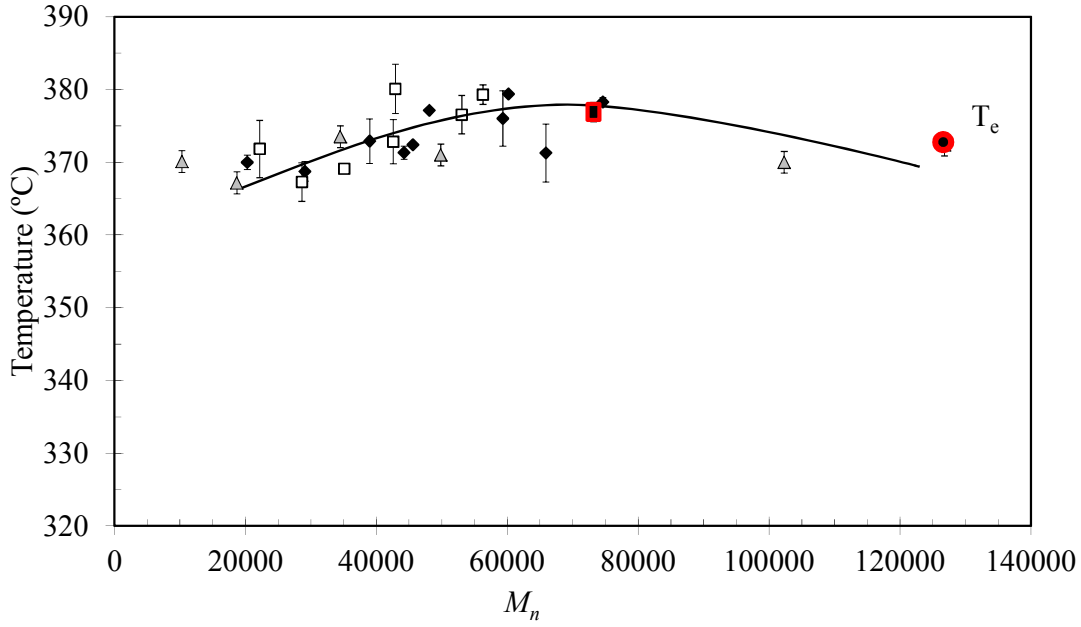

Figure 4-41 T_e vs. M_n at 10ºC/min for (●) Pellets, (■) Plates, (△) Thermal degradation (◆) Biodegradation and (□) Photodegradation.

In general, the profile of all the temperatures seems to follow a common pattern with molar mass regardless of the degradation process, with a maximum at around 60000. Temperature variations are in the ΔT = 10ºC range. However in the case of the thermal degraded samples is practically negligible. The minimum values are observed for T_o of photodegraded samples at small M_n, as Figure 4-39 showed.

All these results suggest that the molar decay controls the thermal stability of the PLA samples, regardless of the degradation type. The results also indicate that any of the temperatures (T_o, T_p and T_e) can be chosen as representative parameters of the thermal decomposition of the samples.

4.3.2 Kinetic analysis

Further analysis was therefore carried out to establish good indicators which correlate the thermal decomposition behavior of PLA with the different degradation processes.

Polylactide presents one single thermal decomposition process (see Figure 4-31) but is considered to involve several complex reactions [47]. Several kinetic models are available in the literature to describe the thermal decomposition of polymers. In general these models do not consider in-depth the description of the chemistry involved in the thermal decomposition and describe the process by rather simplified reaction pathways. The kinetic behavior is governed by the kinetic triplet (ln(A), Ea, $f(\alpha)$, see Chapter 3, The theoretical decomposition mechanisms and their mathematical models, the so-called kinetic functions $f(\alpha)$ were given in Table 3-1.

The apparent activation energy (Ea) of the PLA thermal decomposition was assessed by the Kissinger (Ea_K), Friedman (Ea_F) and Flynn-Wall-Ozawa (Ea_{FWO}) methods, which do not require assumption of any conversion model. The analyses were focused in the conversion degree (α) range of 0.2 and 0.7, since the main mass loss decomposition process occurs in this range.

The fit of the data to the different methods was very accurate and linear trends were obtained for all the samples under study, regardless of the particular degradation processes. Figure 4-42 and Figure 4-43 show the application of these methods to the pellets and plates, respectively.

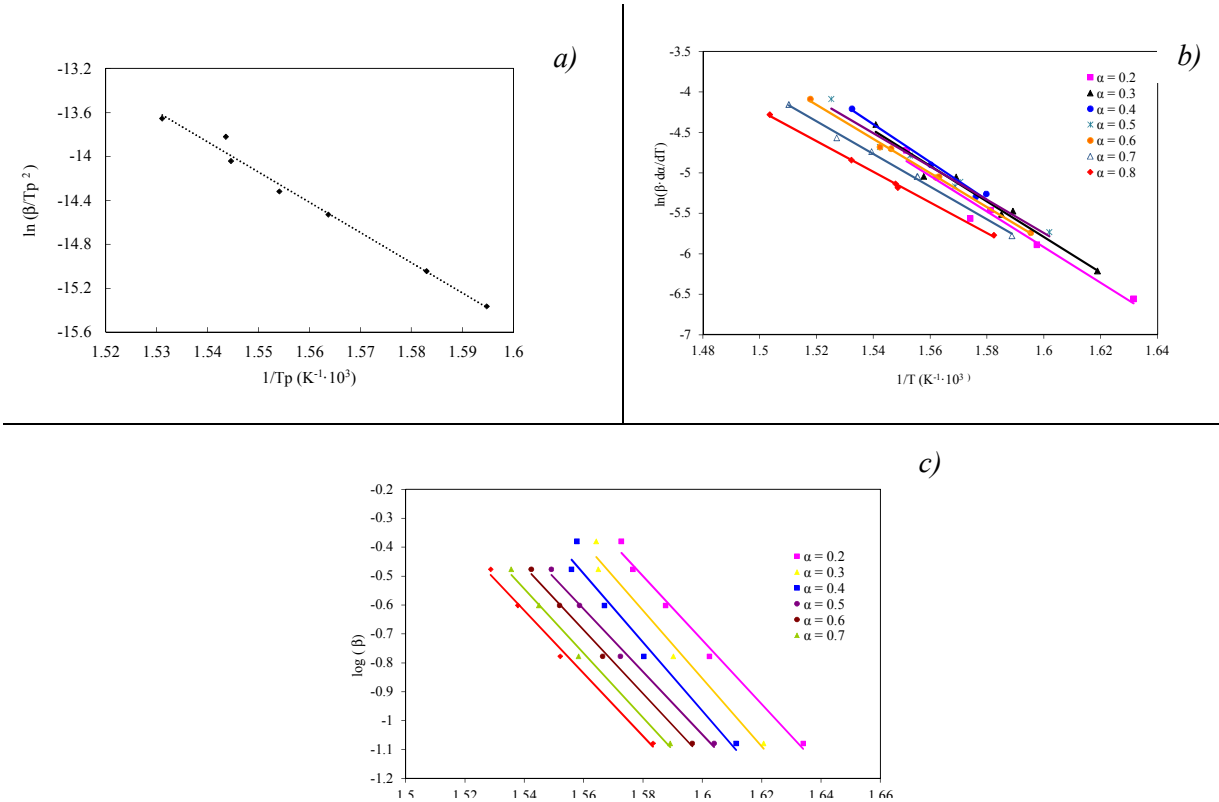

Figure 4-42 Kinetic methods applied to pellets *a*) Kissinger, *b*) Friedman and *c*) Flynn-Wall-Ozawa.

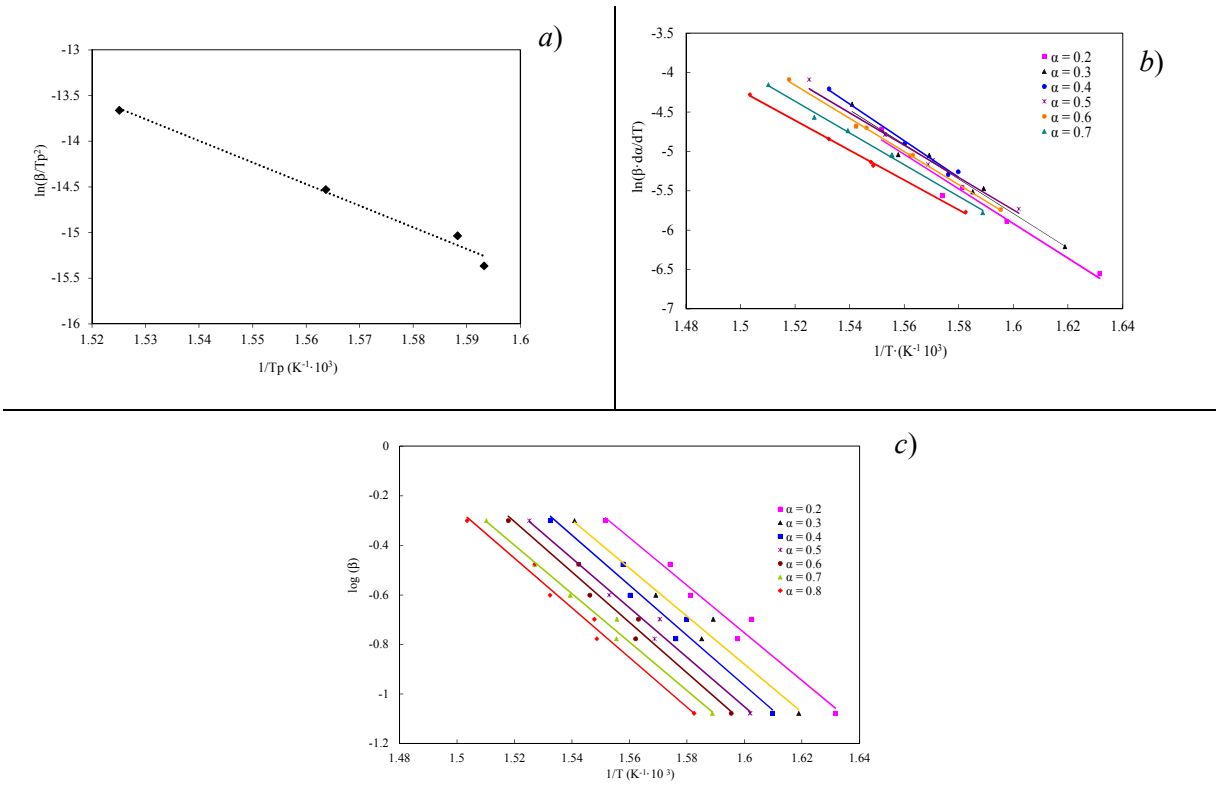

Figure 4-43 Kinetic methods applied to plates: *a*) Kissinger, *b*) Friedman and *c*) Flynn-Wall-Ozawa.

The application of the Kissinger, Friedman and Flynn-Wall-Ozawa methods provided good fits, in the case of all the PLA samples. For selected examples, samples submitted to each kind of degradation are plotted in Figures 4-44, 4-45 and 4-46 (thermally, bio and photo degraded samples, respectively).

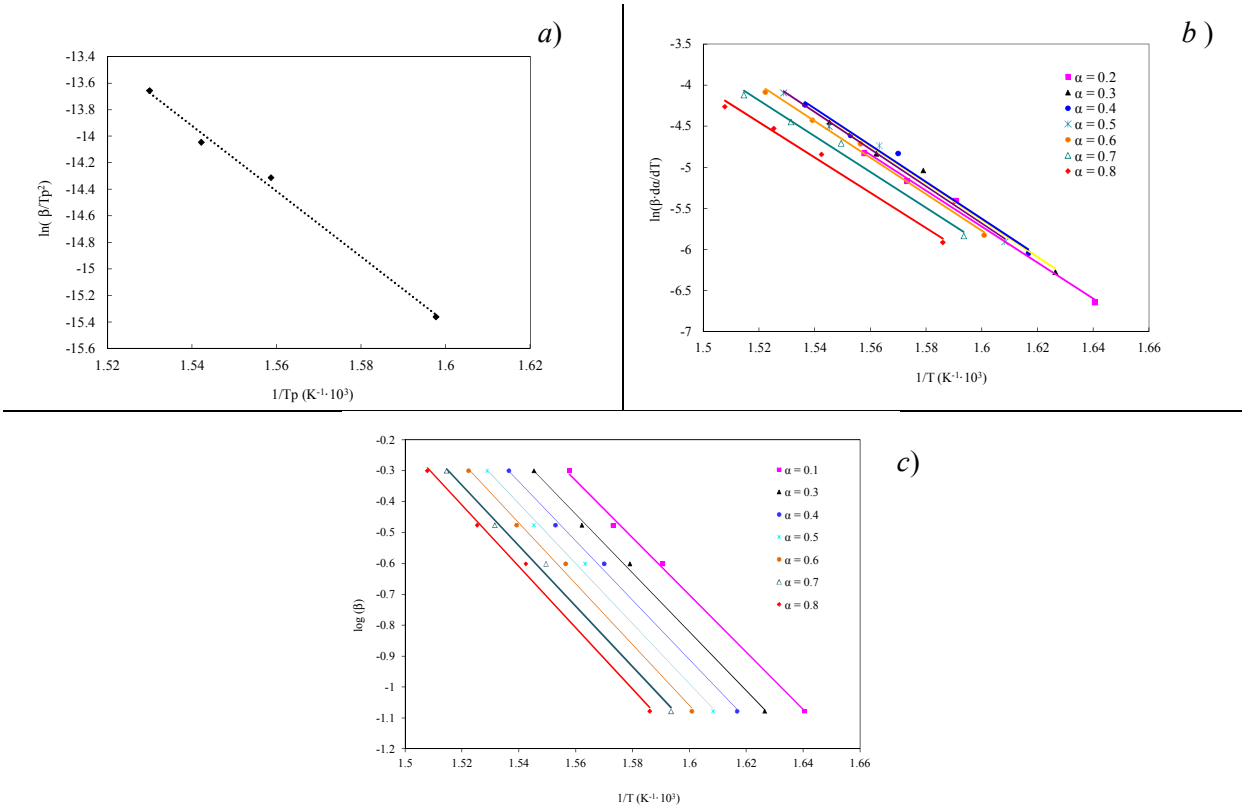

Figure 4-44 Kinetic methods applied to the 3 min sample *a*) Kissinger, *b*) Friedman and *c*) Flynn-Wall-Ozawa.

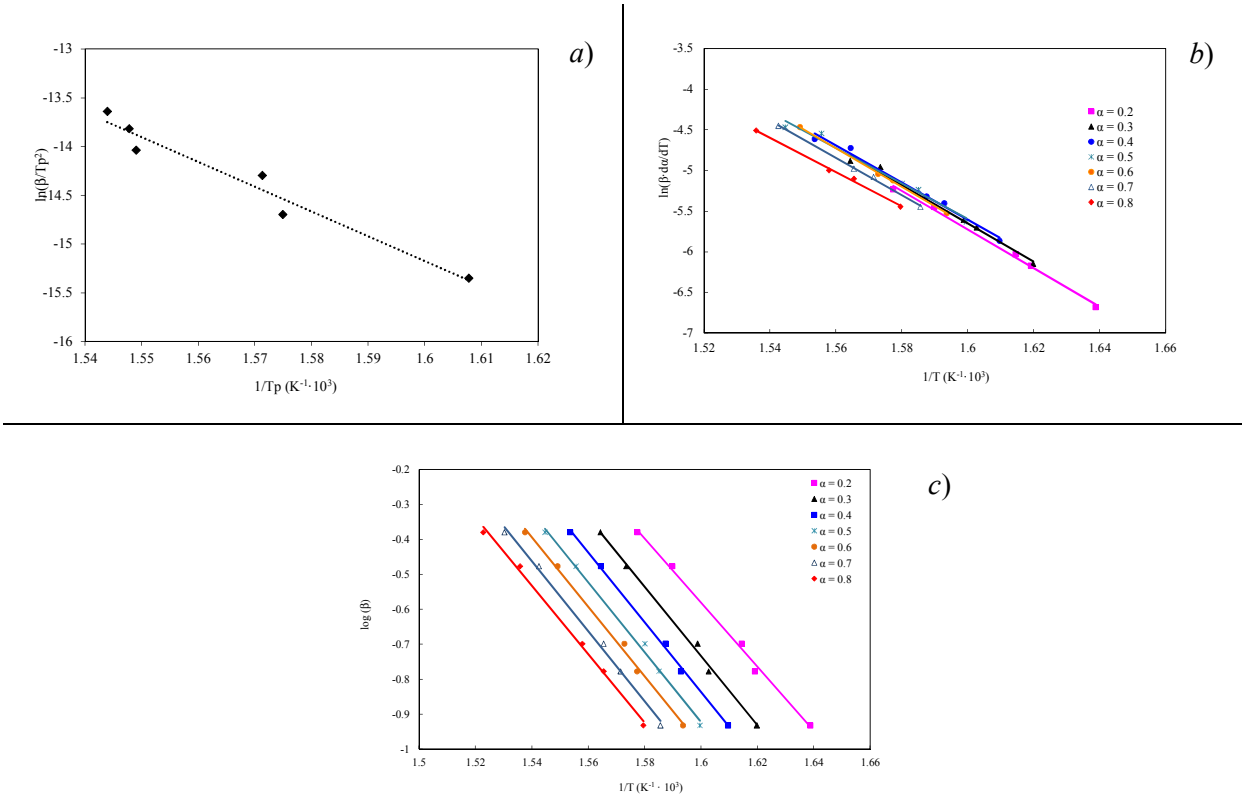

Figure 4-45 Kinetic methods applied to the 35 m sample: *a*) Kissinger, *b*) Friedman and *c*) Flynn-Wall-Ozawa.

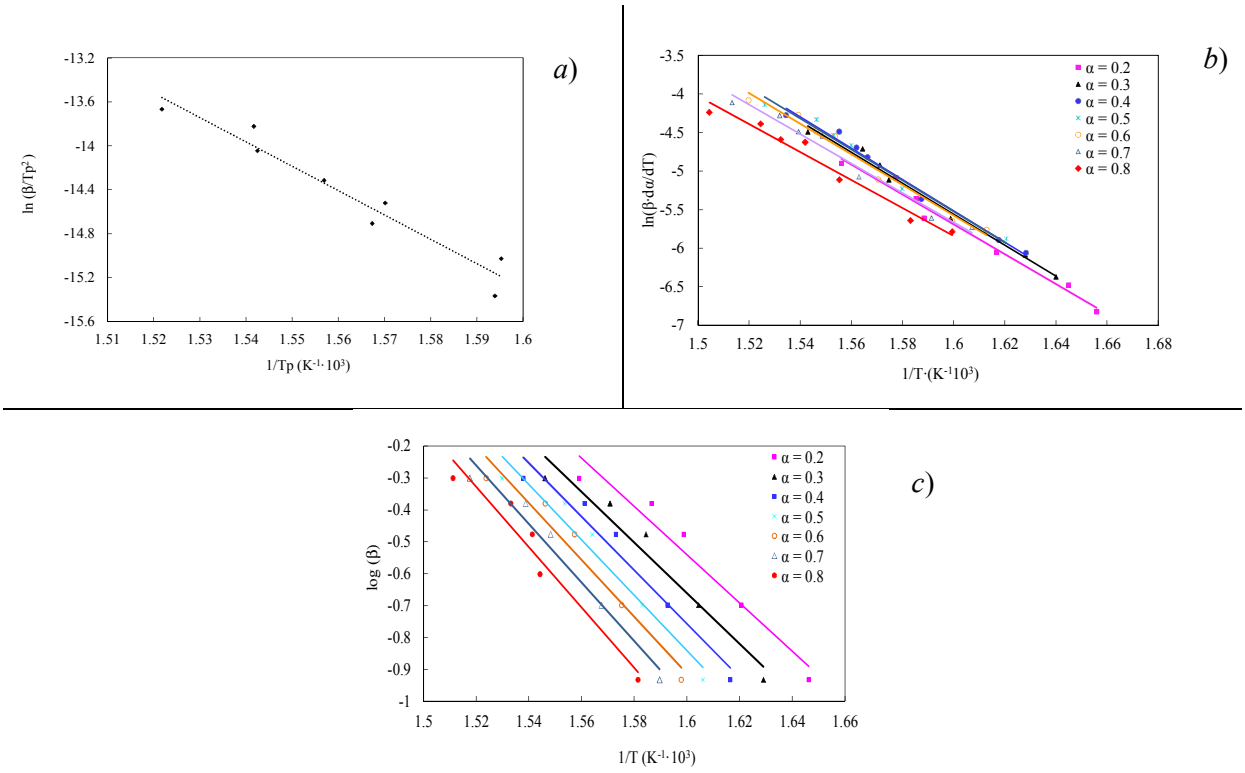

Figure 4-46 Kinetic methods applied to the-400h-1.7m sample *a*) Kissinger, *b*) Friedman method and *c*) Flynn-Wall-Ozawa method.

The results of the apparent activation energy, *Ea*, obtained from these methods are displayed in Tables 4-12, 4-13 and 4-14 for the thermal, bio and photo degradation, respectively.

Table 4-12 Apparent activation energies (Ea_F, Ea_{FWO}, Ea_K) for the thermally degraded samples.

	Pellets			3 min			30 min		
α	Ea_F kJ/mol	Ea_{FWO} kJ/mol	Ea_K kJ/mol	Ea_F kJ/mol	Ea_{FWO} kJ/mol	Ea_K kJ/mol	Ea_F kJ/mol	Ea_{FWO} kJ/mol	Ea_K kJ/mol
0.2	210	201		182	168		219	181	
0.3	207	214		186	173		216	185	
0.4	202	216		186	175		206	176	
0.5	205	197	**229**	188	176	**205**	198	179	**226**
0.6	204	200		185	179		179	173	
0.7	210	202		181	178		156	-	
Average	**206**	**205**		**185**	**175**		**196**	**179**	

	62 min			120 min			330 min		
α	Ea_F kJ/mol	Ea_{FWO} kJ/mol	Ea_K kJ/mol	Ea_F kJ/mol	Ea_{FWO} kJ/mol	Ea_K kJ/mol	Ea_F kJ/mol	Ea_{FWO} kJ/mol	Ea_K kJ/mol
0.2	182	168		155	-		164	153	
0.3	186	172		169	169		172	161	
0.4	182	175		176	170		169	164	
0.5	179	176	**197**	180	173	**194**	163	165	**192**
0.6	176	177		176	170		161	165	
0.7	170	177		170	171		154	165	
Average	**179**	**174**		**171**	**171**		**164**	**162**	

Table 4-13 Apparent activation energies (Ea_F, Ea_{FWO}, Ea_K) for the biodegraded samples.

	Plates			1 m			5 m		
α	Ea_F kJ/mol	Ea_{FWO} kJ/mol	Ea_K kJ/mol	Ea_F kJ/mol	Ea_{FWO} kJ/mol	Ea_K kJ/mol	Ea_F kJ/mol	Ea_{FWO} kJ/mol	Ea_K kJ/mol
0.2	183	175		178	152		189	170	
0.3	183	176		186	157		179	177	
0.4	194	184		183	160		199	179	
0.5	171	182	**197**	181	165	**192**	197	177	**204**
0.6	175	185		173	167		194	180	
0.7	167	178		160	165		186	177	
Average	**179**	**180**		**177**	**161**		**191**	**177**	

	10 m			15 m			20 m		
α	Ea_F kJ/mol	Ea_{FWO} kJ/mol	Ea_K kJ/mol	Ea_F kJ/mol	Ea_{FWO} kJ/mol	Ea_K kJ/mol	Ea_F kJ/mol	Ea_{FWO} kJ/mol	Ea_K kJ/mol
0.2	186	168		177	168		198	194	
0.3	192	169		176	172		202	200	
0.4	197	173		173	174		206	204	
0.5	199	176	**215**	168	177	**174**	205	206	**195**
0.6	197	180		161	177		210	209	
0.7	197	192		151	171		205	210	
Average	**195**	**176**		**168**	**173**		**204**	**204**	

	24 m			30 m			35 m		
α	Ea_F kJ/mol	Ea_{FWO} kJ/mol	Ea_K kJ/mol	Ea_F kJ/mol	Ea_{FWO} kJ/mol	Ea_K kJ/mol	Ea_F kJ/mol	Ea_{FWO} kJ/mol	Ea_K kJ/mol
0.2	171	143		196	186		197	167	
0.3	186	155		197	191		196	180	
0.4	175	158		204	195		190	181	
0.5	173	159	**190**	205	197	**219**	181	182	**211**
0.6	172	160		207	201		197	181	
0.7	162	164		209	203		190	182	
Average	**173**	**156**		**203**	**195**		**192**	**179**	

	40 m			60 m		
α	Ea_F kJ/mol	Ea_{FWO} kJ/mol	Ea_K kJ/mol	Ea_F kJ/mol	Ea_{FWO} kJ/mol	Ea_K kJ/mol
0.2	158	160		196	156	
0.3	162	158		202	174	
0.4	159	157		204	180	
0.5	157	176	**198**	195	183	**232**
0.6	161	179		198	189	
0.7	159	179		191	187	
Average	**159**	**168**		**198**	**178**	

Table 4-14 Apparent activation energies (Ea_F, Ea_{FWO}, Ea_K) for the photodegraded samples.

	400h-1.7m			800h-3.3m			1850h-7.7m		
α	Ea_F kJ/mol	Ea_{FWO} kJ/mol	Ea_K kJ/mol	Ea_F kJ/mol	Ea_{FWO} kJ/mol	Ea_K kJ/mol	Ea_F kJ/mol	Ea_{FWO} kJ/mol	Ea_K kJ/mol
0.2	163	137		161	143		193	185	
0.3	200	144		166	146		195	191	
0.4	209	153		169	151		155	192	
0.5	225	158	185	167	152	163	161	195	184
0.6	199	162		165	155		194	190	
0.7	197	167		159	156		148	194	
Average	**199**	**154**		**164**	**150**		**174**	**191**	

	2250h-9.4m			3000h-12.6m			4100h-17.2m		
α	Ea_F kJ/mol	Ea_{FWO} kJ/mol	Ea_K kJ/mol	Ea_F kJ/mol	Ea_{FWO} kJ/mol	Ea_K kJ/mol	Ea_F kJ/mol	Ea_{FWO} kJ/mol	Ea_K kJ/mol
0.2	191	184		179	162		131	-	
0.3	188	189		191	168		146	122	
0.4	185	195		195	176		155	128	
0.5	183	190	**209**	196	180	**187**	163	133	**170**
0.6	180	192		198	188		166	136	
0.7	170	187		192	186		171	142	
Average	**183**	**189**		**192**	**177**		**155**	**132**	

Figures 4-47 to 4-49 show the dependence of the average apparent activation energy values, obtained by the different isoconversional methods (Tables 4-12 to 4-14), with the degradation time. The results corresponding to the PLA pellets and plates are also displayed.

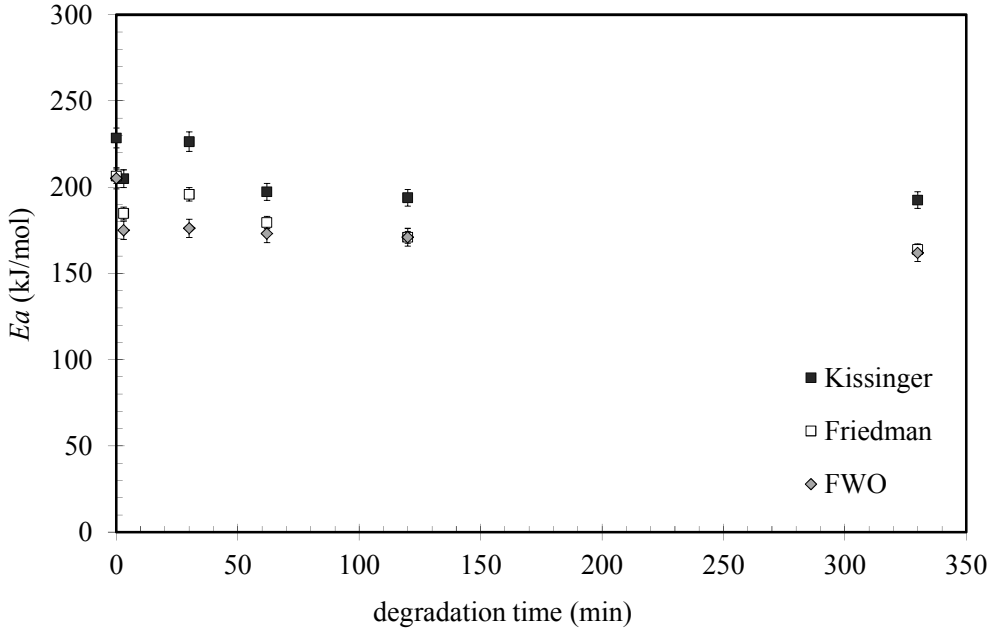

Figure 4-47 Plot of Ea_K and Ea_F, Ea_{FWO} versus time for the thermally degraded samples (pellets correspond to t = 0).

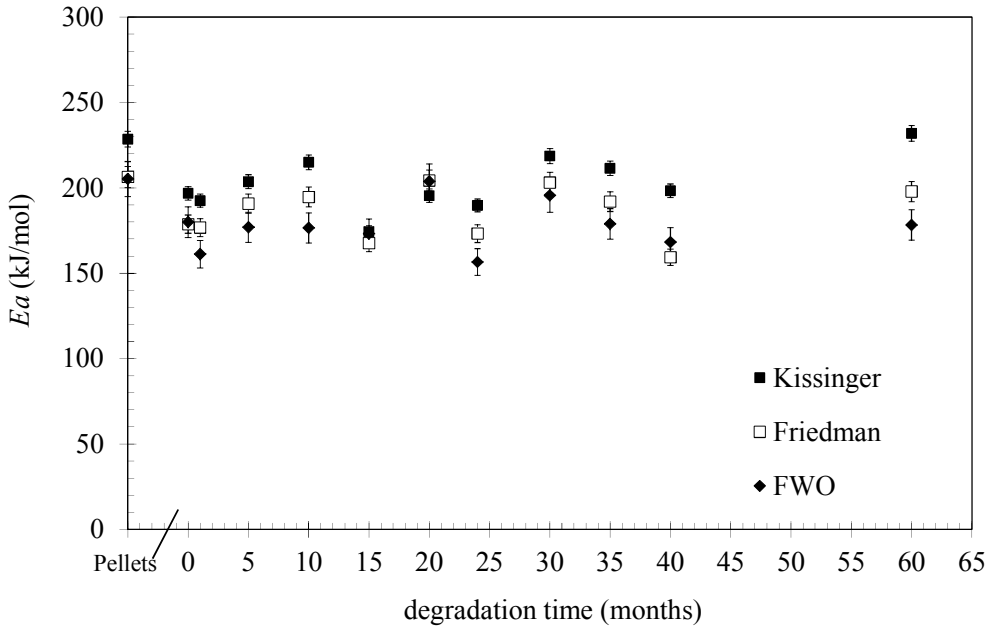

Figure 4-48 Plot of Ea_K and Ea_F, Ea_{FWO} versus time for the biodegraded samples (plates correspond to t = 0)

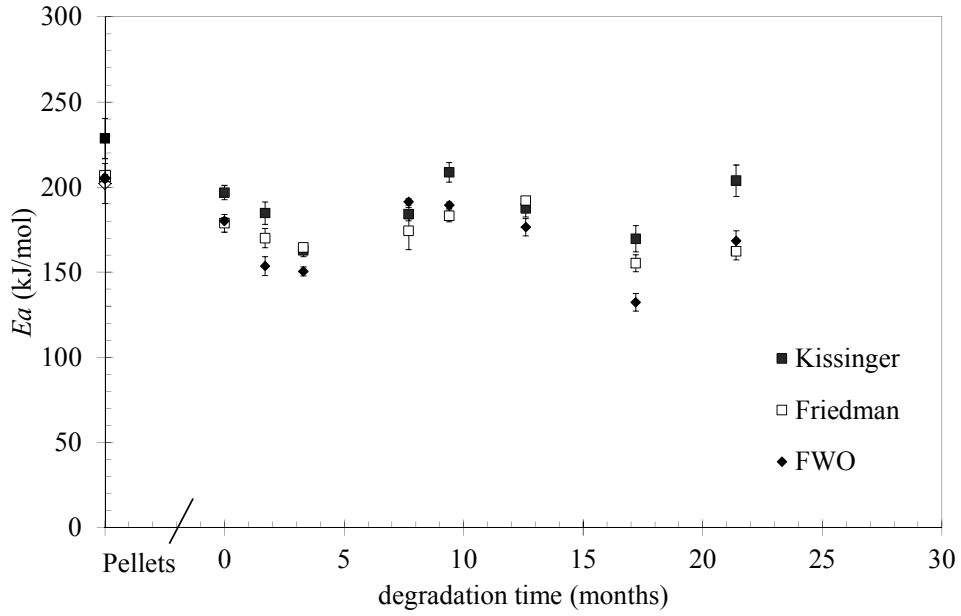

Figure 4-49 Plot of Ea_K and Ea_F, Ea_{FWO} versus time for the photodegraded samples (plates correspond to t = 0).

The three methods provide similar trends of *Ea*, and this is applicable to all the degradation types and samples, although the Kissinger values are usually higher than the others. Thermal degradation promotes a decrease in the apparent activation energies of PLA. This is visible by comparing the *Ea* values of pellets and plates, and also when the pellets are further degraded at different times (Figure 4-47). On the other hand, sinusoidal shapes of *Ea* are obtained in the bio and photo degraded samples. Taking the plates as the reference, biodegraded samples undergo a slight increase in *Ea* values after 60 months degradation, while the results for the photodegraded samples show no appreciable variations after 21 months of exposure.

The same *Ea* results were evaluated respect to the molar mass decay. Since all the methods provide activation energy values following the same trend with degradation time, and the variations of *Ea* within different methods were not higher than 12%, an average apparent activation energy was calculated as $Ea_{iso} = (Ea_K + Ea_F + Ea_{FWO})/3$. The values of Ea_{iso} and the corresponding standard deviations (SD) were summarized in Table 4-15.

Table 4-15 Average apparent activation energies Ea_{iso}

Samples	Ea_{iso} kJ/mol	*SD*
Pellets	213	13
Plates	185	10
Thermally degraded		
3 min	188	15
30 min	200	24
62 min	183	12
120 min	167	25
330 min	173	17
Biodegraded		
1 m	177	16
5 m	190	13
10 m	195	19
15 m	172	4
20 m	201	5
24 m	176	17
30 m	206	12
35 m	194	16
40 m	175	20
60 m	203	23
Photodegraded		
400h-1.7m	179	23
800h-3.3m	159	8
1850h-7.7m	183	9
2250h-9.4m	193	6
3000h-12.6m	185	8
4100h-17.2m	152	19
5100h-21.4m	178	22

Figure 4-50 to 4-52 show the evolution of the average apparent activation energy for the thermally, bio and photo degraded PLA respectively, which ranged from 150 to 215 kJ/mol.

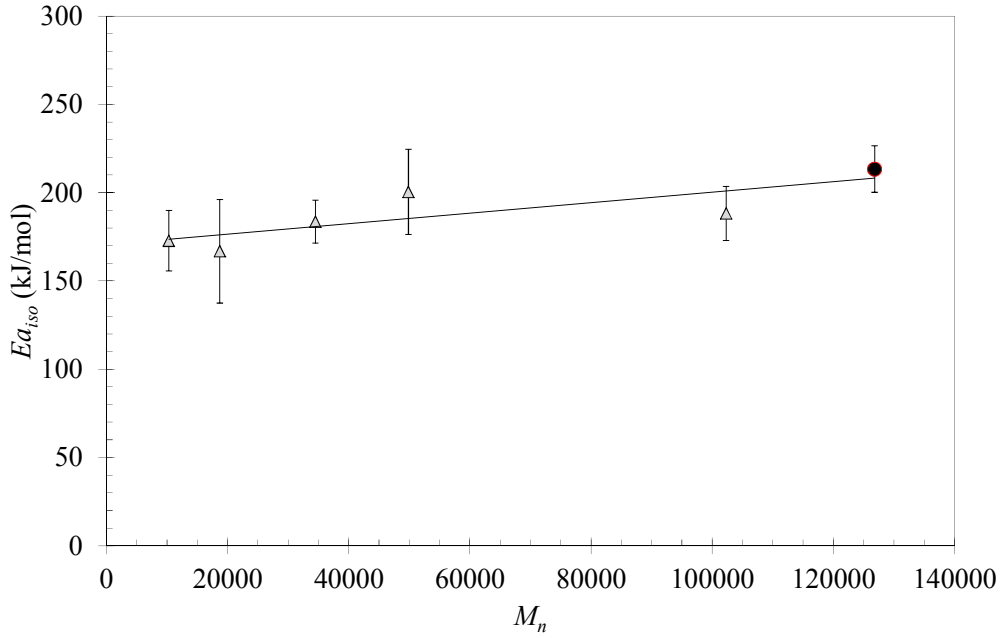

Figure 4-50 Ea_{iso} versus M_n for the thermally degraded samples.

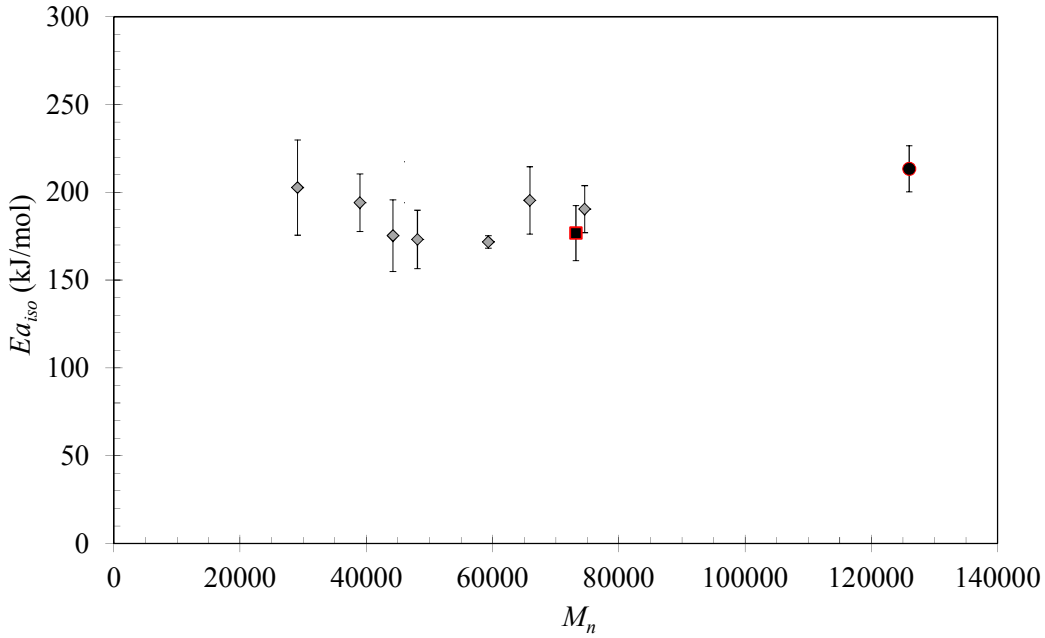

Figure 4-51 Ea_{iso} versus M_n for the for the biodegraded samples, (●) Pellets and (■) Plates

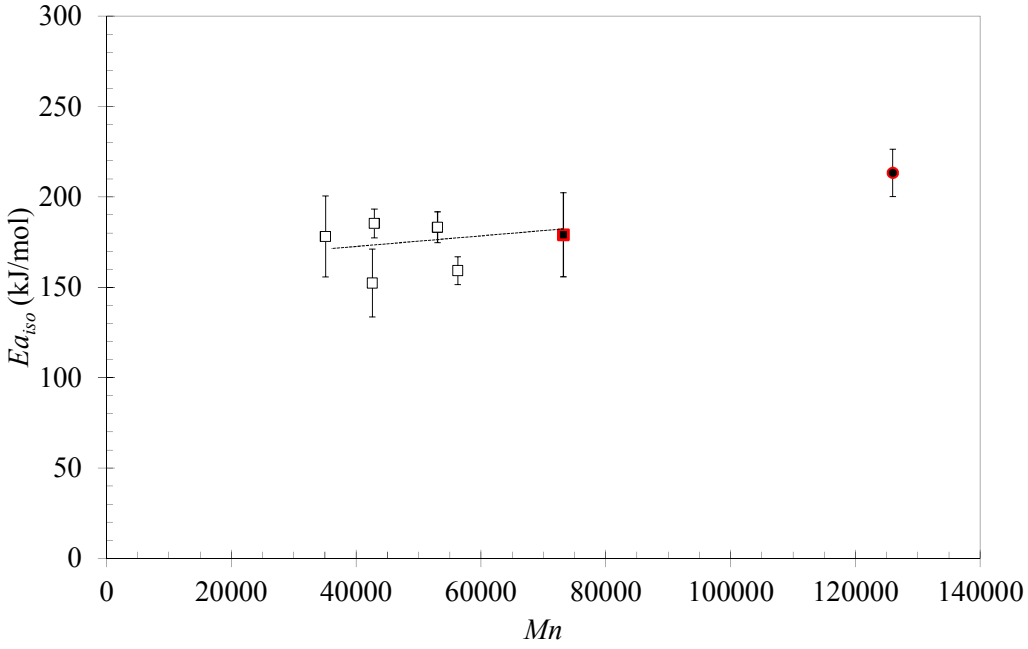

Figure 4-52 Ea_{iso} versus M_n for the photodegraded samples, (●) Pellets and (■) Plates

All the degradation processes promote a decrease in the Ea_{iso} values, respect to the PLA pellets, and such reduction can be approached to a linear trend with M_n. This result is according to different previous studies in polylactide of thermally degraded samples [48,49,50]. Processing PLA plates (from pellets) provokes a reduction of 13 % on Ea_{iso} and thermal degradation at long times promotes a further reduction in Ea_{iso} of 19% (after 330 min at 220ºC). On the other hand, less acute reductions in Ea_{iso} are observed for samples submitted to photodegradation respect to plates (4%) and in the case of biodegradation, Ea_{iso} show a slight increase (9%).

The Ea_{iso} values obtained for pellets and plates were 213 kJ/mol and 185 kJ/mol respectively. These activation energy values were compared with the 320 and **280 kJ/mol** obtained from TG data for unprocessed and **processed** polylactide respectively and by using Kissinger method considering n=1 [50]. This latest value of **280 kJ/mol** is 24% higher if comparing with Ea_{iso} 213 kJ/mol from pellets (similar M_n) and 19 % higher of Ea_K ~ 229 kJ/mol obtained for pellets by Kissinger method. Similarly, other types of isoconversional kinetic models for non-isothermal TG data, *Fan et al.* obtained Ea ~ 176 kJ/mol for comparable molar masses than plates [51,52].

In addition if comparing the Ea_{iso} values with the obtained in the section 4.1 (Figure 4-12) from the isothermal data, Ea_A ~105 kJ/mol is smaller than the obtained from thermogravimetric data (TG). These differences can be explained because the type of data analyzed. While a major decrease in chain length during thermal degradation of PLA is observed quickly after heating at relatively low temperatures, mass loss is not occurring till the temperature is greater than about 300°C. It is hence likely that to activate reactions favored at high temperatures that lead to volatile and small molecules requires much higher activation energy than for the ester cleavage and/or intramolecular esterification.

Criado method for calculating the kinetic function

The kinetic function, *f (α)*, was evaluated by a methodology combining the Criado method [53], which compares the experimental data to theoretical reduced master-curves, and the Coats-Redfern [54] method, which gives a linear fitting for a given kinetic model function. This methodology results in the selection of the *f (α)* function and ultimately completion of the kinetic triplet (*A*, *f (α)* and *Ea*) of the thermal decomposition.

The experimental normalized curve for the thermal decomposition of the PLA pellets is shown in Figure 4-53.

$$\frac{\mathrm{z}(\alpha)}{\mathrm{z}(0.5)} = \frac{f(\alpha)\cdot g(\alpha)}{f(0.5)\cdot g(\alpha)} = \left(\frac{T_\alpha}{T_{0.5}}\right)^2 \cdot \frac{(\frac{d\alpha}{dt})_\alpha}{(\frac{d\alpha}{dt})_{0.5}}$$

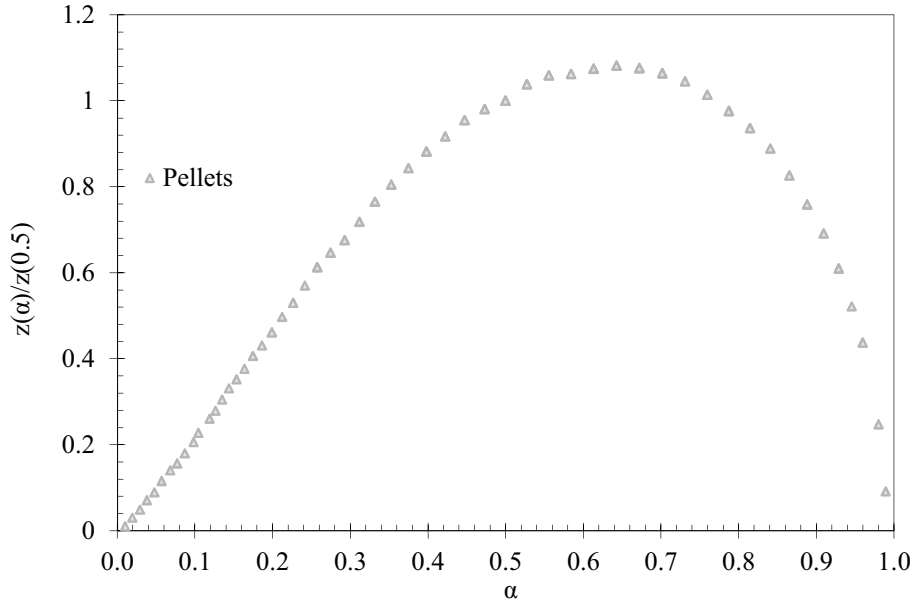

Figure 4-53 Plot of the Criado model for the pellets experimental data.

The theoretical curves, representing the different kinetic model functions, $f(\alpha)$ and $g(\alpha)$, were calculated as $\frac{\mathrm{z}(\alpha)}{\mathrm{z}(0.5)} = \frac{f(\alpha)\cdot g(\alpha)}{f(0.5)\cdot g(\alpha)}$, and are plotted versus α in Figure 4-54.

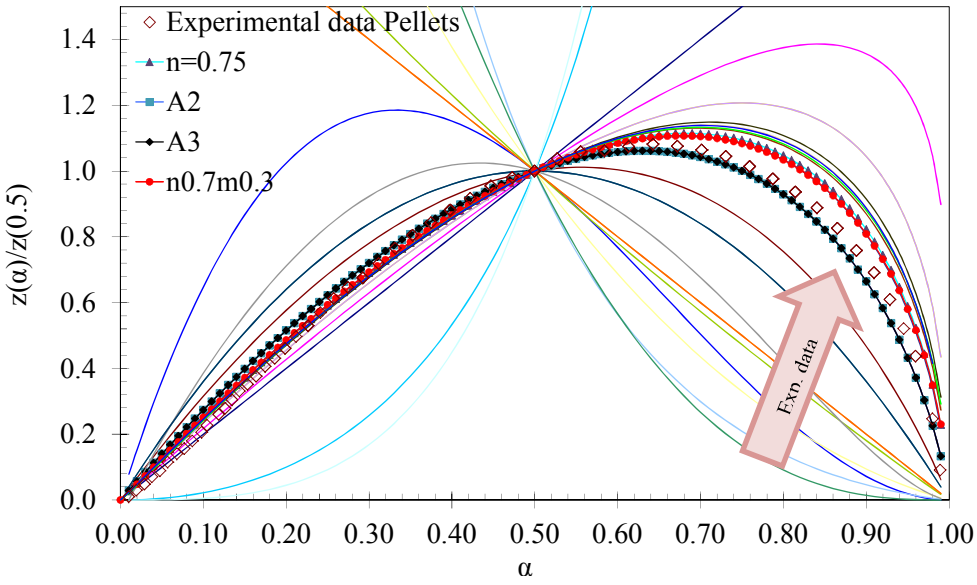

Figure 4-54 Criado method plot for pellets data and some of the kinetic model functions.

Four models were selected to fit with the experimental normalized curves of the pellets, and are shown in Table 4-17. The apparent activation energy for these models was calculated by the Coats-Redfern method (Ea_C). The A2 model provided most similar values for Ea_{iso} and Ea_C, and thus it was selected as the most appropriate to describe the thermal decomposition of PLA pellets (Figure 4-55).

Table 4-16 Results of kinetic methodology for pellets.

	Criado analysis	***Coats Redfern***			**Isoconversional analysis**
	***f (α)* scope reduction**	***Ea*$_C$ kJ/mol**	***ln (A)* (s^{-1})**	**R^2**	***Ea*$_{iso}$ kJ/mol**
Pellets	**A2**	**200**	**39.8**	**0.998**	213 ± 13
	A3	97	12.9	0.996	
	n0.7m0.3	200	33.7	0.997	
	n=0.75	289	50.0	0.997	

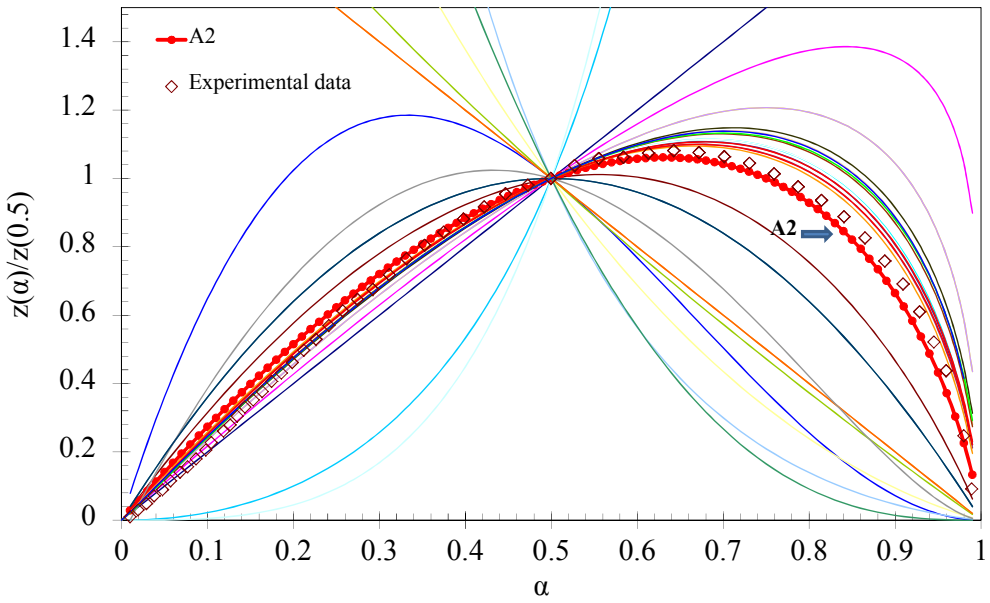

Figure 4-55 Criado plot for pellets and the selected kinetic function.

This kinetic model is quite common in crystallization processes, but has been also reported in thermal decomposition of polymers and in polylactide [55,56,57,58]. The A2 model suggests the presence of active zones (nuclei), more chemically liable to thermal decomposition [59]. Alternatively, when the Criado method is applied to plates, the results indicate the occurrence on an autocatalytic model (n = 0.65; m = 0.3), which has shown a better correlation with the experimental data than the A2 model (see Figure 4-56 and Table 4-17). Other approaches suggested that the kinetic function of polylactides of M_n=69000 to 43000 was $f(\alpha) = (1-\alpha)^n$ with an n varying from 0.63 to 1, depending on the method used and the molar mass [50].

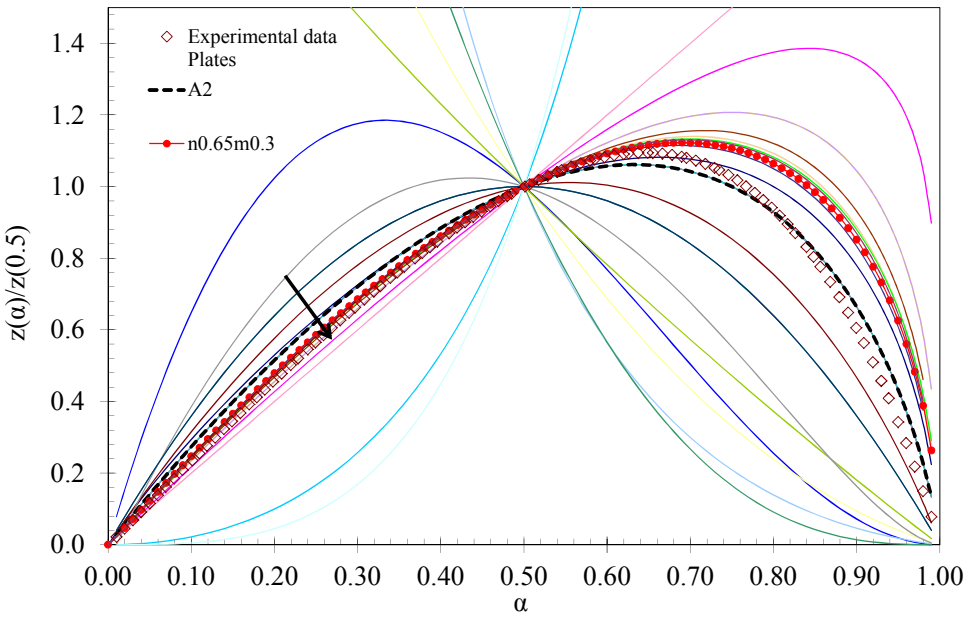

Figure 4-56 Criado plot for plates and some of the kinetic model functions.

Table 4-17 Results of kinetic methodology for plates.

	Criado analysis	*Coats Redfern*			Isoconversional analysis
	***f (α)* scope reduction**	***Ea*$_C$ kJ/mol**	***ln (A)* (s^{-1})**	**R^2**	***Ea*$_{iso}$ kJ/mol**
Plates	**n0.65m0.3**	**192**	**31.6**	**0.999**	185 ± 10
	n0.6m0.4	164	26.4	0.999	
	n0.7m0.1	221	37.0	0.998	
	A2	164	37.9	0.999	

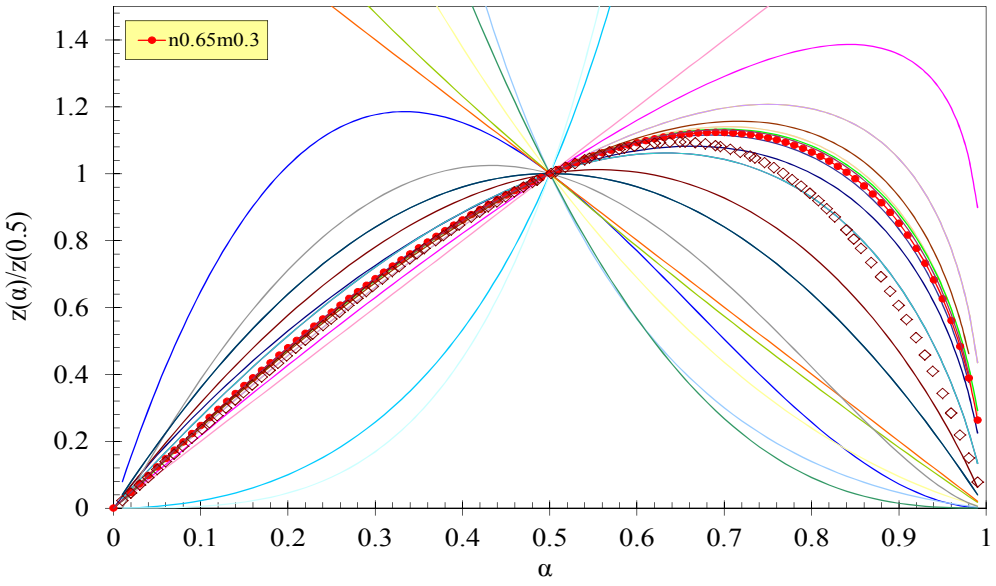

Figure 4-57 Criado plot for plates data and the selected kinetic function.

Figure 4-58 shows the experimental normalized curves for all the biodegraded samples. As degradation time advances, the $\frac{z(\alpha)}{z(0.5)}$ curves take lower values when α<0.5 (Figure 4-58 *b*) and higher when α>0.5 (Figure 4-58 *c*).

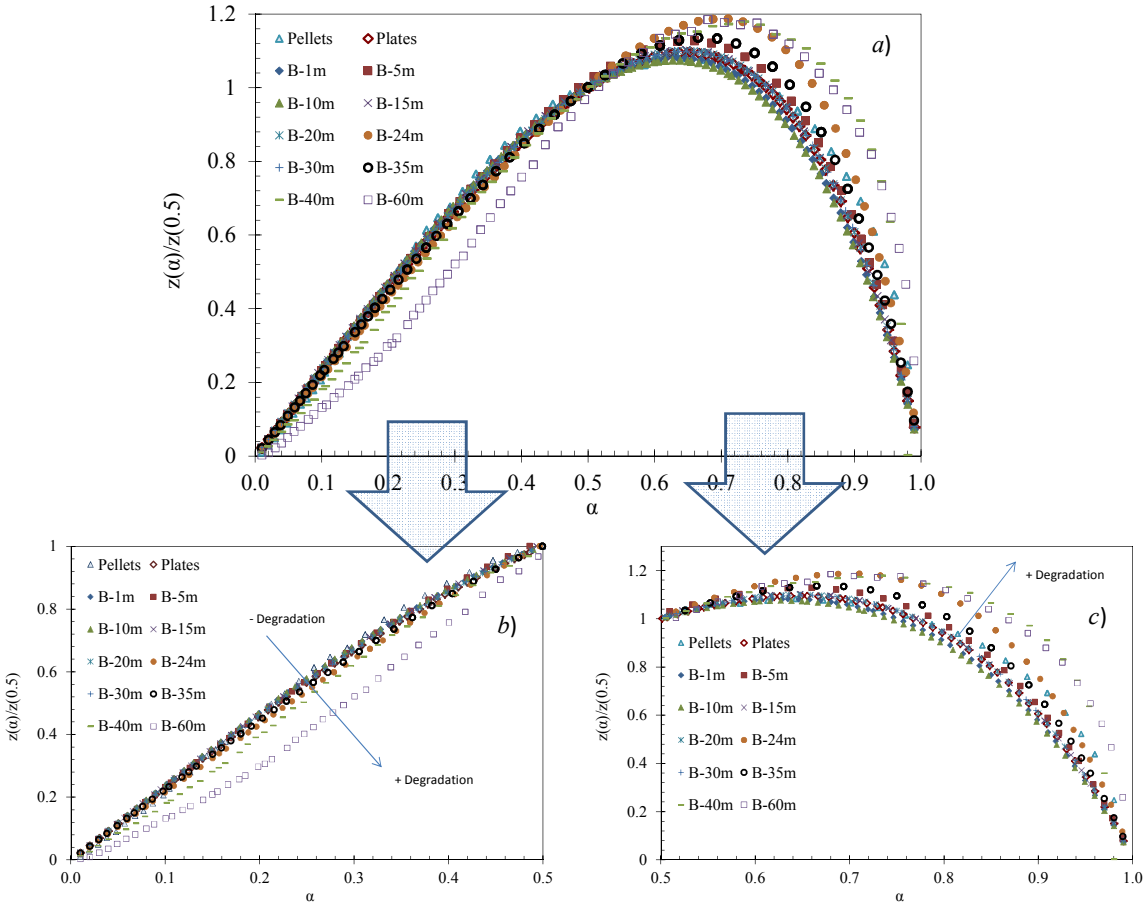

Figure 4-58 Criado curves for the experimental data of the biodegraded samples: general (*a*); *α<0.5 (b) and α>0.5 (c)*

Due to the high influence of the *n* and *m* exponents on the autocatalytic function, prior to the study of the kinetic function, *f(α)*, the effect of *n* and *m* on $f(\alpha) = \alpha^m(1-\alpha)^n$ was evaluated. When *m* is equal to zero the evolution of the kinetic models with *n* is plotted in Figure 4-59. As *n* increases, the maximum of the curve is shifted to lower α values.

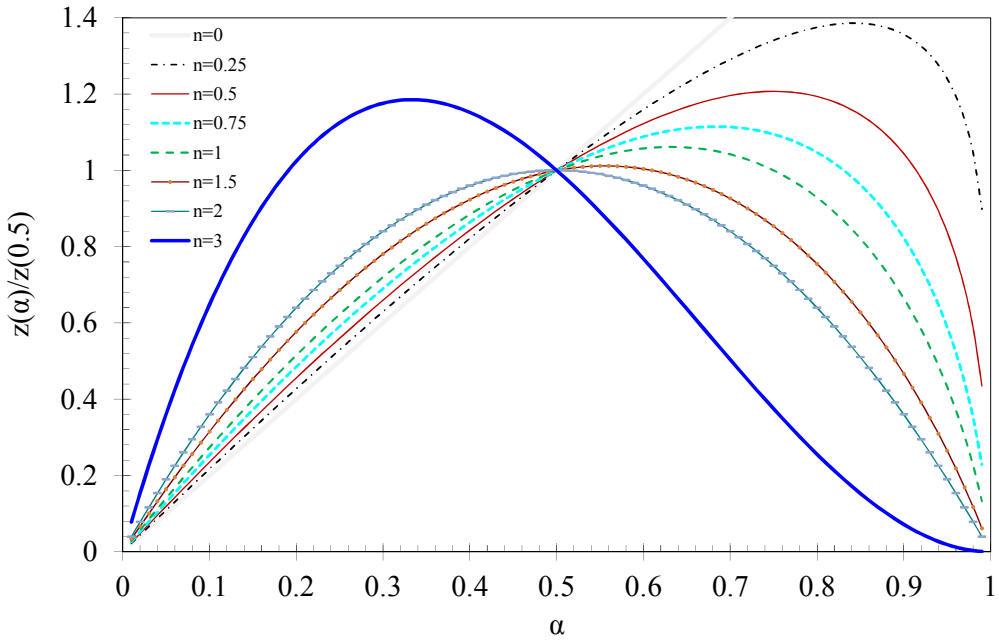

Figure 4-59 Variation of *n*-kinetic functions in the autocatalytic model.

When fixing the *n* value and changing *m*, the variation is not so acute, so smaller changes are obtained leading to more accurate fits, as seen Figure 4-60.

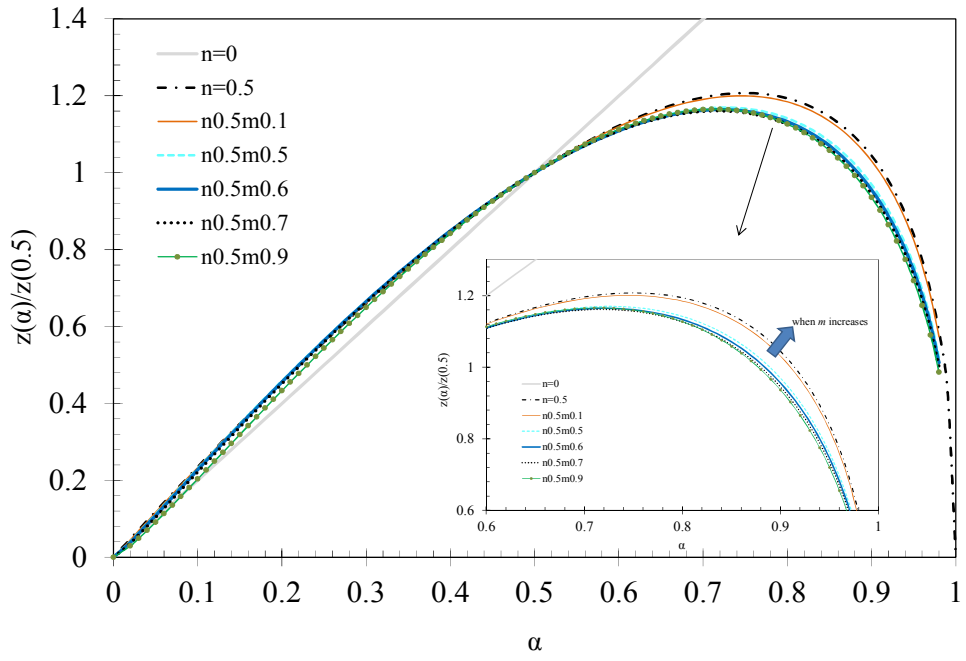

Figure 4-60 Variation of m-kinetic functions in the autocatalytic model.

Finally, when fixing $m \neq 0$, changes in *n* leads to more pronounced variations, see Figure 4-61. The best fitting will be obtained by a combination of the two values.

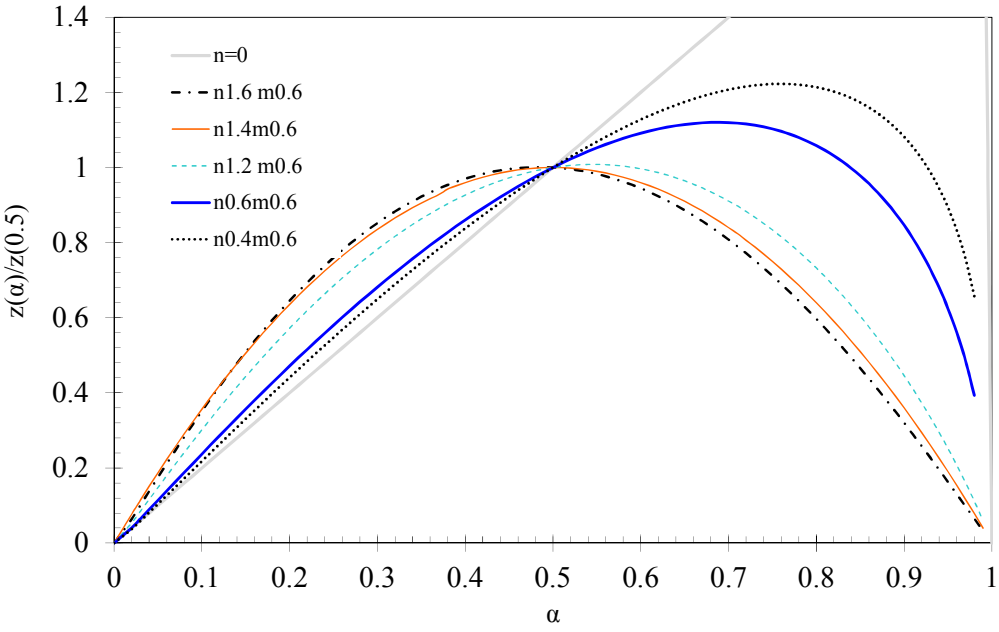

Figure 4-61 Criado method applied to the autocatalytic function fixing *m* and varying *n*.

Figure 4-62 shows the selected kinetic functions corresponding to experimental data of some biodegraded samples, and the resulting values of the kinetic triplet after application of the Criado/Coats Redfern methodology are depicted in Table 4-18. All samples follow an autocatalytic function, however at very high stages of degradation (60 months), the mechanism cannot be explained by one solely model.

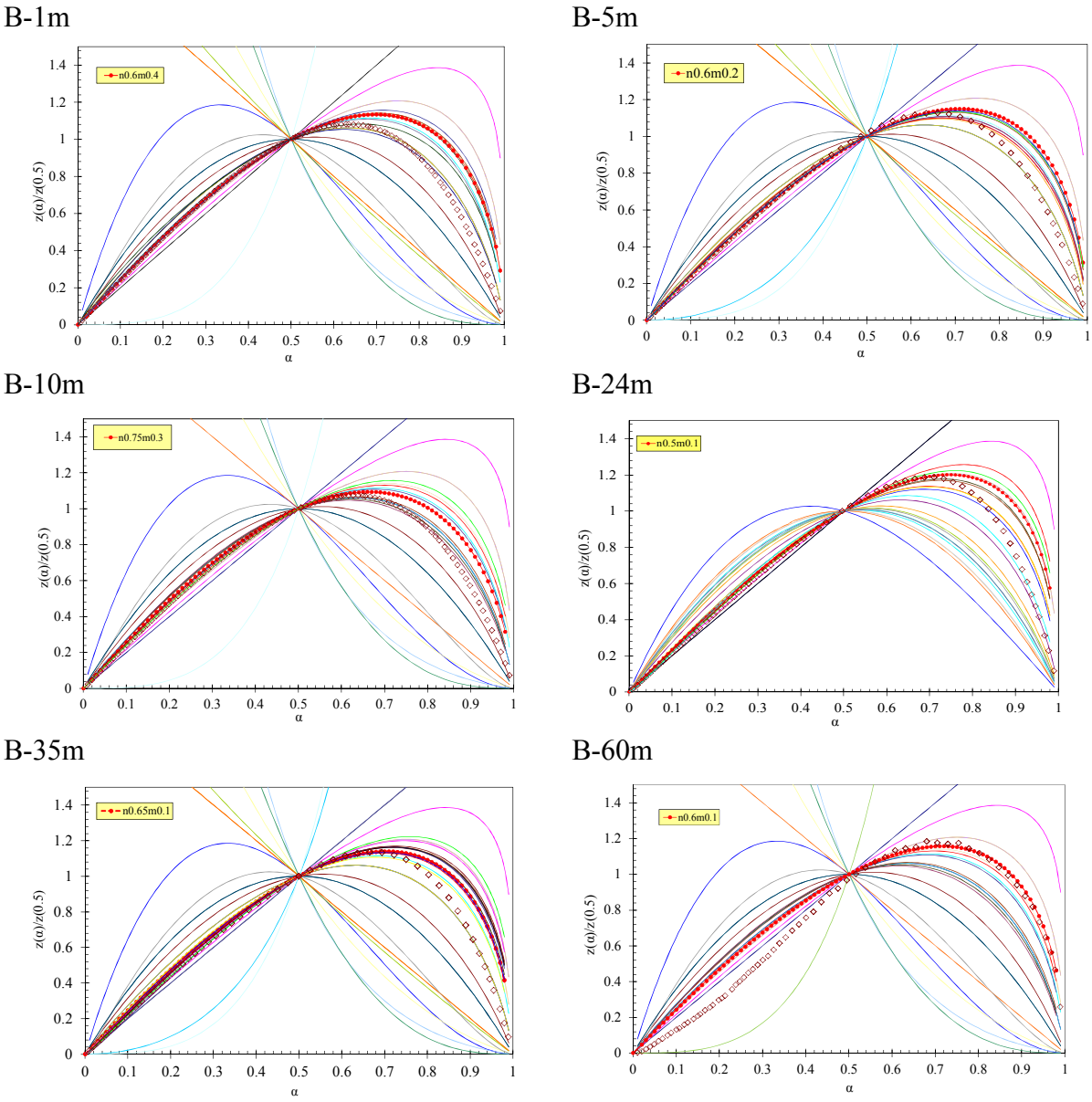

Figure 4-62 Criado plots for some of the biodegraded samples.

Table 4-18 Evolution of kinetic triplet of PLA thermal decomposition through the biodegradation process.

Biodegraded samples		*Criado analysis*	*Coats Redfern*			*Kinetic triplet. Decomposition function*		
		$f(\alpha)$ scope reduction	Ea_C kJ/mol	*ln (A)* (s^{-1})	R^2	Ea_{iso} kJ/mol	$f(\alpha)$	*ln (A)* (s^{-1})
Pellets		A2	196	39.5	0.998	213± 13	A2	39.5
		A3	97	12.9	0.996			
		n0.7m0.3	200	33.7	0.997			
		N=0.75	289	50.0	0.997			
Plates		n0.65m0.3	192	31.6	0.999	185 ± 10	n0.65m0.3	31.6
		n0.6m0.4	164	26.4	0.999			
		n0.7m0.1	221	37.0	0.998			
		A2	164	37.9	0.999			
1 m		n0.6m0.4	165	26.6	0.999	177 ± 16	n0.6m0.4	26.6
		n0.6m0.1	240	40.6	0.998			
		n0.6m0.3	190	31.3	0.999			
		n0.7m0.1	223	37.4	0.999			
5 m		n0.65m0.2	182	30.0	0.998	190 ± 13	n0.6m0.2	29.2
		n0.75m0.2	185	30.6	0.999			
		n0.6m0.2	178	29.2	0.999			
		n0.6m0.4	134	21.0	0.996			
10 m		n0.75m0.3	195	32.2	0.998	195 ± 19	n0.75m0.3	32.2
		n0.65m0.1	240	40.5	0.999			
		n0.9m0.4	182	30.0	0.999			
		n0.6m0.4	163	26.1	0.999			
15 m		n0.6m0.4	182	29.6	0.997	172 ± 4	n0.6m0.4	29.6
		n0.55m0.4	178	29.0	0.997			
		n0.7m0.3	216	36.1	0.997			
		n0.65m0.3	212	35.4	0.997			
20 m		n0.6m0.3	190	31.2	0.999	201 ± 5	n0.6m0.3	31.2
		n0.7m0.2	222	37.2	0.999			
		n0.65m0.7	97	14.0	0.999			
		n0.5m0.1	233	39.0	0.999			
24 m		n0.4m0.1	145	23.0	0.998	176 ± 17	n0.5m0.1	25.0
		R2	167	26.5	0.987			
		n1,1m0,3	133	37.0	0.993			
		n0.5m0.1	157	25.0	0.998			
30 m		n0.6m0.4	172	27.9	0.999	206 ± 12	n0.5m0.3	31.4
		n0.5m0.3	191	31.4	0.999			
		n0.65m0.4	175	28.6	0.999			
		F2	174	28.7	0.999			
35 m		n0.5m0.7	205	35.5	0.998	194 ± 16	n0.65m0.1	31.1
		F2	151	24.6	0.929			
		n0.65m0.1	186	31.1	0.998			
		n0.55m0.6	136	32.4	0.996			
40 m		n1.5m0.5	186	34.0	0.996	175 ± 20	n0.6m0.3	29.2
		n0.6m0.4	153	28.8	0.995			
		n0.75m0.25	198	29.6	0.993			
		n0.6m0.3	169	29.2	0.998			
60 m	$\alpha<0.5$	n=0	161	25.1	0.993	203 ± 27	R1	25.1
		R1	161	25.1	0.993			
	$\alpha>0.5$	n0.6m0.1	193	31.9	0.986		R3	34.9
		R3	215	34.9	0.996			

The kinetic triplets of the photodegraded samples were analyzed following a similar procedure, and the results are shown in Figure 4-63 and 4-64, and summarized in Table 4-19. Similarly to the biodegraded samples, the degradation follow an autocatalytic function, except at very high stages of degradation (17.2 months) where the mechanism cannot be explained by one solely model.

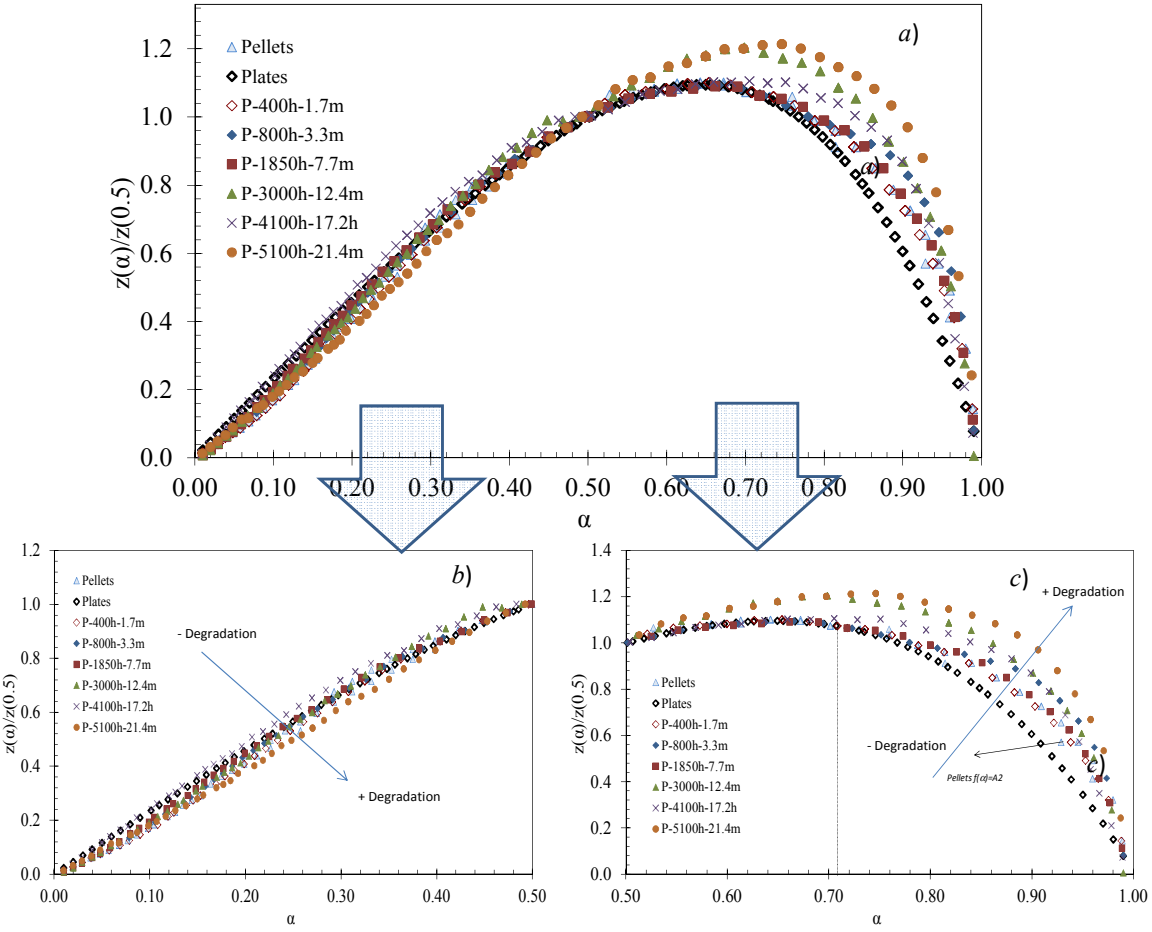

Figure 4-63 Criado curves for the experimental data of the photodegraded samples general *(a);* *$\alpha<0.5$ (b) and $\alpha>0.5$ (c)*

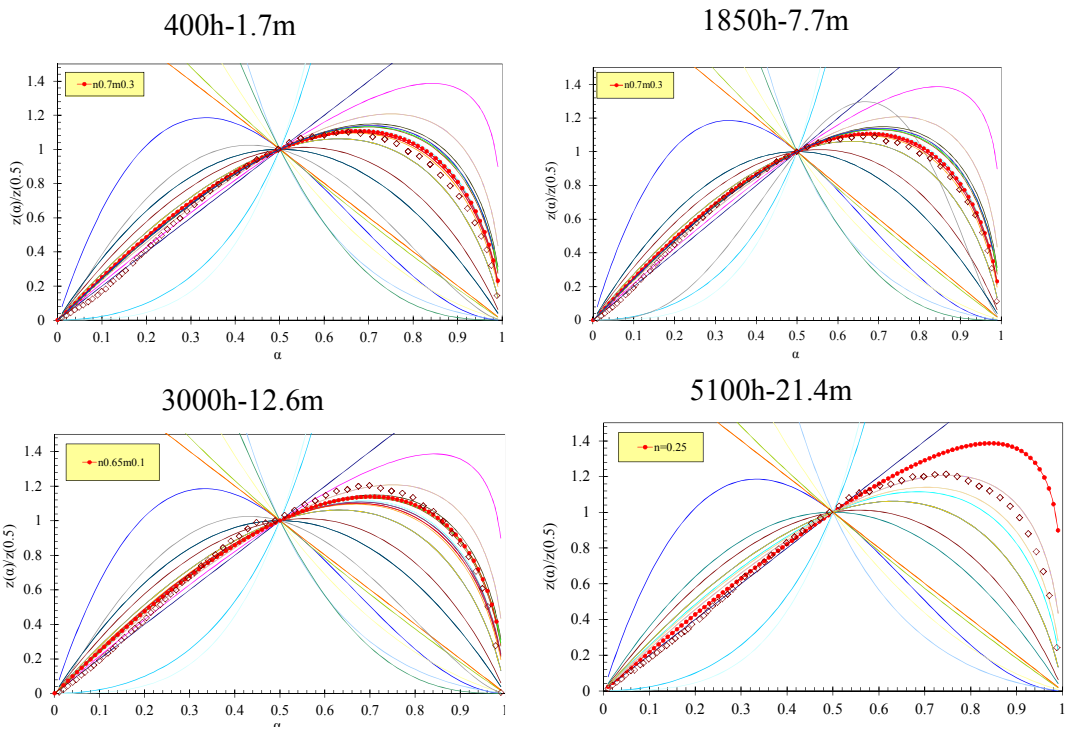

Figure 4-64 Criado plot for experimental and theoretical kinetic functions for some of the photodegraded samples.

Table 4-19 Kinetic triplet of PLA thermal decomposition thought the photodegradation process.

Photodegraded samples	*Criado analysis*	*Coats Redfern*			*Kinetic triplet. Decomposition mechanism*		
	$f(\alpha)$ scope reduction	Ea_C kJ/mol	$ln\ (A)$ (s^{-1})	R^2	Ea_{iso} kJ/mol	$f(\alpha)$	$ln\ (A)$ (s^{-1})
400h-1.7m	n0.65m0.1	200	36.4	0.996	179 ±23	n0.65m0.1	36.4
	n0.7m0.3	165	28.3	0.990			
	n0.7m0.4	163	26.0	0.997			
	n0.8m0.1	222	37	0.994			
800h-3.3m	R2	250	41.6	0.997	159 ± 8	n0.7m0.4	41.6
	n0.7m0.2	200	33.0	0.995			
	n0.7m0.3	180	29.3	0.997			
	n0.7m0.4	168	27.1	0.997			
1850h-7.7m	n0.6m0.2	209.6	34.7	0.998	183 ± 9	n0.7m0.3	31.2
	n0.65m0.1	237.2	39.9	0.998			
	n0.7m0.3	190.3	31.2	0.996			
	n0.6m0.4	140.0	21.7	0.988			
2250h-9.4m	n0.6m0.1	233.1	39.7	0.997	193 ± 6	n=0.75m0.3	30.9
	n=0.75m0.3	186.1	30.9	0.995			
	n0.75m0.25	207.1	35.0	0.997			
	m0.65m0.2	212.3	35.9	0.997			
3000h-12.6m	n0.65m0.1	175.5	28.7	0.997	185 ± 8	n0.65m0.1	28.7
	n0.7m0.3	140.3	22.0	0.994			
	R2	192.5	31.1	0.998			
	n=0.25	178.0	28.8	0.998			
4100h-17.2 m	F1	227.6	40.0	0.998	152± 19	n=0.75	36.1
	n=0.75	165.0	36.1	0.998			
	n0.7m0.3	149.5	28.2	0.998			
	n0.65m0.1	186.8	31.0	0.999			
5100h-21.4m	R2	183.7	29.3	0.998	178 ± 22	n=0.25	27.2
	R1	156.8	24.5	0.998			
	n=0.25	169.8	27.2	0.998			

The same methodology was applied to the thermally degraded samples, being the results summarized in Figure 4-66 and Table 4-20. The thermally degraded samples cannot be fitted to one single process, even at low degradation times

.

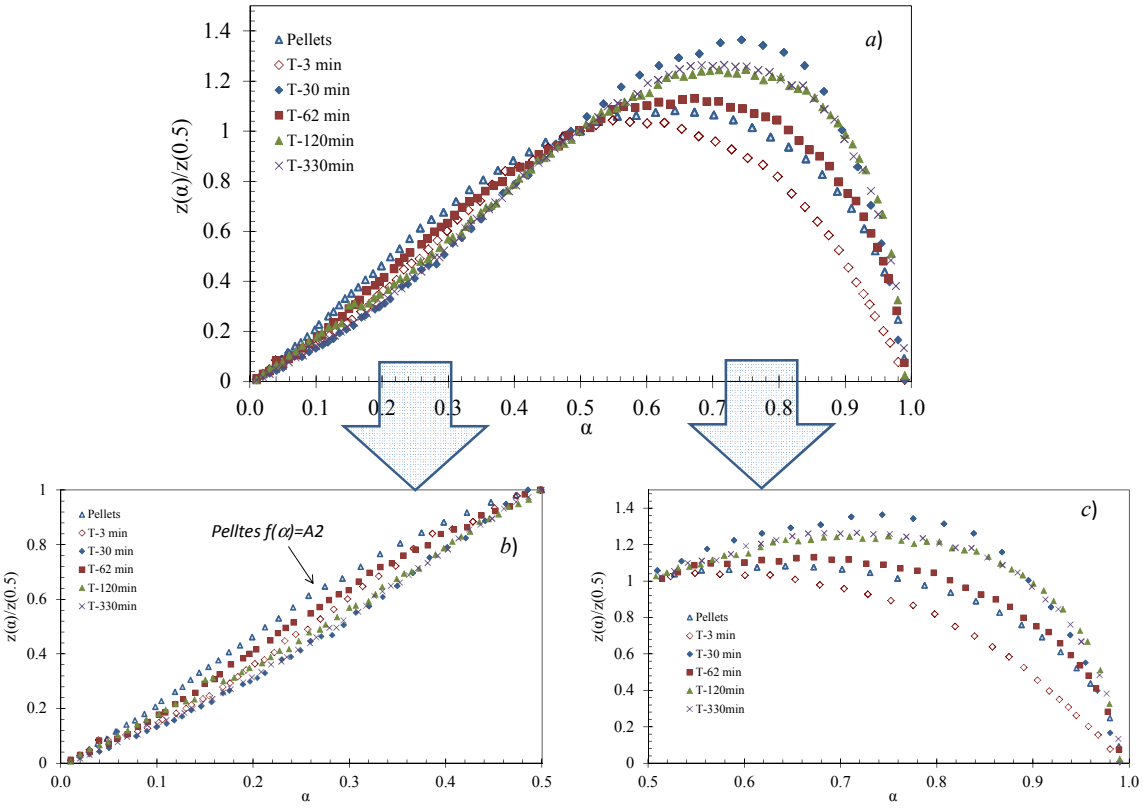

Figure 4-65 Criado plot for the experimental data of the thermally degraded samples, the insets represent the plots at $\alpha<0.5$ and $\alpha>0.5$.

This particular effect of thermal degradation on the kinetic profile was further investigated by studying each sample separately, in Figure 4-66 to 4-70, comprising degradation times from 3 to 330 minutes. All the figures suggest that, at low α values, the curves can be fitted to chemical reaction models, with $n < 0.5$. Moreover, the normalized curves deviate from the results corresponding to the pellets at increasing degradation times, which is also visible in Figure 4-65 *b*.

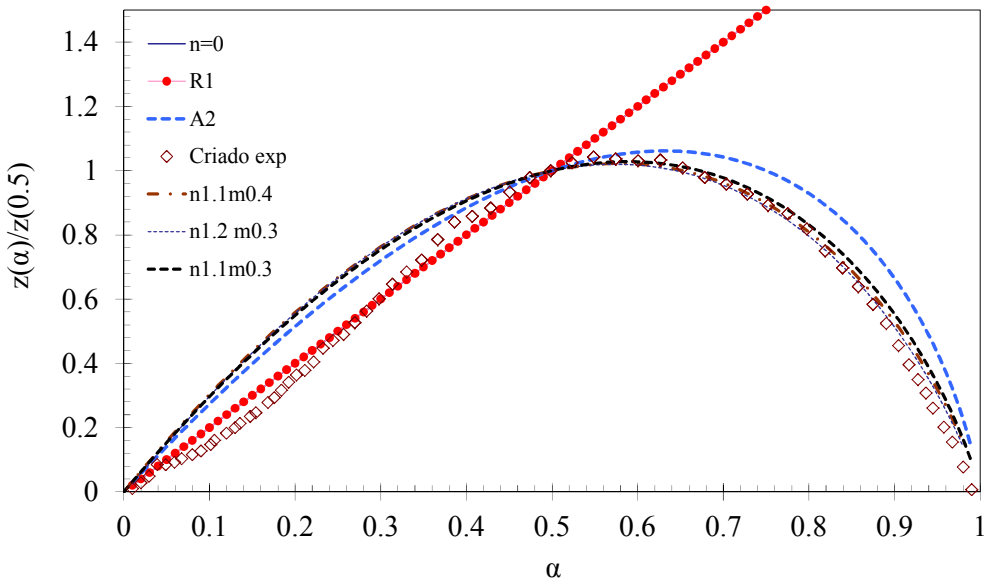

Figure 4-66 Criado plot for the experimental data of the thermally degraded sample at 3 min with some theoretical functions.

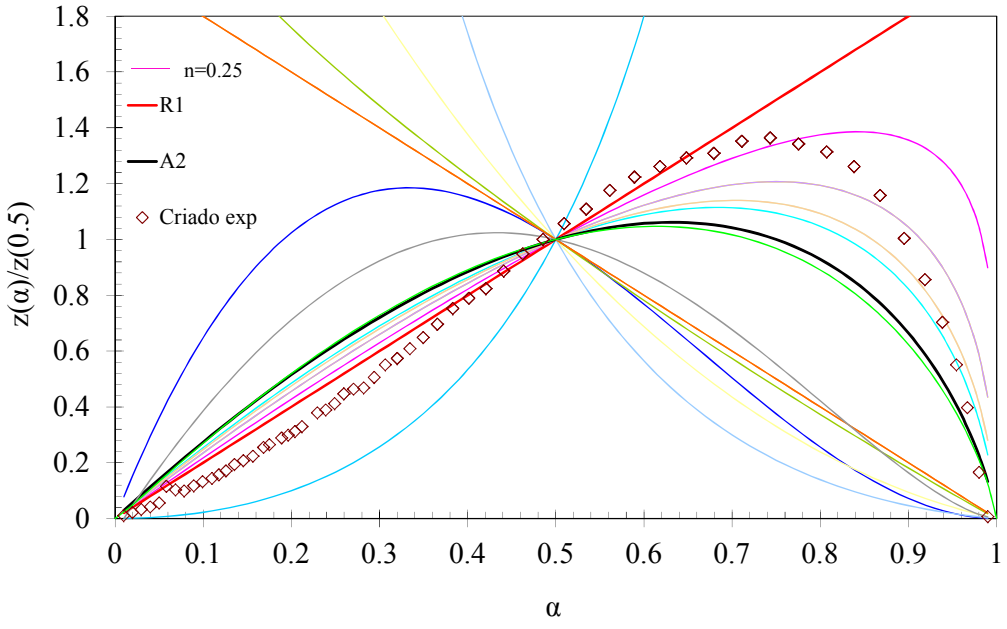

Figure 4-67 Criado plot for the experimental data of the thermally degraded samples at 30 min with some theoretical functions.

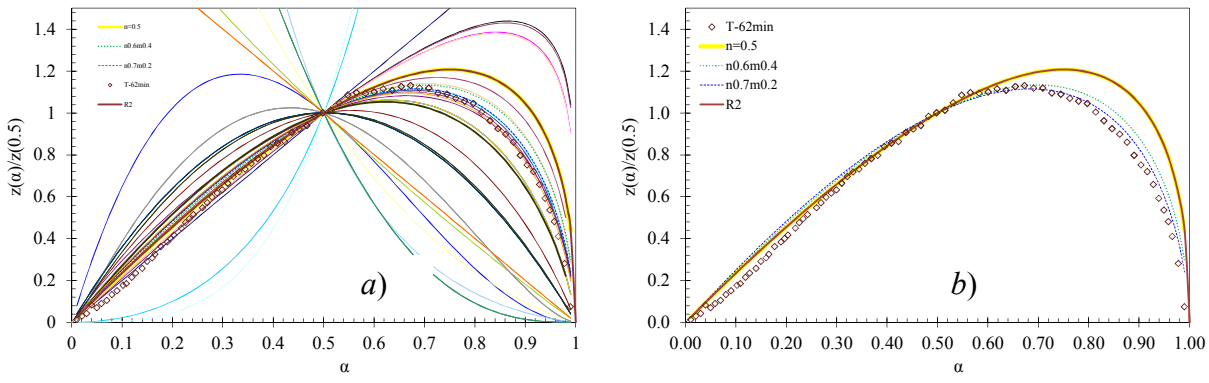

Figure 4-68 Criado plot for the experimental data of the thermally degraded samples at 62 min *a*) some theoretical functions and *b*) the selected curves.

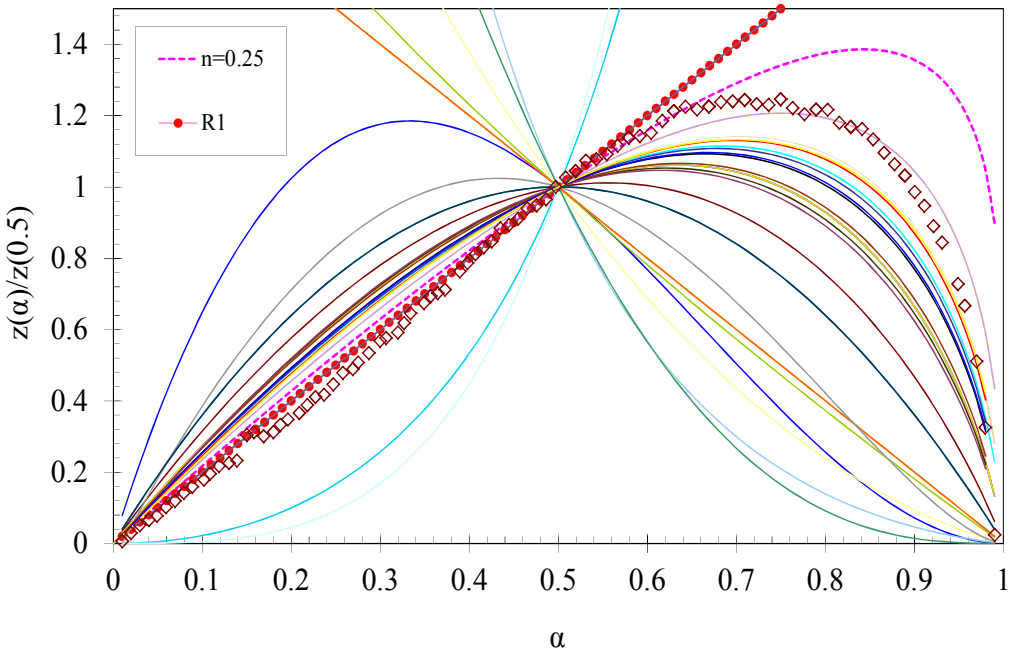

Figure 4-69 Criado plot for the experimental data of the thermally degraded samples at 120 min with some theoretical functions.

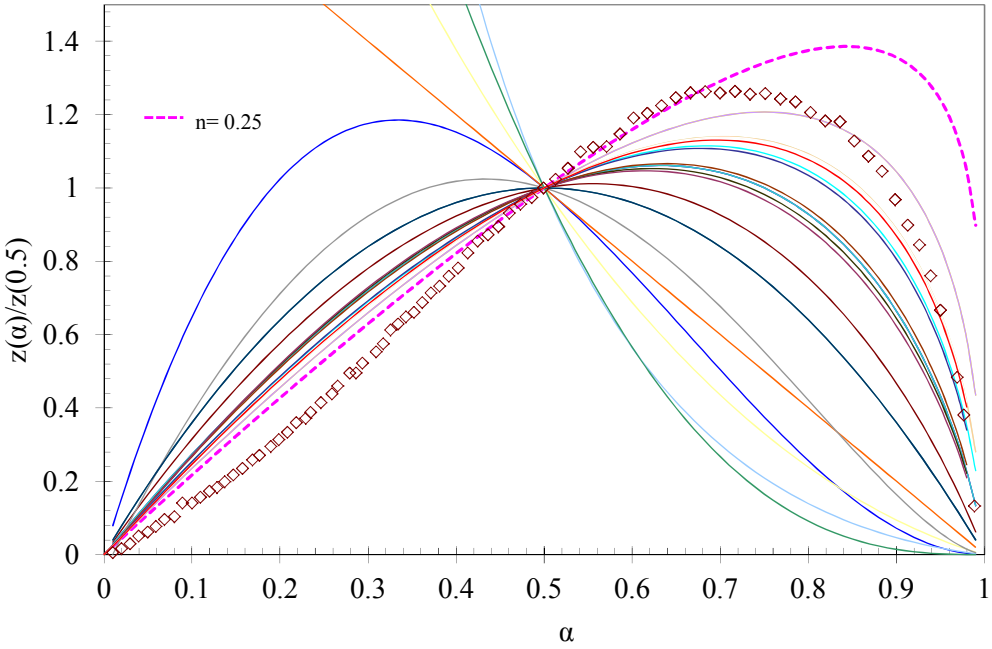

Figure 4-70 Criado plot for the experimental data of the thermally degraded samples at 330 min with some theoretical functions.

Table 4-20 Kinetic triplet of PLA thermal decomposition through the thermal degradation process.

Thermally degraded samples		***Criado analysis***	***Coats Redfern***			**Isoconversional analysis**
		f (α) scope reduction	Ea_C kJ/mol	ln (A) (s^{-1})	R^2	Ea_{iso} kJ/mol
3 min	α<0.5	R1 **n=0**	330	59.1	0.995	188 ±15
	α>0.5	n=1.1m0.3	375	69.0	0.983	
		n=1.1m=0.4	331	60.5	0.983	
		n=1.2m=0.3	399	73.6	0.983	
30 min	α=0.2–0.7	R1	287	48.4	0.996	199 ± 25
		n=0.25	289	42.1	0.991	
62 min	α<0.5	**n=0.5** R=2	256.1	41.5	0.998	184 ± 12
	α>0.5	**n0.6m0.**4	165.3	24.5	0.998	
		n0.7m0.2	213.0	33.6	0.997	
120 min	α=0.2–0.7	R1/n=0	129.6	19.4	0.999	177 ± 13
		n=0.25	140.6	21.7	0.998	
330 min	α>0.5	**n=0.25**	227.4	38.5	0.994	173 ± 17

The application of the methodology has revealed that the kinetic function of the thermal decomposition of photo and biodegraded samples follows an autocatalytic model, in opposition to pellets, which exhibit an A2 model. Moreover, in samples submitted to very high times of bio ($M_n \leq$ 20300) and photo ($M_n \leq 26700$) degradation, the processes cannot be fitted to one solely mechanism. This happens occurs even at low degradation times in thermally degraded samples ($M_n \leq 102000$). For these samples, while the curves can be fitted to autocatalytic processes at high conversion degrees, the process seems to be controlled by a chemical reaction model

All these results obtained the by thermogravimetry indicate significant differences in the thermal decomposition kinetics of the PLA due to the different degradation types, probably by the presence of different subproducts, rather than to a mere molar mass decay.

.

4.4 Surface effects of degradation

The effect of the different types of degradation on the surface morphology was examined by scanning electron microscopy. The SEM micrographs corresponding to the different PLA samples submitted to photo and biodegradation are shown in Figures 4-71 to 4-92. All the SEM observations were performed directly on the surfaces at different magnification.

The results in this section have been organized as follows:

- Figure 4-71 and 4-73 show the micrographs of the PLA plates.
- Figures 4-74 to 4-83 show the micrographs of the biodegraded PLA samples.
- Figures 4-84 to 4-92 show the micrographs of the photodegraded PLA samples.

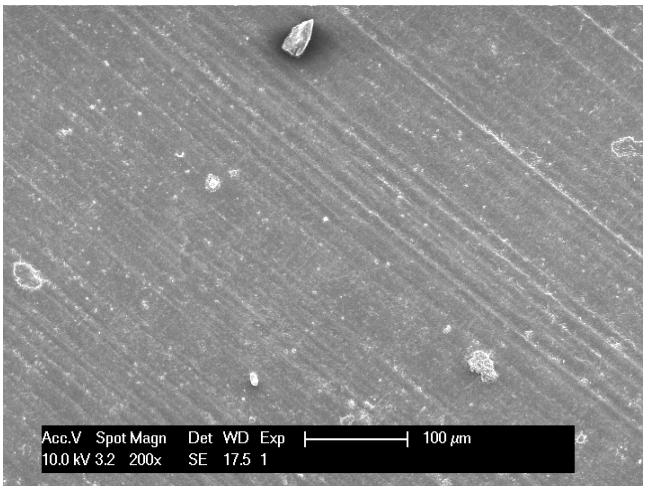

Figure 4-71 SEM micrograph showing the surface of the plate sample (200x).

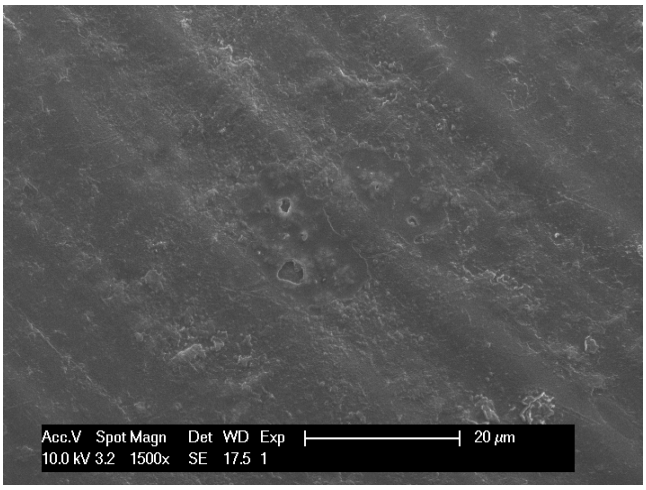

Figure 4-72 SEM micrograph showing the surface of the plate sample (1500x).

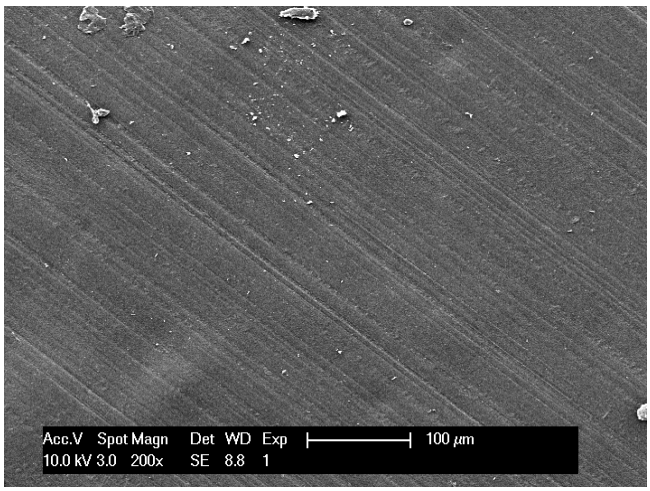

Figure 4-73 SEM micrograph showing the surface of the plate sample (200x).

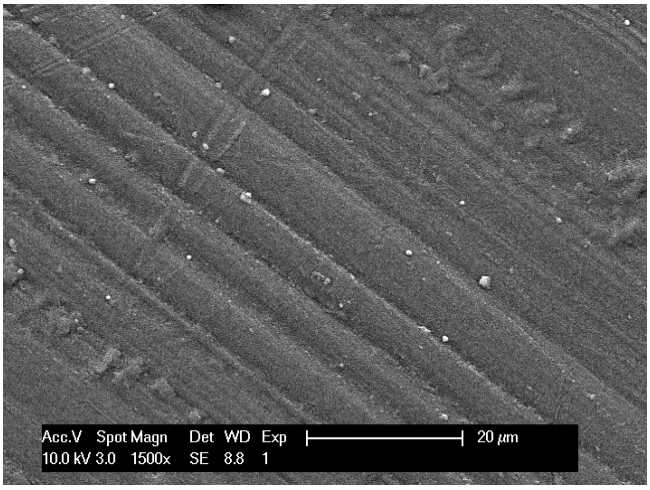

Figure 4-74 SEM micrograph of the sample biodegraded during 10 months (1500x).

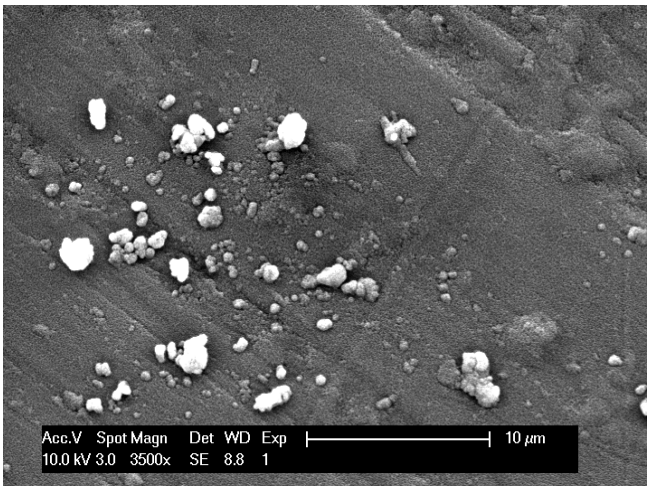

Figure 4-75 SEM micrograph of the sample biodegraded during 10 months (3500x).

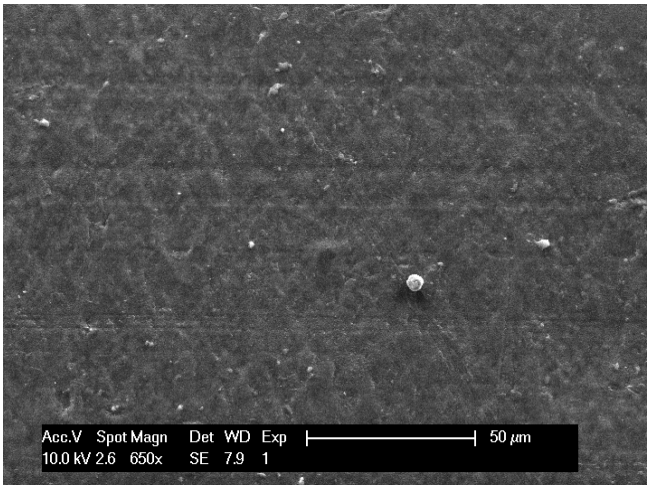

Figure 4-76 SEM micrograph of the sample biodegraded during 24 months (650x).

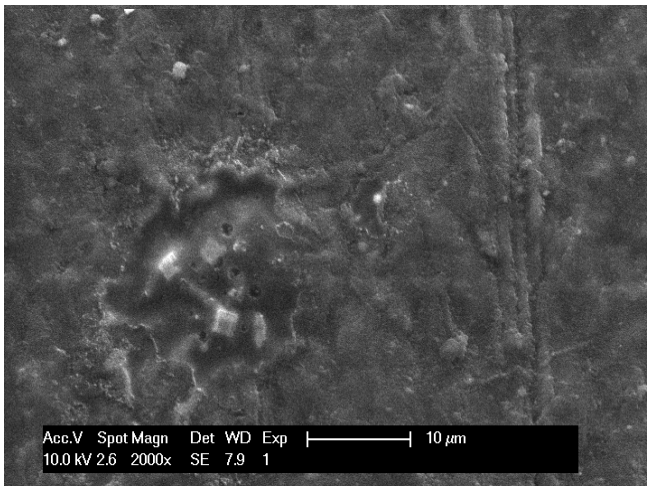

Figure 4-77 SEM micrograph of the sample biodegraded during 24 months (2000x).

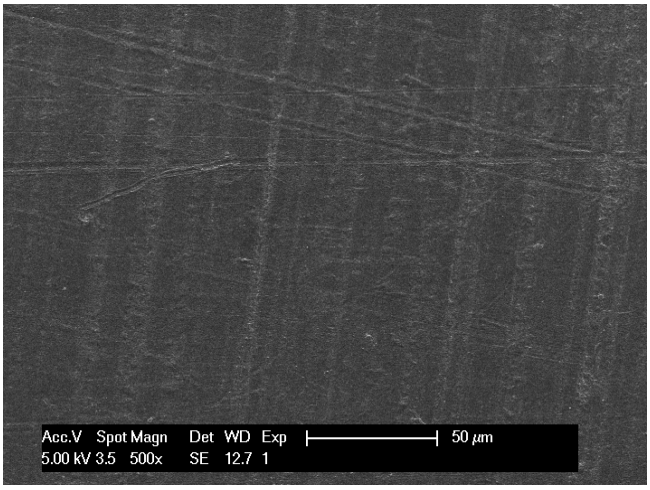

Figure 4-78 SEM micrograph of the sample biodegraded during 30 months (500x).

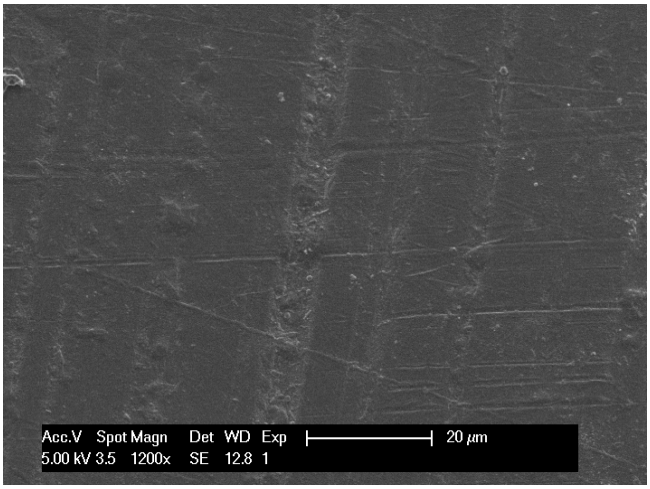

Figure 4-79 SEM micrograph of the sample biodegraded during 30 months (1200x).

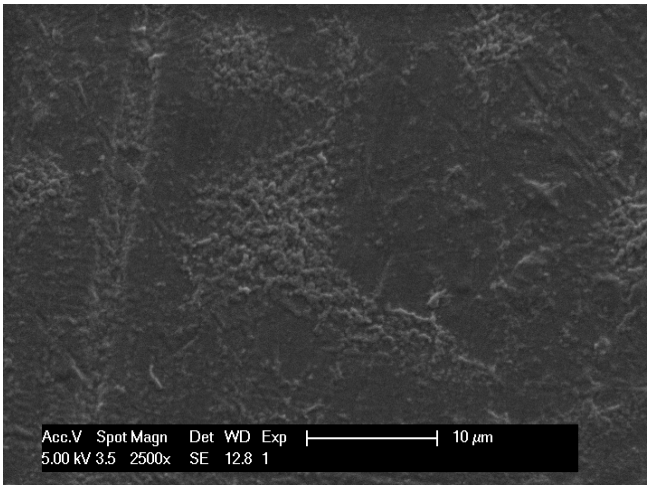

Figure 4-80 SEM micrograph of the sample biodegraded during 30 months (2500x).

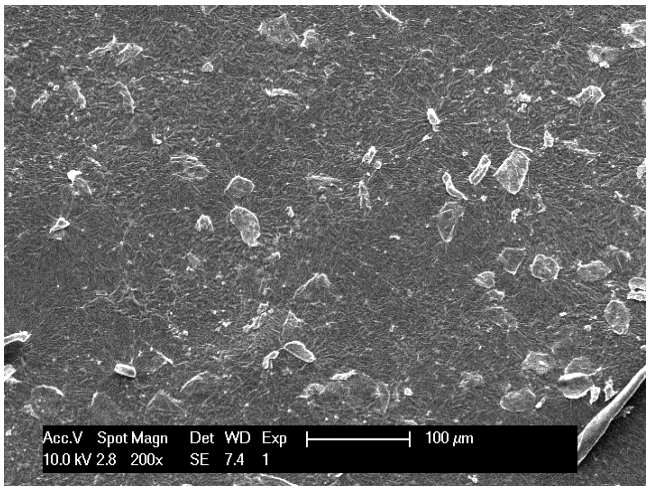

Figure 4-81 SEM micrograph of the sample biodegraded during 35 months (200x).

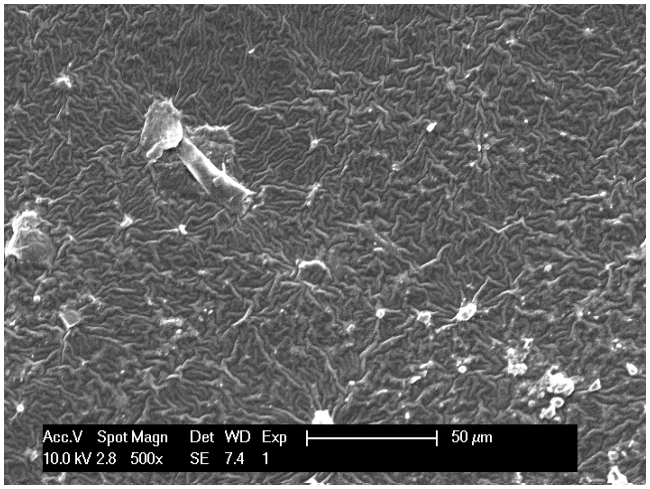

Figure 4-82 SEM micrograph of the sample biodegraded during 35 months (500x).

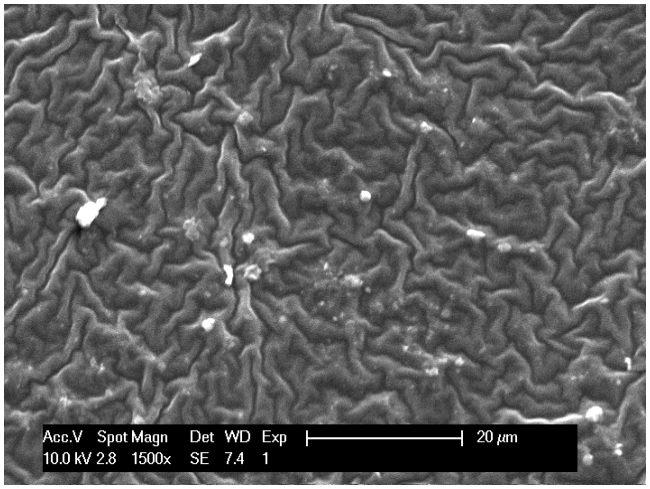

Figure 4-83 SEM micrograph of the sample biodegraded during 35 months (1500x).

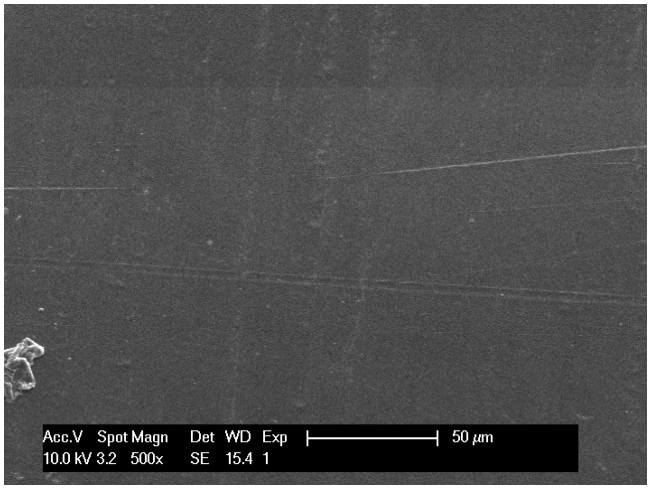

Figure 4-84 SEM micrograph of the sample photodegraded during 400h-1.7m (500x).

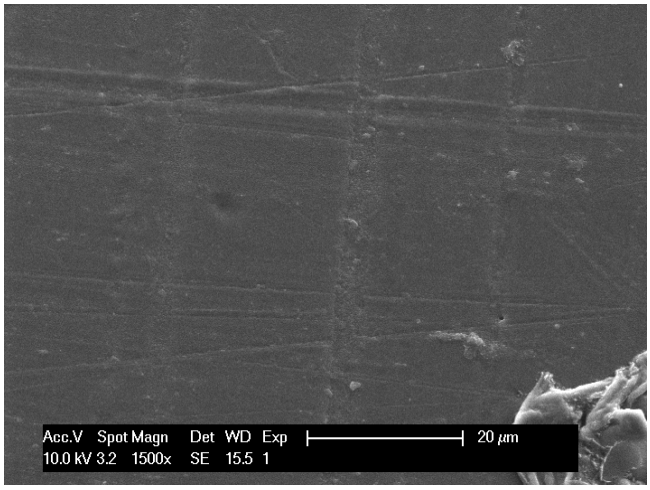

Figure 4-85 SEM micrograph of the sample photodegraded during 400h -1.7m (1500x).

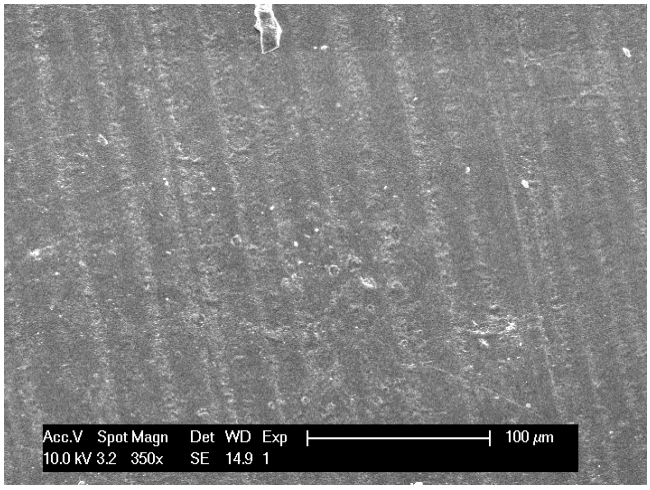

Figure 4-86 SEM micrograph of the sample photodegraded during 1850 hours -7.7 months (350x).

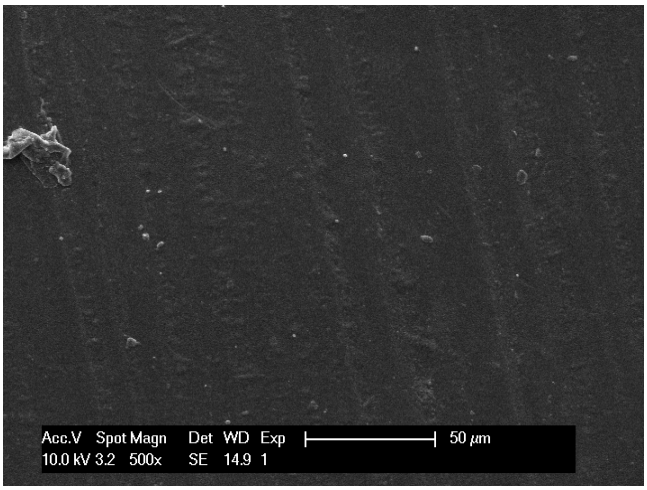

Figure 4-87 SEM micrograph of the sample photodegradedduring 1850 hours -7.7 months (500x).

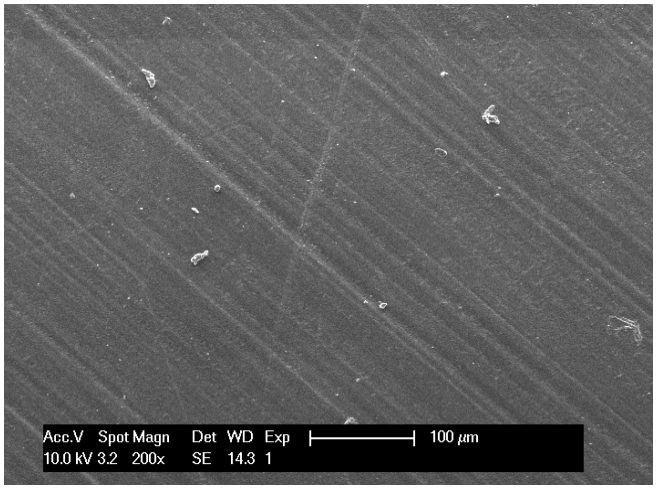

Figure 4-88 SEM micrograph of the sample photodegraded during 2250h -9.4 m (200x).

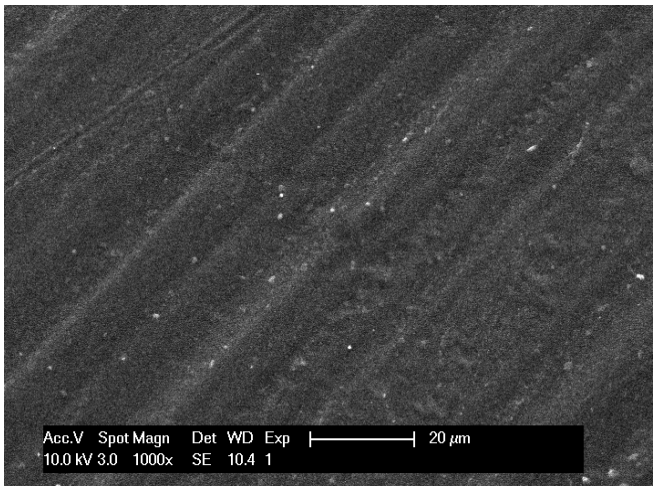

Figure 4-89 SEM micrograph of the sample photodegraded during 2250 hours -9.4 months (1000x).

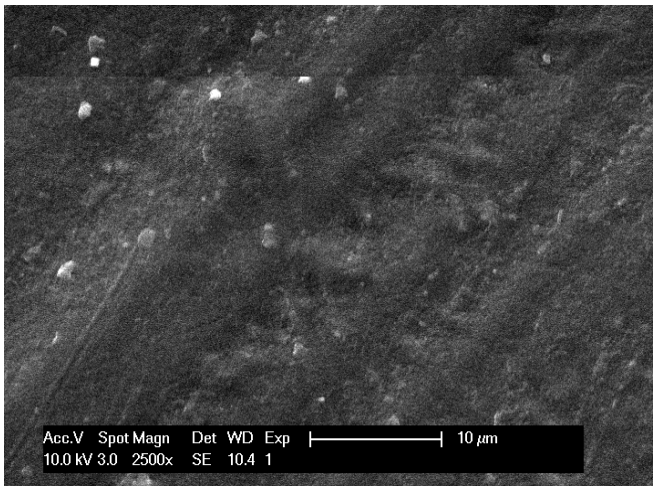

Figure 4-90 SEM micrograph of the sample photodegraded during 2250 hours -9.4 months (2500x).

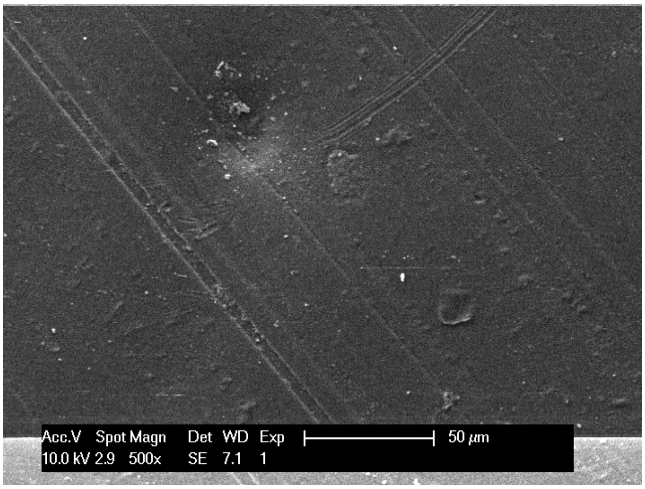

Figure 4-91 SEM micrograph of the sample photodegraded during 4100 hours -17.2 months (500x).

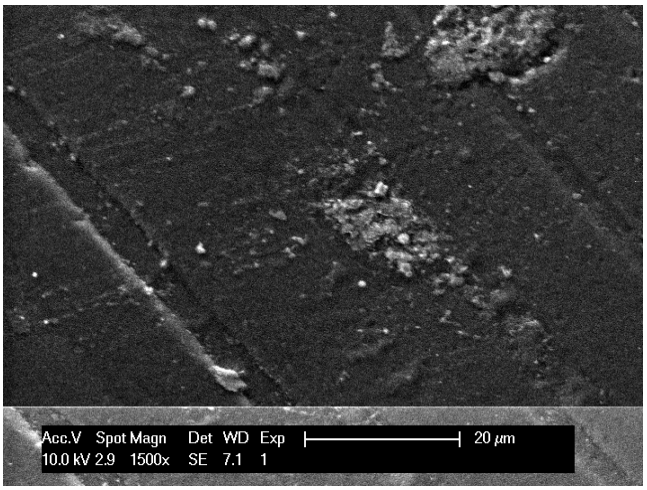

Figure 4-92 SEM micrograph of the sample photodegraded during 4100 hours -17.2 months (1500x).

Based on visual examination no cracks were found in PLA pellets, although some lines on the surfaces can be seen, probably attributed to material processing.

There are no significant changes in the SEM micrographs of the PLA samples subjected to photodegradation, even at high exposure times, which suggests that the surface of the samples is not significantly modified.

Contrarily, progressive changes were observed on the surface of the samples submitted to biodegradation. Such changes are first visible at low biodegradation times (t=10 months, M_n=59300). When passing 24 months (M_n=45600) some canals in the surface are observed and after 35 months (M_n=35100) the surface presents a particular view of canals and the deterioration is patent. This fact indicates that the surface of the materials is highly affected. The formation of these channels can be due to water transport to the core of the sample and to the diffusion to the media of small molar masses that can be bio assimilated, and reinforces the view of heterogeneous degradation.

4.5 Evaluation of the viscoelastic behavior

4.5.1 Dynamic mechanical relaxation spectra

The changes on the PLA structure may also have important effects on its thermal properties, and this was further evaluated by DMTA, DSC and OM. The dynamic-mechanical spectra of the different samples were obtained in terms of the storage modulus (*E'*), delta tangent (tan δ) and loss modulus (*E''*) versus temperature at different frequencies. As an example, Figures 4-93 and 4-94 show the results corresponding to the viscoelastic response of plates at 1 Hz. Since the values of tan δ and *E''* are related, all the results were discussed in terms of *E'* and *E''*, expressed in Pa units.

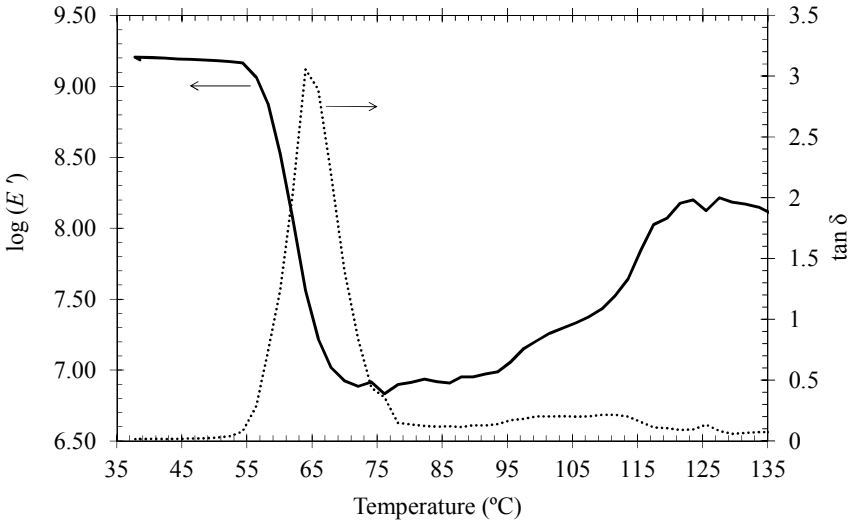

Figure 4-93 log (*E'*) and tan δ versus temperature for plates.

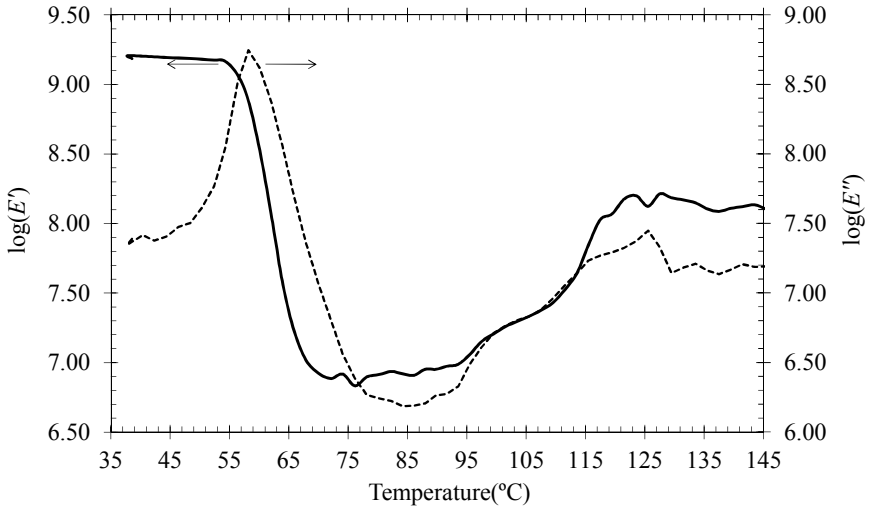

Figure 4-94 log (*E'*) and log (*E''*) versus temperature for plates.

The dependence of *E'* and *E''* with the temperature and frequency is shown in Figure 4-95 for the particular case of the 10 months biodegraded sample. As expected, the curves are displaced to higher temperatures at higher frequencies.

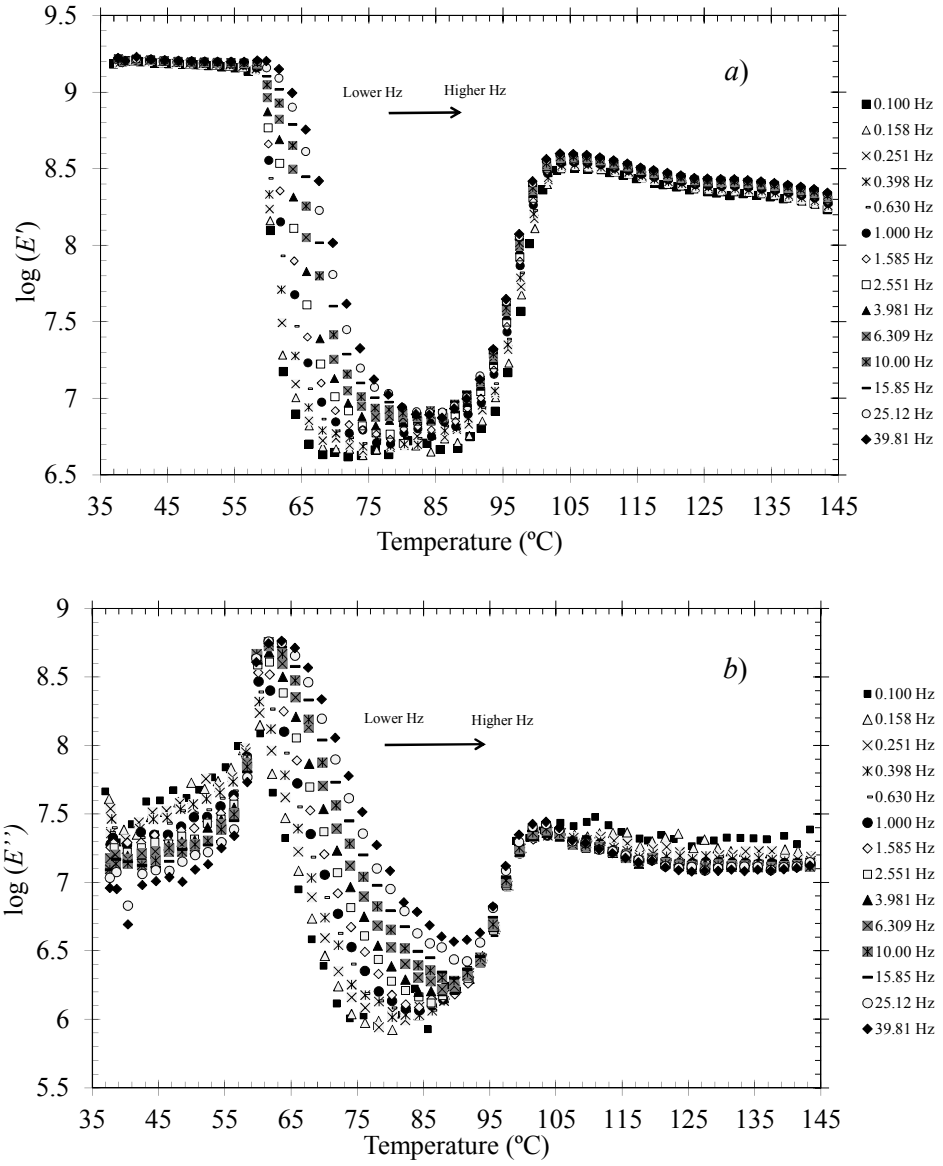

Figure 4-95 *a*) log (*E'*) and *b*) log (*E''*) versus temperature for the bio-10months (frequencies from 0.1 to 39 Hz)

The dynamic-mechanical spectra show different relaxation zones (see Figure 4-96), which can be assigned at increasing temperatures to: a glass/rubber transition (T ≈ 55-75ºC), a rubbery plateau (T ≈ 75-85ºC), crystallization (T ≈ 85-140ºC) and melting (from T ≈ 140ºC) [60,61,62]. Similar regions are observed in the spectra of all samples under study.

In order to compare the effects of degradation on the viscoelastic response of the PLA samples, several parameters were calculated from the log(E') and log(E'') plots versus temperature (see Figures). The values of the storage and loss modulus in the glass state, log(E_g') and log(E_g''), and in the crystallization region, log(E_c') and log(E_c''), were obtained, all of them at f = 1 Hz.

In the case of plates (Figure 4-94) a drop in *E'* and *E''* is indicative of the glass-rubber relaxation of PLA. *E'* is about 2 GPa (log(E_g') ~ 9.20) at room temperature, and decreases significantly to 2MPa (log(E_g') ~ 8.00), at about 75ºC, these values are in good agreement with data in similar experimental conditions [63]. The increase in the *E'* and *E''* values in the 85 to 125ºC region denotes higher polymer stiffness, caused by crystallization above the glass transition.

The structural and morphological changes due to degradation may be reflected in the dynamic mechanical relaxation spectra of the bio and photo degraded PLA samples.

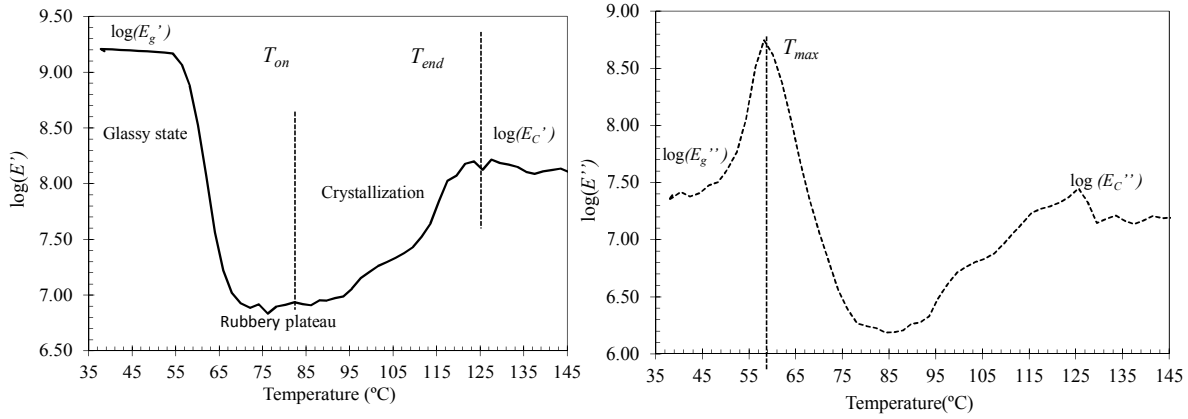

Figure 4-96 Parameters of study from DMTA spectrum

Figure 4-97 *a* and *b* show the storage and loss moduli spectra, respectively, of the samples submitted to **biodegradation** at different times. The parameters obtained from the spectra are displayed in Table 4-21. A slight increase in both E_g' and E_g'' is observed, compared to plates. Such increment is accompanied with increasing brittleness of the samples due to degradation. Indeed, after 35 months samples were too fragile and could not be measured by DMTA. Biodegradation also promotes changes in the depth and temperature range of the rubbery plateau, which is shifted to lower temperatures. These results, together with a slight variation on the E_c' and E_c'', are indicative of faster crystallization process.

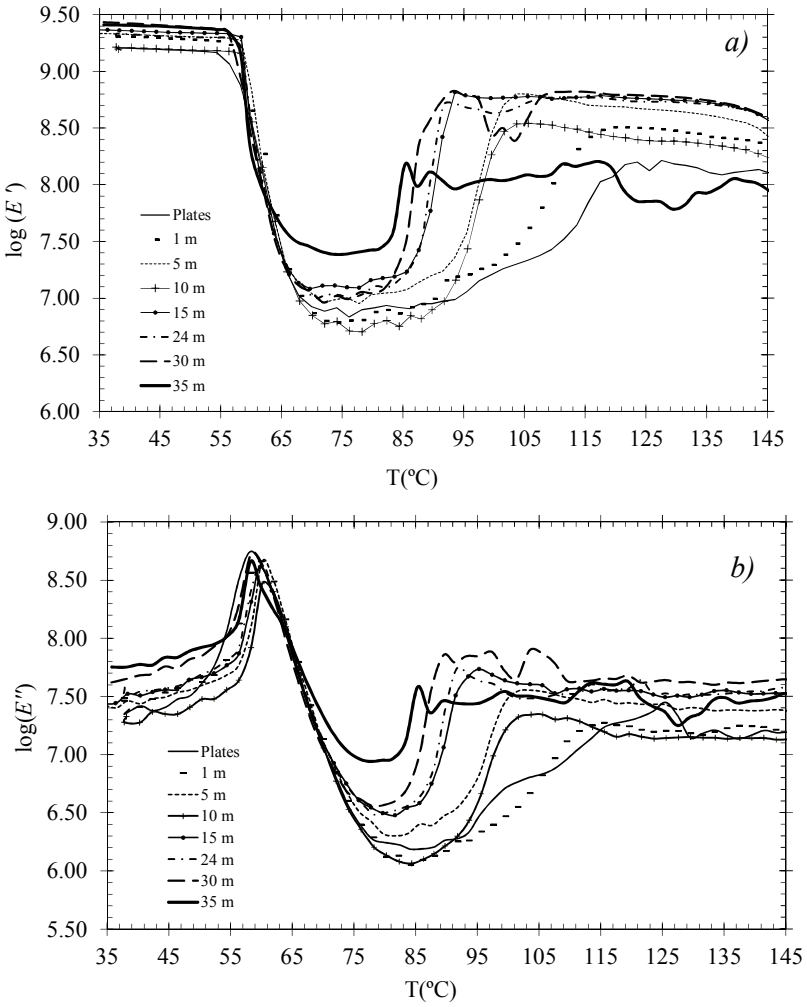

Figure 4-97 *a*) log (*E'*) and *b*) log (*E''*) versus *T* for biodegradation at 1Hz.

Table 4-21 *E'* and *E''* in the glassy and crystalline state for the biodegraded samples.

Biodegraded sample	log(E_g')	log(E_g'')	log(E_c')	log(E_c'')
Plates	9.22 ± 0.10	7.45 ± 0.10	8.00 ± 0.15	6.92 ± 0.25
1 m	9.30 ± 0.12	7.60 ± 0.14	8.48 ± 0.06	7.20 ± 0.33
5 m	9.36 ± 0.12	7.61 ± 0.11	8.50 ± 0.13	7.32 ± 0.25
10 m	9.35 ± 0.08	7.42 ± 0.18	8.50 ± 0.38	7.15± 0.16
15 m	9.30 ± 0.12	7.43 ± 0.07	8.73 ± 0.27	7.53 ± 0.28
24 m	9.40 ± 0.02	7.43 ± 0.06	8.70 ± 0.10	7.50± 0.20
30 m	9.41 ± 0.13	7.30 ± 0.04	8.75± 0.31	7.63 ± 0.10
35 m	9.45 ± 0.05	7.80 ± 0.05	8.00 ± 0.11	7.52 ± 0.34

The results of log(*E'*) and log(*E''*) corresponding to the **photodegraded** samples are shown in Figure 4-98 *a-b*, respectively, and the values of the moduli in Table 4-21. The samples 3000h-12.6m and 4100h-17.7m were difficult to measure because of their high brittleness. Photodegradation promotes increases in log(E_g'') and log(E_g') and a displacement to lower temperatures of the crystallization process. In this case, a slightly reduction in E_c' is observed, accompanied with higher E_c'' values.

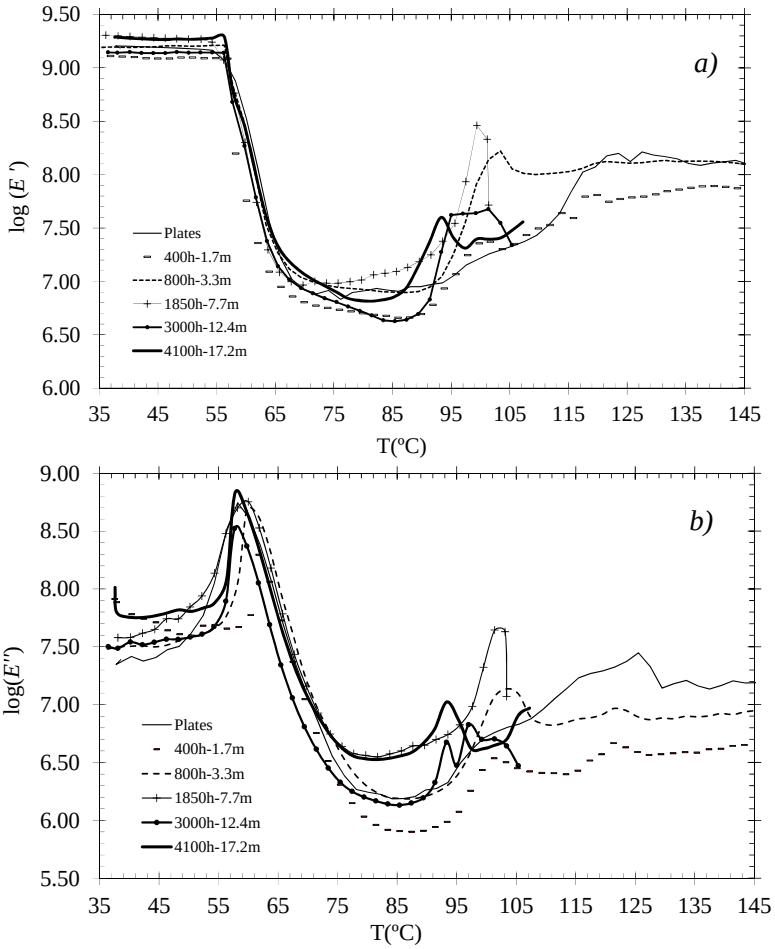

Figure 4-98 *a*) log(*E'*) and *b*) log (*E''*) versus *T* for the photodegraded samples at 1Hz.

Table 4-22. *E'* and *E''* in the glassy and crystalline state for the photodegraded samples

Photodegraded sample	log (E_g')	log (E_g'')	log (E_c')	log (E_c'')
400h-1.7m	9.10 ± 0.14	7.67 ± 0.08	7.90 ± 0.12	7.35 ± 0.50
800h-3.3m	9.20 ± 0.15	7.5 ± 0.04	8.00 ± 0.13	8.11 ± 0.10
1850h-7.7m	9.30 ± 0.12	7.6 ± 0.05	8.50 ±0.50	8.44 ±0.70
3000h-12.6m	9.15± 0.06	7.5± 0.10	7.70 ±0.12	7.56 ±0.19
4100h-17.2m	9.30± 0.09	7.8 ± 0.07	7.60 ±0.09	7.60 ±0.19

In general, the moduli corresponding to all the degraded samples fall in a narrow range. The two degradation processes increases the stiffness of PLA, as the values of E_g' indicate. This is more visible in the case of the biodegraded samples, probably due to a more acute aging effect, which may also account for the more marked effect on the crystallization[64].

4.5.2 Modeling the relaxation spectra

The study of the viscoelastic response was completed by analyzing the temperature dependence of the different regions:

- T_{max} was obtained from the log(E'') plots, as a representative value of the glass transition. The maximum of tan δ appears a few degrees above the peak in log(E'') and closer to the inflection point of log(E'), while the maximum of log(E'') fits more to the beginning of the fall in log(E'). The maximum loss modulus, log(E''), seems to be more appropriate since in practice, the maximum operating temperature of many polymers amorphous is the "softening point", and the value given by the peak of tan δ exceeds this temperature [65].

- The crystallization temperature, T_{on}, is taken as the onset of the increase of log(E') from the rubbery plateau, while the endset temperature, T_{end}, of the crystallization phenomenon is taken as the temperature when the increase in the storage modulus achieves a second plateau.

Table 4-23 reports the T_{max} values for the degraded samples, indicating the corresponding molar masses. These results are plotted versus the degradation time and the molar mass in Figure 4-99 *a* and *b*, respectively.

Table 4-23 T_{max} values corresponding to the bio and photo degraded samples.

Biodegraded sample	M_n	T_{max} (ºC)
Plates	73200	59.7 ± 0.6
1 m	74600	60.1 ± 0.5
5 m	65900	62.0 ± 0.7
10 m	59300	61.1 ± 0.4
15 m	60200	60.2 ± 0.6
24 m	45600	59.4 ± 0.6
30 m	39000	58.3 ± 0.5
35 m	35100	58.1 ± 0.4
Photodegraded samples	M_n	T_{max} (ºC)
400h-1.7m	56300	59.1 ± 0.6
800h-3.3m	55000	59.4 ± 0.6
1850h-7.7m	41300	59.2 ± 0.3
3000h-12.6m	35100	58.0 ± 0.6
4100h-17.2m	26700	57.7 ± 0.6

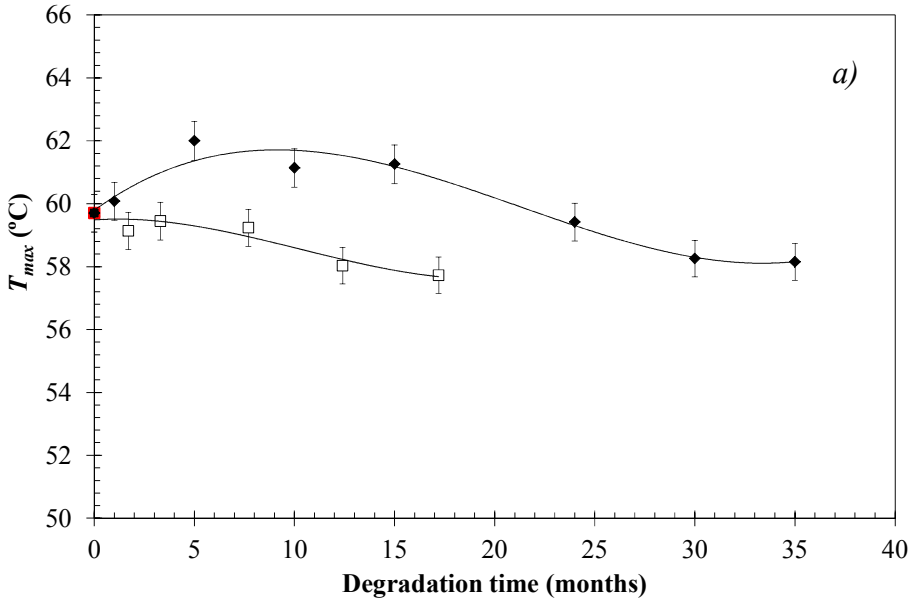

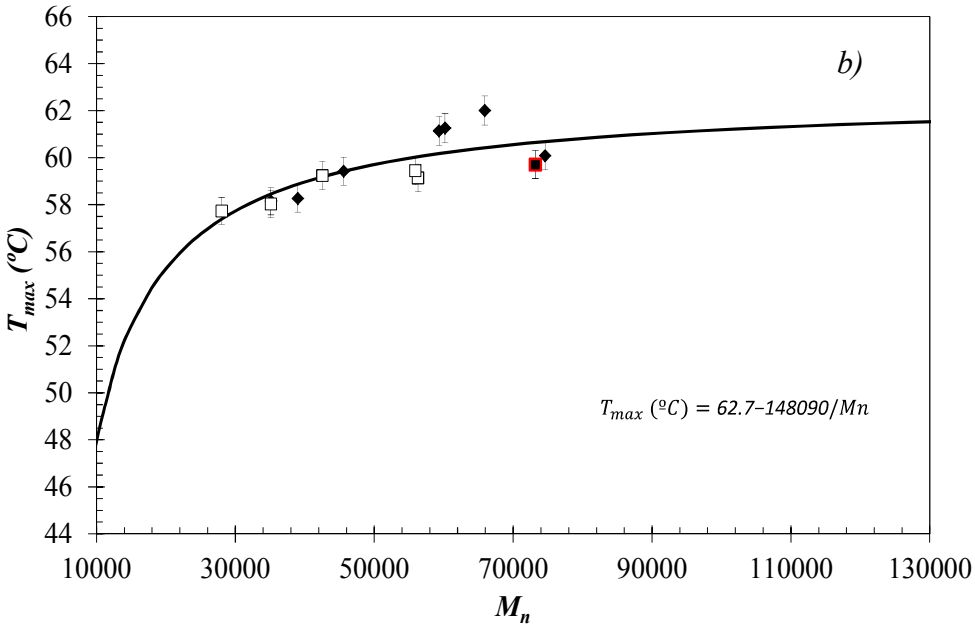

Figure 4-99 a) T_{max} vs. degradation time and b) T_{max} vs. M_n for (■) Plates, (◆) Biodegradation and (□) Photodegradation.

While a sinusoidal trend of T_{max} with time is observed for the biodegraded samples, photodegradation promotes slightly decreases in the values. The overall variations are not greater than 4ºC, and biodegraded samples exhibit higher T_{max} at similar degradation times.

The evolution of T_{max} with molar mass is consistent with the Fox-Flory equation, $T_{g,DMTA}^{\infty} = T_{max} + \frac{K}{M}$, where T_g^{∞} is the glass transition temperature for a polymer sample of infinite molar mass, M is the molar mass and K is a constant [66]. The experimental results were fitted to plots of T_{max} versus 1/ M_n, obtaining values of K=14.8·10^4 ºC/Da and $T_{g,DMTA}^{\infty}$ =62.7ºC.

Free volume study

The changes in the free volume occurring near the glass transition were evaluated by studying the relation between the temperature and the relaxation times, and ultimately calculating the thermal expansion coefficient (α_f) (see Chapter 3). In a first approach, the value of α_f was calculated using the Vogel-Fulcher-Tammann-Hesse equation, *VFTH* (Equation 3-74)

$$\ln f = A - \frac{m_v}{T - T_\infty} \tag{3-74}$$

where f is the frequency, $T_\infty = T_g - C_2$ and m_v can be calculated from the experimental data at $T = T_{max}$ of the E'' curve. The parameter m_v is inversely proportional to the free volume:

$$m_v = 2.3 \cdot C_1 \cdot C_2 = \frac{B}{\phi_g}(T_g - T_\infty) = \frac{B}{\alpha_f} \tag{3-75}$$

where $\phi_\infty = 0 = \phi_g + (T_\infty - T_g)\cdot\alpha_f$ and $\alpha_f = \frac{B}{m_v}$

The maxima of the relaxation processes of the samples under study were fitted using the Origin 7.5 software, following two suppositions. The first one is fitting Equation 3-74 to three parameters A, m_v and T_∞ and obtaining the best approximation of the equation. Alternatively, T_∞ was fixed as T_{max} - 51.6 K (taken from the universal value of C_2), and then only m_v and A were fitted.

Figure 4-100 *a* and *b* shows the Arrhenius map corresponding to the bio and photo degradation data, respectively. The experimental data follow a typical behavior of a glass transition.

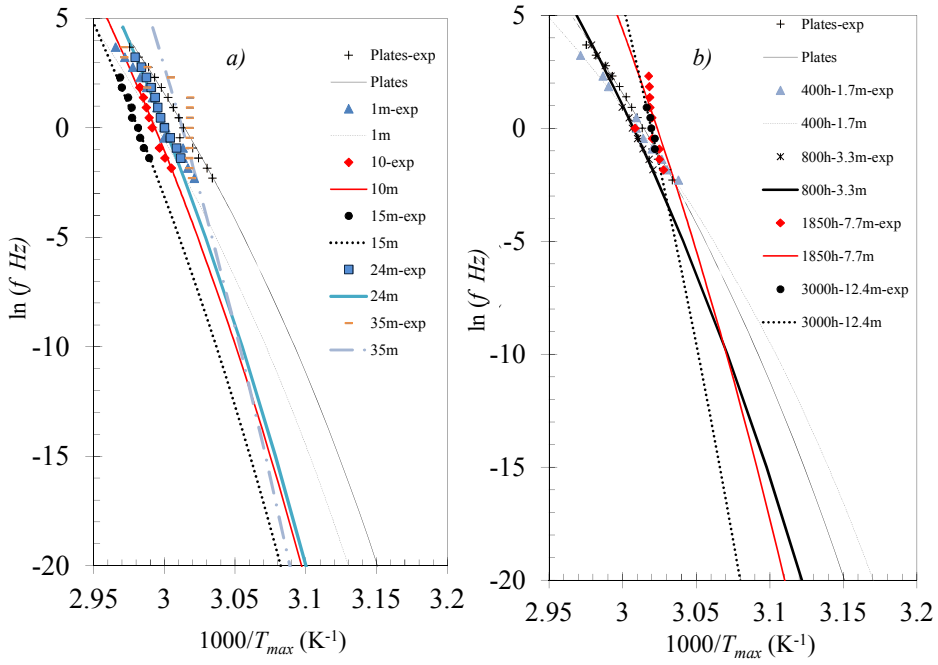

Figure 4-100 Arrhenius maps for *a*) biodegradation and *b*) photodegradation using the data of the fitting to 3 parameters (*A*, m_v and T_∞).

The VFTH curves shift to lower temperatures at increasing biodegradation times, except in the case of 35 months *a*). The same decreasing trend is occurring for photodegradation *b*). Using 3 parameters provides the highest R^2 values (≈ 1). The values obtained are shown in Table 4-24.

Table 4-24 VFTH parameters from fitting the 3 parameters of the equation.

Biodegraded samples	***A***	***m_v* (K)**	***T_∞* (K)**	**Photodegraded samples**	***A***	***m_v* (K)**	***T_∞* (K)**
Plates	26.6	683	306	Plates	26.6	683	306
1 m	24.9	582	310	400h-1.7m	61.6	4713	255
5 m	23.7	321	322	800h-3.3m	67.8	3667	278
10 m	18.4	203	323	1850h-7.7m	96.1	3999	290
15 m	16.0	161	325	3000h-12.6m	119.4	5298	287
24 m	10.7	53	328	4100h-17.2m	125.1	6250	285
30 m	6.0	11	332				
35 m	7.0	13	329				

Although comparison between the two types of degradation is difficult due to the different magnitude orders, opposite trends are observed for m_v with degradation time for bio and photodegraded samples. On the other hand biodegraded samples show lower values of T_∞ than the photodegraded ones.

In order to obtain more comparable parameters, a second approach was applied to fit the experimental results, by fixing T_∞. The theoretical and experimental curves of the Arrhenius maps were plotted in Figure 4-101, and the corresponding parameters are summarized in Table 4-25.

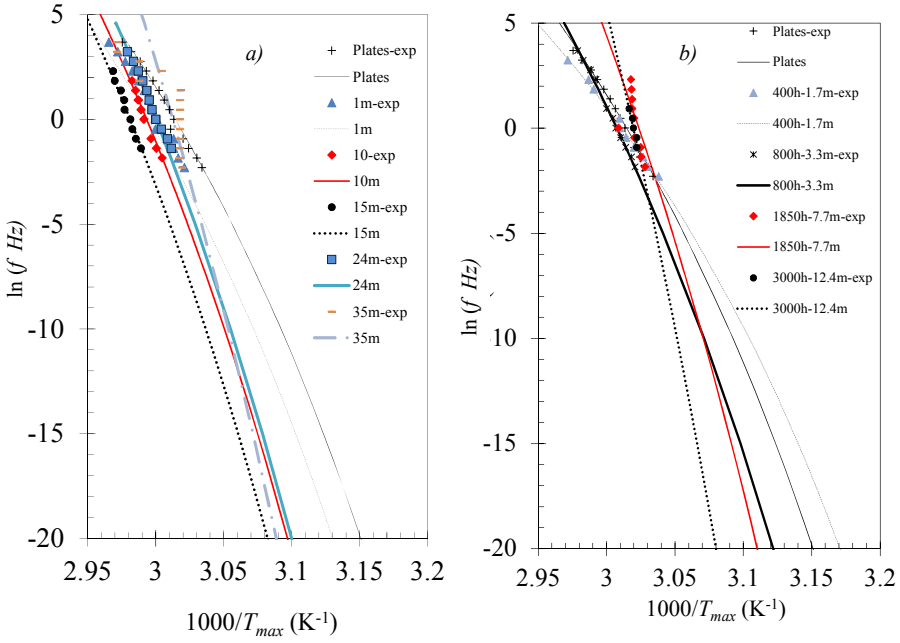

Figure 4-101 Arrhenius maps for *a*) biodegradation and *b*) photodegradation using the data of the fitting to 2 parameters (*A* and m_v).

Table 4-25 VFTH parameters, fixing T_∞ and fitting 2 parameters (*A* and m_v).

Biodegraded samples	*A*	m_v (K)	T_∞ (K)	Photodegraded samples	*A*	m_v (K)	T_∞ (K)
Plates	51.8	2670	280	0-Plates	51.8	2670	280
1	52.6	2750	282	400h-1.7m	41.6	2139	281
5	43.2	2164	284	800h-3.3m	64.6	3328	281
10	72.0	3699	283	1850h-7.7m	88.5	3300	281
15	75.7	3985	283	3000h-12.6m	138.6	7150	280
24	77.5	4054	281	4100h-17.2m	314	16461	279
30	102.1	4501	280				
35	107.8	5632	280				

More comparable parameters are observed when fixing T_∞. After an initial slight decrease, the values of *A* and m_v increases at long degradation times for photo and bio degraded samples. The values of α_f were calculated according to Equation 3-74, and considering *B*=1, and the results are shown in Figure 4-102 as a function of the degradation time.

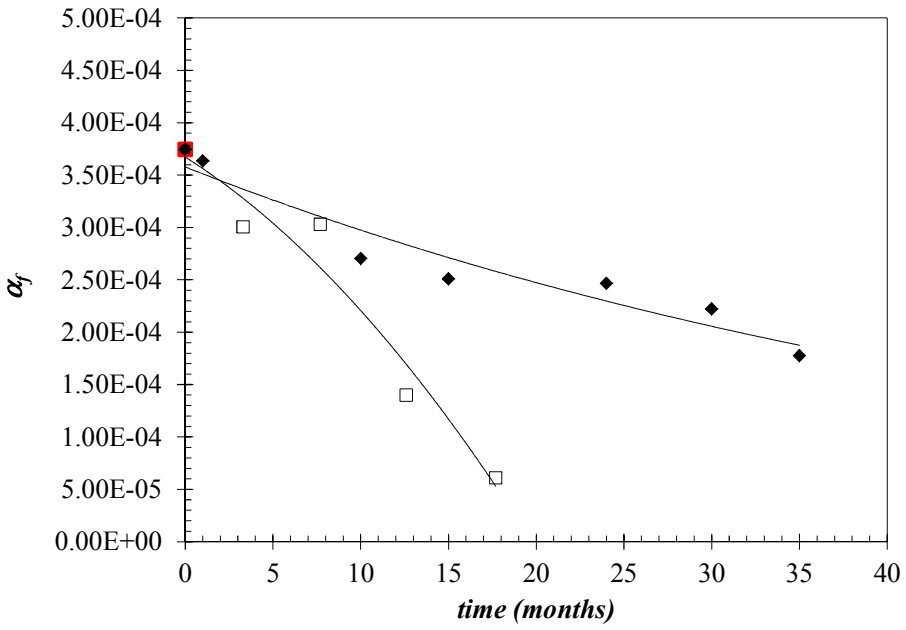

Figure 4-102 α_f vs. degradation time for (■) Plates, (◆) Biodegradation and (□) Photodegradation.

The values of α_f are in the 10^{-4} magnitude order, which is in agreement for most of the amorphous polymers [67,68], and decrease with bio and photo degradation time. The results are also depicted as a function of the molar mass in Figure 4-103.

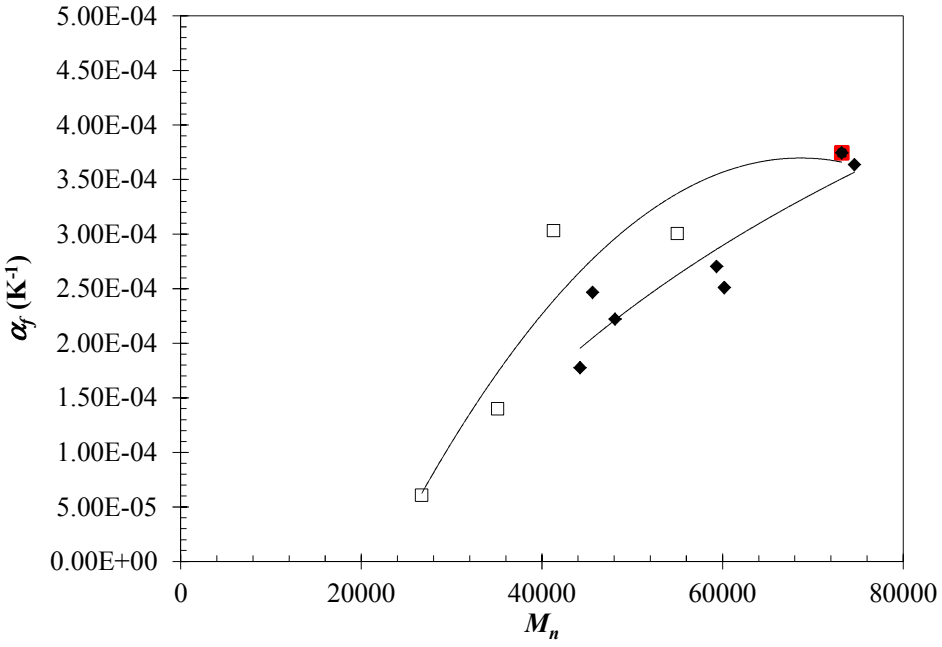

Figure 4-103 α_f vs. molar mass for (■) Plates, (◆) Biodegradation and (□) Photodegradation

α_f decreases when decreasing molar mass for all the samples regardless of the type of degradation. However, at similar molar masses, α_f is slightly smaller for the biodegraded

samples indicating less free volume. The distinct compaction of the samples, visible in the free volume effects, may account for differences in the crystallization processes in photo and bio degraded samples.

Table 4-26 compares the T_{on} and T_{end} values obtained in the DMTA traces for the crystallization process, and the results are plotted in Figure 4-104 as a function of the degradation time.

Table 4-26 Crystallization temperatures for the biodegraded samples.

Biodegraded samples	T_{on} (ºC)	T_{end} (ºC)	ΔT (ºC)
0	85.0 ± 0.1	120.0±1.4	40.0 ± 1.5
1	84.8± 0.2	114.2±1.0	29.4 ± 1.2
5	85.1 ± 0.3	103.1±0.8	18.0 ± 1.1
10	84.8± 0.2	103.8±0.5	19.0 ± 0.7
15	84.0 ± 0.4	95.8 ± 0.7	11.8 ± 1.1
24	80.6 ± 0.7	92.2 ± 0.2	11.6 ± 0.9
30	78.0 ± 1.0	89.9 ± 0.9	11.9 ± 1.9
35	79.0 ± 1.2	85.9 ± 0.4	6.0 ± 1.6

Photodegraded samples	T_{on} (ºC)	T_{end} (ºC)	ΔT(ºC)
0	85.1 ± 0.1	120.0 ± 1.0	40.0 ±1.1
400h-1.7m	86.9 ± 0.6	101.3 ± 1.1	14.4 ±1.7
800h-3.3m	86.2 ± 1.0	103.1 ± 1.0	17.0 ±2.0
1850h-7.7m	83.1 ± 0.8	102.1 ± 0.9	19.0 ±1.7
3000h-12.6m	83.0 ± 1.3	93.9 ± 0.8	8.9 ±2.1
4100h-17.2m	81.0 ± 1.2	92.0 ± 0.6	11.0 ±1.8

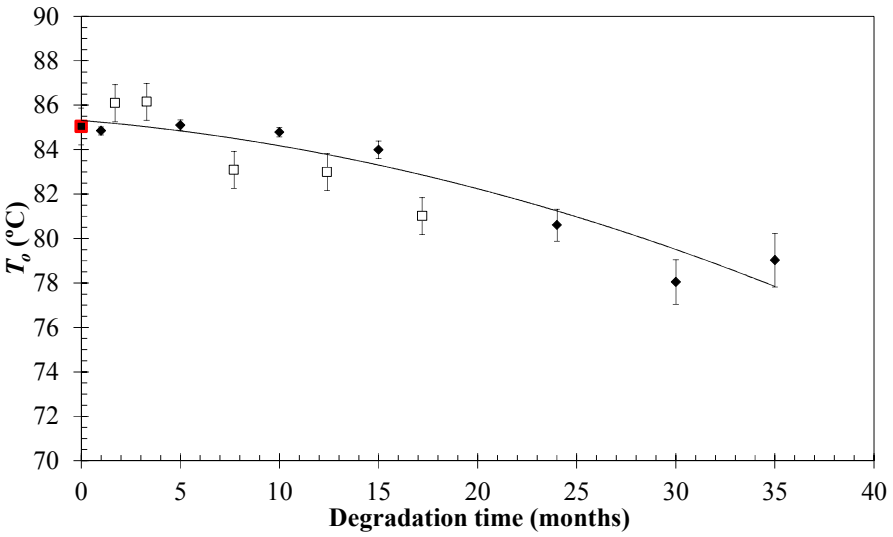

Figure 4-104 T_{on}versus degradation time for (■) Plates, (◆) Biodegradation and (□) Photodegradation.

Higher degradation times promote reductions of $\Delta T = T_{end} - T_{on}$ *and* T_{on}, which are especially visible after15 months. The values of T_{on} are also plotted in Figure 4-105 as a function of the molar mass.

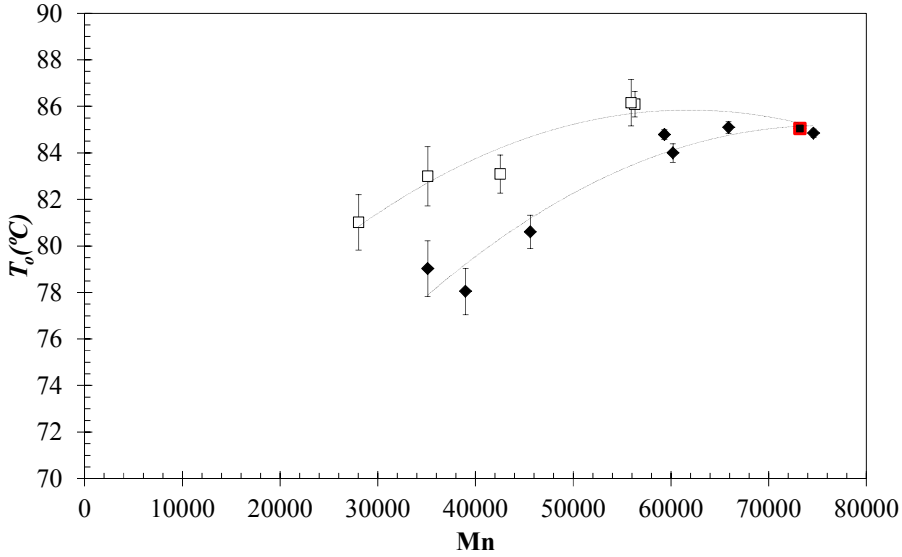

Figure 4-105 T_o vs. molar mass for (■) Plates, (◆) Biodegradation and (□) Photodegradation.

At similar molar masses, T_{on} is higher for the photodegraded samples than for the biodegraded ones, indicating an earlier start of the crystallization. Furthermore, this difference seems to be more acute at lower molar masses, following similar trend as for the free volume (Figure 4-103).

These results suggest that the different degradation mechanism can influence the free volume and the crystallization processes of the degraded samples [69].These results should be study with further detail to elucidate the origin of the effects of each type of degradation on the crystallization temperature observed by DMTA.

4.6 Analysis of thermal transitions

4.6.1 DSC thermograms for the thermally, bio and photo degraded samples

In order to study the thermal transitions of polylactide, the pellets, plates and degraded PLA samples were analyzed by DSC, following heating and cooling scans at 10ºC/min, as explained in Chapter 3.

Figure 4-106 and Figure 4-107 show the DSC thermograms corresponding to pellets and plates, respectively.

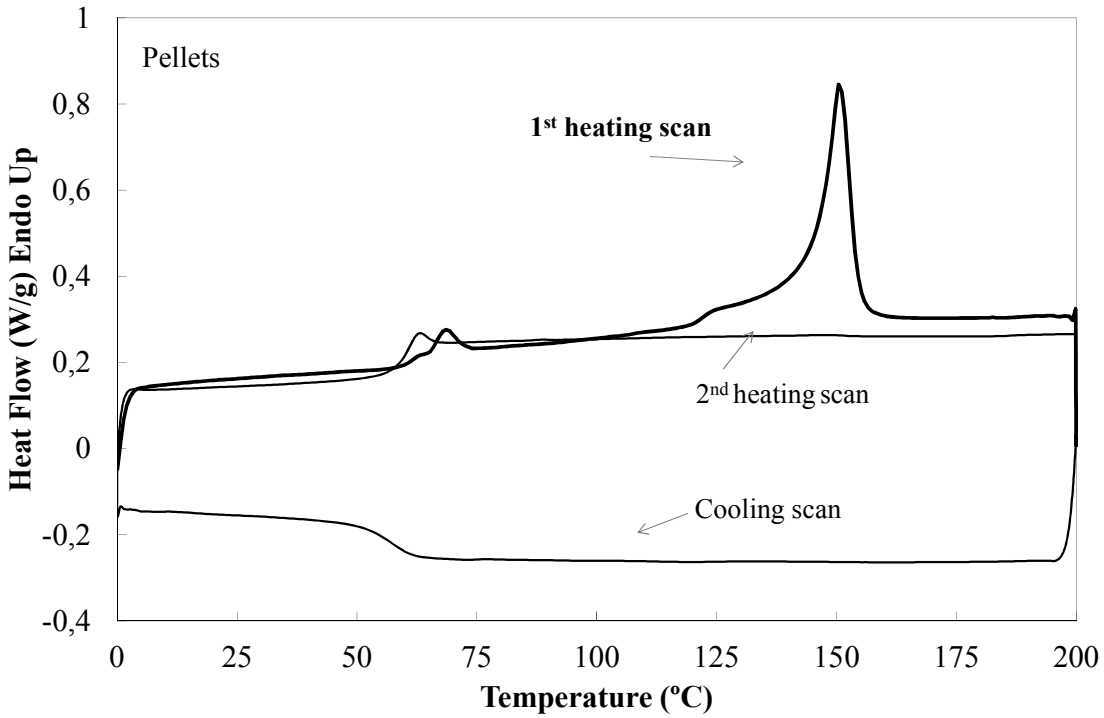

Figure 4-106 Calorimetric thermogram of pellets.

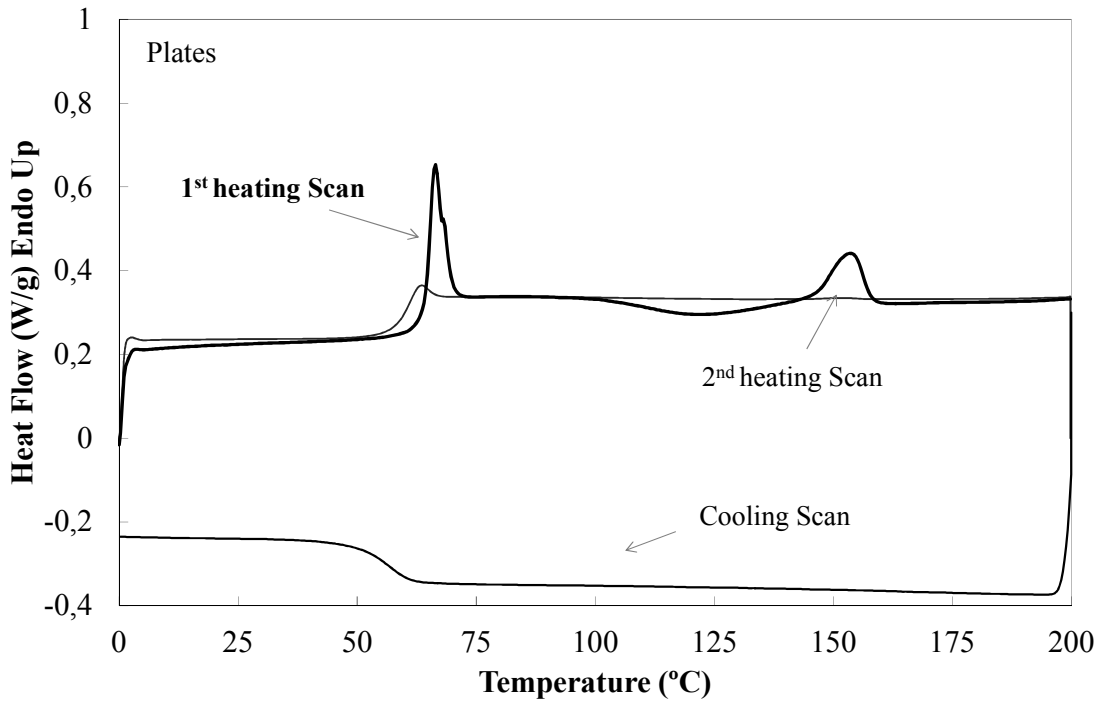

Figure 4-107 Calorimetric thermogram of plates.

In the first heating scan, the structural relaxation is visible overlapped with the glass transition relaxation, in the vicinity of 60ºC for pellets and plates. In the case of plates, the cold crystallization exotherm is observed at higher temperature, with the onset at around T_{on}≈85ºC and the minimum at T_c≈121ºC. The last thermal transition is the melting situated around T_m=150ºC for pellets and plates. The absence of the cold crystallization in the pellets indicates that the sample was initially crystalline, while plates are amorphous and only crystallize during heating. In the cooling scan only the glass transition is visible at around T_g≈56ºC, which is also seen in subsequent heating scans, overlapped with the enthalpic relaxation. T_g is calculated from the cooling scan as the inflection point of the transition. As expected, the glass transition is smaller than the corresponding mechanical relaxation observed by DMTA.

The first heating, the cooling and the second heating thermograms of some of the thermally, bio and photo degraded samples are shown in Figure 4-108 to 4-110 respective.

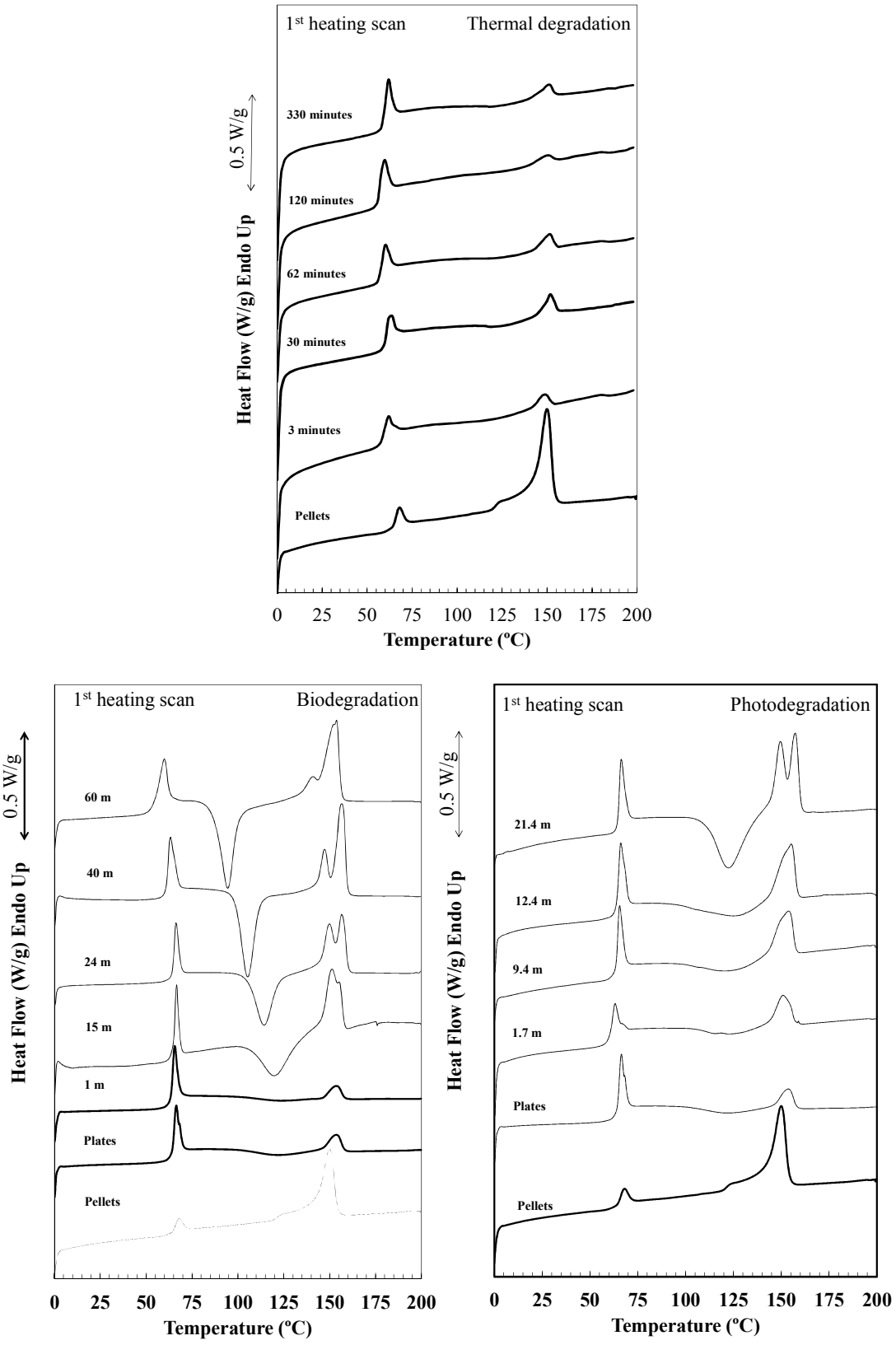

Figure 4-108 DSC first heating scans at 10ºC/min for the thermally, bio and photo degraded samples.

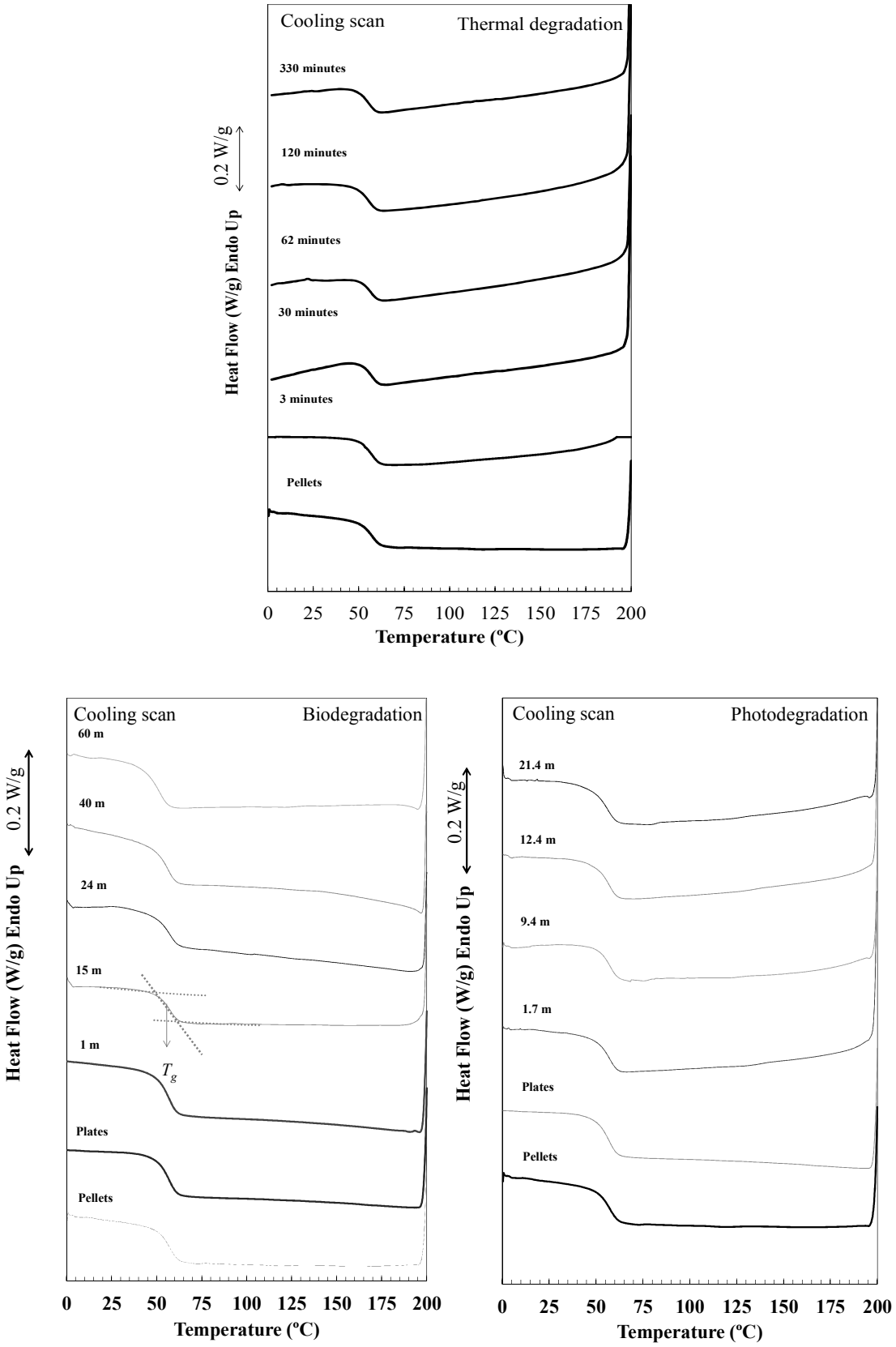

Figure 4-109 DSC cooling scans at 10ºC/min for the thermally, bio and photo degraded samples.

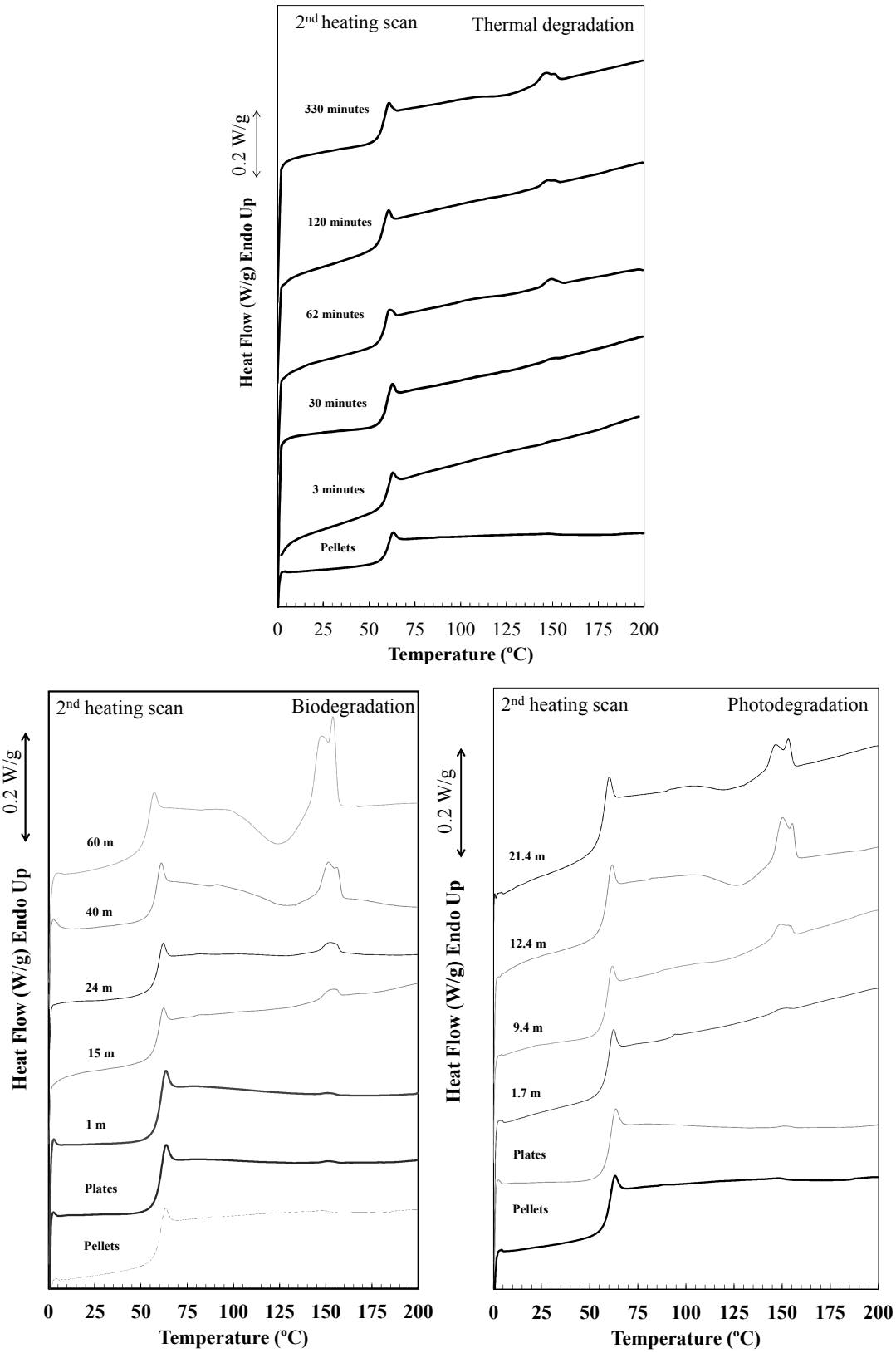

Figure 4-110 DSC second heating scans at 10ºC/min for the thermally, bio and photo degraded samples.

As degradation time advances more distinguishable crystallization and melting processes appear. In similar experimental conditions (10ºC/min from the glass), the thermally degraded samples exhibit lower crystallization than the rest of degraded samples

4.6.2 Double melting behavior

A double melting endotherm appeared when increasing degradation times for bio and photo degraded samples, contrarily to single crystallization processes exhibited by pellets and plates PLA. The origin of this phenomenon was investigated by studying the lower melting (1) and higher melting (2) endotherms. Several studies have reported the existence of double peak melting in several semicrystalline polymers [70,71]. This phenomenon has been explained by a melting-recrystallization-melting model. In melt-recrystallization a quantity of crystals previously formed, recrystallize after the first melting and melt again at higher temperatures. Under this view, the two melting peaks in a DSC thermogram correspond to: melting of some amount of the crystals formed during the crystallization process (low temperatures) and melting of the formed crystallites during the recrystallization (high temperatures).

When increasing the heating rate, this phenomenon can be inhibited and only one peak may be observed. Contrarily, at slow rates, the second melting endotherm is more pronounced since most of the crystals have time to recrystallize. *Yasuniwa et al* studied the non-isothermally melt-crystallization of poly(L-lactide) (PLLA) at different heating and cooling rates [72]. They created a profile of the appearance of the double melting phenomenon, reported as melting-recrystallization-melting process

In order to assess double melting in the degraded samples, isothermal crystallization experiments were performed at 130ºC, to ensure the formation of the crystal phase. Samples were heated at 5ºC/min from the glass to 130ºC, held during 5 min and heated to 200ºC at different heating rates β = 2, 5, 10, 20, 30 and 40ºC/min (see Table 4-27) The experiments were conducted on two samples: polylactide Bio 24 months and Photo 21.4 months. The two transitions were defined by the peak temperatures (T_{m1} and T_{m2}), the enthalpy involved (ΔH_{m1} and ΔH_{m2}) and the height of the endotherm (h_1 and h_2).

Table 4-27 Method for studying the double melting.

First Heating Step	Isothermal Crystallization	Second Heating step
45 to 130ºC at 5ºC/min	130ºC during 5 minutes	130 to 200ºC at 2ºC/min
		130 to 200ºC at 5ºC/min
		130 to 200ºC at 10ºC/min
		130 to 200ºC at 20ºC/min
		130 to 200ºC at 30ºC/min
		130 to 200ºC at 40ºC/min

Figure 4-111 shows the melting endotherms of the biodegraded sample at different heating rates, obtained during the second heating step. The individual enthalpies were calculated by separating the contribution of each peak by using Grams software. The results of T_{m1}, T_{m2}, ΔH_{m1}, ΔH_{m2}, h_1 and h_2 are shown in.

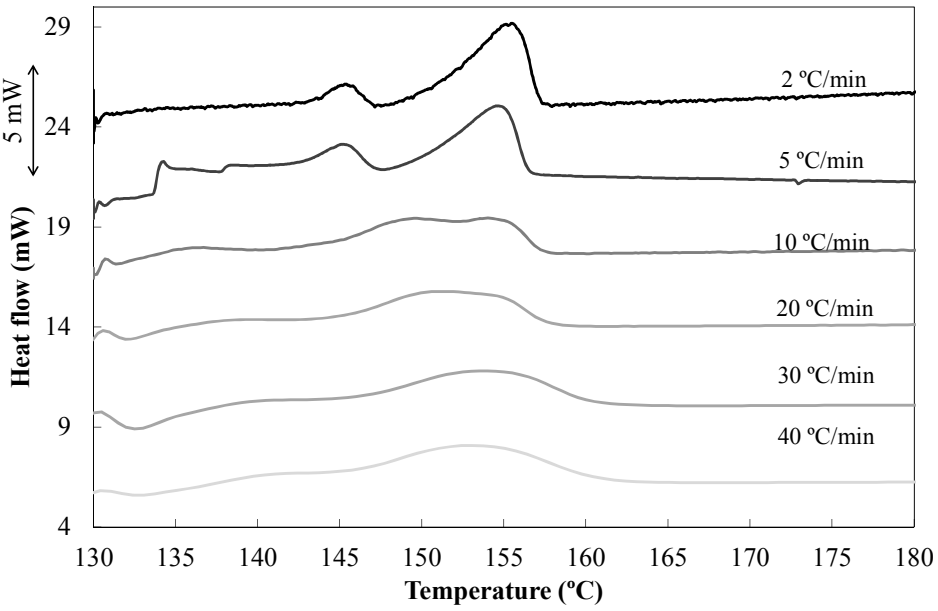

Figure 4-111 Biodegraded sample at 24 months crystallized from glass and heating at different heating rates.

Table 4-28 Results of the double melting peaks study for the 24 months biodegraded sample.

β (ºC/min	T_{m1}(ºC)	ΔHm_1 (J/g)	Height h_1	T_{m2} (ºC)	ΔHm_2 (J/g)	Height h_2
2	146	28.30	1.25	156	73.27	4.25
5	146	23.02	1.30	155	38.45	3.00
10	149	16.76	1.85	154	12.88	1.80
20	152	8.40	1.85	155	5.88	1.45
30	154	6.48	1.89	155	3.56	0.40
40	153	4.47	1.92	155	2.55	0.28

The influence of the heating rate on the relative magnitude of the two melting processes, the ratios of the enthalpies $\frac{\Delta H_{m2}}{\Delta H_{m1}}$ and heights $\frac{h_2}{h_1}$ were calculated and shown in Table 4-29.

Table 4-29 Enthalpy $\frac{\Delta H_{m2}}{\Delta H_{m1}}$ and the height $\frac{h_2}{h_1}$ ratios for the 24 months biodegraded sample.

β (ºC/min)	$\frac{\Delta H_{m2}}{\Delta H_{m1}}$	$\frac{h_2}{h_1}$
2	2.59	3.40
5	1.67	2.31
10	0.80	0.97
20	0.70	0.78
30	0.55	0.21
40	0.57	0.14

The same methodology was applied to the photodegraded sample under study (see Figure 4-112 and Table 4-30 to 4-31)

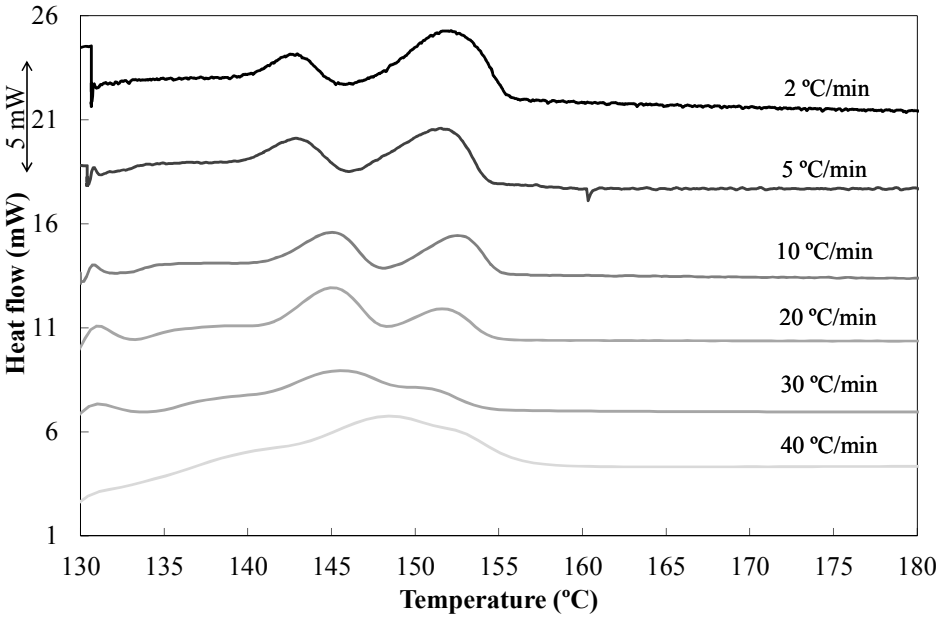

Figure 4-112 Photodegraded sample at 21.4 months crystallized from cooled and heating at different heating rates.

Table 4-30 Results of the double melting peaks study for the 5100h-21.4m photodegraded sample.

β (ºC/min	T_{m1}(ºC)	ΔHm_1 (J/g)	Height h_1	T_{m2} (ºC)	ΔHm_2 (J/g)	Height h_2
2	143	32.61	2.00	152	111.70	3.60
5	143	21.63	2.20	152	37.24	2.80
10	145	12.08	1.90	152	13.10	1.60
20	145	11.93	2.40	151	4.15	1.40
30	145	12.35	2.03	151	1.33	1.03
40	148	19.66	2.50	153	1.21	0.90

Table 4-31 Enthalpy ratio $\frac{\Delta H_{m2}}{\Delta H_{m1}}$ and the Height ratio $\frac{h_2}{h_1}$ for the 5100h-21.4 m photodegraded sample.

β (ºC/min)	$\frac{\Delta H_{m2}}{\Delta H_{m1}}$	$\frac{h_2}{h_1}$
2	3.43	1.80
5	1.72	1.27
10	1.08	0.84
20	0.35	0.58
30	0.11	0.51
40	0.06	0.36

Figure 4-113 *a* and *b* shows the enthalpy and height ratios, respectively, for the two samples, showing a progressive decrease of the ratios at increasing heating rates. This indicates that the formation of crystals from the first melt is not fast enough to permit the recrystallization process ($\Delta H_{m1} > \Delta H_{m2}$). These results evidence the occurrence of the melting-recrystallization-melting process in the PLA samples, which may be taken into account in further discussion of the calorimetric results, and also the possibility to inhibit it at high heating rates.

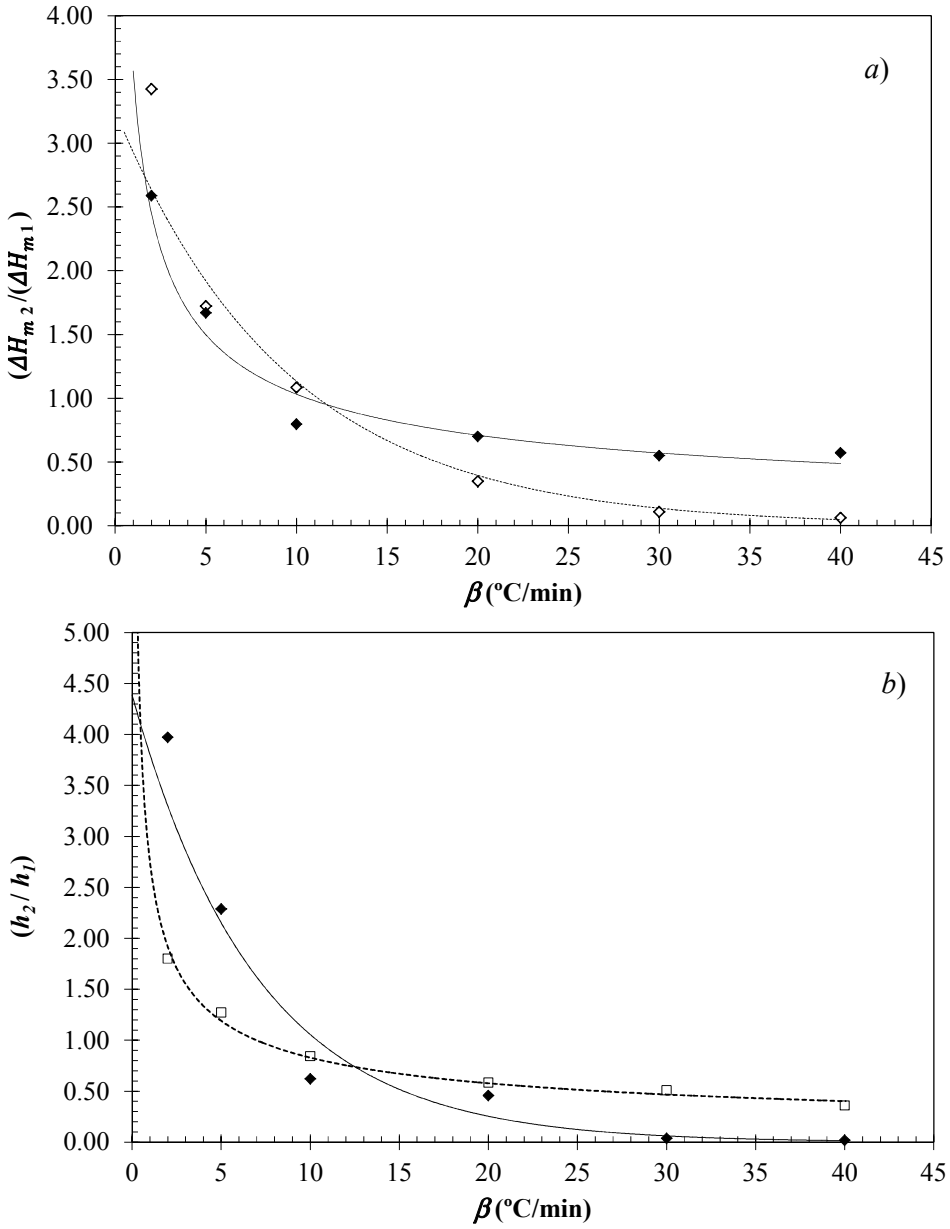

Figure 4-113 *a*) Enthalpy ratio $\frac{\Delta H_{m2}}{\Delta H_{m1}}$ and *b*) height ratio $\frac{h_2}{h_1}$ versus the heating rate for (◆) Bio 24 months and (□) Photo 5100h-21.4 months.

4.6.3 Thermal parameters

The influence of degradation on the glass transition (T_g), the crystallization (T_c) and the melting (T_m) temperatures was analyzed from the calorimetric thermograms of all the samples. The temperature values obtained from the first heating and cooling scans are listed in Table 4-32, while the values obtained from the second heating scan are displayed in Table 4-33. In samples showing double melting, the melting temperature listed, T_m, corresponds to the first endotherm (T_{m1}, lower temperature), as the second one corresponds to the melting of the previously recrystallized crystals. The experimental results were completed with data of biodegraded samples with higher molar masses from *ref.* 22, in order to investigate the influence of the molar mass on the PLA thermal properties.

Table 4-32 Characteristic temperature values for the thermally, bio and photo degraded samples obtained from the 1st heating and cooling scan.

Sample Name	T_g (ºC)	T_c (ºC)	T_m (ºC)
Pellets	57.0 ± 0.1	-	149.6 ± 0.7
Plates	55.7 ± 0.4	121.6 ± 1.0	152.5 ± 1.1
Thermally degraded			
3 min	56.4 ± 0.2	119.0 ± 0.2	148.1 ± 0.2
30 min	56.0 ± 0.3	123.1 ± 1.5	150.9 ± 0.5
62 min	55.6 ± 0.3	121.2 ± 0.4	151.6 ± 0.5
120 min	55.1 ± 0.1	122.8 ± 0.5	146.6 ± 1.5
330 min	53.0 ± 1.5	118.9 ± 0.7	147.9 ± 2.0
Biodegradation *ref*. 22			
0 m	56.5 ± 1.0	123.0 ± 1.0	151.6 ± 2.0
1 m	56.1 ± 0.8	119.0 ± 1.3	151.7 ± 0.8
5 m	56.7 ± 1.0	125.2 ± 1.6	151.8 ± 1.6
10 m	55.7 ± 0.7	123.2 ± 1.1	151.4 ± 1.2
15 m	55.9 ± 0.6	119.7 ± 1.2	151.8 ± 1.3

Biodegraded-			
1 m	55.7 ± 0.3	120.5 ±1.5	150.5 ± 1.2
5 m	56.0 ± 0.1	120.5 ± 0.9	150.6 ± 0.4
10 m	56.4 ± 0.3	123.8 ± 0.6	153.7 ± 0.5
15 m	56.8 ± 0.2	121.1 ± 1.0	151.3 ± 0.5
20 m	56.0 ± 0.2	114.1 ± 0.1	150.0 ± 1.3
24 m	57.1 ± 0.7	113.0 ± 3.0	148.7 ± 0.4
30 m	56.1 ± 0.2	109.8 ± 0.8	148.8 ± 0.3
35 m	56.1 ± 0.3	107.4 ± 0.3	147.7 ± 0.1
40 m	56.5 ± 0.7	105.4 ± 0.1	145.6 ± 1.0
60 m	50.0 ± 0.2	94.8 ± 0.3	140.8 ± 0.1
Photodegradation			
400h-1.7 m	56.5 ± 0.2	121.5 ± 0.7	150.8 ±0.2
800h-3.3 m	56.1 ± 0.2	124.9 ± 3.0	155.3 ± 0.6
1850h-7.7 m	56.2 ± 0.2	121.9 ± 2.0	154.9 ± 0.1
2250h-9.4 m	56.8 ± 0.1	121.5 +/ -1.5	148.2 ± 0.5
3000h-12.6 m	55.4 ± 0.2	121.6 ± 1.3	148.0 ± 1.0
4100h-17.2 m	54.9 ± 0.2	122.2 ± 1.2	147.5 ± 0.1
5100h-21.4 m	55.6 ± 0.5	120.9 ± 2.0	147.1 ± 0.7

Table 4-33 Characteristic temperature values for the thermally, bio and photo degraded samples obtained from the 2nd heating scan.

Sample Name	T_c (ºC)	T_m (ºC)
Plates	*130.7 ± 2.3	*151.1 ± 0.7
Thermally degraded		
3 min	-	-
30 min	*129.2 ± 0.5	*149.0 ± 0.8
62 min	129.5 ± 0.4	148.1 ± 0.6
120 min	123.8 ± 0.4	145.7 ± 0.6
330 min	122.7 ± 0.4	143.1 ± 0.5
Biodegradation *ref.* 22		
1 m	127.4 ± 2.0	150.7 ± 1.6
5 m	124.6 ± 2.1	151.5 ± 2.6
10 m	123.5 ± 1.9	149.8 ± 2.5
15 m	124.3 ± 3.0	151.3 ± 1.8

Biodegraded		
1 m	*126.1 ± 2.7	*148.7 ± 1.7
15 m	*126.6 ± 2.4	*151.6 ± 2.1
24 m	127.9 ± 3.1	151.3 ± 2.5
30 m	127.3 ± 0.2	151.9 ± 0.2
35 m	127.2 ± 0.5	151.7 ± 0.2
40 m	127.0± 1.9	151.4 ± 1.9
60 m	123.2 ± 1.8	147.1 ± 1.0
Photodegraded		
400h-1.7 m	*127.2 ± 1.9	*149.2 ± 0.9
1850h-7.7 m	*127.1 ± 1.2	*150.7 ± 0.1
2250h-9.4 m	123.7 ± -2.5	146.2 ± 1.4
3000h-12.6 m	127.0 ± 1.8	150.1 ± 0.4
4100h-17.2 m	126.1 ± 2.3	147.3 ± 0.7
5100h-21.4 m	124.1 ± 2.0	145.8 ± 1.0

*Temperatures obtained with a huge magnification of the spectra

Figure 4-114 shows the evolution of the glass transition temperature, T_g, with the degradation time for all the degraded samples.

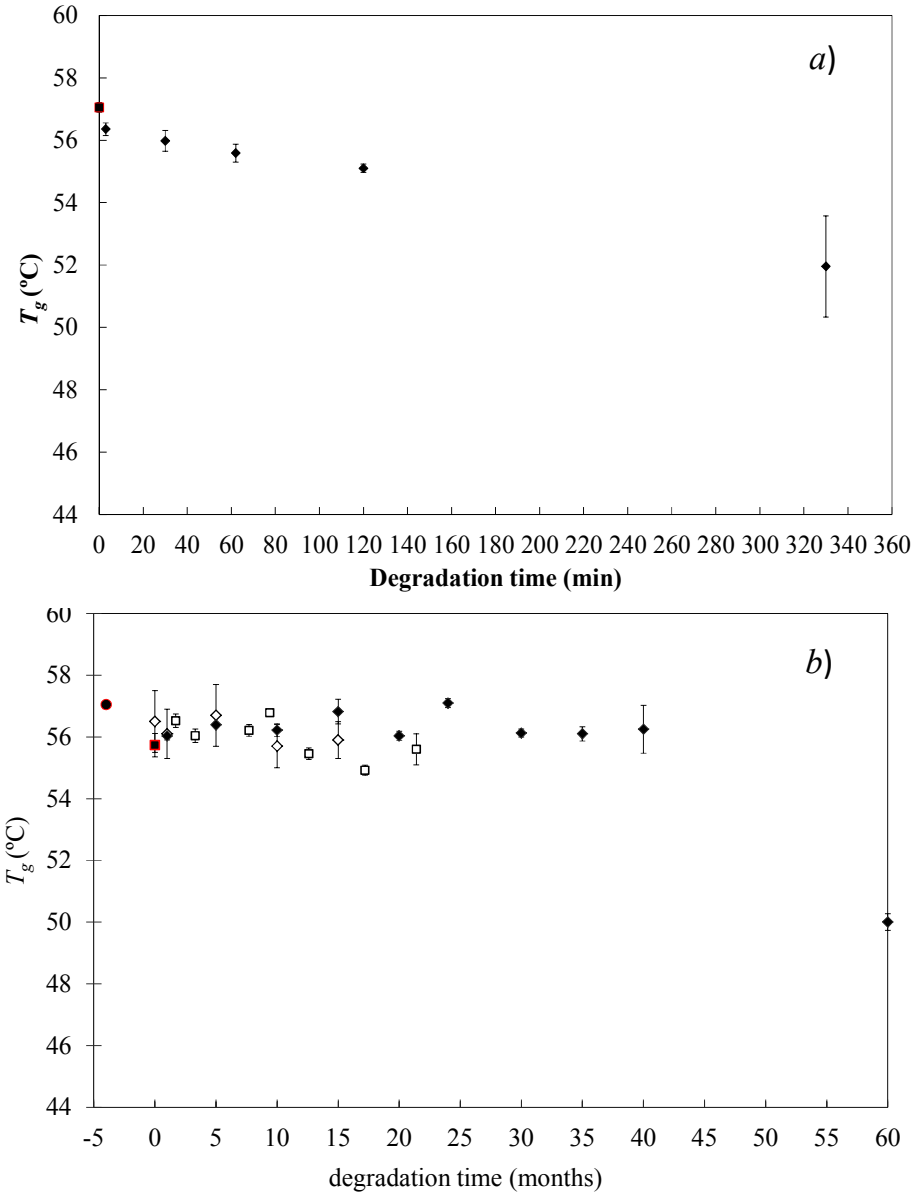

Figure 4-114 T_g vs. degradation time *a*) Thermal degradation and *b)* (●) Pellets, (■) Plates, (◆) Biodegradation, (◇) bio-*ref.* 22 and (□) Photodegradation.

The glass transition temperature slightly decreases upon thermal exposure at 220ºC while no significant decrease is observed by photodegradation. In the case of bio degraded samples, no apparent effects are observed at low-medium degradation times, while the sample degraded during 60 months exhibits a sudden drop in its T_g.

Figure 4-115 shows the crystallization and melting temperatures versus degradation time for all degraded samples, obtained from the first heating scan.

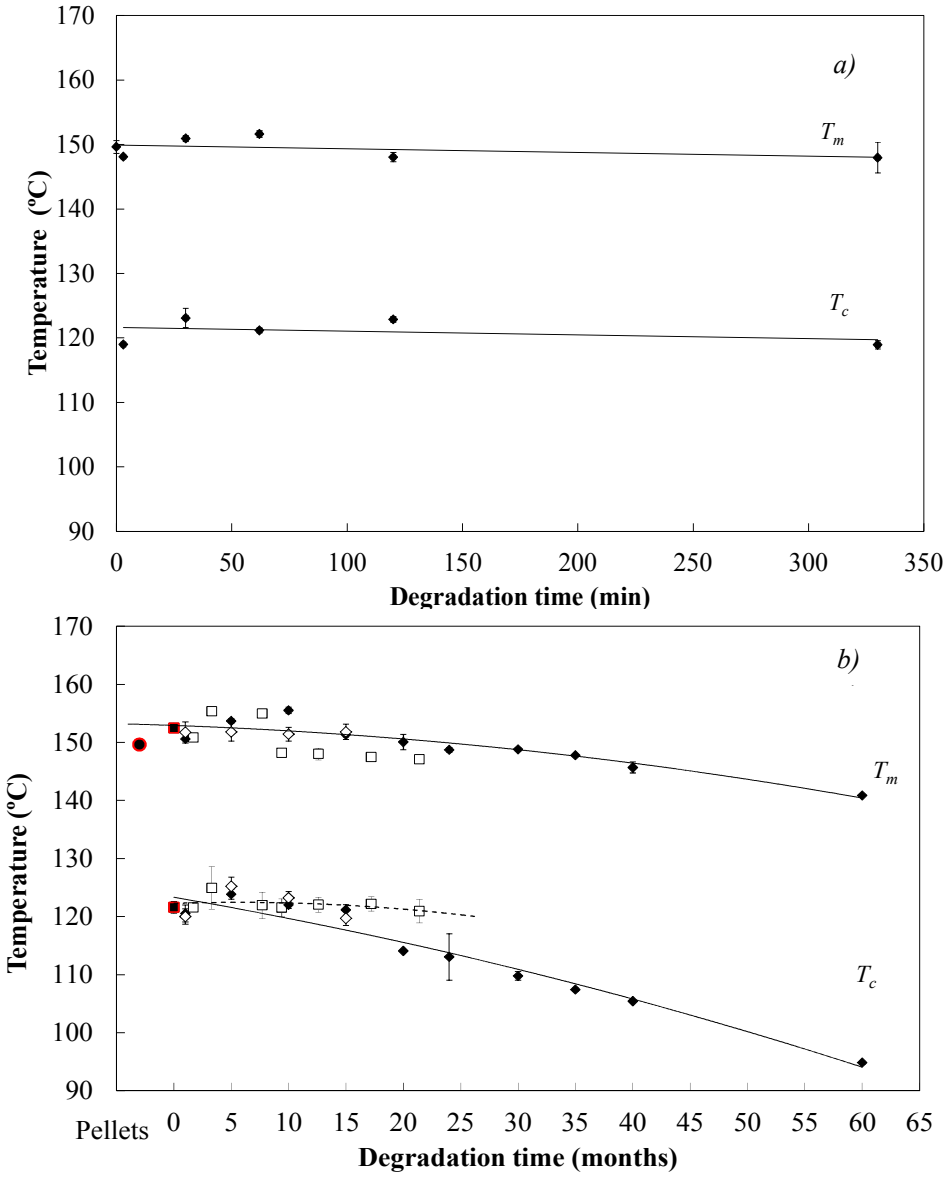

Figure 4-115 T_c and T_m vs. degradation time for *a*) Thermal degradation and *b*) (●) Pellets, (■) Plates, (◆)Biodegradation, (◇) bio-*ref.* 22 and (□) Photodegradation from the 1st heating scan.

A slightly decrease is observed in the crystallization and melting temperatures with degradation time for the thermally and photo degraded samples. A more pronounced decrease occurs for samples biodegraded over 15 months in soil.

The previous parameters were studied as a function of the molar mass, with the aim to compare the effect of each degradation type on the thermal behavior of polylactide. The experimental results are shown in Figure 4-116, which also includes the values reported in *ref.* 22.

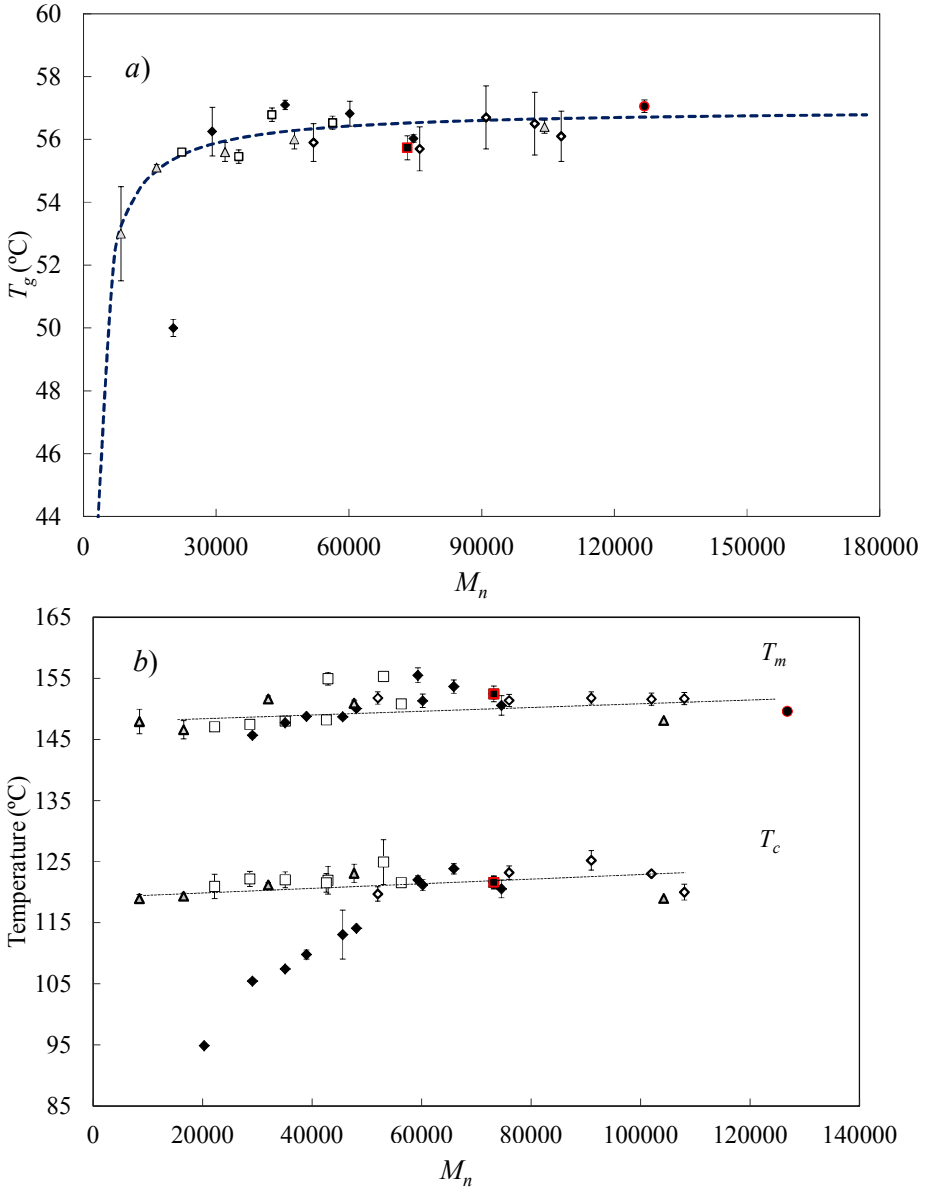

Figure 4-116 *a)* T_g vs. M_n and *b)* T_c and T_m vs. M_n for (●) Pellets, (■) Plates, (△) Thermal Degradation, (◆) Biodegradation , (◇)bio- *ref.* 22 and (□) Photodegradation from the 1st heating scan

The glass transition undergoes changes only at values of M_n lower than 29000. The influence of the molar mass decay on T_g follows the Fox equation, $T_g^{\infty} = T_g + \frac{K}{M_n}$, where T_g^{∞} is the glass transition temperature for a polymer sample of infinite molar mass and K is a constant [66]. Fitting the experimental T_g values to Fox equation provides values of $K=4.7 \cdot 10^4$ and T_g^{∞} =57 ºC. The corresponding law is also plotted in Figure 4-116 -*a*) as a dashed line, evidencing a good fit. This result is comparable to the values of K in the literature, K= 5.5· 10^4 and 7.3·10^4, for PLLA and PDLLA, respectively [20].

Representations of T_c and T_m vs M_n display similar decreasing patterns for all the degradation types above M_n=50000, when the tendency of T_c deviates by decreasing more drastically after biodegradation. This result implies differences in the morphological features controlling the crystallization above the glass transition, resulting from different degradation types. If the sub-products of all the degradation mechanisms had similar structures, the variation of the T_c with M_n would be very similar, due to the strong dependence of T_c on the molar mass. This supports the view of biodegradation lowering the crysallisation temperature at low molar masses, which was already seen by DMTA. On the other hand, the similar tendencies of T_m suggest the formation of similar crystal sizes, during cold crystallization, although it is worth remarking that usually the dependence of T_m with molar mass is not as sensible as T_c (differences are only detected below 29000).

Results from the second heating were examined in order to remove the effect of the thermal history on the thermal parameters. The corresponding values of T_m and T_c are shown in Figure 4-117 as a function of degradation time, for plates and all the degraded samples.

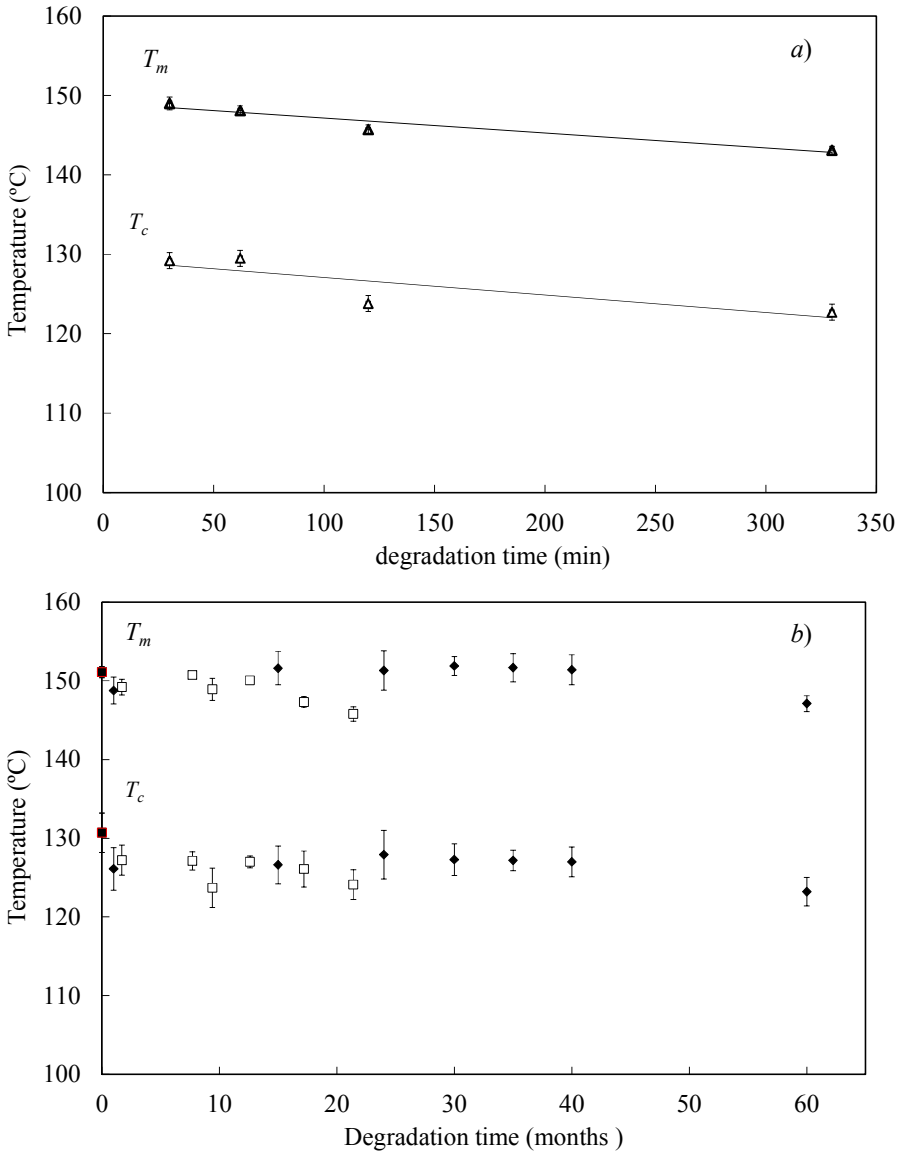

Figure 4-117 T_c and T_m vs. degradation time from the 2nd heating scan for (a) Thermal degradation and (b) (■) Plates, (◆) Biodegradation and (□) Photodegradation.

The crystallization and melting temperatures slightly decreases with time, and the differences could fall within the experimental error. The same slightly decreasing trend in T_c and T_m is observed as a function of M_n, see Figure 4-118.

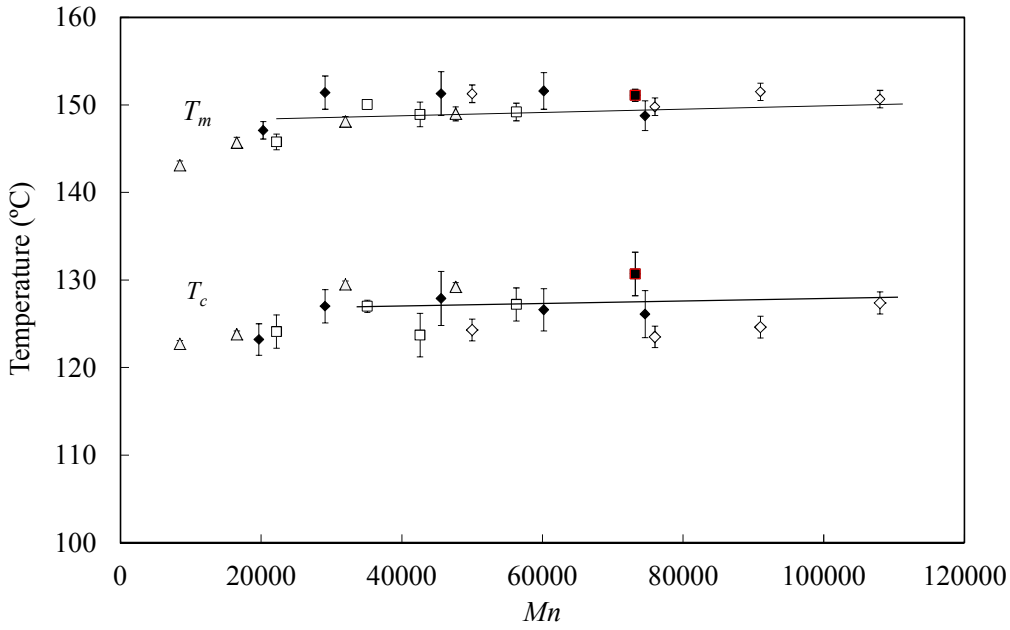

Figure 4-118 T_c and T_m vs. M_n for ((■) Plates, (△) Thermal Degradation, (◇) *ref.* 22, (◆) Biodegradation and (□) Photodegradation.

The enthalpies involved in the transitions observed in the thermograms were also obtained and analyzed respect to time and molar mass. The structural relaxation enthalpy (ΔH_s), the crystallization enthalpy (ΔH_c) and the melting enthalpy (ΔH_m) were calculated from the first and second heating scans and the results shown in Table 4-34 and 3-35, respectively, for all the samples under study. In general, less degraded samples present a very small crystallization enthalpy, as the crystallization process is hindered at high molar masses.

Table 4-34. Characteristic enthalpy values obtained from the first heating for the thermally, bio and photo degraded samples.

Sample Name	ΔH_s (J/g)	ΔH_c (J/g)	ΔH_m (J/g)
Pellets	3.16 ± 0.1	-	32.64 ± 0.7
Plates	7.56 ± 0.4	4.68 ± 1.0	5.70 ± 1.1
Thermally degraded			
3 min	4.00 ± 0.10	4.49 ± 2.15	2.00 ± 0.82
30 min	4.29 ± 0.12	4.60 ± 1.89	4.25 ± 1.71
62 min	5.98 ± 0.25	5.27 ± 1.37	2.42 ± 1.10
120 min	6.40 ± 0.21	2.66 ± 0.54	1.92 ± 0.47
330 min	7.00 ± 0.30	4.66 ± 1.73	2.37 ± 0.72
Biodegraded- *ref.* **22**			
0 m	5.70 ± 2.00	6.95 ± 0.32	7.27 ± 0.30
1 m	5.92 ± 2.10	7.14 ± 0.39	8.61 ± 0.34
5 m	6.55 ± 1.90	12.12 ± 0.51	13.90 ± 0.56
10 m	6.60 ± 3.00	18.42 ± 0.69	18.50 ± 0.74
15 m	8.90 ± 3.00	30.02± 1.15	30.70± 1.23
Biodegraded			
1 m	7.86 ± 0.13	3.27 ± 0.02	4.05 ± 0.05
5 m	8.28 ± 0.01	12.50 ± 0.10	13.00 ± 0.15
10 m	8.16 ± 0.05	18.85 ± 0.40	18.90 ± 0.25
15 m	8.46 ± 0.01	29.60 ± 0.10	25.00 ± 0.15
20 m	8.34 ± 0.07	26.60 ± 0.05	27.45 ± 0.02
24 m	8.25 ± 0.07	30.52 ± 0.05	30.70 ± 0.45
30 m	11.26 ± 0.04	36.12 ± 0.20	33.20 ± 0.35
35 m	10.44 ± 0.01	35.22 ± 0.13	35.90 ± 0.10
40 m	11.64 ± 0.20	35.10 ± 0.40	34.00 ± 0.40
60 m	11.82 ± 0.12	40.10 ± 0.15	40.00 ± 0.05
Photodegraded			
400h-1.7 m	7.80 ± 0.13	7.15 ± 0.64	7.40 ±0.90
800h-3.3 m	8.00 ± 0.32	9.30 ± 0.90	8.65 ±1.00
1850h-7.7 m	8.30 ± 0.90	13.60 ± 1.30	11.15 ±1.80
2250h-9.4 m	9.15 ± 0.01	13.40 ± 1.90	14.10 ±1.70
3000h-12.6 m	9.30 ± 0.40	18.30 ± 0.13	17.00 ±0.30
4100h-17.2 m	9.60 ± 0.20	28.40 ± 5.00	28.00 ±3.40
5100h-21.4 m	11.15 ± 0.80	31.90 ± 3.50	32.10 ±5.10

Table 4-35 Characteristic enthalpy values from the second heating scan for the thermally, bio and photo degraded samples obtained.

Sample Name	ΔH_s (J/g)	ΔH_c (J/g)	ΔH_m (J/g)
Pellets	2.44± 0.50	~0	~0
Plates	1.56± 0.08	1.60 ± 0.50	1.58 ± 0.54
Thermal degradation			
3 min	1.77 ± 0.20	~0	~0
30 min	1.62 ± 0.26	~0	~0
62 min	2.46 ± 0.54	0.85 ± 0.09	0.80 ± 0.09
120 min	2.30 ± 0.38	1.45 ± 0.10	1.48 ± 0.10
330 min	2.75 ±0.84	3.00 ± 0.15	3.10 ± 0.15
Biodegradation- *ref.* **22**			
0 m	1.60 ± 0.22	1.14 ± 0.11	1.21 ± 0.15
1 m	1.42 ± 0.03	0.66 ± 0.10	0.70 ± 0.14
5 m	1.65 ± 0.05	2.10 ± 0.21	2.00 ± 0.18
10 m	1.68 ± 0.11	1.56 ± 0.16	1.62 ± 0.19
15 m	1.90± 0.11	3.18 ± 0.33	3.10 ± 0.40
Biodegraded			
1 m	1.62 ± 0.02	1.80 ± 0.10	2.2 ± 0.12
15 m	1.38 ± 0.03	3.80 ± 0.17	3.75 ± 0.15
24 m	1.32 ± 0.01	4.10 ± 0.20	4.00 ± 0.20
30 m	1.94 ± 0.01	4.40 ± 0.15	4.43 ± 0.23
35 m	1.89 ± 0.02	5.58 ± 0.08	5.68 ± 0.03
40 m	1.74 ± 0.02	6.64 ± 0.17	6.22 ± 0.15
60 m	1.92 ± 0.01	11.46 ± 0.22	11.40 ± 0.22
Photodegradation			
400h-1.7 m	1.34 ± 0.11	1.65± 0.60	1.70 ± 0.70
800h-3.3 m	1.60 ± 0.12	2.60 ± 0.47	1.80 ± 0.37
1850h-7.7 m	2.34 ± 0.34	3.20 ± 0.60	3.13 ± 0.20
2250h-9.4 m	1.71 ± 0.40	4.10 ± 1.20	4.10 ± 1.40
3000h-12.6 m	1.82 ± 0.20	3.95 ± 0.30	3.24 ± 0.39
4100h-17.2 m	1.94 ± 0.08	4.40 ± 1.00	3.66 ± 1.00

*Enthalpies obtained with a high magnification of the spectra

Enthalpy relaxations occur when the samples are heated above the T_g after annealing in the glass stat [61,73,74,75,76,77,78]. Other authors correlated the changes in structural relaxation of glassy state of PET, this parameters was also studied for the degradation of PLA [79].

Figure 4-119 and Figure 4-120 plot the structural relaxation enthalpy (ΔH_s) values, obtained from the 1st heating scan, versus time and molar mass, respectively, for all the samples under study.

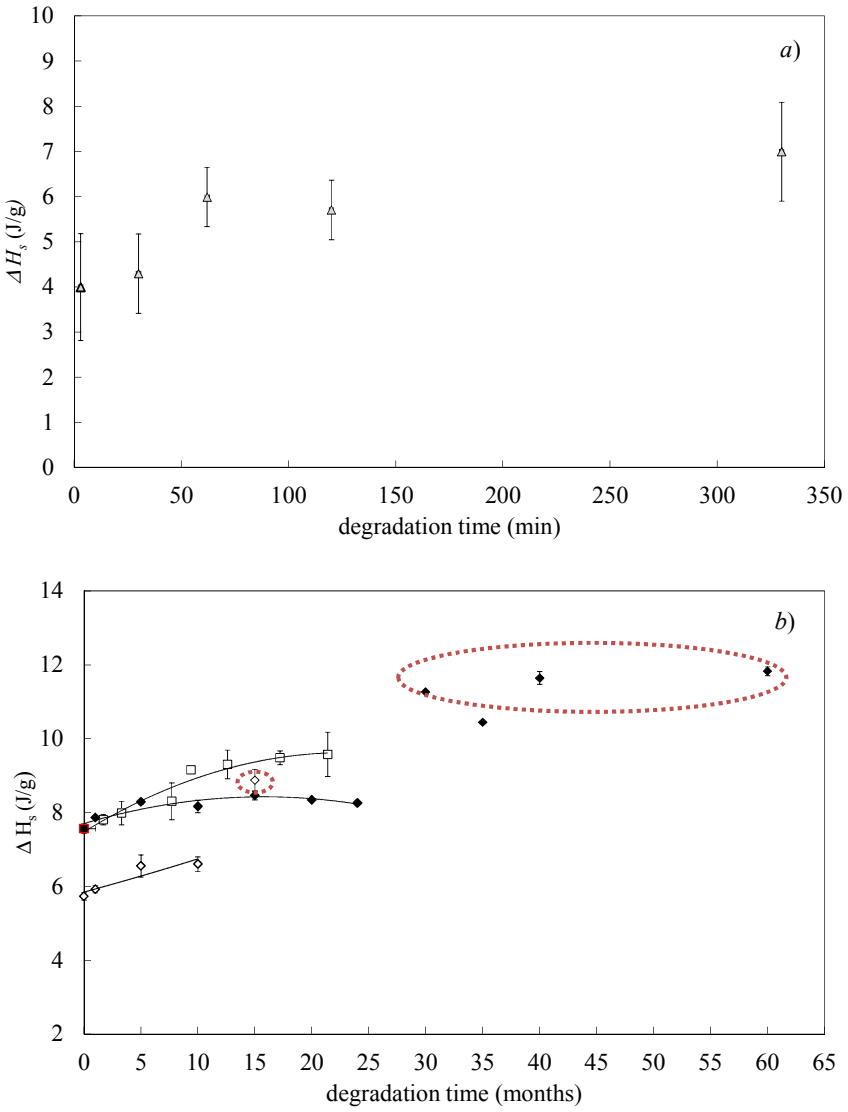

Figure 4-119 ΔH_s vs. degradation time for *a*) Thermal degradation and *b*) (■) Plates, (◆) Biodegradation, (◇) *ref.* 22 and (□) Photodegradation. Data obtained from the 1st scan.

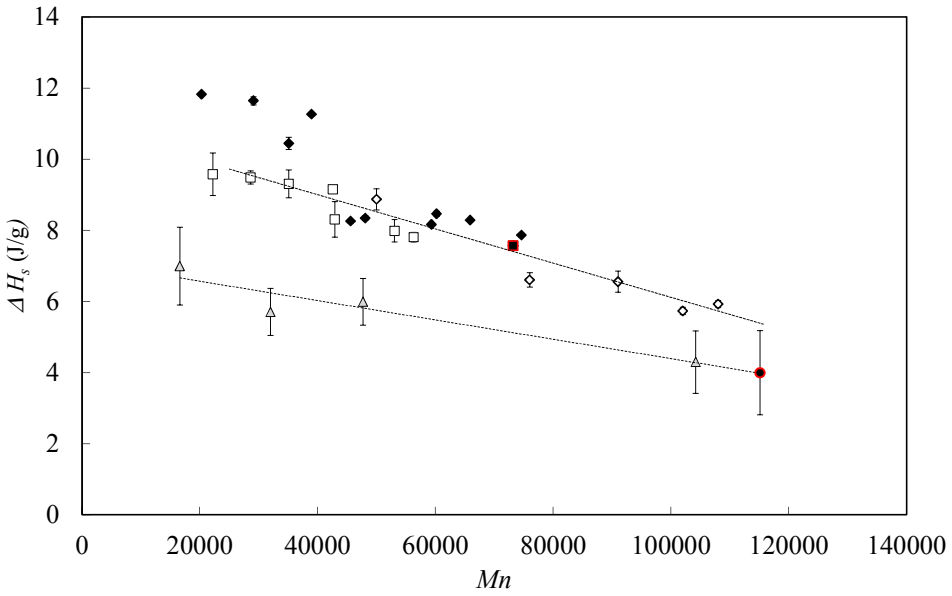

Figure 4-120 ΔH_s vs. molar mass for (●) Pellets , (■) Plates, (△) Thermal degradation (◆) Biodegradation, (◇)*ref.* 22 and (□) Photodegradation. Data obtained from the 1st scan.

Figure 4-119 *a* and *b* shows slightly higher ΔH_s values when increasing the degradation time. For the photo degraded samples, ΔH_s increases faster with time, while the thermally and bio degraded samples present lower values. This can be probably attributed to different degradation temperatures.

Figure 4-120 displays an increase in ΔH_s with decreasing molar mass, in all the degraded samples. The values of ΔH_s of the thermally degraded samples are lower and present more deviation than those obtained for the bio and photo degraded ones (these samples were melted during different times and directly analyzed by DSC). The values from all the biodegraded samples present a common trend versus molar mass. Moreover, below M_n=50000, a change of the trend is observed.

PLA samples by studying the crystallization enthalpies obtained from the 1st heating scan (ΔH_c). Figure 4-121 and Figure 4-122 show plots of ΔH_c versus the degradation time and molar mass, respectively. The total melting enthalpy was not shown since the values and trends were nearly the same as those obtained for the crystallization enthalpy (Figure 4-121).

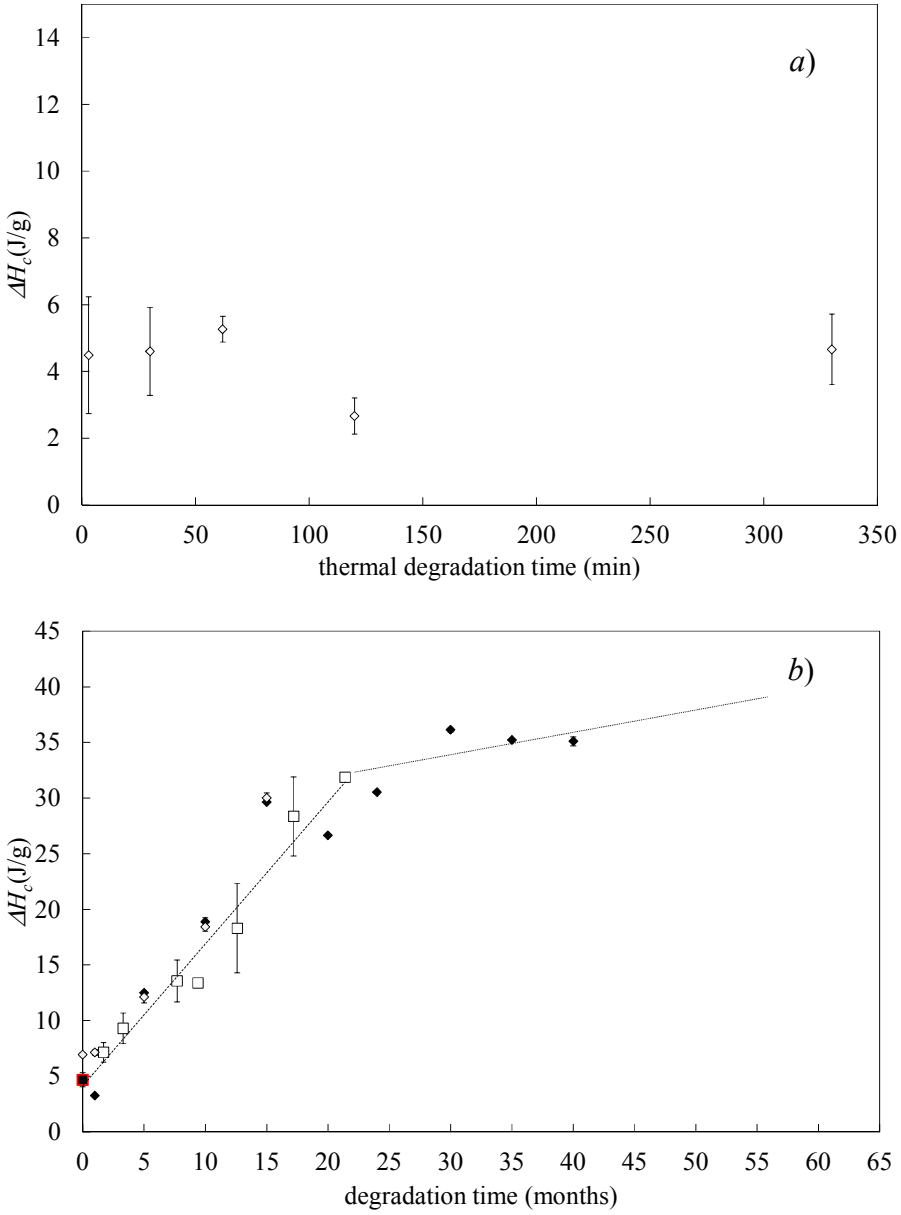

Figure 4-121 ΔH_c vs. degradation time for *a*) Thermal degradation and *b*) (■) Plates, (◆) Biodegradation, (◇) *ref.* 22 and (□) Photodegradation. Data obtained from the 1st scan.

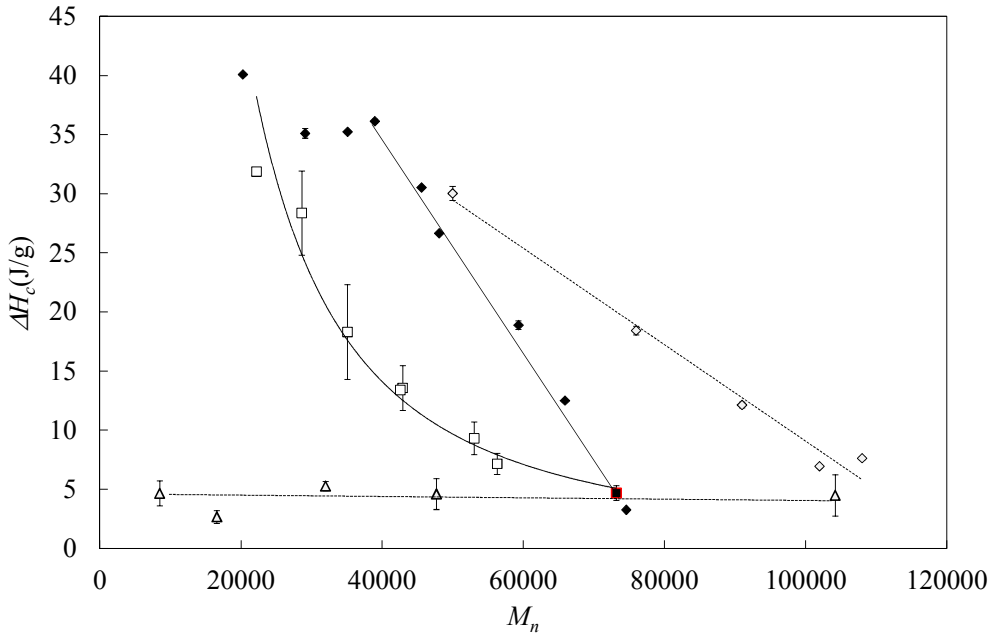

Figure 4-122 ΔH_c versus M_n for (■) Plates, (△) Thermal degradation (◆) Biodegradation, (◇) ref. 22 and (□) Photodegradation. Data obtained from the 1st scan.

The values of crystallization enthalpy in Figure 4-121 a) for the thermally degraded samples were considerably smaller than those obtained for the other degradations, see Figure 4-121 b). The amount of crystals formed during heating in the thermally degraded samples were very small, the crystallinity is about 5% in all the temperature range, taking $\Delta H_m^0 = 93$ J/g as the melting enthalpy of totally crystallized PLA [80]. However for the bio and photo degraded samples a linear increasing trend for ΔH_c with time was observed until 24 months of biodegradation, where a change is detected. The crystallinity can reach values till 40% for bio and photodegraded samples.

On the other hand Figure 4-122 evidences differences in the trends of ΔH_c with M_n, depending on the degradation type. While the values corresponding to thermally degraded samples do not vary to a great extent, photodegradation and biodegradation show exponential and linear increments, respectively. These changes observed in ΔH_c, due to the different degradation processes, can be related to the distinct crystallization of the sub-products produced by different mechanisms.

The crystallization study was completed by analysis of the data from the 2nd heating scan, which is shown in Figure 4-123.

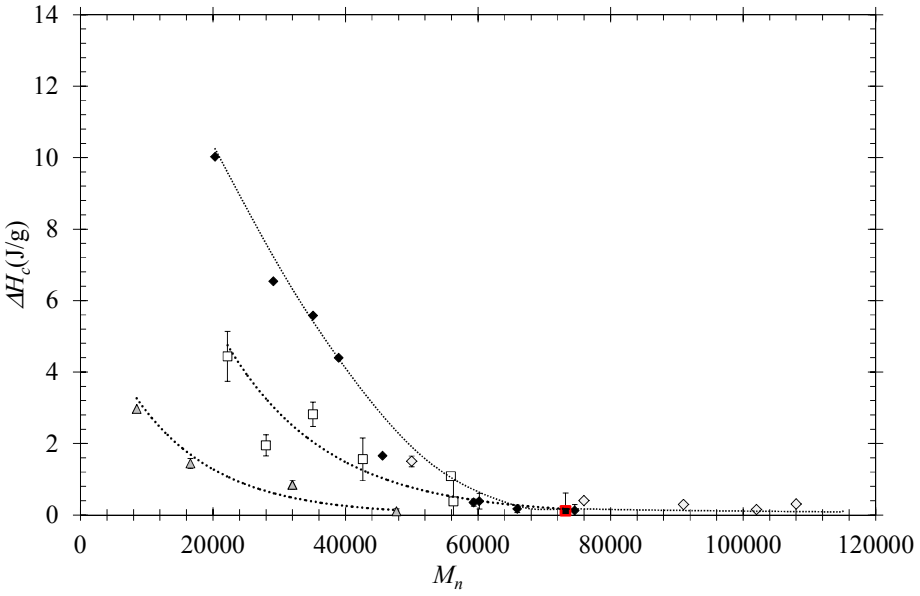

Figure 4-123 ΔH_c vs M_n (■) Plates, (△), Thermal degradation, (◆) Biodegradation, (◇) *ref.* 22 and (□) Photodegradation

Some remarks can be extracted from the ΔH_c vs M_n plot:

- The crystallization enthalpies are very small and the values of thermal degradation can present some uncertainty.
- The crystallization enthalpy follows a common tendency with molar mass for both biodegradation processes.
- Different influence on the crystallization processes due to thermal, bio and photo degradation is verified. The slowest crystallization process is occurring in the thermally degraded samples, followed by the photo and by the bio degraded samples. ΔH_c vs M_n follow exponential behavior in thermal and biodegradation, and polynomial second order in photodegradation.

4.7 Kinetics of the crystallization from the melt

4.7.1 Spherulitic Morphology

The effect of degradation on the formation of crystalline structures in PLA was evaluated by studying the formation of spherulites during isothermal crystallization.

With that purpose, thin films of PLA of 50 μm thickness of were crystallized isothermally at different temperatures, T_c, from the melt at 180ºC, and optical micrographs were obtained between crossed polarizers in an optical microscope. The spherulitic morphology was detected in all the films regardless T_c, although more open spherulites were presented at higher temperatures. The spherulites principally showed negative birefringence, as reported by many authors [81].

Non-significant differences were observed in the number of nuclei activated at each temperature between the samples, regardless of the degradation process. On the other hand, at lower molar mass different spherulites and dispersity on the growth rates were observed depending on the degradation type, especially visible in photodegradation.

The micrographs showed higher nucleation at increasing molar masses, and vice-versa, as can be seen in Figure 4-124.

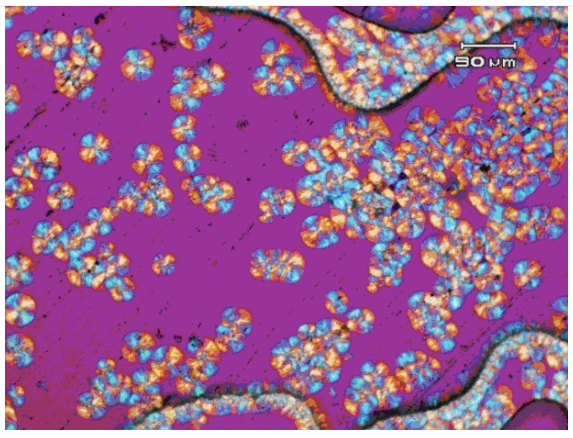

M_n= 126800 T_c =116.5ºC t= 90 min
Pellets

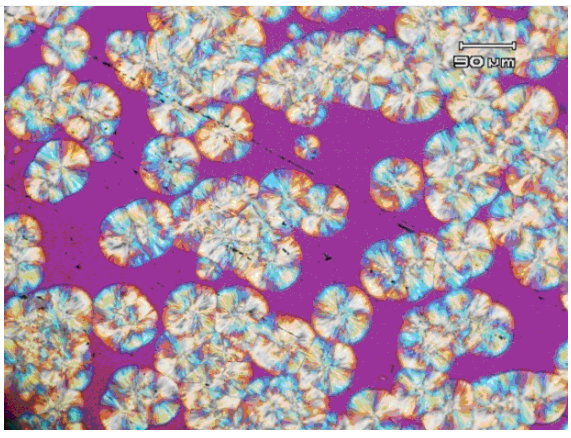

M_n = 73200 T_c =116.5ºC t= 90 min
Plates

Figure 4-124 Micrographs at 116.5ºC for studying the effect of the molar mass on the nucleation and growth, rate for pellets and plates.

The influence of undercooling, $\Delta T = (T_m^0 - T_c)$ in the crystallization rate, where T_m^0 is the temperature at which a crystal without any surface would melt and T_c is the crystallization temperature, is this is visible in Figure 4-125, that shows that for high undercooling, the nucleation is the predominant effect, since the growth is enhanced with time for low undercooling.

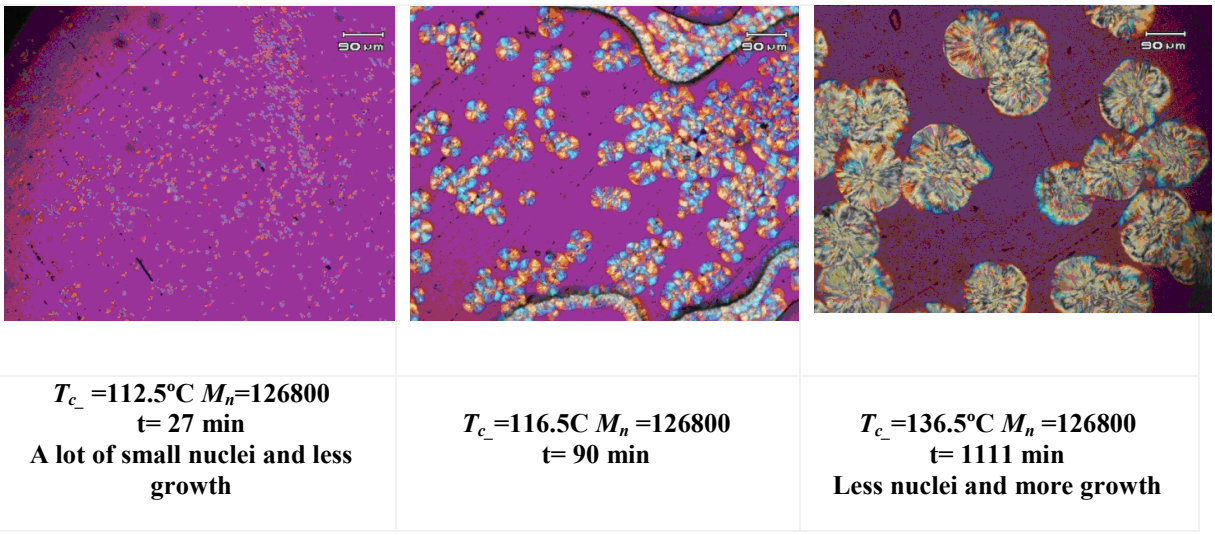

$T_{c\_}$ =112.5ºC M_n=126800 t= 27 min A lot of small nuclei and less growth	**$T_{c\_}$=116.5C M_n =126800 t= 90 min**	**$T_{c\_}$=136.5ºC M_n =126800 t= 1111 min Less nuclei and more growth**

Figure 4-125 Micrographs for comparing the undercooling effect in polylactide for plates.

The effect of each degradation type on the crystallization process of PLA was evaluated from the optical micrographs and the corresponding kinetic study. For selected examples, Figure 4-126 *a* and *b* show the micrographs for the pellets and the thermally degraded sample at 220ºC during 3 minutes (similar M_n) providing non-noticeable differences between them. The same can apply to Figure 4-126 *c* and *d* show, where the micrographs for lower molar mass samples: plates and the biodegraded sample at 1 month are shown. Thus, in general, non-appreciable effects on the spherulites micrographs were observed after degradation of PLA.

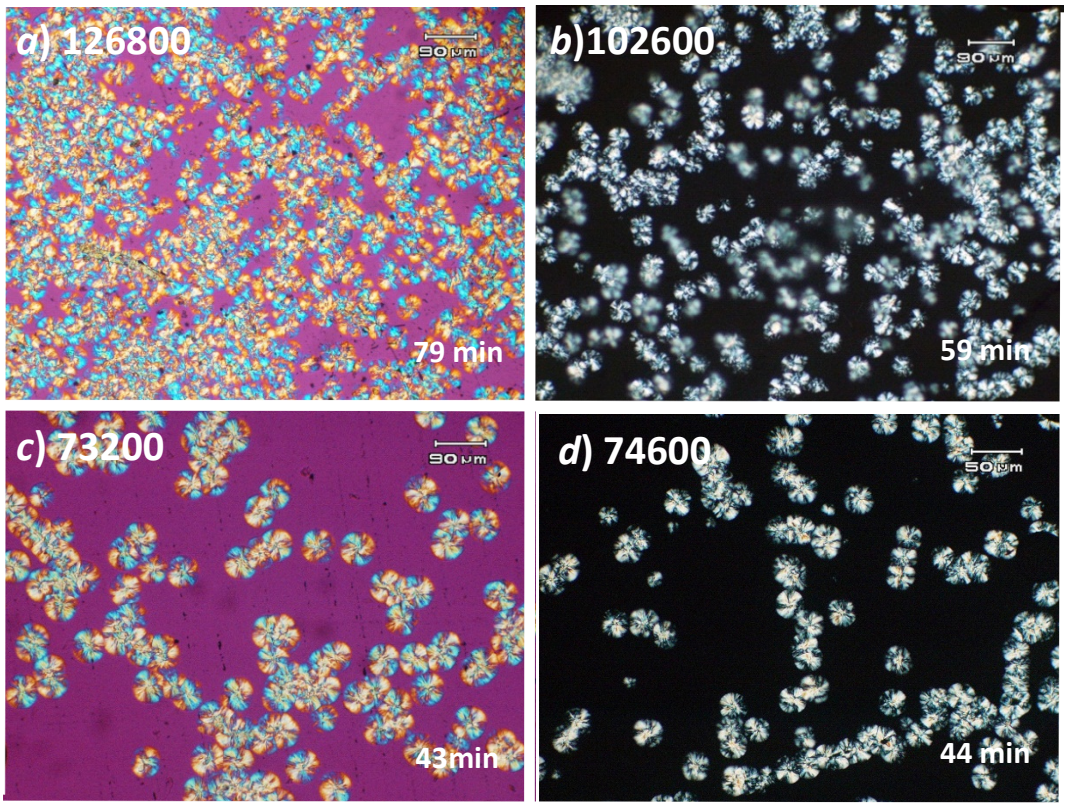

Figure 4-126 Micrographs at 121.5 ºC for *a*) Pellets, *b*)Thermal 3 min, *c*) Plates and *d*) Bio 1 month.

A similar comparison was made between samples degraded by different degradation types, at different molar mass and at T_c =121.5ºC. At similar molar masses biodegradation lead to higher spherulites, being this effect particularly noticeable at M_n below 50000. These results indicated that the growth rate is higher in bio than in the thermally or photo degraded samples, even when nucleation is similar. The most significant can be seen below M_n =22000, as the micrograph from thermally degraded present some nuclei but very fuzzy.

The information provided by the micrographs can give some insight on the DSC results. The thermally degraded samples barely presented a crystallization exotherm in the DSC heating scans from the glass (see Figure 4-110), in comparison to the bio and photo degraded samples. This could be then attributed to a lower spherulitic growth rate, although these results should be further analyzed by the assessment of the crystallization kinetics.

Thermal degradation	Biodegradation	Photodegradation
	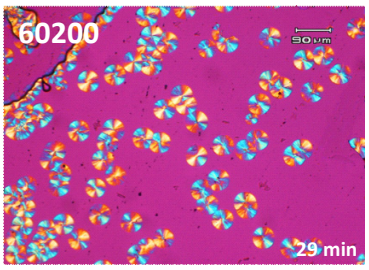	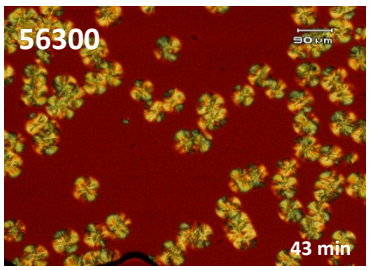
	Bio 15m	**Photo 400h-1.7m**
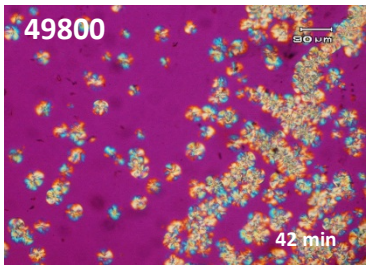	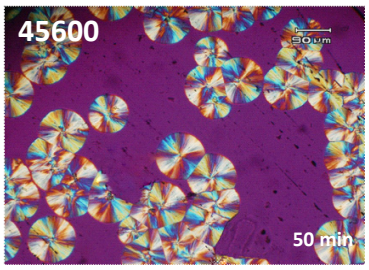	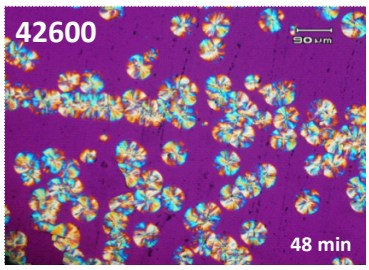
Thermal 30min	**Bio 24m**	**Photo 2250h-7.4m**
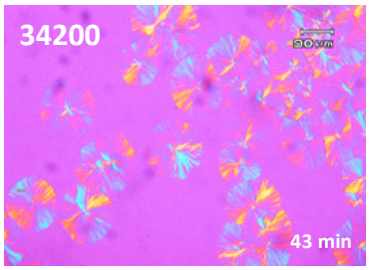	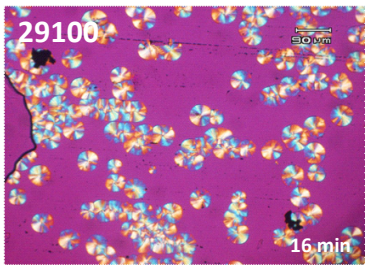	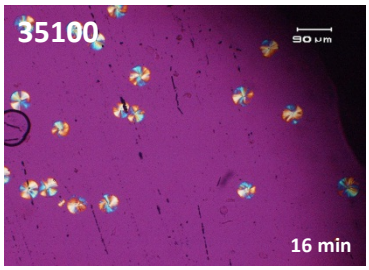
Thermal 62min	**Bio 40m**	**Photo 3000h-12.6m**
	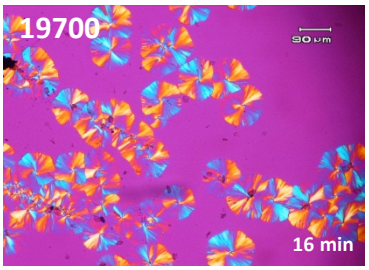	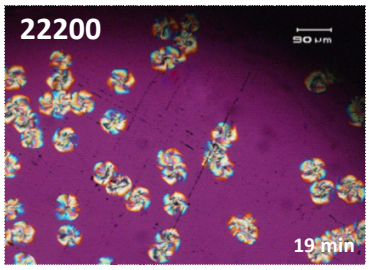
Thermal 120min	**Bio 60m**	**Photo 5100h-21.4m**

Figure 4-127 Micrographs at 121.5 ºC for thermal, bio and photo degraded samples with similar M_n .

4.7.2 Crystallization Kinetics

The linear growth rates (*G*) of the all polylactide samples during isothermal crystallization from the melt were measured in the range of 110 to 140ºC. As expected, the variation of the radius with time was linear and *G* was obtained from the different slopes. A selected example from plates is given in Figure 4-128. The spherulites nucleation depends on the temperature, although all measurements of growth rate started in the first five minutes of experiment.

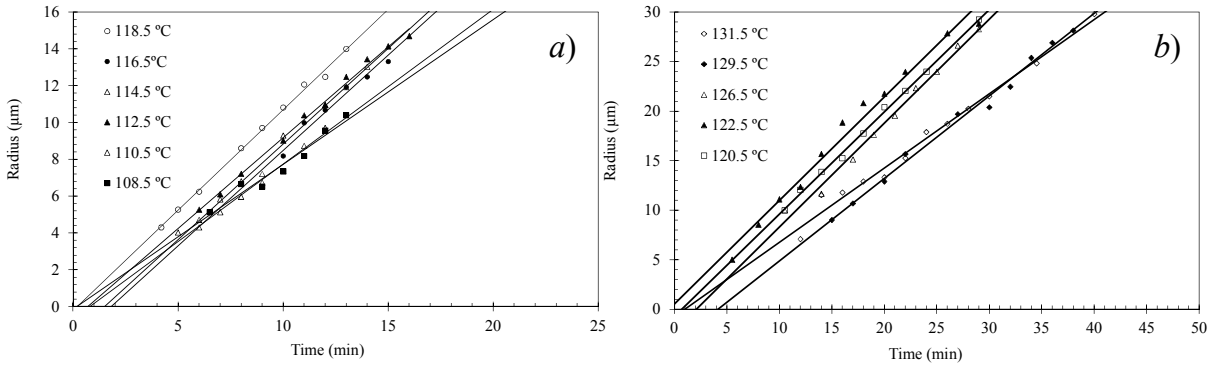

Figure 4-128. Radius vs. time obtained for plates *a*) lower temperatures *b*) higher temperatures.

Prior to the analysis of the growth rate, Table 4-36 and Figure 4-129 evidence the dispersity of some of the measurements of *G* for pellets (a), plates (b), 40 months bio (c) and 21.4 months photo (d), showing the average and representative standard deviation in measurements from 100 to 140ºC. It can be noticed that biodegraded samples, represented as (c), had less experimental uncertaties in *G* than in the photodegraded samples, (d). Pellets and plates exhibit relatively small standard deviation, rarely exceeding 4.5 % in spherulite size of pellets. On the other hand biodegraded samples yield a maximum of standard deviation of 7 % and photodegraded samples reach a maximum of 15 %. For the sake of clarity, the analysis of the *G* data will be based on the average *G* values hereinafter.

Table 4-36 Deviation of the measures of G for some crystallization temperatures

Sample name	T_{c_iso} (ºC)	G (µm/min)	Average	SD	% deviation
Pellets	106.5	0.316			
		0.324	0.320	0.003	0.87
	114.5	0.393			
		0.342			
		0.335	0.357	0.016	4.45
	116.5	0.346			
		0.323			
		0.369	0.346	0.011	3.29
Plates	114.5	0.643			
		0.615	0.629	0.010	1.57
	115.5	0.608			
		0.683	0.646	0.027	4.12
40 m	106.5	1.003			
		0.947	0.975	0.020	2.06
	122.5	2.274			
		2.118	2.196	0.055	2.52
60 m	106.5	3.601			
		3.004	3.303	0.211	6.39
	122.5	4.569			
		3.831	4.200	0.261	6.21
5100h-21.4m	110.5	1.999			
		1.454	1.726	0.193	11.16
	113.5	1.741			
		2.124	1.933	0.135	7.01
	116.5	1.911			
		2.123	2.017	0.075	3.72

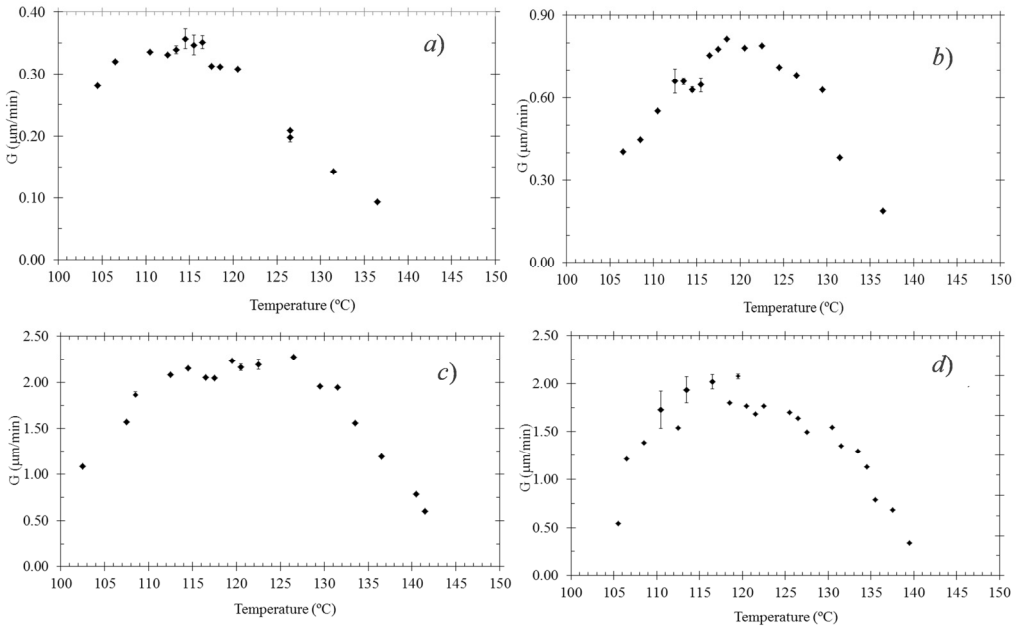

Figure 4-129 Dispersity of the *G* experimental data. *a*) pellets, *b*) plates, *c*) 40 m and *d*) 5100h-21.4m.

The uncertainties may partially arise from the dependence of crystallization on the molar mass and the formation of new groups during degradation. This can explain the similar values of growth rate deviation observed for the PLA pellets and plates. In the case of photodegradation, the increasing deviation in *G* can be attributed to the evolution of more heterogeneous samples as degradation proceeds, in accordance to the higher FWHH values in the molar mass distribution.

Plots of *G* versus temperature are shown in Figure 4-133, 4-134 and 4-315 for the thermal, bio and photo degraded samples, respectively. The results corresponding to the pellets and plates are also included. The growth rates exhibited one maximum at temperatures around 120ºC for all the samples except for pellets, which was observed at 114ºC.

The dependence of the growth rate on the crystallization temperature of PLLA was studied by some authors. In general, one single bell was observed in the *G* vs T_{iso} representations [81,82], although the existence of two bell-shaped curves was also reported [83,84]. This effect was assigned to crystallization following regimes II and III, and was related to a change in the isothermal thickening coefficient which favors an accelerated growth rate. It should be remarked that the transition from regime II to III is not accompanied with variations in spherulite morphology. *Yasuniwa et al*. claimed that the origin of the two different behaviors was polymorphism of the samples, changing from α form (T< 113ºC) to β form (T>130ºC) [85,86]. In previous results of PLA copolymers with less than 10% of D- content, only a single bell behavior for the growth rate versus the crystallization temperature was observed [83,87,88,108].

PLLA can crystallize into various crystalline forms: α, β, and γ [82,89]. Crystallization from the melt or from solution leads to α form crystals, which is the most common polymorph form [90,91,92]. In the α form, two chains with 10_3 helical conformation are packed into an orthorhombic unit cell with dimensions: a = 10.7 Å, b = 6.45 Å, and c =27.8 Å (fiber axis) [93]. A modification of the α-form, the so-called α' form, can also be formed when PLLA is crystallized below 90ºC [94].

In order to assess polymorphism, polylactide samples crystallized at 100ºC and 133ºC during 4 hours were analyzed by X-ray diffraction (Wide-angle X-ray diffractograms (WAXD) were collected at room temperature using a Bruker Nanostar diffractometer). The results are shown in Figure 4-130 and 4-133. Due to some overlapping, the X-ray data were analyzed after subtraction of the scattering pattern of the amorphous phase of PLA.

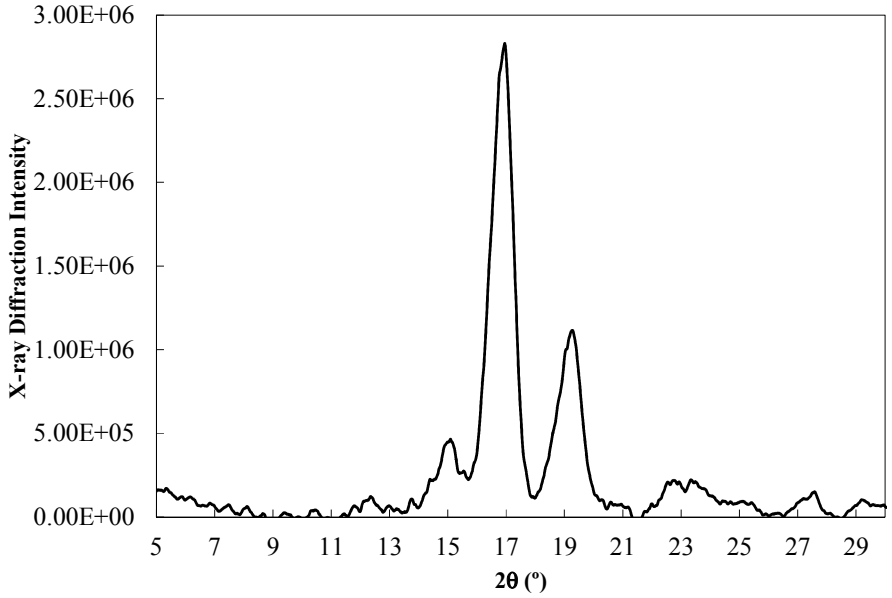

Figure 4-130 X-ray diffraction pattern for isothermally crystallized plates at 100ºC

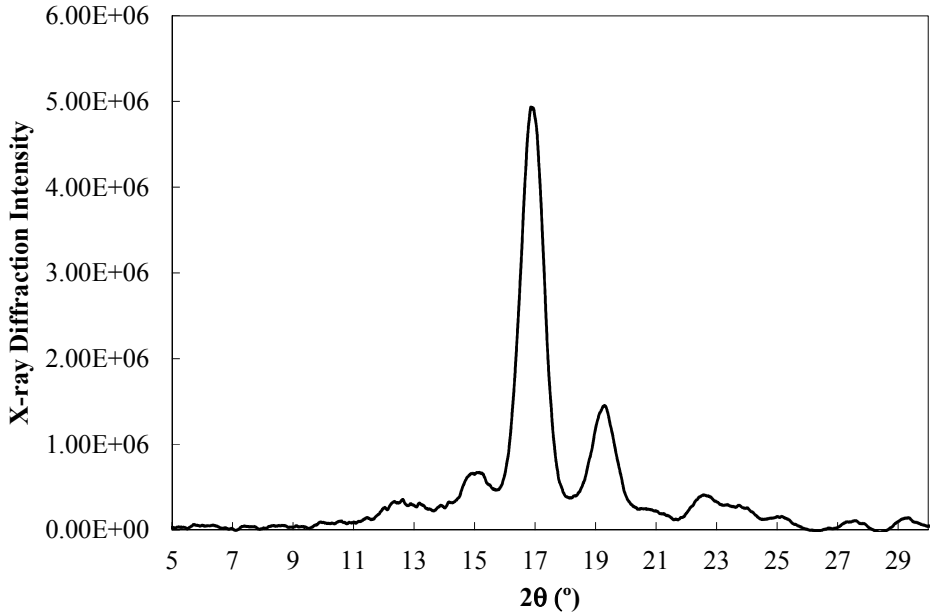

Figure 4-131 X-ray diffraction pattern for isothermally crystallized plates at 133ºC

The diffraction maxima at 14.7 and 22.5 Å are presented in both samples in Figure 4-132, indicating that the possible polymorphisms suggested by *ref.* 85 are not presented, and this is valid for all the PLA samples under study.

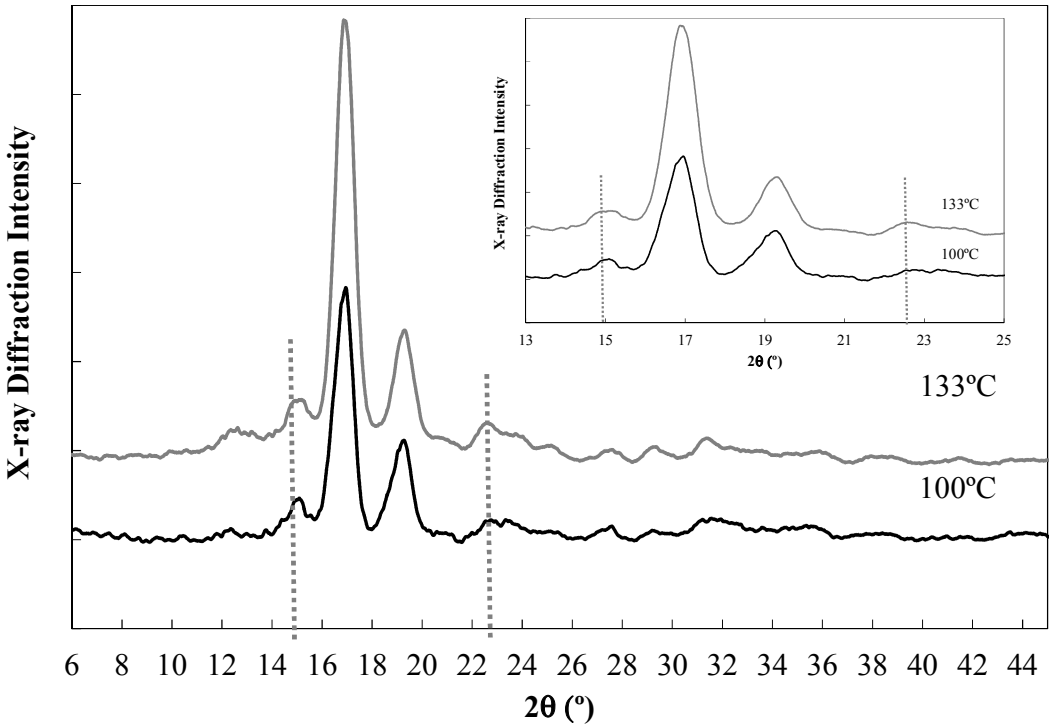

Figure 4-132 Compared X-ray diffraction pattern from isothermally crystallized polylactide at 100ºC and 133ºC.

The X-ray analysis confirms the absence of polymorphism and the existence of a single bell shape curve in plots of growth rate versus the crystallization temperature in the PLA samples under study.

Figure 4-133, 4-136 and 4-137 show that the experimental data of G versus T_c for thermally, bio and photo degraded samples, respectively, fall in the nucleation and transport limited temperature ranges. The lines correspond to the fit of the experimental data according to secondary nucleation, which will be further discussed. It is well known that *G* decreases when increasing the molar mass. Differences in *G* found between pellets and melt-pressed plates indicate that thermal degradation confirming the chain excision. Figure 4-133 shows a progressive increase of *G* for the thermally degraded samples below 120ºC, however *G* decreases for the 330 min sample regardless of the molar mass decrease, which is typical for polymers with very small M_n [95].

Figure 4-134 displays a slightly decrease in *G* for the 1 month biodegraded sample respect to plates. This decrease is reflected in a slightly increase of the molar mass also reported by other authors [22,12]. As degradation advances, *G* increases for the bio and photodegraded samples as Figure 4-135 indicates.

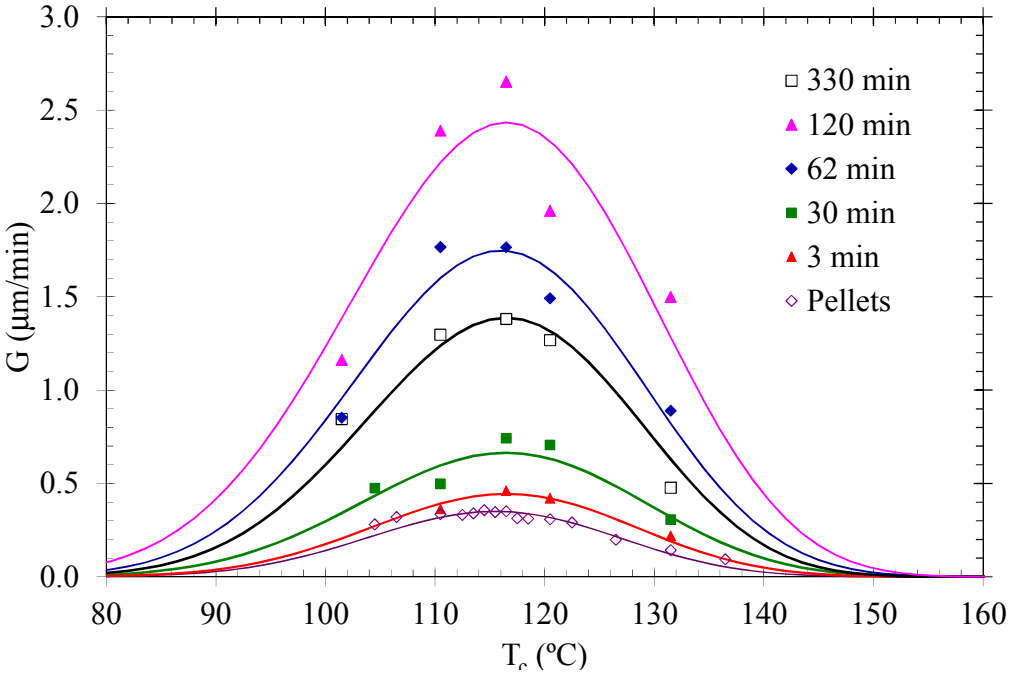

Figure 4-133 Experimental data and fitting to the secondary nucleation theory of G vs Tc for thermally degraded samples.

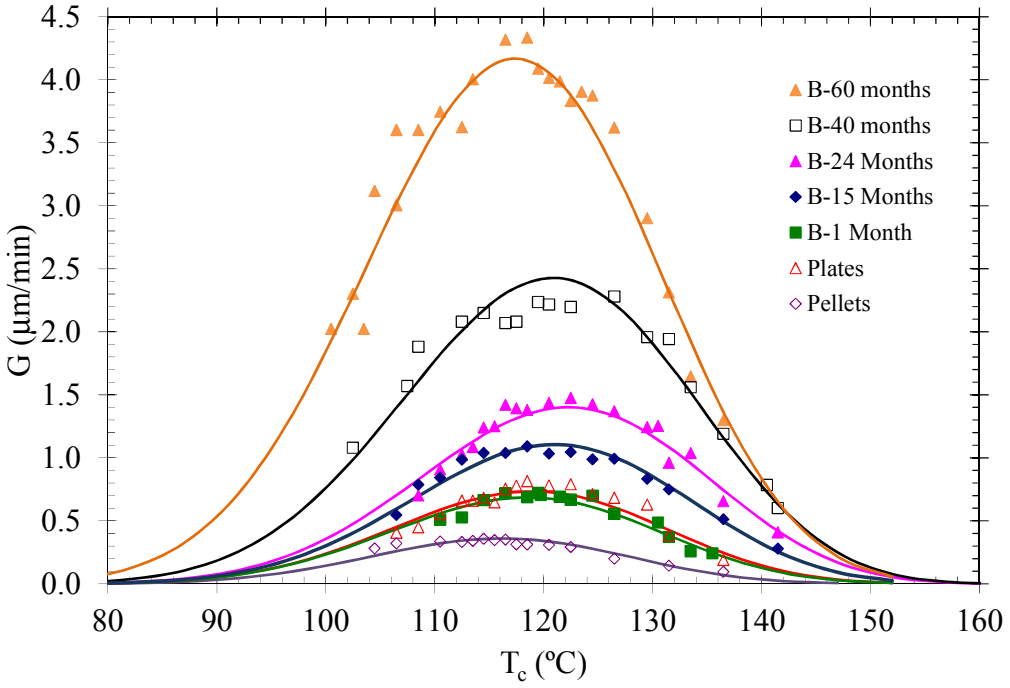

Figure 4-134 Experimental data and fitting to the secondary nucleation theory of *G* vs *Tc* for biodegraded samples.

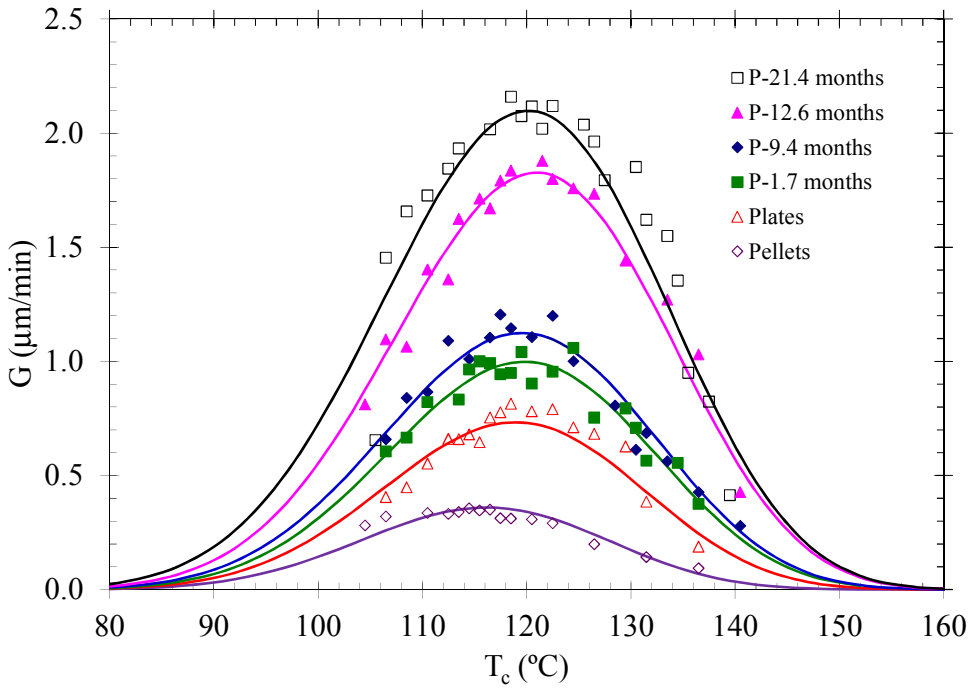

Figure 4-135 Experimental data and fitting to the secondary nucleation theory of *G* vs *Tc* for photodegraded samples.

Figure 4-136 shows the G vs.T_c plots for pellets, plates and two samples bio and photo degraded during similar degradation times. The results indicate that crystallization is faster for samples photodegraded than biodegraded.

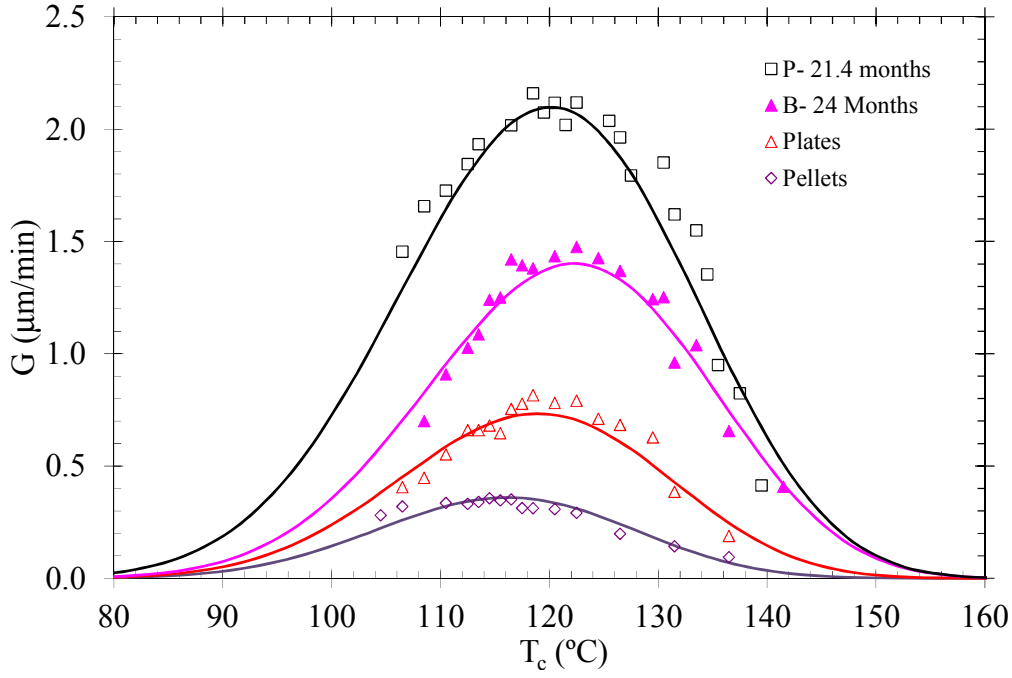

Figure 4-136 Data of *G* versus T_c for pellets, plates and 24m and 5100h-21.4 samples. Comparing at similar time.

Figure 4-137 G versus T_c of pellets, plates and three samples thermal, bio and photo degraded **with similar molar masses** is displayed.

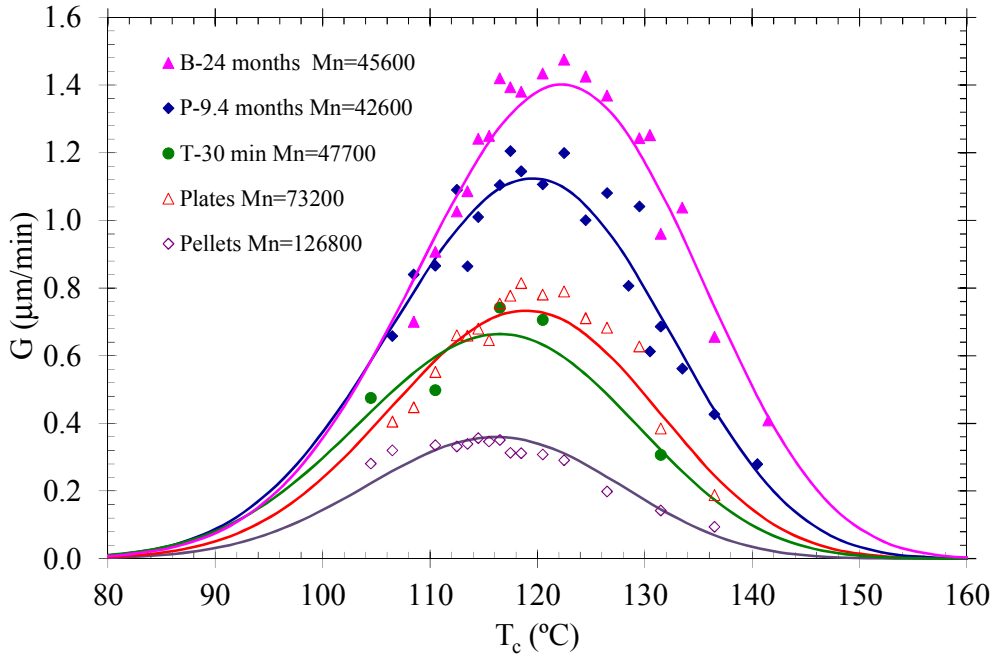

Figure 4-137 Data of G versus T_c for pellets, plates and 30 min, 24 m and 2250h-9.4m samples, with similar molar masses.

At similar molar masses, the growth rates of biodegraded PLA were considerably faster than the G values of photo and thermally degraded samples, the difference increasing with decreasing molar mass. For example, at T_c=120º C and for M_n ~ 43000, the difference in the growth rate is only about 0.3 µm/min (1.1 to 1.4 µm/min) while for M_n ~ 21000 the difference in G increases to 2.2 µm/min (2.1 to 4.3 µm/min). In other words, at the lowest molar mass studied, the linear growth rates of photodegraded specimens were about half the value of equivalent chain length biodegraded specimens, thus corroborating the observed differences in cold crystallization during dynamic heating. The case of thermal and photo degradation basically kept the differences of growth rate during all the range of molar masses.

Thermal degradation is the slowest process followed by photo and bio degradation. The slow rate of photodegradation can be explained by the additional groups that act as defects for crystallization (anhydrides) or some other new groups formed during degradation. The case of the thermal degradation is more unexpected, and the slow crystallization may be due to:

- Heterogeneity of the molar mass distribution due to increased number of chain ends because of the combination of different mechanisms.
- The formation of other functional groups overlapped with the bands studied and not detectable in FTIR.
- The influence of cyclic oligomers in the crystallization [96], as occurred for poly(ε-caprolactone) in a determined range of molar masses or their combination with linear chains [97].

Figure 4-138 *a*), *b*) and *c*) shows the growth rate measured at 112.5ºC, 120.5ºC and 126.5ºC versus time for thermal, bio and photo degradation respectively, in order to confirm the independence of T_c in the trend of *G vs.* time.

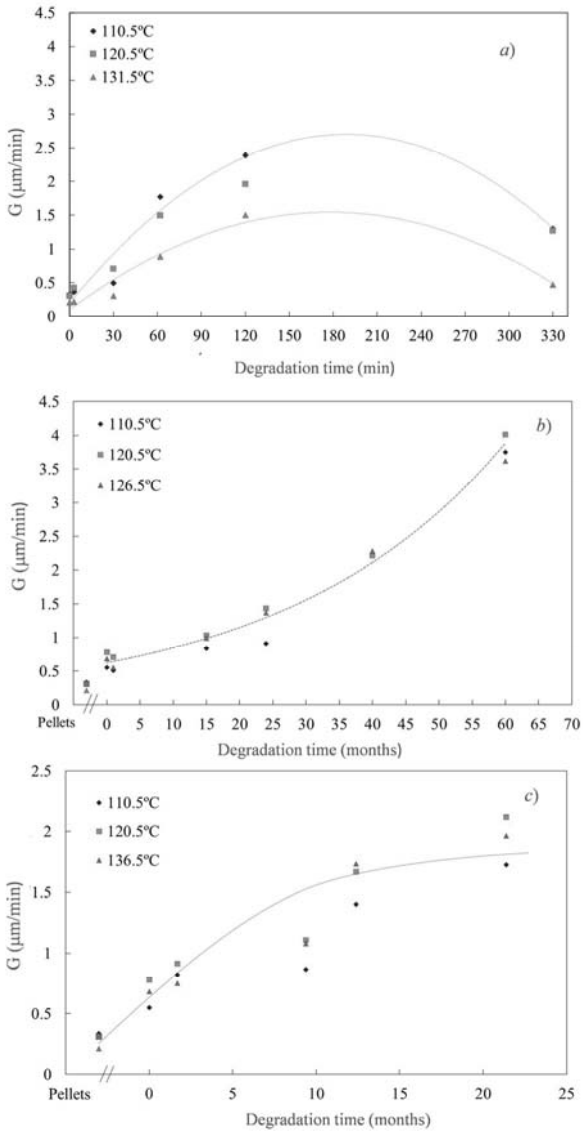

Figure 4-138 Evolution of *G* vs time *a*) thermal degradation *b*) biodegradation and *c*) photodegradation at 110.5, 120.5 and 126.5 ºC.

The effect of molar mass on the growth rate, for the different degradation types, is given in Figure 4-139 at T_c = 120.5º C (at which G_{max} is detected). The dependence of G_{max} with the molar mass has been described as a power law function, $M_w{}^{\alpha}$, for several crystalline polymers [82,98,99]. The value of α depends on the polymer and is strongly dependent on the degree of undercooling and on the molar mass [95]. Although the values of M_w from thermal degradation can present uncertainty due to the unknown molar mass distribution (and thus unknown polydispersity) they were also represented considering polydispersity = 1.82 (section 4.1- Figure 4-3).

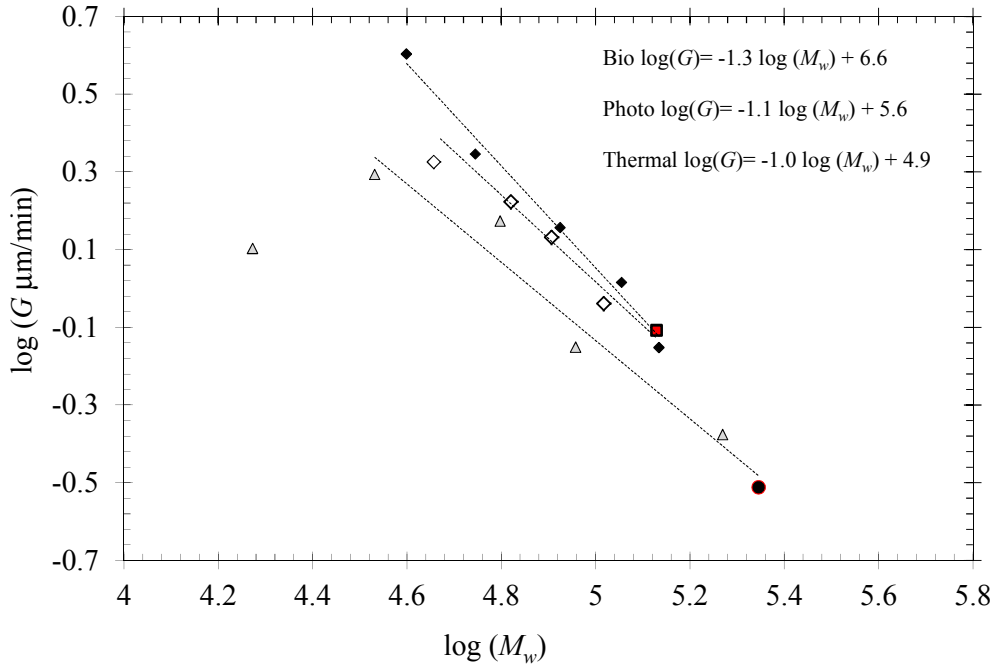

Figure 4-139 Plots of logarithm of the crystal growth rate at 120.5ºC against logarithm of the molar mass for (●) pellets, (■) plates, (△) Thermal Degradation, (◆) Biodegradation and (◇) Photodegradation.

Except for low molar masses, all data in Figure 4-139 decrease following a straight line with very similar exponents: -1.3 for bio, -1.1 for photo and -1.0 for thermal degradation. The dependence is in consonance with $G \propto M^{\alpha}$, inferred from models based on molecular reptation toward the growth front. *Okui et al*. [100] analyzed the G vs M_w dependence for a set of crystalline homopolymers, including PLLA data from *Vasanthakumari and Pennings* and *Miyata and Masuko* [82], and they found a unique dependence when the maximum value of G was used, G_{max} α $M^{0.5}$ [101,102]. They reported that large undercooling, higher than 60ºC, provides α values close to -0.50, and these value increase when the undercooling is lower. At 130ºC a value of α= -0.766 was

reported for PLLA, which is slightly higher than the expected α=-0.5 [83]. The data for those copolymers lead to a higher negative slope, indicating a more pronounced effect of molar mass on *G*. It is well known the effect of *D* units in lowering the linear growth rates and overall crystallization rates of the PLLA chain [87,102]. The data of Figure 4-139 demonstrate the values of *G* were systematically lower for photo and thermal samples at any fixed T_c.

The lower values of *G* observed for the photodegraded samples compared to those from biodegraded specimens at similar molar masses cannot be attributed to differences in polydispersity, since all polydispersity indexes (M_w/M_n) are ~1.82 for all samples. The decrease in *G* must be associated with a change in the chemical structure intrinsically due to photodegradation. A signature of this type of degradation, not found in bio or thermal degradation, is the presence of anhydride groups in photodegraded specimens. These were most likely non-crystalline groups that act as defects retarding crystallization of PLA. The differences in crystallization rates between bio and photodegraded samples at similar molar masses give further support for the formation of non-crystallizable groups (such as the anhydride) during photo degradation.

Although less *G* data were collected on thermally degraded PLA specimens, the trends with molar mass were similar to those of bio or photodegraded samples, except for the sample with the smallest molar mass. The crystallization of the thermally degraded sample during 330 min is unusual. This sample has the lowest molar mass (M_n=10300), yet the growth rate is not higher but about half the rate of the sample kept at the same temperature for 120 min (M_n =18700).

4.7.3 Analysis of temperature coefficient of the growth rate

The temperature coefficient of the growth rate was analyzed according to the secondary nucleation theory described in detail in Chapter 2. Lauritzen, Hoffman and co-workers proposed growth of primary nuclei as a sequence of two events with competitive rates [103]. One is formation of secondary nuclei on the growth front (at a rate *i*), and the second the lateral growth of these nuclei along the face (at rate, *g*). Three possible regimes were identified for the overall growth rate, in the high T_c range: Regime I, i<<g and G ∝ (*i*); Regime II, occurring as undercooling increases and *i* becomes comparable to *g*, and *G* is proportional to $(i,g)^{1/2}$; Regime III, occurring at large undercoolings, when excessive surface nucleation leads to effectively zero spreading rates, and the overall *G* is again proportional to *i*. The temperature coefficient of *G* in Regimes I, II and III changes proportionally as a 1,1/2, 1 ratios.

The experimental data of *G* were first analyzed according to the linear form in Equations (4-22) and (4-21).

$$G = Go\cdot\exp\left(\frac{-U^*}{R(T_c - T_\infty)} - \frac{n\cdot\sigma_e\cdot\sigma\cdot T_m^0\cdot b_0}{\Delta H_m\cdot R\cdot\Delta T\cdot T_c}\right) = Go\cdot\exp\left(\frac{-U^*}{R(T_c - T_\infty)} - \frac{Kg}{\Delta T\cdot T_c}\right) \qquad (4\text{-}21)$$

n=4 in Regime I and III and *n*= 2 in Regime II

$$\ln(G) + \frac{U^*}{R(T_c - T_\infty)} = \ln(Go) - \cdot\frac{Kg}{\Delta T\cdot T_c} \qquad (4\text{-}22)$$

Crystal melting is usually described by the Gibbs-Thomson equation, based on the correlation between lamellar thickness and crystal stability, providing a consistent estimation of T_m^0 of the lamellar crystals of sufficiently large lateral dimensions [104]. *Baratian et al.* have provided T_m^0= 202 ºC for a PLA copolymer with 6% *D* content [87].

The values of the parameters used were:

$T_m^0 = 202\ ^oC$ [87], $\rho = 1.25\ g/cm^3$ [80], $b_0 = 0.517\ nm$ [81], $\sigma = 12\ erg/cm^2$ [81], $k = 1.38\cdot10^{-23}\ J/K$; $\Delta H_m^0 = 93\ J/g$ [80]

Some investigations have studied the regimes in the growth rate of some polylactides by using the "universal" values of U^*= 1500 cal/mol and C_2 = 30 K. [105,106,107]. Applying these assumptions, the first term of Equation (4-22) is plotted against $1/Tc\Delta$ in Figure 4-140. The data of pellets do not follow any regime, as was also reported for PLLA in *ref. 87.*

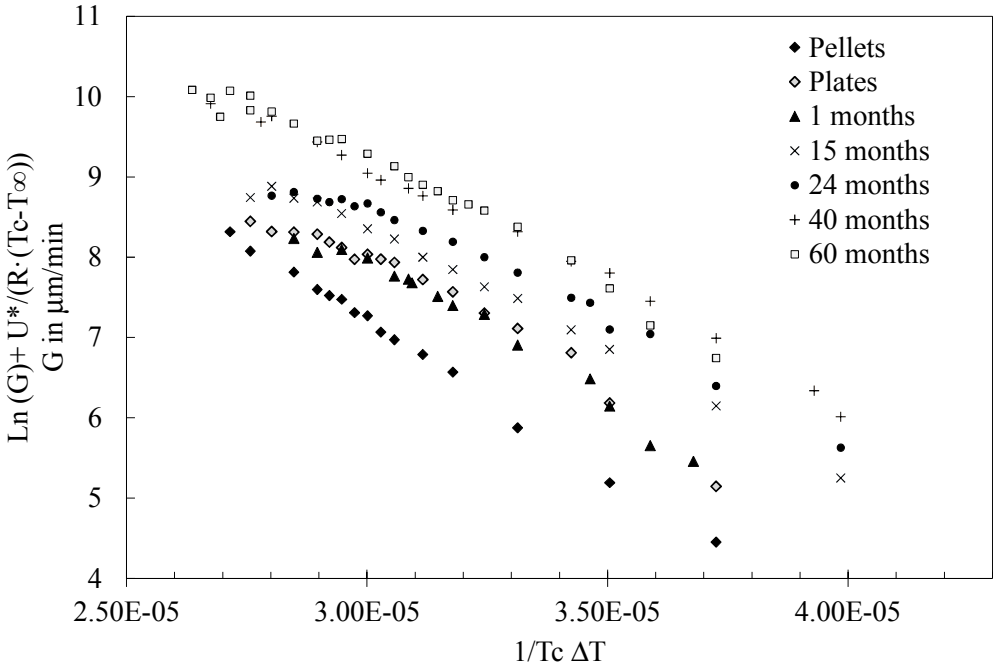

Figure 4-140 Plots of ln $(G) + U^*/R(Tc - T_\infty)$ against $1/Tc{\cdot}\Delta T$ for biodegraded PLA at different times (U^*=1500 cal/mol and C_2 =30 K).

The other pair proposed in the literature is U^*= 4200 cal/mol and C_2= 51.6 K [108]. Although some points corresponding to the sample biodegraded during 24 months do not fall into the linear tendency, in general this pair of U^* and C_2 provide more uniform analysis of the data, see Figure 4-141.

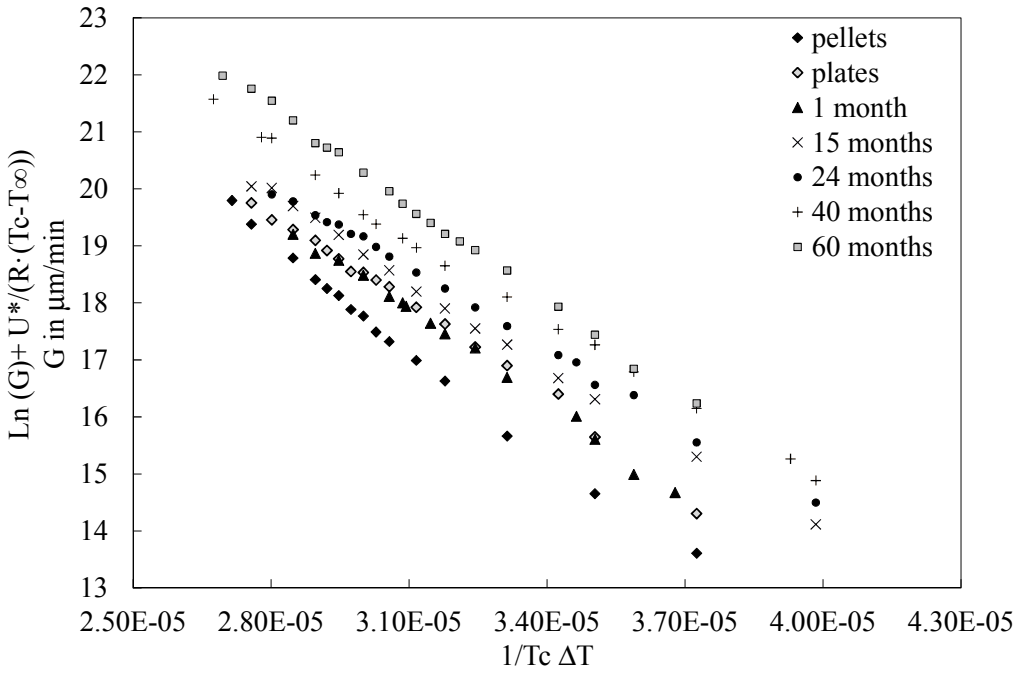

Figure 4-141 Plots of ln *(G) + U*/R(Tc - T_∞)* against *1/Tc·ΔT* for biodegraded PLA at different times (*U=4200 cal/mol and C_2= 51.6 K).**

The variability of *U** with molar mass should be taken into account. Observation of the maximum in the *G* vs. T_c plots allowed reducing the degrees of freedom to two parameters, *Kg* and *Go,* and thus *U** can be calculated [109]. At the maximum, $dG/dT_{cmax} = 0$, *U** can be expressed as Equation (4-23):

$$U^* = R(T_{c\max} - T_\infty)^2 \cdot \left(\frac{Kg}{T_{c\max}(T_m^0 - T_{c\max})^2} - \frac{Kg}{T_{c\max}{}^2 (T_m^0 - T_{c\max})} \right) \qquad (4\text{-}23)$$

When fitting *Kg* and *Go*, no decreasing tendency for *U** with molar mass was observed, for all the biodegraded samples. In that case the study was performed selecting *U**= 4200 cal/mol, from pellets, and *U**=3474 cal/mol, obtained for 40 m sample. These two values were plotted with the respective logarithm of the average-weight molar mass, see Figure 4-142.

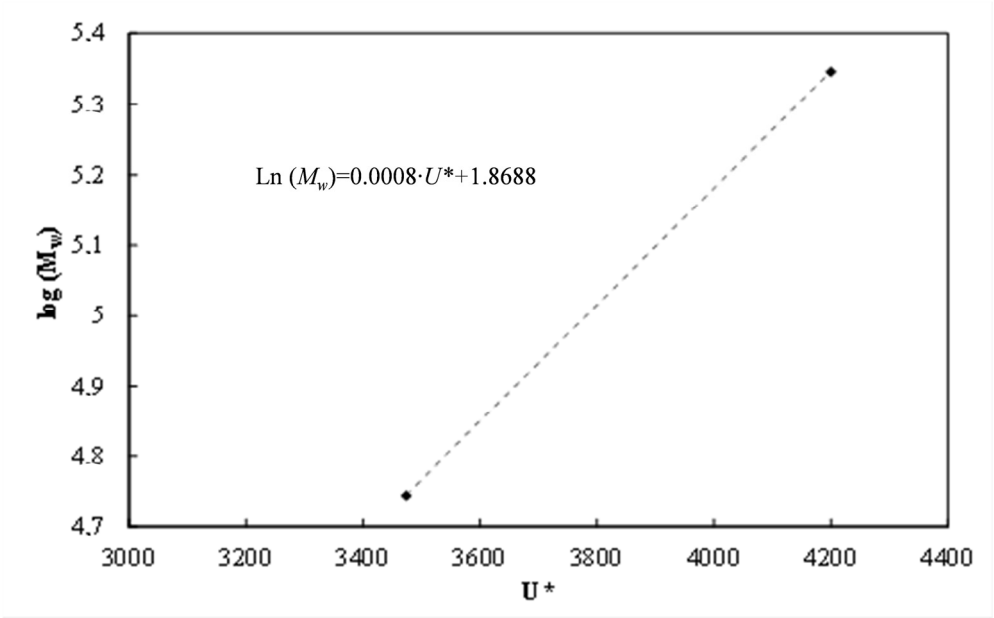

Figure 4-142. Plot of log (M_w) versus U* for pellets and bio 40 months.

From the equation in Figure 4-142, the values of U* were obtained at different M_w for the degraded samples and the theoretical value of G was calculated using Equation (4-23), with C_2 51.6 K. Figure 4-143 and Figure 4-144 show a linear trend when plotting ln(G)+ U*/R·(T_c-T_∞) versus 1/$T_c\Delta$T for bio and photo degradation, respectively. Table 4-37 show the parameters obtained from the linearization (Kg and ln(G_o)).

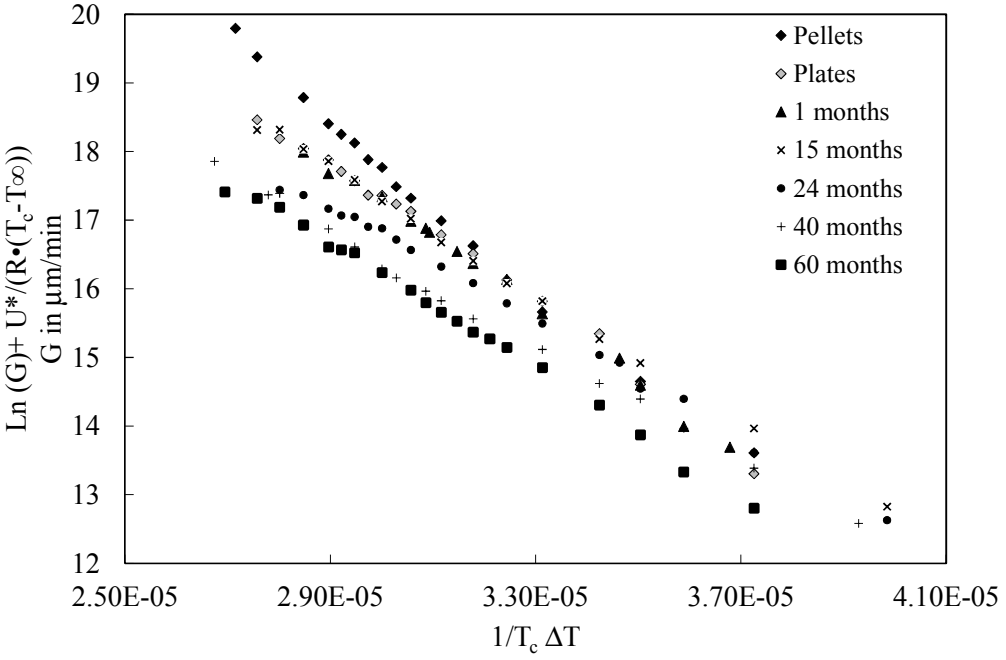

Figure 4-143 Plots of ln (G) + U*/R(T_c - T_∞) against 1/T_c·ΔT for biodegraded PLA at different times (U* variable and C_2= 51.6 K).

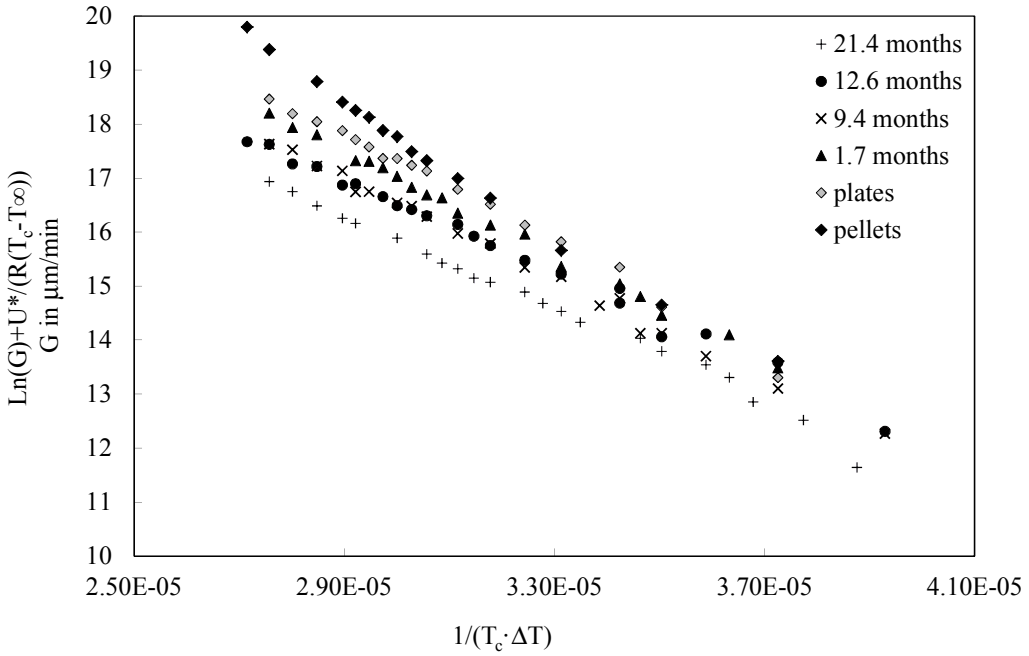

Figure 4-144 Plots *of ln (G) + U*/R(T_c - T_∞)* against 1/T_c·*ΔT* for photodegraded PLA at different times. (*U variable and C_2= 51.6 K).**

Table 4-37 Parameters for bio and photo degraded PLA determined through the secondary nucleation approach (*U variable and C_2= 51.6 K).**

Sample name	M_n	*Go* (µm min^{-1})	*Kg* (K^2)	*U** (cal/mol)	σ_e (erg/cm^2)
Pellets	126800	5.6E+15	6.2 E+05	4200	84
Plates	73200	1.8 E+14	5.2 E+05	3938	70
Biodegradation					
1 m	74600	2.3E+14	5.3 E+05	3944	71
15 m	60200	3.4 E+13	4.6 E+05	3849	63
24 m	45600	5.6 E+12	4.2E+05	3690	57
40 m	29100	3.8 E+12	4.2 E+05	3474	57
60 m	20300	1.1 E+13	4.6 E+05	3298	62
Photodegradation					
1.7 m	56300	4.5 E+13	4.8 E+05	3803	65
9.4 m	42600	1.9 E+13	4.7 E+05	3669	63
12.6 m	35100	5.9 E+12	4.3 E+05	3565	58
21.4 m	22200	2.2 E+12	4.2 E+05	3368	57

The continuous lines plotted in Figure 4-134 and Figure 4-135 correspond to theoretical linearization using data from Table 4-37. Thus, it can be concluded that this approach provided a consistent fit of the experimental data.

In the case of the thermally degraded samples, Figure 4-145 displays plots of ln *(G) + U*/R(T_c - T∞)* versus $1/T_c \cdot \Delta T$ with *U** calculated from the equation in Figure 4-142 and C_2= 51.6 K.

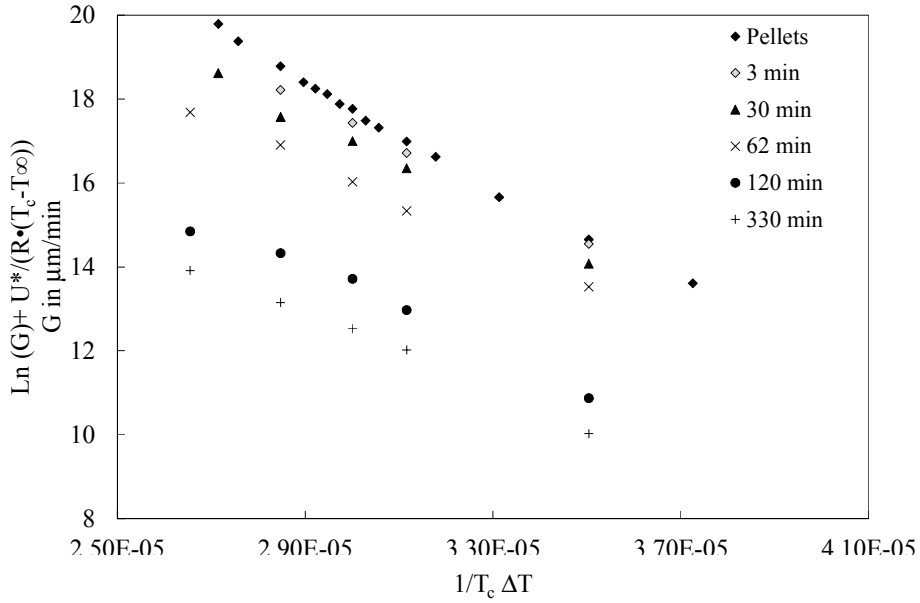

Figure 4-145 Plots of *ln (G) + U*/R(T_c - T∞)* against $1/T_c \cdot \Delta T$ for thermally degraded PLA at different times. (*U variable and C_2= 51.6 K).**

The results did not evidence any trend, probably due to the low number of experimental points. The results from the fitting of the thermal degradation data are displayed in Table 4-38 and Figure 4-146.

Table 4-38 Parameters for thermally degraded PLA determined through the secondary nucleation approach (*U variable and C_2= 51.6 K).**

Sample name Thermal degradation	M_n	*Go* (µm min^{-1})	*Kg* (K^2)	*U** (cal/mol)	σ_e (erg/cm^2)
3 min	102600	1.4 E+15	5.7 E+05	4117	77
30 min	49800	8.0 E+13	5.4 E+05	3707	74
62 min	34200	6.1 E+13	5.2 E+05	3498	69
120 min	18700	9.1 E+13	5.2 E+05	3152	71
330 min	10200	5.0 E+11	4.6 E+05	2800	63

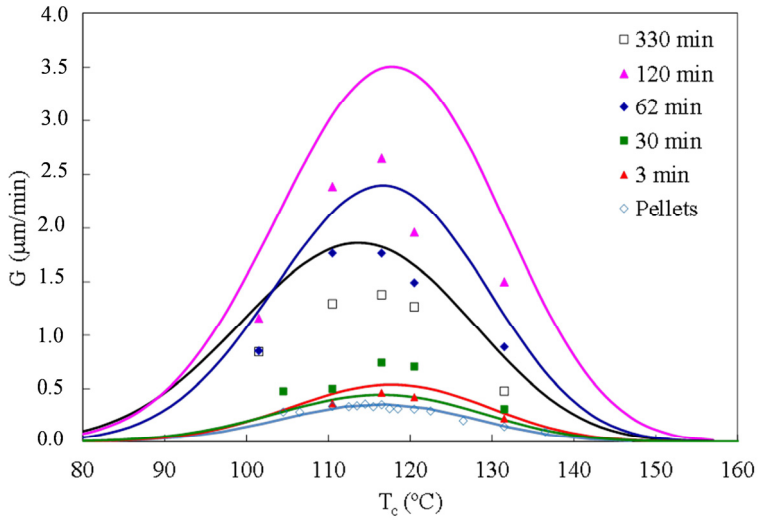

Figure 4-146 Experimental data and fitting to the secondary nucleation theory of *G* vs T_c for thermally degraded samples using a variable *U calculated from Figure 4-142 and C_2= 51.6 K.**

Due to the deviation between the experimental and theoretical values, in thermal degradation *U** could not be calculated from Figure 4-142. Alternatively, *U**, *Go* and *Kg* were obtained by fitting Equation (4-21) and using (4-23). The values obtained from this fit are shown in Table 4-39, leading to satisfactory fit, as seen in Figure 4-133.

Table 4-39 Parameters for thermally degraded PLA determined through the secondary nucleation approach fitting to Equation (4-23)

Sample name	M_n	*Go* (µm min^{-1})	*Kg* (K^2)	*U** (cal/mol)	σ_e (erg/cm^2)
Pellets	126800	5.6 E+15	6.16 E+05	4200	84
Thermal degradation					
3 min	102600	2.90 E+15	5.99 E+05	4064	81
30 min	49800	2.75 E+13	5.16 E+05	3544	70
62 min	34200	3.10 E+13	5.07 E+05	3412	69
120 min	18700	5.82 E+15	5.82 E+05	3195	79
330 min	10200	2.36 E+14	5.39 E+05	2723	73

The value of *U** decreases by about 1000 cal/mol in a M_n range from 126000 to 25000, reflecting a favored activation for segmental transport due to the decrease in melt viscosity. The data of basal surface free energy (σ_e) were plotted against the number-average molar mass in Figure 4-147. The value of the lowest molar masses for thermal and biodegradation do not fall in the decreasing tendency, probably due to the increase of chains end or the use of a non-appropriate T_m^0 when the molar mass is very small.

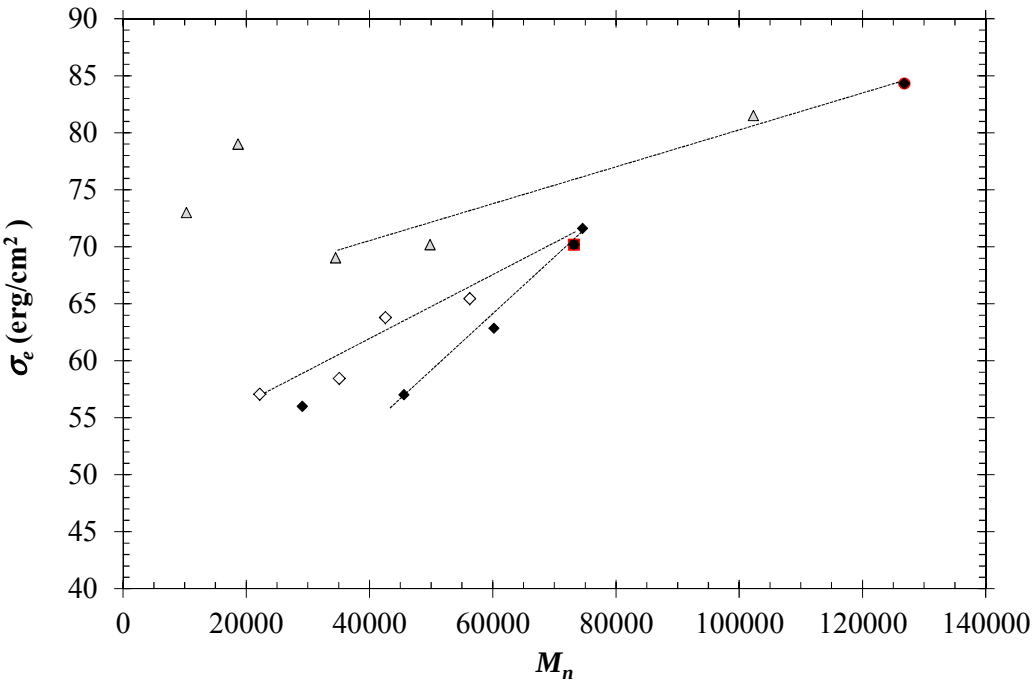

Figure 4-147 (●) pellets, (■) plates, (△) thermal degradation (◆) biodegradation and (◇) photodegradation usingT_m^0 = 202°C for all the samples.

It is well known that $T_m{}^o$ may decrease at lower molar mass. For the thermal degraded samples, T_m^0 was calculated according to *Mandelkern et al.* [110]. This study considers that the T_m^0 variation is related to the carbon units of the molecule of n-alkenes. In order to apply a similar procedure, and considering the molar mass of the polylactide repeating units, 72, the total carbons per repeating unit were calculated, and the results are shown in Table 4-40.

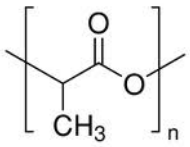

Figure 4-148 PLA repeating unit ($C_3H_4O_2$)

Table 4-40 Calculus of the carbons in the molecule for 120 and 330 minutes thermally degraded samples.

Thermally degraded samples M_v	M_n	Repetitive units M_n/72	Total carbons: 3 C per repeating unit
32000	18700	260	780
17600	10300	143	429

The experimental data are out of range of the plot given in the reference, and thus the increment of T_m^0 could not be read for polylactide. Considering that in the case of n-alkenes with 200 carbons T_m^0 was around 125ºC and 135 ºC for 400 carbons, for samples degraded for 120 and 330 minutes, a correction of T_m^0= 202ºC - 8 ºC was used for the calculation of σ_e. Figure 4-149 shows the plot of σ_e versus M_n, using the new values for $T_m^0$and these new σ_e values are shown in Table 4-41.

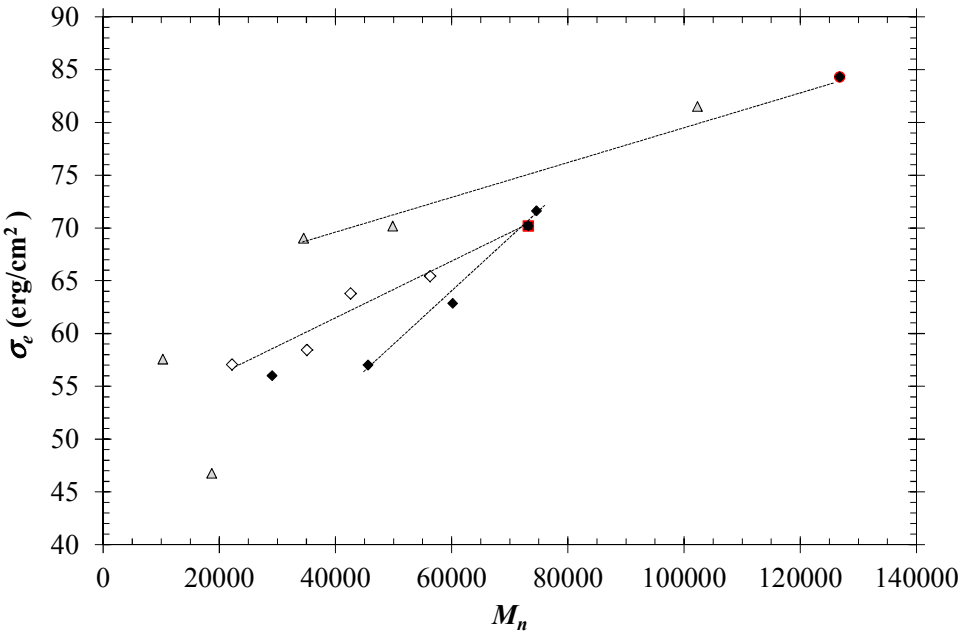

Figure 4-149 (●) pellets, (■) plates, (△) thermal Degradation (◆) biodegradation and (◇) photodegradation (using T_m^0 = 202 ºC -8ºC for thermally degraded samples during 120 and 330 min).

Table 4-41 σ_e value for the 120 and 330 min samples taking T_m^0 = 202 ºC -8ºC

Sample name	M_w	σ_e (erg/cm^2)
120 min	34000	48
330 min	18700	58

The results of σ_e do not follow a defined tendency neither in Figure 4-147 nor in Figure 4-149, considering the results of growth rate and the micrographs. The changes occurred at lower molar masses should be attributed to the increase in the chains end.

The values of σ_e decrease from about 85 to 55 erg/cm^2 with decreasing molar mass for thermal, bio and photo degradation, permitting a favored folding of the shorter molecules. The change of σ_e with molar mass is also explained by an increasing crowdedness of entanglements and loops on the surface of the higher molar mass crystallites that make chain folding on the basal surface more impeded. The range of σ_e values obtained for pellets, plates and from exposure to soil or UV radiation, are similar to those reported in the literature [81,84]. Although *Tsuji et al*. did not report values for σ_e, the authors listed *Kg* values for the homopolymer and copolymers with increasing D content [83]. The corresponding σ_e value (75 erg/cm^2) for a copolymer with M_n = 60000 is in good agreement with the experimental results obtained in the present work.

Most literature works have analyzed the kinetics of the linear growth rates of PLA copolymers considering Regime II, with U^* = 1500 cal/mol and C_2 = 30 K. The present choice of Regime I was based on a better linearity and the fact that the actual Regime and expressions for the transport term are unknown. However, in order to compare the kinetics with other reported data, values of *Kg* and σ_e were also obtained from the linear portions of Figure 4-140. The values of σ_e obtained are 10 – 15 cal/mol higher than those listed in Table 4-41.

The trends of σ_e versus molar mass for thermal degradation were very different respect to the other degradation processes, confirming slower rates of crystallization. In the case of bio and photo degraded specimens, the values of σ_e were closer at high molar masses and differ when increasing the degradation time. These results confirmed the different nature of the degradation mechanisms and their influence in crystallization.

4.8 Bibliographical references

[1] Sakai W, Sadakane T, Nishimoto W, Nagata M, Tsutsumi N, Photosensitized degradation and crosslinking of linear aliphatic polyesters studied by GPC and ESR. Polymer 2002;43:6231-6238.

[2] Sakai W, Kinoshita M, Nagata M, Tsutsumi N, ESR studies of photosensitized degradation of poly(L-lactic acid) via photoionization of dopant. J Polym Sci Part A: Polym Chem 2001;39:706-714.

[3] Stevens MP. Polymer Chemistry: An Introduction, 3rd ed.; Oxford University Press: New York, 1999.

[4] Garlotta, D. A literature review of poly(lactic acid). J Polym Environ 2001;9,2:63-84.

[5] Spinu M, Jackson C, Keating MY, Gardner KH. Material design in poly(lactic acid) systems: block copolymers, star homo and copolymers, and stereocomplexes. J Macromol Sci Pure Appl Chem 1996;A 33:1497–1530.

[6] Dorgan J, "Rheology of poly(lactic acid)," in poly(lactic acid): Synthesis, structures, properties, processing and applications, edited by Auras R, Lim LT, Selke SEM and Tsuji H. John Wiley & Sons, Inc, 2010 pp. 125-139.

[7] Flory PJ. Principles of Polymer Chemistry; Cornell University Press: Ithaca, NY, 1953.

[8] CRC Standard Mathematical Tables and Formulae Zwillinger D, ed., CRC Press, Boca Raton, Florida, 1996, pp. 497.

[9] McNeill I.C and Leiper H.A. Degradation studies of some polyesters and polycarbonates 1. polylactide: general features of the degradation under programmed heating conditions Polym Degrad Stab 1985;11: 267-285.

[10] Liu X, Zou Y, Li W, Cao G, Chen W. Kinetics of thermo-oxidative and thermal degradation of poly(D,L-lactide) (PDLLA) at processing temperature. Polym Degrad Stab 2006;91:3259–3265.

[11] Saha SK, Tsuji H. Effects of molecular weight and small amounts of D-lactide units on hydrolytic degradation of poly(L-lactic acid)s. Polym Degrad Stab 2006;91,8:1665–73.

[12] Kale G, Auras R, Paul S Singh, Narayan R. Biodegradability of polylactide nottles in real and simulated conditions. Polymer Testing 2007:26:1049–61.

[13] Schliecker G, Schmidt C, Fuchs S, Kissel T. Characterization of a homologous series of D,L - lactic acid oligomers; A mechanistic study on the degradation kinetics in vitro. Biomaterials 2003;24:3835–44.

[14] Shih C. Chain-end excision in acid catalyzed hydrolysis of poly(D,L-lactide) in solution. J Control Release 1995;34:9–15.

[15] So1dergard A, Na1sman JH. Melt stability study of various types of Poly(L-lactide). Ind Eng Chem Res 1996;35:732–735.

[16] Tsuji H. Polylactides. In:Doi Y, Steinbuchel A, editors. Polyesters 3. Biopolymers, vol. 4. Weinheim, Germany:Wiley- VCH, 2002 p. 129–77.

[17] Tsuji H, Ikarashi K. In vitro hydrolysis of poly(L-lactide) crystalline residues as extended-chain crystallites. Part I: long-term hydrolysis in phosphate-buffered solution at 37°C. Biomaterials 2004;25:5449–5455.

[18] Tsuji H. In vitro hydrolysis of blends from enantiomeric poly(lactide)s. Part 4:well-homo-crystallized blend and nonblended films. Biomaterials 24 (2003) 537–47.

[19] Tsuji H, Mizuno A, Ikada Y. Properties and morphology of poly(l-lactide). III. Effects of initial crystallinity on long-term in vitro hydrolysis of high molar mass poly(L-lactide) film in phosphate-buffered solution. J Appl Polym Sci 2000;77:1452–64.

[20] Jamshidi K, Hyon S-H, Nakamura T, Ikada Y, Shimizu Y, Teramatsu T. In vitro and in vivo degradation of poly-l-lactide fibers. In: Christel P, Meunier A, Lee AJC, editors. Biological and biomechanical performance of biomaterials. Amsterdam: Elsevier Science Publishers BV; 1986. p. 227–232.

[21] Pistner H, Bendix DR, Muhling J, Reuther JF. Poly(l-lactide): A long-term degradation study in vivo. Part III: Analytical characterization. Biomaterials 1993;14:291–98.

[22] Santonja-Blasco L, Moriana R, Badía JD, Ribes-Greus A. Thermal analysis applied to the characterization of degradation in soil of polylactide: I. Calorimetric and viscoelastic analyses. Polym Degrad Stab 2010;95:2185–2191.

[23] Cam D, Marucci M. Influence of residual monomers and metals on poly (L-lactide) thermal stability. Polymer 1997;38:1879–1884.

[24] Liau L C-K, Tung M-T. Kinetic investigation of photocatalytic effects on poly(vinyl butyral) photodegradation. Ind Eng Chem Res 2006;45:2199–2205.

[25] Calmon A, Guillaume S, Bellon-Maurel V, Feuilloley P, Silvestre F. Evaluation of material biodegradability in real conditions-development of a burial test and an analysis methodology based on numerical vision. J Environ Polym Degrad 1999;7:157–166.

[26] Ho KLG, Pometto III AL, Hinz PN. Effects of temperature and relative humidity on polylactic acid plastic degradation. J Environ Polym Degrad 1999;7:83–92.

[27] Tsuji H, Echizen Y, Nishimura Y. Photodegradation of biodegradable polyesters: A comprehensive study on poly(L-lactide) and poly(ε-caprolactone). Polym Degrad Stab 2006;91:1128–1137.

[28] Janorkar AV, Metters AT, Hirt DE. Degradation of poly(L-lactide) films under ultraviolet-induced photografting and sterilization conditions. J Appl Polym Sci 2007;106:1042–1047.

[29] Ikada E. Photo-and bio-degradable polyesters. Photodegradation behaviours of aliphatic polyesters. J Photopolym Sci Technol 1997;10,2:265–270.

[30] Zaidi L, Kaci M, Bruzaud S, Bourmaud A, Grohens Y. Effect of natural weather on the structure and properties of polylactide/Cloisite 30B nanocomposites. Polym Degrad Stab 2010;95:1751–1758.

[31] McNeill IC, Leiper HA. Degradation studies of some polyesters and polycarbonates 2. Polylactide: degradation under isothermal conditions, thermal degradation mechanism and photolysis of the polymer. Polym Degrad Stab 1985;11:309–326

[32] Kopinke FD, Remmler M, Mackenzie K, Moder M, Wachsen O. Thermal decomposition of biodegradable polyesters. 2. Poly(lactic acid). Polym Degrad Stab 1996;53(3):329–342.

[33] Wachsen O, Reichert K.-H, Kruger R.-P, Much H, Schulz G. Thermal decomposition of biodegradable polyesters- III. Studies on the mechanisms of thermal degradation of oligo-L-la&de using SEC, LACCC and MALDI-TOF-MS. Polym Degrad Stab 1997;55:225–31.

[34] Jamshidi K, Hyon S.-H, Ikada Y. Thermal characterization of polylactides. Polymer 1988;29:2229–2234.

[35] Merkli A, Tabatabay C, Gurny R, Heller J. Biodegradable polymers for the controlled release of ocular drugs. Prog Polym Sci 1998;23(3):563–580.

[36] Hakkarainen M, Karlsson S, Albertsson AC. Influence of low molecular weight lactic acid derivatives on degradability of polylactide. J Appl Polym Sci 2000;76(2):228–39.

[37] Lucas N, Bienaime C, Belloy C, Queneudec M, Silvestre F, Nava-Saucedo JE. Polymer biodegradation: Mechanisms and estimation techniques A review. Chemosphere 2008;73,4: 429–442.

[38] Li S. Hydrolytic degradation characteristics of aliphatic polyesters derived from lactic and glycolic acids. J. Biomed Mater Res (Appl Biomater) 1999;48:342–353.

[39] Vert M, Mauduit J, Li S. Biodegradation of PLA/GA polymers: increasing complexity. Biomaterials 1994;15:1209–1213.

[40] Bocchini S, Fukushima K, Di Blasio A, Fina A, Frache, Geobaldo F. Polylactic acid and polylactic acid-based nanocomposite photooxidation. Biomacromolecules, 2010;11,11:2919–2926.

[41] Kister G, Cassanas G, Vert M. Effects of morphology, conformation and configuration on the IR and Raman spectra of various poly (lactic acid)s. Polymer 1998;39,2:267–273.

[42] Zhang JM, Sato H, Tsuji H, Noda I, Ozaki Y. Differences in the CH3.OC interactions among poly(L-lactide), poly(L-lactide)/poly(D-lactide) stereocomplex,and poly(3-hydroxybutyrate) studied by infrared spectroscopy. J Mol Struct 2005;735-736:249–257.

[43] Carrasco F, Pagès P, Gámez-Pérez J, Santana OO, Maspoch ML. Processing of poly(lactic acid): Characterization of chemical structure, thermal stability and mechanical properties. Polym Degrad Stab 95;2010:116–125.

[44] Meaurio E, López-Rodríguez N, Sarasua JR. Infrared Spectrum of poly(L-lactide): application to crystallinity studies. Macromolecules 2006;39:9291–9301.

[45] Saenz de Juano Arbona, V. Doctoral Thesis Contribución al estudio de la degradación ambiental de poliolefinas fotoestabilizadas Universidad Politécnica de Valencia. 2008.

[46] Contat Rodrigo L. Estudios de degradación de poliolefinas aditivadas con materiales biodegradables. Universidad Politécnica de Valencia. 2000.

[47] Wunderlich B. Thermal analysis of Polymeric Materials. Berlin, ed. Springer. 2005.

[48] Yang M-H, Lin Y-H. Measurement and simulation of thermal stability of oly(lactic acid) by thermogravimetric analysis. J Test Eval 2009;37,4:1-6.

[49] Aoyagi Y, Yamashita K, Doi Y. Thermal degradation of poly[(R)-3-hydroxybutyrate], poly[ε-caprolactone], and poly[(S)- lactide]. Polym Degrad Stab 2002;76:53.

[50] Carrasco F, Pagès P, Gámez-Pérez J, Santana OO, Maspoch ML. Kinetics of the thermal decomposition of processed poly(lactic acid). Polym Degrad Stabil 2010;10:2508–2514.

[51] Fan Y, Nishida H, Hoshihara S, Shirai Y, Tokiwa Y, Endo T. Pyrolysis kinetics of poly(l-lactide) with carboxyl and calcium salt end structures. Polym Degrad Stab 2003;79:547–562.

[52] Fan YJ, Nishida H, Shirai Y, Endo T. Racemization on thermal degradation of poly(l-lactide) with calcium salt in structure. Polym Degrad Stab 2003;80:503-511.

[53] Criado JM. Kinetic analysis of DTG data from master curves. Thermochim Acta 1978; 24:186–189.

[54] Coats AW, Redfern JP. Kinetic parameters from thermogravimetric data. Nature 1964;201,4914: 68–69.

[55] Li L, Guan C, Zhang A, Chen D, Qing Z. Thermal stabilities and the thermal degradation kinetics of polyimides. Polym Degrad Stab 2004;84:369–373.

[56] Sun JT, Huang YD, Gong GF, Cao HL. Thermal degradation kinetics of poly (methylphenylsiloxane) containing methacryloyl groups. Polym Degrad Stab 2005;91:339–346.

[57] Badia JD, Santonja-Blasco L, Martínez-Felipe A, Ribes-Greus A. Reprocessed polylactide: Studies of thermo-oxidative decomposition. Bioresource Technol 2012;114: 622–628.

[58] Badia JD, Santonja-Blasco L, Moriana R. Ribes-Greus A. Thermal analysis applied to the characterization of degradation in soil of polylactide: II. On the thermal stability and thermal decomposition kinetics Polymer Degradation and Stability 2010; 95:2192–2199.

[59] Grausea G, Ishibashia J, Kamedaa T, Bhaskarb T, Yoshioka T. Kinetic studies of the decomposition of flame retardant containing high-impact polystyrene. Polym Degrad Stab 2010;95:1129–1137.

[60] Martin O, Avérous L. Poly(lactic acid): plasticization and properties of biodegradable multiphase systems. Polymer, 2001;42:6209–6219.

[61] Celli A, Scandola M. Thermal properties and physical ageing of poly (L-lactic acid). Polymer 1992;33,13:2699–2703.

[62] Starkweather HW, Avakian P. Fontanella JJ, Wintersgill MC. Internal motions in polylactide and related polymers. Macromolecules 1993;26:5084–5087.

[63] Petersson L, Oksman K. Biopolymer based nanocomposites: Comparing layered silicates and microcrystalline cellulose as nanoreinforcement. Compos. Sci. Technol. 2006;66: 2187–2196.

[64] Pluta M. Morphology and properties of polylactide modified by thermal treatment, filling with layered silicates and plasticization. Polymer 2004;45:8239–8251.

[65] Turi E. Thermal characterization of polymeric materials, Academic Press: New York, 1997.

[66] Fox TG, Jr, Flory PJ. Second-order transition temperatures and related properties of polystyrene.I. Influence of molecular weight. J Applied Physics 1950;21:581–591.

[67] Schubach HR, Nagy E, Heise B. Short range order of amorphous polymers derived by WAXS. Colloid Polym Sci 1981;259, 8:789–796.

[68] Wang F, Saeki S, Yamaguchi T. Temperature and pressure dependence of thermal expansion coefficient and thermal pressure coefficient for amorphous polymers. Polymer 1997;38,14:3485–3492.

[69] Tsuji H, Ikada Y. Properties and morphologies of poly (L-lactide): Annealing conditions effect on properties and morphologies of poly (L-lactide). Polymer 1995;36,14:2709-2716.

[70] Ling X, Spruiell JE. Analysis of the complex thermal behavior of poly(L-lactic acid) film. II. Samples crystallized from the melt. J Polym Sci Part B: Polym Phys 2006;44:3378–3391.

[71] Shieh YT, Liu GL. Temperature-modulated differential scanning calorimetry studies on the origin of double melting peaks in isothermally melt-crystallized poly(L-lactic acid). J Polym Sci Polym Phys 2007;45:466–474.

[72] Yasuniwa M, Tsubakihara S, Sugimoto Y, Nakafuku C. Thermal Analysis of the double-melting behavior of poly(L-lactic acid). Journal of Polymer Science: Part B: Polym Phys 2004;42:25–32.

[73] Kovacs AJ, Transition vitreuse dans les polymeres amorphes: etude phenomenologique Fortschr. Hochpolym.-Forsch. 1963;3:394–507.

[74] Goldstein M, Nakoneczny M. Volume relaxation in zinc chloride glass. Phys Chem Glasses 1965;6:126.

[75] Suga H, Seki S. Thermodynamic investigation on glassy states of pure simple compounds. J. Non-Cryst. Solids 1974;16:171–194.

[76] Yoshida H. Enthalpy relaxation of polymeric glasses. Netsu-Sokutei 1986;13:191–199.

[77] Yoshida H. Relationship between enthalpy relaxation and dynamic mechanical relaxation of engineering plastics. Thermochim Acta 1995;266:119–127.

[78] Struik LCE. Physical aging in amorphous polymers and other materials. Elsevier, Amsterdam, 1878.

[79] Yoshii T, Yoshida H, Kawai T. Effect of structural relaxation of glassy PET on crystallization process observed by the simultaneous DSC–XRD and DSC–FTIR. Thermochim Acta 2005;431:177–181.

[80] Fischer EW, Sterzel HG, Wegner G. Kolloid ZZ. Investigation of the structure of solution grown crystals of lactide copolymers by means of chemical reactions. Polymer 1973;251:980–990.

[81] Vasanthakumari R, Pennings AJ. Crystallization kinetics of poly(L-lactic acid). Polymer 1983;24:175-178.

[82] Miyata T, Masuko T. Crystallization behaviour of poly(L-lactide). Polymer 1998;39:5515–5521.

[83] Tsuji H, Tezuka Y, Saha SK, Suzuki M, Itsuno S. Spherulite growth of L lactide copolymers: Effects of tacticity and comonomers. Polymer 2005;46:4917–4927.

[84] Abe H, Kikkawa Y, Inoue Y, Doi Y. Morphological and kinetic analyses of regime transition for poly[(S)-lactide] crystal growth. Biomacromolecules 2001;2:1007–1014.

[85] Yasuniwa M, Tsubakihara S, Iura K, Ono Y, Dan Y, Takahashi K. Crystallization behavior of poly(L-lactic acid). Polymer 2006; 47:7554–7563.

[86] Yasuniwa M, Sakamo K, Ono Y, Kawahara W. Melting behavior of poly(L-lactic acid): X-ray and DSC analyses of the melting process. Polymer 2008;49:1943–1951.

[87] Baratian S, Hall ES, Lin JS, Xu R, Runt J. Crystallization and solid-state structure of random polylactide copolymers: Poly(L-lactide-*co*-D-lactide)s. Macromolecules 2001;34:4857–4864.

[88] Yuryev Y, Wood-Adams P, Heuzey M-C, Dubois C, Brisson J. Crystallization of polylactide films: an atomic force microscopy study of the effects of temperature and blending. Polymer 2008;49:2306–2320.

[89] Cartier L, Okihara T, Ikada Y, Tsuji H, Puiggali J, Lotz B. Epitaxial crystallization and crystalline polymorphism of polylactide. Polymer 2000;41:8909–8919.

[90] De Santis P, Kovacs AJ. Molecular conformation of poly(S-lactic acid). Biopolymer 1968;6:299–306.

[91] Hoogsteen W, Postema AR, Pennings AJ, Ten Brinke G, Zugenmaier P. Crystal structure, conformation, and morphology of solution-spun poly(L-lactide) fibers. Macromolecules 1990;23:634–642.

[92] Sasaki S.; Asakura T. Helix distortion and crystal structure of the α-form of poly(L-lactide). Macromolecules 2003;36:8385–8390.

[93] Kobayashi J, Asahi T, Ichiki M, Okikawa A, Suzuki H, Watanabe T, Fukuda E, Shikinami Y. Structural and optical properties of poly-lactic acids. J Appl Phys. 1995;77:2957–2973.

[94] Zhang JM, Duan Y, Sato H, Tsuji H, Noda, I, Yan S, Ozaki Y. Crystal modifications and thermal behavior of poly(L-lactic acid) revealed by infrared spectroscopy. Macromolecules 2005;38:8012–8021.

[95] Mandelkern L. Crystallization of Polymers, vol. 2, Cambridge University Press, Cambridge, UK, 2004. 2nd ed.

[96] Badia JD, Strömberg E, Ribes-Greus A,. Karlsson S. Assessing the MALDI-TOF MS sample preparation procedure to analyze the influence of themo-oxidative ageing and themo-mechanical degradation on poly (Lactide). Eur Polym J 2011;692:85–95.

[97] Shin EJ, Jeong W, Brown HA, Koo BJ, Hedrick JL. Waymouth RM. Crystallization of cyclic polymers: Synthesis and crystallization behavior of high molecular weight cyclic Poly(ε-caprolactone)s. Macromolecules 2011;44:2773–2779.

[98] Hoffman JD, Miller RL. Response of criticism of nucleation theory as applied to crystallization of lamellar polymers. Macromolecules 1988;21:3038–3051.

[99] Gomez MA, Fatou JG, Bello A. Spherulitic growth rates of poly(3,3-diethyl oxetane). Eur Polym J 1986;22:661–664.

[100] Okui N. Umemoto S. Polymer Crystallization, ed. Sommer JU, Reiter G. Springer, Berlin, 2003 Chapter 19.

[101] Lovering EG. The relationship between molecular weight and spherulitic growth rates in trans-1,4-polyisoprene. J Polym Sci 1970;C-30:329–338.

[102] Tsuji H, Ikada Y. Crystallization from the melt of poly(lactide)s with different optical purities and their blends Macromol Chem Phys 1996;197:3483–99.

[103] Hoffman JD, Davis GT, Lauritzen JI. Jr. In treatise on solid state chemistry. Hannay NB, Ed. Plenum Press New York, 1976.

[104] Hoffman JD, Davis GT, Lauritzen, JL. Jr. The rate of crystallization of linear polymers with chain folding. In treatise on solid state chemistry Hannay, NB. Ed. Plenum Press: New York, 1976; Vol. 3; Chapter 7, pp 566.

[105] Pantani R, De Santis F, Sorrentino A, De Maio F, Titomanlio G. Crystallization kinetics of virgin and processed poly lactic acid. Polym Degrad Stab 2010;95:1148–1159.

[106] Tsuji H, Tezuka Y, Saha SK, Suzuki M, Itsuno S. Spherulite growth of L-lactide copolymers: Effects of tacticity and comonomers. Polymer 2005;46:4917–4927.

[107] Di Lorenzo ML. Determination of spherulite growth rates of poly(L-lactic acid) using combined isothermal and non-isothermal procedures. Polymer 2001;42:9441–9446.

[108] Williams ML, Landel RF, Ferry JD. The temperature dependence of relaxation mechanisms in amorphous polymers and other glass-forming liquids. J Am Ceram Soc 1955;77:3701–3707.

[109] Jeon K, Chiari YL, Alamo RG. Maximum rate of crystallization and morphology of random propylene ethylene copolymers as a function of comonomer content up to 21 mol%. Macromolecules 2008;41:95–108.

[110] Mandelkern L, Prasad A, Alamo RG, Stack GM. Melting temperature of the n-alkanes and the linear polyethylenes. Macromolecules 1990**;**23,15:3696–3700.

Chapter 5 Conclusions

5.1 Conclusions

A complete degradation study of Polylactide (PLA) under different environments has been carried out. Samples of PLA have been subjected to thermal, bio and photo degradation at different times, with the aim to understand the effect of the different degradation agents on the polymer structure. A methodology was set up and successfully applied combining the use of several analytical techniques. Changes in molar mass were measured by Gel Permeation Chromatography and viscometry and the effect of degradation on the physical-chemical properties of the materials was assessed by using Fourier Transform Infrared Spectroscopy, Thermogravimetric Analysis, Scanning Electron Microscopy, Dynamic Mechanical Thermal Analysis, Differential Scanning Calorimetry and Optical Microscopy. The combination of the analytical techniques provided with selected parameters as reliable indicators useful to monitor the degradation process, evaluate each degradation effect on the polylactide characteristics and detect differences between the mechanisms.

The conclusions of this thesis have been organized by first presenting the most relevant information provided by each technique, followed by the concluding remarks based on the combination of all the information.

Temporal molar mass variation

As expected, all the different degradation processes decreased the PLA molar mass with time, but at different rates. Thermal degradation at 220ºC was found to be the fastest in minutes scale, while in the case of long exposure (months scale) photodegradation is faster than biodegradation. Exposing the PLA pellets to thermal degradation during some minutes provides similar reductions in the molar mass as photodegradation in months and biodegradation in years. At equivalent degradation times, photo degraded specimens have about half the molar mass of soil degraded samples.

The rate of molar mass decay by biodegradation follows a first order, while the decrease in thermal and photodegradation can be explained by second order processes. The difference of the kinetic order of the molar mass decay with time could be due to the fact that the

mechanism of hydrolysis is principally starting in the end chains of the molecules whereas for thermal and photo degradation the mechanism is randomly occurring in the ester groups.

The equations modeling the trend of the molar mass with time for all the degradation processes are next listed:

- Thermal degradation 2nd order $\frac{1}{M_v} = 9.99 \cdot 10^{-3}\,\mathrm{t} + \frac{1}{192.2}$ t in hours
- Biodegradation 1st order: ln M_n= ln(73.2)-0.021·t t in months
- Photodegradation 2nd order $\frac{1}{M_n} = 1.37 \cdot 10^{-3}\,\mathrm{t} + \frac{1}{73.2}$ t in months

These models were successfully applied in general terms to some literature results, confirming their broad range of application for each degradation type. Indeed an extended correlation of the thermal degradation law was correlated with literature data at different temperatures providing Arrhenius temperature dependence, T in K.

- Thermal degradation $\frac{1}{M_v} = e^{-12.64\cdot/T+21.15} \cdot \mathrm{t} + \frac{1}{192.2}$ t in hours

The literature analysis remarked that degradation in soil is the slowest biodegradation processes in comparison to pure hydrolysis and composting that exhibited the fastest biodegradation rate. In the case of photodegradation, lower UV wavelengths of radiation exposure provoke a drastic acceleration of the degradation rate.

Mechanisms of polylactide degradation

Thermal degradation occurs via random cleavage of the ester bonds, via either transesterification or cis-elimination. In the case of the former, the formation of cyclic molecules and the consequent decrease in the OH groups could not be quantified by FTIR, since the concentration was below the threshold detectable.

Hydrolysis is the central process in the biodegradation of PLA and the enzymatic activity of the microorganism can be developed after reaching a threshold at low molar masses. The polylactide hydrolysis can take place by random or end-chain cleavage of ester

groups, generating new carboxylic groups and thus increasing the OH concentration. According to the molar masses calculated during degradation, the percentage of molecules with OH groups was very low, and could not be measured by FTIR.

Photodegradation of PLA follows a Norrish II mechanism, involving the random cleavage and the formation of carbonyl groups and vinyl end groups. An alternative mechanism for outdoor exposure has been recently proposed by *Bocchini et al.*, involving the formation of anhydrides. Low intensity bands related to these groups were observed by FTIR following a linear increase with the degradation time, indicating the occurrence of the *Bocchini* mechanism, probably simultaneously with the Norrish II mechanism.

Influence of the structure on the thermal decomposition

Polylactide submitted to degradation followed a single thermal decomposition stage, and this occurs regardless of the degradation type. The onset ($T_o \approx 345$ºC), endset ($T_e \approx 375$ºC) and the peak decomposition ($T_p \approx 360$ºC) temperatures can be chosen as representative parameters of the thermal decomposition of the degraded samples.

The variation of these temperatures was not very acute but all of them exhibited a sinusoidal trend with degradation time. In general, the profile of all the temperatures seems to follow a common decreasing pattern with molar mass regardless of the degradation process, with temperature decreases in the $\Delta T \approx 10$ºC range. The minimum values are observed for T_o of photodegraded samples at small M_n. The molar decay controls the thermal stability of the PLA samples.

The application of a kinetic analysis methodology described the influence of all types of degradation on the apparent activation energy of the thermal decomposition process of the degraded samples. A combination of five different methods was used, namely, *Friedman*, *Flynn-Wall-Ozawa*, *Kissinger*, *Criado* and *Coats-Redfern*, to determine the PLA kinetic triplet evolution throughout the degradation processes. The values of *Ea* calculated by the different methods follow the same trend. All the thermal degraded samples exhibit a linear decreasing trend for *Ea* with degradation time, while the variation of *Ea* for bio and photo is sinusoidal. The apparent activation energy from the (*Ea*) slightly decreases with decreasing

the molar mass and the values are ranging from 150 to 210 KJ/mol, being the results from the all isoconversional methods consistent. The decrease in *Ea* with molar presents a linear trend for the thermal degradation while bio and photodegradation present scattering probably due to the combination of processing degradation, followed by bio or photo degradation.

The thermal decomposition can be described by an autocatalytic function in the case of samples submitted to bio and photo degradation. On the other hand, the thermal decomposition of thermally degraded samples is more complex and cannot be explained by one solely model. However, bio and photo degraded samples also reach this change in the mechanism at sufficient degradation times, following a chemical controlled process. This fact points out that the mechanism depends on the degradation state and justifies the presence of several models in the bibliography for the thermal decomposition of PLA.

Influence of degradation on the surface of polylactide

Visual changes caused by bio and photo degradation were also monitored by Scanning Electron Microscopy (SEM). No significant changes were observed on the surface of the photodegraded samples, while biodegradation promotes fast appearance of formations and rough surfaces. After 24 months in soil, some canals were observed on the surface of samples with M_n of about 45600. Such changes may enhance water access to the core of the sample and also the diffusion to the media of small molar masses, which can be easily bio assimilated.

Influence of the viscoelastic behavior on the samples

The viscoelastic response of all the degraded samples was monitored by the storage modulus (*E'*) and loss modulus (*E''*) versus the temperature and frequency. The spectra showed a unique relaxation related to the glass transition, followed by an increase in the moduli due to the crystallization of the PLA.

Photo and bio degradation promotes the increase of the stiffness in the glassy and crystalline regions, accompanied with an increase of the samples brittleness. Both types of degradation also promote changes in the depth and temperature range of the rubbery plateau, which is shifted to lower temperatures, indicating a faster crystallization process.

Crystallization is a slower process for bio than for photo degradation as the higher values of crystallization onset temperature show.

The maximum temperature of *E''* for bio and photo degraded samples followed similar trends with molar mass, obeying the Fox-Flory equation and the maximum temperature drastically changes for M_n values below 28000.

The evolution of the free volume was monitored through the thermal expansion coefficient, α_f, which was calculated taking $T_\infty = T_g$ - 51.6ºC to enable a comparison between the bio and photo degraded samples. The free volume decreases at decreasing molar mass, and such reduction is more acute for biodegraded samples than for photodegraded ones, at equivalent molar masses.

Thermal transitions and crystallization from the glass

The thermal transitions were studied with detail by DSC. The glass transition, the crystallization and melting processes of the different degraded samples yielded valuable information regarding the different degradation processes. All the degraded samples undergo melting-recrystallization-melting phenomenon at low molar masses.

The evolution of the crystallization temperature before erasing the thermal history showed differences between bio and photo degradation, in coherence with the DMTA results. Further analysis of the enthalpies revealed different rates of crystallization from the glass, depending on the degradation process. It was found that thermal degradation provokes the slowest rate of crystallization followed by photodegradation and biodegradation. The effect of the sub products of each degradation process has a marked influence on the crystallization phenomenon. The potential presence of cyclic molecules could account for the reduction on the crystallization rate in thermal degraded samples. Other potential inhibition agents of crystallization are intramolecular groups formed by photodegradation, such as anhydrides, that would act as defects in the crystalline lattice.

Crystallization kinetics from the melt

The comparison between the effect of the thermal, biological and photodegradation on the isothermal crystallization from the melt of polylactide was completed with a kinetic study of the degraded samples, correlating the results with the molar mass reduction. Processing from pellets to melt-pressed plates causes an abrupt variation in the crystalline grow rate promoted by the decrease in molar mass, indicating significant chain excision due to thermal degradation. The crystallization growth rate (G) of the photo and bio degraded samples also increases at decreasing molar mass, according to: **biodegraded** > **photodegraded** > **thermally** degraded samples, at comparable molar masses. This can be explained by the formation of cyclic molecules and additional anhydride groups by thermal and photodegradation, respectively, acting as defects in the crystallization process.

Plots of log(G) was plotted versus log(M_w) at the temperature of the maximum growth rate (120.5ºC) showed that the effect of the different degradation processes on G is only noticeable above M_w ≈103000 (M_n~*80000)*. Approximately straight lines have been obtained for each degradation type, with G proportional to M_w^a, with a = -1.3, -1.1 and -1.0 for bio, photo and thermal degradation, respectively. At sufficient low molar masses the presence of chain ends or defects may modify the trend in the crystallization process.

In addition, the analysis of the kinetic data according to the secondary nucleation theory has been performed. The temperature coefficient of the growth rate, analyzed according to secondary nucleation, leads to linear dependence following Regime I for both bio and photo degraded specimens.

The values of surface free energy (σ_e) and segmental transport (U^*) decrease with the molar mass of PLA submitted to thermal, bio and photo degradation. The reduction in σ_e (which occurs in general from 85 to 55 erg/cm^2) is more acute for the biodegraded samples, followed by the photo and finally the thermal degraded samples, in accordance with the growth rate results. The decreasing infers an energetically favored folding in shorter PLA molecules.

Final remarks

Several parameters have been monitored as indicators of the degradation processes of PLA: the molar mass decay, the chemical structure, the surface morphology, thermal transitions, the characteristic temperatures and enthalpies, the decomposition kinetics or crystallization phenomena. The combination of molar mass characterization, FTIR, SEM and Thermal Analysis has proved as a useful strategy to assess and discriminate macroscopic changes on PLA structure induced by different types of degradation. More precisely, the work performed during this PhD thesis has underlined the importance of the crystalline phase formed as an indicator of the degradation degree and as a distinctive characteristic for each degradation process.

The main features of each degradation type are summarized as follows:

- ***Thermal degradation***. This degradation is remarkably fast in time (hours), reaching a 90% molar mass decrease after 330 min at 220ºC, and following a 2nd order equation (k_T= 9.99 10^{-3} mol/kg·hour). The sub products of thermal degradation could not be detected properly by FTIR, and the kinetic function of the thermal decomposition is complex and cannot be explained by one solely model, involving chemical controlled processes. The main particularity of this type of degradation is that crystallization of the molecules exhibited the slowest rate, resulting in smaller sized spherulites respect to bio and photodegraded samples, at equivalent molar masses.

- ***Biodegradation.*** Hydrolysis plays a central role in soil degradation, since bio assimilation is only feasible at molar masses (<10000). Thus, this process can be considered as a synergetic combination of hydrolysis of high molar mass molecules and bio assimilation of smaller ones. The temporal molar mass decay yields a 1st order model with time (exponential) having a rate constant of k_B = 0.021 months^{-1}. The acidic hydrolytic mechanism is considered to start at the chains ends of the molecules, accounting for the origin of the 1st order model. The experimental FTIR spectra do not exhibit significant changes in the characteristic bands of PLA for a quantitative analysis. Other important feature is that thermal decomposition of the degraded polylactide followed an autocatalytic model, with the

activation energy, *Ea*, ranging from 185 to 200 kJ/mol. Hydrolysis and deterioration of the surface permit the migration of the low molar masses and the penetration of water. This fact is observed after 24 months of exposure, according to SEM observation. Regarding the crystallization from the glass and the melt, biodegraded samples undergo the fastest crystallization processes, exhibiting the lowest σ_e.

- ***Photodegradation***. The molar mass decay due to this process follows a 2nd order equation ($k_P = 1.37 \cdot 10^{-3}$ mol/kg·months), being faster than biodegradation in comparable time scales. Photodegraded polylactide followed an autocatalytic model, with the activation energy, *Ea*, ranging from 178 to 185 kJ/mol. FTIR confirmed the presence of anhydride groups, which may be affecting the crystallization from the glass and the crystallization kinetics from the melt of photodegraded samples.

The results obtained in this thesis have established an equivalent molar mass reduction at different times depending on the degradation process. The synergies between the techniques used, and specially the characterization of the crystallization processes, have stated that the degradation of polylactide cannot be explained by a mere process of chain excision. Furthermore, the sub products of each degradation differ and influence the different thermal, viscoelastic and physical properties of the polylactide.

All these results can be especially useful in order to select disposal management processes to control the residue volume. Considering radiation conditions characteristic of Spain, the sunlight exposition could be more effective to eliminate polylactide disposal than degradation in soil, avoiding the drawbacks related to thermal treatment.

5.2 Future Research

The protocol created for the study of PLA can be applied to compare the degradation of several polymers or to study the synergetic effect of different degradations in one polymer. Furthermore, the protocol could be complemented by implementing alternative techniques.

Several possible strategies to continue and broaden this research line can be focused on studying the synergetic effect of different degradation types, on characterizing the resulting chemical structure and determining the effects on morphology.

More concretely:

- To study the synergetic effect of photo and bio degradation in order to simulate initial exposure of polylactide to sunlight followed by further deposition in soil. To characterize the effects of both degradations on the molecule structure following the methodology protocol of this thesis.
- To study the synergetic effect of thermal and photo degradation, in order to simulate the effect of initial recycling and further sunlight exposure after deposition. To characterize the effects of both degradations on the molecule structure following the methodology protocol of this thesis.
- To extend the study varying different parameters, such as changing the wavelength range in photodegradation or increasing the temperatures in thermal degradation.
- To quantify the extent of the cyclic molecules formed during thermal degradation at different temperatures.
- To use other analytical techniques to detect further degradation products to determine the degradation mechanism (chromatography, MALDI-TOF, NMR…)
- To analyze the effect of ageing on the resulting morphology and its effect on the structural relaxation and crystallization of PLA.
- To extend the degradation study to other polymers.

Annex

Publications during the research period

1. Hygrothermal ageing of reprocessed polylactide

2. Reprocessed polylactide: Studies of thermo-oxidative decomposition

3. A methodology to assess the energetic valorization of bio-based polymers from the packaging industry: Pyrolysis of reprocessed polylactide

4. Thermal analysis applied to the characterization of degradation in soil of polylactide: I. Calorimetric and viscoelastic analyses

5. Thermal analysis applied to the characterization of degradation in soil of polylactide: II. On the thermal stability and thermal decomposition kinetics

6. A thermogravimetric approach to study the influence of a biodegradation in soil test to a poly(lactic acid)

7. Thermal characterisation of photo-oxidized HDPE/Mater-BI and LDPE/Mater-BI blends buried in soil

8. Thermal characterization of polyethylene blends with a biodegradable masterbatch subjected to thermo-oxidative treatment and subsequent soil burial test

Accepted Manuscript

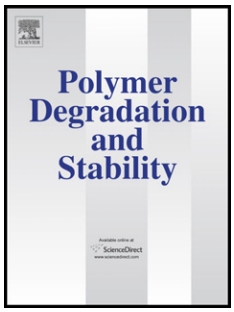

Hygrothermal ageing of reprocessed polylactide

J.D. Badia, L. Santonja-Blasco, A. Martínez-Felipe, A. Ribes-Greus

PII: S0141-3910(12)00216-9

DOI: 10.1016/j.polymdegradstab.2012.06.001

Reference: PDST 6691

To appear in: *Polymer Degradation and Stability*

Received Date: 11 November 2011

Revised Date: 23 May 2012

Accepted Date: 4 June 2012

Please cite this article as: Badia JD, Santonja-Blasco L, Martínez-Felipe A, Ribes-Greus A, Hygrothermal ageing of reprocessed polylactide, *Polymer Degradation and Stability* (2012), doi: 10.1016/j.polymdegradstab.2012.06.001.

HYGROTHERMAL AGEING OF REPROCESSED POLYLACTIDE

J.D. Badia, L. Santonja-Blasco, A. Martínez-Felipe, A. Ribes-Greus*

Instituto de Tecnología de Materiales (ITM),

Universitat Politècnica de València

Camino de Vera s/n, E-46022 Valencia, Spain

* Corresponding author: A. Ribes-Greus

+34 963879817

e-mail: aribes@ter.upv.es

HYGROTHERMAL AGEING OF REPROCESSED POLYLACTIDE

J.D. Badia, L. Santonja-Blasco, A. Martínez-Felipe, A. Ribes-Greus*

Abstract

The influence of an accelerated hygrothermal ageing simulation test on a commercial PLA and its three subsequent mechanically-reprocessed materials was studied. The analysis was focused on the water diffusion kinetics and the physico-chemical changes induced by the hygrothermal degradation. Water diffusion proceeded faster than chain relaxation processes, as defined by a Case II absorption model. It was proved that the water diffusion rate decreased with subsequent reprocessing cycles and increased with higher hygrothermal ageing temperatures. Hydrolytic chain scission provoked significant molar mass decays and consequent general losses of thermal and mechanical performance. The rearrangement into crystalline fractions of shorter chains provoked by hygrothermal ageing was qualitatively and quantitatively followed by both Fourier-Transform Infrared Spectroscopy and Differential Scanning Calorimetry. The microstructural changes were monitored by the cold-crystallization temperature, the crystallinity degree X_C and the absorbance intensity ratio I_{921}/I_{955}. A Weibull model showed that the crystallites were formed faster at higher reprocessing cycles and at lower hygrothermal ageing temperatures. All these effects were particularly significant for PLA reprocessed more than one time.

Keywords

Polylactide (PLA)

Hygrothermal ageing

Water absorption kinetics

Crystallinity

Differential Scanning Calorimetry (DSC)

Fourier-Transform Infrared Analysis (FT-IR)

Bioresource Technology 114 (2012) 622–628

Contents lists available at SciVerse ScienceDirect

Bioresource Technology

journal homepage: www.elsevier.com/locate/biortech

Reprocessed polylactide: Studies of thermo-oxidative decomposition

J.D. Badia, L. Santonja-Blasco, A. Martínez-Felipe, A. Ribes-Greus *

Instituto Tecnológico de Materiales. Universidad Politécnica de Valencia, Camino de Vera, s/n, 46022 Valencia, Spain

ARTICLE INFO

Article history:
Received 21 December 2011
Received in revised form 23 February 2012
Accepted 24 February 2012
Available online 5 March 2012

Keywords:
Energetic valorization
Polylactide (PLA)
Thermal stability
Thermo-oxidative decomposition kinetics
Evolved-Gas Analysis (EGA)

ABSTRACT

The combustion process of virgin and reprocessed polylactide (PLA) was simulated by multi-rate linear non-isothermal thermogravimetric experiments under O_2. A complete methodology that accounted on the thermal stability and emission of gases was thoroughly developed. A new model, Thermal Decomposition Behavior, and novel parameters, the Zero-Decomposition Temperatures, were used to test the thermal stability of the materials under any linear heating rate. The release of gases was monitored by Evolved Gas Analysis with in-line FT-IR analysis. In addition, a kinetic analysis methodology that accounted for variable activation parameters showed that the decomposition process could be driven by the formation of bubbles in the melt. It was found that the combustion technologies for virgin PLA could be transferred for the energetic valorization of its recyclates. Combustion was pointed out as appropriate for the energetic valorization of PLA submitted to more than three successive reprocessing cycles.

1. Introduction

The research in the packaging industry within a framework of sustainable development is focused on the use of bio-based materials which accomplish the benefit of coming from renewable resources, and being biodegradable once discarded, within a rational time. In this sense, polylactide (PLA) is an aliphatic polyester that can be obtained from agricultural resources, and reintroduced into the carbon cycle after being used. The increasing know-how in the technology of production of PLA (Gupta and Kumar, 2007) enhances its performance as suitable candidate for replacing commodities at the packaging sector.

Despite the potential of PLA for being treated by biological valorization in composting facilities, the foreseeable high amount of plastic waste invites to diversify and combine the available technologies of valorization. Among current procedures, material valorization by mechanical recycling is widely established (Vilaplana and Karlsson, 2008). It mainly consists in recovery, washing, drying, shredding and processing by means of extrusion or injection. The inherent thermo–mechanical degradation may modify the polymeric structure (Badia et al., 2009, 2011a) and consequently affect the thermal, rheological and mechanical properties (Strömberg and Karlsson, 2009; Badia et al., 2012a), thus reducing the performance rates of recycled goods.

A viable solution to manage bio-based recycled plastics waste, when no better performance can be guaranteed, could be the application of thermally-induced valorization technologies, such as pyrolysis and combustion (Al-Salem et al., 2009).

The application of these thermal operations must be carefully handled by technologists during the design of energetic valorization facilities, taking into account the knowledge of the thermal stability and the detection of emitted gases. As well, the characterization of the decomposition kinetics should be considered.

Thermogravimetric analysis (TGA) is a widely used technique to assess the thermal stability and reaction kinetics of biomass (Barneto et al., 2010) and bio-based polymers (Carrasco et al., 2010). On the other hand, detection techniques such as Fourier transform-infrared spectroscopy (FT-IR) are widely used hyphenated to TGA for gas detection (Materazzi and Vecchio, 2010).

The majority of current studies on the combustion behavior of PLA are reported from the point of view of the flame retardancy (Bourbigot and Fontaine, 2010), but not approached from the point of view of the management of their wastes. The aim of this work was thus to assess the behavior of mechanically-recycled polylactide submitted to a combustion process, with the purpose of assuring the performance of energetic valorization processes as a contribution for further plastic waste management solutions.

2. Experimental procedure

2.1. Reprocessing simulation and sample preparation

Polylactide (PLA) 2002D is a thermo-forming grade PLA obtained from NatureWorks LLC (Minnetonka, MN) in the form of pellets. Prior to processing, virgin PLA (VPLA) pellets were dried during 2 h at 80 °C in a dehumidifier Conair Micro-D FCO 1500/3

* Corresponding author.
E-mail address: aribes@ter.upv.es (A. Ribes-Greus).

0960-8524/$ - see front matter © 2012 Elsevier Ltd. All rights reserved.
http://dx.doi.org/10.1016/j.biortech.2012.02.128

List of abbreviations

α	degree of conversion
A	pre-exponential factor
AIC	Advanced Isoconversional Method
β	TGA heating rate
DTG	first-derivative thermogravimetric curve
Ea	activation energy
Ea_α	apparent Ea at a fixed α
EGA	Evolved Gas Analysis
$f(\alpha)$	kinetic function
FT-IR	Fourier transform-infrared spectroscopy
FWO	Flynn–Wall–Ozawa
KAS	Kissinger–Akahira–Sunose
MP	master-plots
n	order in kinetic functions $f(\alpha)$
n_β	n averaged from experiments at different β
n'	n averaged from n_β
n''	n averaged from the n obtained analytically–Eq. (4)
p	power
RPLA-i	reprocessed polylactide
TDB	Thermal Decomposition Behavior
TG	thermogravimetric curve
TGA	thermogravimetric analysis
VPLA	virgin polylactide
ZDT	Zero-Decomposition Temperature

(UK), in order to remove as much humidity as possible from PLA flakes. Afterward, samples were processed by means of injection molding with an Arburg 420 C 1000–350 (Germany) injector, single-screw model (diameter $\Phi = 35$ mm, length/$\Phi = 23$). Successive processing steps were applied under the same conditions (temperature gradient set from hopper to die: 160, 170, 190, 200 and 190 °C; molds set at 15 °C; cooling time residence ~40 s and total residence time ~60 s). Samples were dried before each processing cycle. After injection, a fraction of the samples were kept as test specimens and the rest was ground by means of a cutting mill Retsch SM2000 (UK), which provide pellets of size $d < 20$ mm to be fed back into the recirculation process. Up to five processing cycles were applied to obtain the different testing specimens of reprocessed PLA (RPLA-i, with i: 1–5).

2.2. Thermogravimetric experiments

Multi-rate linear non-isothermal thermogravimetric experiments were carried out in a Mettler–Toledo TGA/SDTA 851 (Columbus, OH). Samples weighing ~5 mg were heated in an alumina holder with capacity for 70 μL. Experiments were performed from 25 to 750 °C at different heating rates ($\beta = 2$, 5, 7, 10, 12, 15 °C min^{-1}), under constant flow of 50 mL min^{-1} of oxygen. Experiments were repeated at least three times, and the averages were considered as representative values. The assessment was performed with the help of the software STAR^e 9.10 from Mettler–Toledo.

Results are plotted in terms of {average, dev_{max}, dev_{min}}, where dev_{max} = max (data)−average (data), and dev_{min} = average (data)−min (data). Tabulated errors were obtained by dividing the standard deviation by the average of data.

2.3. Evolved Gas Analysis

Evolved Gas Analysis (EGA) was applied to fumes released by combustion by means of coupled TGA/FT-IR. In this case, the TGA analysis was focused on a temperature range in which the main decomposition range of PLA occurred, from 180 to 500 °C, by means of a heating rate of 1 °C min^{-1}. Samples weighing ~40 mg were heated in an alumina holder with capacity for 900 μL. The flow rate of the oxygen was set to 25 mL min^{-1}, according to technical specifications. FT-IR gas-phase spectra were collected by a previously calibrated Thermo Nicolet 5700 FT-IR Spectrometer (MA, USA), from 4000 to 600 cm^{-1} of wavenumber, at a resolution of 4 cm^{-1}. Both transfer line and gas cell were kept at 250 °C to prevent gas condensation. Sixteen co-added spectra were recorded every 30 s to assure accuracy of the temperature scanning. The Gram–Schmidt plots as well as its corresponding 3D FT-IR spectra were analyzed with the help of software OMNIC 7.0. 2D-IR correlation spectroscopy was performed by means of the software 2D Shige (Morita, 2005).

3. Results and discussion

The potential of the use multi-rate thermogravimetric analysis, coupled to FT-IR, to approach the behavior of PLA and its subsequent recyclates under a thermo-oxidative decomposition process is discussed in detail in this section. The assessment comprises (i) the description of the decomposition profiles; (ii) the use of a novel model to functionalize the thermal stability at different heating rates; (iii) the application of a thorough kinetic strategy pursued for ascertaining the kinetics of decomposition accounting for variable activation parameters and (iv) the detection of gases evolved during the decomposition.

3.1. Description of the thermo-oxidative decomposition profiles

Fig. 1a shows the thermogravimetric curve at the heating rate $\beta = 5$ °C min^{-1} of virgin and fifth reprocessed PLAs. The rest of reprocessed materials showed intermediate profiles. As expected, higher β led to shift the thermograms towards higher temperatures, but the graphs have not been shown for the sake of clarity. The thermo-oxidative decomposition took place through a two-stage profile. The first mass-loss took place from 250 to 370 °C, consuming nearly 96–98% of the material, which can be addressed to the decomposition of the backbone. Immediately afterward, the second step appeared from 370 to 400 °C, eliminating 4–2% of the polymer, without presence of char, as can be seen in the inset of Fig. 1a. As expected, lower temperatures than those used in inert conditions (Badia et al., 2012c) were necessary under an oxidizing environment. For further calculations, the second step under O_2 was considered negligible if compared with the main decomposition and therefore the study was focused on the first mass-loss region.

A complete description of the thermo-oxidative decomposition of PLA recyclates is given in terms of thermal stability, decomposition kinetics, and detection of evolved gases, as the first approach to be used in combustion facilities.

3.2. On the use of the TDB model to describe the thermal stability of PLA under any linear heating rate

With the aim of assessing the thermal stability of PLA and its further recyclates, the corresponding decomposition onset T_0 and endset T_e temperatures were obtained by a tangential intercept method onto the thermogravimetric curves for the whole process.

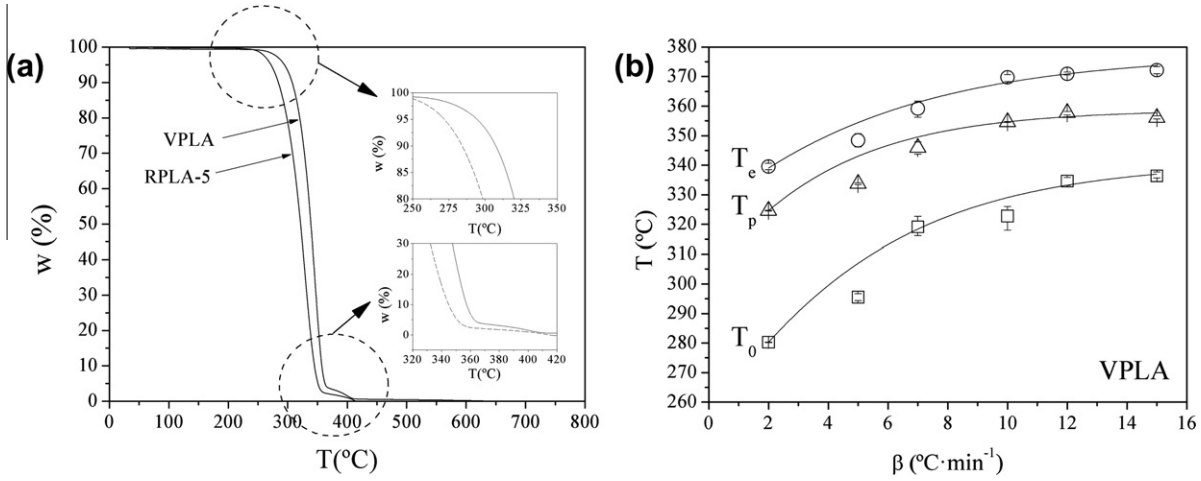

Fig. 1. (a) Mass-loss profiles of virgin PLA and PLA reprocessed five times. Inset: detail of onset and endset of decomposition. (b) Application of the TDB model to fit the evolution of the characteristic thermogravimetric temperatures (0: onset, p: peak, e: endset), for the case of virgin PLA.

Table 1
Results of fitting $T_0 = f(\beta)$ to Eq. (1), along with the onset Zero-Decomposition Temperature obtained by extrapolating Eq. (1) to $\beta \to 0$.

Material	T_0	Value	e (%)	Value	e (%)	Value	e (%)	R^2 (%)	ZDT_0 (°C)
		TDB fitting values for T_0							
		a		b		k			
VPLA		340.9	1.45	0.34	0.53	0.22	2.76	99.7	254.4
RPLA-1		345.4	0.63	0.35	0.34	0.19	0.10	99.3	255.8
RPLA-2		362.5	2.89	0.26	0.35	0.09	3.17	99.8	287.7
RPLA-3		337.3	0.08	0.45	1.02	0.49	0.99	99.8	232.6
RPLA-4		340.1	0.92	0.36	1.38	0.31	2.36	92.9	250.1
RPLA-5		339.2	1.12	0.40	2.03	0.26	2.07	96.5	242.3

Likewise, the temperature at the maximum decomposition rate, i.e. the peak temperature T_p of the differential thermogravimetric curve was also considered for all applied heating rates β. To help enhance the analysis of the influence of the β on the characteristic decomposition temperatures and functionalize the thermal stability of PLA under combustion processes, the so-called Thermal Decomposition Behavior TDB model given in Eq. (1) was proposed. An example of its validity[1] is shown in Fig. 1b for the case of VPLA.

$$TDB(\beta) = a \cdot (1 + b \cdot e^{-k \cdot \beta})^{-1} \quad (1)$$

In order to evaluate the differences in thermal stability under combustion conditions due to reprocessing, instead of choosing the experimental temperatures obtained at a specific β, the so-called onset Zero-Decomposition Temperature ZDT_0 was used, since this parameter is related to the trigger of the decomposition, and was obtained by extrapolating the TDB fitting of T_0 to infinitely low β (Badia et al., 2012c). Table 1 shows the results of the proposed procedure. A sharp increase in ZDT_0 of ~30 °C was registered from virgin PLA up to the second recyclate, dropping ~50 °C when passed the third recyclate. A previous study by means of Differential Scanning Calorimetry (Badia et al., 2012b) showed that the influence of reprocessing on PLA structure formed shorter chains up to the third recyclate. Thus the apparition of new sites liable to O_2 in the PLA structure may promote faster decomposition at lower temperatures at high reprocessing cycles, which may need lower temperatures to start their decompositions.

[1] See results of fitting in the Supplementary material.

3.3. Studies on the kinetics of thermo-oxidative decomposition

The intrinsic kinetics of solid-state decompositions, are usually described by a simplified reaction pathway in terms of three parameters: apparent activation energy *Ea*, pre-exponential factor *A* and kinetic function $f(\alpha)$ with reaction order *n*, conforming the so-called kinetic triplet. In this section, the results of the application of a detailed strategy are shown, according to the following steps: (i) the application of isoconversional methods to assess the evolution of the apparent activation energy, along with the proposal of a novel model to mathematically describe this evolution; (ii) the evaluation of the kinetic model, in terms of variable apparent activation energy and reaction order; (iii) the assessment of the variation of the pre-exponential factor, in order to complete the kinetic triplet. As a result, instead of a kinetic triplet comprised by three constant parameters, this methodology provides the variation of the kinetic triplet along the decomposition process. Finally, the differences between the decomposition of virgin PLA and its recyclates are discussed.

3.3.1. Evolution of the apparent activation energy

A significant variation in activation energy (Ea_α) along the conversion range α ($\alpha = (m_0 - m_t)/(m_0 - m_\infty)$, where *m* was the mass and subscripts 0, *t* and ∞ stand for initial, actual and final, respectively), was found, as shown in Fig. 2. This variation was detected by the application of three suitable integral isoconversional methods, namely linear Flynn–Wall–Ozawa (FWO) (Flynn and Wall, 1966) (Ozawa, 1970), linear Kissinger–Akahira–Sunose (KAS) (Kissinger, 1957) (Akahira and Sunose, 1971), and nonlinear Advanced Isoconversional Method (AIC) (Vyazovkin, 1997). As can be seen in Fig. 2a, the three methods offered similar Ea_α values for the assessment of virgin PLA, showing a good coincidence along the decomposition reaction, as also obtained for the rest of reprocessed materials. Fig. 2b and c show the evolution of the Ea_α averaged from the application of the three isoconversional methods at each α, while Table 2 gathers the averaged *Ea* values obtained by each method averaged along the whole α range. The Ea_α behaved increasing from values ~40–60 kJ mol^{-1} at low conversions α to values ~150–170 kJ mol^{-1} at the end of the decomposition. It should be pointed out that the large obtained deviation values (ε, 18–40%) did not permit to apply a simplified kinetic triplet (Badia et al., 2012c) that is, with constant activation parameters, and therefore the variation of *Ea*, *A* and *n* in $f(\alpha)$ was considered.

The physical meaning underlying the evolution of the apparent activation energy has been a matter of profuse debate (Galwey,

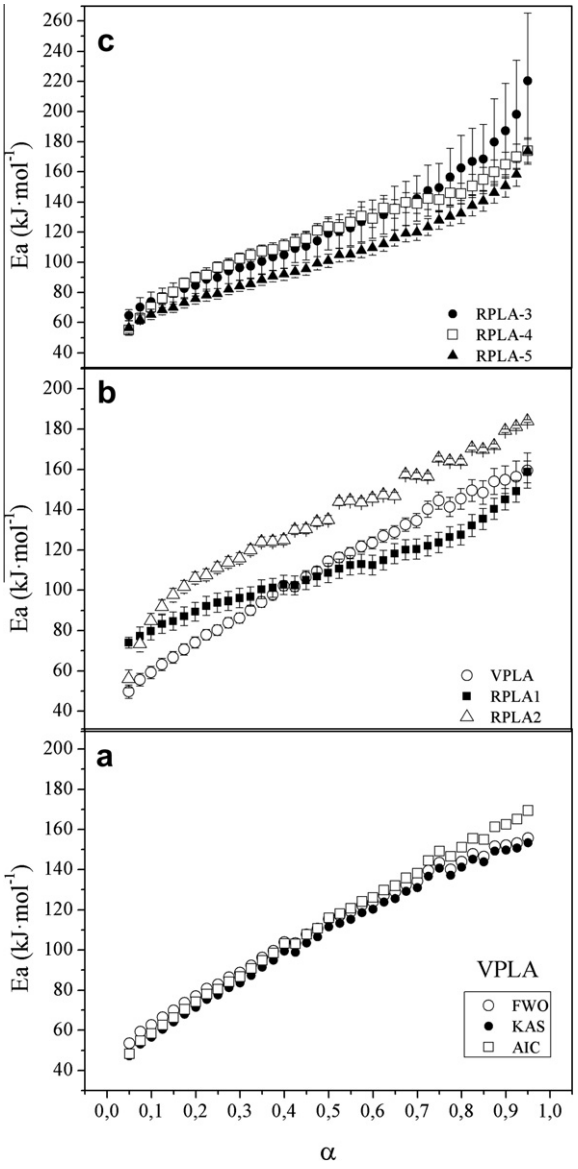

Fig. 2. (a) Apparent *Ea* obtained for VPLA by means of FWO, KAS and AIC methods; (b) average isoconversional activation energy of VPLA, RPLA-1 and RPLA-2 and (c) evolution of average isoconversional activation energy for RPLA-3, RPLA-4 and RPLA-5.

Table 2
Average activation energy along the thermo-oxidative decomposition process, as obtained by different isoconversional methods.

Material	Activation energy averaged from the α range					
	FWO		KAS		AIC	
	Ea (kJ mol^{-1})	*e* (%)	*Ea* (kJ mol^{-1})	*e* (%)	*Ea* (kJ mol^{-1})	*e* (%)
VPLA	101	30.7	96	31.2	112	25.0
RPLA-1	106	19.8	102	21.5	97	23.7
RPLA-2	127	30.6	123	33.3	120	31.0
RPLA-3	114	29.8	116	28.4	103	27.3
RPLA-4	121	21.8	119	19.6	114	18.5
RPLA-5	97	27.8	92	30.4	89	39.3

2003) (Vyazovkin, 2003). It seems reliable to understand that the increase of Ea_α is consistent with the decomposition of the residual material which is becoming more refractory as temperature increases (Vyazovkin et al., 2011). In any case, the mathematical characterization of its evolution may help to control its kinetics. In order to define the evolution of Ea_α throughout the thermo-oxidative decomposition process, a powered equation was chosen, based on the Freundlich model (Freundlich, 1928) for growing behaviors, according to Eq. (2):

$$Ea(\alpha) = Ea_0^* + \sum_i b_i \cdot \alpha^{p_i} \tag{2}$$

where i was the number of slopes in the curve, Ea_0^* a fictive activation energy at $\alpha = 0$, b a fitting parameter and p a power that accounted for the shape of the curve; whether $p < 1$, the increase is decelerative, and if $p > 1$, the increase is accelerative. Table 3 shows the powers resulted from the fitting of Eq. (2) to the Ea_α evolution of all materials. Generally, two slopes could be considered, as described by Ea_α in Fig. 2b and c, and thus $i = 1, 2$ in Eq. (2). As can be seen, virgin PLA only showed a decelerative curve, while the recyclates started with a decelerative trend and presented a change in tendency at advanced conversions, rapidly increasing its Ea_α in an accelerative fashion. Accordingly, it can be also observed how the smaller $p1$ the faster initial increases and vice versa, as clearly happened from VPLA to RPLA-2; on the other hand, the smaller $p2$, the brusquer changes in tendency to faster Ea_α increases along the reaction, as shown for RPLA-3–5. The functionalizing of Ea_α will be useful for further analysis in which the variation of the activation energy is considered.

3.3.2. How to obtain the kinetic model with varying Ea?

The next step in order to complete the kinetic triplet was to achieve the mathematical model of the decomposition that should best describe the combustion process along the valorization process. Thus, the kinetic function $f(\alpha)$ was approached by the use of reduced differential Master-Plots MPf_e (Gotor et al., 2000). Eq. (3) was thus used for determining which family of theoretical curves MPf_t, namely, nucleation and growth (A_n), n-order reaction (F_n), reaction-controlled (R_n) and diffusion-controlled (D_n) – see description elsewhere (Khawan and Flanagan, 2006) – was more suitable to describe the experimental behavior of virgin and reprocessed PLAs facing combustion.

$$\Phi(f,\alpha) = \sum_\beta \left(\sum_{\alpha=0}^{1} [MPf_t(\alpha) - MPf_e(\alpha)]^2 \right); \quad \Delta\alpha = 0.025; \quad \forall f \tag{3}$$

The minimization of Φ in Eq. (3) was achieved by the model A_n, with n ranging from 2 to 4 depending on the heating rate β of the analysis, as shown in Table 4. Fig. 3 shows the abacus of the theoretical differential master plots in comparison with those experimental for VPLA and RPLA-1, as an example of the accuracy of this methodology to predict the model of decomposition.

The next step consisted in determining the value of n for each conversion degree α, which was achieved by the minimization of ξ in Eq. (4), being i the counter of the h experiments carried out at different heating rates β. This equation compared the Ea_α obtained by the isoconversional methods to the *Ea* given by the Coats–Redfern (Coats and Redfern, 1964) method in Eq. (5), using the mathematical expression of the kinetic model A_n, and took into account the Perez-Maqueda et al. criterion (Pérez-Maqueda et al., 2002); that is, the independence of the activation parameters on β. Since the analysis was performed at particular α values, considering all results obtained at all β, the analysis could be considered also isoconversional.

$$\xi(n,\alpha) = \sum_i^h \left| (-R) \cdot \frac{d}{dt} \left(\frac{ln\left(\beta_i \cdot T^{-2} (-ln(1-\alpha))^{\frac{1}{n}}\right)}{T^{-1}} \right) - Ea_\alpha \right| \tag{4}$$

Fig. 4 shows the evolution of n along the α range, which could be assumed to be almost constant within a confidence margin lower than 7%, as shown by n'' in Table 3. Therefore, the suitability of

Table 3
Results of fitting of *Ea* and *lnA* to Eq. (2).

Material	Activation energy/*Ea*					Pre-exponential factor/*lnA*				
	p_1		p_2		R^2 (%)	p_1		p_2		R^2 (%)
	Value	*e* (%)	Value	*e* (%)		Value	*e* (%)	Value	*e* (%)	
VPLA	0.791	2.61	–	–	99.82	0.746	2.82	–	–	99.64
RPLA-1	0.591	6.39	9.352	7.81	99.85	0.672	7.99	9.467	8.30	99.80
RPLA-2	0.413	2.46	11.783	2.89	99.06	0.399	7.22	10.63	4.11	99.64
RPLA-3	0.746	6.55	5.737	8.40	99.82	0.712	7.86	5.732	8.51	99.79
RPLA-4	0.357	8.40	8.294	3.96	99.81	0.342	7.08	10.47	4.23	99.68
RPLA-5	0.807	6.93	7.545	6.10	99.79	0.775	7.65	7.377	6.52	99.69

Table 4
n_β: values of n of the A_n model found for the thermo-oxidative decomposition of PLA and its recyclates at different β; n': average of n_β; n'': values obtained from the minimization method, using Eq. (4).

Material	n_β						n'	n''	
	β (°C min^{-1})								
	2	5	7	10	12	15		Average	*e* (%)
VPLA	2.0	2.5	2.5	2.5	3.0	3.0	2.58	2.65	6.2
RPLA-1	2.0	2.0	2.5	2.5	3.0	3.0	2.50	2.41	6.9
RPLA-2	2.0	2.0	2.5	2.5	2.5	3.0	2.41	2.26	6.5
RPLA-3	2.0	2.5	2.5	2.5	3.0	4.0	2.76	2.76	5.3
RPLA-4	3.0	3.0	3.0	4.0	3.5	4.0	3.40	3.49	6.8
RPLA-5	2.5	2.5	3.0	4.0	4.0	4.0	3.33	3.38	6.4

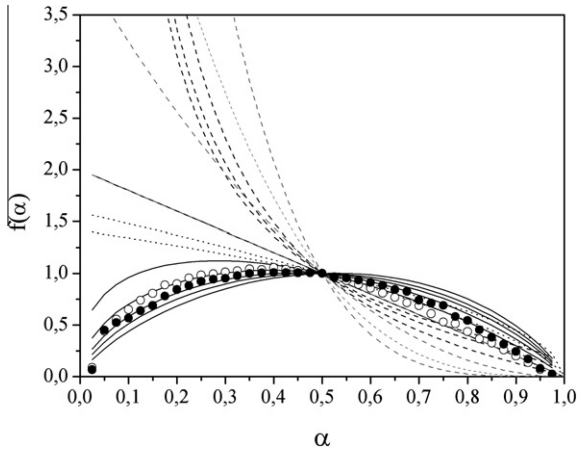

Fig. 3. Master plots based on the differential form of the general kinetic law compared to experimental data obtained for thermo-oxidative decomposition of VPLA (hollow circles) and RPLA-1 (full circle). Kinetic models: A_n (nucleation and growth, solid black lines), F_n (n-order reactions, solid gray lines), R_n (reaction-controlled, pointed lines), D_n (diffusion-controlled, dashed lines).

the model A_n was strengthened. In addition, the possibility of using n' (average of $n\beta$, those are, the n individually obtained for each material at each heating rate β) was remarked, since closer values to those given by the analytical procedure (n'') were obtained, thus permitting to continue the calculations with less time-consuming computations.

3.3.3. Closing the kinetic triplet: pre-exponential factor

Finally, the evolution of the pre-exponential factor along the α decomposition range (lnA_α) was also isoconversionally obtained from the intercept at the origin in Eq. (5), considering the data at all heating rates β.

$$\left[ln\frac{\beta\cdot(-ln(1-\alpha))^{\frac{1}{n}\big|_\alpha}}{T^2}\right]_y = ln\frac{A_\alpha\cdot R}{Ea_\alpha}+\frac{Ea_\alpha}{R}\cdot\left[\frac{1}{T}\right]_x \quad (5)$$

Fig. 5a shows the evolution of lnA_α for VPLA and RPLA-2 as example. The rest are not presented to prevent overlapping curves. It can be seen how lnA_α was strongly connected to the behavior of Ea_α, since both presented similar profiles along the α range. Therefore, one may suggest that the application of Eq. (2) might also be suitable for fitting the experimental data and thus provide a mathematical description of lnA_α evolution. The accuracy of the fitting can be seen at Fig. 5a and assessed at Table 2. The powers $p1$ and $p2$ were of the same order than those obtained for Ea_α, thus permitting the use of the powers previously obtained for Ea_α as initialization values in the iteration process of the fitting of lnA_α.

Finally, the kinetic triplet was completed and the mathematical description of the combustion process of PLA and its recyclates was resolved. Fig. 5b shows for virgin PLA the comparison between the experimental points of the differential thermogravimetric curve in terms of conversion degree, and the mathematical description obtained by the kinetic analysis for variable activation parameters. Similar results were found for the rest of recyclates. The proposed methodology thus stands out as a suitable and effective tool to model the kinetic behavior of virgin and reprocessed PLA under thermally-induced energetic valorizations.

3.3.4. Effects of reprocessing on the decomposition kinetics of PLA

Results concluded that virgin PLA and its recyclates followed an A_n kinetic model (growth of previously formed nuclei) during their combustion. This kind of kinetic model is scarcely reported in studies dealing with thermal decomposition processes of polymers -see discussion elsewhere (Badia et al., 2010)-. However, the model A_n indicates the presence of active zones more chemically liable to thermo-oxidative decomposition, which activate the formation and growth of gas bubbles in the polymer melt.

With regards to the evolution of the apparent activation energy, as expected, the Ea_α needed to trigger the decomposition under oxidative conditions was lower than under inert conditions, i.e. pyrolysis (Badia et al., 2012c), since the reactions were enhanced by oxidation processes which led to the formation of radical species such as carboxylic-ended species that accelerated the decomposition (Bikiaris and Karayannidis, 1999) (Liu et al., 2006). Concerning the differences in Ea_α among virgin material and recyclates facing the thermo-oxidative decomposition, it was assessed in terms of the apparent activation energy at the initial stages of combustion. For instance, selecting the Ea_α at a conversion rate of 0.2 (that is, $Ea_{0.2}$), a similar profile than that shown by the onset Zero-Decomposition Temperature ZDT_0 at the studies of thermal stability was found. An increase up to the second recyclate was registered, which was not followed by the successive reprocessed materials, which kept their $Ea_{0.2}$ at lower values. Thus the apparition of reaction sites liable to O_2 in the PLA structure promoted the decomposition with less demanded energy from the third reprocessing cycle on, also pointing out the feasibility of combustion to valorize highly reprocessed polylactide.

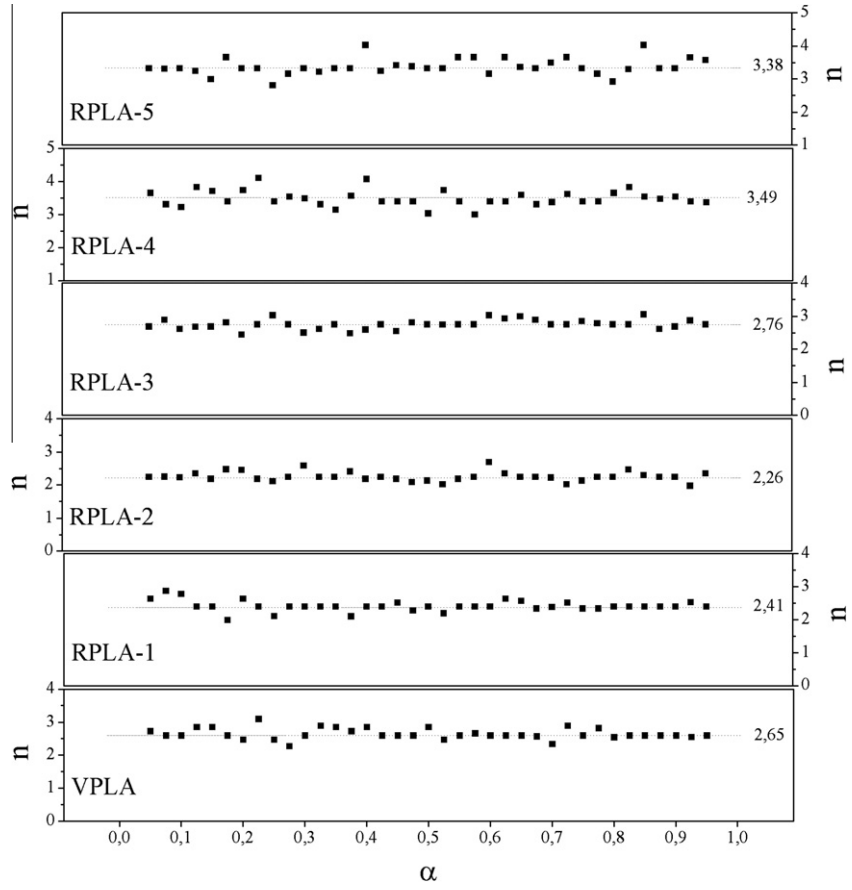

Fig. 4. Evolution of n in the A_n model of thermo-oxidative decomposition of virgin PLA and its successive recyclates. The number is the average of data (n'' in Table 3).

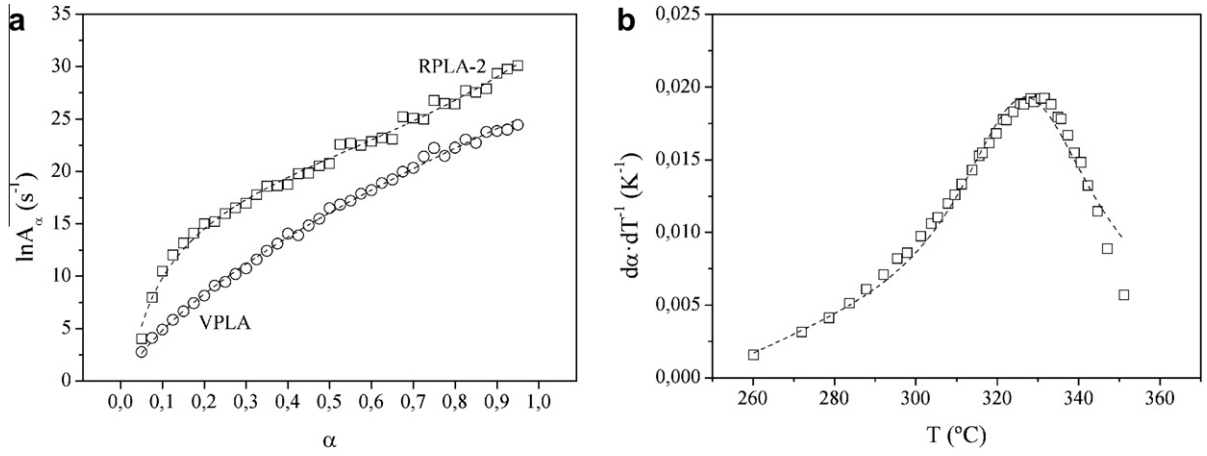

Fig. 5. (a) *lnA* evolution given for VPLA and RPLA-2 as an example of the goodness of fitting of Eq. (2) to explain its behavior along the α range. Hollow symbols: obtained lnA_α values; dashed lines: computed fittings. (b) Comparison of experimental DTG curves (symbols) to compute kinetic functions (dashed lines) obtained from the kinetic methodology.

3.4. Evolved Gas Analysis by in-line FT-IR

Finally, to exploit the potential of TGA to simulate the thermo-oxidative decomposition of PLA under combustion conditions, the emission of gases was monitored by in-line FT-IR analysis. Main detected evolved species were: carbon dioxide [2349 cm^{-1} υ_{as}(O═C═O)]; carbon monoxide [2174/2116 cm^{-1} υ(C≡O)]; acetaldehyde [2968 cm^{-1} $\upsilon(CH_3)$, 2740 cm^{-1} υ(CHO), 1762 cm^{-1} υ(C═O), 1414/1371 cm^{-1} $\delta(CH_3)$ and 1127 cm^{-1} υ(C—O)] and acetic acid [3586 cm^{-1} υ(H—O), 1778 cm^{-1} υ(C═O)], which may be formed by oxidation of acetaldehyde; short-chain acids and their dimers and trimers [3589 cm^{-1} υ(OH), 2952 cm^{-1} $\upsilon(CH_2)$, 2816 cm^{-1} υ(CH), 1778 cm^{-1} υ(C═O), and 1164/1107 cm^{-1} υ(C—O)] (Vogel and Siesler, 2008) and traces of lactide [3008 cm^{-1} υ(CH), 2952 cm^{-1} $\upsilon_{as}(CH_3)$, 2893 cm^{-1} $\upsilon_s(CH_3)$, 1796 cm^{-1} υ(C═O), 1365 cm^{-1} $\delta(CH_3)$, 1248/1108 cm^{-1} υ(C—O—C) and 932 cm^{-1} corresponding to the ring skeletal vibration] and water [3900–3400 cm^{-1} υ(H—O), 1800–1300 cm^{-1} δ(H—O)].The gases were similar to those obtained during the pyrolysis (Badia et al., 2012c). As main differences, carbon mono- and di-oxides

evolved with bigger intensity, due to the combustion processes were enhanced; the bands of acetaldehyde decreased, and those related to acetic acid slightly increased, due to the oxidation effect of O_2; as well, lactide still appeared, but its bands were overlapped along with those corresponding to short-chain acids and their dimers and trimers and thus a finer identification was complicated. The application of 2D-correlation spectra (Noda, 1990) gave an asynchronous spectrum, where positive cross-peaks at (2378, 1796) and (2316, 1796) and a negative cross-peak at (2116, 1796), which exposed that CO_2 was evolved before the main decomposition products with υ(C=O) vibrations, while CO was released afterward.

After mechanical reprocessing, the chemical nature of polylactide was essentially the same (Badia et al., 2011b), though shorter chains can be obtained (Badia et al., 2012b), and thus no differences were found at the IR spectra of the evolved gases of reprocessed PLAs. The necessary facilities for detecting the emission of evolved gases from the combustion of reprocessed PLAs could thus be the same than those needed for virgin PLA, which may reduce costs of investing and implementation in new technologies.

4. Conclusions

Multi-rate linear-non-isothermal thermogravimetric (TGA) experiments under oxidative (O_2) conditions, coupled to FT-IR analysis for gas detection, were suitable to simulate the thermal behavior of virgin and multiple-injected PLA facing combustion. A kinetic methodology was applied accounting for the evolution of the activation parameters along the decomposition. A powered equation was used to explain the variations of activation energy and pre-exponential factor along the decomposition process. A nucleation and growth model which gave importance to the formation of gas bubbles in the polymer melt was valid for all materials. Reprocessed PLA did not modify the profile of evolved gases.

Acknowledgements

The authors would like to acknowledge the Spanish Ministry of Science and Innovation for the financial support through the Research Projects ENE2007-67584-C03, UPOVCE-3E-013, ENE2011-28735-C02-01, IT-2009-0074, as well as for the pre-doctoral research position for L. Santonja-Blasco through the FPI program. The Spanish Ministry for Education is acknowledged for the concession of a pre-doctoral research position to J.D. Badia and A. Martinez-Felipe by means of the FPU program. The authors thank the financial support of the Generalitat Valenciana through the ACOMP/2011/189, the Grisolia research position for A. Martínez-Felipe, and for the Forteza technician position. Universitat Politècnica de València (UPV, Spain) is thanked for additional support through the PAID 05-09-4331 and PAID 06-11-2037 projects. AIMPLAS (Technological Institute of Plastic) is acknowledged for providing and processing the material.

Appendix A. Supplementary data

Supplementary data associated with this article can be found, in the online version, at doi:10.1016/j.biortech.2012.02.128.

References

Akahira, T., Sunose, T., 1971. Res. Rep. Chiba Inst. Technol. 16, 22–31.
Al-Salem, S.M., Lettieri, P., Baeyens, J., 2009. Recycling and recovery routes of plastic solid waste (PSW): a review. Waste Management 29, 2625–2643.
Badia, J.D., Vilaplana, F., Karlsson, S., Ribes-Greus, A., 2009. Thermal analysis as a quality tool for assessing the influence of thermo–mechanical degradation on recycled poly(ethylene terephthalate). Polymer Testing 28, 169–175.
Badia, J.D., Santonja-Blasco, L., Moriana, R., Ribes-Greus, A., 2010. Thermal analysis applied to the characterization of degradation in soil of polylactide: II. On the thermal stability and thermal decomposition kinetics. Polymer Degradation and Stability 95, 2192–2199.
Badia, J.D., Strömberg, E., Ribes-Greus, A., Karlsson, S., 2011a. A statistical design of experiments for optimizing the MALDI–TOF–MS sample preparation of polymers. An application in the assessment of the thermo–mechanical degradation mechanisms of poly(ethylene terephthalate). Analytica Chimica Acta 692, 85–95.
Badia, J.D., Strömberg, E., Ribes-Greus, A., Karlsson, S., 2011b. Assessing the MALDI–TOF MS sample preparation procedure to analyze the influence of thermo-oxidative ageing and thermo–mechanical degradation on poly(lactide). European Polymer Journal 47, 1416–1428.
Badia, J.D., Strömberg, E., Karlsson, S., Ribes-Greus, A., 2012a. The role of crystalline, mobile amorphous and rigid amorphous fractions in the performance of recycled poly(ethylene terephthalate) (PET). Polymer Degradation and Stability 97, 98–107.
Badia, J.D., Strömberg, E., Karlsson, S., Ribes-Greus, A., 2012b. Material valorisation of amorphous polylactide. Influence of thermo–mechanical degradation on the morphology, segmental dynamics, thermal and mechanical performance. Polymer Degradation and Stability 97, 670–678.
Badia, J.D., Santonja-Blasco, L., Martínez-Felipe, A., Ribes-Greus, A., 2012c. A methodology to assess the energetic valorization of bio-based polymers from the packaging industry: pyrolysis of reprocessed polylactide. Bioresource Technology 111, 468–476.
Barneto, A.G., Carmona, J.A., Alfonso, J.E.M., Serrano, R.S., 2010. Simulation of the thermogravimetry analysis of three non-wood pulps. Bioresource Technology 101, 3220–3229.
Bikiaris, D.N., Karayannidis, G., 1999. Effect of carboxylic end groups on thermooxidative stability of PET and PBT. Polymer Degradation and Stability 66, 213–218.
Bourbigot, S., Fontaine, G., 2010. Flame retardancy of polylactide: an overview. Polymer Chemistry 1, 1413–1422.
Carrasco, F., Pagès, P., Gámez-Pérez, J., Santana, O.O., Maspoch, M.L., 2010. Kinetics of the thermal decomposition of processed poly(lactic acid). Polymer Degradation and Stability 95, 2508–2514.
Coats, A.W., Redfern, J.P., 1964. Kinetic analysis from thermogravimetric data. Nature 68, 4914.
Flynn, J.H., Wall, L.A., 1966. A quick, direct method for the determination of activation energy from thermogravimetric data. Journal of Polymer Science 4, 323–342.
Freundlich, H., 1928. Colloid and Capillary Chemistry. Duton & Co, New York.
Galwey, A.K., 2003. What is meant by the term 'variable activation energy' when applied in the kinetic analyses of solid state decompositions (crystolysis reactions)? Thermochimica Acta 397, 249–268.
Gotor, F.J., Criado, J.M., Malek, J., Koga, K., 2000. Kinetic analysis of solid-state reactions: the universality of Master Plots for analyzing isothermal and non-isothermal experiments. Journal of Physical Chemistry A 104, 10777–10782.
Gupta, A.P., Kumar, V., 2007. New emerging trends in synthetic biodegradable polymers–polylactide: a critique. European Polymer Journal 43, 4053–4074.
Khawan, A., Flanagan, D.R., 2006. Solid-state kinetic models: basics and mathematical fundamentals. Journal of Physical Chemistry B 110, 17315–17328.
Kissinger, H.E., 1957. Reaction kinetics in differential thermal analysis. Analytical Chemistry 29, 1702–1706.
Liu, X., Zou, Y., Li, W., Cao, G., Chen, W., 2006. Kinetics of thermo-oxidative and thermal degradation of poly(D, L-Lactide) (PDLLA) at processing temperature. Polymer Degradation and Stability 91, 3259–3265.
Materazzi, S., Vecchio, S., 2010. Evolved gas analysis by infrared spectroscopy. Applied Spectroscopy Reviews. 45, 241–273.
Morita, S., 2004–2005. 2D Shige (c). Kwansei–Gakuin University.
Noda, I., 1990. Two-dimensional infrared (2D IR) spectroscopy: theory and applications. Applied Spectroscopy. 44, 550–561.
Ozawa, T., 1970. Kinetic analysis of derivative curves in thermal analysis. Journal of Thermal Analysis 2, 301.
Pérez-Maqueda, L.A., Criado, J.M., Gotor, F.J., Málek, J., 2002. Advantages of combined kinetic analysis of experimental data obtained under any heating profile. Journal of Physical Chemistry A 106, 2862–2868.
Strömberg, E., Karlsson, S., 2009. The design of a test protocol to model the degradation of polyolefins during recycling and service life. Journal of Applied Polymer Science 112, 1835–1844.
Vilaplana, F., Karlsson, S., 2008. Quality concepts for the improved use of recycled polymeric materials: a review. Macromolecular Materials and Engineering. 293, 274–297.
Vogel, C., Siesler, H.W., 2008. Thermal degradation of poly(ε-caprolactone), poly(L-lactic acid) and their blends with poly(3-hydroxy-butyrate) studied by TGA/FT-IR spectroscopy. Macromolecular Symposia 265, 183–194.
Vyazovkin, S., 1997. Advanced isoconversional method. Journal of Thermal Analysis 49, 1493–1499.
Vyazovkin, S., 2003. Reply to "What is meant by the term 'variable activation energy' when applied in the kinetics analyses of solid state decompositions (crystolysis reactions)?". Thermochimica Acta 397, 269–271.
Vyazovkin, S., Burnham, A.K., Criado, J.M., Pérez-Maqueda, L.A., Popescu, C., Sbirrazzuoli, N., 2011. ICTAC kinetics committee recommendations for performing kinetic computations on thermal analysis data. Thermochimica Acta 520, 1–19.

Bioresource Technology 111 (2012) 468–475

Contents lists available at SciVerse ScienceDirect

Bioresource Technology

journal homepage: www.elsevier.com/locate/biortech

A methodology to assess the energetic valorization of bio-based polymers from the packaging industry: Pyrolysis of reprocessed polylactide

J.D. Badia, L. Santonja-Blasco, A. Martínez-Felipe, A. Ribes-Greus *

Instituto de Tecnología de Materiales, Universitat Politècnica de València, Camino de Vera, s/n, 46022 Valencia, Spain

ARTICLE INFO

Article history:
Received 5 December 2011
Received in revised form 30 January 2012
Accepted 2 February 2012
Available online 14 February 2012

Keywords:
Pyrolysis
Polylactide (PLA)
Reprocessing
Thermal decomposition kinetics
Evolved Gas Analysis (EGA)

ABSTRACT

The energetic valorization process of bio-based polymers is addressed in this study, taking polylactide (PLA) as model. The pyrolysis of virgin and multiple-injected PLA was simulated by means of multi-rate linear-non-isothermal thermogravimetric experiments. A complete methodology, involving control of gases, thermal stability and thermal decomposition kinetics was proposed. The release of gases was monitored by Evolved Gas Analysis of the fumes of pyrolysis, by in-line FT-IR, with the aid of 2D-correlation IR characterization. A novel model to establish the thermal stability of PLAs under any linear heating profile was proposed. A kinetic strategy was methodically applied to assess the thermal decomposition in terms of activation energy and kinetic model. It was found that the pyrolysis technologies for virgin PLA could be straightforwardly transferred for the valorization of its recyclates.

1. Introduction

The packaging industry is a highly important economic sector that involves big quantities of plastic materials. The current research is focused on bio-based polymers which accomplish the double benefit of coming from renewable resources, and being biodegradable once discarded, within a rational time. Polylactide (PLA) was used in this study as polymer model due to its good processability, mechanical properties, thermal stability and low environmental impact (Gupta and Kumar, 2007), which enhance its performance as suitable candidate for replacing commodities at the packaging sector. However, adding another material into the market chain will imply a new source of polymeric waste, which will have to be managed. Despite its potential of compostability, it would be advisable to explore the possibilities of extending its use during service life, recovering it and obtaining an added value from its discard. Among all recovery methods, material valorization by mechanical recycling is widely established (Vilaplana and Karlsson, 2008; Badia et al., 2011a), but the performance of recyclates may arrive to a threshold (Strömberg and Karlsson, 2009; Badia et al., 2009, 2012), when no suitable properties can be guaranteed. Then, a viable solution to manage recycled plastics waste is the application of thermally-induced recovery technologies, such as pyrolysis, gasification or combustion (Al-Salem et al., 2009). The application of these thermo-chemical operations must be carefully tackled by technologists when designing energetic valorization facilities, taking into account three basic pillars. Firstly, healthy and environmental issues must be addressed, and thus the management of emitted gases should be guaranteed. Previous lab-scale experiments such as Evolved Gas Analysis (EGA) permits testing the hazard of the released fumes, as well as helps identify the order of emitted compounds, which is related to the thermal decomposition mechanism. Secondly, the stability of the material under a specific heating profile should be known, in order to delimit the temperature ranges where the efficiency of the thermal process is improved. Finally, the thermal performance in terms of decomposition kinetics should be handled, with the aim of understanding the behavior of the polymer under the thermo-chemical process, and thus selecting the proper operational parameters for the correct performance of the valorization. Thermogravimetric analysis (TGA) is a widely used technique to assess the thermal stability and reaction kinetics of biomass (Barneto et al., 2010) and bio-based polymers (Carrasco et al., 2010). As well, detection techniques such as Fourier Transform-InfraRed Spectros-

Abbreviations: 2D-IR, two-dimensional InfraRed Spectroscopy; 3D-FTIR, three-dimensional plot from EGA; α, degree of conversion; A, pre-exponential factor; A_β, A at a defined β; AIC, Advanced Isoconversional Method; β, TGA heating rate; DTG, first-derivative thermogravimetric curve; Ea, activation energy; Ea_α, apparent Ea at a fixed α; Ea_{av}, average of Ea along the α range; Ea_{iso}, average of Ea for the three isoconversional methods; EGA, Evolved Gas Analysis; FT-IR, fourier-transform infrared spectroscopy; FWO, Flynn–Wall–Ozawa; KAS, Kissinger–Akahira–Sunose; MALDI-TOF-MS, matrix-assisted laser desorption/ionization – time of flight – mass spectrometry; *MP*, Master-Plots; MP_e, experimental MP; MP_β, differential form of MP; MP_{fg}, differential/integral form of MP; MP_g, integral form of M-P; MP_t, theoretical MP; PM_C, *Perez-Maqueda* et al criterion; RPLA-i, reprocessed polylactide; *TDB*, thermal decomposition behavior; TG, thermogravimetric curve; TGA, thermogravimetric analysis; VPLA, virgin polylactide; *ZDT*, Zero-Decomposition Temperatures.

* Corresponding author.
E-mail address: aribes@ter.upv.es (A. Ribes-Greus).

0960-8524/$ - see front matter © 2012 Elsevier Ltd. All rights reserved.
doi:10.1016/j.biortech.2012.02.013

copy (FT-IR) can be hyphenated to TGA for the gas identification (Materazzi and Vecchio, 2010).

The pyrolysis process of PLA is addressed in this study. Current related studies report the impact of zeolites (Yuzay et al., 2010), hydrolytic fillers (Liu et al., 2010) or burial in soil (Badia et al., 2010) on PLA decomposition kinetics during pyrolysis. Concerning the assessment of the pyrolysis of mechanically reprocessed PLA, the literature describes the influence of several extrusion cycles on the thermal stability (Żenkiewicz et al., 2009) and the effect of one stage of extrusion, injection and annealing on the thermal decomposition kinetics (Carrasco et al., 2010), but no studies have been found reporting the pyrolytic process of multi-injected PLA.

Thus, the aim of this work was to define a suitable methodology to assess the pyrolysis on mechanically reprocessed PLA in terms of (i) emitted gases, (ii) thermal stability, and (iii) thermal decomposition kinetics, as a contribution to further plastic waste management solutions.

2. Methods

2.1. Reprocessing simulation and sample preparation

Polylactide (PLA) 2002D was a thermo-forming grade PLA obtained from Natureworks LLC (Minnetonka, MN) in the form of pellets. Prior to processing, virgin PLA (VPLA) pellets were dried during 2 h at 80 °C in a dehumidifier Conair Micro-D FCO 1500/3 (UK), in order to remove as much humidity as possible from PLA flakes. Afterwards, samples were processed by means of injection molding by means of an Arburg 420 C 1000-350 (Germany) injector, single-screw model (diameter Φ = 35 mm, length/Φ = 23). Successive processing steps were applied under the same conditions (temperature gradient set from hopper to die: 160, 170, 190, 200 and 190 °C; moulds set at 15 °C; cooling time residence ~40 s and total residence time ~60 s). Samples were dried before each processing cycle. After injection, a fraction of the samples was kept as test specimen and the rest was ground by means of a cutting mill Retsch SM2000 (UK), which provided pellets of size lower than 20 mm to be fed back into the recirculation process. Up to five processing cycles were applied to obtain the different testing specimens of reprocessed PLA (RPLA-i, with i: 1–5).

2.2. Thermogravimetric experiments

Multi-rate linear non-isothermal thermogravimetric experiments were carried out in a Mettler-Toledo TGA/SDTA 851 (Columbus, OH). Samples weighing ~5 mg were heated in an alumina holder with capacity for 70 μL. Experiments were performed from 25 to 750 °C at different heating rates (β = 2, 5, 7, 10, 12, 15 °C min^{-1}), under constant flow of 50 mL min^{-1} of Argon to ensure inert conditions. Experiments were repeated at least three times, and the averages were considered as representative values. Characterization was assessed with the aid of the software STAR^{e} 9.10 from Mettler-Toledo.

2.3. Evolved Gas Analysis

Evolved Gas Analysis (EGA) was applied to the fumes released by pyrolysis by means of coupling Fourier-Transform Infrared Analysis to the TGA (TGA/FT-IR). In this case, the TGA analysis was focused on a temperature range in which the main decomposition range of PLA occurred, from 180 to 500 °C, by means of a heating rate of 1 °C min^{-1}. Samples weighing ~40 mg were heated in an alumina holder with capacity for 900 μL. The flow rate of the carrier gas was set to 25 mL min^{-1}, according to technical specifications. FT-IR gas-phase spectra were collected by a previously calibrated Thermo Nicolet 5700 FT-IR Spectrometer (MA, USA), from 4000 to 600 cm^{-1} of wavenumber, at a resolution of 4 cm^{-1}. Both transfer line and gas cell were kept at 250 °C to prevent gas condensation. 16 co-added spectra were recorded every 30 s to assure accuracy of the temperature scanning. The Gram-Schmidt plots as well as its corresponding 3D and 2D FT-IR spectra at different constant temperatures were analyzed with the help of software OMNIC 7.0. In addition, 2D-correlation spectroscopy was performed by means of the software 2Dshige (Morita, 2005).

3. Results and discussion

The thermal decomposition of virgin PLA took place through a single-step process between 250 °C and 370 °C, consuming nearly 98–99% of mass when the polymeric chains broke down to evolve to the gaseous phase, as shown elsewhere (Badia et al., 2010). The formation of char was thus negligible, which pointed out the suitability of PLA wastes to be used in pyrolysis facilities due to the high efficiency of conversion. The thermogravimetric curves of PLA recyclates showed a similar mass-loss profile. A thorough analysis of their suitability in terms of evolved gases, thermal stability and decomposition kinetics is given hereafter in order to consider if the same operating conditions for VPLA could be assimilated for RPLA-i.

3.1. Evolved Gases Analysis

The FT-IR analysis of the evolved gases from the thermal decomposition of PLA showed that the main detected species were lactide, acetaldehyde, carbon monoxide and, in traces, carbon dioxide, water, and acetic acid. The vibration and wavenumbers of the corresponding functional groups are gathered in Table 1. It is known that the thermolysis of PLA occurs through a predominant pathway in which intramolecular hydroxyl end-initiated transesterifications of PLA mainly give rise to the formation of cyclic oligomers of lactic acid and lactide. Simultaneously, β-elimination, recombination of cyclic oligomers with linear polyesters through insertion reactions, hydrolytic reactions, or other radical degradation reactions may occur, giving rise to the release of the aforementioned gaseous species (Mc Neill and Leiper, 1985;Kopinke and Mackenzie, 1997). Accordingly, different mechanisms might take place in the formation of each compound: acetaldehyde might have been formed by homolytic reactions, along with CO, whereas lactide might have been formed by transesterification and/or by chain homolysis of PLA.

In order to offer deeper information, 2D-correlation spectroscopy (hereafter 2D-IR) was applied. Basically, in 2D-IR, a spectrum is obtained as a function of two independent IR wavenumbers υ_1 and υ_2, due to the application of an external perturbation, such as temperature. These measurements provide information that cannot be drawn from conventional one-dimensional IR spectra (Noda, 1990). The synchronous spectra $\varphi(\upsilon_1,\upsilon_2)$ reflect the correlation of simultaneously variation of spectral intensity, whereas on the other hand the asynchronous spectra $\psi(\upsilon_1,\upsilon_2)$ reflect the non-comparability of spectral intensity variations, being both signals out-of-phase. The discussion of both types of graphs is given in terms of auto and cross-peaks. The auto-peaks (υ_1,υ_1), (υ_2,υ_2) in synchronous spectra rely on a diagonal line and their intensities reflect the influence of the external perturbation on the molecular groups of wavenumbers υ_1 and υ_2. The asynchronous spectrum has not auto-peaks by definition. The cross-peaks (υ_1,υ_2), (υ_2,υ_1) are located off-diagonal, and represent the synchronicity of groups corresponding to wavenumbers υ_1 and υ_2, highlighting the strong cooperation or interaction between their different molecular groups. A positive cross-peak thus describes the increase or decrease of the intensities of both υ_1 and υ_2, while a negative cross-peak indicates an increase in the intensity of υ_1 during a decrease of υ_2, or vice versa. The cross-peaks in this case represent the

Table 1
IR absorption bands of evolved gases from thermal decomposition of PLA.

Compound	Wavenumber (cm^{-1})	Vibrations[a]
Acetaldehyde	3475	2 X υ(C=O)
	2968	$\upsilon(CH_3)$
	2740	υ(CHO)
	1762	υ(C=O)
	1414 + 1371	$\delta(CH_3)$
	1127	υ(C–O)
Lactide	3008	$\upsilon(CH_3)$
	2952	$\upsilon_{as}(CH_3)$
	2893	$\upsilon_{s}(CH_3)$
	1795	υ(C=O)
	1365	$\delta(CH_3)$
	1248 + 1108	υ(C–O–C)
Short-chain acids + their dimers and trimers	3589	υ(H–O)
	2952	$\upsilon(CH_2)$
	2816	υ(CH)
	1778	υ(C=O)
	1164 + 1107	υ(C–O)
CO_2	2349	υ_{as}(O=C=O)
CO	2174 + 2116	υ(C≡O)
H_2O	3900–3400 + 1800–1300	υ(H–O) + δ(H–O)

υ, stretching; δ, in-plane bending; s, symmetric; as, asymmetric.
[a] Notation on vibrations.

sequential changes of the spectral intensities υ_1 and υ_2 due to the asynchrony of the variations in their intensities. This characteristic is also very useful for distinguishing between overlapped bands that arise from different spectral variations.

The rules for determination of the sequence of spectral intensity changes are determined according to the sign of the peaks at the synchronous spectrum, which can be positive ($\varphi(\upsilon_1,\upsilon_2) > 0$), or negative ($\varphi(\upsilon_1,\upsilon_2) < 0$).

If the sign in the synchronous spectrum is positive ($\varphi(\upsilon_1,\upsilon_2) > 0$), a positive cross-peak in the asynchronous spectrum ($\psi(\upsilon_1,\upsilon_2) > 0$) states that the change in intensity of υ_1 occurs before the change in υ_2, whereas a negative cross-peak in the asynchronous spectrum ($\psi(\upsilon_1,\upsilon_2) < 0$) states that the change in intensity of υ_2 occurs before the change in υ_1.

If the sign in the synchronous spectrum is negative ($\varphi(\upsilon_1,\upsilon_2) < 0$), the abovementioned rules are reversed.

Fig. 1 shows the synchronous and asynchronous spectra at different infrared regions, for the study of the thermal decomposition of VPLA. Note that negative cross-peaks are grey-shadowed. In the 2400–1600 cm^{-1} region, the synchronous spectrum shows (Fig. 1a) a wide positive auto-peak corresponding to the υ(C=O) region, which reflects the strong influence of the temperature on this spectral vibration. In the 1600–800 cm^{-1} region (Fig. 1c), two positive auto-peaks (1371,1371), (1127,1127) for acetaldehyde and a positive auto-peak (1248,1248) for lactide were detected. The asynchronous spectra (Fig. 1b, d, e) completed the information, taking into account positive and negative cross-peaks. Lactide evolved before acetaldehyde, as can be guessed from fthe positive cross-peaks at (1248,1127)-Fig. 1d and (1795,1762)-Fig. 1e, and negative cross-peaks at (1414,1248)-Fig. 1d and (1376,1248)-Fig. 1d. Carbon dioxide traces evolved before acetaldehyde and lactide, as drawn from positive cross-peaks at (2349,1795)-Fig. 1b, and (2349,1762)-Fig. 1b. Carbon monoxide evolved before lactide, as shown by the negative cross-peak at (2116,1795)-Fig. 1b. Summing up, the emission profile followed the sequence: CO, CO_2, lactide, acetaldehyde, due to different mechanisms, as introduced above.

After reprocessing, the gas emission profile gave similar IR spectra. Since the chemical nature of polylactide was essentially the same (Badia et al., 2011b) when it comes to the evolved gases, no differences were likely to be found. The necessary facilities for controlling the emission of evolved gases from reprocessed PLAs could thus be the same than those needed for VPLA, which may reduce costs of investing and implementation in new technologies.

3.2. Studies on the thermal stability

In order to assess the thermal stability of PLA and its further recyclates, the corresponding decomposition onset T_0 and endset T_e temperatures were initially obtained by a tangential intercept method onto the thermogravimetric curves *TG* for the whole process. Likewise, the temperature at the maximum decomposition rate, i.e. the peak temperature T_p of the differential thermogravimetric curve *DTG*, which is related to the inflection temperature of the *TG* curve, was also considered. Technologists may be interested in finding the relationship between the influence of the heating rate β and the characteristic decomposition temperatures (T_0,T_e,T_p) to model the thermal stability behavior of bio-based plastics in thermo-chemical processes. Despite other authors have proposed linear relationships to describe the evolution of the thermogravimetric characteristic temperatures with β (Liu et al., 2003), Fig. 2a clearly shows for VPLA that, when considering lower β, the linear assumption may not be operative. Therefore, other models must be used in order to functionalize this evolution under any β. The exponential relationship shown in Eq. (1), named thermal decomposition behavior (*TDB*), where *a*, *b* and *k* are parameters of the fitting, was proposed and successfully applied for this purpose[1].

$$TDB(\beta) = a \cdot (1 + b \cdot \exp(-k \cdot \beta))^{-1} \quad (1)$$

In order to evaluate the influence of multiple reprocessing on PLA's thermal stability in terms of its characteristic temperatures, instead of choosing the experimental temperatures (T_0, T_e, *or* T_p) obtained at one specific β, which can be locally affected by both experimental errors and misleading calculation assumptions (i.e. the tangent slope is strongly dependent on the points chosen for drawing), the so-called Zero-Decomposition Temperatures *ZDT*, those are, the values obtained when the heating rate tends to zero ($TDB(\beta \to 0)$) were proposed, due to the fitting of *TDB* smoothens the possible variations in local temperatures. Fig. 2b shows the evolution of the Zero-Decomposition Temperatures along the reprocessing cycles, for onset (ZDT_0), peak (ZDT_p) and endset (ZDT_e). As well, the evolution of ΔZDT (ZDT_e–ZDT_0) is also depicted.

ZDT_0 showed a ~10 °C increase up to the third recyclate, whereas ZDT_p and ZDT_e showed a small decrease. Afterwards, all *ZDTs* followed the same steady trend, slightly decreasing the ΔZDT, as a consequence of the diminution of thermal stability. These results are in agreement to the conclusions given in a previous study (Badia et al., 2011b) in which a significant increase of methoxyl-terminated linear species was found, specially up to the third recyclate, accompanied by a decrease of initially predominant cyclic species, as well as a diminution of hydroxyl/carboxyl terminated linear species. Despite the chemical nature of polylactide did not essentially change, these variations in the oligomeric distribution affected to the heterogeneity of the material, weakening its polymeric structure. Thus the increase of ZDT_0 may be assigned to the disappearance of cyclic structures, which possess latent ring tension and need less temperature to depolymerize than the new methoxyl-terminated linear species. When operating the pyrolysis of reprocessed PLA, higher initial decomposition temperatures should then be used.

The changes in thermal stability of virgin and reprocessed PLA were governed by modifications in their thermal decomposition

[1] See results of fitting in the supplementary material.

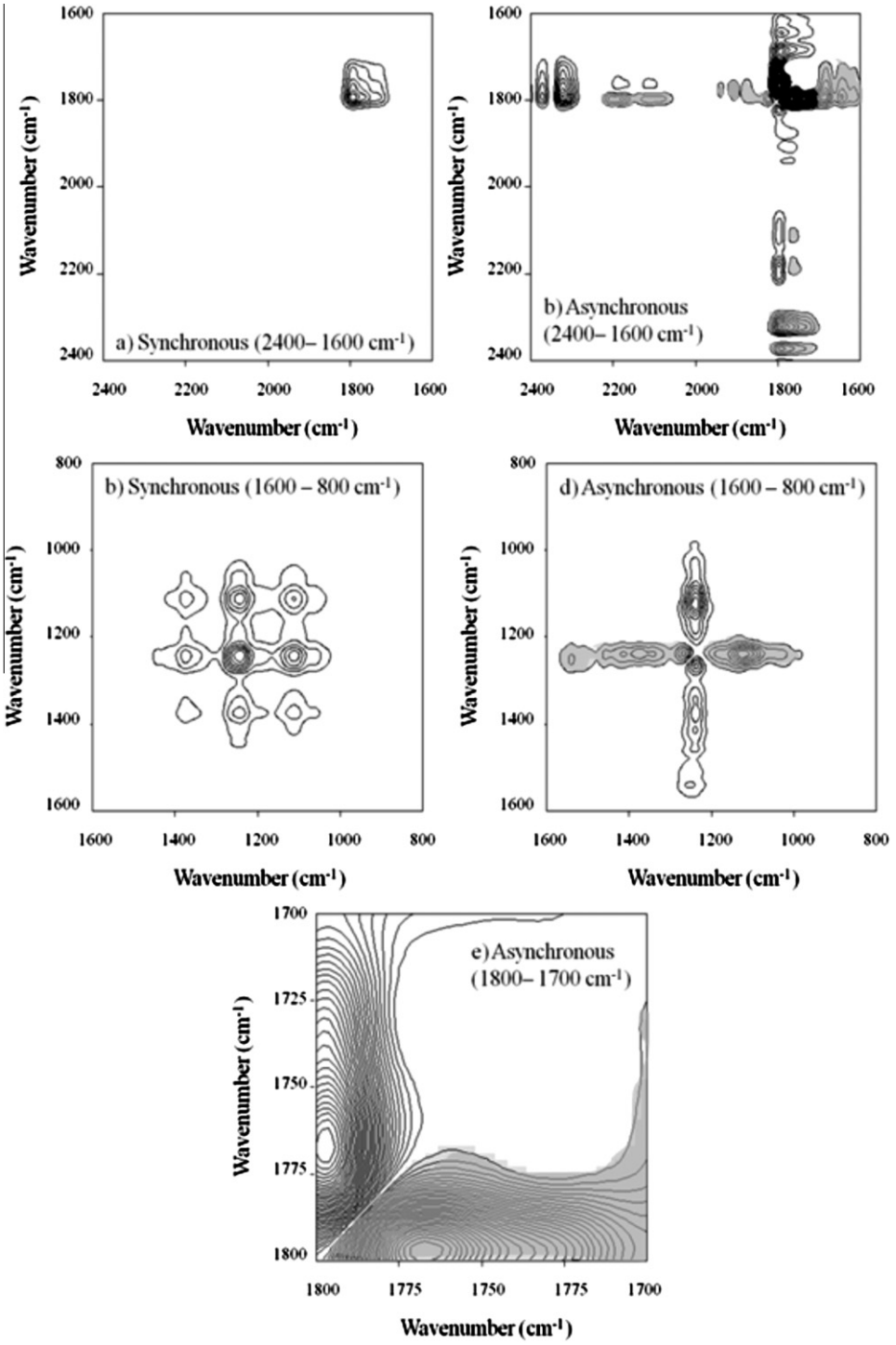

Fig. 1. 2D correlation spectra of VPLA under inert conditions at different wavenumber ranges. Negative cross-points are grey-shadowed.

behavior. Subsequent analysis was therefore needed to establish a suitable methodology to model their pyrolysis for full-scale energetic valorization facilities.

3.3. Assessment of the thermal decomposition kinetics

The thermo-chemical transformation of solid raw materials to diverse gaseous products is highly dependent on the kinetic rates of the pyrolytic reactions, and thus accurate kinetic models are needed to design the pyrolysis process in the best conditions. Macroscopic solid-state kinetics is complex, since it might give information about multiple steps taking place simultaneously. In the attempt to develop a model for plastic thermal behavior in full-scale systems, the main purpose is to describe the thermal decomposition in terms of an intrinsic kinetics, without taking into account the rigorous chemistry of decomposition, thus describing the process by means of a simplified reaction pathway, representative of a complex network of reactions. Literature indicates that different researchers use different kinetic models and diverse kinetic methodologies to perform their studies. This fact often provokes confusion concerning which model is more suitable and therefore should be used to best represent the system under study.

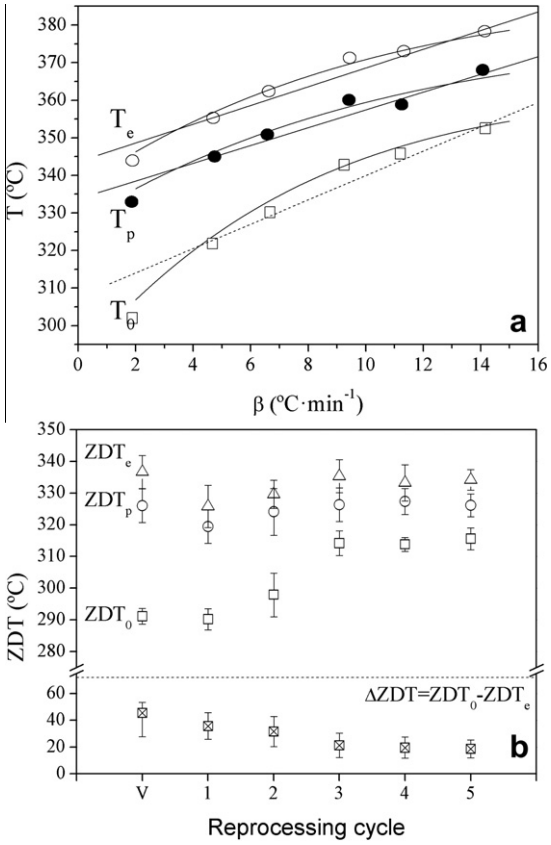

Fig. 2. Thermal stability results. (a) Fittings applied to the evolution of the characteristic TGA temperatures for VPLA (dashed line: linear regression; solid line: regression applied according to *TDB*. (b) Evolution of zero-decomposition temperatures along the reprocessing cycles.

With the aim of shedding light on this matter, a detailed methodology is presented in this work.

3.3.1. Description of the kinetic triplet

The intrinsic kinetics of solid-state decompositions are usually described by three parameters: activation energy (Ea), pre-exponential factor (A/lnA) and kinetic function ($f(\alpha)$), conforming the so-called kinetic triplet. These kinetic functions mathematically express different physical kinetic models. The relationship between the theoretical decomposition mechanisms and their mathematical models can be found in literature (Khawan and Flanagan, 2006). These reaction models may adopt various expressions, based on nucleation and nuclei growth, phase boundary reactions, diffusion or order reactions[2]. The kinetic analysis of non-isothermal processes is generally performed by using a single step kinetic equation:

$$\frac{d\alpha}{dt} \equiv \beta \cdot \frac{d\alpha}{dt} = A \cdot f(\alpha) \cdot k(T) = A \cdot f(\alpha) \cdot e^{-\frac{Ea}{RT}}, \tag{2}$$

where t is the time (s), T is the temperature (K), α is the conversion degree and R is the ideal gas constant (8.31 J mol^{-1} K^{-1}). For thermogravimetric experiments, $\alpha = (m_0 - m_t)/(m_0 - m_\infty)$, where m stands for mass (g), and subscripts 0, ∞ and t respond to initial, final and actual mass values. The integration of Eq. (2), after rearranging, leads to:

$$g(\alpha) = \int_0^\alpha \frac{d\alpha}{f(\alpha)} = \frac{A \cdot Ea}{\beta \cdot R} \cdot \int_0^\infty \frac{e^{-x}}{x^2} = \frac{A \cdot Ea}{R \cdot T} \cdot p(x), \quad x = \frac{Ea}{R \cdot T}, \tag{3}$$

[2] See the expressions of the different kinetic models in the supplementary material.

where $g(\alpha)$ is the inverse integral kinetic function. Under linear heating rate program, Eq. (3) has not an exact analytical solution to the temperature integral $p(x)$ and therefore a vast number of publications have performed approximated equations to approach the best values within the lowest error margin (Pérez-Maqueda et al., 2005). In this work, the Senum-Yang approximation shown at Eq. (4) truncated at its fifth term was used, since it gives deviations lower than 10^{-8}% from the exact value of the temperature integral for $x > 10$ (Pérez-Maqueda and Criado, 2000), which permits its application in solid-state decomposition reactions, where x is usually higher.

$$p(x) = \frac{e^{-x}}{x^2} \cdot \sum_n \frac{n \cdot (1-n)}{x + 2 \cdot (n+1)} \tag{4}$$

3.3.2. Assessment of the activation energy

The first step in the study of decomposition kinetics is the assessment of the evolution of the apparent activation energy (Ea_α). It should be noted that solid-state kinetics adopted the theory for reaction kinetics in homogeneous systems (i.e. gases and liquids), and it is generally assumed that the Ea_α and the pre-exponential factor (A) remain constant. However, it has been proved that these kinetic parameters may vary with the progress of the decomposition. This variation can be detected by isoconversional methods, which use data from different multi-linear non-isothermal experiments and do not take modelistic assumptions for the analysis, main source of error of simpler model-fitting methods. The most broadly used isoconversional methods are those integral linear methods developed by Flynn–Wall–Ozawa (*FWO*) (Flynn and Wall, 1966; Ozawa, 1970) (supported on Doyle's integral approximation (Doyle, 1965) and Kissinger–Akahira–Sunose (*KAS*) (Kissinger, 1957; Akahira and Sunose,1971), which are represented at Eqs. (5) and (6), respectively. These methods give rise to linear functions from which slopes the Ea_α at a fixed decomposition degree α are obtained.

$$[\log(\beta)]_y = \log\left(\frac{A_\alpha \cdot Ea_\alpha}{R \cdot g(\alpha)}\right) - 2.315 - \frac{0.457 \cdot Ea_\alpha}{R} \cdot \left[\frac{1}{T_\alpha}\right]_\infty \tag{5}$$

$$\left[\ln\left(\frac{\beta}{T^2}\right)\right]_y = \ln\left(\frac{A_\alpha \cdot R}{Ea_\alpha \cdot g(\alpha)}\right) - \frac{Ea_\alpha}{R} \cdot \left[\frac{1}{T_\alpha}\right]_x \tag{6}$$

The results were compared to those obtained by the non-linear Advanced Isoconversional method (*AIC*) (Vyazovkin, 1997), in order to test the consistency of the results. This method, which accounts for variable β and systematic errors in the Ea_α, is given at Eq. (7)

$$\Omega = \left|\sum_{i=1}^{h} \sum_{j \neq i}^{h} \frac{J(Ea_\alpha, T_i(t_\alpha))}{J(Ea_\alpha, T_j(t_\alpha))}\right|. \quad J(Ea_\alpha, T(t)) = \int_{t\alpha-\Delta\alpha}^{t_\alpha} e^{-\frac{Ea_\alpha}{RT(t)}} \cdot dt, \tag{7}$$

where i and j are counters through the h experiments performed at β,$T(t) = T_0 + \beta \cdot t$, where T_0 is the initial temperature, and $\Delta\alpha = (m^{-1})$, with $m = 40$, the number of α segments chosen for integration. The integral $J(Ea_\alpha, T(t))$ was numerically evaluated by the Simpson 1/3 method. The Ea_α was the value that minimized Ω at Eq. (7) for a particular α. This method required the tool Solver of MS Excel software, by applying the Newton method with progressive derivatives, setting an accuracy of 10^{-6} and a tolerance of 10^{-4}. Kinetic analyses were carried out in the conversion degree α range from 0,1 to 0,8 since the main reaction took place in this region. In order to check the suitability of using a constant value for the activation energy, the averages of those obtained by *FWO*, *KAS* and *AIC* methods are gathered at Table 2. The average values (Ea_{av}) lay within coincident values among all methods, with low dispersion values. Therefore, it was assumed that the average isoconversional energy (Ea_{iso} = aver-

age of Ea_{av}, given in Table 3) may be used as constant, i.e. $Ea_{\alpha} \sim Ea_{iso}$, throughout the decomposition process for the following calculations.

The Ea_{iso} of virgin PLA gave out a value of 152 kJ·mol^{-1}, which was comparable to the values reported in different studies for PLA grades in the same order of molecular weight (Li et al., 2009; Zhou and Xanthos,2009). After the first reprocessing step, a sharp 26.5% increase was registered up to 207 kJ·mol^{-1}, keeping this order of value within a 5% margin along the successive recyclates. In accordance to the results found for the thermal stability, this change can be related to the presence of more linear methoxyl- terminated species in the oligomeric distribution of PLA recyclates, to a detriment of mainly predominant cyclic species in virgin PLA (Badia et al., 2011b), which may vary the principal thermal decomposition mechanisms.

3.3.3. The use of master-plots for determining the kinetic model

To achieve the mathematical decomposition model will help design the proper pyrolysis systems, regardless the specific decomposition pathway. Thus, the kinetic function $f(\alpha)$ was approached for virgin and reprocessed PLA by the use of reduced Master-Plots (MP) which are reference theoretical curves dependent on the kinetic model, but generally independent of the kinetic parameters of the process. The comparison of the experimental with the theoretical master curves, i.e. $MP_e \equiv MP_t$, allows for the selection of the appropriate kinetic model of the process under investigation or, at least, reducing the span of suitable kinetic models (Gotor et al., 2000). There exist three main types of MP_t, those based on the differential form (MP_f) of the generalized kinetic equation, Eq. (2); those based on the integral form (MP_g), according to Eq. (3); and the most common one that combines both differential and integral forms (MP_{fg}), that are usually reduced at $\alpha = 0.5$ for better visualization. The mathematical description of each curve can be found elsewhere (Gotor et al., 2000). They are described after the introduction of the so-called generalized time θ, which denotes the reaction time taken at a particular conversion degree α at infinite temperature, defined as:

$$\theta = \int_0^t e^{-\frac{Ea}{RT}} \cdot dt, \tag{8}$$

which differentiation in combination with Eq. (2), one obtains:

$$\frac{d\alpha}{d\theta} = A \cdot f(\alpha) = \frac{d\alpha}{dt} \cdot e^{\frac{Ea}{RT}} \tag{9}$$

Therefore, assuming A and Ea constant, due to interdependence of kinetic parameters, and using a reference point at $\alpha = 0.5$, the theoretical MP_f and MP_g and the expression for their corresponding reduced form of the experimental data can be drawn from the following expressions:

$$\frac{\frac{d\alpha}{d\theta}}{\frac{d\alpha}{d\theta}|_{0.5}} = \frac{f(\alpha)}{f(0.5)} = MP_t \equiv MP_e = \frac{\frac{d\alpha}{dt} \cdot e^{x}}{\frac{d\alpha}{dt}|_{0.5} \cdot e^{x_{0.5}}} \tag{10}$$

$$\frac{\theta}{\theta_{0.5}} = \frac{g(\alpha)}{g(0.5)} = MP_t \equiv MP_e = \frac{p(x)}{p(x_{0.5})} \tag{11}$$

The advantage of using MP_f and MP_g is that the former clearly disperse among different $f(\alpha)$ in the range $\alpha < 0.5$ while the latter disperse for $\alpha > 0.5$ and therefore permits a straightforward identification. Contrarily, the use of the common MP_{fg} tends to produce confusion due to the coincidence of different kinetic models under the same line. In order to select the best kinetic model, the condition of minimization of Φ in Eq. (12) was applied, taking into account experiments performed at all heating rates:

Table 2
Ea averages (Ea_{av}) of the thermal decompositions obtained by the isoconversional methods (FWO: Flynn–Wall–Ozawa, KAS: Kissinger–Akahira–Sunose, AIC: Advanced Iso-Conversional).

Material	Isoconversional methods					
	FWO		KAS		AIC	
	Ea_{av}(kJ mol^{-1})	e (%)	Ea_{av} (kJ mol^{-1})	e (%)	Ea_{av} (kJ mol^{-1})	e (%)
VPLA	153	6.3	151	6.9	152	7.1
RPLA-1	208	1.2	208	1.3	205	1.9
RPLA-2	202	2.9	202	3.1	198	6.0
RPLA-3	219	6.1	220	6.3	213	6.7
RPLA-4	205	4.7	207	4.9	202	5.8
RPLA-5	216	1.1	216	1.2	205	2.1

Table 3
Simplified kinetic triplet for virgin PLA and its subsequent recyclates.

Material	Kinetic triplet					
	Model		Activation energy		Pre-exponential factor	
	Function	n	Ea_{iso} (kJ mol^{-1})	e (%)	lnA (s^{-1})	e (%)
VPLA	A_n	1.611	153	6.1	24.4	5.2
RPLA-1		1.354	207	2.5	34.7	2.7
RPLA-2		1.510	201	4.3	32.6	4.1
RPLA-3		1.231	217	1.5	40.1	6.1
RPLA-4		1.529	204	6.0	33.7	5.6
RPLA-5		1.346	212	3.9	35.7	4.1

$$\phi(f_t, g_t, \alpha) = \sum_{\beta} \left(\sum_{\alpha=0}^{0.5} [MPf_t(\alpha) - MPf_e(\alpha)]^2 + \sum_{\alpha=0.5}^{1} [MPg_t(\alpha) - MPg_e(\alpha)]^2 \right); \quad \Delta\alpha = 0.025; \quad \forall f_t, g_t, \tag{12}$$

where MPf_t and MPg_t are the theoretical differential and integral forms of the kinetic models and MPf_e and MPg_e the experimental form of the reduced curves given by the right-hand part of Eqs. (10) and (11), respectively. Fig. 3 shows as an example the comparison of the experimental master curves of RPLA-2 at $\beta = 5$ °C min^{-1} with the differential (Fig. 3a) and integral (Fig. 3b) abaci. Similar plots were obtained for the rest of characterized materials. Results conclude that virgin PLA and its recyclates followed an A_n kinetic model, ascribed to a model of growth of previously formed nuclei, with n close to 1.5. This kind of kinetic model is quite common in crystallization processes, though scarcely reported in studies dealing with thermal decomposition processes of polymers, as discussed elsewhere (Badia et al., 2010), where the controversy of the relationship between the mathematical models and the physical mechanisms was addressed. The model A_n indicates the presence of active zones more chemically liable to thermal decomposition, which activate the formation and growth of gas bubbles in the polymer melt.

3.3.4. Determination of the pre-exponential factor

In order to complete the kinetic triplet and thus obtain a full mathematical description of the kinetics of pyrolysis, the pre-exponential factor A had to be found, along with the n of the kinetic model. Taking into account that a suitable kinetic triplet should fulfill the *Perez-Maqueda* et al. criterion (Pérez-Maqueda et al.,2002); that is, the independence of the activation parameters *Ea*. *A* on the heating rate β, the minimization of ξ in Eq. (13) provided the best n for the model, and thereafter endowed with the most accurate A, by averaging the A_β obtained from the intercept

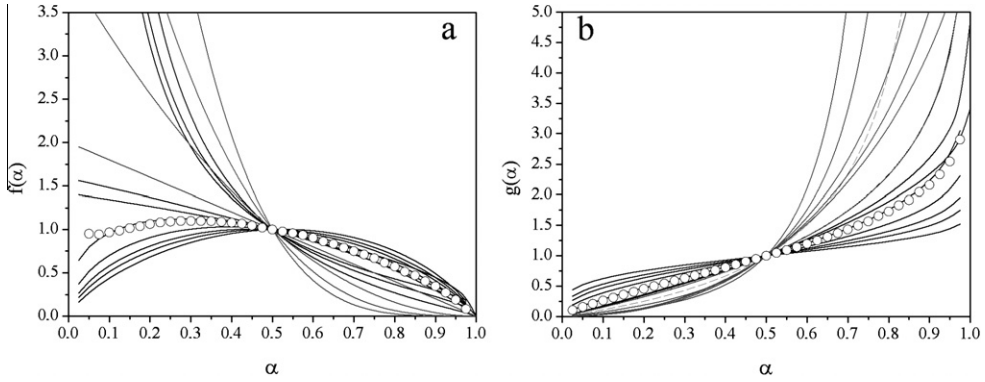

Fig. 3. Master plots based on the differential (a) and integral (b) forms of the general kinetic law compared to experimental data obtained for thermal decomposition of RPLA-2 (hollow circles). (Black solid lines: nucleation; grey solid lines: n-order; dashed grey lines: diffusion, pointed black lines: reaction.)

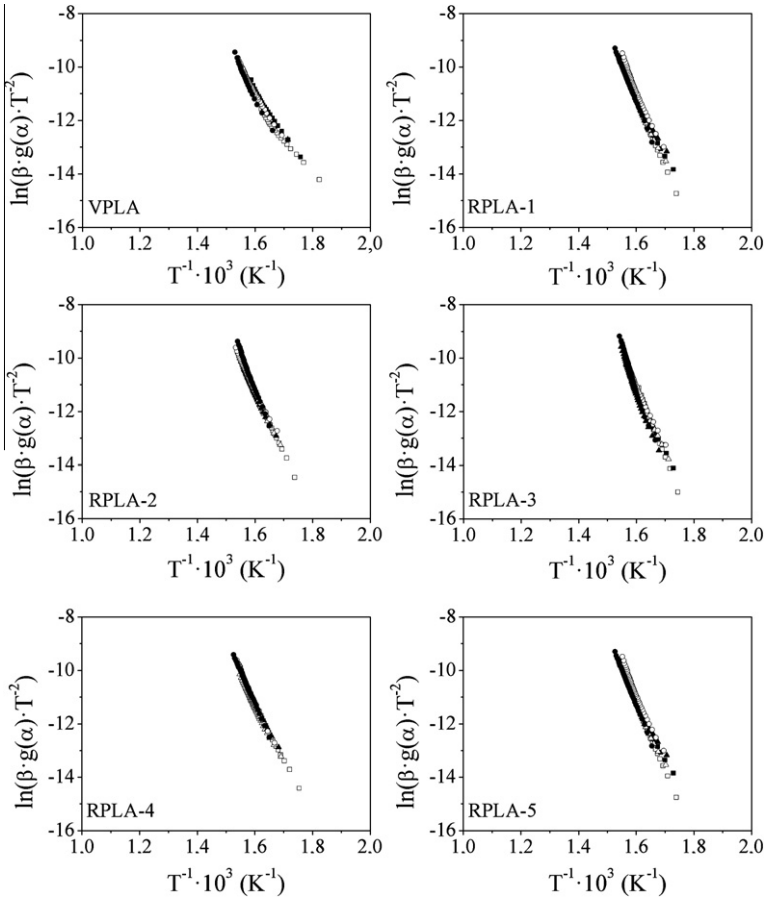

Fig. 4. Application of *Perez-Maqueda* et al. criterion to virgin PLA and subsequent recyclates. Symbols correspond to experiments at different heating rates (°C min^{-1}): □-2, ■-5, Δ-7, ▲-10, ○-12, ●-15.

at $y = 0$ of Coats–Redfern (Coats and Redfern 1964) equation (Eq. (14)) at each experiment with different heating rates β:

$$\xi(n,\alpha) = \sum_{i}^{h} \left| (-R)\cdot \frac{d}{dt}\left(\frac{\ln\left(\beta_i \cdot T^{-2}(-\ln(1-\alpha))^{\frac{1}{n}}\right)}{T^{-1}} \right) - Ea_{iso} \right| \quad (13)$$

$$\ln\left[\frac{\beta\cdot(-\ln(1-\alpha))^{\frac{1}{n}}}{T^2}\right]_y = \ln\frac{A\cdot\beta}{Ea_\beta} + \frac{Ea_\beta}{R}\cdot\left[\frac{1}{T}\right]_x \quad (14)$$

Table 3 shows the results obtained by this methodology completing the kinetic triplet of the thermal decomposition of virgin and reprocessed PLA. Fig. 4 shows the fulfillment of the *Perez-Maqueda criterion* by virgin and all subsequent reprocessed materials as a proof of the goodness of the fitting procedure. It is important to notice that technologist may use the same experimental settings for the pyrolysis of PLA to the rest of its recyclates, by only smoothly adjusting three parameters, since the thermal behavior of the materials was essentially the same after recycling.

4. Conclusions

A complete methodology in terms of gas control, thermal stability and decomposition kinetics, was thoroughly applied.

The gas control facilities could be transferable to reprocessed PLA.

A new model (*TDB*) and novel parameters (*ZDT*) to test the thermal stability of the materials was useful.

An increase in the trigger of the thermal decomposition as well as in the average activation energy indicated was found up to the third recyclate.

Similar experimental settings for the pyrolysis of virgin PLA could be applied for the valorization of reprocessed PLA with minimum corrections in the initial decomposition stages.

Acknowledgements

The authors would like to acknowledge the Spanish Ministry of Science and Innovation for the financial support through the Research Projects ENE2007-67584-C03, UPOVCE-3E-013, ENE2011-28735-C02-01, IT-2009-0074, as well as for the pre-doctoral research position for L. Santonja-Blasco through the FPI program. The Spanish Ministry for Education is acknowledged for the concession of a pre-doctoral research position to J.D. Badia and A. Martinez-Felipe by means of the FPU program. The authors thank the financial support of the Generalitat Valenciana through the ACOMP/2011/189, the Grisolia research position for A. Martínez-Felipe, and for the Forteza technician position for J.D. Badia. Universitat Politècnica de València (UPV, Spain) is thanked for additional support through the PAID 05-09-4331 and PAID 06-11-2037 projects. AIMPLAS is acknowledged for providing and processing the material. This paper is warmly dedicated to Gael Badia-Ombuena, in commemoration of his birth.

Appendix A. Supplementary data

Supplementary data associated with this article can be found, in the online version, at doi:10.1016/j.biortech.2012.02.013.

References

Akahira, T., Sunose, T., 1971. Res. Rep. Chiba Inst. Technol 16, 22–31.
Al-Salem, S.M., Lettieri, P., Baeyens, J., 2009. Recycling and recovery routes of plastic solid waste (PSW): a review. Waste management 29, 2625–2643.
Badia, J.D., Vilaplana, F., Karlsson, S., Ribes-Greus, A., 2009. Thermal analysis as a quality tool for assessing the influence of thermo-mechanical degradation on recycled poly(ethylene terephthalate). Polymer Testing 28, 169–175.
Badia, J.D., Santonja-Blasco, L., Moriana, R., Ribes-Greus, A., 2010. Thermal analysis applied to the characterization of degradation in soil of polylactide: II. On the thermal stability and thermal decomposition kinetics. Polymer Degradation and Stability 95, 2192–2199.
Badia, J.D., Strömberg, E., Ribes-Greus, A., Karlsson, S., 2011a. A statistical design of experiments for optimizing the MALDI-TOF-MS sample preparation of polymers. An application in the assessment of the thermo-mechanical degradation mechanisms of poly (ethylene terephthalate). Analytica Chimica Acta 692, 85–95.
Badia, J.D., Strömberg, E., Ribes-Greus, A., Karlsson, S., 2011b. Assessing the MALDI-TOF MS sample preparation procedure to analyze the influence of thermo-oxidative ageing and thermo-mechanical degradation on poly (lactide). European Polymer Journal 47, 1416–1428.
Badia, J.D., Strömberg, E., Karlsson, S., Ribes-Greus, A., 2012. Material valorisation of amorphous polylactide. Influence of thermo-mechanical degradation on the morphology, segmental dynamics, thermal and mechanical performance. Polymer Degradation and Stability 97, 670–678.
Barneto, A.G., Carmona, J.A., Alfonso, J.E.M., Serrano, R.S., 2010. Simulation of the thermogravimetry analysis of three non-wood pulps. Bioresource Technology 101, 3220–3229.
Carrasco, F., Pagès, P., Gámez-Pérez, J., Santana, O.O., Maspoch, M.L., 2010. Kinetics of the thermal decomposition of processed poly(lactic acid). Polymer Degradation and Stability 95, 2508–2514.
Coats, A.W., Redfern, J.P., 1964. Kinetic analysis from thermogravimetric data. Nature 68, 4914.
Doyle, C.D., 1965. Series approximations to the equation of thermogravimetric data. Nature 207, 209.
Flynn, J.H., Wall, L.A., 1966. A quick, direct method for the determination of activation energy from thermogravimetric data. Journal of Polymer Science 4, 323–342.
Gotor, F.J., Criado, J.M., Malek, J., Koga, K., 2000. Kinetic analysis of solid-state reactions: the universality of Master Plots for analyzing isothermal and non-isothermal experiments. Journal of Physical Chemistry A 104, 10777–10782.
Gupta, A.P., Kumar, V., 2007. New emerging trends in synthetic biodegradable polymers – Polylactide: a critique. European Polymer Journal 43, 4053–4074.
Khawan, A., Flanagan, D.R., 2006. Solid-state kinetic models: basics and mathematical fundamentals. Journal of Physical Chemistry B 110, 17315–17328.
Kissinger, H.E., 1957. Reaction kinetics in differential thermal analysis. Analytical Chemistry 29, 1702–1706.
Kopinke, F.D., Mackenzie, K., 1997. Mechanistic aspects of the thermal degradation of poly(lactic acid) and poly(beta-hydroxybutyric acid). Journal of Analytical and applied Pyrolysis 41, 43–53.
Li, J., Zheng, W., Li, L., Zheng, Y., Lou, X., 2009. Thermal degradation kinetics of g-HA/PLA composite. Thermochimica Acta 493, 90–95.
Liu, B., Zhao, X., Wang, X., Wang, F., 2003. Thermal degradation kinetics of poly(propylene carbonate) obtained from the copolymerization of carbon dioxide and propylene oxide. Journal of Applied Polymer Science 90, 947–953.
Liu, X., Khor, S., Petinakis, E., Yu, L., Simon, G., Dean, K., Bateman, S., 2010. Effects of hydrophilic fillers on the thermal degradation of poly(lactic acid). Thermochimica Acta 509, 147–151.
Materazzi, S., Vecchio, S., 2010. Evolved gas analysis by infrared spectroscopy. Applied Spectroscopy Reviews 45, 241–273.
Mc Neill, I.C., Leiper, H.A., 1985. Degradation studies of some polyesters and polycarbonates – 2: polylactide: degradation under isothermal conditions, thermal degradation mechanisms and photolysis of the polymer. Polymer Degradation and Stability 11, 309–326.
Morita, S., 2005. 2D Shige (c). – Kwansei-Gakuin University-. 2004–2005.
Noda, I., 1990. Two-dimensional infrared (2D IR) spectroscopy: theory and applications. Applied Spectroscopy 44, 550–561.
Ozawa, T., 1970. Kinetic analysis of derivative curves in thermal analysis. Journal of Thermal Analysis 2, 301.
Pérez-Maqueda, L.A., Criado, J.M., 2000. The accuracy of Senum and Yang's approximations to the Arrhenius Integral. Journal of Thermal Analysis and Calorimetry 60, 909–915.
Pérez-Maqueda, L.A., Criado, J.M., Gotor, F.J., Málek, J., 2002. Advantages of combined kinetic analysis of experimental data obtained under any heating profile. Journal of Physical Chemistry A 106, 2862–2868.
Pérez-Maqueda, L.A., Sánchez-Jiménez, P.E., Criado, J.M., 2005. Kinetic analysis of solid-state reactions: precision of the activation of the activation energy calculated by integral methods. International Journal of Chemical Kinetics 37, 658–666.
Strömberg, E., Karlsson, S., 2009. The design of a test protocol to model the degradation of polyolefins during recycling and service life. Journal of Applied Polymer Science 112, 1835–1844.
Vilaplana, F., Karlsson, S., 2008. Quality concepts for the improved use of recycled polymeric materials: a review. Macromolecular Materials and Engineering 293, 274–297.
Vyazovkin, S., 1997. Advanced isoconversional method. Journal of Thermal Analysis 49, 1493–1499.
Yuzay, I.E., Auras, R., Soto-Valdez, H., Selke, S., 2010. Effects of synthetic and natural zeolites on morphology and thermal degradation of poly(lactic acid) composites. Polymer Degradation and Stability 95, 1769–1777.
Żenkiewicz, M., Richert, J., Rytlewski, P., Moraczewski, K., Stepczyńska, M., Karasiewicz, T., 2009. Characterisation of multi-extruded poly(lactic acid). Polymer Testing 28, 412–418.
Zhou, Q., Xanthos, M., 2009. Nanosize and microsize clay effects on the kinetics of the thermal degradation of polylactides. Polymer Degradation and Stability 94, 327–338.

Polymer Degradation and Stability 95 (2010) 2185–2191

Contents lists available at ScienceDirect

Polymer Degradation and Stability

journal homepage: www.elsevier.com/locate/polydegstab

Thermal analysis applied to the characterization of degradation in soil of polylactide: I. Calorimetric and viscoelastic analyses

L. Santonja-Blasco, Rosana Moriana, J.D. Badía, A. Ribes-Greus*

Instituto de Investigación en Tecnología de Materiales, Universidad Politécnica de Valencia, Camino de Vera s/n 46071 Valencia, Spain

ARTICLE INFO

Article history:
Received 30 November 2009
Received in revised form
26 July 2010
Accepted 6 August 2010
Available online 14 August 2010

Keywords:
Polylactide (PLA)
Degradation in soil
Differential Scanning Calorimetry (DSC)
Dynamic-Mechanical-Thermal Analysis (DMTA)
Free volume
Lamellar thickness distribution

ABSTRACT

An accelerated soil burial test has been performed on a commercial polylactide (PLA) for simulating non-controlled disposal. Degradation in soil promotes physical and chemical changes in polylactide properties, which can be characterized by Thermal Analysis techniques. Physical changes occurred in polylactide due to the degradation in soil were evaluated by correlating their calorimetric and viscoelastic properties. It is highly remarkable that each calorimetric scan offers specific and enlightening information. Degradation in soil affects the polylactide chains reorganization. A multimodal melting behavior is observed for buried PLA, degradation in soil also promotes the enlarging the lamellar thickness distribution of the population with bigger average size. Morphological changes due to degradation in soil lead to an increase in the free volume of the polylactide chains in the amorphous phase that highly affected the bulk properties. Thermal Analysis techniques provide reliable indicators of the degradation stage of polylactide induced by degradation in soil, as corroborated by molecular weight analysis.

1. Introduction

Polylactide (PLA) is an aliphatic, biodegradable, and compostable polyester which can be easily processed with standard equipment to yield articles that can be used in many applications such as in industrial packaging, in the building area, in medical, agriculture and textile field, etc [1–3]. Initially, polylactide products were produced for biomedical purposes and thus their hydrolysis processes captured the whole research attention [4,5]. Studies performed in neutral media such as phosphate-buffered solution, in vivo solution and water, have been extensively analyzed in order to determine the hydrolytic degradation mechanism [6–10]. Nowadays PLA stands out as a reliable alternative to commodities in packaging applications. This solution will therefore imply an increase of a new source of plastic waste. Hence, to correctly manage the PLA disposal, its biodegradability performance has been studied in several environmental conditions, such as composting, microbiological cultures, biological degradation and disposal in soil [11–14].

Extensive work has been performed by several researchers for understanding the degradation in soil of polymers. Former PLA biodegradation studies stated that hydrolytic reactions seem to act in the initial stage of the overall PLA biodegradation, proceeding by chain-end scission in the PLA matrix, which eases the successive biotic assimilation [11,15–17]. A biotic environment implies chain scissions and the physical and chemical properties of the polymer can be severely modified. Thus, the common characterization is mainly carried out by means of the measurement of the molecular weight or the weight loss changes. Ho et al. found that about 20% of a PLA film was mineralised to CO_2 after 182 days in a laboratory respirometer charged with soil at 28 °C [18]. Calmon et al. found that PLA films had weight losses varying from 0 to 100% after burial in soil for 24 months depending on PLA type and location [19]; in contrast Urayama et al. only found a decrease of a 20% in molecular weight of PLA (100% L) plates after 20 months in soil [14]. In addition, it has been suggested that traditional techniques as the measurement of the weight loss changes for studying polymer biodegradation have some limitations especially after 3 months, because of the adhesion of soil and fungi to the polymer, which can mask real results and thus induce misleading information [14,20,21]. Fast, cost-effective and reliable characterization procedures for testing the biodegradation effects on polymers should be developed and implemented. Thermal Analysis techniques have been successfully applied in our research group to monitor and control the degradation effects on the macroscopic properties of polymers submitted to different degradative environments since

* Corresponding author. Fax: +34963879817.
E-mail address: aribes@ter.upv.es (A. Ribes-Greus).

0141-3910/$ – see front matter © 2010 Elsevier Ltd. All rights reserved.
doi:10.1016/j.polymdegradstab.2010.08.005

they offer a huge amount of parameters that can act as indicators of the extent of degradation [22–26]. Fig. 1 summarizes the Thermal Analysis techniques proposed for the study of the extent of degradation on PLA: Thermogravimetry (TGA), Differential Scanning Calorimetry (DSC) and Dynamic-Mechanical-Thermal Analysis (DMTA), as well as the principal parameters selected for the study. The first paper is focused on the DSC and DMTA study, whereas a forthcoming second paper will report on TGA data.

The aim of this work is to simulate the degradation in the environmental conditions that PLA is subjected during non-controlled disposal. In this set of papers, the physical changes occurred to polylactide properties throughout the degradation in soil process are analyzed by Thermal Analysis, making efforts on establishing new insights in studying the degradation in soil process on polymers. The study is complemented with the analysis of the evolution of the average molecular weight in number and weight by Gel Permeation Chromatography, aiming to test the reliability and consistency of the techniques proposed in the assessment of degradation in soil effects on PLA.

2. Experimental section

2.1. Material and sample preparation

A commercial polylactide (PLA), obtained from renewable resources by ring opening polymerization supplied by Natureworks (Minnetonka, USA) was used in this study. This PLA is a commercial resin with 3.8% meso-lactide and with a number-average molecular weight of 102.230 g/mol, as measured by Gel Permeation Chromatography.

PLA pellets were previously dried with demoisturized air at 80 °C during 4 h. Rectangular plates were prepared by melt compression in a Collin PCS-GA Type Press 800 (GA, USA) at an initial temperature of the hot plates of 195 °C and a final temperature of 60 °C. Five pressure steps were performed as follows starting with an 5 min at 6 bar, 8 min at 75 bar, 8 min at 155 bar, 4 min at 215 bar, and 11 min at 45 bar. Specimens of 145 × 10 × 2 mm were cut from the melt-pressed plates for the degradation in soil tests. Since this work approaches the degradation in soil of non-controlled landfilling of consumer goods, which are obtained by means of, at least, one processing step, "non-buried PLA" has been considered the reference material of the study.

2.2. Accelerated soil burial test

PLA plates were subjected to a controlled degradation in soil test under controlled conditions (temperature, water content and pH), following the ISO 846-1997 International Norm, method D [27]. Samples were buried in biologically active soil and kept in a Heraeus B12 (Hanau, Germany) culture oven at 28 °C. The soil used in these tests was a red soil extract taken from a culture field in Alginet (Valencia). Microbial activity of soil was monitored with cotton along the extension of the experiment. The soil was maintained at approximately pH 7 and a relative humidity of 0.87 g water/g wet soil. To ensure the oxygenation of the soil, a protocol of periodical air oxygen supply was followed. Test specimens were extracted at 30, 150, 300 and 450 days, cleaned and kept in a desiccator during 4 days in order to ensure water desorption before being analyzed.

2.3. Analytic procedures

Samples were thermally characterized by means of Differential Scanning Calorimetry (Mettler Toledo DSC822, Columbus, OH, USA). The calibration of the DSC was previously checked by In and Zn standards. Three calorimetric scans were performed to each sample at a heating/cooling rate of 10 °C/min. Samples of around 4 mg were introduced in a pierced aluminium crucible, with capacity for 40 μL. The first heating scan, in which the thermal history is suppressed, was performed from 0 to 200 °C; the cooling scan went from 200 °C to 0° and the third heating scan from 0 to 200 °C. All experiments were performed under N_2 dry gas as protective gas (50 ml/min) to avoid the water condensation in the equipment and purged with N_2 (200 ml/min) in the furnace.

The mechanical and viscoelastic properties were assessed by means of a Rheometric Scientifics Dynamic-Mechanical-Thermal Analyser Mark IV (USA). The deformation force was set at 0.01 N. The displacement was checked before each experiment. Experiments were performed by using dual cantilever clamping in bending mode. Specimens of 40 × 10 × 2 mm were heated from 35 to 150 °C in iso-step mode every 2 °C in the frequency (f) range from 0.1 to 39 Hz measuring 5 points per decade.

In order to correlate the results obtained by Thermal Analysis with the molecular weight changes, the number and weight average molecular weights ($\overline{M}_n$ and $\overline{M}_w$ respectively) of the

ANALYSIS OF CHEMICAL AND PHYSICAL PROPERTIES		THERMAL ANALYSIS Technique	Experiment	Direct observation	Further data analysis
	1 st Paper	**Differential Scanning Calorimetry (DSC)**	Heating/ Cooling/ Heating	→ Glass transition temperature → Crystallization temperatures and enthalpies → Melting temperatures and enthalpies → Crystallinity degree	→ Structural relaxation / physical ageing → Lamellar thickness distribution → Multi-modal melting behaviour characterisation
		Dynamical-Mechanical Thermal Analysis (DMTA)	Multi-frequency	→ Storage and Loss Moduli → Loss tangent	→ Activation energies of relaxations → Free-volume ratio (thermal expansion coefficient)
	2nd Paper	**Thermogravimetry (TGA)**	Non-isothermal analysis Multi-heating rates	→ Decomposition temperatures (thermal stability) → Percentage of mass loss and residue	→ Safety decomposition temperatures → Activation energies evolution → Kinetic models

Fig. 1. Summary of parameters used to assess the extent of degradation in soil on polylactide.

samples were evaluated in tetrahydrofuran (THF) at 25 °C by means of a GPC Agilent 1100 Series, using a PL Gel 5 μm 104 Å column, of 300 × 7.5 mm, from Polymer Laboratories.

3. Results and discussion

The extent of biodegradation of polylactide (PLA) has been deeply characterized by means of Differential Scanning Calorimetry (DSC) and Dynamic-Mechanical-Thermal Analysis (DMTA) experiments. A parallel DSC/DMTA results interpretation along the study will thus provide specific indicators to monitor the extent of degradation, by understanding the role of both amorphous and crystalline fractions of PLA. Furthermore, these results have been associated with the average molecular weight evolution in order to validate the suitability of Thermal Analysis techniques for monitoring degradation in soil on PLA.

Fig. 2a and b show the calorimetric thermogram and the mechanical relaxation spectrum of non-buried PLA, respectively. In the Fig. 2a, the three calorimetric (heating, cooling, and second heating) scans are plotted. From the first heating scan, the degradation in soil effect on PLA was assessed, since it represents the current status of the buried polymer and because the second cooling scan does not offer information. The following transitions are observed along the increasing temperature-axis: glass transition (between 40 °C and 75 °C), cold crystallization (between 90 °C and 140 °C) and melting process (between 140 °C and 160 °C). From each calorimetric transition, sensitive indicators were studied to evaluate degradation. The cooling DSC scan only shows the glass transition and the second DSC heating scan shows the glass transition, overlapped with the structural relaxation. In the second heating scan, the PLA amorphous phase does not crystallize at 10 °C/min.

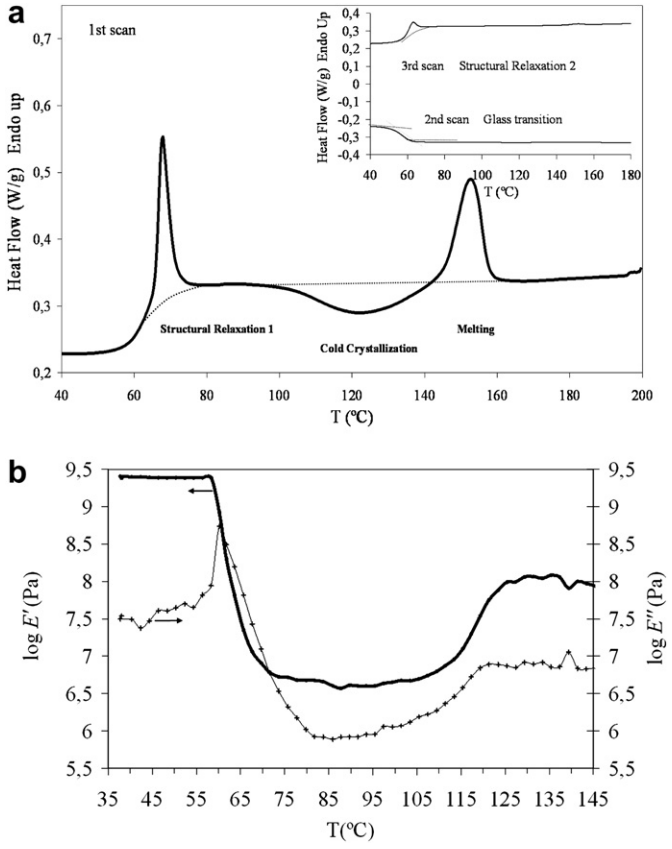

Fig. 2. Calorimetric and viscoelastic behavior of non-buried polylactide (a) calorimetric thermogram and (b) log (*E'*) and log (*E''*) versus temperature.

In the Fig. 2b the storage (*E'*) and loss (*E''*) moduli versus temperature at the commonly used frequency of 1 Hz are plotted. Similar curves are obtained for all the other frequencies between 0.1 and 39 Hz, but are not displayed for the sake of clarity. The mechanical relaxation spectra show different relaxation zones which can be assigned to the calorimetric transitions along the increasing temperature-axis: glass/rubber transition (55–75 °C), rubbery plateau (75–90 °C), crystallization (90–140 °C).

Fig. 3 shows the effect of degradation in soil on the first DSC heating scan. The effect of the degradation in soil is basically appreciate in the changes on the crystallization transition and consequently in the melting. The degradation in soil modifies the storage and loss moduli spectra as can be seen at Fig. 4a and b, respectively. Taking into account that the first calorimetric thermogram (first DSC scan) and the mechanical relaxation spectrum (DMTA scan) are directly related; the discussion of the results is focused in the three important transitions observed in the first calorimetric thermogram and the corresponding mechanical relaxation spectrum.

3.1. Glass transition assessment

The study of the glass transition region from the calorimetric and the mechanical techniques enables analyzing the effect of degradation on the amorphous molecular chains. At the first calorimetric scan (Fig. 2) an endothermic phenomenon, the structural relaxation, overlapped to the glass transition relaxation, is observed

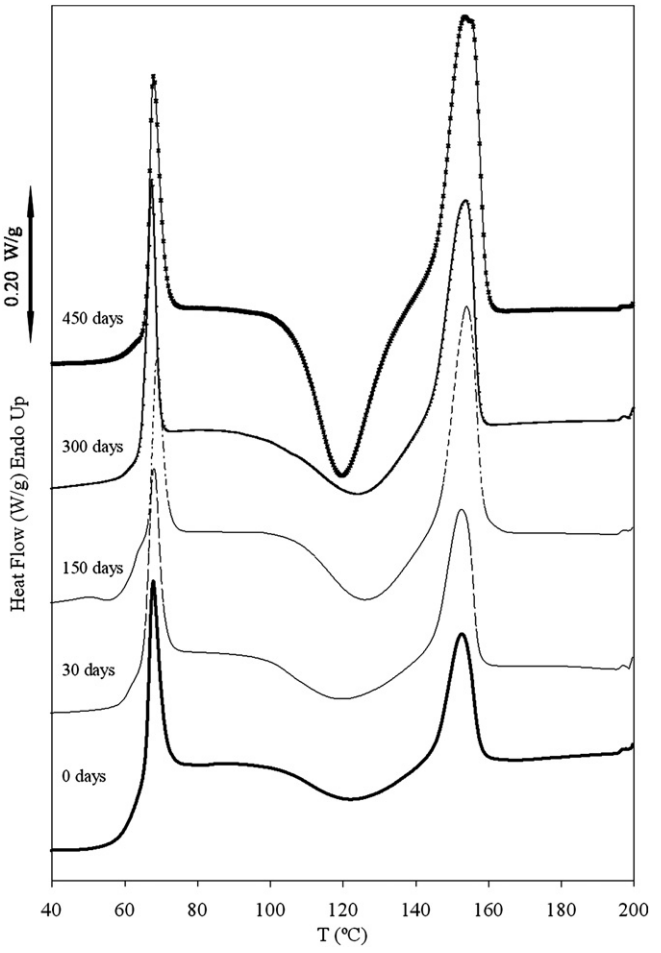

Fig. 3. Comparative first scan of the calorimetric thermograms at different degradation times.

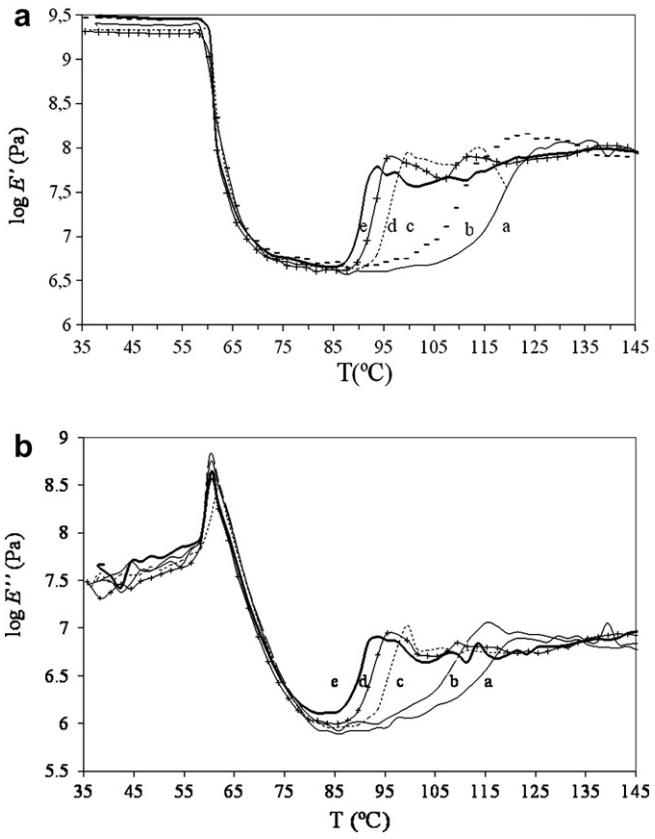

Fig. 4. (a) Effect of degradation in soil on log E' vs. temperature. (b) Effect of degradation in soil of polylactide on log E'' vs. temperature. (a. 0 days; b. 30 days; c. 150 days; d. 300 days; e. 450 days).

at 61 °C. In order to assess this phenomenon, the relative structural relaxation enthalpy (ΔH_R) is proposed as indicator. The enthalpies were calculated by the specific area (J/g) of the consequent endotherm using a spline baseline. The relative structural relaxation enthalpy (ΔH_R) is obtained by the subtraction of the structural relaxation enthalpy of the first scan (ΔH_{R1}) to the one related obtained in the second heating scan (ΔH_{R3}). It is provided in relative terms with regards to the non-buried sample (sample"o") to study the "i" times of degradation in soil $\Delta H_{Ri} = (\Delta H_{R1i} - \Delta H_{R3i})/(\Delta H_{R1o} - \Delta H_{R3o})$. Table 1 shows the changes of ΔH_R. It can be seen that when the soil burial test advances, there is an increasing tendency of this indicator reaching a 70% increase at 450 days.

The glass transition temperature (T_g) is obtained from the second heating DSC scan in which this is the only phenomenon shown, due to the applied cooling rate does not allow crystallization. The T_g is calculated as the temperature at the inflection point of the phenomenon, and for non-buried PLA it is located around 56 °C.

The glass-rubber relaxation of PLA appears in DMTA as a drop of E' to very low values. The peak temperature (T_{max}) taken from the maximum of E'' related to the glass transition gives a value of approx. 60 °C at the frequency of 1 Hz. As was expected, the temperature related to the glass-rubber relaxation is higher than the calorimetric glass transition temperature.

Table 1
Calorimetric and viscoelastic parameters related to the glass transition relaxation.

Time in soil (days)	DSC			DMTA
	T_g (°C)	ΔH_{R1} (J/g)–ΔH_{R3} (J/g)	ΔH_R (J/g)	T_{max} (°C)
0	56.5 ± 1.0	4.3 ± 0.1	1.0 ± 0.02	60.9 ± 0.5
30	56.1 ± 0.8	4.7 ± 0.1	1.1 ± 0.02	60.9 ± 0.3
150	56.7 ± 1.0	5.2 ± 0.2	1.2 ± 0.04	62.0 ± 0.7
300	55.7 ± 0.7	6.0 ± 0.3	1.4 ± 0.07	60.7 ± 0.2
450	55.9 ± 0.6	7.3 ± 0.3	1.7 ± 0.04	60.8 ± 0.7

The values of T_g and T_{max} obtained for PLA submitted to degradation in soil are shown at Table 1. These parameters do not offer significant changes with burial, because are sensitive to large-scale morphological changes. With the aim of assessing the morphological rearrangements of PLA amorphous chains, a closer inspection has been carried out.

The calculation of the Arrhenius maps has thus been performed (Fig. 5) in order to predict the influence of the degradation in soil on the viscoelastic performance of PLA. As expected, the relationship of ln (f) and T_{max}^{-1} can be fitted to the Vogel-Fulcher-Tamman-Hesse (VFTH) equation (1) for obtaining the thermal expansion coefficient [28]:

$$\ln f = A - m_v \cdot \frac{1}{T_{max} - T\infty} \quad (1)$$

where f represent the selected frequencies in Hz, T_{max} in K, is the temperature obtained at the maximum value of E″, $m_v = B/\alpha_f$, being α_f the thermal expansion coefficient and $B \cong 1$, T_∞, is the temperature at which the free volume would be zero and A is a pre-exponential factor. The thermal expansion coefficient trend during the degradation in soil for all samples is shown in Fig. 6. The thermal expansion coefficient presents an increasing tendency when degradation time becomes longer. The increase is more noticeable from 300 days on.

Therefore, the free volume existing among the amorphous chains is higher as the extent of degradation rises up. This may be a direct consequence of chain cleavages in the amorphous phase, caused by degradation in soil agents (water and microorganisms) on the PLA matrix. Specifically in the presence of water it has been found to proceed through two alternative mechanisms: surface or heterogeneous, and bulky or homogeneous erosion [29]. The free volume of the studied PLA arises with degradation in soil strengthening the suggestion of easy molecular motions as degradation in soil advances.

3.2. Cold-crystallization evaluation

When the glass transition relaxation is overcome other phenomenon very significant presented by PLA is the cold crystallization. In the first heating DSC scan, the cold crystallization is observed in an onset (T_{0n}) around 85 °C (Fig. 2 and Table 2), since the chains which were constrained have the condition to freely

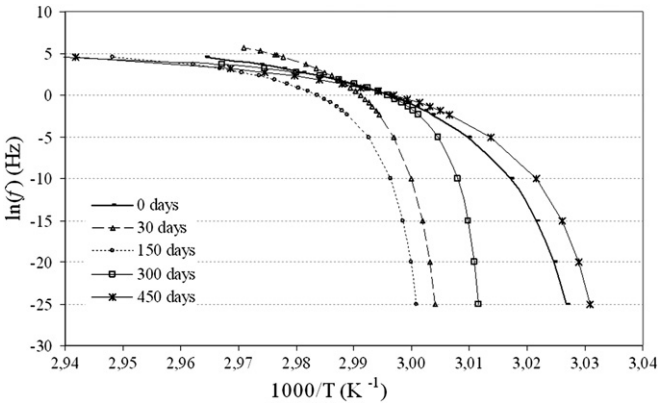

Fig. 5. Arrhenius Maps obtained from multi-frequency DMTA analysis.

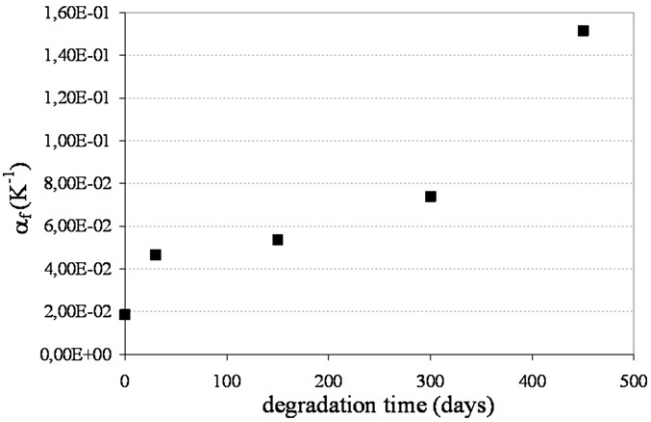

Fig. 6. Thermal expansion coefficient vs. degradation time.

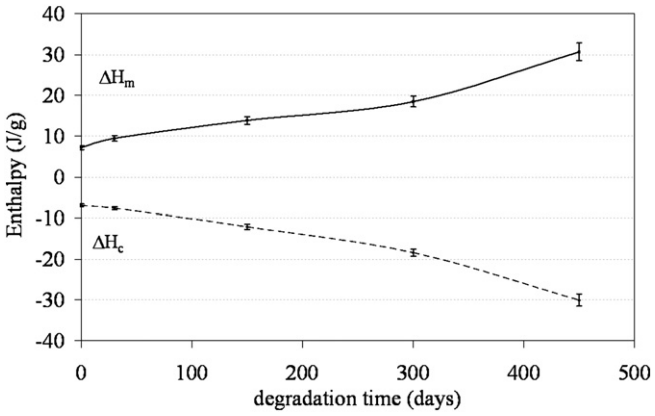

Fig. 7. Crystallization and melting enthalpies vs. degradation time.

crystallize and at around 123 °C the exothermic peak (T_c) is situated. The mechanical relaxation spectrum shows that the storage modulus increases again after the glass transition, at a determined temperature named onset crystallization temperature (T_o), around 85 °C (Fig. 4 and Table 2), which is in good agreement with the DSC results. The endset temperature (T_e) of the crystallization phenomenon is taken as the temperature reached when the increase in both viscoelastic modulus achieve a second plateau, being for the non-buried sample around 125 °C. This increase in the storage modulus indicates an increase of the rigidity of the material. The slow heating rate enhances the crystallization process during the DMTA measurement and the development of spherulites as other authors have confirmed using Thermal Optical Analysis and X-Ray Diffraction methods [30].

Significant changes due to the degradation in soil are observed by both techniques. The principal parameters evaluated for the analysis of the cold crystallization are listed in Table 2. Degradation in soil principally modifies the magnitude of the cold crystallization exotherm (ΔH_C), especially from 300 days of burying in soil on. The increase of this parameter indicates the presence of more polymeric chains involved in the crystallization process as the degradation time is higher, thus strengthening the hypothesis of morphological changes previously drawn from the glass transition assessment.

Changes are also observed in the mechanical spectra; the rubbery plateau is narrower as samples are more degraded, since the crystallization ends at lower temperatures. These results may suggest that the effect of degradation in soil on the amorphous regions is forming shorter chains that easily rearrange in spherulites, since the mobility is enhanced by the availability of more free volume.

3.3. Melting characterization

The study of the PLA melting process allows the determination of new parameters that will reinforce the knowledge of the degradation in soil effects on PLA morphology and thermal properties. The melting process of non-buried PLA has been analyzed by the deconvolution of the melting endotherms that represent two different crystalline distributions. The lowest melting temperature peak, corresponding to the population with lower size (peak 1) is located at 151 °C and the highest, corresponding to crystalline conformations with larger size (peak 2), appears at 155 °C, (T_{m1}) and (T_{m2}) respectively. Fig. 7 represents the evolution of both melting (ΔH_m) and cold crystallization (ΔH_c) enthalpies along the degradation test. It is obtained that the melting enthalpy slightly differs from the immediately previous cold-crystallization enthalpy regardless the time of the experiment, confirming that PLA is initially amorphous. Higher degradation time leads to equally increase both enthalpies: as can be seen, the initially melting enthalpy was around 7 J/g and at 300 days it reached 18 J/g but it is up to this time when the increase is more significant, achieving at 450 days, 30 J/g.

Nonetheless, it has been considered interesting to perform an accurate study of the morphology of the coldly obtained crystallites. Hence, from the obtained results of the melting process during the first scan, the lamellar thickness distribution "l_c" in Ámstrongs (1 Å = 10^{-10} m) of the newly grown crystallites was calculated by means of Thompson equation.

$$l_c = \frac{2 \cdot \sigma_e}{\Delta h_m^{\infty}\left(1 - \frac{T}{T_m^o}\right)} \tag{2}$$

where: T = observed melting temperature (K), T_m^o = equilibrium melting temperature (K), σ_e = free surface energy of the basal plane (J m^{-2}) and Δh_m^{∞} = melting enthalpy per volume unit for a crystalline phase (J m^{-3}). For PLA the values used for calculating the lamellar thickness are, T_m^0 = 480 K, $\sigma_e = 60.89 \cdot 10^{-3}$ J m^{-2}, and $\Delta h_m^{\infty} = 111.083 \times 10^8$ J m^{-3} [31]. According to the Thompson equation, Eder assumes that at a given temperature for a sample of molten polymer, the rate of heat consumption is proportional to the fraction of lamellar which thickness is l_c [32]. The plot has been done subtracting the baseline of the endotherm and normalized to the maximum value of the enthalpy. For the non-buried material, l_c relays between 75 and 115 Å. The influence of degradation in soil on the lamellar thickness of the crystallites is shown at Fig. 8. The plots slightly shift to higher l_c values with longer degradation in soil, showing the continuous formation of crystalline zones with higher lamellar size. The lamellar thickness distribution is splitting into two different shoulders. A multimodal endothermic behavior, attributed to segregation into two main populations can be observed. A deconvolution procedure was applied to the melting thermograms in order to individually characterize the behavior of each population and their contribution to the overall effect using

Table 2
Calorimetric and viscoelastic parameters related to the cold crystallization.

Cold Crystallization					
DSC			DMTA		
Time in soil (days)	T_{0n} (°C)	T_c (°C)	log E′ (Pa)	T_o (°C)	T_e (°C)
0	84.9 ± 1.5	123.0 ± 1.0	7.9 ± 0.2	85.5 ± 1.0	125.3 ± 1.0
30	84.3 ± 1.0	119.0 ± 1.3	7.8 ± 0.3	85.1 ± 1.0	125.4 ± 1.4
150	86.6 ± 1.8	125.2 ± 1.6	7.9 ± 0.2	85.0 ± 0.8	99.5 ± 1.0
300	84.3 ± 1.6	123.2 ± 1.1	7.8 ± 0.3	85.1 ± 0.9	95.6 ± 0.6
450	89.9 ± 1.3	119.7 ± 1.2	7.7 ± 0.1	85.0 ± 0.7	93.6 ± 1.2

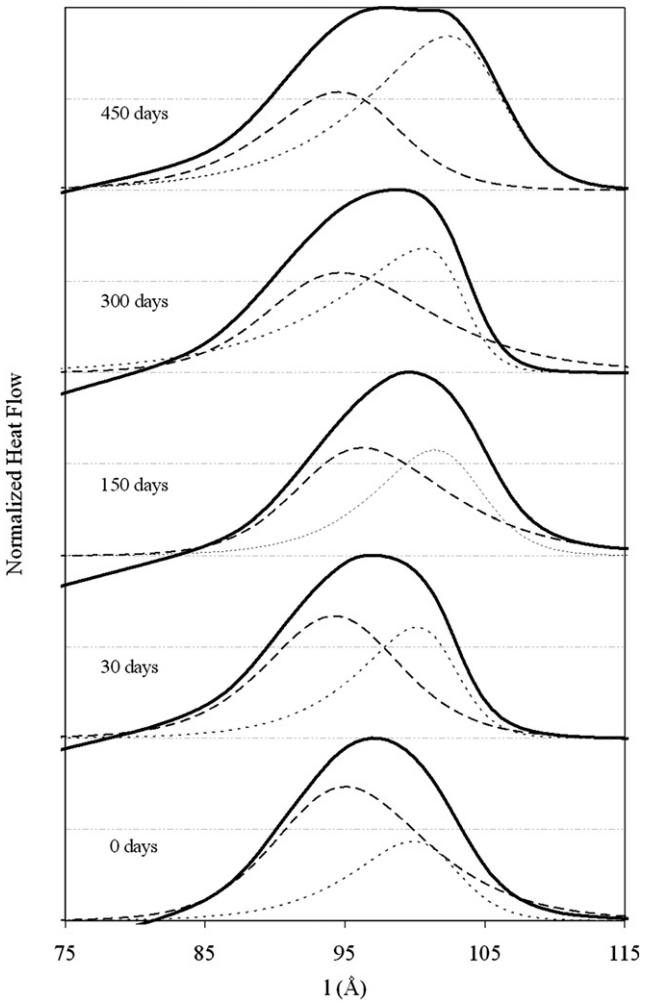

Fig. 8. Influence of degradation in soil on the lamellar thickness distribution of polylactide. (▬) overall endotherm, (—) 1st deconvoluted lamellar thickness distribution with lower crystalline sizes and (—) 2nd deconvoluted lamellar thickness distribution with higher crystalline sizes.

a partial areas study [33]. The following expression was employed as deconvolution.

$$y_i = y_0 + A\cdot\left(\frac{1}{1+\exp\left(\frac{-(x-x_c+\frac{w_1}{2})}{w_2}\right)}\right)\cdot\left(1-\frac{1}{1+\exp\left(\frac{-(x-x_c+\frac{w_1}{2})}{w_3}\right)}\right) \quad (3)$$

where y_i is the normalized heat flow for each deconvoluted curve, x are the l_c values, x_c is a position parameter related to maximum value of the curve ($l_{c\ max}$), A is an amplification parameter and w_1, w_2, w_3 describe the dispersion and symmetry of the curve.

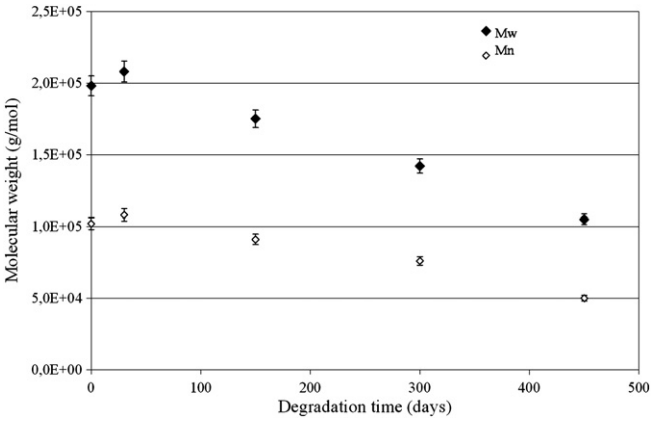

Fig. 9. $\overline{M}_n$ and $\overline{M}_w$ evolution calculated by GPC.

The curve of the normalized heat flow is expressed as $y = y_0 + \sum_{i=1}^{n} y_i$ where y_0 is the y value of the baseline of the curve and n is the number of deconvoluted curves. Deconvoluted peak temperatures, as well as the lamellar thickness at the maximum of both populations are gathered at Table 3. As can be seen, T_{m1} remains almost constant and T_{m2} slightly increases with degradation. The integration of the individual curves have been calculated from l_c = 75 to 115 Å (Fig. 8) and the values obtained are named $Area_1$ and $Area_2$, corresponding to the curves with a maximum in T_{m1} and T_{m2} respectively. The values are expressed in % percentage respect the total integration value ($Area_{total}$) and are listed at Table 3, indicating that degradation in soil promotes the growing of the lamellar distribution with higher crystalline sizes. These results indicate that as a consequence of the degradation, the heterogeneity of this material increase. Both techniques indicate that the crystallization process as an important indicator of the samples degradation.

Summing up, the increase of the relative structural relaxation enthalpy and the thermal expansion coefficient manifest the chain cleavages induced by degradation in soil of PLA. The increased free volume between the molecular chains that form the amorphous phase allows a major mobility of the free chains. The apparition of shorter chains is monitored by the continuous increase in the cold-crystallization enthalpy, especially after 300 days of burying. The raise of crystallization is confirmed by the increase of the relative area of the melting endotherm related to the coldly-formed crystalline population with higher lamellar thickness.

Results provided by Thermal Analysis have been correlated with the obtained by directly measuring the molecular weight. Fig. 9 shows the behavior of average molecular weight in number and weight ($\overline{M}_n$ and $\overline{M}_w$, respectively) as a function of the days in soil. A slight increase in the molecular weight after 30 days due to the rearrangements that PLA underwent in contact with water and soil is shown [34]. The molecular weight continuously decreases from 30 days on and it specially drops after 300 days, reaching a 50% decrease of the initial molecular weigh of PLA at 450 days.

Table 3
Calorimetric parameters related to the melting transition.

Melting parameters						
Time in soil (days)	T_{m1} (°C)	l_{cmax1} (Å)	$Area_1$ (% $Area_{total}$)	T_{m2} (°C)	l_{cmax2} (Å)	$Area_2$ (% $Area_{total}$)
0	151.6 ± 2.0	93.7 ± 1.2	61	154.9 ± 2.0	101.3 ± 1.4	39
30	151.7 ± 1.8	94.5 ± 0.8	56	155.1 ± 1.4	101.6 ± 1.2	44
150	151.8 ± 1.6	94.4 ± 1.0	49	155.6 ± 1.7	102.7 ± 1.1	51
300	151.4 ± 1.2	92.8 ± 1.2	46	154.9 ± 2.0	102.6 ± 0.8	54
450	151.8 ± 1.3	95.9 ± 0.8	37	156.9 ± 1.3	104.5 ± 0.9	63

The correlation of Thermal Analysis assessment with the molecular weight characterization has been therefore shown to be complementary and interesting, since the stage of degradation can be effectively examined by both types of analysis. DSC and DMTA techniques are very sensitive to study the molecular rearrangements occurring before large-scale degradation processes, and therefore capable of explaining the morphological changes induced during degradation in soil. Likewise, Thermal Analysis techniques have effectively monitored the effects of burial when the molecular weight experiences a remarkable decrease, thus confirming the suitability of these techniques for understanding the influence of degradation in soil on polylactide.

4. Conclusions

Polylactide was buried in active soil in order to simulate its disposal stage following an international standard, and the changes in their physical properties were assessed by Differential Scanning Calorimetry and Dynamic Mechanical Thermal Analysis.

Along the degradation in soil process, indicators such as the relative structural relaxation enthalpy and the thermal expansion coefficient have given an idea about the free volume generated within the amorphous matrix. Onset, endset and peak cold crystallization temperatures and enthalpies showed the variation of the crystalline phase, due to the liability of shorter chains to rearrange in spherulites after cleavages induced by degradation in soil. The melting behavior of the crystalline fraction formed, especially after 300 days of burial, show that the lamellar thickness distribution experiences a change towards higher sizes, coinciding with the molecular weight decrease. These facts stress the relation between the heterogeneity acquired by PLA after chain scissions and the notable change of properties, also corroborated by molecular weight reduction.

The combination of both Thermal Analysis and Molecular Weight Characterization stands out as a very interesting option for assessing not only the macroscopic changes on PLA structure induced by degradation in soil, but also for establishing new insights on the morphological rearrangements involved during the whole process.

Acknowledgements

Partial funding of this work by Ministerio de Educación y Ciencia, Project ENE2007-67584-C03-02 and for a pre-doctoral grant scholarship FPU to J.D. Badía, and by the Ministerio de Ciencia e Innovación for a pre-doctoral grant scholarships FPI to L. Santonja Blasco and Rosana Moriana, is gratefully acknowledged.

References

[1] Doi Y, Fukuda K, editors. Biodegradable plastic and polymers. Amsterdam, The Netherlands: Elsevier; 1994.
[2] Scott G, editor. Biodegradable polymers. Principles and applications. 2nd ed. Dordrecht, The Netherlands: Kluwer Academic Publishers; 2002.
[3] Vert M, Schwach G, Coudane J. Present and future of PLA polymers. J Macromol Sci Pure Appl Chem 1995;A32:787–96.
[4] De Jong SJ, Arias ER, Rijkers DTS, van Nostrum CF, Kettenes-van den Bosch JJ, Hennink WE. New insights into the hydrolytic degradation of poly(lactic acid): anticipation of the alcohol terminus. Polymer 2001;42:2795–802.
[5] Kronenthal RL, Oser Z, Martin E, editors. Polymers in medicine and surgery. New York, NY: Plenum Press; 1975. p. 119–37.
[6] Li S, Garreau H, Vert M. Structure-property relationships in the case of the degradation of massive aliphatic poly-(α-hydroxy acids) in aqueous media. J Mater Sci Mater Med 1990;1:123–30.
[7] Migliaresi C, Fambri L, Cohn D. A study on the *in vitro* degradation of poly (lactic acid). J Biomater Sci Polym Ed 1994;4:591–606.
[8] Södergård A, Selin J-F, Näsman JH. Hydrolytic degradation of the peroxide modified poly (L-lactide). Polym Degrad Stab 1996;51:351–9.
[9] Tsuji H, Mizuno A, Ikada Y. Properties and morphology of poly(L-lactide). III. Effects of initial crystallinity on long-term in vitro hydrolysis of high molecular weight poly(L-lactide) film in phosphate-buffered solution. J Appl Polym Sci 2000;77:1452–64.
[10] Tsuji H, Ikada Y. Properties and morphology of poly(L-lactide) 4. Effects of structural parameters on long-term hydrolysis of poly(L-lactide) in phosphate-buffered solution. Polym Degrad Stab 2000;67:179–89.
[11] Hakkarainen M. Aliphatic polyesters: abiotic and biotic degradation and degradation products. Adv Polym Sci 2002;157:113–38.
[12] Shogren RL, Doane WM, Garlotta D, Lawton JW, Willett JL. Biodegradation of starch/polylactic acid/poly(hydroxyester-ether) composite bars in soil. Polym Degrad Stab 2003;79:405–11.
[13] Torres A, Li SM, Roussos S, Vert M. Poly(lactic acid) degradation in soil or under controlled conditions. J Appl Polym Sci 1996;62:2295–302.
[14] Urayama H, Kanamori T, Kimura Y. Properties and biodegradability of polymer blends of poly(L-lactide)s with different optical purity of the lactate units. Macromol Mater Eng 2002;287:116–21.
[15] Siepmann J, Göpferich A. Mathematical modeling of bioerodible, polymeric drug delivery systems. Adv Drug Deliv Rev 2001;48(2–3):229–47.
[16] Schliecker G, Schmidt C, Fuchs S, Kissel T. Characterization of a homologous series of D, L-lactic acid oligomers; a mechanistic study on the degradation kinetics in vitro. Biomaterials 2003;24:3835–44.
[17] Aso Y, Yoshioka S, Li Wan Po A, Terao T. Effect of temperature on mechanisms of drug release and matrix degradation of poly(DL-lactide) microspheres. J Control Release 1994;31(1):33–9.
[18] Ho KLG, Pometto III AL, Hinz PN. Effects of temperature and relative humidity on polylactic acid plastic degradation. J Environ Polym Degrad 1999;7:83–92.
[19] Calmon A, Guillaume S, Bellon-Maurel V, Feuilloley P, Silvestre F. Evaluation of material biodegradability in real conditions-development of a burial test and an analysis methodology based on numerical vision. J Environ Polym Degrad 1999;7:157–66.
[20] Iman HS. Adhesive properties of a symbiotic bacterium from a wood-boring shipworm. Appl Environ Microbiol 1990;56:1317–22.
[21] Goheen RP, Wool RP. Degradation of polyethylene-starch blends in soil. J Environ Polym Degr 1991;42:2691–701.
[22] Santonja-Blasco L, Contat-Rodrigo L, Moriana-Torro R, Ribes-Greus A. Thermal characterization of polyethylene blends with a biodegradable masterbatch subjected to thermo-oxidative treatment and subsequent soil burial test. J Appl Polym Sci 2007;106:2218–30.
[23] Badía JD, Vilaplana F, Karlsson S, Ribes-Greus A. Thermal analysis as a quality tool for assessing the influence of thermo-mechanical degradation on recycled poly(ethylene terephthalate). Polym Test 2009;28:169–75.
[24] Contat-Rodrigo L, Ribes-Greus A, Díaz-Calleja R. Characterization by thermal analysis of PP with enhanced biodegradability. J Appl Polym Sci 2001;82:2174–84.
[25] Vallés-Lluch A, Contat-Rodrigo L, Ribes-Greus A. Influence of previous annealing on the first stage of degradation of LDPE-Mater-Bi blends aged in soil. Comparative study by thermal analysis. J Appl Polym Sci 2003;90:3359–73.
[26] Contat-Rodrigo L, Ribes-Greus A. Viscoelastic behavior of degradable polyolefins aged in soil. J Appl Polym Sci 2000;78:1707–20.
[27] ISO 846, 1997. Plastics–determination of behaviour under the action of microoganisms. Evaluation by visual examination or measurement of changes in mass or physical properties.
[28] Vogel H. The temperature dependence law of the viscosity of fluids. Phys Z 1921;22:645–6.
[29] Heya T, Okada H, Ogawa Y, Toguchi H. In-vitro and in-vivo evaluation of thyrotropin-releasing-hormone release from copoly(DL-lactic/glycolic acid) microspheres. J Pharm Sci 1994;83(5):636–40.
[30] Pluta M. Morphology and properties of polylactide modified by thermal treatment, filling with layered silicates and plasticization. Polymer 2004;45:8239–51.
[31] Vasanthakumari R, Pennings AJ. Crystallization kinetics of poly(L-lactic acid). Polymer 1983;24:175–8.
[32] Wlochowicz A, Eder M. Distribution of lamella thicknesses in isothermally crystallized polypropylene and polyethylene by differential scanning calorimetry. Polymer 1984;25:1268.
[33] Moriana-Torró R, Contat-Rodrigo L, Santonja-Blasco L, Ribes-Greus A. Thermal characterisation of photo-oxidized HDPE/Mater-Bi and LDPE/Mater-Bi blends buried in soil. J Appl Polym Sci 2008;109:1177–88.
[34] Liua X, Zoub Y, Lia W, Caoa G, Chen W. Kinetics of thermo-oxidative and thermal degradation of poly(D,L-lactide) (PDLLA) at processing temperature. Polym Degrad Stab 2006;91(12):3259–65.

Polymer Degradation and Stability 95 (2010) 2192–2199

Contents lists available at ScienceDirect

Polymer Degradation and Stability

journal homepage: www.elsevier.com/locate/polydegstab

Thermal analysis applied to the characterization of degradation in soil of polylactide: II. On the thermal stability and thermal decomposition kinetics

J.D. Badía, L. Santonja-Blasco, Rosana Moriana, A. Ribes-Greus*

Instituto de Tecnología de Materiales, Universidad Politécnica de Valencia, Camino de Vera, s/n, 46071, Valencia, Spain

ARTICLE INFO

Article history:
Received 1 December 2009
Received in revised form
19 April 2010
Accepted 3 June 2010
Available online 12 June 2010

Keywords:
Polylactide
Degradation in soil
Thermal decomposition kinetic analysis
Isoconversional methods

ABSTRACT

The disposal stage of polylactide (PLA) was assessed by burying it in active soil following an international standard. Degradation in soil promotes physical and chemical changes in the polylactide properties. The characterization of the extent of degradation underwent by PLA was carried out by using Thermal Analysis techniques. In this paper, studies on the thermal stability and the thermal decomposition kinetics were performed in order to assess the degradation process of a commercial PLA submitted to an accelerated soil burial test by means of multi-linear-non-isothermal thermogravimetric analyses. Results have been correlated to changes in molecular weight, showing the same evolution as that described by the parameters of thermal stability temperatures and apparent activation energies. The decomposition reactions can be described by two competitive different mechanisms: Nucleation model (A2) and Reaction Contracting Volume model (R3). The changes in the kinetic parameters and kinetic models are in agreement with the calorimetric and dynamic–mechanical–thermal results, presented in the Part I of the study [1].

1. Introduction

Due to the significant impact of plastic waste on the environment, to find eco-friendly solutions to manage the disposal of synthetic plastics is a key challenge. A promising solution is the use of biodegradable polymers for packaging, as well as many other applications. Due to its good thermal, mechanical and processing properties, economic and environmental advantages [2–12], one of the most potential candidates is polylactide (PLA), which is being currently established at the polymer industry. However, the use of new materials would also imply the generation of a new and huge source of polymeric materials waste in the near future, which should be carefully managed. Therefore, the degradation process involved the disposal stage of PLA must be assessed, with the aim of ensuring the completion of its life cycle.

The necessity of developing and implementing fast, cost-effective and reliable characterization testing procedures has been stated in order to ascertain a deeper knowledge about the ongoing interaction of the polymer with its disposal environment [1]. Thermal Analysis techniques have demonstrated to be very appropriate and reliable methodologies to monitor and control the influence of several degradation phenomena on biodegradable polymers, such as hydrolysis, photo-oxidation, swelling, or degradation in soil [13–15]. Chain cleavage processes induce morphological and mechanical changes, as observed by Differential Scanning Calorimetry and Dynamical Mechanical Thermal Analysis [1]. These morphological changes may alter the thermal decomposition process of the bulk PLA and thus its characterization would also provide a complementary interpretation on the macroscopic effects of degradation in soil on PLA. As discussed in previous studies [16,17], the decomposition of PLA during thermal treatment is mainly caused by intramolecular transesterification reactions leading to cyclic oligomers of lactic acid and lactide. Simultaneously, there is a recombination of the cyclic oligomers with linear polyesters through insertion reactions, whereas molecules with longer chains lengths are favoured. Evolved gases in inert atmosphere also contain acetaldehyde, carbon monoxide, carbon dioxide and methylketene, among others [18].

Due to its applicability in the macroscopic scale, the modeling of the thermal decomposition processes in inert or reactive conditions has been broadly applied by using isoconversional and non-isoconversional methods proposed by different authors with good acceptance because of its versatility in different materials [19,20]. The completion of the kinetic triplet, consisting in kinetic model function f(α), apparent activation energy (Ea), and pre-exponential factor (A) can furnish with the knowledge of the polymer thermal decomposition behaviour, and thus be related to the ongoing degradation stage.

* Corresponding author. Tel.: +34 963879817.
E-mail address: aribes@ter.upv.es (A. Ribes-Greus).

0141-3910/$ – see front matter © 2010 Elsevier Ltd. All rights reserved.
doi:10.1016/j.polymdegradstab.2010.06.002

The aim of this work is to test by thermal Analysis techniques the thermal changes that PLA suffers through degradation in soil. To mimic the environmental conditions at which PLA is subjected in non-controlled disposals, PLA is submitted to a standardized accelerated degradation in soil test. Physical and chemical changes occurred to the polylactide properties, throughout the degradation in soil process are analyzed, making efforts on establishing new insights in studying the degradation in soil process on polymers by other accurate methods; alternative and complementary to the chemical analytical techniques. The current paper is focused on the influence of degradation in soil on the thermal stability and the thermal decomposition kinetics of PLA. Once assessed the effect of degradation in soil on PLA molecular weight (MW), parameters such as the characteristic thermal stability temperatures (T_{on}, T_{end}, T_p) and the components of the kinetic triplet (f (α), A and Ea) have been correlated to MW evolution and consequently evaluated as indicators of degradation.

2. Theoretical background

The primary purpose of the kinetic analysis is to obtain the aforementioned kinetic triplet. Recently, Khawan and Flanagan [21,22] have reviewed the relationship between the theoretical decomposition mechanisms and their mathematical models, the so-called kinetic functions f (α). A list of the most common f (α) applied to polymers is given at Table 1.

Macroscopic kinetics are complex since they might give information about multiple steps simultaneously occurring, and therefore induce to misleading results [23]. Some investigations have been hence carried out in order to focus on the challenge of clarifying the interpretation of macroscopic kinetics; and have settled isoconversional methods as suitable analysis procedures to evaluate the apparent activation energy (Ea) [23,24]. These methods, which require experiments at several linear heating rates, are based on the assumption that at a constant extent of conversion α, the decomposition rate $d\alpha/dt$ is a function only of the temperature, and do not need any conversion model assumption at the initial stages of the analysis. The most broadly used isoconversional methods are those developed by Friedman [25] and Flynn-Wall-Ozawa [26,27] (supported on Doyle's integral approximation [28]). These methods give rise to linear functions from which slopes the Ea at a constant α is obtained. Likewise, the model free kinetic method established by Kissinger [29] is widely employed by many authors in order to check their results. This method calculates the activation energy from the slope of a linear function which takes into account the relationship between the peak temperature of the first-derivative thermogravimetric curve and the heating rate employed in the experiment.

Table 1
List of common kinetic functions to explain the thermal decomposition mechanisms in bulk polymers.

model	Differential form $f(\alpha) = 1/k \cdot d\alpha/dt$	Integral form $g(\alpha) = k \cdot t$
Nucleation models		
Avrami–Erofeyev (A2)	$2 \cdot (1-\alpha)[-\ln(1-\alpha)]^{1/2}$	$[-\ln(1-\alpha)]^{1/2}$
Avrami–Erofeyev (A3)	$3 \cdot (1-\alpha)[-\ln(1-\alpha)]^{2/3}$	$[-\ln(1-\alpha)]^{1/3}$
Avrami–Erofeyev (A4)	$4 \cdot (1-\alpha)[-\ln(1-\alpha)]^{3/4}$	$[-\ln(1-\alpha)]^{1/4}$
Geometrical contraction models		
Contracting area (R2)	$2 \cdot (1-\alpha)^{1/2}$	$1-(1-\alpha)^{1/2}$
Contracting volume (R3)	$3 \cdot (1-\alpha)^{1/3}$	$1-(1-\alpha)^{1/3}$
Reaction-order models		
Zero-order (F0/R1/$n=0$)	1	α
First-order (F1, $n=1$)	$(1-\alpha)$	$-\ln(1-\alpha)$
Second-order (F2, $n=2$)	$(1-\alpha)^2$	$\frac{1}{1-\alpha}-1$
Third-order (F3, $n=3$)	$(1-\alpha)^3$	$1/2 \cdot [\frac{1}{(1-\alpha)^2}-1]$

Regarding the kinetic function f (α) evaluation, the most common methodologies are those proposed by Criado [30], which allows the comparison of the experimental data to theoretical reduced master-curves, and Coats-Redfern [31], which gives a linear fitting for a given kinetic model function. By combining both methods, Coats-Redfern method is applied to those theoretical kinetic functions f (α) that better fit the experimental behaviour according to the results drawn from the Criado method. A comparison of the apparent activation energy Ea obtained from the slope for each f (α) with the average apparent activation energy given by the Friedman, Flynn-Wall-Ozawa and Kissinger methods Ea_{iso} will be deciding in the selection of the f (α). The pre-exponential (A) is also obtained from this method, and the kinetic triplet is thus achieved, which is automatically related to the physical decomposition mechanism. An extended explanation of these methods can be found elsewhere [32]. To summarize, Fig. 1 schematically represents the theoretical description of these methods and the kinetic strategy followed at this paper.

3. Experimental procedures

3.1. Material and sample preparation

A commercial polylactide with 3. 8% content of meso-lactide, obtained from renewable resources by ring opening polymerization supplied by Natureworks (Minnetonka, USA) was used in this study. This PLA is a commercial resin with a number-average molecular weight of 102.130 g/mol, as measured by Gel Permeation Chromatography.

Pellets of PLA were dried with demoisturized air at 80 °C during 4 h. Rectangular bars were prepared by compression moulding in a Collin PCS-GA Type Press 800 (GA, USA) at an initial temperature of the hot plates of 195 °C and final temperature of 60 °C. Five pressure steps were performed as follows: 5 min at 6 bar, 8 min at 75 bar, 8 min at 155 bar, 4 min at 215 bar, and 11 min at 45 bar. Test specimens were presented as bars of ($145 \times 10 \times 2$ mm). Since this work approaches the degradation in soil of discarded consumer goods, which are obtained by means of, at least, one processing step, "non-buried PLA" has been considered the starting material of the study.

3.2. Accelerated soil burial test

PLA plates were subjected to a controlled degradation in soil test under controlled conditions (temperature, water content and pH), following the ISO 846-1997 International Norm [33], according to method D. Samples were buried in biologically active soil and kept in a Heraeus B12 (Hanau, Germany) culture oven at 28 °C. The soil used in these tests was a red soil extract taken from a culture field in Alginet (Valencia). To ensure the oxygenation of the soil, a protocol of periodical air oxygen supply was followed. Microbial activity of soil was monitored with cotton along the extension of the experiment. According to norm, if the activity of the cellulose-degrading micro-organisms is in order, the case is also applicable to the rest of flora. The soil was maintained at approximately pH 7 and a relative humidity of 0.87 g water/g wet soil. Test specimens were extracted at 30, 150, 300 and 450 days, cleaned and kept in a desiccator during 4 days in order to ensure water desorption before being analyzed.

3.3. Thermogravimetric analysis

Experiments were carried out in a Mettler-Toledo TGA/SDTA 851 (Columbus, OH), from 25 to 750 °C at different heating rates ($\beta = 5$, 10, 15, 20, 25, 30 °C/min), under constant flow of 50 mL/min of Argon atmosphere.

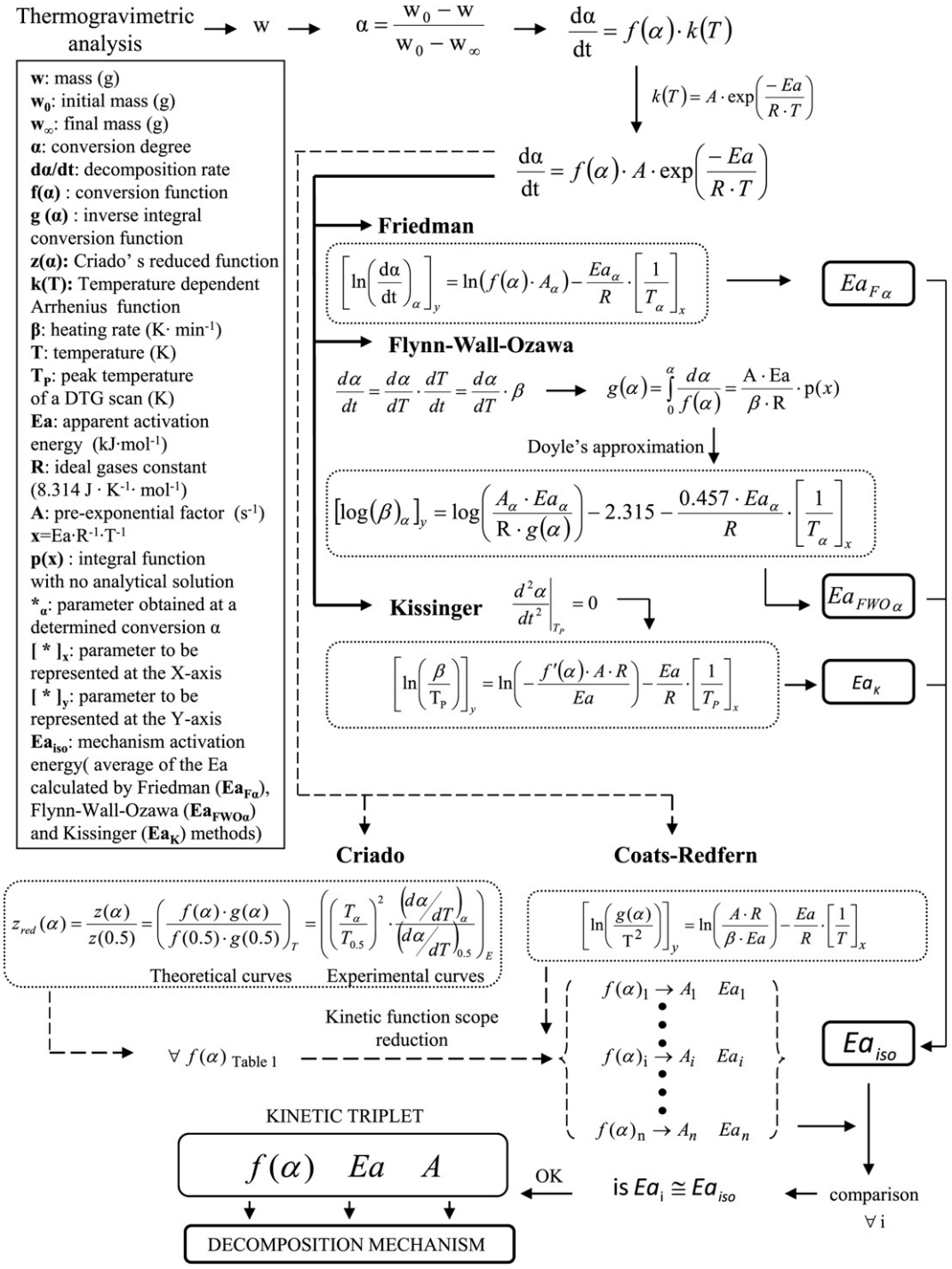

Fig. 1. Methodology applied for the characterisation of the thermal decomposition kinetics of PLA submitted to degradation in soil.

4. Results and discussion

The influence of degradation in soil on polylactide has been deeply characterized by Thermogravimetry (TGA). The changes in the thermal stability have been firstly studied. A further assessment of the thermal decomposition behaviour in the bulk PLA is performed. Results are related to those showed by Differential Scanning Calorimetry (DSC) and Dynamical Mechanical Thermal Analysis (DMTA), reported in the Part I of the study [1]. Discussion is given in terms of both the effects of degradation in soil on the physical–chemical properties of PLA, and the reliability of these thermal analysis techniques to offer reliable indicators of the degradation extent.

4.1. Thermal stability

A preliminary analysis of the differences observed in thermal stability temperatures for non-buried PLA and samples submitted to the accelerated soil burial test was performed. For this purpose, the thermal decomposition (TG) curves and their first-order

derivative (DTG) curves for samples extracted at 30, 150, 300 and 450 of burying have been analyzed at different heating rates and compared to the TG and DTG curves of the non-buried PLA. Fig. 2 shows the influence of the degradation process on the TG and DTG curves in terms of the conversion degree evolution displayed for non-buried and 450-days-buried PLA samples; the other soil burial experiments were omitted for the sake of clarity.

As usual, higher heating rates (β) lead to shift the thermograms to higher temperatures. PLA thermal decomposition occurs through a single decay stage, regardless the degradation in soil time and the β employed for the thermogravimetric analysis. The mass loss was around 98–99% in all cases. The corresponding decomposition onset and endset temperatures (T_{on}, T_{end}) were obtained by a tangential intercept method onto the TG curve. Likewise, the peak temperature of the DTG curve, which is related to the inflection temperature of the TG curve (T_P) was also considered. Fig. 3 displays the T_{on}, T_{end} and T_P evolution along the degradation in soil process at the experiment of lower β (5 °C min^{-1}), since it is supposed to offer the best accuracy and the major independence with the experimental TGA conditions [23]. All thermal stability temperatures describe the same behaviour, clearly differenced in two stages: firstly, an overall increase of around 5 °C is stated; afterwards, the decomposition temperatures continuously diminish, describing an attenuated decreasing tendency. These results suggest modifications in the arrangement of chains in the bulk PLA matrix. Initial hydrolytic reactions might give out smaller free chains able to react or reorganize, thus offering a slightly higher resistance to the thermal decomposition [34]. Later on, the degradation weakens the structure of the bulk polymer, and thus lower temperatures are capable of overcoming its thermal stability. The results from thermogravimetric analysis lead to guess that degradation in soil produces small changes in the bulk polymer, since the interaction of the polymer and the testing environment takes place slowly, as it has been shown in other studies [13,14]. However, these small variations might indicate modifications in the thermal decomposition kinetic model. Further analysis is therefore carried out to establish good indicators which correlate the thermal decomposition behaviour of PLA with its degradation in soil stage.

4.2. Thermal decomposition kinetic model

In the attempt to develop a model for plastic thermal behaviour in full scale systems, the main purpose is to describe the thermal decomposition of polymers in terms of an intrinsic kinetics, in which heat and mass transfer limitations are not included. Generally, kinetic models are proposed in literature for plastics and biomasses.

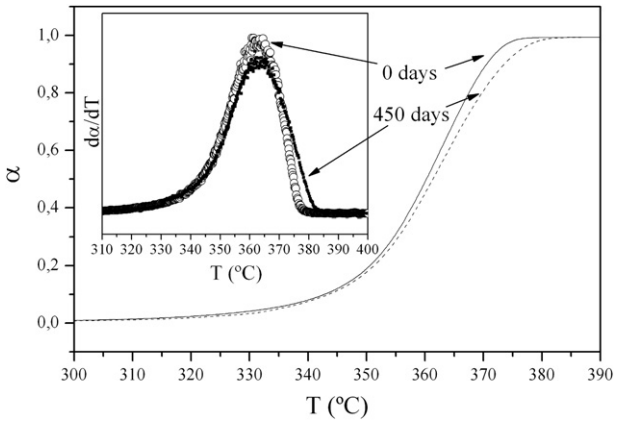

Fig. 2. Comparison of the conversion degree evolution and its first-derivative thermogravimetric curve plot for non-degraded PLA and PLA buried during 450 days.

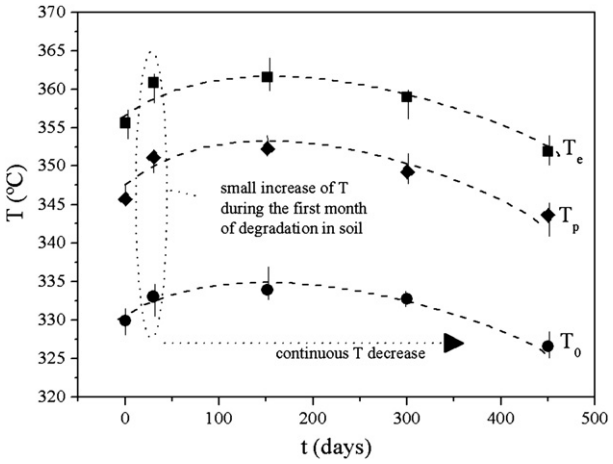

Fig. 3. Effect of degradation in soil on the thermal stability temperatures obtained from TGA experiments at 5 °C/min.

These models do not take into account the rigorous and exhaustive description of the chemistry of thermal decomposition of polymers and describe the process by means of a simplified reaction pathway. Each single reaction step considered is representative of a complex network of reactions [21]. The obtaining of the aforementioned kinetic triplet may provide new knowledge regarding the kinetic model of PLA thermal decomposition. A deep kinetic analysis according to the kinetic methodology formerly proposed in Fig. 1 has been performed. The Friedman, Flynn-Wall-Ozawa and Kissinger methods have been initially applied to evaluate the degradation in soil effect on the apparent activation energy (Ea) of the PLA thermal decomposition. These three methods offer good experimental data fittings to straight lines, for all degradation in soil times studied. Fig. 4 (a, b, c) shows the application of these methods to the non-buried PLA.

The Ea for every constant conversion degree α value has been obtained from the slope of each line. Since the main mass loss decomposition process occurs in the α domain comprised between 0.2 and 0.7 for all samples, the analyses have been focused in that range. Table 2 shows the isoconversional apparent activation energy Ea_α values for all samples submitted to the soil burial test. In order to investigate the degradation consequences on the PLA thermal decomposition kinetics, the average apparent activation energy Ea_{iso} value has been taken. Fig. 5 represents the Ea_{iso} evolution with the soil burial time for the three employed methods. As can be seen, a consistent behaviour in a small confidence range has been given by all of them. The Ea_{iso} tendency is similar to the evolution described by all the characteristic thermal stability temperatures and molecular weights [1]. In a first stage, a slight increase in molecular weight ($Mn = 1.02 \times 10^5$ g mol^{-1} at 0 days and 1.08×10^5 g mol^{-1} at 30 days) strengthens the suggestion previously drawn on molecular recombinations of smaller chains into the polymeric backbone for the action of the humidity of the soil [34], which is further supported by the increase of the Ea_{iso}, since more energy is needed to trigger the thermal decomposition. Later on, the Ea_{iso} continuously decreases, which indicates a progressive weakening of the PLA structure, related to a continuous decrease in molecular weight ($Mn = 9.1 \times 10^4$ g mol^{-1} at 150 days, 7.6×10^4 g mol^{-1} at 300 days, and 5×10^4 g mol^{-1} at 450 days) as a consequence of the degradation in soil subjected, as it was shown [1]. These changes support the hypothesis previously drawn, which considered modifications on the thermal decomposition mechanism as a degradation in soil effect, as it is shown as follows.

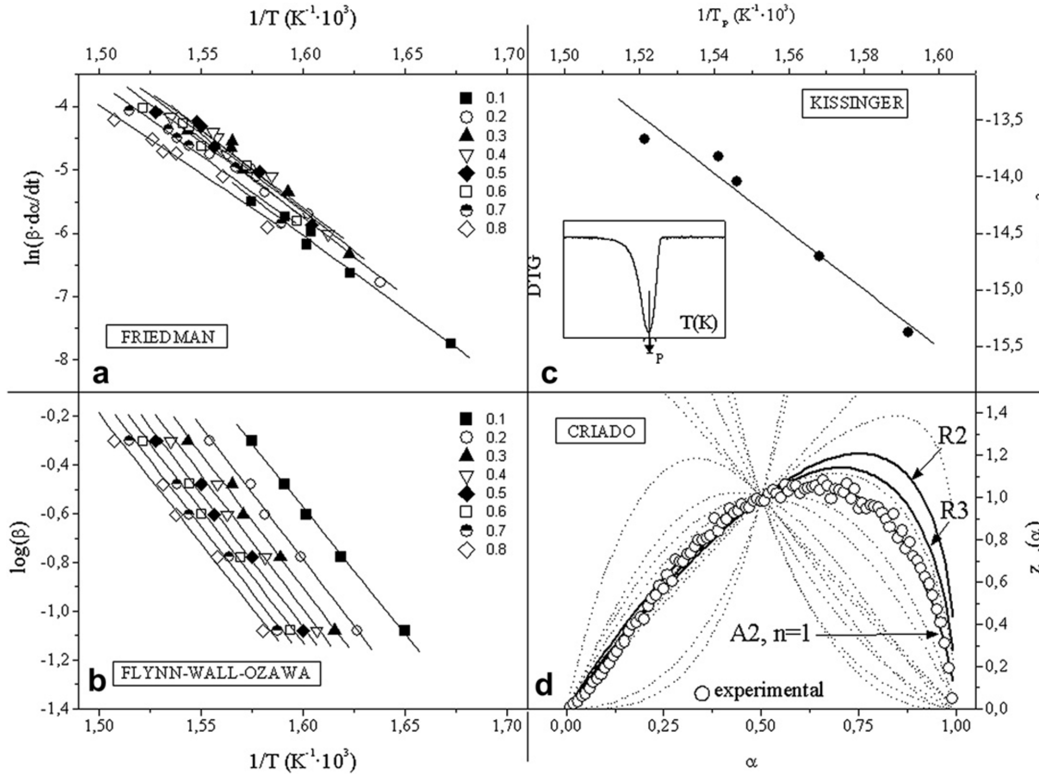

Fig. 4. Kinetic methods applied to non-degraded PLA. a) Friedman method; b) Flynn-Wall-Ozawa method. c) Kissinger method. d) Criado method.

Concerning the completion of the kinetic triplet, the kinetic model function f (α), and the pre-exponential factor (A) should be obtained. Criado method has been applied for all the theoretical f (α) related at Table 1. Fig. 4 (d) shows the comparison of the reduced Criado functions of non-buried PLA to the master-curves for the experiments carried out at the slower heating rate (5 °C·min^{-1}), which are supposed to offer more accurate results [23]. This method allows for the discrimination of the most possible kinetic models which can explain the thermal decomposition behaviour of polymers. Nevertheless, a parallel evaluation of the apparent activation energies Ea is required to verify the chosen kinetic function f (α). Among the different methods that calculate the Ea from a given f (α), Coats-Redfern method has been demonstrated to offer the most precise results [35]. In that way, the results of the combination of the analyses performed by means of the application of Criado, Coats-Redfern and the isoconversional methods are shown at Table 3, together with the kinetic triplet obtained and the corresponding physical thermal decomposition model for each soil burial time. The knowledge of the complete kinetic triplet allows mathematically describing the thermal degradation process at any time of the soil burial experiment. As can be seen at Fig. 6, the theoretical kinetic models drawn from the analysis to all samples perfectly fit to the thermogravimetric experimental data.

The kinetic analysis methodology has permitted to accurately model the thermal decomposition process along the degradation in soil test. The kinetic triplet interpretation eases the complexity of the decomposition processes taking place, and permits to relate the changes induced by degradation in soil to the changes in the morphology of the bulk PLA. The non-buried PLA thermal decomposition mechanism is described by a Nucleation model (A2). This kind of kinetic model is quite common in crystallization processes, but have only been observed in few studies dealing with thermal decomposition processes of polymers [36–42]. In these studies, the controversy of the relationship between the mathematical models and the physical mechanisms is patent. Even being aware of the limitations of these studies, a physical approach of the influence of degradation in soil on the bulk PLA have been drawn from our kinetic analysis. Therefore, the A2 model indicates the presence of active zones (nuclei), more

Table 2
Apparent activation energies values obtained by the Friedman (Ea_F), Flynn-Wall-Ozawa (Ea_{FWO}) and Kissinger (Ea_K) methods.

	PLA_0 days			PLA_30 days			PLA_150 days			PLA_300 days			PLA_450 days		
α	Ea_F (kJ mol^{-1})	Ea_{FWO} (kJ mol^{-1})	Ea_K (kJ mol^{-1})	Ea_F (kJ mol^{-1})	Ea_{FWO} (kJ mol^{-1})	Ea_K (kJ mol^{-1})	Ea_F (kJ mol^{-1})	Ea_{FWO} (kJ mol^{-1})	Ea_K (kJ mol^{-1})	Ea_F (kJ mol^{-1})	Ea_{FWO} (kJ mol^{-1})	Ea_K (kJ mol^{-1})	Ea_F (kJ mol^{-1})	Ea_{FWO} (kJ mol^{-1})	Ea_K (kJ mol^{-1})
0.2	205.5	206.0		235.7	260.9		217.7	233.0		180.5	215.3		195.2	222.6	
0.3	207.6	212.4		259.8	261.3		224.3	241.7		201.7	218.8		199.2	214.3	
0.4	208.0	202.5	206.7	271.8	265.9	259.7	229.1	238.9	239.0	211.7	217.2	214.3	201.7	203.3	199.7
0.5	206.1	202.7		283.9	272.0		231.6	237.4		219.8	207.1		199.3	193.2	
0.6	205.4	197.0		274.8	263.9		233.9	240.3		222.5	202.5		194.8	179.7	
0.7	204.1	191.8		252.7	261.7		235.7	235.7		222.9	186.0		193.6	176.4	

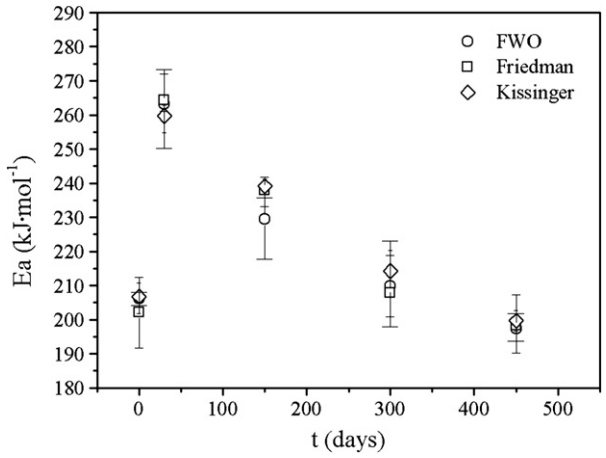

Fig. 5. Evolution of the apparent activation energy throughout the degradation in soil process.

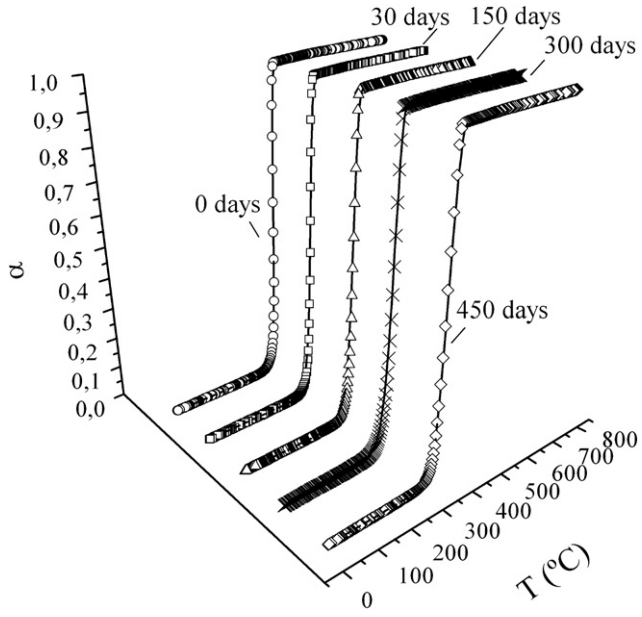

Fig. 6. Comparison of experimental TG curves (symbols) to fitted kinetic functions (solid lines) obtained from the kinetic methodology.

chemically liable to thermal decomposition [34], which activate the formation and growth of gas bubbles in the polymer melt [42]. However, the degradation in soil process alters the thermal decomposition behaviour of PLA. When PLA samples are submitted to the accelerated soil burial test, changes in the kinetic triplet are involved, due to the humidity and the presence of micro-organisms, which mainly induce chemical changes in the polymeric structure [43–46]. In this first stage, humidity may affect the PLA structure and the effect of ingestion and coalescence nuclei processes could difficult the molecules release and produce a change in the thermal decomposition mechanism, which may be primarily controlled by a Reaction Contracting model (R3). This model explains the thermal decomposition in a generalized fashion throughout the bulk PLA, where the gas release is controlled in the phase boundaries. After this first stage, the thermal decomposition mechanism remains being described by an R3 model but, due to the continuous interaction between the polymer and the degrading environment, low molecular weight compounds might be released. Hence, the characteristic temperatures and the Ea_{iso} of the thermal decomposition process show a decrease, which is a sign of the progressive weakening of PLA structure, since it requires lower energy to activate its thermal decomposition process as longer is PLA submitted to degradation in soil. The R3 kinetic model is maintained during almost 300 days but after this time, in agreement with the morphological variations stated by the DSC and DMTA results [1], a rearrangement of chains into weaker conformations is produced and the generalized decomposition may be therefore disabled, giving relevance to the decomposition in specific sites (nuclei) and thus the thermal decomposition process is again governed by an A2 Nucleation model.

Table 3
Results of kinetic methodology. Evolution of kinetic triplet of PLA thermal decomposition throughout the degradation in soil process.

PLA degradation in soil								
Burial in soil	Criado analysis	Coats-Redfern analysis			Isoconversional analysis	Kinetic triplet Decomposition mechanism		
Time (days)	f (α) scope reduction	Ea (kJ mol−1)	lnA (s−1)	R2	Average Ea (kJ mol−1)	f (α)	Ea (kJ mol−1)	lnA (s−1)
0	$n = 1$	378.7	67.4	0.998	205.0	A2	205.0	46.1
	A2	205.1	46.1	0.999		Nucleation		
	R2	318.9	55.0	0.997				
	R3	337.7	58.3	0.998				
30	$n = 1$	300.3	50.3	0.998	262.4	R3	262.4	43.0
	A2	161.1	37.4	0.995		Reaction		
	R2	244.9	40.6	0.998		Contracting volume		
	R3	259.3	43.0	0.999				
150	$n = 1$	240.4	40.2	0.956	232.5	R3	232.5	36.9
	A2	135.7	32.2	0.949		Reaction		
	R2	224.7	36.3	0.969		Contracting volume		
	R3	229.8	36.9	0.975				
300	$n = 1$	253.9	43.5	0.985	210.7	R3	210.7	34.8
	A2	142.4	33.6	0.987		Reaction		
	R2	227.0	36.9	0.993		Contracting volume		
	R3	214.6	34.8	0.996				
450	$n = 1$	354.7	62.1	0.997	198.4	A2	198.4	43.1
	A2	193.2	43.1	0.997		Nucleation		

5. Conclusions

Commercial polylactide was buried in active soil in order to mimic its disposal stage following an international standard, and the changes in their physical and chemical properties were assessed by Thermal Analysis techniques. The research in this second paper focuses on the thermal stability and thermal decomposition kinetics of PLA. Multi-rate linear-non-isothermal thermogravimetric experiments have been performed and indicators for monitoring the influence of degradation in soil on the bulk PLA have been proposed.

A single thermal decomposition stage has been stated for all PLA degraded in soil samples, regardless the burial time and the heating rate employed. The effect of degradation in soil on PLA thermal stability has been evaluated in terms of onset, endset and the peak decomposition temperatures. All temperature indicators follow the same double-stage behaviour: a first increase related to the major degrading activity in the polymer; and a continuous attenuated decay along the degradation in soil process. These changes have been also assessed by the evolution of the apparent activation energy, being in this case the difference between both stages more noticeable. The correlation of these parameters to the evolution observed for the molecular weight strengthens the usefulness of thermogravimetry as a means for monitoring the influence of degradation on polymers.

A kinetic analysis methodology, consisting in the combination of five different methods (namely Friedman, Flynn-Wall-Ozawa, Kissinger, Criado and Coats-Redfern) has been successfully applied and has allowed the determination of the PLA kinetic triplet evolution throughout the degradation in soil process. The PLA thermal decomposition mechanism is influenced, since it can be described by two competitive different decomposition models: on the one hand, a Nucleation model (A2), which gives importance to specific decomposition sites; and on the other hand, a Reaction Contracting model (R3), which represents a particles release generalized on the whole polymer surface. Therefore, the knowledge of the thermal decomposition model at each degradation stage has permitted to interpret from a macroscopic point of view the degradation in soil consequences on PLA bulk morphology.

Acknowledgements

The authors would like to acknowledge the Ministerio de Educación y Ciencia (Spanish Government) and the European Regional Development Fund for the economical support through the Project ENE2007/67584/C03-02 and the research position granted through the FPU pre-doctoral program to J.D. Badía. The Ministerio of Ciencia e Innovación is acknowledged by L.Santonja-Blasco and Rosana Moriana for the research position by means of the FPI pre-doctoral programme.

References

[1] Santonja-Blasco L, Moriana R, Badía JD, Ribes-Greus A. Thermal analysis applied to the characterization of degradation in soil of polylactide: I. Calorimetric and viscoelastic analyses. Polymer Degradation and Stability 2010;95:2185–91.
[2] Tsuji H, Doi Y, Steinbückel A, editors. Biopolymers. Polyesters III. Applications and commercial products. Weinheim: Wiley-VCH Verlag GmbH; 2002.
[3] Auras R, Harte B, Selke S. An overview of polylactides as packaging materials. Macromolecular Bioscience 2004;4:835–64.
[4] Gupta AP, Kumar V. New emerging trends in synthetic biodegradable polymers-polylactide: a critique. European Polymer Journal 2007;43(10):4053–74.
[5] Holland SJ, Tighe BJ. Biodegradable polymers in advances in pharmaceutical sciences. London: Academic Press London; 1992.
[6] Bogaert JC, Coszach P. Poly(lactic acids): a potential solution to plastic waste dilemma. Macromolecular Symposia 2000;153:287.
[7] Dorgan JR, Lehermeier HJ, Palade LI, Cicero J. Thermal and rheological properties of commercial-grade poly(lactic acid)s. Macromolecular Symposia 2001;175:55.
[8] Tsuji H, Ikada Y. Crystallization from the melt of poly(lactide)s with different optical purities and their blends. Macromolecular Chemistry and Physics 1996;197:3483.
[9] Sarasua JR, Prud'homme RE, Wisniewski M, Le Borgne A, Spassky N. Crystallization and melting behavior of polylactides. Macromolecules 1998;31:3895.
[10] Miyata T, Masuko T. Crystallization behaviour of poly (L-lactide). Polymer 1998;39:5515.
[11] Dattaa R, Tsaia SP, Bonsignorea P, Moona SH, Frank JR. Technological and economical potential of poly(lactic acid) and lactic acid derivatives. FEMS Microbiology Reviews 1995;16:221.
[12] Vink ETH, Rabago KR, Glassner DA, Gruber PR. Applications of life cycle assessment to nature works polylactide (PLA) production. Polymer Degradation and Stability 2003;80(3):403–19.
[13] Santonja-Blasco L, Contat-Rodrigo L, Moriana-Torró R, Ribes-Greus A. Thermal characterization of polyethylene blends with a biodegradable masterbatch subjected to thermo-oxidative treatment and subsequent soil burial test. Journal of Applied Polymer Science 2007;106:2218–30.
[14] Moriana-Torró R, Contat-Rodrigo L, Santonja-Blasco L, Ribes-Greus A. Thermal characterisation of photo-oxidized HDPE/Mater-Bi and LDPE/Mater-Bi blends buried in soil. Journal of Applied Polymer Science 2008;109:1177–88.
[15] Torres A, Li SM, Roussos S, Vert M. Poly(lactic acid) degradation in soil or under controlled conditions. Journal of Applied Polymer Science 1998;62 (13):2295–302.
[16] Hakkarainen M. Aliphatic polyesters: abiotic and biotic degradation and degradation products. Advances in Polymer Science 2002;157:113–38.
[17] Ho KGL, Pometto AL, Hinz PN. Effects of temperature and relative humidity on polylactic acid plastic degradation. Journal of Environmental Polymer Degradation 1999;7:83–92.
[18] Mc Neill IC, Leiper HA. Degradation studies of some polyesters and polycarbonates. II: polylactide: degradation under isothermal conditions, thermal degradation mechanism and photolysis of the polymer. Polymer Degradation and Stability 1985;11(4):309–26.
[19] Ramis XC, Salla JM, Morancho JM, Vallés A, Contat L, Ribes A. Thermal degradation of polypropylene/starch-based materials with enhanced biodegradability. Polymer Degradation and Stability 2004;86:483–91.
[20] Alvarez VA, Vázquez A. Thermal degradation of cellulose derivatives/starch blends and sisal fibre biocomposites. Polymer Degradation and Stability 2004;84:13–21.
[21] Wunderlich B, editor. Thermal analysis of polymeric materials. Berlin: Springer; 2005.
[22] Khawam A, Flanagan DR. Solid-state kinetic models: basics and mathematical fundamentals. Journal of Physical Chemistry Part B 2006;110:17315–28.
[23] Techniques and Applications. In: Brown M, editor. Introduction to thermal analysis. 2nd ed. Secaucus, NJ, USA: Kluwer Academic Publishers; 2001.
[24] Brown ME, Vyazovkin S, Nomen R, Sempere J, Burnham A, Opfermann J, et al. Computational aspects of kinetic analysis. Part A: the ICTAC kinetics project-data, methods and results. Thermochimica Acta 2000;355:125–43.
[25] Friedman HL. Kinetics and gaseous products of thermal decomposition of polymers. Journal of Macromolecular Science Part A 1967;1(1):57–79.
[26] Flynn JH, Wall LA. A quick, direct method for the determination of activation energy from thermogravimetric data. Journal of Polymer Science 1966; 4:323–42.
[27] Ozawa T. Kinetic analysis of derivative curves in thermal analysis. Journal of Thermal Analysis 1970;2:301.
[28] Doyle CD. Series approximations to the equation of thermogravimetric data. Nature 1965;207:290.
[29] Kissinger HE. Reaction kinetics in differential thermal analysis. Analytical Chemistry 1957;29(11):1702–6.
[30] Criado JM. Kinetic analysis of DTG data from master curves. Thermochimica Acta 1978;24:186–9.
[31] Coats AW, Redfern JP. Kinetic parameters from thermogravimetric data. Nature 1964;68(201):4914.
[32] Moriana Rosana, Badia JD., Santonja-Blasco L, Ribes-Greus A. Assessing the mechanical enhancement and the thermostabilising effect of adding cotton fibres to a starch-based matrix using thermal analysis, in preparation.
[33] ISO 846, 1997. Plastics – determination of behaviour under the action of microoganisms. Evaluation by visual examination or measurement of changes in mass or physical properties.
[34] Liua X, Zoub Y, Lia W, Caoa G, Chen W. Kinetics of thermo-oxidative and thermal degradation of poly(D, L-lactide) (PDLLA) at processing temperature. Polymer Degradation and Stability 2006;91(12):3259–65.
[35] Pérez-Maqueda LA, Sánchez-Jiménez PE, Criado JM. Kinetic analysis of solid-state reactions: precision of the activation energy calculated by integral methods. International Journal of Chemical Kinetics 2005;37:658–66.
[36] Stoeva St, Gjurova K, Zagorcheva M. Thermal analysis study on the degradation of the solid-state chlorinated poly (ethylene). Polymer Degradation and Stability 2000;67:117–28.
[37] Li L, Guan C, Zhang A, Chen D, Qing Z. Thermal stabilities and the thermal degradation kinetics of polyimides. Polymer Degradation and Stability 2004;84:369–73.
[38] Sun JT, Huang YD, Gong GF, Cao HL. Thermal degradation kinetics of poly (methylphenylsiloxane) containing methacryloyl groups. Polymer Degradation and Stability 2005;91:339–46.
[39] Meng X, Huang Y, Yu H, Lu M. Thermal degradation kinetics of polyimide containing 2,6-benzobisoxazole units. Polymer Degradation and Stability 2007;92:962–7.

[40] Chen Y, Wang Q. Thermal oxidative degradation kinetics of flame-retarded polypropylene with intumescent flame-retardant master batches in situ prepared in twin-screw extruder. Polymer Degradation and Stability 2007;92:280–91.
[41] Budrugeac P, Segal E, Pérez-Maqueda LA, Criado JM. The use of the IKP method for evaluating the kinetic parameters and the conversion function of the thermal dehydrochlorination of PVC from non-isothermal data. Polymer Degradation and Stability 2004;84(2):311–20.
[42] Grausea G, Ishibashia J, Kamedaa T, Bhaskarb T, Yoshioka T. Kinetic studies of the decomposition of flame retardant containing high-impact polystyrene. Polymer Degradation and Stability 2010;95:1129–37.
[43] Proikakis CS, Mamouzelos NJ, Tarantili PA, Andreopoulos AG. Swelling and hydrolytic degradation of poly(D, L-lactic acid) in aqueous solutions. Polymer Degradation and Stability 2006;91(3):614–9.
[44] Zhang X, Wyss UP, Pichora D, Goosen MFA. An investigation of poly (lactic acid) degradation. Journal of Bioactive and Compatible Polymers 1994;9:80.
[45] Gupta AP, Deshmukh VG. Thermal oxidative degradation of poly-lactic Acid; Part I: activation energy of thermal degradation in air. Colloid and Polymer Science 1982;260:11.
[46] Kopinke FD, Remmler M, Mackenzie K, Möder M, Wachsen O. Thermal decomposition of biodegradable polyesters—II. Poly(lactic acid). Polymer Degradation and Stability 1996;53(3):329–42.

A Thermogravimetric Approach to Study the Influence of a Biodegradation in Soil Test to a Poly(lactic acid)

*J. D. Badía, R. Moriana, L. Santonja-Blasco, A. Ribes-Greus**

Summary: An amorphous grade Poly (lactic acid) (PLA) was selected for an accelerated burial in soil test during 450 days. Thermogravimetric analyses were carried out to study the effects of degradation in soil on the thermal stability and the thermal decomposition kinetics. A single stage decomposition process is observed for all degradation times. It is shown that the thermal stability of PLA is slightly affected by degradation in soil. Concerning the study of the thermal decomposition kinetics, Criado master curves were plotted from experimental data to focus the study of the thermodegradation kinetic model.The kinetic methods proposed by Broido and Chang were used to calculate the apparent activation energies (Ea) of the degradation mechanism. These results were compared to the Ea values obtained by the method developed by Coats and Redfern in order to prove the applicability of the former methods to the kinetic study. As expected, non-linear tendency is found out for Ea variation along the degradation times, which can be explained as an evolution by stages.

Keywords: activation energy; biodegradation in soil; kinetics (polim.); poly(lactic acid); thermogravimetry analysis (TGA)

Introduction

Poly(lactic acid) (PLA) is a well-known green polymer, since it can be obtained from renewable resources and can be compostable when its service life has finished. Last decades it is been widely employed because of its biomedical and pharmaceutical applications.[1] Its good mechanical and gas barrier qualities also confer on the polymer the capability to compete with other commodities such as PE, PS or PET at the packaging sector.[2] Although this application is not well established yet, the increasing interest in PLA will raise the consumption ratios and therefore the disposal problems. The knowledge of the degradation mechanisms concerning the disposal stage of PLA must be hence assessed, in order to assure the complete material loop of the biodegradable material.

Some studies have revealed that degradation in soil tests are suitable to analyze the degradation phenomena in bio-based polymers.[3–5] Thermal analysis techniques represent a powerful tool to control and monitor the degradation evolution in polymers.[6–8] In this work, thermogravimetric experiments have been performed in order to characterize the effects of a degradation in soil test on the thermal stability and the thermal decomposition kinetics of an amorphous PLA.

Theoretical Background

In an heterogeneous reaction $A(s) \rightarrow B(s) + C(g)$, the decomposition rate for

Instituto de Tecnología de Materiales. Escuela Técnica Superior de Ingeniería del Diseño. Universidad Politécnica de Valencia. Camino de Vera, s/n, 46022, Valencia (Spain)
E-mail: aribes@ter.upv.es

A(s) can be defined as follows:

$$\frac{d\alpha}{dt} = k(T) \cdot f(\alpha) \quad (1)$$

where α is the conversion degree of A(s) at time t (further defined for thermogravimetric analyses); $f(\alpha)$ is a temperature-independent function of conversion (kinetic model); and $k(T)$ is a temperature-dependent function assumed as an Arrhenius equation:

$$k(T) = A \cdot \exp\left(\frac{-Ea}{R \cdot T}\right) \quad (2)$$

where A is the frequency factor (also called pre-exponential factor); R is the ideal gases constant (8.31 $J \cdot mol^{-1} \cdot K^{-1}$); T is the temperature; and Ea is the activation energy of the equation. Substituting the Arrhenius equation into Equation (1), we obtain:

$$\frac{d\alpha}{dt} = A \cdot \exp\left(\frac{-Ea}{R \cdot T}\right) \cdot f(\alpha) \quad (3)$$

If the temperature of a sample varies as a function of a controlled and constant value of heating rate β ($\beta = dT/dt$), the decomposition rate can be expressed as a function of the temperature:

$$\frac{d\alpha}{dT} = \frac{A}{\beta} \cdot \exp\left(\frac{-Ea}{R \cdot T}\right) \cdot f(\alpha) \quad (4)$$

Separating variables, rearranging and integrating Equation (4), we obtain:

$$g(\alpha) = \int_{\alpha_0}^{\alpha_f} \frac{d\alpha}{f(\alpha)} = \frac{A}{\beta} \cdot \int_{T_0}^{T_f} \exp\left(\frac{-Ea}{R \cdot T}\right) \cdot dT \quad (5)$$

For thermogravimetric experiments, the conversion degree is defined as:

$$\alpha = \frac{m_0 - m}{m_0 - m_f} \quad (6)$$

where m is the mass of the sample at time t; and 0 and f represent the initial and final times, respectively.

In this article, several fitting methods have been employed, which are described as follows. By representing the lefth-hand of Equation (7), Equation (8) and Equation (9) versus 1/T, the Ea can be obtained from the slope of the different plots.

Chang Method[9]

Assuming $f(\alpha) = (1-\alpha)^n$, being n the reaction order into Equation (3), rearranging and taking logarithms, Chang proposed the following differential model:

$$\ln\left(\frac{\frac{d\alpha}{dt}}{(1-\alpha)^n}\right) = \ln A - \frac{Ea}{R \cdot T} \quad (7)$$

Broido Method[10]

This method is valid for $n = 1$ and employs the following model:

$$\ln\left(\ln\left(\frac{1}{1-\alpha}\right)\right) = \frac{-Ea}{R \cdot T} + \ln\left(\frac{R \cdot C}{Ea \cdot \beta} \cdot T_m^2\right) \quad (8)$$

where C is an integration constant and T_m the temperature of the maximum reaction velocity.

Coats-Redfern Method[11]

This model applies an asymptotic approximation to solve Equation (5) at different conversion values. If $(2RT/Ea) \rightarrow 0$ is true for the Doyle approximation,[12] and taking natural logarithms, the model adopts the following form:

$$\ln\frac{g(\alpha)}{T^2} = \ln\left(\frac{A \cdot R}{\beta \cdot Ea}\right) - \frac{Ea}{R \cdot T} \quad (9)$$

Criado Method[13]

By combining Equation (3) and (9) without logarithms, Criado described the obtaining of reduced master curves of the type:

$$\frac{z(\alpha)}{z(0.5)} = \frac{f(\alpha) \cdot g(\alpha)}{f(0.5) \cdot g(0.5)} = \left(\frac{T}{T_{0.5}}\right)^2 \cdot \frac{\left(d\alpha/dt\right)}{\left(d\alpha/dt\right)_{0.5}} \quad (10)$$

where 0.5 refers to the conversion degree of 0.5. The left-hand of the Equation (10) is the reduced theoretical curve, which is

characteristic of each reaction mechanism, whereas the right-hand is associated with the reduced decomposition rate and can be obtained from the experimental data. A comparison of both sides of Equation (10) indicates the kinetic model which best describes the experimental decomposition process.

Experimental Part

PLA with a 3.8% of meso-lactide content samples (supplied by Natureworks.DDL, Minnetonka, U.S.A) were submitted to accelerate soil burial test in a culture oven Heraeus 12 at 28 ± 0.5°C during 450 days following the DIN 53739 standard.[14] Specimens extracted at 0, 30, 150, 300 and 450 days were analyzed by thermogravimetry. Measures were carried out in a Mettler-Toledo TGA/SDTA 851, from 25 to 750 °C at a heating rate of 20 °C/min, under Ar atmosphere.

Results and Discussion

Thermal Stability

Figure 1 (a,b) illustrates the thermogravimetric curves and derivative thermogravimetric curves (in advanced called TG and

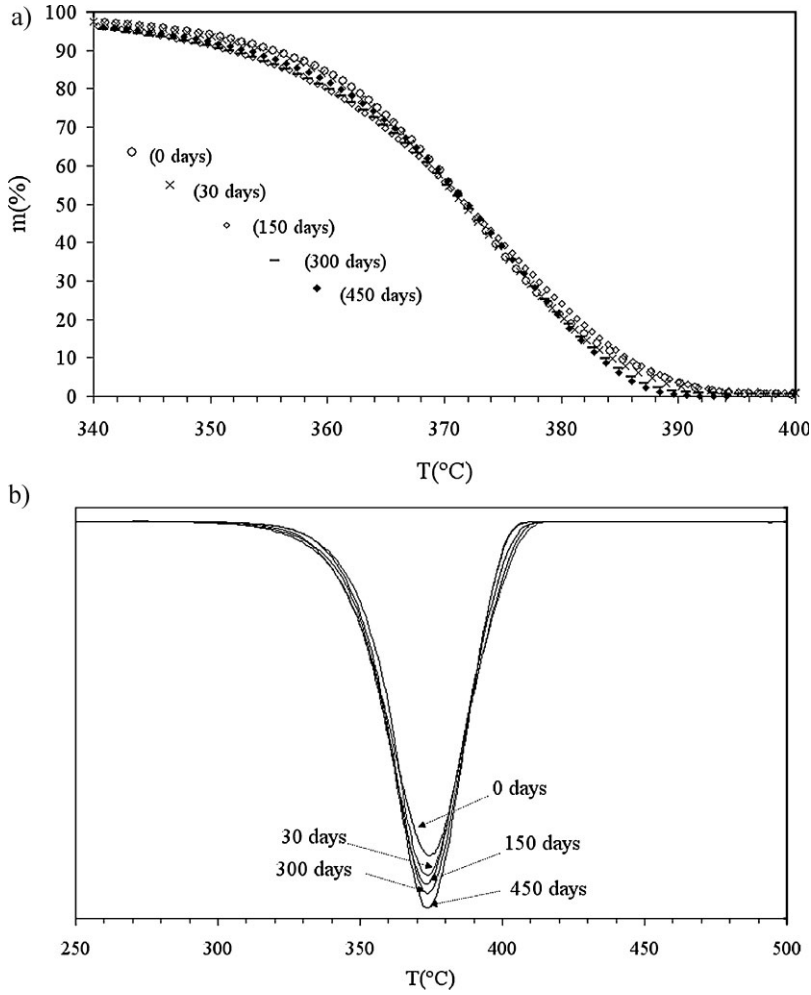

Figure 1.
TG (a) and DTG (b) curves of PLA thermal degradation.

DTG, respectively), of the thermal decomposition of PLA for all the degradation in soil times. The DTG curves show only one maximum, which is related to a single-stage decomposition process, regardless of the degradation time studied. The DTG temperature peak (T_{peak}), the degradation onset (T_{onset}) and endset (T_{endset}), as well as the temperature range between T_{onset} and T_{endset} (ΔT_{deg}), were selected as characterization parameters. Results are listed at Table 1.

There are not remarkable changes in the T_{peak} as the exposure in soil time becomes longer, whereas the T_{onset} evolution presents a slight overall decrease. Regarding the T_{endset} tendency, an approx. 8 °C decrease is seen, with leads to sharpen the degradation temperatures interval. It might be explained as an effect of biodegradation in soil, which produces chain scission processes to the polymer that seems to slightly decrease the thermal resistance of PLA, according to literature.[15] However, no conclusions should be given out yet, since little changes at the degradation temperatures are seen after 450 days.

Thermal Decomposition Kinetics

According to the literature, several molecular as well as radical reactions are involved in PLA decomposition, mainly considering non-radical intra or intermolecular exchange reactions involving –OH groups, as well as cis-elimination or radical and non-radical concerted reactions.[15] The characterization of the thermal decomposition mechanism is hence complicated, due to the relative action of all the competitive reactions above mentioned.

Nonetheless, it is generally possible to mathematically study the overall decomposition process kinetics from the TG-DTG data of polymers [16]. In that sense, several methods which can be applied to a single TG run have been chosen (Criado, Broido, Chang and Coats-Redfern) as a first approach of the problem. The apparent activation energy (Ea) of the thermal decomposition mechanisms is the monitoring parameter selected to assess the effects of degradation in soil. Since the conversion degree related to the maximum decomposition rate (which corresponds to the DTG peak temperature, T_{peak}) is 0.6, all kinetic measurements have been performed in the interval $\alpha\,\varepsilon\,(0.01–0.6)$.

Criado master curves were plotted from experimental data to focus the study of the thermodegradation kinetics. Figure 2 shows the comparison between the experimental curves of the original and the last tested samples (0 and 450 days) with the theoretical master curves. It is seen that curves lie between the theoretical curves for $f(\alpha) = (1–\alpha)^n$ with reaction order n between 1 and 1.5, behavior proved for all times of exposure in soil studied.

In order to evaluate the differences between employing $n = 1$ or $n = 1.5$ to describe the thermodegradation mechanism at each degradation time studied, the kinetic methods developed by Broido (for $n = 1$) and Chang (for $n = 1$ and $n = 1.5$) to obtain the Ea of the thermodegradation process were applied. The results were compared to the Ea values obtained by the kinetic method worked out by Coats and Redfern, which is considered as reference by many authors.[16–18] Table 2 lists the Ea values obtained by all methods and reaction

Table 1.
Thermal stability parameter of PLA submitted to soil burial test.

Burial in soil time (days)	T_{onset} (°C)	T_{endset} (°C)	T_{peak} (°C)	ΔT_{deg} (°C)
0	360,4	415,0	373,6	54,5
30	358,0	412,9	373,2	54,8
150	356,4	411,0	374,5	54,6
300	356,4	407,8	373,8	51,4
450	358,9	407,8	373,6	48,4

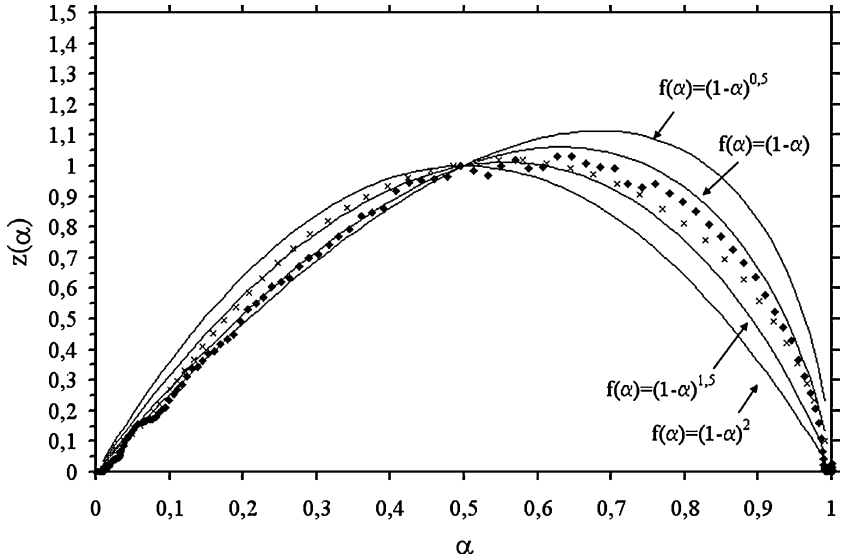

Figure 2.
Comparison of the experimental data of virgin (X) and 450 days (◆) buried PLA with the theoretical master curves.

orders for PLA at all times of exposure in soil studied. The behaviour of the Ea evolution plotted by each methodology is shown at Figure 3.

Regarding the Ea values, they should be defined between the Ea boundary values obtained by the Coats-Redfern method for $n = 1$ and $n = 1.5$. The differences observed in Ea values from each kinetic method might be attributed to the different mathematical approaches employed at each one.[16] Although neither Chang method nor Broido one provide Ea values in that region, the later shows exactly the same Ea tendency as the evolution described by the Ea calculated by Coats-Redfern method. It could be hence solved that to approach the reaction order to $n = 1$ and to use Broido method is useful, due to the qualitative interpretation of the influence of degradation in soil on the Ea of the thermal decomposition kinetics of PLA does not change.

Concerning the Ea evolution behaviour, no linear trend was established for the Ea variation along the degradation in soil time. As it is been proved to other polymers submitted to soil burial test,[3] the Ea evolution evidences a behaviour by stages, with an underlying overall 20% decrease.

Table 2.
Activation energies obtained by the Broido, Chang and Coats-Redfern methods for PLA at all exposure in soil times analyzed.

Burial in soil time (days)	$n = 1$			$n = 1.5$	
	Ea (Broido) (kJ/mol)	Ea (Chang) (kJ/mol)	Ea (Coats-Redfern) (kJ/mol)	Ea (Chang) (kJ/mol)	Ea (Coats-Redfern) (kJ/mol)
0	387	315	324	318	344
30	379	352	317	332	337
150	313	236	262	239	278
300	311	275	266	284	281
450	336	241	279	244	295

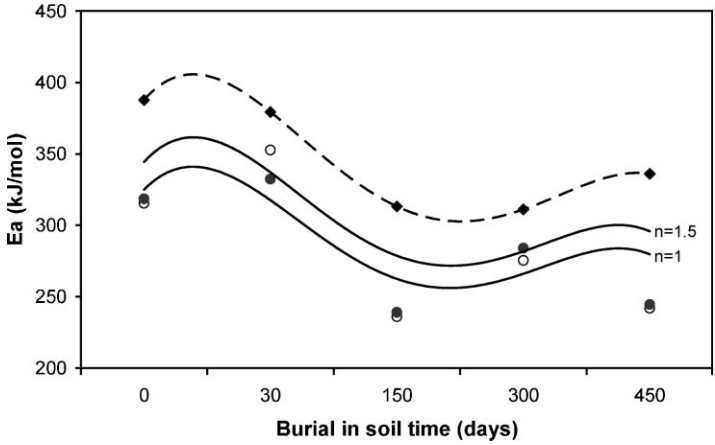

Figure 3.
Ea evolution shown by the different kinetic methodologies (Coats-Redfern: –; Broido: -◆-; Chang with $n = 1$: ○, and with $n = 1.5$: ●).

Conclusion

The thermodegradation mechanism is governed by a single-stage decomposition process regardless of the burial in soil time studied, which can be modelled by a kinetic function $f(\alpha) = (1-\alpha)^n$ with n between 1 and 1.5.

The Ea evolution can be qualitatively explained by using the Coats-Redfern and Broido methods, which describe the same behaviour. As expected, non-linear tendency is found out for Ea variation along the exposure in soil time, which may be understood as an evolution by stages, which overall decreases.

The thermal resistance of PLA has not been too affected by degradation in soil after 450 days of experiment, due to its thermal properties have not significantly changed.

Acknowledgements: The authors would like to acknowledge the Ministerio de Educación y Ciencia (Spanish Government) and the European Regional Development Fund for the economical support through the Project CTM2004-04977/TECNO and for the concession of the pre-doctoral grants through the programmes FPI and FPU.

[1] H. Tsuji, Polylactides, Biopolymers. in: *Polyesteres III. Applications and Commercial Products*, Y. S. Doi, A., Eds., Wiley-VCH, Weinheim **2002**, p. 129–177.
[2] N. H. Naitove, *Plast. Tech.* **1998**, *44*, 13.
[3] L. Santonja-Blasco, et al. Thermal characterization of polyethylene blends with a biodegradable masterbach subjected to thermo-oxidative treatment and subsequent soil burial test. *Journal of Applied Polymer Science*, **2007**, Pendent of publication.
[4] L. Contat-Rodrigo, A. Ribes-Greus, Thermal and Viscoelastic Properties of some commercial Starch products. *Journal of Applied Polymer Science* **2003**, *88*, 1242–1251.
[5] L. Contat-Rodrigo, A. Ribes-Greus, Biodegradation Studies of LDPE Filled with Biodegradable Additives: Morphological Changes. I. *Journal of Applied Polymer Science* **2002**, *83*, 1683–1691.
[6] F. Vilaplana, A. Ribes-Greus, S. Karlsson, Degradation of recycled high-impact polystyrene. Simulation by reprocessing and thermo-oxidation. *Polymer Degradation and Stability* **2006**, *91*(9), 2163–2170.
[7] F. Vilaplana, A. Ribes-Greus, S. Karlsson, Analytical strategies for the quality assessment of recycled high-impact polystyrene: A combination of thermal analysis, vibrational spectroscopy, and chromatography. *Analytical Chimica Acta*, Available online 27 April **2007**, In Press, Corrected Proof.
[8] L. Contat-Rodrigo, A. Ribes-Greus, C. T. Imrie, Thermal Analysis of High-Density Polyethylene and Low-Density Polyethylene with Enhanced Biodegradability. *Journal of Applied Polymer Science* **2002**, *86*, 764–772.
[9] W. L. Chang, *J. of Apply. Polym. Sci.* **1994**, *53*, 1759.
[10] A. Broido, A simple, sensitive graphical method of treating thermogravimetric analysis data. *Journal of Polymer Science Part A-2: Polymer Physics* **1969**, *7*(10), 1761–1773.
[11] A. Coats, A. Redfern, *Nature* **1964**, *68*(201), 4914.
[12] C. D. Doyle, *Nature* **1965**, *207*, 290.
[13] J. M. Criado, Kinetic Analysis of DTG data from master curves. *Thermochimica Acta* **1978**, *24*, 186–189.

[14] DIN 53739. Testing of Plastics. Influence of fungi and bacteria. Visual Evaluation. Change in Mass and Physical Properties. **1984**.
[15] F. D. Kopinke,, et al. Thermal decomposition of biodegradable polyesters–II. Poly(lactic acid). *Polymer Degradation and Stability* **1996**, *53*(3), 329–342.
[16] M. Brown, *Introduction to Thermal Analysis. Second Edition. Techniques and Applicattions*, Kluwer Academic Publishers, Secaucus, NJ, USA **2001**.
[17] X. C. Ramis, A. Salla, J. M. Morancho, A. Vallés, L. Contat, A. Ribes, Thermal Degradation of Polypropylene/starch-based materials with enhanced biodegradability. *Polymer Degradation & Stability* **2004**, *86*, 483–491.
[18] B. Z. Liu, X. Wang, F. Wang, Thermal Degradation Kinetics of Poly(propylene carbonate) Obtained from the Copolymerization of Carbon Dioxide and Propylene Oxide. *J. of Apply. Polym. Sci.* **2003**, *90*, 947–953.

Thermal Characterisation of Photo-Oxidized HDPE/Mater-BI and LDPE/Mater-BI Blends Buried in Soil

R. Moriana-Torró, L. Contat-Rodrigo, L. Santonja-Blasco, A. Ribes-Greus

Instituto de Tecnología de Materiales, Escuela Técnica Superior de Ingeniería del Diseño, Universidad Politécnica de Valencia, 46071 Valencia, Spain

Received 21 March 2007; accepted 21 January 2008
DOI 10.1002/app.28171
Published online 15 April 2008 in Wiley InterScience (www.interscience.wiley.com).

ABSTRACT: Blends of high and low density polyethylene with a commercial biodegradable material (Mater-Bi) were subjected to an accelerated soil burial test. A set of samples was previously photo-oxidized to evaluate the effects of UV-irradiation on the degradation in soil process of these blends. Thermogravimetric as well as calorimetric analysis were performed to study the biodegradation, photo-degradation and their synergetic effects. Differential scanning calorimetry was carried out to analyze the morphological changes as a consequence of the photo-oxidation process. UV-irradiation slightly modifies the crystalline content of HDPE/Mater-Bi blends, increasing the heterogeneity of this blend. Criado master curves were plotted to analyses the degradation kinetic model. Broido and Coats-Redfern methods have been used for calculating the Ea of the thermal decomposition mechanisms. Thermogravimetric results reveal that noncomplexed starch is more affected by biodegradation than the polyethylene matrix and the starch/EVOH complexes chains from Mater-Bi. However, the effects of both photo-oxidation and biodegradation processes on the thermal decomposition of Mater-Bi is influenced by the polymeric matrix used. Previous photo-oxidation finds to slow down the degradative effects caused by the soil burial test on the HDPE/Mater-Bi blends. © 2008 Wiley Periodicals, Inc. J Appl Polym Sci 109: 1177–1188, 2008

Key words: thermogravimetric analysis; polyethylene; Mater-Bi; biodegradation; photo-oxidation

INTRODUCTION

The increasing problems posed by plastics waste management have stimulated the interest in developing different strategies to find out a solution to this environmental problem.[1–3] Among them, many efforts have been made these last years in promoting the development of degradable materials that could replace conventional synthetic polymers.[4–13] Although the contribution of such biodegradable polymers to the reduction of plastics waste is obvious, nowadays these materials still cannot compete from an economical point of view with conventional polymers.

A viable solution, already employed by producers, is to combine the different features and benefits of both synthetic and biodegradable materials to produce blends fulfilling the requirements of both good cost-performance ratio as well as being environmentally-friendly. This is the case of polyolefins that are still considered as one of the most important plastic materials due to their good mechanical properties and low cost but as it is well-known, they are resistant to microbial attack. Thus, blends of polyolefins with other commercial biodegradable polymers contain parts that may enhance their sensitivity to degradation. To assess the potential applications of these blends, their characterization, as well as the study of their degradation process must be performed. As it has already been shown in previous works.[14–17] Thermal Analysis can provide useful information about the irreversible changes in the properties of polymers caused by degradation in soil of polymeric materials.

In this study, blends of high and low density polyethylene with a commercial biodegradable material containing thermoplastic starch and ethylene vinyl alcohol were analyzed. Such blends were exposed to a soil burial test to study their degradation and to investigate the influence of the polyolefinic matrix. Some of these blends were subjected to photo-oxidation before the soil burial test to evaluate the effects of UV-irradiation on this biodegradation process. Thermogravimetric and calorimetric methods were used for this purpose, since they provide qualitative and quantitative information about the degradation processes of these materials. Biodegradation exhibits a complex mechanism, so that the interaction of different oxidative processes may produce a synergetic effect that may modify the biodegradation rate.

Correspondence to: Ribes-Greus (aribes@ter.upv.es).
Contract grant sponsor: Ministerio de Educación y Ciencia of Spain; contract grant number: CTM2004-04977/TECNO.

EXPERIMENTAL

Materials

Low-density polyethylene (LDPE 710) and high-density polyethylene (HDPE 10062) from Dow Chemical (Spain) were used as polymeric matrices. These polyolefins were blended with a commercial biodegradable material, Mater-Bi AF05H, supplied by Novamont North America (USA). This starch-based material contains about 60% of maize starch and natural additives, and 40% of [40/60 (mol/mol)] ethylene-vinyl alcohol copolymer (EVOH).[18]

Samples preparation

Homogeneous blends of 50/50 wt % of the corresponding polyethylene (LDPE 710 or HDPE 10062) and Mater-Bi AF05H were prepared from the molten state in a Brabender Plasti-Corder PL 2100 rheometer. The HDPE/Mater-Bi blends were processed at 170°C and the LDPE/Mater-Bi blends at 150°C. The processing time was 7 min for all the blends.

The samples for the burial test were prepared from the blends by compression molding with a Carver M press. The compression program consisted on decreasing temperature steps from 160 to 100°C for the LDPE 710/Mater-Bi blends, and from 125 to 90°C for the HDPE 10062/Mater-Bi blends. When the blends reached the final temperature a pressure step of 14 atm was applied. The resulting sheets were then submerged into cool water. Pure HDPE and LDPE samples were used as references. Finally all the samples were cut into rectangular bars with dimensions $68 \times 12 \times 1.8$ mm^3.

Photo-oxidation test

A set of samples was subjected to an accelerated photo-oxidation test before the soil burial test. Pure and blended samples were irradiated in an Atlas XLS+ Suntest with UV-radiation. Samples were exposed to a total radiation of 138,000 kJ/m^2 during 98.7 h, while they were submerged in water at 38°C, continuously pumped around in close circuit.

Soil burial test

According to the DIN 53739 international Norm,[19] samples were buried in active soil contained in plastic rectangular boxes. The soil burial test was carried out during 6 months, periodically controlling the humidity, pH and temperature of the soil. Samples were taking out after different periods of time: 20 days, 2 months, 4 months, and 6 months. Pure samples were only removed at the end of the test. Once removed, samples were washed with a soap solution to stop the degradation process.

TGA measurements

Thermogravimetric measurements were performed using a Mettler Toledo TGA/SDTA 851 analyzer. Dynamic measurements were carried out from 25 to 600°C, at a heating rate of 10°C/min under Argon atmosphere with a flow rate of 200 mL/min. The initial sample mass was between 10 and 12 mg.

Differential scanning calorimetry measurements

The DSC measurements were carried out in a Perkin–Elmer DSC-4 Calorimeter (Norwalk, CT), previously calibrated with indium standard. Samples of 6–7 mg were placed in standard aluminum pans that were sealed, pierced and scanned from 0 to 200°C, at a heating rate of 10°C/min under nitrogen atmosphere. Measurements were repeated to limit errors to ± 0.01°C for the melting temperature and ± 0.05% for the crystalline content.

RESULTS AND DISCUSSION

Samples have been initially characterized by thermogravimetric analysis. Figures 1 and 2 show the differential thermogravimetric curves of pure HDPE and LDPE, respectively. The thermograms of both pure polyethylenes display a single weight-loss zone, centered at 486.7°C for HDPE and 483.5°C for LDPE.

As it has been previously mentioned, Mater-Bi AF05H is a starch-based material that contains starch and poly(ethylene-vinyl alcohol) copolymers (EVOH). This material is a blend with complex interactions between its components.[18] Because of the

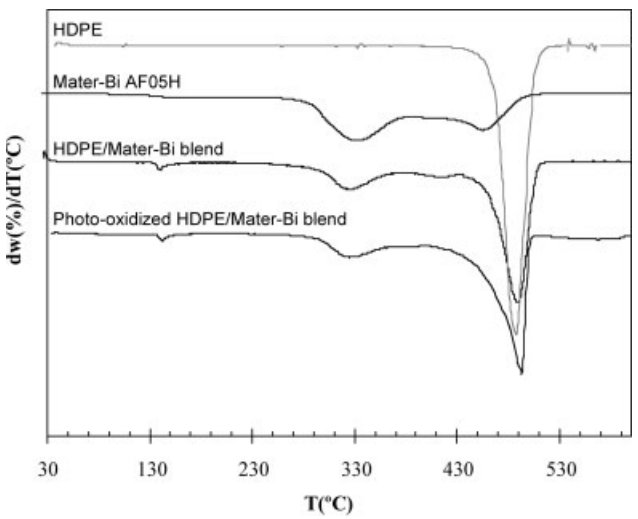

Figure 1 Differential thermogravimetric curves of pure HDPE, pure Mater-Bi AF05H, HDPE/Mater-Bi blend, and the photo-oxidized HDPE/Mater-Bi blend.

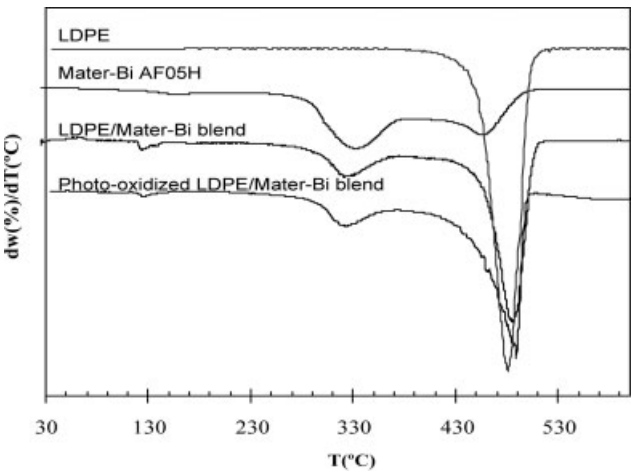

Figure 2 Differential thermogravimetric curves of pure LDPE, pure Mater-Bi AF05H, LDPE/Mater-Bi blend, and the photo-oxidized LDPE/Mater-Bi blend.

reported hydrophobic and hydrophilic interactions within starch, ethylene, and vinyl alcohol,[11,18] the differential thermogravimetric curve of this pure Mater-Bi displays multiple degradation zones (Figs. 1 and 2).

The first weight-loss region appears around 155°C and displays a mass loss of 4.6%. Such region can be attributed to the loss of low molecular weight molecules, like water absorbed by the starch or other compounds included in the Mater-Bi formulation.[4,10,20]

The second weight-loss zone appears around 260–360°C, with a peak at 331.1°C and a mass loss of 47.7%. This peak can be attributed to the pyrolysis of the starch present in the Mater-Bi, since this native polysaccharide shows a complex degradation in this temperature interval.[4,5,21,22]

The third weight-loss region is a complex zone with overlapped mechanisms that take place between 390 and 500°C. The main peak of this region appears around 455°C with a mass loss of 22.7%. Other authors related this peak to the pyrolysis of the synthetic component in Mater-Bi.[21,23,24]

According to its formulation, Mater-Bi AF05H contains 60% starch and 40% EVOH.[18] However, the experimental weight losses determined for these two components are inferior to those expected. A closer inspection of the differential thermogravimetric curve of pure Mater-Bi revealed the presence of various small shoulders overlapped to the second and third decomposition peaks, previously assigned to starch and to the synthetic component, respectively. To characterize this overlapped weight-loss region, a deconvolution method has been applied. Each individual contribution of the differential thermogravimetric curve has been fitted to the following equation:

$$y_i = A\left(\frac{1}{1+\exp\left(\frac{-(x-x_c+\frac{w_1}{2})}{w_2}\right)}\right)\left(1-\frac{1}{1+\exp\left(\frac{-(x-x_c+\frac{w_1}{2})}{w_3}\right)}\right)$$

where x_c is a position parameter related to the curve maximum, A is an amplification parameter and w_1, w_2, w_3 describe the dispersion and symmetry of the curve.

This proposed deconvolution model considers that the measured value of $(dw(\%)/dT) = y$ is equivalent to $y = y_0 + \sum_{i=1}^{n} y_i$, where y_0 is the onset of each differential thermogravimetric curve and n is the total number of deconvoluted peaks.

Figure 3 shows the application of this deconvolution method for the differential thermogravimetric curve of pure Mater-Bi. Besides from displaying the two prominent peaks centered at 335°C and 455°C, which have been previously related to the pyrolysis of starch and the ethylene chains from the synthetic component (EVOH), the deconvolution also shows two small peaks at 393°C and 421°C. These small peaks may be assigned to the pyrolysis of the rest of more thermally stable starch chains and the vinyl alcohol chains, since literature shows that pure EVOH undergoes a complex thermal degradation under inert atmosphere.[25] EVOH pyrolysis consists of two partially overlapped peaks: the first peak that can be associated to the thermal degradation of vinyl alcohol chains appears in the 390–410°C interval at a heating rate of 10°C/min; the second peak at higher temperatures (450–455°C) can be assigned to thermal degradation of the ethylene chains. Thus, as the degradation in soil process undergoes and certain chain scission of starch occurs, the evolution of these small peaks (between 390 and 450°C) may be observed.

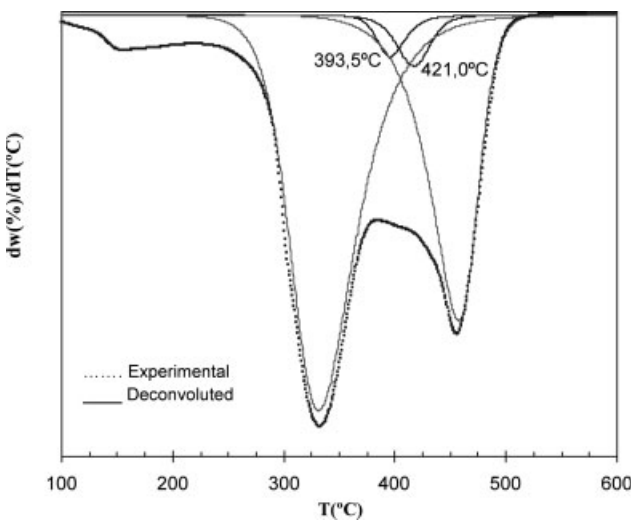

Figure 3 Deconvolution of the differential thermogravimetric curve of Mater-Bi AF05H.

TABLE I
Thermogravimetric Parameters of the HDPE/Mater-Bi Blends as a Function of the Exposure Time in Soil

	HDPE/Mater-Bi blends							
	Weight loss (%)	T Peak (°C)	Weight loss (%)	T Peak (°C)	Weight loss (%)	T Peak (°C)	Weight loss (%)	T Peak (°C)
0 days	2.0	142.0	24.7	328.0	6.6	398.0	66.0	489.0
20 days	–	–	13.0	324.0	8.7	396.0	70.0	490.0
2 months	–	–	6.0	320.0	14.7	391.0	75.1	489.0
4 months	–	–	–	–	18.0	392.6	77.0	489.0
6 months	–	–	–	–	18.0	392.0	77.2	487.2

Figures 1 and 2 also show the differential thermogravimetric curves of HDPE/Mater-Bi and LDPE/Mater-Bi blends that display several decomposition regions, which can consequently be attributed to both PE and Mater-Bi components.

As in pure Mater-Bi, the first weight loss region (around 140°C), can be assigned to the thermal decomposition of the low molecular weight compounds present in this material.

The second weight-loss (between 275°C and 435°C) is a complex region also associated to Mater-Bi contributions. For the differential thermogravimetric curves of LDPE/Mater-Bi blends only one peak centered at 328°C can be distinguished. For the HDPE/Mater-Bi blends, two peaks can be observed in this region. The first one (275–360°C) is a prominent peak, which can be attributed to the thermal degradation of most part of the starch. The second peak (360–435°C) appears as a very small shoulder that may have the origin in the pyrolysis of the more thermally stable starch chains and the vinyl alcohol chains.

The third weight-loss is located between 435 and 530°C and is the main decomposition region. Since differential thermogravimetric curves of both HDPE/Mater-Bi and LDPE/Mater-Bi blends display a single peak in this region, they must include two contributions overlapped; one of them assigned to the thermal decomposition the backbones chains of pure polyethylenes and the other to ethylene chains of Mater-Bi.

Thermogravimetric parameters of these blends are summarized in Tables I and II, respectively. The blending process does not modify the thermogravimetric parameters of both pure components. This may be an indication of the heterogeneity of polyethylenes/Mater-Bi blends.

Figures 1 and 2 also show the differential thermogravimetrics curves of photo-oxidized HDPE/Mater-Bi and LDPE/Mater-Bi blends. The thermogravimetric parameters of these photo-oxidized blends are summarized in Tables III and IV, respectively. These results show that photo-oxidation does not modify the initial weight loss region, which has been associated to the thermal decomposition of the low molecular weight compounds. However, photo-oxidation affects the pyrolysis of both Mater-Bi and the polyethylene components of the blends.

When HDPE/Mater-Bi and LDPE/Mater-Bi blends are subjected to photo-oxidation, the main thermogravimetric peak overlaps with the small shoulders at 360–435°C related to the more thermally stable starch and vinyl alcohol chains. Furthermore, an increase of the thermal stability of both blends types has been observed. In contrast, the thermal stability of the starch slightly decreases for the HDPE/Mater-Bi blend, and remains unmodified for the LDPE/Mater-Bi. These results suggest that the behavior of the starch during photo-oxidation depends on the polyolefinic matrix used.

On the other hand, derivative thermogravimetric curves of the HDPE/Mater-Bi blends and the LDPE/Mater-Bi blends subjected to the soil burial test are plotted in Figures 4 and 5. Substantial modifications appeared in the region associated to Mater-Bi (275–435°C). Thus, a careful study of the degradation in soil of pure Mater-Bi is very important to understand the degradation in soil of these blends.

TABLE II
Thermogravimetric Parameters of the LDPE/Mater-Bi Blends as a Function of the Exposure Time in Soil

	LDPE/Mater-Bi blends							
	Weight loss (%)	T Peak (°C)	Weight loss (%)	T Peak (°C)	Weight loss (%)	T Peak (°C)	Weight loss (%)	T Peak (°C)
0 days	2.3	125.3	22.2	325.0	–	–	64.5	485.6
20 days	1.0	125.0	14.0	325.0	10.0	399.0	69.2	486.0
2 months	0.8	125.0	8.0	327.0	13.0	397.0	75.0	485.3
4 months	0.9	121.5	8.1	323.4	13.0	397.6	75.0	485.3
6 months	0.8	120.2	8.2	324.0	13.0	397.5	75.1	486.7

TABLE III
Thermogravimetric Parameters of the Photo-Oxidized HDPE/Mater-Bi Blends as a Function of the Exposure Time in Soil

	Photo-oxidized HDPE/Mater-Bi blends							
	Weight loss (%)	T Peak (°C)	Weight loss (%)	T Peak (°C)	Weight loss (%)	T Peak (°C)	Weight loss (%)	T Peak (°C)
0 days	1.0	142.1	21.3	325.6	–	–	69.5	493.0
20 days	1.0	141.0	13.0	322.5	8.0	388.0	70.9	495.0
2 months	0.2	142.6	7.0	322.5	12.0	385.6	73.6	492.5
4 months	–	–	–	–	20.0	387.0	75.6	493.2
6 months	–	–	–	–	20.2	389.2	75.0	494.5

TABLE IV
Thermogravimetric Parameters of the Photo-Oxidized LDPE/Mater-Bi Blends as a Function of the Exposure Time in Soil

	Photo-oxidized LDPE/Mater-Bi blends							
	Weight loss (%)	T Peak (°C)	Weight loss (%)	T Peak (°C)	Weight loss (%)	T Peak (°C)	Weight loss (%)	T Peak (°C)
0 days	1.8	125.0	24.3	324.7	–	–	66.0	489.0
20 days	1.2	123.5	17.8	319.4	–	–	74.0	493.2
2 months	0.2	126.7	7.9	327.0	14.0	400,0	71.5	492.7
4 months	0.1	127.0	5.7	323.5	16.6	402,4	72.4	492.4
6 months	0.4	128.0	6.7	320.4	14.0	401,7	73.1	493.9

Figure 6 shows differential thermogravimetric curve of the pure Mater-Bi submitted to the burial soil test. Table V displays the thermogravimetric parameters related to the decomposition zones of pure Mater-Bi. These plots show that substantial changes are related to the thermal decomposition of starch.

Figure 6 also displays the deconvolution method of the differential thermogravimetric curves of the biodegraded Mater-Bi, to characterize this complex zone. The original contribution at 331°C, attributed to thermal degradation of starch chains, is continuously reduced as the degradation time increases. These results confirm the degradation of most of starch by the biodegradation process in soil.

Furthermore, as the degradation test in soil progresses, the small shoulders in the 360–435°C interval that above have been related to the remaining more thermally stable starch chains and vinyl alcohol chains, considerably develop into a single and main contribution. After 20 days of exposure time in soil, this single contribution is centered at 391°C. As the degradation time increases, this peak slightly shifts towards lower temperatures (386°C).

Figure 6 also displays that the weight-loss peak associated with the ethylene chains of poly(vinyl

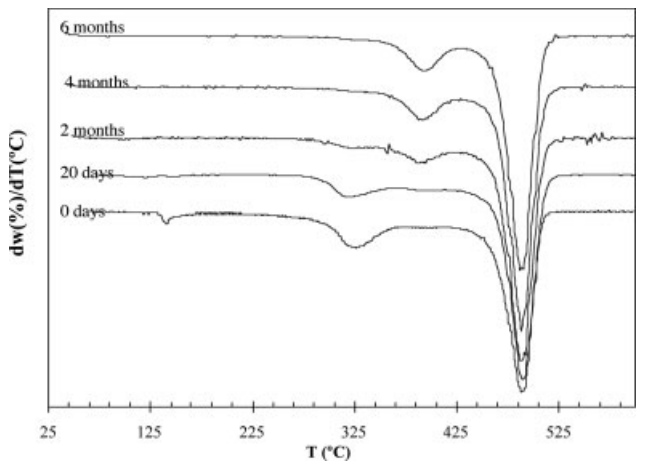

Figure 4 Differential thermogravimetric curves of the HDPE/Mater-Bi blends as a function of the exposure time in soil.

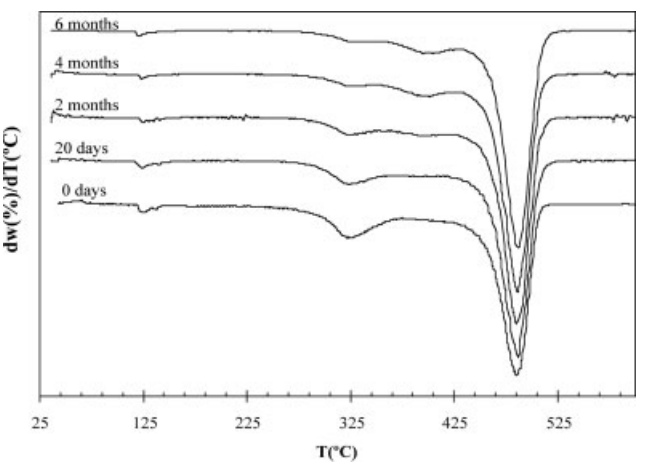

Figure 5 Differential thermogravimetric curves of the LDPE/Mater-Bi blends as a function of the exposure time in soil.

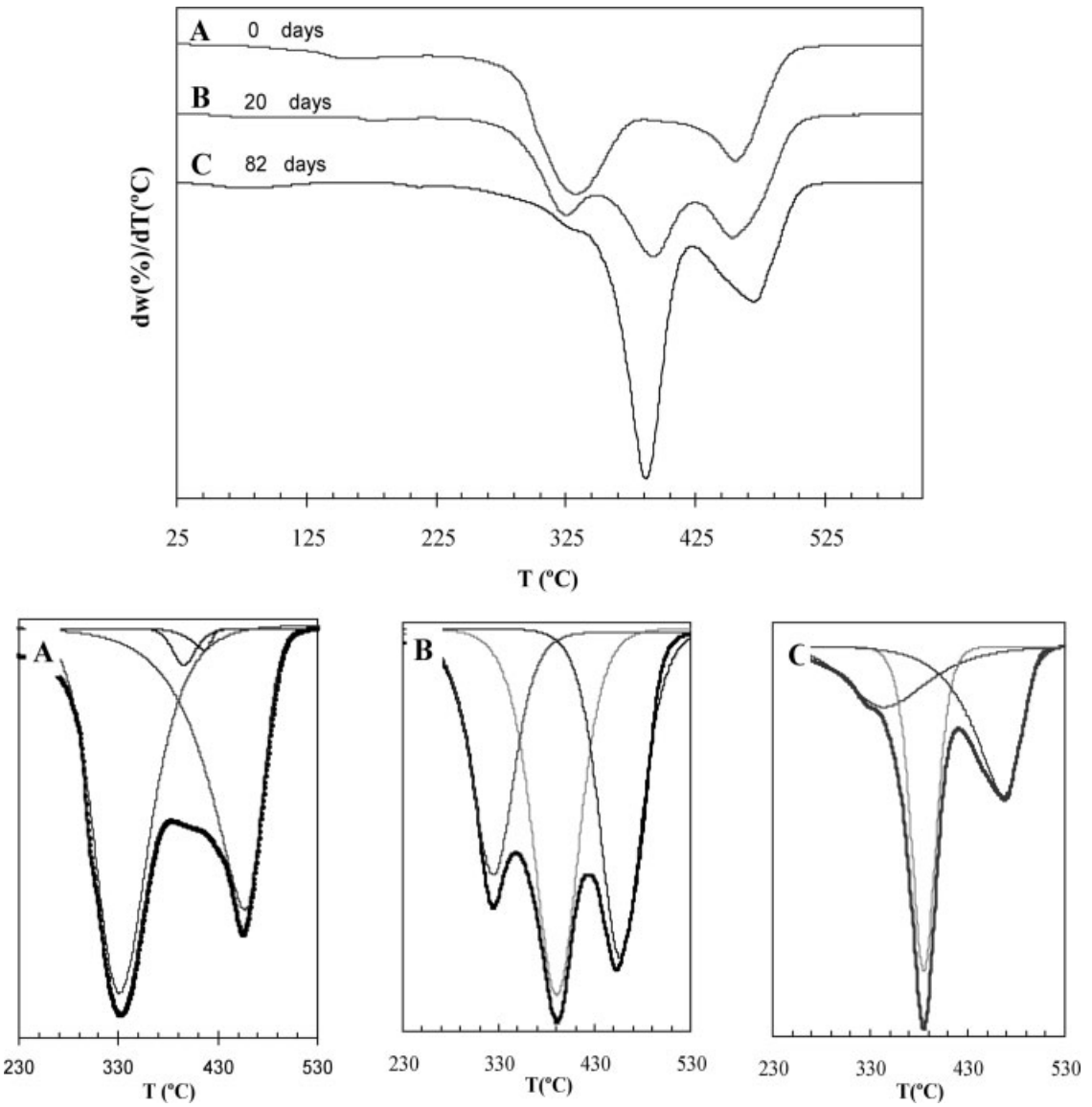

Figure 6 Differential thermogravimetric curves of Mater-Bi AF05H as a function of the exposure time in soil. (A) deconvolution of the DTG curve of Mater-Bi AF05H (B) deconvolution of the DTG curve after 20 days and (C) after 82 days of exposure time in soil.

alcohol) is not significantly modified as a result of the biodegradation process in soil; a shift of that peak towards higher temperatures (468°C) is only noted as the degradation time increases.

These results seem to indicate that the starch chains exhibit diverse behavior when Mater-Bi is subjected to degradation in soil. Most of the more labile, easily accessible and biodegradable starch chains in Mater-Bi, disappear. The rest of the more thermally stable and/or less accessible starch remains, probably for the influence of the vinyl alcohol.[26] These results may be understood taking into

TABLE V
Thermogravimetric Parameters of Mater-Bi AF05H as a Function of the Exposure Time in Soil

	Mater-Bi AF05H							
	Weight loss (%)	T Peak (°C)	Weight loss (%)	T Peak (°C)	Weight loss (%)	T Peak (°C)	Weight loss (%)	T Peak (°C)
0 days	4.6	155.0	47.7	331.1	–	–	22.7	456.5
20 days	1.6	176.5	35.0	325.6	35.0	391.2	24.7	453.7
80 days	–	–	–	–	55.5	385.5	24.5	469.7

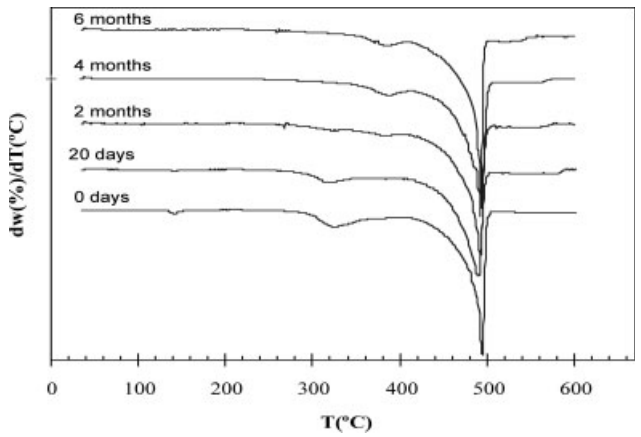

Figure 7 Differential thermogravimetric curves of the photo-oxidized HDPE/Mater-Bi blends as a function of exposure time in soil.

consideration previous studies made by Bastioli et al.[11,18]; they have proposed a model considering large individual amylopectine molecules, interconnected at several points per molecule, as a result of hydrogen bonds and entanglements, by chains of amylose/EVOH complexes. Thus, Mater-Bi AF05H adopts a complex droplet structure, with a core of an almost amorphous amylopectine surrounded by amylose/EVOH complexes that make amylopectine unsoluble. The droplets can interact by means of hydrogen bonds, producing a gel-like structural skeleton. During the soil burial test, the droplets structure core and the ethylene chains of Mater-Bi should be degraded slower than the noncomplexed starch.[27]

For the HDPE/Mater-Bi and LDPE/Mater-Bi blends submitted to degradation in soil, the same behavior as the one described for the pure Mater-Bi is observed in the region between 275 and 435°C. The thermogravimetric parameters are showed at Tables I–IV from both kinds of blends.

Derivative thermogravimetric curves of the HDPE/Mater-Bi and LDPE/Mater-Bi blends subjected to both the photo-oxidation and the soil burial tests are displayed in Figures 7 and 8. Their parameters are also showed at Tables I–IV. As it has been previously stated, the small shoulders in the 360–435°C interval, which may be related to the core of droplets structure, cannot be identified when these blends are photo-oxidized, since they overlap with the main decomposition zone associated to polyethylene chains. However, as the exposure time in soil increases, the main peak becomes narrower, and the development of small shoulder associated to Mater-Bi can be distinguished.

To analyze in more detail the thermogravimetric results and assessed the mechanisms involved, the kinetic behavior of all the blends has been studied. Criado method[28] was employed to analyze the decomposition mechanism of the ethylene chains in the HDPE/Mater-Bi and LDPE/Mater-Bi blends. Criado equation allows obtaining reduced master curves, which are used to assess the kinetic model that describes the studied thermal decomposition process.

$$\frac{z(\alpha)}{z(0,5)} = \frac{f(\alpha)g(\alpha)}{f(0,5)g(0,5)} = \left(\frac{T}{T_{0,5}}\right)^2 \frac{(d\alpha/dt)}{(d\alpha/dt)_{0,5}}$$

where $\frac{d\alpha}{dt}$ is the rate equation, T is the absolute temperature, α is the degree of degradation or conversion, $f(\alpha)$ is the differential conversion function and $g(\alpha)$ is the integral conversion function.

The left side of this equation is a reduced theoretical curve, where the digit 0.5 refers to the conversion of 0.5. This side of equation is characteristic for each reaction mechanism, whereas the right side of the equation can be obtained from experimental data. Different algebraic expressions for $f(\alpha)$ and $g(\alpha)$ have been used to describe the employed kinetics models.[29]

Figure 9 displays the reduced master curves of HDPE/Mater-Bi and LDPE/Mater-Bi blends, proving that the thermodegradation mechanism of the ethylene chains of the blends follows a kinetic model of $f(\alpha) = (1-\alpha)^n$, being $n = 1$.

The Broido method[30] has also been used for the kinetic analysis of the main thermal decomposition process for the both kind of blends as has already been successfully applied in previous works for polyolefins.[15–17] Broido equation could be used to calculate the activation energy.

$$\ln\ln\left(\frac{1}{x}\right) \cong -\frac{E_a}{RT} + \text{constant}$$

where R is the gas constant, T is the absolute temperature, E_a is the activation energy and x is the

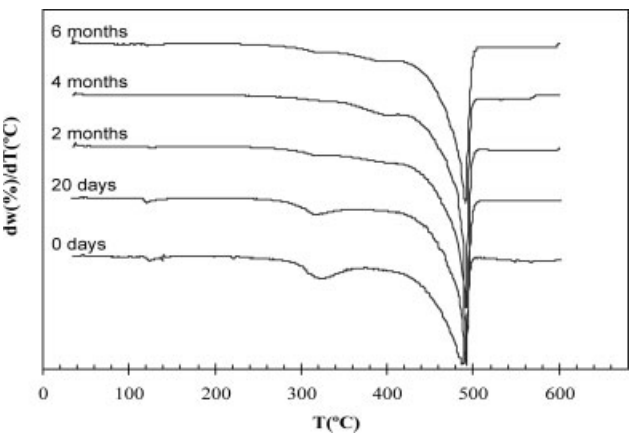

Figure 8 Differential thermogravimetric curves of the photo-oxidized LDPE/Mater-Bi blends as a function of exposure time in soil.

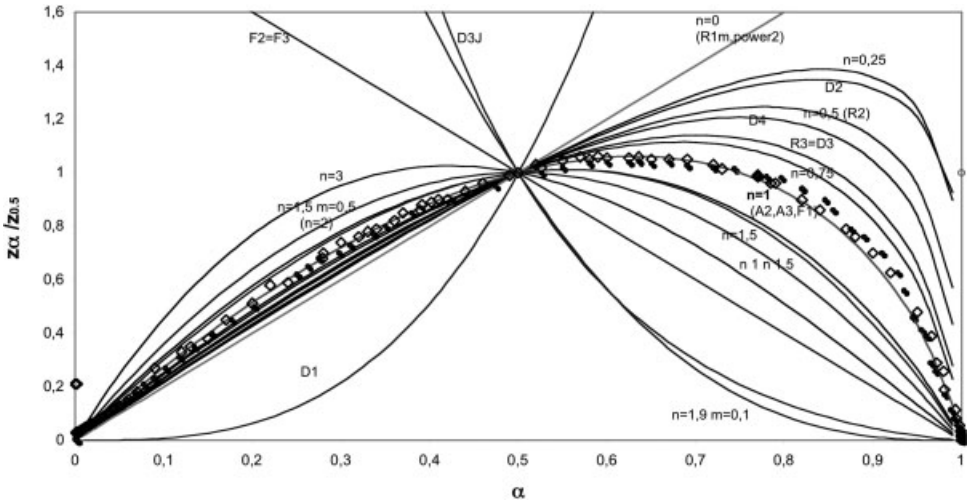

Figure 9 Reduced master curves of different kinetic models and experimental data for the main thermal decomposition processes of the (●) HDPE/Mater-Bi and the (◇) LDPE/Mater-Bi blends.

residual fraction, calculated as $(w-w_\infty)/(w_0-w_\infty)$, where w_0 is the initial mass, w is the sample mass at time t and w_∞ is the final mass.

The activation energy values of the pyrolysis process of the ethylene chains as a function of the soil burial time can be observed in Table VI. Similar activation energy values have been obtained for the HDPE/Mater-Bi and LDPE/Mater-Bi blends in the same temperature interval. It is noted that the activation energy increases in both types of blends with the exposure time in soil, but the increase is higher in the HDPE/Mater-Bi blend (85 kJ/mol) than in the LDPE/Mater-Bi blend (54 kJ/mol).

Photo-oxidation leads to the decrease of the activation energies for both polyethylenes/Mater-Bi blends. This decrease in the activation energy affects to a higher extent the HDPE/Mater-Bi blends (42 kJ/mol) than the LDPE/Mater-Bi blends (17 kJ/mol). When these previous photo-oxided blends were submitted to soil burial test, the activation energy values of the pyrolysis process of the ethylene chains also increase, but the effects caused by the soil burial test are slowed down. These results may indicate that some changes in the morphology of these blends may be produced during the photo-oxidative process.[31]

To analyze these possible morphological changes as a consequence of both the photo-oxidative treatment and the degradation process in soil, calorimetric measurements have also been performed. In previous studies,[16,17,32] the melting temperature were directly determined from the thermogram as the value of the maximum of each endothermic peak. Pure polyethylenes showed their typical thermogram, with a main endothermic peak around 113°C for LDPE and 130°C for HDPE. Two endothermic peaks around 133 and 156°C can be observed in the DSC thermogram of pure Mater-Bi: the low temperature peak is associated to the crystalline phase of starch and the high temperature peak is related to the crystalline phase of EVOH.

Figures 10 and 11 display the calorimetric thermograms of HDPE/Mater-Bi and LDPE/Mater-Bi blends, respectively. The synergetic effects caused by the previous photo-oxidation process on the calorimetric thermograms have also displayed in the same

TABLE VI
Activation Energies of the HDPE/Mater-Bi and LDPE/Mater-Bi Blends as a Function of the Exposure Time in Soil Calculated Using Broido Method

	HDPE/Mater-Bi blends		LDPE/Mater-Bi blends	
	Non photo-oxidized	Photo-oxidized	Non photo-oxidized	Photo-oxidized
	E_a (kJ/mol) 475–490°C	E_a (kJ/mol) 475–490°C	E_a (kJ/mol) 475–490°C	E_a (kJ/mol) 475–488°C
0 days	218	176	222	205
20 days	254	189	240	181
2 months	277	202	261	202
4 months	297	195	278	202
6 months	304	201	277	196

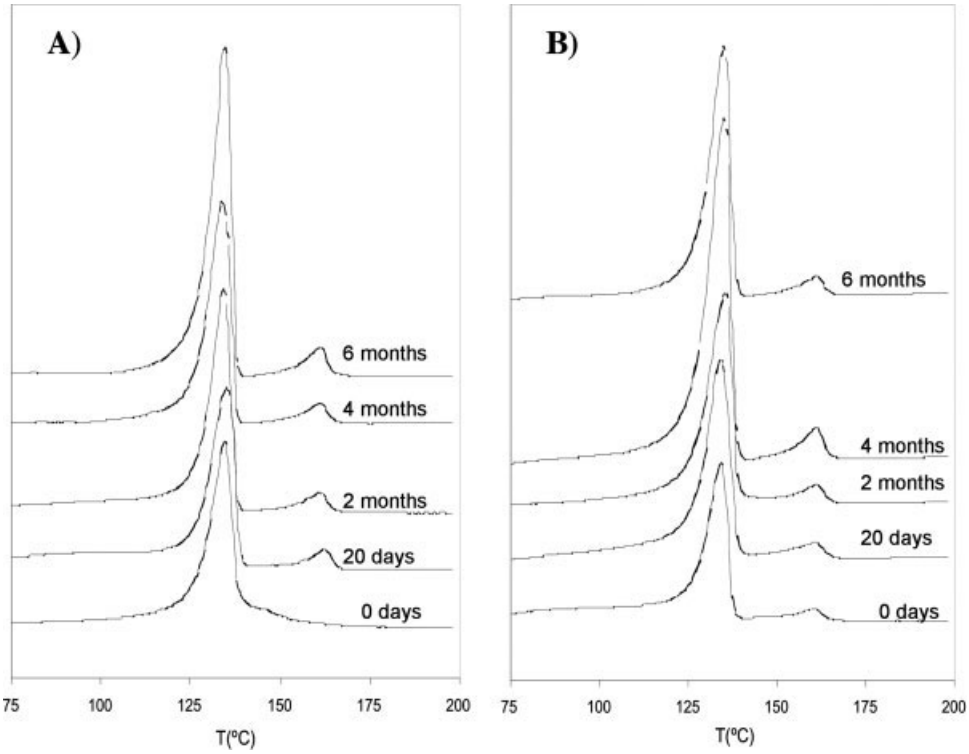

Figure 10 (A) DSC thermograms of the HDPE/Mater-Bi blend as a function of the exposure time in soil. (B) DSC thermograms of the photo-oxidized HDPE/Mater-Bi blend as a function of the exposure time in soil.

figures. The calorimetric thermograms of HDPE/Mater-Bi blends exhibit a prominent endothermic peak assigned to the polyethylene chains. Other small endothermic peaks associated to the Mater-Bi components cannot be distinguished, probably due to their overlapping with the ethylene contribution.

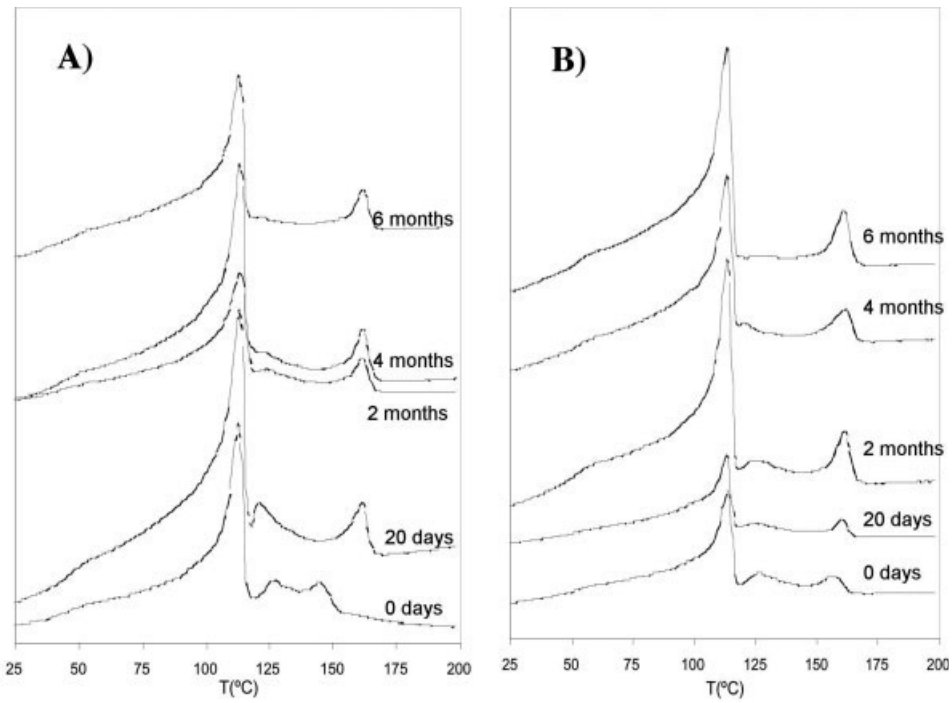

Figure 11 (A) DSC thermograms of the LDPE/Mater-Bi blend as a function of the exposure time in soil. (B) DSC thermograms of the photo-oxidized LDPE/Mater-Bi blend as a function of the exposure time in soil.

TABLE VII
Activation Energies of Mater-Bi as a Function of the Exposure Time in Soil

	Mater-Bi AF05H					
	T (°C)	E_a (kJ/mol)	T (°C)	E_a (kJ/mol)	T (°C)	E (kJ/mol)
0 days	300–360	65	–	–	450–490	50
20 days	285–335	72	350–420	45	450–490	51
82 days	285–335	49	365–402	114	450–490	55

However, LDPE/Mater-Bi blends exhibited three peeks, which could be assigned to both polyethylene and Mater-Bi components.

The photo-oxidative treatment modifies more the calorimetric thermograms of the HDPE/Mater-Bi (Fig. 10) than the LDPE/Mater-Bi blends (Fig. 11). The endothermic peaks assigned to Mater-Bi in the HDPE/Mater-Bi blends appear as a small and a broad peak separated by the ethylene contribution. This fact suggests that photo-oxidative treatment may cause chain scission, enhancing the crystallization and segregation of the different components of the HDPE/Mater-Bi blends, and thus increasing the heterogeneity of these blends. These calorimetric results are in agreement with the activation energy values determined for the thermal decomposition process of the ethylene chain. In general, photo-oxidation enhances the degradation in soil by means of chain scission reactions, but at the same time crystallization processes may be caused, which slow down the biodegradation effects caused by the soil burial test.

No significant changes can be observed in the endotherms associated with the Mater-Bi. Thus, a careful analysis of this region in the derivative thermogram by means of kinetic analysis is very important to understand the degradation of this Mater-Bi in the blends.

In previous studies,[33] the decomposition mechanisms of the different thermal degradation processes of pure Mater-Bi were calculated using Criado method. It has been assessed that at least two mechanisms coexist, and the main thermal decomposition processes follow an Rn type mechanism, being the algebraic expression $f(\alpha) = 3(1 - \alpha)^{2/3}$. The activation energies of the two main thermal decomposition processes of pure Mater-Bi could not be calculated by Broido method, since this method is proposed for reaction order equal to one. Thus, they were calculated using Coats-Redfern method.[34]

Table VII shows also the activation energy values for degraded pure Mater-Bi as the degradation process in soil undergoes. Two different behaviors have been observed when the exposure time in soil increases: (i) the activation energy of the thermal decomposition of the noncomplex starch and more accessible and biodegradable starch diminishes and (ii) the activation energy related to the less accessible to microorganisms complex starch with vinyl alcohol (complex droplet structure) increases. Moreover, the activation energy associated to the thermal decomposition of ethylene chains scarcely is modified. These results agree with the biodegradation mechanisms suggested by Bastioli et al.,[11] who proposed that starch is first hydrolyzed by extracellular enzymes, whereas the synthetic component is biodegraded by surface erosion by the microorganisms. This surface adsorption is enhanced by the increase of available surface area during the hydrolysis of the natural component.

Tables VIII and IX show the activation energy values of thermal decomposition of noncomplex and more accessible starch, the complex starch with vinyl alcohol chains of HDPE/Mater-Bi, LDPE/Mater-Bi blends and the previous photo-oxidized blends, respectively, as a function of the soil burial time.

The differences obtained between the activation energy values from both kinds of PE/Mater-Bi blends suggest that the degradation in soil of Mater-Bi can be conditioned by the matrix used. In the

TABLE VIII
Activation Energies of the HDPE/Mater-Bi Blends as a Function of the Exposure Time in Soil Using Coats-Redfern Method

	HDPE/Mater-Bi blends							
	Non photo-oxidized				Photo-oxidized			
	T (°C)	E_a (kJ/mol)	T (°C)	E_a (kJ/mol)	T (°C)	E_a (kJ/mol)	T (°C)	E_a (kJ/mol)
0 days	296–321	69	–	–	280–341	102	–	–
20 days	290–328	173	–	–	250–320	117	–	–
2 months	315–328	185	354–390	73	283–321	120	350–410	48
4 months	–	–	350–390	111	–	–	350–410	75
6 months	–	–	349–392	117	–	–	350–410	75

TABLE IX
Activation Energies of the LDPE/Mater-Bi Blends as a Function of the Exposure Time in Soil Using Coats-Redfern Method

	LDPE/Mater-Bi blends							
	Non Photo-oxidized				Photo-oxidized			
	T (°C)	E_a (kJ/mol)	T (°C)	E_a (kJ/mol)	T (°C)	E_a (kJ/mol)	T (°C)	E_a (kJ/mol)
0 days	299–340	64	–	–	295–309	66		–
20 days	233–340	83	–	–	260–317	75		–
2 months	265–340	129	352–429	50	264–317	110	335–416	42
4 months	268–340	97	356–429	48	290–346	83	351–419	61
6 months	267–333	119	356–429	53	267–317	104	351–411	51

HDPE/Mater-Bi blends, the noncomplex starch disappears in less time than in the LDPE/Mater-Bi blends. When PE/Mater-Bi blends are submitted to both degradation in soil and photo-oxidation, differences in the activation energy profiles can be observe. In the HDPE/Mater-Bi blends, kinetic parameters seem to indicate that photo-oxidation slows down the changes caused during the soil burial test. In the LDPE/Mater-Bi blends, photo-oxidation faintly modifies the activation energy during biodegradation.

CONCLUSIONS

The thermal decomposition process of blends of polyolefins (HDPE and LDPE) and Mater-Bi AF05H, a starch-based material that contains starch and poly(ethylene-vinyl alcohol) copolymers is a complex degradation that results from its complex structure. Several decomposition regions are displayed in the differential thermogravimetric curves of HDPE/Mater-Bi and LDPE/Mater-Bi blends display, which can therefore be attributed to both PE and Mater-Bi components.

A deconvolution method has been applied to characterize each individual contribution from the differential thermogravimetric curves of all the studied samples. The thermal decomposition mechanism of the ethylene chains of HDPE/Mater-Bi and LDPE/Mater-Bi blends was proved to follow a kinetic function of order 1 $f(\alpha) = (1 - \alpha)$. On the other hand, the two main thermal decomposition mechanisms of pure Mater-Bi were proved to follow a Rn type kinetic model mechanism, $f(\alpha) = 3(1 - \alpha)^{2/3}$.

Photo-oxidized blends of HDPE/Mater-Bi and LDPE/Mater-Bi exhibit the same weight-loss regions than non photo-oxidized blends. Previous photo-oxidation enhances the thermal stability and decrease the activation energy of the pyrolysis process of the ethylene chains in both types of blends. However, the effect of the photo-oxidation on the thermal decomposition of the starch chains depends on the polyolefinic matrix used. HDPE/Mater-Bi blends are more affected by photo-oxidation than LDPE/Mater-Bi blends.

Degradation in soil, on the other hand, mainly affects the noncomplexed starch in both blends; ethylene chains from Mater-Bi and polyethylene prove to be more resistant to biodegradation. The behavior of noncomplexed starch in the blends during the soil burial test is influenced by the used polymeric matrix, being faster in HDPE/Mater-Bi blends than in the LDPE/Mater-Bi blends.

The synergetic effects caused by both degradation processes, the photo-oxidation and the degradation in soil on both types of PE/Mater-Bi blends can be monitorized by the activation energy parameters. In the HDPE/Mater-bi blends seems that the previous photo-oxidation slow down the effects caused by the soil burial test in all thermal decomposition regions.

References

1. La Mantia, F. Handbook of Plastics Recycling; Rapra Technology: Shawbury, 2002.
2. Albertsson, A.-C.; Huang, S. J., Eds. Degradable Polymers, Recycling and Plastics Waste Management; Marcel Dekker: New York, 1995.
3. Smits, M. Polymer Products and Waste Management; Marcel Dekker: New York, 1995.
4. Griffin, G. J. L., Ed. Chemistry and Technology of Biodegradable Polymers; Blackie: Glasgow, 1994.
5. Chandra, R.; Rustgi, R. Polym Degrad Stabil 1997, 56, 185.
6. Erlandsson, B.; Karlsson, S.; Albertsson, A.-C. Polym Degrad Stabil 1997, 55, 237.
7. Albertsson, A.-C.; Erlandsson, B.; Hakkarainen, M.; Karlsson, S. J Environ Polym Degrad 1998, 6, 187.
8. Scott, G. Degradable Polymers; Kluwer Academic: Netherlands, 2002.
9. Clarinval, A.; Halleux, J. In Biodegradable Polymers for Industrial Applications; Smith, R., Ed.; Woodhead Publishing: London, 2005.
10. Bastioli, C. Polym Degrad Stabil 1998, 59, 263.
11. Bastioli, C. Handbook of Biodegradable Polymers. Rapra Technology: Shrewsbury, 2005.
12. Mohanty, A. K.; Misra, M., Drzal, T. D., Eds. Natural Fibers, Biopolymers and Biocomposites; Taylor & Francis: Boca Raton, 2005.
13. Marcelo, A. V.; Edwin, L. T.; Amstrong, R. C. Polymer 1995, 36, 1869.

14. Contat-Rodrigo, L.; Ribes-Greus, A. J Appl Polym Sci 2000, 78, 1707.
15. Contat-Rodrigo, L.; Ribes-Greus, A.; Día-Calleja, R. J Appl Polym Sci 2001, 82, 2174.
16. Contat-Rodrigo, L.; Ribes-Greus, A. J Appl Polym Sci 2002, 83, 1683.
17. Contat-Rodrigo, L.; Ribes-Greus, A.; Imrie, CT. J Appl Polym Sci 2002, 86, 764.
18. Bastioli, C.; Belloti, V.; Rallis A. Rheologica Acta 1994, 33, 307.
19. DIN 53739 Testing of Plastics. Influence of Fungi and Bacteria. Visual Evaluation. Change in Mass and Physical Properties, November 1984.
20. Contat-Rodrigo, L.; Ribes-Greus, A.; Imrie, C. T. J Appl Polym Sci 2002, 86, 174.
21. Jiang, W.; Qiao, X.; Sun. K. Carbohydr Polym 2006, 65, 139.
22. Wang, X.-L.; Yang, K.-K.; Wang, Y.-Z.; Wu, B.; Liu, Y.; Yang, B. Polym Degrad Stabil 2003, 81, 415.
23. Mano, F.; Koniarova, D.; Reis, R. L. J Mater Sci Mater Med 2003, 14, 127.
24. Cabedo, L.; Jiménez, E.; Lagaron, J. M.; Gavara, R.; Saura, J. J Polym 2004, 45, 5233.
25. Alvarez, V. A.; Ruseckaite, R. A.; Vázquez, A. J Appl Polym Sci 2003, 90, 3157.
26. Aráujo, M. A.; Cunha, A. M.; Mota, M. Biomaterials 2004, 25, 2687.
27. Simmons, S.; Thomas, E. L. J Appl Polym Sci 1995, 58, 2259.
28. Criado, J. M. Thermochim Acta 1978, 24, 86.
29. Vayazovkin, S. Int Rev Phys Chem 2000, 19, 45.
30. Broido, A. J Polym Sci Part A-2: Polym Phys 1969, 7, 1761.
31. Scott, G. Mechanisms of Polymer Degradation and Stabilisation; Elsevier: New York, 1990.
32. Santonja-Blasco, L.; Contat-Rodrigo L.; Moriana-Torró, R.; Ribes-Greus A. J Appl Polym Sci 2007, 106, 2218.
33. Ramis, X.; Cadenato, A.; Salla, J. M.; Morancho, J. M.; Valles, A.; Contat, L.; Ribes, A. Polym degrad Stabil 2004, 86, 483.
34. Coats, A. W.; Redfern, J. P. Nature 1964, 201, 68.

Thermal Characterization of Polyethylene Blends with a Biodegradable Masterbatch Subjected to Thermo-Oxidative Treatment and Subsequent Soil Burial Test

L. Santonja-Blasco, L. Contat-Rodrigo, R. Moriana-Torró, A. Ribes-Greus

Instituto de Tecnología de Materiales, Escuela Técnica Superior de Ingeniería del Diseño, Universidad Politécnica de Valencia, 46071 Valencia, Spain

Received 2 March 2007; accepted 6 April 2007
DOI 10.1002/app.26667
Published online 25 July 2007 in Wiley InterScience (www.interscience.wiley.com).

ABSTRACT: The viability of producing environment-friendly blends of HDPE and LDPE with a commercial biodegradable masterbatch containing starch and polyethylene was studied. The service life of these blends was simulated by means of a thermo-oxidative treatment, and their further disposal in landfill was modeled using an accelerated soil burial test. Characterization was carried out in terms of their calorimetric and thermogravimetric properties. Thermo-oxidative treatment causes an increase in the crystalline content of both components of the blends, and promotes a segregation of the crystallite sizes of polyethylene. The soil burial test leads to changes in the crystalline content of the biodegradable material, which is influenced by the polyolefinic matrix used. The kinetics of the thermal decomposition of these blends was studied using the Hirata and the Broido models. Thermogravimetric results reveal that the thermo-oxidative treatment causes a decrease in the activation energy of the thermal decomposition process of both components in the blends, regardless of the type of polyethylene used. The thermo-oxidative treatment mainly modifies the thermal properties of starch during the degradation process in soil, especially in the LDPE blends. Synergetic degradation of these blends is a complex process that is dependent on the polyolefinic matrix used and mainly causes morphological changes. © 2007 Wiley Periodicals, Inc. J Appl Polym Sci 106: 2218–2230, 2007

Key words: calorimetric analysis; thermogravimetric analysis; polyethylene; degradation; thermo-oxidation

INTRODUCTION

It is well-known that plastics disposal has become a very important environmental problem. The development of degradable polymers offers an effective approach for minimizing plastics wastes.[1,2] Nowadays, most interest is focused on the use of degradable materials that can replace conventional synthetic polymeric materials, both in terms of the production cost and performance. In this sense, a viable solution that has been already employed by producers is to combine the different features and benefits of materials from both petroleum and natural resources, to produce useful blends that may satisfy both economical and environmental requirements.[3]

Conventional plastics like polyolefins are slowly degraded by the environment. However, their sensitivity to degradation can be enhanced by blending them with different commercial biodegradable masterbatches.[4–9] Such blends should be designed to guarantee suitable performance during service life and short degradation times during further disposal. Only an accurate characterization of the degradation process of these blends can validate their future applications.

The aim of this work is to simulate the service life and further disposal of high and low density polyethylene (LDPE) blends with a biodegradable masterbatch, to study their viability for future applications. Simulation of the degradative conditions, under which polymeric materials are exposed during their service life, can be done using many procedures, depending on the application of the studied material. These include reprocessing and thermo-oxidative treatments, among others.[10,11] In this work, the service life was modeled by means of a previous thermo-oxidative treatment in air atmosphere, and further disposal in landfill was simulated using an accelerated soil burial test.

In previous works, the biodegradation process under soil burial conditions of different polyolefin blends with commercial starch products has been characterized.[12,13] The important effect of a previous

Correspondence to: A. Ribes-Greus (aribes@ter.upv.es).

Contract grant sponsor: Ministerio de Educación y Ciencia of Spain; contract grant number: CTM2004-04,977/TECNO.

Contract grant sponsor: Conselleria de Empresa, Universidad y Ciencia (Ayuda Complementaria GV Project); contract grant number: CTM2004-04,977/TECNO.

Journal of Applied Polymer Science, Vol. 106, 2218–2230 (2007)

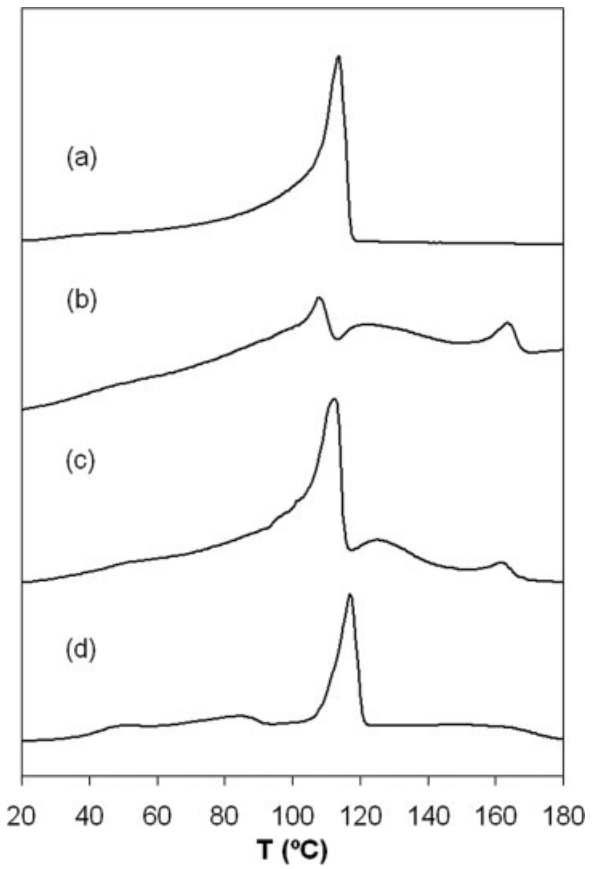

Figure 1 DSC thermograms of (a) LDPE, (b) Cornplast, (c) LDPE/Cornplast blend, and (d) LDPE/Cornplast blend subjected to thermo-oxidative treatment.

thermo-oxidative treatment on the biodegradation process of polyethylene blends with enhanced biodegradability has also been reported in terms of their morphological changes.[14] As a continuation of the aforementioned studies, this work is focused on the assessment of the effect that different polyethylene types may have on the degradation process of these blends.

It is well-established that thermal analysis allows the characterization of the degradation effects on the structure and on other important properties of the polymers. In this work, morphological changes of the different components of the blends have been monitored by Differential Scanning Calorimetry (DSC). Thermogravimetric analysis has been selected to provide information about the thermal stability and the kinetic parameters of the thermal decomposition process of these materials. These parameters are related to the breakdown of the molecular chains, as a result of degradation. Thus, the influence of both the thermo-oxidative treatment and the soil burial test on the properties loss of each type of polyethylene blends was able to be analyzed by means of these thermal analysis techniques.

MATERIALS AND METHODS

Materials

LDPE 710 and high density polyethylene 10,062 (HDPE) supplied by Dow Chemical (Spain) were used as polymeric matrices.

Cornplast, produced by the National Corn Grower Association (USA), is a commercial biodegradable material with 20% of polyethylene and 80% of a promoter of biodegradation containing starch.

Samples

Two types of blends were prepared, consisting of a mixture of 50/50% by weight of polymeric matrix (either HDPE or LDPE) and Cornplast. The blends were prepared from the melt in a Brabender Plastic-Corder PL 2100 rheometer (Druisburg, Germany). The mixture was cut as nut coal and thereafter processed by compression molding into rectangular samples (68 mm $\times$ 12 mm $\times$ 1.8 mm), using a Carver M press (Wabash, IN).

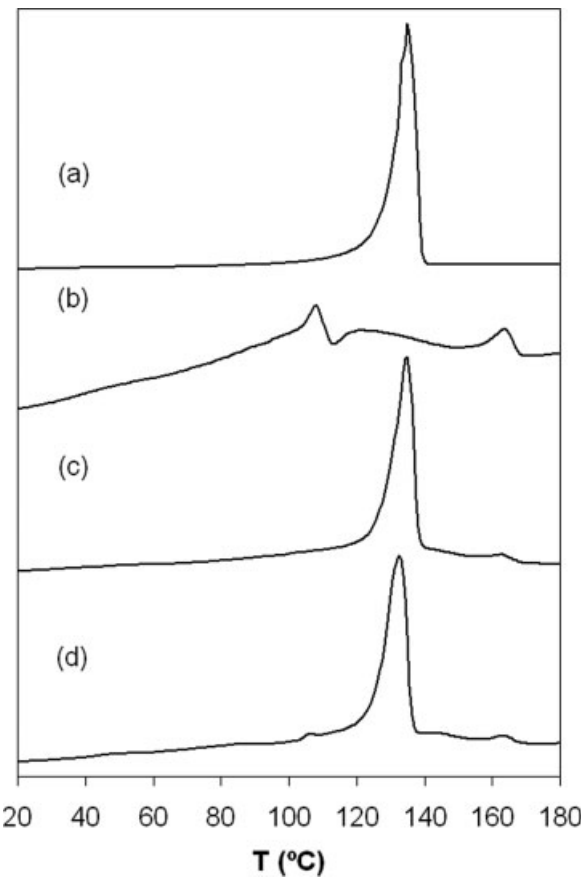

Figure 2 DSC thermograms of (a) HDPE, (b) Cornplast, (c) HDPE Cornplast blend, and (d) HDPE/Cornplast blend subjected to thermo-oxidative treatment.

TABLE I
Melting Temperatures of the Main Endotherm of the LDPE/Cornplast Blends

Exposure time in soil	LDPE/Cornplast blends	LDPE/Cornplast blends with thermo-oxidative treatment
	T_m (°C)	T_m (°C)
0 Days	112.3	117.0
20 Days	112.6	116.5
2 Months	113.0	115.0
4 Months	112.0	116.1
6 Months	113.7	116.4

Thermo-oxidative treatment

A set of samples was subjected to a thermo-oxidative treatment, prior to the soil burial test. This was carried out in a Heraeus UT 6060 oven (Germany) at (100 ± 1)°C during 360 h in air atmosphere. Samples were then immediately quenched in a water and ice bath at 0°C.

Soil burial test

All samples (previously submitted to the thermo-oxidative treatment or not) were subjected to an accelerated soil burial test according to the DIN 53,739 standard norm.[15] Samples were buried for 6 months in biologically active soil in a plastic container, which was kept opened to ensure a fresh oxygen supply. The soil burial test was performed in a Heraeus B12 culture oven (Germany) at a constant temperature of (28 ± 0.5)°C. The soil was a 50/50% by weight mixture of a soil extract from a cultivated field and a soil typically used in pine tree nurseries. The pH of the soil measured in water was 6.75. Samples were removed periodically, cleaned with a soap solution, and dried, to stop the degradation process.

Differential scanning calorimetry

The DSC measurements were carried out in a Perkin–Elmer DSC-4 Calorimeter (Norwalk, CT), previously calibrated with indium standard. Samples of 6–7 mg were placed in standard aluminum pans that were sealed, pierced, and scanned from 0 to 200°C, at a heating rate of 10°C/min under nitrogen atmosphere. Measurements were repeated to limit errors to ±0.01°C for the melting temperature and ±0.05% for the crystalline content.

Thermogravimetric analysis

Changes in the thermal properties of the samples were studied by Thermogravimetric Analysis (TGA). Measurements were carried out in a Mettler-Toledo TGA/SDTA 851 module (Switzerland). Dynamic measurements were performed from 25 to 600°C at a heating rate of 10°C/min, under argon atmosphere (flow rate of 200 mL/min). Measurements were repeated to limit errors to ±0.01°C for the peak temperatures.

RESULTS AND DISCUSSION

Calorimetric results

Calorimetric analysis was performed to study the morphological changes of the samples, as a consequence of the thermo-oxidative treatment and the degradation process in soil. The melting temperature, the total and partial crystalline contents, and the lamellar thickness distribution were analyzed.

Figures 1 and 2 show the DSC thermograms of pure LDPE, HDPE, and Cornplast, and their blends. The DSC thermogram of pure polyethylene consists of a main endotherm with a maximum around 113°C for LDPE and 130°C for HDPE. On the other hand, three endothermic peaks can be observed in the DSC thermogram of pure Cornplast. The first endotherm (around 108°C) could be assigned to the polyethylene present in the composition of this product. Cornplast also displays other overlapped peaks at higher temperatures: A broad peak located at about 122°C, and a narrower peak centered at 163°C, which can be associated to the starch present in Cornplast.[16,17] Different types of morphological structures have been proposed to describe the crystalline zone of starch,[18] basically organized as highly crystalline lamellae intermitted by less perfect crystalline regions, which could explain this complex melting behavior of starch.

The DSC thermogram of the LDPE/Cornplast blend shows three peaks that can be related to the two components of the blend (Fig. 1). The first one is a main peak around 112°C that can be originated by the carbonated chains of both the LDPE and the polyethylene contained in Cornplast. This thermo-

TABLE II
Melting Temperatures of the Main Endotherm of the HDPE/Cornplast Blends

Exposure time in soil	HDPE/Cornplast blends	HDPE/Cornplast blends with thermo-oxidative treatment
	T_m (°C)	T_m (°C)
0 Days	134.7	132.5
20 Days	133.1	133.6
2 Months	132.3	133.9
4 Months	134.1	133.6
6 Months	131.6	133.1

TABLE III
Calorimetric Parameters of the LDPE/Cornplast Blends

	LDPE/Cornplast blends			LDPE/Cornplast blends with thermo-oxidative treatment			
Exposure time in soil	Area LDPE	Area cornplast	$l_{máx}$ (Å)	Area 1 HDPE	Area 2 LDPE	Area cornplast	$l_{máx}$ (Å)
0 Days	1.00	1.00	61	1.00	1.00	1.00	71
20 Days	0.84	–	61	1.06	2.01	–	70
2 Months	1.08	1.47	62	1.05	1.84	0.29	66
4 Months	0.93	1.06	59	1.08	2.00	0.20	70
6 Months	1.86	1.47	63	1.09	1.89	0.00	70

$l_{máx}$, relative partial areas and average lamellar thickness.

gram also clearly displays two small peaks at 122 and 163°C, which have already been observed in pure Cornplast. These two endotherms can therefore be related to the biodegradable material. Thus, the blending process does not seem to produce any interaction between the two components of the blend, since the different characteristic peaks of the blend correspond to the endothermic peaks of the pure components.

Unlike the LDPE/Cornplast blend, the DSC thermogram of the HDPE/Cornplast blend exhibits only two peaks (Fig. 2). The main peak (around 130°C) is associated to the melting of the polyethylene chains. Concerning the Cornplast component, only its peak around 163°C can be observed. The other small peaks (around 108 and 122°C) cannot be distinguished, probably due to overlap with the polyethylene contribution.

The thermo-oxidative treatment modifies the DSC thermogram of the LDPE/Cornplast blend (Fig. 1). The endotherm assigned to the ethylene chains is divided into two peaks, suggesting a possible segregation of the crystalline zones. Furthermore, the endotherms related to starch develops into a single peak at 164°C. It has been reported for dry starch that a broad endotherm with a peak around 163°C is attributed to both the melting and recrystallization of the amylase and amylopectin components of starch.[19]

The thermo-oxidative treatment has different effects on the morphological behavior of both components of the HDPE/Cornplast blend, as compared with the LDPE blend (Fig. 2). The main endotherm related to the ethylene chains shifts slightly to lower temperatures. Moreover, several small peaks related to the biodegradable material now can be distinguished. Thus, the thermo-oxidative treatment seems to provoke a diffusion of the molecular chains and a subsequent separation of the different heterogeneous components of the HDPE/Cornplast blend, highlighting the heterogeneity of this blend.

The main melting temperature of all the samples during the soil burial test is summarized in Tables I and II. This parameter scarcely changes with the exposure time in soil. Therefore, a study of the crystalline content and the lamellar thickness distribution has been performed as well, to more accurately characterize the degradation process of these blends.

Crystalline content

The total crystalline content of pure polyethylenes has been obtained using the equation:

$$X = \frac{(H_a - H_c)}{H_m}$$

where H_a and H_c are the enthalpies in the melt state and the crystalline state, respectively. Their difference is directly obtained from the thermogram. H_m is the change in the melting enthalpy of a perfect

TABLE IV
Calorimetric Parameters of HDPE Blends

	HDPE/Cornplast blends			LDPE/Cornplast blends with thermo-oxidative treatment			
Exposure time in soil	Area HDPE	Area cornplast	$l_{máx}$ (Å)	Area 1 HDPE	Area 2 HDPE	Area cornplast	$l_{máx}$ (Å)
0 Days	1.00	1.00	272	1.00	1.00	1.00	196
20 Days	1.07	2.09	211	0.75	2.00	0.46	228
2 Months	1.38	2.95	196	1.05	2.71	1.49	228
4 Months	1.19	2.00	248	0.78	0.29	1.05	228
6 Months	1.54	3.32	183	1.08	0.43	1.21	211

$l_{máx}$, relative partial areas and average lamellar thickness.

crystal of infinite size. For polyethylene, H_m = 290.3 J/g.[20] Crystalline contents of 0.48 for pure LDPE and 0.75 for pure HDPE have been found.

To study the evolution of the crystalline content of the blends during the soil burial test, a calculation method of partial areas has been used, which was already developed in previous works.[21,22] This method is based on the determination of the area of the main peaks, and the later subtraction of all the other contributions. After the peak separation, the area of each peak is calculated. This area is directly proportional to the necessary heat flow for the melting of this crystalline fraction. It can also be assumed that this heat flow is in turn directly proportional to the crystalline content. To obtain the relative partial area, the area of the corresponding peak of the original sample divides this area.

For the studied LDPE/Cornplast and HDPE/Cornplast blends, the area related to polyethylene has been evaluated, together with the area of the endotherm at higher temperatures assigned to the starch in Cornplast, because these are the endothermic peaks that persist in time. Tables III and IV list the values of the relative partial areas of all the samples.

A common increase of the areas of the two components can be observed for both blends after the thermo-oxidative treatment performed for the simulation of their service life. Thus, such treatment seems to lead to a recrystallization process, which results in an increase in the crystalline content. The area related to the starch in the LDPE/Cornplast blend exhibits the most significant increase. Concerning polyethylene, a segregation of its crystalline zones is observed in both types of polyethylene blends.

To simulate the further disposal of the LDPE/Cornplast and HDPE/Cornplast blends, these were submitted to a soil burial test. The area related to the biodegradable material of the LDPE/Cornplast blend under soil burial conditions does not change significantly (Table III). In contrast, the area related to polyethylene increases with the exposure time in soil.

In the LDPE/Cornplast blend subjected to both the thermo-oxidative treatment and the soil burial test, the area associated to the biodegradable material tends to disappear as the exposure time in soil increases (Table III). Moreover, both areas related to polyethylene increase with the degradation time in

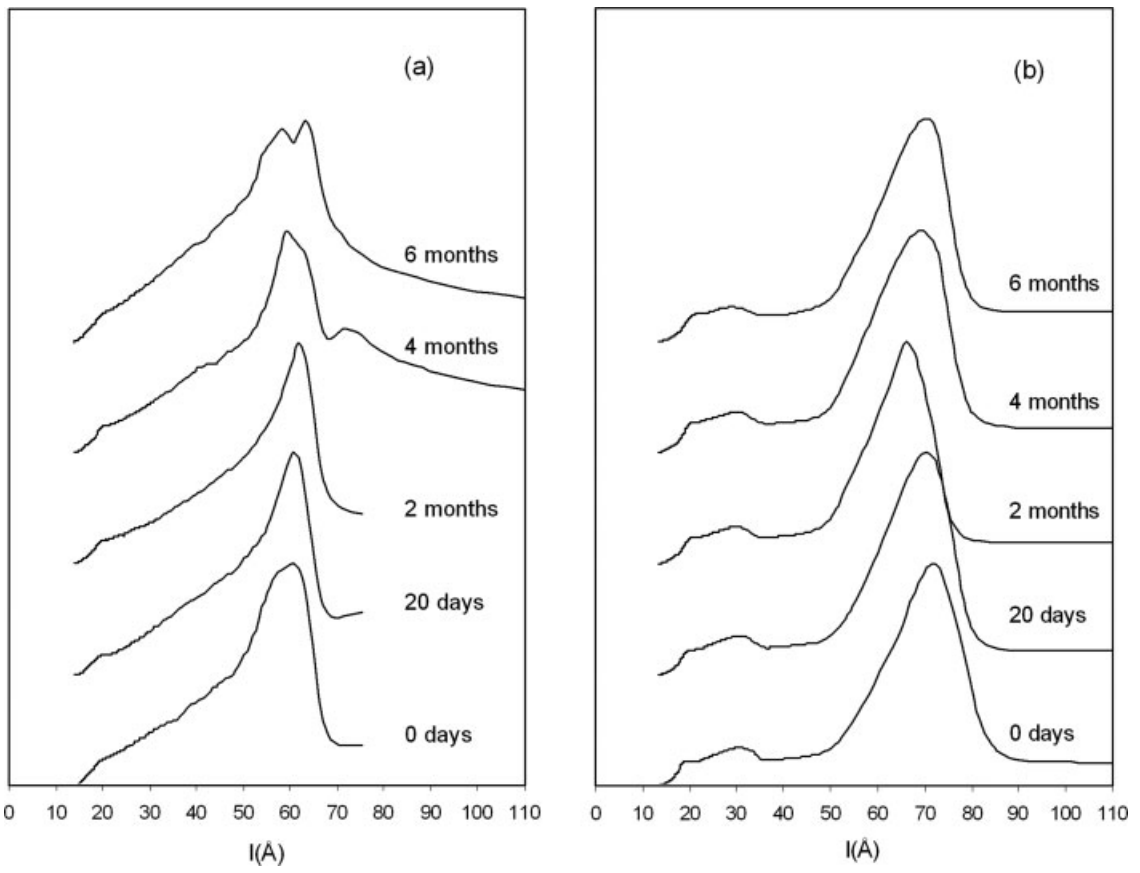

Figure 3 Evolution with the exposure time of the lamellar thickness distribution of the (a) LDPE/Cornplast blends and (b) LDPE/Cornplast blends subjected to thermo-oxidative treatment.

soil. These results may indicate that the thermo-oxidative treatment mainly modifies the degradation process in soil of the starch.

On the other hand, for the HDPE/Cornplast blends that were submitted to the burial soil test, it has been found that the areas related to both the biodegradable material and polyethylene increase with the exposure time in soil (Table IV).

Concerning the HDPE/Cornplast blends subjected to both the thermo-oxidative treatment and the soil burial test, a similar evolution of the two polyethylene areas and the Cornplast area is observed (Table IV). This consists of an initial increase followed by a later decrease of these areas as a function of the exposure time in soil. Comparing with the HDPE blends directly buried in soil, these results suggest that the thermo-oxidative treatment accelerates the degradation process in soil. This could be probably due to the fact that the thermo-oxidative treatment has promoted heterogeneity of these blends.

Thus, from the analysis of the crystalline content it can be stated that the thermo-oxidative treatment has a different effect on both types of blends. Whereas in the LDPE/Cornplast blends, starch is affected to a greater extent, in the HDPE/Cornplast blends both components are significantly modified by such treatment.

These results reveal that degradation is a complex process into which a great variety of molecular mechanisms are involved, such as crystallization and segregation processes. To analyze in more detail the changes taking place in the crystalline zone, the lamellar thickness distributions of the polyethylene contributions have also been calculated.

Lamellar thickness distribution

The lamellar thickness distribution of polyethylene was determined for each sample, using the method proposed by Wlochowicz and Eder,[23] based on the Thompson equation:

$$T_m = T_m^0\left(1 - \frac{2\sigma_e}{\Delta h_m l}\right)$$

where T_m is the observed melting point of lamellae of thickness l, σ_e is the surface free energy of the basal plane, Δh_m is the melting enthalpy per unit volume, and T_m^0 is the equilibrium melting point of an infinite crystal. These parameters have the following values for polyethylene: $T_m^0 = 414.6$ K,[23], $\sigma_e = 60.9 \times 10^{-3}$ J/m^2,[24] and $\Delta h_m = 2.88 \times 10^8$ J/m^3.[24]

The lamella thickness corresponding to each melting temperature can be calculated by means of the

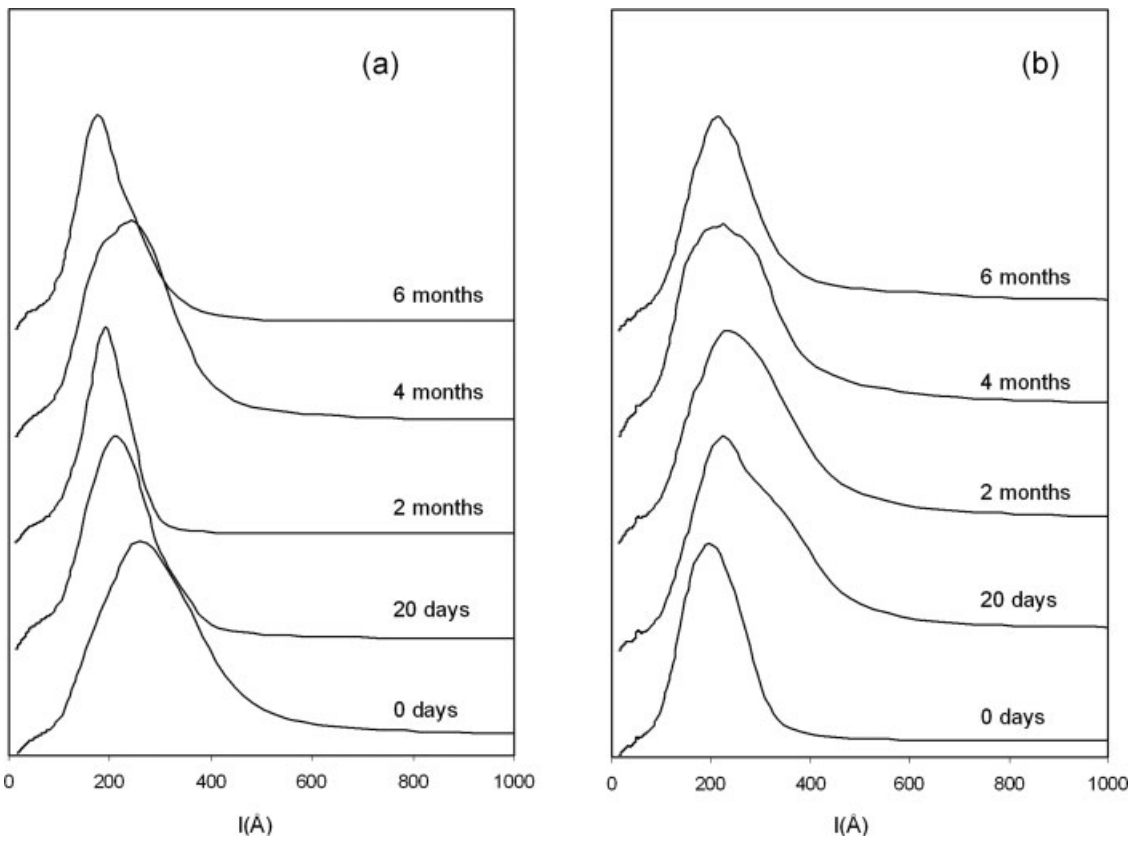

Figure 4 Evolution with the exposure time of the lamellar thickness distribution of the (a) HDPE/Cornplast blends and (b) HDPE/Cornplast blends subjected to thermo-oxidative treatment.

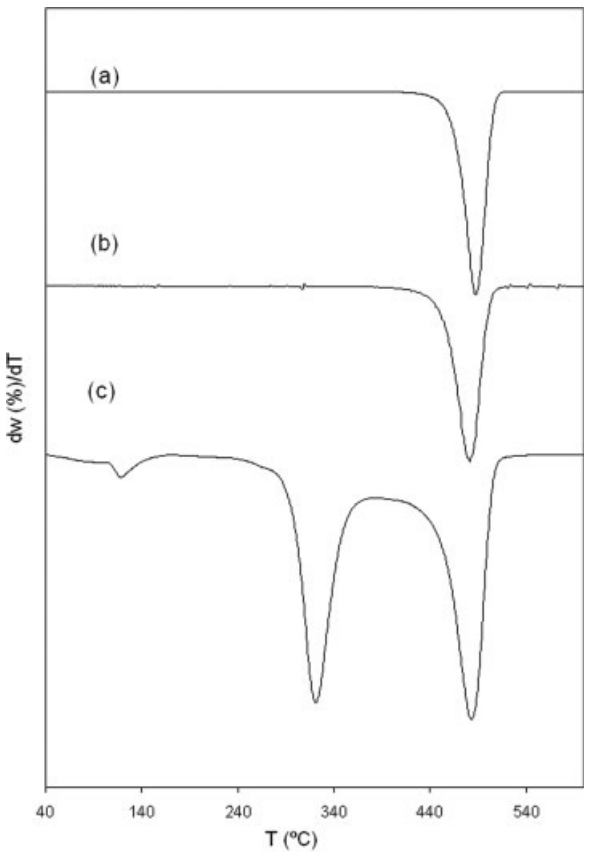

Figure 5 DTG thermograms of pure components. (a) LDPE, (b) HDPE, and (c) Cornplast.

Thomson equation and the earlier parameters. This method leads to the distribution curves of lamellae thicknesses. The lamellar thickness distribution of all the samples is plotted in Figures 3 and 4. The average lamellar values, corresponding to the maximum of each distribution, are listed in Tables III and IV.

The thermo-oxidative treatment leads to a shift towards higher values of the average lamellar thickness of the LDPE/Cornplast blends. Furthermore, a segregation of lamellae with very small thicknesses is also observed (Fig. 3).

Figure 3 reveals that the previous thermo-oxidative treatment leads to a different evolution of the lamellar thickness distribution of the LDPE/Cornplast blends during the soil burial test. The blends that were not subjected to the thermo-oxidative treatment exhibit two evolution stages as a function of the exposure time in soil. In a first stage, the distribution tends to become more homogeneous. In a second stage, a segregation of the crystallite sizes is observed. This phenomenon indicates a rearrangement of the crystalline phase, maybe promoted by the diffusion of the chains of the interspherulitic zone to the crystalline region. However, in the LDPE/Cornplast blends previously subjected to the thermo-oxidative treatment, the shape of their distribution does not change with the exposure time in soil. A slight decrease of the average lamellar thickness can also be observed in these blends (Table III).

The morphological behavior of the HDPE/Cornplast blends is different from that observed for the LDPE/Cornplast blends, regardless if they were subjected to the thermo-oxidative treatment or not (Fig. 4). For the HDPE/Cornplast blends directly buried in soil, the average lamellar thickness shifts to lower values with the exposure time in soil (Table IV). However, the average lamellar thickness of the HDPE/Cornplast blends subjected to the thermo-oxidative treatment first increases and finally tends to decrease with the exposure time in soil.

The lamellar thickness distribution of the HDPE/Cornplast blends that were directly buried in soil tends to become more homogeneous as the exposure time in soil increases. In contrast, in the HDPE blends that were previously subjected to the thermo-oxidative treatment, a broadening of their lamellar thickness distribution can be noted as a function of the exposure time in soil. This could probably be due to the heterogeneity promoted by the thermo-oxidative treatment in the HDPE/Cornplast blend.

These results confirm that degradation of the studied blends is a complex process involving various molecular mechanisms, such as homogeneity and segregation of the crystalline sizes. These are competitive processes that can occur simultaneously during degradation. Many factors like moisture, morphology of the blends, etc., may provoke one process prevailing over the others.

Thus, the thermal treatment leads to different morphological effects on the studied blends, depending on the polyethylene type. In the LDPE/Cornplast blends, the thermo-oxidative treatment promotes the degradation in soil of the biodegradable material, but it increases the crystalline zone of polyethylene and apparently hinders the degradation in soil of

TABLE V
Thermogravimetric Parameters of Pure LDPE, HDPE, and Cornplast

	LDPE		HDPE		CORNPLAST		
Exposure time in soil	*T* peak (°C)	Residue (%)	*T* peak (°C)	Residue (%)	*T* peak starch (°C)	*T* peak carbonated chains (°C)	Residue (%)
0 Days	483.5	1.6	486.7	0.36	322.0	484.0	7.0

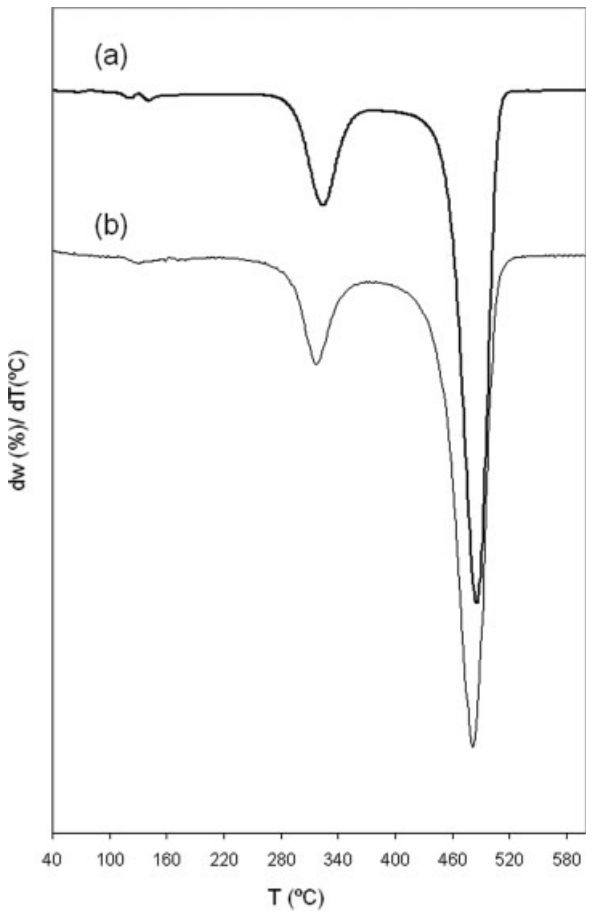

Figure 6 DTG thermograms of (a) LDPE/Cornplast blend and (b) LDPE/Cornplast blend subjected to thermo-oxidative treatment.

this component. In contrast, in the HDPE blends, the main modification is observed in the crystalline zone related to polyethylene. The thermo-oxidative treatment enhances the segregation of different lamellar thickness under soil burial conditions.

To analyze the occurrence of possible scissions of the molecular chains as result of the degradation process, and to confirm the different behavior of both polyethylene types, thermogravimetric measurements have also been performed.

TGA results

All the samples have been analyzed using TGA to study their thermal stability and to obtain their kinetic parameters. The latter allows the characterization of the thermal decomposition process of these blends, since these parameters may reveal the changes that occur in the molecular chains as a result of the degradation process.

The thermogram of pure polyethylenes can be observed in Figure 5. It displays a single degradation zone, which appears at 483°C for LDPE and 487°C for HDPE. These values agree with those reported in the literature for the thermal decomposition of the carbonated chains of these types of polyethylenes.[25,26] The amount of residue for both polyethylenes is less than 2% (Table V).

The thermogram of pure Cornplast displays two degradation steps (Fig. 5). The first one that appears at 321°C has been associated with the pyrolysis of starch.[27,28] The second step is centered on 482°C, and appears in the same temperature range as pure LDPE. Thus, this step has been related to the thermal decomposition of the polyethylene present in Cornplast. The amount of residue for pure Cornplast is 7% (Table V).

The thermograms of the LDPE/Cornplast and HDPE/Cornplast blends are displayed in Figures 6 and 7, respectively. The values of the residue and the peak temperature, corresponding to the temperature of the maximum rate of the thermal decomposition, are reported for these blends in Tables VI and VII, respectively. Three well-defined mass loss stages can be observed in both types of blends. The first mass loss is located around 130°C. It is well-known

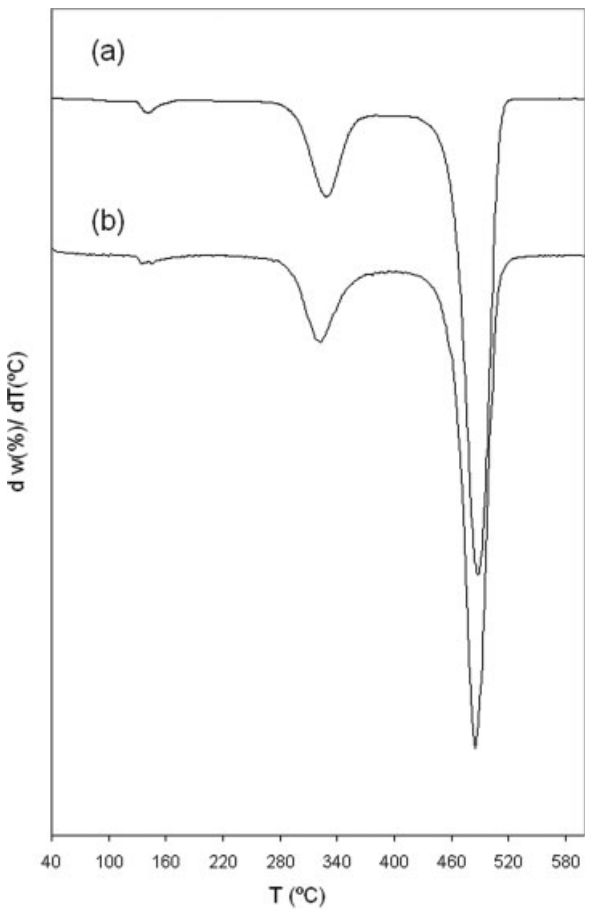

Figure 7 Thermograms of (a) HDPE/Cornplast blend and (b) HDPE/Cornplast blend subjected to thermo-oxidative treatment.

TABLE VI
Thermogravimetric Parameters of the LDPE/Cornplast Blends

	LDPE/Cornplast blends			LDPE/Cornplast blends with thermo-oxidative treatment		
Exposure time in soil	*T* peak secondary stage (°C)	*T* peak main stage (°C)	Residue (%)	*T* peak secondary stage (°C)	*T* peak main stage (°C)	Residue (%)
0 Days	324.1	485.6	5.3	316.0	481.3	6.2
20 Days	324.4	485.7	5.4	318.0	482.0	6.3
2 Months	326.2	485.9	4.7	317.0	481.2	6.1
4 Months	327.0	485.2	5.5	318.0	482.0	6.1
6 Months	329.6	485.5	4.9	319.0	482.0	6.0

that the loss of water retained by starch takes place in this temperature range. Thus, this stage can be attributed to the water absorbed by the starch present in Cornplast. This mass loss does not represent in any case more than 2%.[7]

The second mass loss appears around 323°C, regardless of the polyolefinic matrix used. Because this peak does not appear in the thermograms of pure LDPE and HDPE, it can be assigned to the thermal decomposition of Cornplast. Moreover, because the thermogram of pure Cornplast exhibits the pyrolysis of starch in this temperature interval, this stage can be associated with the thermal decomposition of the starch present in this biodegradable product.

The third mass loss corresponds to the main stage, which appears at 486°C for LDPE and at 489°C for HDPE, and can be associated to the overlapped thermal decomposition of the carbonated chains of both polyethylene and Cornplast. The temperature of this peak increases slightly as compared with their corresponding pure polyethylenes. This suggests that these blends have a thermal stability similar to that of pure polyethylene.

Regardless of the polyethylene used, all blends exhibit a similar amount of residue (6%). The fact that the residue of pure LDPE and HDPE is less than 2% and that of Cornplast is 7%, indicates that the origin of the residue in the blends may be mainly due to Cornplast.

To simulate the service life of the LDPE/Cornplast and HDPE/Cornplast blends, they were submitted to a previous thermo-oxidative treatment. The thermograms of these blends are displayed in Figures 6 and 7, and their thermogravimetric parameters are summarized in Tables VI and VII. It can be observed that the thermo-oxidative treatment causes a slight decrease of the peak temperature of starch in both types of blends. However, the peak temperature of the polyethylene chains changes slightly as a consequence of the thermo-oxidative treatment. These thermogravimetric results also show that the thermo-oxidative treatment increases the residue percentage in the same proportion for both types of blends.

The further disposal in landfill of the LDPE/Cornplast and HDPE/Cornplast blends was modeled with a soil burial test. It is observed for both blends that the peak temperature of the polyethylene backbones does not change significantly with the exposure time in soil, regardless of whether the blends were previously subjected to the thermo-oxidative treatment or not (Figs. 6 and 7). This indicates that the polyethylene chains of all the components of the blends are basically not modified during the degradation process in soil, regardless of thermo-oxidative treatment. However, a slight increase in the peak temperature of starch is noted, regardless of the polymeric matrix used.

Furthermore, the soil burial test leads to a slight decrease in the amount of residue in both blends, regardless of thermo-oxidative treatment (Tables VI

TABLE VII
Thermogravimetric Parameters of the HDPE/Cornplast Blends

	HDPE/Cornplast blends			HDPE/Cornplast blends with thermo-oxidative treatment		
Exposure time in soil	*T* peak secondary stage (°C)	*T* peak main stage (°C)	Residue (%)	*T* peak secondary stage (°C)	*T* peak main stage (°C)	Residue (%)
0 Days	328.3	488.6	5.5	322.0	485.6	6.6
20 Days	324.1	488.5	5.4	323.0	486.4	6.0
2 Months	324.5	488.7	4.4	324.9	485.2	6.2
4 Months	329.0	488.0	4.6	325.7	486.4	6.3
6 Months	331.4	488.7	5.4	326.0	486.0	6.1

TABLE VIII
Activation Energies (Ea) of Pure LDPE, HDPE, and Cornplast

	LDPE		HDPE		CORNPLAST			
	Ea (kJ/mol)		Ea (kJ/mol)		Ea (kJ/mol)			
Exposure time	Broido	Hirata	Broido	Hirata	Broido		Hirata	
in soil	(475–505°C)	(450–485°C)	(475–505°C)	(450–485°C)	(300–330°C)	(475–485°C)	(290–315°C)	(450–485°C)
0 Days	399.5	405.8	518.8	502.0	132.2	199.1	214.2	265.6

and VII). Because the residue has been attributed to the presence of Cornplast, this decrease in the amount of residue may indicate the degradation of Cornplast. As Cornplast is mainly made up of starch and this degradation is expected to be related to the degradation of the starch.

Because the temperature of the maximum rate of the thermal decomposition scarcely changes, a kinetic analysis was performed as well. This has allowed the calculation of the activation energy, to more accurately characterize the degradation process.

The activation energies of all thermal decomposition zones have been determined using the Broido integral method and the Hirata differential method. In previous works, it was concluded that the integral methods seem to better define the thermal decomposition stages at high temperatures when there are several overlapped processes, because these methods provide an average activation energy value.[13] On the other hand, the differential methods seem to better describe the low-temperature stages, since they allow the identification of different stages taking place in the same thermal decomposition process.

The Broido model[29] is based on the equation:

$$\ln\ \ln\left(\frac{1}{x}\right) = -\frac{E_a}{RT} + \text{const}$$

where R is the gas constant, T is the absolute temperature, E_a is the activation energy, and x is the residual fraction defined as $x = \frac{\omega_0 - \omega}{\omega_0 - \omega_\infty}$, where ω_0, ω_∞, and ω are the initial, residual, and actual mass, respectively.

The activation energy values estimated with the Broido model for the different processes involved in the thermal decomposition of all the samples are shown in Tables VIII, IX, and XI.

The Hirata model[30] is directly deduced from a kinetic function in its derivative form. This method describes the kinetics of a system undergoing chemical changes in terms of the weight of the sample ω at time t. The Hirata model is based on the equation:

$$\ln\left(-\frac{d\omega}{dt}\right) - \ln(\omega) = \ln\ A - \frac{E_a}{RT}$$

where A is the pre-exponential factor. R is the gas constant, T is the absolute temperature, and E_a is the activation energy.

The activation energies calculated with the Hirata model for the pure components and their blends are summarized in Tables VIII, X, and XII.

The results obtained with the Broido and the Hirata methods lead to the same decomposition stages. Nevertheless, the Hirata method allows the identification of more differences between the activation energy associated with each type of degradation.

As it has been previously mentioned, the thermal decomposition of pure LDPE and HDPE takes place in a single stage, which can be associated to the

TABLE IX
Activation Energies (Ea) of the LDPE/Cornplast Blends Calculated with the Broido Model

	LDPE/Cornplast blends		LDPE/Cornplast blends with thermo-oxidative treatment	
	Ea (kJ/mol)		Ea (kJ/mol)	
Exposure time	P2[a]	P1[b]	P2[a]	P1[b]
in soil	(300–330°C)	(475–505°C)	(290–330°C)	(475–505°C)
0 Days	118.8	297.4	118.8	255.2
20 Days	131.7	297.4	92.8	261.5
2 Months	117.9	304.6	88.2	268.6
4 Months	123.0	300.8	82.8	274.0
6 Months	112.1	302.0	84.5	271.1

[a] Related to the starch.
[b] Related to the carbonated chains.

TABLE X
Activation Energies (Ea) of the LDPE/Cornplast Blends Calculated with the Hirata Model

Exposure time in soil	LDPE/Cornplast blends		LDPE/Cornplast blends with thermo-oxidative treatment	
	Ea (kJ/mol)		Ea (kJ/mol)	
	P2 (290–315°C)	P1 (450–485°C)	P2 (290–315°C)	P1 (450–480°C)
0 Days	200.8	389.1	178.6	300.4
20 Days	196.6	401.6	131.3	301.2
2 Months	193.0	402.2	119.2	306.2
4 Months	184.0	414.6	99.1	309.6
6 Months	167.3	408.7	107.9	313.8

decomposition of their carbonated chains. Table VIII displays the activation energies assigned to this stage, calculated according to the Broido and the Hirata methods. It is well-known that the activation energy of the thermal decomposition process of LDPE is lower than that of HDPE.

The characteristic activation energies of the thermal decomposition process of pure Cornplast have also been determined (Table VIII). These correspond to the two thermal decomposition processes that were previously identified, related to starch and the polyethylene chains in the biodegradable material.

Activation energies for the LDPE/Cornplast and the HDPE/Cornplast blends are shown in Tables IX and X, and Tables XI and XII (where P2 is related to the starch and P1 to the carbonated chain), respectively. In general, kinetic results show that the LDPE/Cornplast blends have slightly lower activation energy values for all the thermal decomposition stages than the HDPE/Cornplast blends.

In contrast, the thermo-oxidative treatment causes a decrease in the activation energies of the thermal decomposition process of both the starch and the carbonated chains, regardless of the polyethylene type. However, this effect is more pronounced for the decomposition process of the polyethylene chains. Therefore, it can be established that the thermo-oxidative treatment affects the carbonated chains of polyethylenes to a greater extent. These results are in good agreement with the previous calorimetric results.

Concerning the LDPE/Cornplast and HDPE/Cornplast blends subjected to the soil burial test, a slight decrease of the activation energy of the starch has been noted, and is most significant in the HDPE/Cornplast blends. In contrast, the activation energy of both polyolefins tends to increase slightly with the exposure time in soil. Hence, degradation in soil affects the starch more significantly than the polyethylene chains. Moreover, the starch seems to degrade faster in the HDPE/Cornplast blends.

Finally, it can also be observed that the thermo-oxidative treatment accelerates the decrease of the activation energy of the decomposition of starch, when the blends are later submitted to the soil burial test. Furthermore, this effect is more significant in the LDPE/Cornplast blends, in contrast to what was noted in the LDPE blends directly buried in soil. These results are also in good agreement with the calorimetric results that have shown that in the LDPE/Cornplast blends, the area associated with the biodegradable material tends to disappear with the exposure time in soil. On the other hand, the

TABLE XI
Activation Energies (Ea) of the HDPE/Cornplast Blends Calculated with the Broido Model

Exposure time in soil	HDPE/Cornplast blends		HDPE/Cornplast blends with thermo-oxidative treatment	
	Ea (kJ/mol)		Ea (kJ/mol)	
	P2 (300–330°C)	P1 (475–490°C)	P2 (290–330°C)	P1 (470–505°C)
0 Days	149.3	305.4	216.0	256.4
20 Days	128.8	310.8	121.3	261.9
2 Months	115.0	330.1	126.7	266.5
4 Months	115.4	336.3	117.1	264.8
6 Months	140.5	324.2	112.9	273.6

TABLE XII
Activation Energies (Ea) of the HDPE/Cornplast Blends Calculated with the Hirata Model

Exposure time in soil	HDPE/Cornplast blends		HDPE/Cornplast blends with thermo-oxidative treatment	
	Ea (kJ/mol)		Ea (kJ/mol)	
	P2 (290–315°C)	P1 (450–485°C)	P2 (290–315°C)	P1 (450–480°C)
0 Days	213.3	397.4	186.6	364.8
20 Days	184.9	442.6	193.7	374.8
2 Months	186.6	442.2	179.0	370.2
4 Months	140.5	447.6	171.5	369.4
6 Months	129.7	449.7	161.0	369.8

thermo-oxidative treatment does not seem to affect significantly the thermal behavior of the polyethylene chains under soil burial conditions.

It could then be suggested that the thermo-oxidative treatment accelerates the degradation process in soil of the starch, especially in the LDPE/Cornplast blends. However, degradation in soil of the polyethylene chains seems not to be so influenced by the thermo-oxidative treatment.

CONCLUSIONS

Mixtures of high and LDPEs and a commercial biodegradable masterbatch containing starch (Cornplast) allow the production of heterogeneous blends with high thermal stability. The heterogeneity of the LDPE/Cornplast and HDPE/Cornplast blends has been demonstrated in the DSC thermograms where it is possible to distinguish the endotherm attributed to polyethylene from those associated with Cornplast.

For both types of blends, the thermo-oxidative treatment mainly affects the morphological and thermal properties of polyethylene. However, the degradation process in soil modifies to a greater extent the morphological and thermal behavior of the starch contained in the biodegradable material, which seems to degrade faster in the HDPE/Cornplast blends.

Synergetic degradation of the LDPE/Cornplast and HDPE/Cornplast blends has proved to be a complex process, in which a great variety of competitive processes are involved that mainly originate morphological changes in both components, especially in polyethylene. During the degradation process of these blends, a simultaneous tendency towards homogeneity and segregation of the crystallite sizes of polyethylene takes place.

In the LDPE/Cornplast blends, the thermo-oxidative treatment promotes the degradation of the biodegradable material under soil burial conditions. However, it also increases the crystalline zone of polyethylene, which apparently hinders its degradation in soil.

In the HDPE/Cornplast blends, the thermo-oxidative treatment promotes its heterogeneity and mainly modifies the crystalline zone of polyethylene. As a consequence, the segregation of different lamellar thicknesses of polyethylene during the soil burial test is enhanced.

References

1. Albertsson, A.-C.; Huang, S. J., Eds. Degradable Polymers, Recycling and Plastics Waste Management; Marcel Dekker: New York, 1995.
2. Smits, M. Polymer Products and Waste Management; Marcel Dekker: New York, 1995.
3. Clarinval, A.; Halleux, J. In Biodegradable Polymers for Industrial Applications; Smith, R., Ed.; Woodhead: London, 2005; Part 1, Chapter 1.
4. Bastioli, C. Handbook of Biodegradable Polymers; Rapra Technology: Shrewsbury, 2005.
5. Vikman, M.; Itavaara, M.; Poutanen, K. J Macromol Sci Pure Appl Chem 1995, 32, 863.
6. Albertsson, A.-C.; Karlsson, S. In Chemistry and Technology of Biodegradable Polymers; Griffin, G. J. L., Ed.; Blackie: Glasgow, 1994; Chapter 2.
7. Griffin, G. J. L., Ed. Chemistry and Technology of Biodegradable Polymers; Blackie: Glasgow, 1994.
8. Gould, J. M.; Gordon, S. H.; Dexter, L. B.; Swanson, C. L. In Agricultural and Synthetic Polymers: Biodegradability and Utilization; Glass, J. E., Swift, G., Eds.; American Chemical Society: Washington, DC, 1990; Chapter 7, p 65. ACS Symposium Series 433.
9. Otey, F. H.; Westhoff, R. P.; Doane, W. M. Ind Eng Chem Prod Res Dev 1987, 26, 1659.
10. Vilaplana, F.; Ribes-Greus, A.; Karlsson, S. Polym Degrad Stab 2006, 91, 2163.
11. Luzuriaga, S.; Kovárová, K.; Fortelny, I. Polym Degrad Stab 2006, 91, 1226.
12. Contat-Rodrigo, L.; Ribes-Greus, A. J Appl Polym Sci 2000, 78, 1707.
13. Contat-Rodrigo, L.; Ribes-Greus, A.; Día-Calleja, R. J Appl Polym Sci 2001, 82, 2174.
14. Vallés-Lluch, A.; Contat-Rodrigo, L.; Ribes-Greus, A. J Appl Polym Sci 2003, 90, 3359.
15. DIN 53739. Testing of plastics. Influence of Fungi and Bacteria. Visual Evaluation. Change in Mass and Physical Properties, Nov. 1984.

16. Contat-Rodrigo, L.; Ribes-Greus, A. J Appl Polym Sci 2003, 88, 1242.
17. Bogracheva, T. Y.; Meares, C.; Headley, C. L. Carbohydr Polym 2006, 63, 323.
18. Blennow, A.; Bay-Smidt, A. M.; Olsen, C. E.; Moller, B. L. Int J Biol Macromol 2000, 27, 211.
19. Kweon, D. K.; Cha, D. S.; ParK, H. J.; Lim, S. T. J Appl Polym Sci 2000, 78, 986.
20. Turi, E. Thermal Characterization of Polymeric Materials; Academic Press: New York, 1997; Vols. I and II.
21. Contat-Rodrigo, L.; Ribes-Greus, A. J Appl Polym Sci 2002, 83, 1683.
22. Vallés-Lluch, A.; Contat-Rodrigo, L.; Ribes-Greus, A. J Appl Polym Sci 2002, 86, 405.
23. Wlochowicz, A.; Eder, M.; Polymer 1984, 25, 1268.
24. Wunderlich, B. Macromolecular Physics; Academic Press: New York, 1973; Vol. 1, p 388.
25. Hawkins, W. Polymer Degradation and Stabilization; Springer-Verlag: Berlin, 1984.
26. Albertsson, A.-C.; Andersson, S. O.; Karlsson, S. Polym Degrad Stab 1987, 18, 73.
27. Aggarwal, P.; Dollimore, D. Thermochim Acta 1997, 291, 65.
28. Mano, J. F.; Koniarova, D.; Reis, R. L. J Mater Sci Mater Med 2003, 14, 127.
29. Broido, A. J Polym Sci Part A-2: Polym Phys 1969, 27, 1761.
30. Hirata, T.; Werner, K. E. J Appl Polym Sci 1987, 33, 1533.